175
Advances in Polymer Science

Advances in Polymer Science

Recently Published and Forthcoming Volumes

Inorganic Polymeric Nanocomposites and Membranes
Vol. 179, 2005

Polymeric and Inorganic Fibres
Vol. 178, 2005

Poly(arylene Ethynylenes)
From Synthesis to Application
Volume Editor: Weder, C.
Vol. 177, 2005

Metathesis Polymerization
Volume Editor: Buchmeiser, M.
Vol. 176, 2005

Polymer Particles
Volume Editor: Okubo, M.
Vol. 175, 2005

Neutron Spin Echo in Polymer Systems
Authors: Richter, D., Monkenbusch, M., Arbe, A., Colmenero, J.
Vol. 174, 2005

Advanced Computer Simulation Approaches for Soft Matter Sciences I
Volume Editors: Holm, C., Kremer, K.
Vol. 173, 2005

Microlithography · Molecular Imprinting
Vol. 172, 2005

Polymer Synthesis
Vol. 171, 2004

NMR · Coordination Polymerization · Photopolymerization
Vol. 170, 2004

Long-Term Properties of Polyolefins
Volume Editor: Albertsson, A.-C.
Vol. 169, 2004

Polymers and Light
Volume Editor: Lippert, T. K.
Vol. 168, 2004

New Synthetic Methods
Vol. 167, 2004

Polyelectrolytes with Defined Molecular Architecture II
Volume Editor: Schmidt, M.
Vol. 166, 2004

Polyelectrolytes with Defined Molecular Architecture I
Volume Editor: Schmidt, M.
Vol. 165, 2004

Filler-Reinforeced Elastomers · Scanning Force Microscopy
Vol. 164, 2003

Liquid Chromatography · FTIR Microspectroscopy · Microwave Assisted Synthesis
Vol. 163, 2003

Radiation Effects on Polymers for Biological Use
Volume Editor: Kausch, H.
Vol. 162, 2003

Polymers for Photonics Applications II
Nonlinear Optical, Photorefractive and Two-Photon Absorption Polymers
Volume Editor: Lee, K.-S.
Vol. 161, 2003

Filled Elastomers · Drug Delivery Systems
Vol. 160, 2002

Statistical, Gradient, Block and Graft Copolymers by Controlled/ Living Radical Polymerizations
Authors: Davis, K. A., Matyjaszewski, K.
Vol. 159, 2002

Polymer Particles

Volume Editor: Masayoshi Okubo

With contributions by
A. Butté · P. Y. Chow · J. M. DeSimone · K. Fontenot · L. M. Gan
K. Ito · S. Kawaguchi · K. A. Kennedy · Y. Luo · M. Nomura
G. W. Roberts · J. P. Russum · F. J. Schork · W. Smulders · K. Suzuki
H. Tobita

Springer

The series presents critical reviews of the present and future trends in polymer and biopolymer science including chemistry, physical chemistry, physics and material science. It is addressed to all scientists at universities and in industry who wish to keep abreast of advances in the topics covered.

As a rule, contributions are specially commissioned. The editors and publishers will, however, always be pleased to receive suggestions and supplementary information. Papers are accepted for "Advances in Polymer Science" in English.

In references Advances in Polymer Science is abbreviated Adv Polym Sci and is cited as a journal.

The electronic content of APS may be found springerlink.com

Library of Congress Control Number: 2004110358

ISSN 0065-3195
ISBN 3-540-22923-X **Springer Berlin Heidelberg New York**
DOI 10.1007/b14102

Springer is a part of Springer Science+Business Media
springeronline.com

Printed in The Netherlands

Cover design: KünkelLopka GmbH, Heidelberg/design & production GmbH, Heidelberg
Typesetting: Fotosatz-Service Köhler GmbH, Würzburg

Printed on acid-free paper 02/3141 xv – 5 4 3 2 1 0

Volume Editor

Prof. Masayoshi Okubo

Kobe University
Fac. Engineering Dept.
Rokko-dai 1-1, Nada-ku
657-8501 Kobe, Japan
okubo@cx.kobe-u.ac.jp

Editorial Board

Advances in Polymer Science
Also Available Electronically

For all customers who have a standing order to Advances in Polymer Science, we offer the electronic version via SpringerLink free of charge. Please contact your librarian who can receive a password for free access to the full articles by registering at:

springerlink.com

If you do not have a subscription, you can still view the tables of contents of the volumes and the abstract of each article by going to the SpringerLink Homepage, clicking on "Browse by Online Libraries", then "Chemical Sciences", and finally choose Advances in Polymer Science.

You will find information about the

– Editorial Board
– Aims and Scope
– Instructions for Authors
– Sample Contribution

at springeronline.com using the search function.

Preface

In this special volume on polymer particles, recent trends and developments in the synthesis of nano- to micron-sized polymer particles by radical polymerization of vinyl monomers in environmentally friendly heterogeneous aqueous and supercritical carbon dioxide fluid media are reviewed by prominent worldwide researchers. Polymer particles are prepared extensively as synthetic emulsions and latexes, which are applied as binders in the industrial fields of paint, paper and inks, and films such as adhesives and coating materials. Considerable attention has recently been directed towards aqueous dispersed systems due to the increased awareness of environmental issues. Moreover, such polymer particles have already been applied to more advanced fields such as bio-, information, and electronic technologies. In addition to the obvious commercial importance of these techniques, it is of fundamental scientific interest to completely elucidate the mechanistic details of macromolecule synthesis in the "microreactors" that the polymer particles in these heterogeneous systems constitute.

In the first chapter, Professor Nomura et al. review features of emulsion polymerization, which is applied for the synthesis of submicron-sized polymer particles, with particular emphasis on particle nucleation and growth and polymer structure development. In the second chapter, Professor Schork describes the basic features of miniemulsion polymerization, which is deeply related to emulsion polymerization, but offers advantages for the synthesis of hybrid particles in which hydrophobic substances are included. This chapter also covers controlled/living radical polymerization, which has been developed over the past 10 years. It is of great importance both from an academic and industrial perspective to make controlled/living radical polymerization compatible with heterogeneous systems. In the third chapter, Professsor Gan and coworkers review microemulsion polymerization and its applications for the synthesis of polymer nanoparticles and nanocomposites of polymeric/inorganic substances. In the fourth chapter, Professors Kawaguchi and Ito review various features of dispersion polymerization, which is a useful technique for the synthesis of micron-sized monodisperse polymer particles, focusing on the preparation of novel functional particles and the control of particle size. In the final chapter, heterogeneous polymerization of fluoroolefins in supercritical carbon dioxide fluids is reviewed. One of the authors,

Professor DeSimone, is the pioneer of heterogeneous polymerizations in supercritical carbon dioxide.

As the editor of this Special Volume on "Polymer Particles", I would like to thank all of the authors who made valuable contributions in spite of their undoubtedly busy schedules. I believe this work will be of great use for scientists in both academia and industry.

Kobe, November 2004 Masayoshi Okubo

Contents

Adv Polym Sci (2005) 175: 1–128
DOI 10.1007/b100116

Emulsion Polymerization: Kinetic and Mechanistic Aspects

Mamoru Nomura (✉) · Hidetaka Tobita · Kiyoshi Suzuki

Department of Materials Science and Engineering, Fukui University, Fukui, Japan
nomuram@matse.fukui-u.ac.jp, tobita@matse.fukui-u.ac.jp, suzuki@matse.fukui-u.ac.jp

Abstract The current understanding of the kinetics and mechanisms of batch and continuous emulsion polymerizations is summarized from the viewpoints of particle formation and growth and polymer structure development. There are numerous factors that affect these processes; among them, studies on the radical transfer and monomer partitioning between phases, which are key factors for particle formation and growth, are reviewed and discussed. Attention is also focused on the effects of initiator type, additives and impurities in the recipe ingredients, and agitation, each of which sometimes exert crucial influences on the processes of particle formation and growth. In relation to polymer structure development, important aspects of the molecular weight distribution and branched/crosslinked polymer formation are highlighted.

Keywords Emulsion polymerization · Kinetics · Particle nucleation · Particle growth · Molecular weight distribution · Nonlinear polymers

Abbreviations

AA	acrylic acid
AAm	acrylamide
AN	acrylonitrile
APS	ammonium persulfate
AIBN	2,2′-azobis-isobutyronitrile
BA	butyl acrylate
Bu	butadiene
CCTVFR	continuous Couette-Taylor vortex flow reactor
CLTR	continuous loop-tubular reactor
CMC	critical micellar concentration
CSTR	continuous stirred tank reactor
CTR	continuous tubular reactor
DVB	divinylbenzene
E	ethylene
KPS	potassium persulfate
MA	methyl acrylate
MAA	methacrylic acid
MC	Monte Carlo
MMA	methyl methacrylate
MWD	molecular weight distribution
NaLS	sodium laurylsulfate
n-BA	*n*-butyl methacrylate
PSD	particle size distribution
PSPC(R)	pulsed sieve plate column (reactor)
PT(R)	pulsed tubular (reactor)
S-E	Smith and Ewart
SEC	size exclusion chromatography
St	styrene
VAc	vinyl acetate
VCl	vinyl chloride
A_m	total surface area of micelles per unit volume of water
A_p	total surface area of polymer particles per unit volume of water
a_s	surface area occupied by a unit amount of emulsifier
d_m	diameter of a micelle
d_p	diameter of a polymer particle
D_w	diffusion coefficient for radicals in the aqueous phase

D_p	diffusion coefficient for radicals inside a polymer particle
$E(t)$	residence time distribution function
F	absorption efficiency factor defined in Eq. 8
f	initiator efficiency
f_i	fraction of i-radicals in the polymer particle phase
I_0, $[I_0]$	initial initiator concentration
k_d	rate constant for initiator decomposition
k_{em}	mass transfer coefficient for micelles defined by Eq. 7
k_{ep}	mass transfer coefficient for polymer particles defined by Eq. 7
k_f	rate coefficient for radical desorption per particle
k_{mf}	chain transfer rate constant to monomer
k_{tw}	rate coefficient for bimolecular radical termination in the aqueous phase
k_{Tf}	chain transfer rate constants to chain transfer agent (CTA)
m_d	partition coefficient for monomer (monomeric radicals) between particle and aqueous phases defined by $m_d=[M]_p/[M]_m$
M_m	aggregation number of emulsifier molecules per micelle
M_0	initial monomer concentration
$[M]_{pc}$	constant monomer concentration in polymer particles at saturation swelling
$[M]_w$	monomer concentration in the aqueous phase
$\bar{n}_A$	average number of A-radicals per polymer particle
N_n	number of polymer particles containing n radicals
R_p	rate of polymerization
$[R_w^\bullet]$	radical concentration in the aqueous phase
S_0	initial emulsifier concentration
S_m	concentration of emulsifier forming micelles
v_p	volume of a polymer particle
X_{Mc}	critical monomer conversion where monomer droplets disappear from the aqueous phase
α_w	nondimensional parameter defined by $\rho_w v_p/k_{tp}N_T$
ε	defined by $(k_{ep}/k_{em})M_m$ in Eq. 37
λ	partition coefficient for radicals between particle and water phase
μ	volumetric growth rate per polymer particle
θ	mean residence time
ρ	radical entry rate per polymer particle defined by Eq. 12
ρ_e	overall rate of radical entry into polymer particles
ρ_p	polymer density
ρ_w	rate of radical generation per unit volume of water

1 Introduction

There are four main types of liquid-phase heterogeneous free-radical polymerization; microemulsion polymerization, emulsion polymerization, miniemulsion polymerization and dispersion polymerization, all of which can produce nano- to micron-sized polymeric particles. Emulsion polymerization is sometimes called macroemulsion polymerization. In recent years, these heterophase polymerization reactions have become more and more important

technologically and commercially, not only as methods for producing high-performance polymeric materials, but also from an environmental point of view. It is well known that microemulsion, miniemulsion and dispersion polymerizations bare many similarities to emulsion polymerization in the kinetics of particle nucleation and growth and in polymer structure development. Therefore, for optimal design and operation of these heterophase free radical polymerizations, it is important to have detailed knowledge of the kinetics and mechanisms of emulsion polymerization. In this article, recent developments in emulsion polymerization are reviewed from kinetic and mechanistic perspectives.

Between 1995 and 1997, three excellent books on emulsion polymerization were published and provide extensive reviews of the subject up to 1995 [1–3]. Therefore, this review article will focus on research work that has appeared since ~1996. We will also include historically important work from before 1995 in this review article.

2
Emulsion Polymerization Kinetics

2.1
Generally Accepted Kinetics Scheme

Emulsion polymerization takes place over a number of steps, where various chemical and physical events take place simultaneously during the process of particle formation and growth. Figure 1 depicts the generally accepted scheme for the kinetics of emulsion polymerization.

Three major mechanisms for particle formation have been proposed to date. Figure 1a shows the proposed scheme for particle formation in emulsion polymerization initiated by water-soluble initiators. Particle formation is considered to take place when either: (1) a free radical in the aqueous phase enters a monomer-swollen emulsifier micelle and propagation proceeds therein (*micellar nucleation*); (2) the chain length of a free radical growing in the aqueous phase exceeds its solubility limit and precipitates to form a particle nucleus (*homogeneous nucleation*), or; (3) a free radical growing in the aqueous phase enters a monomer droplet and propagation proceeds therein (*droplet nucleation*). However, if the resultant polymer particles are not stable enough, the final number of polymer particles produced, regardless of the mechanism of particle formation, is determined by coagulation between the existing particles (*coagulative nucleation*).

In the process of particle growth, various chemical and physical events occur in both the aqueous and particle phases, as illustrated in Fig. 1b [1]. We now know that the polymerization takes place exclusively in the resultant polymer particle phase, wherever the free radicals are generated. Smith and Ewart [4] were the first to establish a quantitative description of the processes of parti-

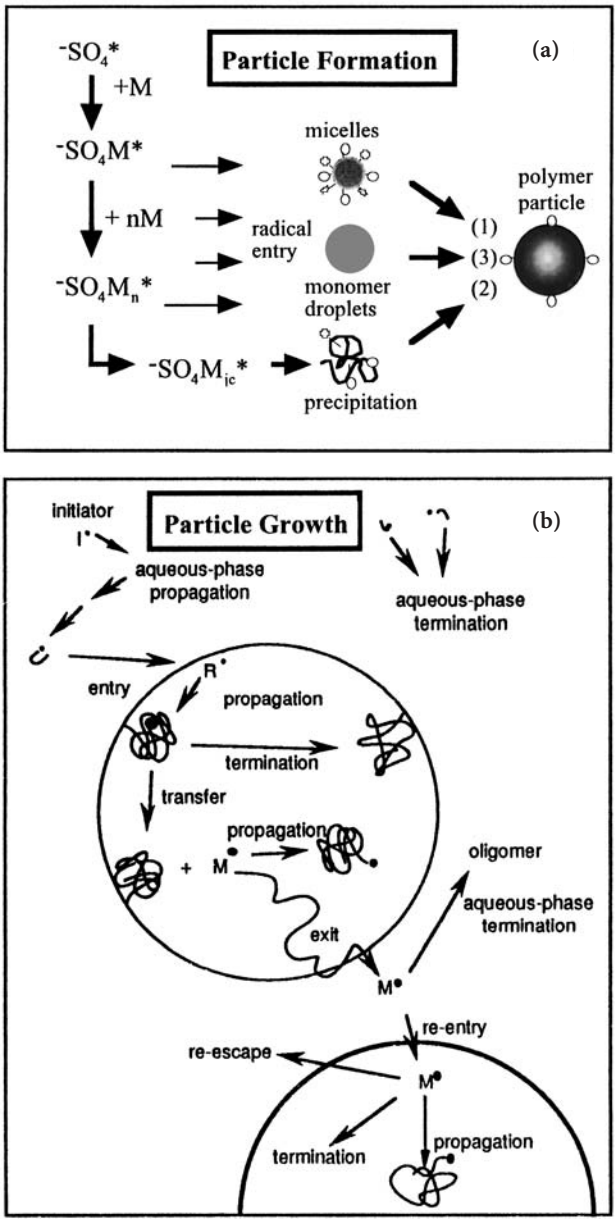

Fig. 1 (**a**) Three major mechanisms of particle formation, and (**b**) various chemical and physical events that occur during the process of particle growth in an emulsion polymerization

cle formation and growth in emulsion polymerization on the basis of the achievements made by Harkins et al. [5]. This is now called the Smith-Ewart theory. It is not an exaggeration to say that almost all of the theoretical developments in emulsion polymerization that have been made so far are based on the Smith-Ewart theory.

2.2 Summary of the Smith-Ewart Theory

The Smith and Ewart theory (the S-E theory) describes the basic concept of emulsion polymerization. Its main points are briefly reviewed here. Smith and Ewart showed that the rate of emulsion polymerization, which proceeds exclusively in the polymer particles, is given by

$$R_p = k_p[M_p]\bar{n}N_T \tag{1}$$

where k_p is the propagation rate constant, $[M]_p$ is the monomer concentration in the monomer-swollen polymer particles, N_T is the number of monomer-swollen polymer particles per unit volume of water and $\bar{n}$ is the average number of radicals per particle, defined as

$$\bar{n} = \sum_{n=1}^{\infty} nN_n \Big/ \sum_{0}^{\infty} N_n = \sum_{n=1}^{\infty} nN_n \Big/ N_T \tag{2}$$

where N_n is the number of polymer particles containing n free radicals. N_n is described by the following balance equation that takes into account three rate processes: (1) radical entry into, (2) radical desorption (exit) from, and (3) bimolecular radical termination inside the polymer particle

$$\begin{aligned} dN_n/dt = {} & (\rho_e/N_T)N_{n-1} + k_f(n+1)N_{n+1} + k_{tp}[(n+2)(n+1)/v_p] \\ & - N_n\{\rho_e/N_T + k_f n + k_{tp}[(n(n-1)/v_p]\} = 0 \end{aligned} \tag{3}$$

where k_f is the rate coefficient for radical desorption per particle, v_p is the volume of a polymer particle, k_{tp} is the rate coefficient for bimolecular radical termination inside the polymer particles, and ρ_e is the overall rate of radical entry into polymer particles, defined by

$$\rho_e = \rho_w + k_f\bar{n}N_T - 2k_{tw}[R_w^*]^2 \tag{4}$$

where ρ_w is the rate of radical production per unit volume of water, k_{tw} is the rate coefficient for bimolecular radical termination in the aqueous phase, and $[R_w^*]$ is the radical concentration in the aqueous phase.

On the other hand, they derived an expression that predicts the number of polymer particles produced, N_T, assuming that (i) a monomer-swollen emulsifier micelle is transformed into a polymer particle by capturing a free radical from the aqueous phase, (ii) the volumetric growth rate per particle μ is constant, at least during particle formation, and (iii) free radical activity does not transfer out of a growing particle

$$N_T = k(\rho_w/\mu)^{0.4}(a_s S_0)^{0.6} \quad (5)$$

where k is a constant between 0.37 and 0.53, a_s is the surface area occupied by a unit amount of emulsifier, S_0 is the initial emulsifier concentration (the concentration of emulsifier forming micelles), and ρ_w is the rate of radical generation per unit volume of water, given by

$$\rho_w = 2k_d f[I_0] \quad (6)$$

where k_d is the rate constant for initiator decomposition, f is the initiator efficiency, and $[I_0]$ is the initial initiator concentration. Since the appearance of the S-E theory, much effort has been directed into investigating the physical meanings of various parameters such as ρ_e, k_f and k_{tp}, and the effects of these parameters on the three key factors of emulsion polymerization, $[M]_p$, $\bar{n}$ and N_T.

3
Kinetics and Mechanisms of Emulsion Polymerization

3.1
Radical Entry

One of the most important parameters in the S-E theory is the rate coefficient for radical entry. When a water-soluble initiator such as potassium persulfate (KPS) is used in emulsion polymerization, the initiating free radicals are generated entirely in the aqueous phase. Since the polymerization proceeds exclusively inside the polymer particles, the free radical activity must be transferred from the aqueous phase into the interiors of the polymer particles, which are the major loci of polymerization. Radical entry is defined as the transfer of free radical activity from the aqueous phase into the interiors of the polymer particles, whatever the mechanism is. It is believed that the radical entry event consists of several chemical and physical steps. In order for an initiator-derived radical to enter a particle, it must first become hydrophobic by the addition of several monomer units in the aqueous phase. The hydrophobic oligomer radical produced in this way arrives at the surface of a polymer particle by molecular diffusion. It can then diffuse (enter) into the polymer particle, or its radical activity can be transferred into the polymer particle via a propagation reaction at its penetrated active site with monomer in the particle surface layer, while it stays adsorbed on the particle surface. A number of entry models have been proposed: (1) the surfactant displacement model; (2) the collisional model; (3) the diffusion-controlled model; (4) the colloidal entry model, and; (5) the propagation-controlled model. The dependence of each entry model on particle diameter is shown in Table 1 [12].

However, some of these models have been refuted, and two major entry models are currently widely accepted. One is the diffusion-controlled model, which assumes that the diffusion of radicals from the bulk phase to the surface

Table 1 Dependence of entry rate coefficient on particle diameter, as predicted by different models [12]

Entry model	Dependence on d_p
Surfactant displacement [7]	none
Collisional [8]	d_p^2
Diffusional [9]	d_p
Colloidal [10]	d_p
Propagational [6, 11]	no dependence

of a polymer particle is the rate-controlling step. The other is the propagation-controlled model, which assumes that since only z-mer radicals can enter the polymer particles very rapidly, the generation of z-mer radicals from (z–1)-mer radicals by a propagation reaction in the aqueous phase is the rate-controlling step.

3.1.1 Diffusion-Controlled Entry

Smith and Ewart [4] first proposed that the transfer of free radical activity into the interior of a polymer particle takes place by the direct entry of a free radical into a polymer particle. They pointed out that the rate of radical entry into a polymer particle is given by the rate of diffusion of free radicals from an infinite medium of concentration $[R_w^*]$ into a particle of diameter d_p with zero radical concentration,

$$\rho_e/N_T = 2\pi D_w d_p [R_w^*] = k_{ep}[R_w^*] \tag{7}$$

where D_w is the diffusion coefficient for the radicals in the water phase and k_{ep} the mass transfer coefficient for radical entry into a particle. However, for simplicity, they actually used a rate coefficient that is proportional to the square of the diameter (the surface area). Since then, most researchers have treated the problem of particle formation by assuming that the rate of radical entry into a micelle and a polymer particle is proportional to the surface area (*the collisional entry model*) [8, 13].

On the other hand, Nomura and Harada [14] proposed a kinetic model for the emulsion polymerization of styrene (St), where they used Eq. 7 to predict the rate of radical entry into both polymer particles and monomer-swollen micelles. In their kinetic model, the ratio of the mass-transfer coefficient for radical entry into a polymer particle k_{ep} to that into a micelle k_{em}, k_{ep}/k_{em}, was the only one unknown parameter (Eq. 37). They determined the value of k_{ep}/k_{em} to be about 10^3 by comparing the model's predictions with experimental results. However, the observed value of k_{ep}/k_{em} was at least two orders of magnitude greater than that predicted by Eq. 7, because $k_{ep}/k_{em}=d_p/d_m$ (d_m is the

diameter of a micelle) according to Eq. 7 and the value of d_p/d_m would be 10 at the most during particle formation. This was considered to indicate that the radical capture efficiency of a micelle is a factor of about 100 less than that of a particle. Taking this into consideration, they implicitly introduced a concept called the "radical capture efficiency of a micelle relative to a polymer particle" to adjust for this disagreement and pointed out two possible reasons for the lower radical capture efficiency of a micelle. One is that the energy barrier against the entry of charged radicals into micelles may be higher than that into polymer particles. The other is that an oligomeric radical, having entered a micelle, may pass through the micelle without adding at least one extra monomer unit because the volume of the micelle is so small that the mean residence time of the radical in the micelle is too short for the radical to add another unit.

The concept of "radical capture efficiency" was further elaborated on by Hansen et al. [15–17]. By applying the theory of mass transfer with simultaneous chemical reactions, they proposed the following expression to represent the *net rate* of radical absorption by a particle, introducing an "*absorption efficiency factor*" *F* into Eq. 8

$$\rho_e/N_T = 2\pi D_w d_p [R_w^*] F = k_{ep}[R_w^*]. \tag{8}$$

Therefore, *F* represents a factor that describes the degree to which absorption is lowered compared to irreversible diffusion, and is given by

$$\frac{1}{F} = \left(\frac{D_w}{\lambda D_p}\right)(X \coth X - 1)^{-1} + W' \tag{9}$$

where $X=(d_p/2)\{(k_p[M]_p+nk_{tp}/v_p)/D_p\}^{1/2}$ and λ is the equilibrium partition coefficient between particles and water for radicals, W' is the potential energy

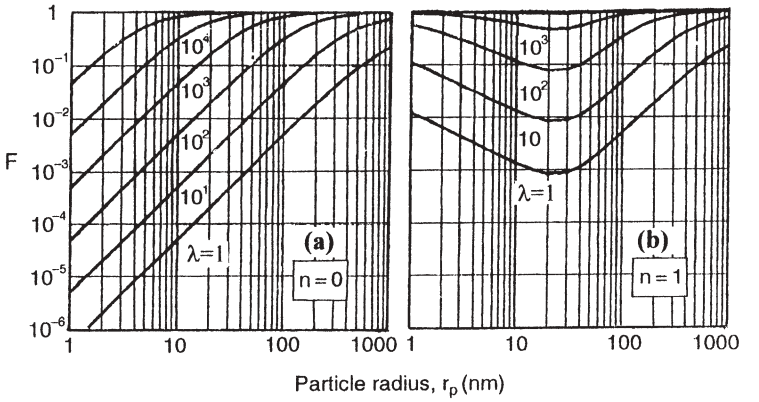

Fig. 2 Capture efficiency *F* as a function of particle size r_p for different values of the partition coefficient, λ, and the number of radicals in a polymer particle for St polymerization; (**a**) n=0 and (**b**) n=1

barrier analogous to Fuchs' stability factor, D_p is the diffusion coefficient for the radicals inside a particle, k_p is the propagation rate constant, $[M]_p$ is the monomer concentration in particles, n is the number of radicals in a particle, N_A is Avogadro's number and v_p is the particle volume. It should be noted that radicals are captured inside the particles only if they react therein; otherwise they will eventually diffuse out and back to the water phase. Figure 2 shows an example of F versus particle radius r_p, calculated from Eq. 9. The important conclusion of Eq. 9 is, as is clear from Fig. 2, that the value of F for a particle containing radicals is higher than that for a particle containing no radicals. According to Fig. 2a, it approximately holds that $F \propto d_p^2$, and hence this model gives $k_{ep}/k_{em}=(d_p/d_m)(F_p/F_m)=(d_p/d_m)^3 \cong 10^3$, the value of which is in good agreement with the result obtained by Nomura et al. in the emulsion polymerization of St [14].

A much simpler model for the radical capture (absorption) efficiency F can be derived by introducing the concept of radical desorption from a polymer particle, developed in Section 3.2.1. The probability F for a radical to be captured inside a particle containing n radicals by any chemical reaction (propagation or termination) is given by

$$F = \frac{k_p[\mathrm{M}]_p + k_{tp}(n/v_p)}{K_o + k_p[\mathrm{M}]_p + k_{tp}(n/v_p)} \tag{10}$$

where K_o is the overall radical desorption rate constant for a particle, defined by Eq. 19 and shown later in Section 3.2.1. For simplicity, no distinction is made here between radicals with and without initiator fragments at their ends. In the case where $K_o \gg k_p[\mathrm{M}]_p$, $k_{tp}(n/v_p)$, substitution of Eq. 19 into Eq. 10 leads to

$$F = k_p[\mathrm{M}]_p/K_o = \left(\frac{k_p[\mathrm{M}]_p m_d}{12D_w}\right)\left(1 + \frac{\psi D_w}{m_d D_p}\right) d_p^2 \propto d_p^2 \tag{11}$$

The result of Eq. 11 agrees with $F \propto d_p^2$ obtained above by Ugelstad and Hansen [15]. Therefore, both Eq. 9 developed by Hansen and Ugelstad and Eq. 11 developed here can explain the value of $k_{ep}/k_{em} \cong 10^3$ found experimentally by Nomura et al. [14], although no direct experimental confirmation of the validity of these radical capture models have been reported yet.

Unzueta et al. [18] derived a kinetic model for the emulsion copolymerization of methyl methacrylate (MMA) and butyl acrylate (BA) employing both the micellar and homogeneous nucleation mechanisms and introducing the radical absorption efficiency factor for micelles, F_m, and that for particles, F_p. They compared experimental results with model predictions, where they employed the values of $F_p=10^{-4}$ and $F_m=10^{-5}$, respectively, as adjustable parameters. However, they did not explain the reason why the value of F_m is an order of magnitude smaller than the value of F_p. Sayer et al. [19] proposed a kinetic model for continuous vinyl acetate (VAc) emulsion polymerization in a pulsed

sieve plate column reactor, where they assumed that both micellar and homogeneous nucleation takes place, and introduced the radical absorption efficiency factor F_m for micelles and F_p for polymer particles, respectively. They could explain the experimental results by employing $F_m=1.0\times10^{-5}$ and $F_p=3.3\times10^{-3}$ in the model predictions, indicating that $k_{ep}/k_{em}=330$. This value agrees fairly well with the value of 100 found for the St system [14], but is 30 times less than $k_{ep}/k_{em}=10^4$ found for the VAc system [20]. Araújo et al. [21] developed a detailed dynamic mathematical model that describes the evolution of particle size distributions (PSDs) during the emulsion copolymerization of VAc and Veova10 in a continuous loop-tubular reactor and compared results from it with their experimental data. They could describe the process of micellar particle formation by introducing radical absorption efficiency factors for micelles of $F_m=1.5\times10^{-4}$ and for particles of $F_p=1.5\times10^{-3}$, respectively, although they also did not provide a reason why the value of F_m is 1/10 of the value of F_p. This gives $k_{ep}/k_{em}=(d_p/d_m)(F_p/F_m)\cong10^2$ if one assumes that $d_p/d_m\cong10$. On the other hand, Herrera-Ordóñez et al. [22] also developed a mathematical model for St emulsion polymerization employing Eq. 8 as the radical capture rate coefficient, where the expression for the capture of monomeric radicals is that used by Hansen and Ugelstad [15, 17], while a more detailed modification was made for the entry of initiator-derived radicals.

3.1.2 Propagation-Controlled Entry

Maxwell et al. [11] proposed a radical entry model for the initiator-derived radicals on the basis of the following scheme and assumptions. The major assumptions made in this model are as follows: An aqueous-phase free radical will irreversibly enter a polymer particle only when it adds a critical number z of monomer units. The entrance rate is so rapid that the z-mer radicals can survive the termination reaction with any other free radicals in the aqueous phase, and so the generation of z-mer radicals from (z–1)-mer radicals by the propagation reaction is the rate-controlling step for radical entry. Therefore, based on the generation rate of z-mer radicals from (z–1)-mer radicals by propagation reaction in the aqueous phase, they considered that the radical entry rate per polymer particle, ρ ($\rho=\rho_e/N_T$) is given by

$$\rho = k_{pw}[\mathrm{IM}^{\star}_{z-1}][\mathrm{M}]_w N_T \tag{12}$$

where k_{pw} is the propagation rate constant in the aqueous phase and $[M]_w$ is the monomer concentration in the aqueous phase. By substituting the steady-state concentration of (z–1)-mer radicals $[\mathrm{IM}^{\star}_{z-1}]$ into Eq. 12, the approximate expressions for ρ and the initiator efficiency, f_{entry} are derived, respectively, as

$$\rho = \frac{2k_d[\mathrm{I}]}{N_p}\left\{\frac{\sqrt{k_d[\mathrm{I}]k_{t,w}}}{k_{p,w}[\mathrm{M}]_w}+1\right\}^{1-z} = \frac{2k_d[\mathrm{I}]}{N_p}f_{entry} \tag{13}$$

$$f_{\text{entry}} = \left\{ \frac{\sqrt{k_{\text{d}}[\text{I}]k_{\text{t,w}}}}{k_{\text{p,w}}[\text{M}]_{\text{w}}} + 1 \right\}^{1-z} \tag{14}$$

There has been discussion on the value of z. Maxwell et al. [11] proposed a semi-empirical thermodynamic model to predict the value of z for persulfate-derived oligomeric radicals, which is given by

$$z \cong 1 + \text{int}\left(-23\ \text{kJmol}^{-1}/\{RT \ln[\text{M}_{\text{sat}}]_{\text{w}}\}\right) \tag{15}$$

where the integer function (int) rounds down the quantity in parentheses to the nearest integer value and $[\text{M}_{\text{sat}}]_{\text{w}}$ is the saturation solubility of the monomer in mol dm^{-3}. On the other hand, Sundberg et al. [23] proposed a thermodynamic method for estimating the critical chain length z of entry radicals with a hydrophilic end group (such as SO_4^-) using a simple two-layer lattice model. The values of z calculated by both Sundberg et al. and by Maxwell et al. (Eq. 15) are listed in Table 2.

Several research articles have been published that deal with the methodology for determining the radical entry rate ρ, the initiator efficiency f_{entry} and the actual values of z. Hawkett et al. [24] developed a method for determining the value of ρ along with the desorption rate coefficient k_{fs}, termed the *slope-and-intercept* method. This method is experimentally simple, but has several drawbacks [25]. For example, it is only applicable to the so-called zero-one system ($\bar{n} \leq 0.5$) with negligible radical termination in the aqueous phase. It is usually very difficult to judge whether or not the radical termination in the aqueous phase is negligible. Moreover, it gives a large error if an induction period caused by any trace of impurity exists. Marestin et al. [26] proposed an experimental method for directly determining the entry rate of a critical size MMA oligomer into the polymer particle using the seeded emulsion polymerization of MMA

Table 2 Predicted Z values for persulfate-derived radicals

Monomer	Z value	
	Maxwell et al., at 50 °C [1]	Sundberg et al., at 25 °C [23]
2-EHA	–	1
Styrene (St)	2–3	2
Butyl methacrylate (BMA)	3	2
Butyl acrylate (BA)	2–3	2
Butadiene (Bu)	3	2
Ethyl acrylate (EA)	–	4
Methyl methacrylate (MMA)	4–5	4
Vinyl acetate (VAc)	–	5
Methyl acrylate (MA)	–	8
Acrylonitrile (AN)	–	>10 (estimate: 12)

initiated by KPS. The initial seed latex used was synthesized so as to have radical traps (TEMPO) covalently bound onto the particle surface. When an aqueous phase-propagating radical entered a seed particle, the nitroxide moiety led to the formation of a stable alkoxyamine. Therefore, the kinetics of radical entry into the seed particles was followed by monitoring the decay of the ESR signal from the nitroxide in the samples withdrawn from the reactor. They obtained f_{entry}=0.36 for KPS at 70 °C and f_{entry}=0.33 for V-50 at 70 °C, respectively. Maxwell et al. [11] obtained the value of $z \cong 2$ by comparing the model predictions with the experimental results in the emulsion polymerization of St. Schoonbrood et al. [27] reported $z \cong 18$ for a 80:20/St:MA emulsion copolymerization system. However, there is an example where it is difficult to explain the kinetic behavior of the emulsion copolymerization of St and AAm without assuming z=(one St monomer unit), as shown later in Section 3.2.3.

3.1.3 Miscellaneous Kinetic Problems in Radical Entry

Two major entry models – the diffusion-controlled and propagation-controlled models – are widely used at present. However, Liotta et al. [28] claim that the collision entry is more probable. They developed a dynamic competitive growth model to understand the particle growth process and used it to simulate the growth of two monodisperse polystyrene populations (bidisperse system) at 50 °C. Validation of the model with on-line density and on-line particle diameter measurements demonstrated that radical entry into polymer particles is more likely to occur by a collision mechanism than by either a propagation or diffusion mechanism.

One of the most basic and important problems to be clarified in emulsion polymerization is what kind of radicals can enter the polymer particles. A proposal now widely accepted is that in the emulsion polymerization of St initiated by, for example, potassium persulfate (KPS), an entering radical must be surface active, so it must be a charged oligomer such as $\cdot M_z SO_4^-$ [11]. Tauer et al. [29] carried out MALDI-TOF-MS investigations of the polymer inside the particles at the end of a persulfate-initiated emulsifier-free emulsion polymerization of St, and showed that besides sulfate end groups, a variety of different end groups for the polymer molecules exist almost independently of the buffer concentration employed during the polymerization. These results support the existence of the following end group combinations: H–H, H–OH, K^{+-}OO–OH, K^{+-}OO–K^{+-}OO, OH–OH, $K^{+-}OSO_3$–H, $K^{+-}OSO_3$–OH, $K^{+-}OSO_3$–$K^{+-}OSO_3$. They concluded from these experimental results that the entering radicals can be either corresponding primary radicals (H, OH, or O_3SO radicals) or oligomer radicals, and therefore surface activity is not a prerequisite condition for the entering radicals.

Another important problem that has been debated for a long time is whether or not the electric charges and the emulsifier layers on the surfaces of the polymer particles affect the radical entry rate of a charged radical (ρ). It is now con-

firmed that for conventional emulsifiers such as sodium lauryl sulfate (NaLS, electrostatic stabilizer), the extent of the surface coverage on a particle and the ionic strength have no effect on radical entry, within experimental error margins [10, 30]. Adams et al. [30] found that the radical entry rate is independent not only of the surface coverage and the ionic strength, but also of differences in the kind of charges between the particle surface and the entering free radical. Furthermore, they refuted, on the basis of experimental data, the proposals that the rate of radical entry is controlled by surfactant displacement [7] and by collision of free radicals with the polymer particles [31]. Penbos et al. [10] carried out the seeded emulsion polymerization of St using a PSt seed latex with negative surface charge in combination with three different initiators: persulfate anions (negatively charged radicals), hydrogen peroxide/iron (II) (neutral radicals) and 2,2′-azobis(2-amidinopropane) (V-50, cationic free radicals). They found that the rate of radical entry showed no significant dependence on the kind of charges of these initiating radicals. El-Aasser et al. [25] examined the effect of an adsorbed layer of the nonionic emulsifier (steric stabilizer) TritonX-405 (octylphenoxypolyethoxy ethanol with an average number of 40 ethylene oxide units) on the rate of radical entry by changing the ratio of anionic (NaLS) and nonionic emulsifiers in the seeded emulsion polymerization of St initiated by KPS. They concluded that any variation in surface coverage by the nonionic emulsifier did not significantly affect the value of ρ within experimental error, suggesting that the adsorbed layer of the nonionic emulsifier on the particle surface would not act as a barrier to radical entry. Contrary to the observations of El-Aasser et al. [25], Kuster et al. [32] observed a large decrease in the desorption rate coefficient for monomeric radicals in the emulsion polymerization of St conducted using poly(ethylene oxide) nonylphenol surfactant with an average number of 30 ethylene oxide units as the steric stabilizer. They concluded from this observation that a "hairy" layer near the particle surface would also act as a barrier for the entry of such uncharged radicals because re-entry of desorbed radicals is the reverse process of desorption. Wang et al. [33] conducted the seeded emulsion polymerization of St using the reactive surfactant sodium dodecyl allyl sulfosuccinate (TREM LF-40) and its polymeric counterpart, poy(TREM), and only observed an increase in the PSt molecular weight when poly(TREM) was used. This was considered to be a consequence of the decrease in the rate of bimolecular radical termination resulting from the decrease in the rate of radical entry into the polymer particles due to the diffusion barrier of the hairy layer near the particle surface to the diffusing radicals.

On the other hand, several reports have been published that point out that when a polymeric surfactant acting as an electrosteric stabilizer is used, the rate of radical entry into a polymer particle should decrease due to a diffusion barrier of the hairy layer built up by the polymeric surfactant adsorbed on the surface of the polymer particles [34–36]. Coen et al. [34] found that in the seeded emulsion polymerization of St using a PSt seed latex stabilized electrosterically by a copolymer of acrylic acid (AA) and St, the electrosteric stabilizer greatly reduced the radical entry rate ρ compared to the same seed latex

with a conventional electrostatic stabilizer. The explanation was that the "hairy" layer on the surface of the polymer particle acted as a diffusion barrier to the entering radicals. Kim et al. [35] also observed the decrease in the value of ρ in the seeded emulsifier-free emulsion polymerization of MMA conducted using KPS as the initiator and a PSt seed latex electrosterically coated by a copolymer of St and styrenesulfonate (NaSS), which constitutes a thick hairly layer on the particle surface. Vorwerg et al. [36] observed a decrease in the value of ρ, although it was dependent on the pH, in the seeded emulsion polymerization of St using seed latexes electrosterically stabilized with poly(acrylic acid). Leeman et al. [37], on the other hand, synthesized amphiphilic water-soluble polyelectrolytes, a poly(methyl methacrylate-*block*-sulfonated glycidyl methacrylate) block copolymer (PMMA-*b*-SPGMA; polyanionic block copolymer) and a poly(methyl methacrylate-*block*-quaternized *N*,*N*′-dimethylaminoethyl methacrylate) block copolymer (PMMA-*b*-QPDMAEMA; polycationic block copolymer). They carried out the emulsion polymerization of MMA at 60 °C in the presence of these two copolymers as surfactants and with the following four types of initiators: KPS producing anionic radicals, H_2O_2 and AIBN both producing neutral radicals and AAP (2,2′-azobis(2-amidinopropane)) which generates cationic radicals in acid medium and neutral radicals in basic medium. There was no major difference in the rate of polymerization R_p when the initiators producing neutral radicals were combined with either of these two oppositely charged copolymer surfactants. But a large decrease in R_p was observed when the charge of the entering radical was different to the charge of the block polyelectrolyte surfactant. Considering the experimental results of El-Aasser et al. [25], the former finding is acceptable, but the latter one is contrary to our expectations and the conclusions given in the articles [34–36]. Therefore, clarifying whether or not the adsorbed layer of polymeric surfactants on the particle surface act as a diffusion barrier to the entering radicals is still an important problem that needs to be solved in the future.

In the emulsion copolymerization of the water-soluble monomer acrylamide (AAm) and the sparingly water-soluble monomer St using KPS as initiator, Kawaguchi et al. [38] observed odd kinetic behavior. Regardless of the fraction of AAm in the monomer feed, the polymerization of both monomers started from the beginning of the reaction, but soon the AAm polymerization slowed down and finally stopped, while the polymerization of St continued very smoothly to the end. Nomura et al. [39] examined the reason for this abnormal kinetic behavior and ascribed the reason to unusual radical entry behavior. They studied the seeded emulsion copolymerization of St and AAm at 50 °C using PSt particles as the seed and KPS as the initiator, and found that the change in the number of PSt seed particles N_s caused a drastic change in the kinetic behavior of this emulsion copolymerization system. When the number of seed particles was less than a certain critical value N_c (~2.5×10^{12} particles/cm^3-water), both St and AAm started polymerizing as soon as the initiator was added. However, when the number of seed particles was higher than N_c, an apparent induction period suddenly appeared for AAm polymerization; in other words,

although more than 99% of the initially charged AAm existed in the aqueous phase, the AAm polymerization did not start until the St conversion exceeded around 75%. Therefore, the apparent induction period was the time necessary for the St conversion to reach 75%. On the other hand, the St polymerization started and continued very smoothly from the beginning to the end of the reaction, independently of the AAm polymerization. We have not yet succeeded in explaining this interesting phenomenon quantitatively, but the reason may be explained qualitatively as follows [40]. Using values for the monomer reactivity ratio and the concentrations of St and AAm in the aqueous phase, it is clear that the addition rate of St radicals to AAm is about 100 times faster than to St and the addition rate of AAm radicals to AAm is about 5 times faster than to St in the aqueous phase. Therefore, once an AAm radical is formed in the aqueous phase, this AAm radical preferentially adds AAm monomer in the aqueous phase without entering the polymer particles due to its hydrophilicity. When the number of initially charged PSt seed particles is higher than N_c, no AAm polymerization occurs in the aqueous phase although all free radicals are produced in the aqueous phase and almost all AAm monomer units exist in the aqueous phase. This implies that KPS radicals preferentially add St monomer units as soon as they are generated in the aqueous phase and enter the seed particles before the resultant St radicals add one AAm monomer unit. This is because the mean residence time of the St radicals in the aqueous phase before they enter the seed particles is shorter than the average time necessary for these radicals to add one AAm monomer unit. On the other hand, when the number of seed particles is less than N_c, the mean residence time of most of the St radicals would become longer than the average time necessary for a St radical to add one AAm monomer unit, and so these St radicals are mostly transformed into AAm radicals, although some of these radicals can enter the seed particles and continue St polymerization inside the particles. Therefore, the St radicals produced continue AAm polymerization in the aqueous phase. The mechanism of radical entry proposed in this copolymerization system contradicts the conclusions of Maxwell et al. [11], who claimed that KPS radicals need to add at least 2–3 St monomer units before entering the monomer-swollen polymer particles.

3.2 Radical Desorption

3.2.1 Desorption in Homopolymer Systems

The desorption (exit) of free radicals from polymer particles into the aqueous phase is an important kinetic process in emulsion polymerization. Smith and Ewart [4] included the desorption rate terms into the balance equation for N_n particles, defining the rate of radical desorption from the polymer particles containing n free radicals in Eq. 3 as $k_f n N_n$. However, they did not give any

detailed discussion on radical desorption. Ugelstad et al. [41] pointed out that the rate coefficient for radical desorption (the desorption rate coefficient) could be a function of particle size, the rate of chain transfer to monomer, the rate of polymerization and the diffusion coefficients involved in the transport processes leading to desorption of radicals, and suggested that, in the emulsion polymerization of VCl, the desorption rate coefficient, k_f might be expressed in the form

$$k_f = kv_p^{-2/3} = k'd_p^{-2} \tag{16}$$

On the other hand, Nomura and Harada [14, 42–45] pointed out that radical desorption from the polymer particles and micelles plays a decisive role in particle formation and growth, and further that there are many examples of kinetic deviations from the S-E theory that are attributable to radical desorption. First, they theoretically derived the desorption rate coefficient from both stochastic [42] and deterministic approaches, [14, 42, 43] based on a scheme consisting of the following three consecutive steps: (1) chain-transfer of a polymeric radical to a monomer molecule or a species like CTA in a polymer particle, followed by (2) diffusional transportation of the resulting low molecular weight radical to the particle-water interface, and (3) successive diffusion into the bulk water phase through a stagnant film adjacent to the surface of the particle. In modeling the rate coefficient for radical desorption, the following assumptions were made:

A1. Polymer particles contain at most one radical (zero-one system).
A2. An oligomeric radical with no more than *s* monomer units can desorb from and re-enter into a polymer particle with the same rate, irrespective of its chain length.
A3. Instantaneous termination takes place when another radical enters a particle already containing a radical.
A4. No distinction is made between radicals with or without an initiator fragment on its end.
A5. Water-phase reactions such as propagation, termination, and chain-transfer to a monomer are negligible for the desorbed radicals. This means that all of the desorbed radicals would re-enter particles and the loss of these radicals occurs only through the event given by the assumption A3).
A6. The physical and chemical properties of chain transfer agent (CTA) radicals are approximately equal to those of monomer radicals.

Based on these assumptions, they derived the desorption rate coefficient k_f as

$$k_f = K_{oI}\left[\frac{\rho_w(1-\bar{n})}{K_{oI}\bar{n} + k_i[M]_p\bar{n}N_p}\right] + K_o\left[\frac{k_{mf}}{k_p} + \frac{k_{Tf}[T]_p}{k_p[M]_p} + \frac{\rho_w(1-\bar{n})k_i}{K_{oI}\bar{n} + k_i[M]_p k_p\bar{n}N_p}\right] \cdot \sum_{j=1}^{S}\left(\frac{k_p[M]_p}{K_o\bar{n} + k_p[M]_p}\right)^j \tag{17}$$

When it is assumed that initiator-derived radicals do not exit and only monomeric and CTA radicals produced by chain transfer to a monomer and/or a CTA can desorb (s=1), Eq. 17 can be simplified as

$$k_f = K_o\left(\frac{k_p[M]_p}{K_o\bar{n} + k_p[M]_p}\right)\left(\frac{k_{mf}}{k_p} + \frac{k_{Tf}[T]_p}{k_p[M]_p}\right) \tag{18}$$

where k_{mf} and k_{Tf} are the chain transfer rate constants to monomer and to CTA, respectively, and K_o is the overall desorption rate constant per particle for monomeric (or CTA) radicals, which is approximately given by [42–44]

$$K_o = \left(\frac{2\pi D_w d_p}{m_d v_p}\right)\left[1 + \frac{\psi D_w}{m_d D_p}\right]^{-1} = \left(\frac{12 D_w \delta}{m_d d_p^2}\right) \tag{19}$$

where δ=$(1+\psi D_w/m_d D_p)^{-1}$ denotes the ratio of the aqueous-side to overall diffusion resistance, ψ is a numerical constant between 1 and 6 that depends on the mass-transfer coefficient employed (ψ=1 if Eq. 7 is assumed to be applicable to the mass-transfer process inside the polymer particles) [42–45], m_d is the partition coefficient for monomer radicals between the polymer particle and aqueous phases, defined by m_d=$[M]_p/[M]_w$, and the term, $\psi D_w/m_d D_p$ is the ratio of the particle-side to water-side diffusion resistance. Ugelstad et al. [9] obtained the same expression as Eq. 19 with ψ=1. On the other hand, Casey et al. [1, 46] also derived the same expression as Eq. 19 with δ=1. However, it must be noted that when the diffusion resistance inside the particle is far greater than that in the aqueous-side effective diffusion film, that is, $D_w/m_d D_p \gg 1$, one gets

$$K_o = \left(\frac{2\pi D_w d_p}{m_d v_p}\right)\left[1 + \frac{\psi D_w}{m_d D_p}\right]^{-1} = \left(\frac{12 D_p}{d_p^2}\right) \tag{19a}$$

For the St emulsion polymerization, for example, in the absence of CTA, it usually holds that $K_o\bar{n} \ll k_p[M]_p$, at least in the range where monomer droplets exist. Then, Eq. 18 is reduced to

$$k_f = K_o\left(\frac{k_{mf}}{k_p}\right) = \left(\frac{12 D_w \delta}{m_d d_p^2}\right)\left(\frac{k_{mf}}{k_p}\right) = \left(\frac{12 D_w C_m \delta}{m_d}\right) d_p^{-2} \tag{20}$$

where C_m is the monomer chain transfer constant. The validity of Eq. 20 has been demonstrated by Nomura et al. [20, 42, 44, 47] and Adams et al. [48]. Equation 18 was derived under the assumption that the physical and chemical properties of a CTA radical are approximately equal to those of a monomeric radical. However, if it is necessary to take into account the differences in the physical and chemical properties between monomeric and CTA radicals, Eq. 18 can be modified approximately as

$$k_f = K_{om}\left(\frac{k_{mf}[M]_p}{K_{om}\bar{n} + k_p[M]_p}\right) + K_{oT}\left(\frac{k_{Tf}[T]_p}{K_{oT}\bar{n} + k_{iT}[M]_p}\right) \tag{18a}$$

where K_{om} and K_{oT} are the overall desorption rate constants per particle for monomeric and CTA radicals, respectively.

Ugelstad et al. [9] later derived almost the same desorption rate coefficient as Eq. 19 given by

$$k_f = \left(\frac{12D_w}{m_d d_p^2}\right)\left(\frac{k_{mf}}{k'_p}\right)\left(1 + \frac{D_w}{m_d D_p}\right)^{-1} = \left(\frac{12D_w\delta}{m_d d_p^2}\right)\left(\frac{k_{mf}}{k'_p}\right) \tag{21}$$

where k'_p is the rate constant for the reaction between a monomeric radical formed by chain transfer and a monomer, the value of which may be different from the value of k_p, the propagation rate constant.

Asua et al. [49–51] modified Eq. 18 in the absence of a CTA to include more general cases, taking into account the fate of the desorbed radicals (both chemical reactions in the water phase and re-entry) as

$$k_f = k_{mf}[M]_p\left(\frac{K_o}{K_o\beta + k_p[M]_p}\right) \tag{22}$$

where β stands for the fraction of desorbed radicals that cannot re-enter because of the aqueous phase termination or propagation, and is given by

$$\beta = \frac{k_p[M]_w + k_{tw}[T^*]_w}{k_p[M]_w + k_{tw}[T^*]_w + k_a N_T} \tag{23}$$

where $[T^*]_w$ is the total radical concentration in the water phase and k_a is the mass-transfer coefficient for radical entry, and $[M]_w$ is the monomer concentration in the water phase.

On the other hand, Casey and Morrison et al. [52, 96] derived the desorption rate coefficient for several limiting cases in combination with their radical entry model, which assumes that the aqueous phase propagation is the rate-controlling step for entry of initiator-derived free radicals. Kim et al. [53] also discussed the desorption and re-entry processes after Asua et al. [49] and Maxwell et al. [11] and proposed some modifications. Fang et al. [54] discussed the behavior of free-radical transfer between the aqueous and particle phases (entry and desorption) in the seeded emulsion polymerization of St using KPS as initiator.

3.2.2 Desorption in Copolymer Systems

As we discuss later in Section 3.3.3, Nomura et al. [45, 47] first derived the rate coefficient for radical desorption in an emulsion copolymerization system by

extending the approach developed for emulsion homopolymerization under the same assumptions as A1–A6 given in Section 3.2.1. This methodology is now termed the "*pseudo-homopolymerization approach*". According to this approach, the average rate coefficient for radical desorption, defined, for example, in a binary emulsion copolymerization system with monomers A and B, $\bar{k}_f$, is given by

$$\bar{k}_f = k_{fA}(\bar{n}_A/\bar{n}_t) + k_{fB}(\bar{n}_B/\bar{n}_t) = k_{fA}f_A + k_{fB}f_B \tag{24}$$

where k_{fA} is the desorption rate coefficient for A-monomeric radicals, $\bar{n}_t$ is the average number of total radicals per particle, $\bar{n}_A$ the average number of A-radicals per particle ($\bar{n}_t = \bar{n}_A + \bar{n}_B$), and f_A is the fraction of A-radicals in the particle phase and is expressed, at steady-state, as a function of the propagation rate constant k_p, the monomer reactivity ratio r', and the monomer concentration in the polymer particles $[M]_p$, in the following form.

$$\bar{n}_t = \bar{n}_A + \bar{n}_B \tag{25}$$

In the case where all the desorbed A-monomeric radicals reenter the polymer particles, the desorption rate coefficient for A-monomeric radicals k_{fA} is given by

$$k_{fA} = K_{oA}\left[\frac{C_{mAA}r_A[M_A]_p + C_{mBA}[M_B]_p}{r_B\{(K_{oA}\bar{n}_t/k_{pAA}) + [M_B]_p\} + [M_A]_p}\right] \tag{26}$$

where K_{oA} is the overall desorption rate constant per particle for A-monomeric radicals given by Eq. 19 in Section 3.2.1 and C_{mBA} is the chain transfer constant for a B-radical to A-monomer.

López et al. [55] investigated the kinetics of the seeded emulsion copolymerization of St and BA in experiments where the diameter and number of seed particles, and the concentration of initiator were widely varied. The experimental data were fitted with a mathematical model in which they used the desorption rate coefficient developed by Forcada et al. [56] for a copolymerization system. The desorption rate coefficient for the A-monomeric radical that they used was a modification of Eq. 22 and Eq. 23, and is given by

$$k_{fA}f_A = (k_{mf,AA}f_A + k_{mf,BA}f_B)[M_A]_p\left(\frac{K_{0A}}{\beta_A K_{0A} + k'_{pAA}[M_A]_p + k'_{pAB}[M_B]_p}\right) \tag{27}$$

where $k_{mf,AB}$ denotes the chain transfer constant of the A-radical to the B-monomer and β_A is the fraction of the desorbed A-monomeric radicals that cannot reenter the polymer particles because of the aqueous phase termination or propagation. Barudio et al. [57], on the other hand, developed a simulation model for emulsion copolymerization based on the pseudo-homopolymerization approach, where they used the average rate coefficient for radical desorption given by $\bar{k}_{de} = (12D_w z/m_d d_p^2)(\bar{k}_{mf}/\bar{k}_p)$. Saldivar et al. have presented a survey of

emulsion copolymerization models that have been published in the literature, and a comprehensive mathematical model for emulsion copolymerization [58], along with its experimental verification [59, 60]. In Appendix A of the former paper, they present a detailed discussion on the average rate coefficient for radical desorption, which is applicable to a multimonomer system.

Only a few experimental studies have been published that aim to demonstrate the validity of the average rate coefficient for radical desorption given by Eqs. 24 to 27 [45, 47] directly. Vega et al. [61] modeled the batch emulsion copolymerization of AN and Bu in order to simulate an industrial process and improve the final polymer quality. The mathematical model they used was an extended version of that developed by Guliotta et al. [62] for the continuous emulsion polymerization of St and Bu. Due to the high solubility of AN in water, the effect of the desorption of AN radicals was taken into consideration in the model. The average rate coefficient for radical desorption used was given by Eqs. 24 and 27. Barandiaran et al. [63] proposed a method to estimate the rate coefficient for radical desorption in emulsion copolymerization and gave the values of this parameter for the MA-VAc and MMA-BA emulsion copolymerization systems.

3.2.3 Miscellaneous Kinetics Problems in Radical Desorption

The rate coefficient for radical desorption was derived by assuming that the adsorbed layer of conventional or polymeric surfactant on the surface of the polymer particle does not act as an interfacial diffusion barrier to the desorbing neutral monomeric radicals. However, Kusters et al. [32] studied the kinetics of particle growth in emulsion polymerization systems with a surface-active initiator (an "inisurf"). The inisurf employed was the diester of 4,4′-azobis(4-cyanopentanoic acid), the initiator moiety, with poly(ethylene oxide) nonylphenol, the surfactant moiety. They observed a large decrease (one order of magnitude) in the desorption rate coefficient for monomeric radicals in the emulsion polymerization of St. They ascribed the reason for the decrease in the rate of radical desorption to a "hairy" layer of the polymeric surfactant, which would play the role of a diffusion barrier. Coen et al. [34] also reported that in the seeded emulsion polymerization of St using a PSt seed latex stabilized electrosterically by a copolymer of AA and St, the electrosteric stabilizer greatly reduced the rate of radical desorption compared to the same seed latex with an electrostatic stabilizer. They interpreted the reason for the decrease in the rate of radical desorption by assuming that the aqueous-phase diffusion of monomeric radicals is slower in the hairy layer. Recently, Vorwerg et al. [36] carried out a kinetic study of the seeded emulsion polymerization of St using PSt seed lattices electrosterically stabilized with poly(acrylic acid) (pAA). They found that seed lattices with a high-coverage of pAA (above 50 μC cm^{-2}) exhibited a significant reduction in radical desorption (by a factor of ~3 compared to the ionically stabilized seed) at low pH.

3.3 Particle Formation and Growth

3.3.1 Particle Formation

As we mentioned in Section 2.1 (Fig. 1a), there are three major models for particle formation in emulsion polymerization. According to these models, polymer particles are formed:

1. When a free radical in the aqueous phase enters a monomer-swollen emulsifier micelle and polymerization proceeds therein (*micellar nucleation*).
2. When the chain length of a free radical growing in the aqueous phase exceeds its solubility limit and precipitates to form a particle nucleus (*homogeneous nucleation*).
3. When a free radical growing in the aqueous phase enters a monomer droplet and polymerization proceeds therein (*droplet nucleation*).

However, when the resultant polymer particles become unstable and coagulate, then whatever the mechanism of particle formation is, the final number of polymer particles produced is determined by a limited coagulation between existing polymer particles (*coagulative nucleation*).

Smith and Ewart [4] derived an expression that can predict the number of polymer particles produced, by assuming that:

1. A monomer-swollen emulsifier micelle is transformed into a polymer particle by capturing a free radical from the aqueous phase [4, 5].
2. The volumetric growth rate per particle μ is constant, at least during particle formation ($\mu = dv_p/dt$=constant).
3. Free radical activity does not transfer out of a growing particle ($k_f \cong 0$).
4. The amount of emulsifier that dissolves in the water phase without forming micelles and adsorbs on the surface of emulsified monomer droplets may be neglected.

Based on these assumptions, two limiting cases were discussed.

Case A: The rate of radical entry into micelles that results in the formation of new particles is approximately equal to the rate of radical generation in the water phase (ρ_w), as long as emulsifier micelles are present; in other words,

$$\frac{dN_T}{dt} = \rho_w \tag{28}$$

Particle formation stops at the time t_c, when the emulsifier micelles have just disappeared because all of the emulsifier molecules comprising the emulsifier micelles have been transferred to the surfaces of growing polymer particles for adsorption. The volume $v_{p,c}$ at time t_c of a particle formed at time τ is $v_{p,c} = \mu(t_c - \tau)$, and so the surface area $a_{p,c}$ of this particle at time t_c is given by

$a_{p,c}=\sigma(t_c-\tau)^{2/3}$ where $\sigma=[(4\pi)^{1/2}3\mu]^{2/3}$. Therefore, the total surface area $A_{p,c}$ of all the polymer particles present at time t_c is given by the integral $A_{p,c}=\int_0^{t_c}\sigma(t_c-\tau)^{2/3}\rho_w d\tau = 3/5\ \sigma\rho_w t_c^{5/3}$. No micelles exist ($A_m=0$) at time t_c, and so all of the charged emulsifier molecules are adsorbed onto the surfaces of polymer particles present. Therefore, it holds that $A_{p,c}=(3/5)\sigma\rho_w t_c^{5/3}=a_s S_0$. In this case, the number of polymer particles produced (N_T) can be obtained by substituting t_c into $N_T=\rho_w t_c$ as

$$N_T = 0.53(\rho_w/\mu)^{0.4}(a_s S_0)^{0.6} \tag{29}$$

where A_m and A_p are the total surface area of the micelles and the total surface area of the polymer particles per unit volume of water, respectively, a_s is the surface area occupied by a unit amount of emulsifier, and S_0 is the amount of initially charged emulsifier per unit volume of water (the initial emulsifier concentration).

Case B: Radicals enter both micelles and polymer particles at rates that are proportional to their surface areas (collision theory), so that the rate of new particle formation is given by

$$dN_T/dt = \rho_w\left(\frac{A_m}{A_m + A_p}\right) = \frac{\rho_w}{1 + A_p/A_m} \tag{30}$$

Then, it follows that

$$N_T = 0.37(\rho_w/\mu)^{0.4}(a_s S_0)^{0.6} \tag{31}$$

On the other hand, Nomura et al. [14] proposed a different approach for predicting the number of polymer particles produced, where the new concept of "radical capture efficiency" of a micelle relative to a polymer particle was proposed. The assumptions employed were almost the same as those of Smith and Ewart, except that the volumetric growth rate μ of a polymer particle was not considered to be constant. It was also assumed that all of the radicals formed in the aqueous phase enter either micelles or polymer particles with negligible termination in the aqueous phase. In this approach, the following elementary reactions and their respective rates were defined.

(1) Particle formation by radical entry into a micelle

$$R^* + m_s \rightarrow N^*,\ k_{em} m_s [R_w^*] \tag{32}$$

(2) Formation of a dead particle by radical entry into an active particle containing a radical

$$R^* + N^* \rightarrow N_0,\ k_{ep} N^* [R_w^*] \tag{33}$$

(3) Formation of an active particle by radical entry into a dead particle containing no radical

$$R^* + N_0 \rightarrow N^*,\ k_{ep} N_0 [R_w^*] \tag{34}$$

where m_s is the number of monomer-swollen micelles, $[R_w^*]$ the concentration of free radicals in the aqueous phase, N^* the number of active particles containing a radical, N_0 the number of dead particles containing no radical, k_{em} the rate constant for radical entry into micelles, and k_{ep} the rate constant for radical entry into particles. Using these rate expressions, the following equations, describing the balance of radicals in the aqueous phase and the rate of particle formation, were obtained:

$$\frac{d[R_w^*]}{dt} = \rho_w - k_{em} m_s [R_w^*] - k_{ep} N_T [R_w^*] \tag{35}$$

$$\frac{dN_T}{dt} = k_{em} m_s [R_w^*] \tag{36}$$

where N_T is the total number of polymer particles produced ($N_T = N^* + N_0$). Introducing the aqueous phase concentration $[R_w^*]$, obtained by applying the steady state assumption to Eq. 35 into Eq. 36, and rearranging leads to

$$\frac{dN_T}{dt} = k_{em} m_s [R_w^*] = \frac{\rho_w}{1 + (k_{ep} N_T / k_{em} m_s)} = \frac{\rho_w}{1 + (\varepsilon N_T / S_m)} \tag{37}$$

where $k_{ep} N_T / k_{em} m_s$ denotes the ratio of the rate of radical entry into polymer particles to that into micelles and is rewritten as $\varepsilon N_T / S_m$, where $\varepsilon = (k_{ep}/k_{em}) M_m$ and ε is the one unknown parameter, which affects the number of polymer particles produced. Here, S_m is the total number of emulsifier molecules forming micelles, and M_m is the aggregation number of emulsifier molecules per micelle, defined by $M_m = S_m / m_s$. By solving a set of simultaneous differential equations describing N_T, N^*, the monomer conversion X_M, and using the balance equation for the number of emulsifier micelles m_s, the number of polymer particles produced N_T can be predicted with respect to the initial emulsifier (S_0) and initiator concentrations (I_0) (or $\rho_w = 2 k_d f [I_0]$) as shown by $N_T \propto \rho_w^{0.3} S_0^{0.7}$. In the case of VAc emulsion polymerization [20], the authors took into account radical desorption from the polymer particles, yielding the following expression in place of Eq. 37.

$$\frac{dN_T}{dt} = k_{em} m_s [R_w^*] = \frac{\rho_w + k_{de} \bar{n} N_T}{1 + (k_{ep} N_T / k_{em} m_s)} = \frac{\rho_w + k_{de} \bar{n} N_T}{1 + (\varepsilon N_T / S_m)} \tag{38}$$

In this derivation, it was assumed that only monomer-transferred radicals could desorb from the polymer particles, and that radical termination in the aqueous phase was negligible. The calculated result was correlated by $N_T \propto \rho_w^{0.04} S_0^{0.94}$, from which it was found that radical desorption from the polymer particles decreases the value of the exponent of the initiator dependence and increases the value of the exponent of the emulsifier dependence. To obtain agreement between the predicted and experimental values of N_T, however, it was necessary

to introduce a value of ε that is far greater than that predicted by using the diffusion theory given by Eq. 7 ($k_{ep}/k_{em}=d_p/d_m$). A value of $\varepsilon=1.28\times10^5$ was necessary for St emulsion polymerization [14], and a value of $\varepsilon=1.2\times10^7$ for VAc emulsion polymerization [20], while the value of ε predicted by diffusion theory (Eq. 7) was ~1000 in both systems because $M_m\approx100$ and $d_p/d_m\approx10$ hold (roughly) in Interval I of particle formation, as already discussed in Sect. 3.1.1. The authors, therefore, proposed the concept of the "radical capture efficiency" of a micelle relative to a polymer particle to correct for this disagreement. The same phenomenon has been encountered by several researchers [18, 19, 21] (Sect. 3.1.1). However, the reason for the disagreement between the predicted and experimental values of ε has not been found yet.

As we discussed in Sect. 3.1.1, Hansen et al. [15] made significant improvements to the concept of the radical capture efficiency proposed by Nomura et al. [14]. Taking this concept into consideration, they examined the effect of radical desorption on micellar particle formation in emulsion polymerization [65]. Assuming that radical entry is proportional to the x^{th} power of the micelle radius and the polymer particle radius, they proposed the following general expression for the rate of particle formation:

$$\frac{dN_T}{dt}=(\rho_w+k_f\bar{n}N_T)\left(\frac{\delta_{ce}m_s d_m^x}{\delta_{ce}m_s d_m^x+N_T d_p^x}\right)=\frac{\rho_w+k_f\bar{n}N_T}{\left[1+\frac{N_T}{\delta_{ce}m_s}\left(\frac{d_p}{d_m}\right)\right]} \tag{39}$$

where δ_{ce} is the radical capture efficiency of a micelle relative to a polymer particle, and is related to ε by $\delta_{ce}=(M_m/\varepsilon)(d_p/d_m)^x$. The condition $x=1$ corresponds to the diffusional entry model, while the condition $x=2$ corresponds to the collisional entry model. Using $x=1$, they calculated the effect of radical desorption in the emulsion polymerizations of St, MMA, VAC, and VCl on the number of polymer particles produced, and demonstrated that the following general rule for initiator and emulsifier exponents, which was first found by Nomura et al. [20, 43], could also be applied to the emulsion polymerizations of these monomers.

$$N_T \propto I_0^{1-z}S_0^z \tag{40}$$

where $0.6<z<1.0$. The value of z increases from 0.6 (a common value for St) to 1.0 (a common value for VAc) with increasing radical desorption.

Particle formation below the critical micellar concentration (CMC) in emulsion polymerization is now accepted to take place according to the homogeneous nucleation mechanism. Among several quantitative treatments of homogeneous particle formation in emulsion polymerization, the best-known model was that proposed by Fitch and co-workers [66]. Their model is based on the assumption that when the chain length of a free radical growing in the aqueous phase reaches its solubility limit (critical chain length), it precipitates to form a primary particle, and that particle formation will be hindered if these growing oligomers are absorbed in polymer particles formed earlier. Hansen

et al. [67] made significant improvements on the Fitch model [the HUFT (Hansen-Ugelstad-Fitch-Tsai) model]. According to Hansen et al, the rate of particle formation is given by

$$\frac{dN_T}{dt} = k_{pw} M_w (R_{Ij_{Icr}} + R_{Mj_{Mcr}}) \tag{41}$$

where k_{pw} and M_w are the propagation rate constant and the monomer concentration in the aqueous phase, respectively, and R_{Ijcr} and R_{Mjcr} are the aqueous phase concentrations of oligomer radicals with critical chain length derived from initiator and monomer radicals, respectively. This equation means that oligomers stemming from initiator and monomer radicals precipitate as particles when they propagate beyond their respective critical degree of polymerization, j_{Icr} and j_{Mcr}. The authors derived the steady-state expressions for R_{Ij} and R_{Mj} and obtained a general equation for homogeneous particle formation by nserting them into Eq. 41. Furthermore, in order to simplify it, they neglected particle formation from oligomers stemming from the desorbed monomeric radicals, along with several other assumptions, and obtained

$$\frac{dN_T}{dt} = \rho_w (1 + k_{tw} R_w / k_{pw} M_w + \bar{k}_c N_T / k_{pw} M_w)^{-j_{Icr}} \tag{42}$$

where $\bar{k}_c$ is the average rate coefficient for radical entry into polymer particles, and R_w is the total radical concentration in the aqueous phase. Assuming that, as an approximation, radical absorption by particles may be neglected in the calculation of R_w, one gets

$$N_T(t) = \{[k_1 \rho_w j_{cr} t + (k_2 + 1)^{j_{cr}}]^{1/j_{cr}} - k_2 - 1\}/k_1 \tag{43}$$

where $R_w = (\rho_w / k_{tw})^{1/2}$ in this case, and $k_1 = \bar{k}_c / k_{pw} M_w$ and $k_2 = (k_{tw} \rho_w)^{1/2} / k_{pw} M_w$.

On the other hand, Tauer et al. [68] developed a framework for modeling particle formation in emulsion polymerization on the basis of a combination of classical nucleation theory with radical polymerization kinetics and the Flory-Huggins theory of polymer solutions. The basic assumption adopted was that water-borne oligomers form stable nuclei under critical conditions. The only adjustable model parameter was the activation energy of nucleation. The model allows us to calculate the chain length of the nucleating oligomers, the number of chains forming one nucleus, the diameter of the nucleus, the total number of nuclei formed, and the rate of nucleation. Further, they experimentally studied particle formation in the very early stages of the emulsifier-free emulsion polymerization of St by monitoring the optical transmission and the conductivity of the reaction mixture on-line [69].

Usually particle formation by initiation in the monomer droplets (*droplet nucleation*) is not considered important in conventional emulsion polymerization. This is because of the low absorption rate of radicals into the monomer droplets, relative to the other particle formation rates. However, when the monomer

droplets are very small, they become an important source of particle formation because the monomer droplets can compete for aqueous phase free radicals with emulsifier micelles. This mode of heterogeneous polymerization is now called "miniemulsion polymerization" and is reviewed in another chapter.

It is accepted that particle formation below the CMC in emulsion polymerization takes place by homogeneous nucleation. However, there have been claims that homogeneous nucleation is the main particle formation mechanism, even above the CMC. Lichti et al. [70] investigated the mechanism of particle formation in the emulsion polymerization of St using sodium dodecyl sulfate (SDS) as an emulsifier, and proposed the concept of "*coagulative nucleation*". They measured the full PSDs by electron microscopy at consecutive times soon after the cessation of particle formation, and found that the PSDs obtained during particle formation (Interval I) were positively skewed, confirming the role of coagulation, even above the CMC. Based on this phenomenon, they concluded that the particle formation process does not occur by either simple micellar entry or homogeneous nucleation mechanisms. Therefore, they suggested a mechanism for particle formation where the homogeneous nucleation of oligomers in the aqueous phase creates small primary polymer particles, and these primary particles coagulate to produce polymer particles. On the basis of this experimental finding, Feeny et al. [71] proposed a detailed theory for coagulative nucleation and the PSDs in emulsion polymerization. The theory combined and extended Müller-Smoluchowski coagulation kinetics with the DLVO theory. Expressions were provided for the time evolutions of the nucleation rate, particle number, and PSD. They showed that with physically reasonable values for the parameters of the coagulation kinetics, agreement was obtained with experimental data for the St emulsion polymerization system. Richards et al. [72] developed a mathematical model for emulsion copolymerization. The model combined the theory of coagulative nucleation of homogeneously nucleated precursors with detailed species material and energy balances to calculate the time evolution of the concentration, size and colloidal characteristics of polymer particles, the monomer conversion, the copolymer composition, and the molecular weight in an emulsion copolymerization system.

Although it is now accepted that particle formation below the CMC in emulsion polymerization takes place according to the homogeneous nucleation mechanism, there has been debate as to whether homogeneous nucleation is still operative even above the CMC, especially when relatively water-soluble monomers are polymerized in emulsion in the presence of emulsifier micelles. To date, most investigators believe that in the emulsion polymerization of partially water-soluble monomers such as MMA and methyl acrylate (MA), polymer particles are generated not by a micellar mechanism, but by homogeneous nucleation even in the presence of emulsifier micelles. This is because the emulsion polymerization involving these monomers does not follow the Smith-Ewart theory, and moreover, because an inflection point cannot be seen around the CMC of the emulsifier on the particle number versus initial emulsifier concentration curve, where an abrupt and sharp decrease in the number

of polymer particles produced is usually observed if particle formation occurs by the micellar mechanism [73, 74]. Nomura et al. [75] carried out the emulsion polymerization of vinylidene chloride (VDC) at 50 °C using NaLS as the emulsifier and KPS as the initiator. They found that $N_T \propto S_m^{0.7} I_0^{0.3} M_0^0$, where S_m is the initial concentration of emulsifier forming micelles, I_0 is the initial initiator concentration and M_0 is the amount of monomer initially charged per unit volume of water. Although the solubility of VDC in water at 25 °C is 2.5×10^{-2} mol/dm^3-water (~0.25 wt%), which is about ten times more water-soluble than St, but is about 1/10 of the water-solubility of MMA, an inflection point was definitely observed around the CMC on the particle number versus initial emulsifier concentration curve. This seems to indicate that micellar nucleation occurred, although Gilbert et al. [70, 71, 76] refuted micellar nucleation even in the emulsion polymerization of sparingly water-soluble monomer St in the presence of SDS micelles. Sajjadi et al. [77] investigated the kinetic features of the batch emulsion polymerization of BA using SDS as the emulsifier and KPS as the initiator. They observed that the number of polymer particles produced was proportional to the 0.54th power of emulsifier concentration, to the 0.39th power of initiator concentration, and was practically independent of the monomer/water ratio. Particle formation was found to occur even during Interval III, when undissociated micelles existed.

Experimental investigations that deal in detail with particle formation in emulsion copolymerization are scarce. Nomura et al. [78] studied the kinetics of particle formation and growth in the emulsion copolymerization of VDC and MMA using NaLS as the emulsifier and KPS as the initiator. The number of polymer particles produced was determined using particle diameters measured by both electron microscopy (TEM) and dynamic light scattering (DLS) for comparison. They found that $N_T \propto S_0^{1.0} I_0^{0.3} \Phi^0$, where S_0 and I_0 are the initial emulsifier and initiator concentrations, respectively, and Φ is the weight fraction of MMA in the initial monomer feed. It was also found that the particle number determined via the DLS particle diameter was always about 1/2~1/3 of that determined by TEM. This is due to the difference between the average particle diameters determined from TEM and DLS. Yuan et al. [79] carried out the emulsion terpolymerization of St, butadiene (Bu) and AA, and found that the mechanism of water-soluble oligomer formation during the emulsion polymerization differed depending on whether the SDS emulsifier concentration was above or below the CMC. This may demonstrate that particle formation is also closely connected to the presence of emulsifier micelles.

Herrera-Ordóñez et al. [22, 80] discussed particle formation during the emulsion polymerization of St above the CMC of the emulsifier used (SDS), based on their detailed mathematical model for emulsion polymerization. By comparing the model predictions with experimental data, they concluded that micellar nucleation dominates over the homogeneous nucleation above the CMC, and that coagulation is not significant, even if it does take place. Furthermore, they [81] concluded that particle formation by micellar nucleation is at all times at least ten orders of magnitude greater than that by homoge-

neous nucleation, even in the emulsion polymerization of relatively water-soluble monomer MMA. Recently, however, Varela de la Rosa et al. [82–84] carried out detailed experimental studies on the emulsion polymerization of St at 50 °C, using SDS as the emulsifier and KPS as the initiator, and proposed the modified description shown by the following, which is very different from the widely accepted classical description of St emulsion polymerization.

1. In Interval I, the rate of polymerization and the number of polymer particles produced increase. Particle formation takes place predominantly by micellar nucleation. Micelles disappear between 5% and 10% conversion, marking the end of this interval.
2. In Stage II (referred to as Stage II to differentiate it from the classical Interval II), the rate of polymerization and the number of polymer particles continue to increase but at a slower rate. Polymer particles are formed by homogeneous nucleation as long as monomer droplets and enough emulsifier (>0.05 mM) are present in the system. The end of this stage is marked by the disappearance of monomer droplets, but particle nucleation may or may not end at this time.
3. The number of polymer particles produced is proportional to the 0.36^{th} power of the initial monomer concentration.

Therefore, the mechanism of particle formation is still anything but a settled question, even in the emulsion polymerization of St.

Only a few papers [85–88] have been published so far that discuss methodologies that could be used to discriminate experimentally between micellar and homogeneous nucleations. Nomura et al. [85, 86] proposed an experimental method to gauge to what extent the homogeneous and micellar nucleations are operative in a given emulsion polymerization system. The method involves the emulsion copolymerization of the sparingly water-soluble monomer St with partially water-soluble monomers such as MMA or MA, followed by measurement of the composition of the copolymers produced at the very beginning of the reaction, including the interval of particle formation. This method is based on the fact that the composition of the copolymer produced at the very beginning of the reaction reflects the comonomer composition at the locus of particle formation. In other words, the copolymer composition serves as a probe of the locus of particle formation. They carried out the emulsion copolymerizations of St-MMA and St-MA, where the weight ratio of two monomers was 1:1. The copolymer compositions observed at the very beginning of the reactions (far less than 1% monomer conversion) in the presence of emulsifier (NaLS) micelles were definitely very different from those observed when the emulsifier micelles were absent, reflecting the comonomer composition in the locus of particle nucleation. These experimental results revealed that the micellar nucleation is the main particle formation mechanism, even in the emulsion polymerization of moderately water-soluble MMA and MA in the presence of emulsifier micelles. Recently, Chern et al. [87, 88] proposed a novel method in which a water-insoluble dye was used as a probe to study the particle nucleation

mechanism. The rationale behind the method was that if particle formation took place by homogeneous nucleation, the resultant polymer particles would contain negligible amounts of dye because the transport of the dye species from the monomer droplet phase to the resultant polymer particles could be neglected due to the insolubility of the dye in the aqueous phase. If, on the other hand, particle formation took place by micellar nucleation, the resultant polymer particles would contain an amount of dye corresponding to that solubilized in the micelles. They carried out the semibatch emulsion polymerization of St and of MMA in the presence of the dye. In the semibatch emulsion polymerization of MMA, for example, the experimental results showed that when the emulsifier (SDS) concentration is above its CMC, mixed mode particle nucleation (micellar and homogeneous nucleation) was the predominant mechanism. However, a question raised for this study is that if the transport of the dye species from the monomer droplets to the resultant polymer particles can be neglected, how is the dye transported from the monomer droplet phase, where the dye is dissolved, to the monomer-swollen micelle phase where the dye is solubilized.

Semibatch seeded emulsion polymerizations are quite common in industrial operations. One of the most important problems in semibatch seeded emulsion polymerization is how to control secondary particle formation. It is well known that the amount of emulsifier must be carefully fed during starved-fed semibatch seeded emulsion polymerization. Too little emulsifier leads to emulsion instability and hence coagulation, while too much emulsifier leads to secondary particle formation by the micellar mechanism. Wang et al. [89] developed a method for controlling the emulsifier level in starved-fed emulsion polymerization. Morrison et al. [90] studied the conditions for secondary particle formation in emulsion polymerization systems where the amount of added emulsifier was below the CMC. They advanced their discussion based on the HUFT model (Eq. 41), incorporating their reaction-controlled entry model, and deduced a simple means for determining conditions for the onset and extent of secondary particle formation. Coen et al. [91] further extended the work of Morrison et al. [90] and proposed an extensive model for the PSD, particle number, particle size and amount of secondary particle nucleation in emulsion polymerization. Prescott et al. [92] proposed a simplified model for particle formation, which is particularly useful for exploring the conditions required for the growth of large particles, while avoiding secondary particle formation. Butucea et al. [93] studied the seeded emulsion polymerization of VCl to establish the conditions needed to avoid the formation of new polymer particles (secondary nucleation), and proposed new parameters: (1) MSA, the minimum surface area of seed particles necessary to capture all initiator-derived (ionic) radicals generated in the aqueous phase at a given initiator concentration; (2) MCCI, the maximum critical concentration of initiator per unit surface of seed particles under which the formation of new polymer particles is avoided; (3) PVR_1, the polymer volume per active growing radical necessary for the radical to be within the particle for one second.

It has been reported that both the surface charge density and the degree of surface coverage by emulsifier on the seed particles affect the behavior of secondary particle nucleation in seeded emulsion polymerization because these factors control the rate of radical entry into seed particles. Vorwerg et al. [36] carried out a kinetic study of seeded emulsion polymerization using PSt seed particles electrosterically stabilized with poly(acrylic acid), and studied the effect of the degree of surface coverage by poly(acrylic acid) on both radical entry (ρ) and desorption (k_f), through which secondary particle nucleation is influenced under the condition of a fixed number of seed particles. The behavior of ρ and k_f for the low-coverage particles was the same as that of the PSt seed stabilized by initiator fragments and adsorbed emulsifier. The high-coverage particles, on the other hand, exhibited strongly reduced k_f values (by a factor of three) at low pH, but ρ was only slightly lower than for the ionically stabilized seed, while at high and neutral pH, secondary particle nucleation and a decreased polymerization rate was observed with increasing pH (despite an increase in particle number), indicating a reduced ρ value. Therefore, an extensive electrosteric stabilizer reduced the rate coefficient for radical entry (and for radical desorption), inducing secondary particle nucleation. Cheong et al. [35, 94] investigated the effects of surface charge density on the kinetics of secondary particle formation. They carried out three emulsifier-free seeded emulsion polymerizations of MMA using monodispersed seed particles with different surface charge densities, prepared from the St and NaSS comonomers using the two-stage shot-growth process. In the case of the highest surface charge density (72.7 μC/cm^2), secondary particle nucleation was observed. They ascribed the reason for this to the reduced rate of radical entry into the seed particles resulting from electrical repulsion between seed particles and entering oligmeric radicals [35]. They [94] proposed a mathematical model to explain the effects of seed particle surface charge density on secondary particle nucleation by introducing a modified Smolchowski equation and the DLVO theory.

Sajjadi [95] examined the conditions for secondary particle formation and coagulation in the seeded semibatch emulsion polymerization of BA under monomer-starved conditions. They arrived at very interesting conclusions: (1) particle coagulation occurred if the particle surface coverage (θ_{cr1}) dropped below θ_{cr1}=0.25±0.05; (2) secondary particle formation occurred above a critical surface coverage of θ_{cr2}=0.55±0.05, indicating that the presence of micelles in the reaction vessel is not the only prerequisite for micellar nucleation to occur; (3) the number of polymer particles remained approximately constant if the critical surface coverage was within (θ_{cr1}=0.25)<θ<(θ_{cr2}=0.55), and; (4) this surface coverage band is equivalent to the surface tension band of 42.50±5.0 dyne/cm that is required to avoid particle formation and coagulation in the course of polymerization. Sajjadi [96] also carried out an experimental investigation on particle formation under monomer-starved conditions in the semibatch emulsion polymerization of St. They observed that the number of polymer particles formed increased with a decreasing monomer feed rate, and

that a much larger number of particles (1–2 orders of magnitude greater) than that generally expected from a conventional batch emulsion polymerization was obtained. It is clear from Eq. 29 that any variation in the formulation or process variables that results in a reduction in the volumetric growth rate per particle μ will enhance particle formation as long as polymer particles are generated from emulsifier micelles. A depressed rate of particle growth can be achieved either by the starvation of polymer particles or by a reduction in the capability of polymer particles to swell monomer, with the exception of impurities (see Sect. 3.5) and radical desorption (see Sect. 3.2). In this case, the former was the reason for an increase in particle formation. The latter could be achieved, for example, if a small amount of crosslinking agent was used in the formulation. It is well known that crosslinking will decrease the extent of particle swelling by a monomer and thereby reduce the rate of particle growth [97]. Sajjadi [98] also investigated particle nucleation in the seeded emulsion polymerization of St in the presence of Aerosol-MA emulsifier micelles and in the absence of monomer droplets (Interval III). A larger number of polymer particles were found to form in Interval III than in the corresponding seeded batch operation in the presence of monomer droplets. The increase in the number of polymer particles could be attributed to the reduced rate of growth of new particles, which retarded the depletion of the emulsifier micelles.

There are an enormous variety of commercial emulsifiers that are employed in emulsion polymerization. Emulsifiers are generally categorized into four major classes: anionic, cationic, nonionic and zwitterionic (amphoteric). The anionic and nonionic emulsifiers are the most widely used. In addition, mixtures of emulsifiers are also often used. Since the effects of the molecular structure and chemical and physical properties of an emulsifier on particle formation are still far from being well understood, numerous experimental investigations on particle formation have been carried out to date with various nonionic emulsifiers [99–102], mixed emulsifiers (ionic and nonionic emulsifiers) [18, 103–106] and reactive surfactants [33, 107–110]. Recently, polymeric surfactants have become widely used and studied in emulsion polymerizations [111–116]. A general review of polymeric surfactants was published in 1992 by Piirma [117]. Recently, emulsion polymerization stabilized by nonionic and mixed (ionic and nonionic) emulsifiers was reviewed by Capek [118].

Özdeğer et al. studied the role of the nonionic emulsifier Triton X-405 (octylphenoxy polyethoxy ethanol) in the emulsion homopolymerization of St [99] and *n*-butyl acrylate (*n*-BA) [100], and in the emulsion copolymerization of St and *n*-BA [101]. In the emulsion homopolymerization of St, they noted two separate nucleation periods, resulting in bimodal PSDs. Although the total concentration of the emulsifier was maintained at a level above its CMC based on the water phase in the recipe, the portion of the emulsifier initially present in the aqueous phase was below the CMC due to partitioning between the oil and aqueous phases. Due to the nature of this emulsifier, the first of the two nucleation periods was attributed to homogeneous nucleation, while the second was

attributed to micellar nucleation. In the case of *n*-BA, contrary to the case of St, the emulsifier was found to partition primarily into the aqueous phase, leading to nucleation in the presence of micelles and unimodal PSDs. Particle formation was accompanied by limited aggregation in the early stages of the reaction with particles being formed past 50% monomer conversion in some cases. In the emulsion copolymerization of St and *n*-BA, unimodal PSDs were observed at the lowest (4.2 mM) and the highest (12.5 mM, 16.2 mM) levels of the emulsifier, while bimodal PSDs were produced at intermediate levels. These results were also attributed to emulsifier partitioning between the oil and aqueous phases. Lin et al. [102] also studied the kinetics of the emulsion polymerization of St in the presence of the nonionic emulsifier NP40 (nonylphenol polyethoxylate with an average of 40 oxyethelene units per molecule). The initially charged emulsifier concentration was well above its CMC. The number of polymer particles produced was proportional to the 2.4^{th} power of the total emulsifier concentration. This deviation of particle formation kinetics from the S-E theory (the 0.6^{th} power) was attributed to the low water solubility of the emulsifier (higher solubility in the monomer droplets), the increased agglomeration of polymer particles for the system with the lower amount of emulsifier, and the increased contribution of miniemulsion polymerization kinetics to the system with a higher emulsifier level.

Anionic emulsifiers provide electrostatic stability to the resultant polymer particles. The efficiency of anionic emulsifiers is dependent on various parameters, such as ionic strength and pH, but this can be a major drawback in terms of the stability of the resultant polymer particles. On the other hand, nonionic polymeric emulsifiers provide the steric stabilization provided by the thermodynamically-favored steric repulsion between particles. It is therefore practical to use mixtures of anionic and nonionic emulsifiers in emulsion polymerization to take advantage of these two different stabilization mechanisms. Chern et al. [104, 105] studied the CMC of the mixed emulsifier SDS/NP40 for various compositions at 25 °C and at 80 °C by performing surface tension measurements. They examined the effect of the mixed emulsifier SDS/NP40 on particle formation in the emulsion polymerization of St at 80 °C. They found that adding only a small amount of SDS to NP40 dramatically increased the number of polymer particles produced, and that the emulsion polymerization of St with the mixed emulsifier SDS/NP40 did not follow the conventional S-E theory. The number of polymer particles produced, N_T, was described by the expression $N_T \propto S_0^{\alpha}$, where S_0 is the concentration of mixed emulsifier, and the values of α were 0.60, 0.76, 1.3 and 1.1 for experiments with molar concentrations of NP40 of 0%, 40%, 70% and 100%, respectively. Colombié et al. [106] investigated the role of mixed anionic-nonionic emulsifier systems in particle formation in the emulsion polymerization of St. They carried out the emulsion polymerization of St using a mixture of SDS and Triton X-405 at 70 °C. They found that adding just 1 mM SDS to 6.4 mM Triton X-405 produced a dramatic increase in the rate of polymerization and the number of polymer particles produced. The increase in the number of polymer particles was 17 times that without SDS. When in-

creased amounts of SDS (3 and 5 mM) were used in combination with 6.4 mM Triton X-405, the number of polymer particles produced increased. No secondary particle nucleation was noted upon the disappearance of the droplets, and the resulting latexes were stable. They attributed this behavior to the change in the partitioning of the Triton X-405 between the oil and aqueous phases by changing the amount of SDS added. When no SDS was used, 95% of the Triton X-405 was associated with the oil phase as opposed to 78% when 5 mM SDS was used. Therefore, increasing the amounts of Triton X-405 in the water phase by increasing the amount of SDS added allowed the formation of mixed emulsifier micelles, resulting in an increase in the number of polymer particles produced and the rate of polymerization. Unzueta et al. [103] carried out the semicontinuous emulsion copolymerization of MMA and *n*-BA using mixed emulsifier systems (anionic sodium lauryl sulfate and nonionic polyethylene oxide lauryl ether (Brij35)) and found that narrower PSDs with larger average particle sizes were obtained with mixed emulsifier systems than those obtained with single anionic systems. Furthermore, they developed a mathematical model for the emulsion copolymerization of MMA and *n*-BA with mixed anionic/nonionic emulsifier systems, where the CMC and micelle composition of mixed emulsifiers was predicted using the thermodynamics of nonideal mixtures [18].

Reactive surfactants have also been used in emulsion polymerization [33, 107–110, 114]. This is because the disadvantages of the surfactants that are typically used in emulsion polymerization, such as instability of the latex and surfactant migration during film formation, can be overcome in theory by using a reactive surfactant. Studies of the use of reactive surfactants in heterophase polymerizations (up to 1997) have already been extensively reviewed [107]. Amalvy et al. [108] investigated the particle formation process in the emulsion polymerizations of St, MMA and VAc stabilized by sodium dodecyl sulfopropyl maleate, a polymerizable surfactant (surfmer), focusing their attention on whether the reactivity of the surfmer with the main monomer(s) and the polymerization locus play critical roles in the particle formation in emulsion polymerization systems. The results obtained suggested that the presence of the surfmer did not affect the particle formation mechanism. They concluded from the shape of the $\log N_T$ vs $\log S_0$ (surfmer concentration) plot that the polymer particles were formed by micellar nucleation in the case of St and by homogeneous nucleation in the case of MMA and VAc. Wang et al. [33, 109, 110, 114] studied the emulsion polymerization of St using the reactive surfactant sodium dodecyl allyl sulfosuccinate (TREM LF-40) and its polymeric counterpart (poly(TREM)) as anionic polymeric emulsifiers in terms of the polymerization kinetics. The use of TREM LF-40 gave $N_T \propto S_0^{0.5-0.6}$ and $R_p \propto N_T^{0.7}$ at constant initiator concentration. The reasons for the unusual kinetics compared to those with SDS ($R_p \propto N_T^{1.0}$) were ascribed to chain transfer to TREM LF-40, copolymerization of St with TREM LF-40, and the influence of the homopolymer TREM LF-40 (poly(TREM)) and/or the copolymer (poly(TREM-*co*-St)) on the entry and the exit rates of the free radicals. In contrast, by

varying the initiator concentration, the kinetics were found to have the same dependencies as the conventional emulsifier ($R_p \propto N_T^{1.0} \propto I_0^{0.4}$). In the case of poly-(TREM), the dependencies of R_p and N_T on S_0 and I_0 varied depending on experimental conditions ($R_p \propto N_T^{1.0} \propto S_0^{0.2-0.4}$, and $R_p \propto N_T^{1.0} \propto I_0^{0.6-0.8}$). It was inferred that homogeneous nucleation was dominant when using poly(TREM), even at concentrations exceeding its CMC. This was different from the monomeric TREM LF-40 emulsifier.

Recently, polymeric surfactants have received considerable attention in industry. They provide the steric repulsion between interacting particles, which gives the latex excellent stability against high electrolyte concentration, freeze-thaw cycling and high shear rates. Cochin et al. [111] carried out a comparative study of the emulsion polymerization of St using conventional, polymerizable and polymeric emulsifiers. Ayoub et al. [112] investigated the emulsion polymerization of St with amphiphatic copolymers [of VAc and methoxy polyoxyethlene (PVAc-b-MPOE)(35:65, 27:73, 19:81 wt/wt) prepared with a macroradical initiator in the presence of benzoyl peroxide] as the emulsifier. The experimental results for the number of polymer particles produced (N_T) versus emulsifier concentration (S_0) were as follows: $N_T \propto S_0^{1.82}$ (65%), $N_T \propto S_0^{2.1}$ (73%) $N_T \propto S_0^{1.66}$ (81%). They [113] also studied the emulsion polymerizations of VAc and St using the polymeric emulsifier prepared from polyoxyethylene methylether (POE, 66%) and St (34%). They did not measure the number of polymer particles produced, but the rate of polymerization was found to be proportional to the 0.9th and 0.76th powers of the initiator (KPS) concentrations, and to the 0.77th and 0.66th powers of the emulsifier concentrations for VAc and St monomers, respectively. Kato et al. [115] investigated the emulsion polymerization of St using poly(methyl methacrylate (MMA)-*co*-methacrylic acid (MAA)) with different copolymer compositions as polymeric emulsifiers. They examined the effect of the copolymer compositions, molecular weights and MAA contents of the polymeric emulsifiers on the number of polymer particles produced. They found that the number of polymer particles produced showed a slight dependence on the copolymer molecular weight, having a maximum when the molecular weight was in the range 5,000–10,000, and decreasing monotonously with the content of MMA in the copolymer. Cheong et al. [116] studied the kinetics of particle nucleation and growth in the emulsion polymerization of St using water-soluble polyurethane resins (PUR) as the emulsifier. They found that the number of polymer particles produced became constant in the early stage of polymerization when the concentration of the initially charged PUR was lower. However, the monomer conversion where the particle number became constant increased with increasing the initial PUR concentration. The constant particle number observed (N_T) was correlated as $N_T \propto [PUR]_0^{0.6-0.7}[KPS]_0^{0.4}$ (where $[PUR]_0$ and $[KPS]_0$ are the PUR and KPS concentrations, respectively). These dependencies are almost the same as those predicted by the S-E theory.

3.3.2 Particle Growth in Homopolymer Systems

As is clear from Eq. 1, the rate of particle growth (R_p/N_T) is proportional to the monomer concentration, $[M]_p$ and the average number of radicals per particle, $\bar{n}$, respectively. Thus, $\bar{n}$ is one of the basic parameters that characterize the kinetic behavior of particle growth in an emulsion polymerization system. Early researchers devoted their efforts to deriving a quantitative description of $\bar{n}$ by solving Eq. 3 for $\bar{n}$ defined by Eq. 2 [4, 119, 120].

Smith and Ewart [4] did not obtain a general solution to Eq. 3, but rather solved it for three limiting cases at steady-state conditions, that is, $dN_n/dt=0$.

Case 1. The number of radicals per particle is smaller than unity.

In this case, it holds that, $\rho_e/N_T \ll k_f$, $(\rho_e/N_T)N_0 \cong k_f N_1$, and $N_0 \cong N_T$. Furthermore,

a. When radical termination in the water phase is dominant; in other words, $\rho_w \cong 2k_{tw}[R_w^*]^2$, then

$$\bar{n} = (\rho_w/2k_{tw})^{1/2} m_d \nu_p \ll 0.5 \tag{44}$$

where k_{tw} is the termination rate constant in the water phase, ρ_w is the rate of radical generation per unit volume of water, $[R_w^*]$ is the concentration of radicals in the water phase, and m_d is the partition coefficient of radicals between the water and the polymer particle phases. However,

b. When termination in the polymer particles is dominant,

$$\bar{n} = (\rho_w/2k_f N_T)^{1/2} \ll 0.5 \tag{45}$$

The requirement for this condition is obtained as $(4\pi^2 D_w^2 d_p^2 N_T/k_f) \gg k_{tw}$ from additional assumptions that $\rho_e = 2\pi D_w d_p [R_w^*] N_T$ and $2k_{tw}[R_w^*]^2 \ll 2(\rho_e/N_T)N_1$, where D_w is the diffusion coefficient for the radicals in the water phase and d_p the diameter of the particles.

Case 2. The number of radicals per particle is approximately equal to 0.5.

The requirements for this case are given as $k_f \ll \rho_e/N_T < k_{tp}/\nu_p$. Then we have

$$\bar{n} = 0.5 \tag{46}$$

Equation 46 usually holds in St emulsion polymerization under normal conditions and is generally well known as the S-E theory.

Case 3. The number of radicals per particle is larger than unity.

This situation will prevail when the average time interval between successive entries of radicals into a polymer particle is much smaller than the average time for two radicals in the same particle to coexist without mutual termination; in other words, $\rho_e/N_T \gg k_{tp}/\nu_p$.

$$\bar{n} = (\rho_e \nu_p/2k_{tp})^{1/2} \gg 0.5 \tag{47}$$

Moreover, when both radical termination in the water phase and radical desorption from the particles are negligible, Eq. 47 is reduced to

$$\bar{n} = (\rho_w \nu_p / 2k_{tp} N_T)^{1/2} \gg 0.5 \tag{48}$$

In this case, the kinetic behavior is quite similar to that of suspension polymerization, except that the polymer particles are supplied with free radicals from the external water phase. When the polymerization proceeds according to Eq. 48, the system is sometimes referred to as obeying "*pseudo-bulk*" kinetics.

A general solution to Eq. 3 was provided by Stockmayer [121] with minor corrections by O'Toole [119]. On the other hand, Ugelstad et al. [120] proposed the most useful and widely applicable expression for $\bar{n}$ given by

$$\bar{n} = (a/4)\frac{I_m(a)}{I_{m-1}(a)} = (1/2)\cfrac{2\alpha}{m+\cfrac{2\alpha}{m+1+\cfrac{2\alpha}{m+2+\ldots}}} \tag{49}$$

where $I_m(a)$ is the modified Bessel function of the first kind, $m=k_f\nu_p/k_{tp}$, and $\alpha=a^2/8=\rho_e\nu_p/k_{tp}N_T$. On the other hand, the radical balance in the water phase (Eq. 4) leads to the following relationship using the non-dimensional parameters, α, α_w, m and Y.

$$\alpha = \alpha_w + m\bar{n} - Y\alpha^2 \tag{50}$$

where $\alpha_w=\rho_w\nu_p/k_{tp}N_T$ and $Y=2k_{tw}k_{tp}/k_a^2N_T\nu_p$. They solved the simultaneous equations, Eq. 49 and Eq. 50 for $\bar{n}$, and plotted the calculated value of $\bar{n}$ against the value of α_w that consisted of variables of known values with m varied as a parameter for various fixed values of Y. Figure 3(a) shows an example of the plot of $\log\bar{n}$ versus $\log\alpha_w$ for varying m and Y=0 [120].

On the other hand, Nomura et al. [122a] provided a semi-theoretical expression for $\bar{n}$ corresponding to Y=0, and compared it with the experimental data shown in Fig. 3(b) [122b].

$$\bar{n} = \frac{1}{2}\left[\left\{\left(\alpha_w + \frac{\alpha_w}{m}\right)^2 + 2\left(\alpha_w + \frac{\alpha_w}{m}\right)\right\}^{1/2} - \left(\alpha_w + \frac{\alpha_w}{m}\right)\right] + \left(\frac{1}{4} + \frac{\alpha_w}{2}\right)^{1/2} - \frac{1}{2} \tag{51}$$

The values predicted by Eq. 51 agree well with those predicted by Eq. 49 within less than 4%. This type of plot is called a "*Ugelstad plot*" and has been applied as a criterion to determine whether a system under consideration obeys either zero-one kinetics ($\bar{n}\leq 0.5$) or pseudo-bulk kinetics ($\bar{n}>0.5$).

Nomura et al. [42, 43, 64] showed that when the value of the term k_{tp}/ν_p is very large (the rate of bimolecular termination in the polymer particles is very rapid), $\bar{n}$ is expressed by

$$\bar{n} = (-C + \sqrt{C^2 + 2C})/2 \tag{52}$$

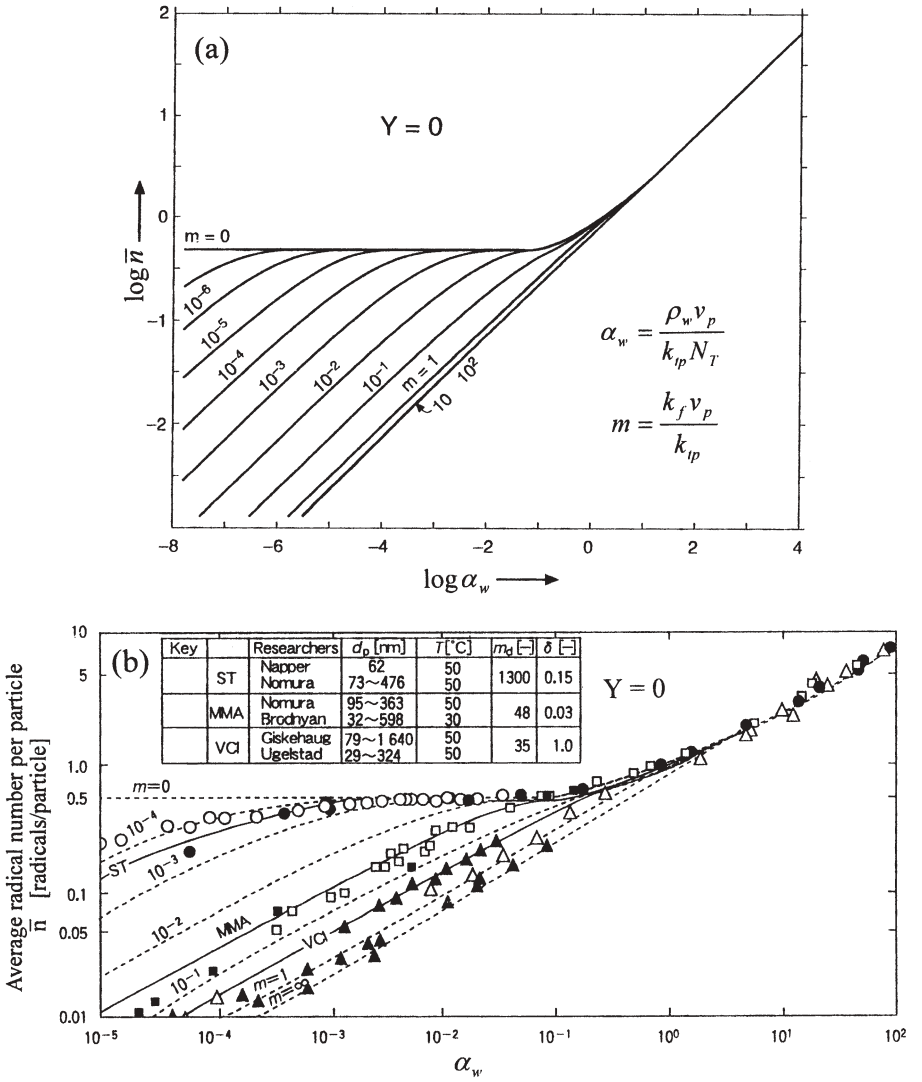

Fig. 3 (**a**) Average number of radicals per particle $\bar{n}$ as predicted by Eqs. 49 and 50, and presented as a function of the parameters α_w and m for Y=0, (**b**) comparison between predicted and observed values of $\bar{n}$.

where $C=\rho_w/k_fN_T$. In Fig. 4, they plotted the value of $\bar{n}$ against the value of C for the monomers of VCl, VAc, MMA, *n*-BMA and St obtained from the literature. It was found that the experimental values of $\bar{n}$ are in fairly good agreement with those predicted by Eq. 52, although the values of the parameters used in this comparison may not necessarily be exact.

An example of a successful application of the Ugelstad plot to determine some of the rate coefficients involved in emulsion polymerization was pre-

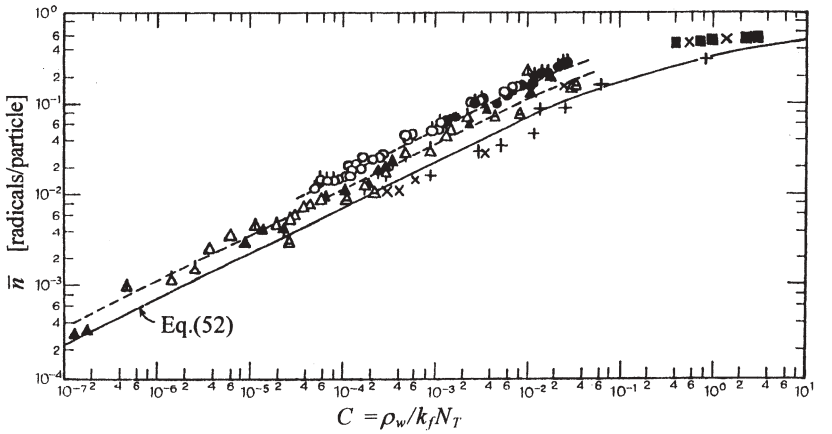

Table 3 Properties of several monomers and reaction conditions

Monomer	Temp. [°C]	k_p [l/mol·sec]	k_{fm}/k_p [–]	m [—]	Key in Fig. 4	$N_T \times 10^{-14}$ [particle/cc]	$\rho_w \times 10^{-12}$ [molecule/cc·sec]	Researcher
Vinyl chloride	50	10000	1.2×10^{-3}	35	△	12	0.73–7.3	
					↑	4.0	0.73–7.3	
					↑	2.2	1.82–3.65	Peggion
					▲	0.43–380	7.4	
					△	1.8–8.5	74	
					▲	66–32400	4.5	Giskehang
					△	0.30–6.4	3.6–28.5	Ugelstad
Vinyl acetate	50	3340	2.0×10^{-4}	28	↓	1.0–1.3	2.8–16.8	
					●	2.2	2.8–16.8	Authors
					○	5.0–6.0	0.7–11.2	
					○	10–15	5.6	
Methyl methacrylate	30	251	1.0×10^{-5}	48	×	0.018–121	0.032–0.95	Brodnyan
n-Butyl methacrylate	30	362	3.2×10^{-5}	830	+	1.5–113	0.19–0.95	
Styrene	50	227	1.2×10^{-5}	1300	■	1.6–10	3.7	Authors

Fig. 4 Comparison of experimental values of $\bar{n}$ with those predicted by Eq. 52

sented by Nomura et al. [123]. Although this approach is rather laborious and time-consuming, they could successfully determine the propagation rate constant k_p and the value of m, from which the desorption rate coefficient k_f could then be deduced, in seeded and unseeded emulsion polymerization of VDC at 50 °C. On the other hand, Hawkett et al. [24] developed a method for determining ρ and k_f termed the *slope-and-intercept* method. This method is simple and straightforward, but has several drawbacks (as stated in Sect. 3.1.2), so care must be taken when this method is used. Asua et al. [12, 124] proposed a new approach for the estimation of kinetic parameters such as the entry and desorption rate coefficients, the termination rate constant in the aqueous phase, the rate coefficient for initiator decomposition and the propagation rate constant in emulsion homopolymerization systems under zero-one conditions.

They claim that accurate values for the parameters are obtainable with this approach provided that a sufficient number of experiments with a minimum range of variation are available.

Recently, several modeling papers have been published which are useful for the design and operation of emulsion homopolymerization processes [22, 80, 81, 125–127]. Mendoza et al. [125] developed a mathematical model that could predict the monomer conversion, particle diameter, number of polymer particles produced, and the number-average and weight-average molecular weights in the unseeded emulsion polymerization of St using *n*-dodecyl mercaptan as CTA. This model was validated by fitting the experimental data to the model's predictions. Kiparissides et al. [126] proposed a comprehensive mathematical model to quantify the effect of the oxygen concentration on the polymerization rate and PSD in the unseeded emulsion polymerization of VCl. Particle formation was assumed to proceed by both the homogeneous and micellar nucleation mechanisms. Asua et al. [127] developed a mathematical model for seeded emulsion polymerization stabilized with polymerizable surfactants (surfmers). The model included the most distinctive features of surfmer polymerization, including partitioning of the unreacted surfmer between the surface of the polymer particles and the aqueous phase, and the surfmer burying itself inside the polymer particles. The model also included the possibility of having radical concentration profiles in the polymer particles. Herrera-Ordóñez et al. [22, 80, 81] proposed a detailed mathematical model of the kinetics of St emulsion polymerization, which was a modification and adaptation of previous works reported in the literature. By comparing model predictions with experimental results, they arrived at the conclusion that initiator-derived radicals with only one monomeric unit also make a significant contribution to the rate of radical capture by polymer particles, which contradicts the conclusion obtained by the Sydney Group [11, 91]. They applied the model to the emulsion polymerization of MMA above the CMC of the emulsifier to discuss the mechanism of particle formation and growth in this system, and concluded that particle formation by micellar nucleation is at all times at least ten orders of magnitude greater than the homogeneous one, although MMA is moderately water-soluble [81].

Although the emulsion polymerization of VAc is already one of the most studied systems, research articles on this topic are still being published [128–132]. Gilmore et al. [128, 129] presented a mathematical model for particle formation and growth in the isothermal semibatch emulsion polymerization of VAc stabilized with poly(vinyl alcohol) (PVA). The model accommodated grafting onto the PVA backbone during particle formation, and polymeric stabilization. When the emulsion recipe, process conditions and kinetic parameters are supplied, the model can predict the various species concentrations along with the monomer conversion and particle size and number profiles. In Part II of a series of papers [129], model predictions were compared with semibatch and batch experimental results. Budhiall et al. [130] investigated the role of grafting in particle formation and growth during the emulsion polymerization of VAc with partially hydrolyzed PVA as the emulsifier and KPS as the initiator.

They found that: (1) the number of polymer particles produced was dependent on the PVA blockiness; (2) the PVA with the higher degree of blockiness led to the formation and stabilization of more polymer particles; (3) particle formation continued to high conversions for the more random PVA (Poval 217), whereas it appeared to stop at intermediate conversions for the blockier PVA (PVA217EE); (4) all systems exhibited limited aggregation of the polymer particles during the polymerization process, and; (5) the greatest amount of grafting of the PVA stabilizer onto the polymer particles occurred early in the reactions (X_M<25%), presumably contributing primarily to the stabilization of the particles. Shaffie et al. [131] studied the kinetics of the emulsion polymerization of VAc initiated by redox initiation systems of different persulfate cations such as KPS, sodium persulfate (NaPS), and ammonium persulfate (APS); each of them was coupled with a developed acetone sodium bisulfate adduct as the reducing agent. In emulsion polymerization, the exhaustion of the separate monomer droplet phase (the onset of Interval III) is usually followed by a decrease in the rate of polymerization due to the decrease in monomer concentration in the polymer particles. This is not the case for the emulsion polymerization of VAc, where the rate of polymerization remains constant throughout most of Interval III (ca. 20~90% conversion). In the case of VAc, Interval III starts from around 20% conversion [20, 64]. In order to explain the reason for the independence of the polymerization rate from the monomer concentration, Nomura et al. [20] developed a model that takes into account the particles containing at most two free radicals, where no instantaneous termination inside the particles is assumed. Based on this model, they ascribed the reason to an increase in the value of $\bar{n}$ due to the gel effect, which compensates for the decrease in monomer concentration with conversion. The decrease in the termination rate constant inside the polymer particles due to an increase in viscosity with conversion (the gel effect) prolongs the coexisting time of two free radicals in the same particle, thereby increasing the value of $\bar{n}$. Chern et al. [133] also developed a model that includes particles containing at most two free radicals. However, they attributed the reason to a decrease in the rate coefficient for radical desorption due to an increase in viscosity with conversion, which results in an increase in the value of $\bar{n}$. On the other hand, Bruyn et al. [132] proposed a kinetic model that considers a zero-one system with instantaneous radical termination inside the particles. The model assumes that radical loss is by transfer to a monomeric species which is very slow to propagate and whose radical activity is lost by desorption and termination, either in the aqueous phase or when it enters a particle containing a radical. Since the transfer step is rate determining, the rate of this process is proportional to monomer concentration, which then cancels the dependence on the monomer concentration in the overall polymerization rate expression. This model also predicts that the radical loss rate coefficient should be either $k_{tr}C_p$ (Limit 2a [1]) or $2k_{tr}C_p$ (Limit 2b [1]), where k_{tr} is the rate coefficient for transfer to monomer and C_p is the monomer concentration in the particles. They [134] also studied the kinetics and mechanisms of the emulsion polymerization of vinyl *neo*-decanete

(VnD), a practically water-insoluble monomer (its water solubility≅4×10^{-5} M at 50 °C) at 50 °C using sodium persulfate (NaPS) as the initiator and SDS as the emulsifier. They found that the polymerization rate was nearly independent of particle number for a given initiator concentration (approximately independent of particle size). They regarded this as consistent with the Limit 2b zero-one kinetics of emulsion polymerization, whereby a monomeric radical resulting from transfer to a monomer goes from particle to particle by desorption and reentry until it eventually enters a particle containing a growing radical, whereupon it undergoes very rapid bimolecular termination. Therefore, they explained the kinetic behavior of this system with the same mechanisms and model applied to the VAc system [132]. The most important claim raised in these articles is that, contrary to the conclusion of Nomura et al. [43, 64], the rate coefficient of radical desorption is independent of the water solubility of a desorbing monomeric radical. Therefore, the validity of their claim is still open for discussion and further studies are needed for its final solution.

Matsumoto et al. [135] studied the kinetics of the emulsion crosslinking polymerization and copolymerization of allyl methacrylate (AMA) with MMA, BMA and ethylene dimethacryllate (EDMA).

3.3.3 Particle Growth in Copolymer Systems

Ballard et al. [136] presented an extended S-E theory that provides a description of the emulsion copolymerization system during Interval II and III and suggested the possibility of using an "*average*" rate coefficient to treat the copolymerization system. On the other hand, Nomura et al. [45, 47, 137] first developed an approach to generalize the S-E theory for emulsion homopolymerization to emulsion copolymerization by introducing "*average (or mean) rate coefficients*" for propagation, termination and radical desorption. This methodology was termed the "*pseudo-homopolymerization approach*" [138] or the "*pseudo-kinetic rate constant method*" [139] and is now widely applied, not only to emulsion copolymerization systems, but also to other homogeneous free radical copolymerization systems. Nomura et al. [47, 122a, 140] demonstrated that the equations derived so far for emulsion homopolymerization can also be applied without any modification to a binary emulsion copolymerization system with monomers A and B by substituting the following "*average rate coefficients*" for the corresponding rate constants for emulsion homopolymerization.

The polymerization rate for the A-monomer is expressed as

$$r_{pA} = \bar{k}_{pA}[M_A]_p \bar{n}_t N_T \tag{53}$$

where $[M_A]_p$ is the concentration of A-monomer in the polymer particles and $\bar{n}_t$ is the average number of total radicals per particle ($\bar{n}_t = \bar{n}_A + \bar{n}_B$). The overall rate of copolymerization is defined by

$$R_p = \overline{k_p}[M]_p \bar{n}_t N_T = r_{pA} + r_{pB} = (\bar{k}_{pA}[M_A]_p + k_{pB}[M_B]_p)\bar{n}_t N_T \tag{54}$$

where $\bar{k}_p$ is the overall propagation rate coefficient defined by Eq. 54 and is a function of the propagation rate constant, monomer reactivity ratio and mole fraction of each monomer in the polymer particles. In the case of a binary emulsion copolymerization system, for example, the average rate coefficients are defined as follows:

1. The average rate coefficient for the propagation of the A-monomer, $\bar{k}_{pA}$, is given by

$$\bar{k}_{pA} = k_{pAA} f_A + (k_{pBB}/r_B) f_B \tag{55}$$

Here

$$f_A = \frac{\bar{n}_A}{\bar{n}_t} = \frac{k_{pBB} r_A [M_A]_p}{k_{pAA} r_B [M_B]_p + k_{pBB} r_A [M_A]_p} \tag{25}$$

where k_{pBA} denotes the rate constant for the propagation of a B-radical to an A-monomer, f_A is the fraction of A-radicals in the particle phase ($f_A+f_B=1$), and r_B is the B-monomer reactivity ratio.

2. The average rate coefficient for radical desorption, $\bar{k}_f$, is defined using the equations

$$k_f = k_{fA}(\bar{n}_A/\bar{n}_t) + k_{fB}(\bar{n}_B/\bar{n}_t) = k_{fA} f_A + k_{fB} f_B \tag{24}$$

and

$$k_{fA} = K_{oA}\left[\frac{C_{mAA} r_A [M_A]_p + C_{mBA} [M_A]_p}{r_B\{(K_{oA}\bar{n}_t/k_{pAA}) + [M_B]_p\} + [M_A]}\right] \tag{26}$$

where k_{fA} is the desorption rate coefficient for the A-monomeric radicals, C_{mBA} is the chain transfer constant of a B-radical to an A-monomer, and K_{oA} is the desorption rate constant for A-monomeric radicals, given by Eq. 19 in Sect. 3.2.1.

3. The average rate coefficient for radical termination in the particle phase, $\bar{k}_{tp}$, is defined by

$$\bar{k}_{tp} = k_{tpAA} f_A^2 + 2k_{tpAB} f_A f_B + k_{tpBB} f_B^2 \tag{56}$$

where k_{tpAB} is the bimolecular radical termination rate constant between A- and B-radicals. Other average coefficients, such as the average chain transfer coefficient, can be defined, if necessary, using the same principle. This approach can be easily extended to multimonomer emulsion polymerization systems [138, 141]. Based on an exact mathematical treatment, Giannetti [142] concluded that the pseudo-homopolymerization approach represents a suitable approximation for most copolymerization systems of practical interest, except for very special cases.

Since the appearance of the pseudo-homopolymerization approach, a wide variety of mathematical models have been developed for emulsion copolymerization systems using this approach, in order to thoroughly understand the mechanisms involved in particle formation, growth processes, and to predict the copolymerization rate, the properties of the copolymer obtained (molecular weight and copolymer composition), and colloidal characteristics (the particle number and PDS) [18, 27, 55, 58–63, 122(a), 140, 143–147]. Nomura et al. [122(a)] first proposed a kinetic model that introduced the pseudo-homopolymerization approach. They showed that the model could fairly accurately predict the monomer conversion versus time histories observed in the emulsion copolymerization of St and MMA. Moreover, they showed that the model could be successfully applied to the MMA-VAc system to predict the propagation rate constant and monomer reactivity ratio for each monomer, respectively. Furthermore, they presented both experimental and modeling work for the unseeded emulsion copolymerization of St and MMA, including the particle formation process [140]. The model was an extension of that used for simulating the kinetic behavior of the emulsion homopolymerization of MMA [74]. This model describes both the number of polymer particles produced and the monomer conversion versus time histories observed in the emulsion copolymerization of St and MMA conducted at 50 °C using KPS as the initiator and NaLS as the emulsifier.

Barandiaran et al. [63] also developed a mathematical model based on the pseudo-homopolymerization approach. Furthermore, they proposed a method to predict the kinetic parameters ($k_d f$, k_{ep}, k_f) in emulsion copolymerization using only calorimetric measurements, and gave the values of these parameters for the MA-VAc, MMA-BA emulsion copolymerization systems. Schoonbrood et al. [27] carried out a kinetic study of the seeded emulsion copolymerization of St with the relatively water-soluble monomer MA to investigate the mechanisms of radical entry into particles, radical desorption from particles, and the fate of radical species in the aqueous phase. For this purpose, they extended their propagation-controlled entry model to an emulsion copolymerimerization system by applying the pseudo-homopolymerization approach. López et al. [55] used calorimetric measurements to study the kinetics of the seeded emulsion copolymerization of St and BA. They varied the diameters of the seed particles, the number of initially charged seed particles, and the initial initiator concentration. A mathematical model was used to fit the experimental data for conversion versus time using the entry and desorption coefficients as adjustable parameters. Martinet et al. [145] carried out the emulsion copolymerization of α-methyl styrene (αMSt) and MMA at various temperatures (60, 70, 85 °C) in order to study the kinetic behavior, investigating the conversion, particle size, and the average number of radicals per particle, as well as the copolymer composition, microstructure, molecular weight distributions (MWDs), and the glass transition temperature (T_g). Unzueta et al. [18] proposed a mathematical model for emulsion copolymerization with mixed emulsifier systems, and carried out the seeded and unseeded emulsion copolymerizations of MMA and BA. Good agreement was found between the experimental results in batch and semicon-

tinous reactors and the corrsponding model predictions. Vega et al. [61, 147] and Dubé et al. [144] both developed mathematical models for the emulsion copolymerization of AN and Bu initiated by a redox initiator system, with the aim of simulating an industrial process and of improving the final polymer quality. Due to the high solubility of AN in water, the following effects were included: (a) the homopolymerization of AN in the aqueous phase; (b) the desorption of AN radicals from the polymer particles, and; (c) homogeneous particle nucleation. Saldívar et al. [58–60, 143] carried out extensive investigations on emulsion copolymerization. In the first paper, they presented a detailed mathematical modeling of emulsion copolymerization reactors along with comprehensive reviews of earlier models [58]. Then, they validated their model with experimental results obtained in the emulsion copolymerization of St and MMA, and demonstrated the generality of the model by applying it to three illustrative problems [143]. Furthermore, they performed a systematic experimental study of ten binary and three ternary emulsion copolymerization systems involving St, MMA, BA, Bu, VAc, AA and E [59]. The predictions for the evolution of conversion and average particle diameter in batch emulsion copolymerizations from the model were compared with experimental data for four emulsion copolymerizations of St with the comonomers MMA, BA, Bu and AA. After data fitting for unknown or uncertain parameters, the model was capable of quantitatively explaining the experimental observations for conversion evolution, but could only qualitatively explain the particle size evolution [59].

In industrial emulsion polymerization processes, a small amount of water-soluble carboxylic monomer (such as AA) is often added to improve the colloidal stability and surface properties of the resulting latex particles. Therefore, numerous studies have been carried out to date to clarify the influence of the AA monomer on the kinetic behavior of the emulsion copolymerization of St and AA [148–152] and of emulsion terpolymerizations including AA [79, 153, 154]. Shoaf et al. [148] presented a kinetic model that describes the reaction behavior of emulsion copolymerization systems where significant polymerization occurs in both the particle and aqueous phases. The model was applied to two seeded carboxylated emulsion copolymerization systems, AA-St and methacrylic acid (MAA)-St. They observed that the reaction behavior is greatly affected by the type of acid monomer used, the partitioning of the monomer between the various phases, and the locus of polymerization, and furthermore that the mechanism for the AA-St system is more complicated than that for the MAA-St system. They suggested that the primary reaction locus in the AA-St system shifts from the particles to the aqueous phase after the hydrophobic monomer, St, has been consumed. Yang et al. [149, 150] studied the effects of the initial comonomer (AA) concentration on the monomer conversion and particle number (N_T) in the emulsifier-free emulsion copolymerization of St and AA. They proposed an end-chain extension model to explain the experimental results where the monomer conversion to the power of 2/3 is proportional to the reaction time and $\log(N_T)=36.00+9.44[AA]_w$. Slawinski et al. [151] investigated the influence of AA on the particle growth process, with pH as the main

parameter in the seeded emulsion copolymerization of St and AA. To avoid the effect of pH on the decomposition of KPS [153, 155], they carried out the copolymerization at pH 2.5 (complete protonation) or pH 7 (neutralization). It was found that pH was the dominating factor in the incorporation of AA onto the particle surface. Wang et al. [152] examined the effect of AA and MAA separately on the total monomer conversion and the distributions of the carboxylic groups at different positions (the surfaces and cores of particles, and in the aqueous phase) in the emulsifier-free emulsion copolymerization of St with AA or MAA. On the other hand, Santos et al. [153] carried out a batch emulsion terpolymerization of St, BA and AA or MAA to study the effect of pH on the polymerization rate, monomer conversion, and glass transition temperature of the polymers produced, as well as the distributions of the carboxylic groups at different positions (the surfaces and cores of particles, and in the aqueous phase). Yan et al. [154] studied the kinetics and mechanisms of an emulsifier-free emulsion terpolymerization of St, MMA and AA. They found that the rates of particle formation and copolymerization increased with increasing concentrations of AA and APS and polymerization temperature. Yuan et al .[79] carried out the emulsion terpolymerization of St, Bu and AA in order to understand the roles of the water-soluble oligomers produced. It was found that increasing the AA concentration in the recipe increased the water-soluble oligomer concentration and the number of polymer particles, thereby increasing the rate of polymerization.

On the other hand, Xu et al. [156] studied the emulsifier-free emulsion terpolymerization of St, BA and the cationic monomer *N*-dimethyl, *N*-butyl, *N*-ethyl metacrylate ammonium bromide (DBMA) using oil-soluble azobis (isobutyl-amidine hydrochloride) (AIBA) as the initiator. They found that with increasing DBMA and AIBA concentrations, the number of oligomeric radicals increased, resulting in an increased polymerization rate, as shown by $R_p \propto [\mathrm{DBMA}]^{0.64}[\mathrm{AIBA}]^{0.67}$. Fang et al. [157] investigated the kinetics and the colloidal properties of the resulting polymer latexes in the emulsifier-free emulsion copolymerization of St and the nonionic water-soluble comonomer AAm, using an amphoteric water-soluble initiator, 2,2′-azobis[*N*-(2-carboxyethyl)-2–2-methylpropionamidine]-hydrate (VA057). They found that the rate of polymerization at 20% conversion was proportional to the initiator concentration to the power of 0.52.

Kostov et al. [158, 159] carried out a kinetic and mechanistic investigation of tetrafluoroethylene and propylene with a redox system containing tert-butylperbenzoate (TBPB). They found that $R_p \propto I_0^{0.54} S_0^{0.42}$, where R_p is the rate of polymerization, I_0 is the initial TBPB concentration, and S_0 is the initial emulsifier ($C_7F_{15}\,COONH_4$) concentration. Noël et al. [160] studied the effect of water solubility of the monomers on the copolymer composition drift in the emulsion copolymerization of MA and vinyl ester combinations. Urretabizkaia et al. [161] investigated the kinetics of the high solids content semicontinuous emulsion terpolymerization of VAc, MMA and BA. The effects of operating variables (feed flow rate, total amount of emulsifier, concentration of initiator and so on)

on the time evolution of the conversion, terpolymer composition, and the total number of polymer particles were investigated. The experimental results were analyzed by means of a mathematical model that incorporated the main features of the system. Ge et al. [162] studied the inverse emulsion copolymerization of (2-methacryloyloxyethyl) trimethyl ammonium chloride and AAm initiated with KPS. Aqueous monomer solutions were emulsified in kerosene with a blend of two emulsifers (Span80 and OP10). Particle formation was supposed to take place by monomer droplet nucleation. The observed rate of polymerization is represented by $R_p \propto I_0^{0.52} S_0^{0.38} M_0^{1.50}$, where M_0 is the monomer concentration.

3.3.4 Monomer Concentration in Polymer Particles

It is clear from Eq. 1 that the monomer concentration in a polymer particle is one of the three key factors that control the particle growth rate, and accordingly, the rate of polymerization. In emulsion polymerization, the course of emulsion polymerization is usually divided into three stages, namely, Intervals I, II and III. In Intervals I and II of emulsion homopolymerization, the monomer concentration in the polymer particles is assumed to be approximately constant. In Interval III, it decreases with reaction time. Two methods are now used to predict the monomer concentration in the polymer particles in emulsion homopolymerization: empirical and thermodynamic methods.

According to the empirical method [14, 20, 163], the monomer concentration in Intervals I and II can be expressed as

$$[\mathrm{M}]_p = [\mathrm{M}]_{pc} \tag{57}$$

Interval III begins when the monomer droplets disappear from the system at the monomer conversion X_{Mc}. The monomer concentration in this interval ($X_M > X_{Mc}$) is approximately given by

$$[\mathrm{M}]_p = [\mathrm{M}]_{pc} \left(\frac{1 - X_M}{1 - X_{Mc}} \right) \tag{58}$$

where $[\mathrm{M}]_{pc}$ is the constant monomer concentration at saturation swelling.

On the other hand, several researchers [164–167] have tried to thermodynamically describe the swelling behavior of polymer particles by one monomer. The thermodynamic approach now used is based on the so-called Morton equation given by

$$\frac{\Delta F_{ip}}{RT} = \ln(1 - \varphi_p) + \varphi_p \left(1 - \frac{1}{\bar{P}_n} \right) + \chi \varphi_p^2 + \frac{2 V_m \gamma \varphi_p^{1/3}}{r_0 RT} = 0 \tag{59}$$

where ΔF_{ip} is the partial molar free energy of the monomer in the polymer particles, φ_p is the volume fraction of polymer in the polymer particles, $\bar{P}_n$ is

the number-average degree of polymerization, χ is the Flory-Huggins interaction parameter, r_0 is the unswollen radius of the particle, R is the gas constant, T is the temperature, V_m is the partial molar volume of the monomer, and γ is the interfacial tension between the particles and the aqueous phase. Since the value of $\bar{P}_n$ is usually very large, the term $1/\bar{P}_n$ can be neglected. Given values of χ and r_0, Eq. 59 can be solved iteratively to yield φ_p. Then, by introducing the value of φ_p into the following equation, one can get the saturation monomer concentration in the polymer particles.

$$[M]_{pc} = \frac{1 - \varphi_p}{V_m} \tag{60}$$

Maxwell et al. [166] discussed the effects of several factors on the saturation and partial swelling of polymer particles by monomers using Eq. 59 and the Vanzo equation [168] that deals with the partial swelling of polymer particles in Interval III. By comparing theory and experiments for the MA and poly(MA-*co*-St) system, the authors showed that the monomer partitioning was insensitive to temperature, particle radius, copolymer composition, polymer molecular weight, polymer cross-linking, the value of the Flory-Huggins interaction parameter, and the particle-water interfacial tension, and that the conformational entropy of mixing of monomer and polymer was the significant term in determining the degree of partial particle swelling by the monomer. Contrary to Maxwell et al. [166], Antonietti et al. [167] observed a pronounced dependence of the swelling ratio on particle size where absolute values of swelling were much lower than those described by the classical Morton equation. In order to explain this phenomenon, the authors presented a modified description that considered size-relevant effects (such as the Kelvin pressure and depletion) using an additional osmotic pressure term, which increases with the inverse of the particle size. They also studied the effect of different types of covalently bound surface stabilizing groups on the degree of swelling, and found that electrically-stabilized particles resulted in higher swelling ratios and significant lower values for the interfacial energy as compared to sterically stabilized particles.

In an emulsion copolymerization, monomer partitioning between the monomer droplet, polymer particle and aqueous phases plays a key role in determining the rate of copolymerization and the copolymer composition. Two approaches (empirical and thermodynamic) have been proposed to predict the monomer concentrations in the polymer particles in an emulsion copolymerization system. In the emulsion copolymerization of St and MMA, Nomura et al. [45, 122, 140] first proposed an empirical approach for predicting the saturated concentration of each monomer in the polymer particles as a function of the monomer composition in the monomer droplets, as shown by

$$[M_i]_p = \frac{1}{a_i + b_i / W_{i,m}} \tag{61}$$

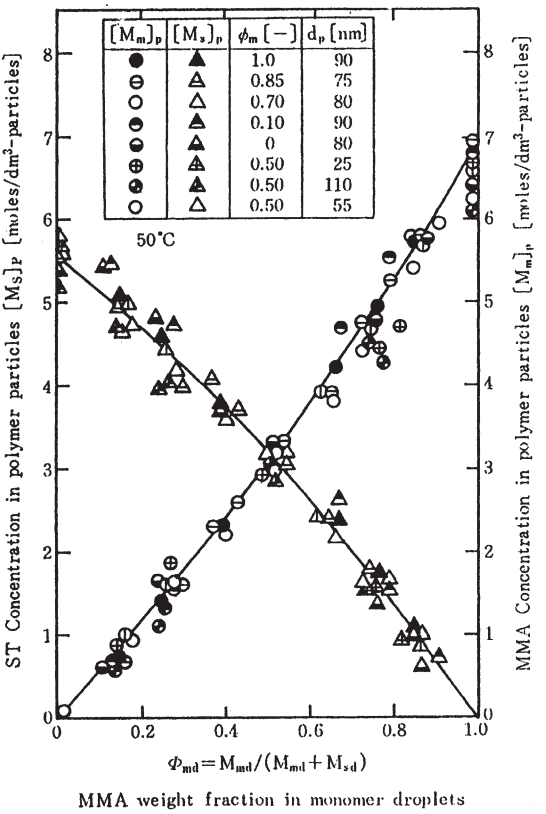

Fig. 5 Comparison of the observed saturation concentrations of St and MMA monomers in polymer particles with those predicted by Eq. 61 [45]

where the subscript i denotes monomer i, a_i and b_i are the numerical constants particular to monomer i, and $W_{i,\mathrm{m}}$ is the weight fraction of monomer i in the monomer droplets. Figure 5 is an example that shows good agreement between the predictions from Eq. 61 and experimental results.

The authors demonstrated experimentally that the saturation monomer concentration in the polymer particles was insensitive to particle radius and copolymer composition, and also that the weight fraction of the monomer i in the polymer particles ($W_{i,\mathrm{m}}$) was approximately equal to that in the monomer droplets ($W_{i,\mathrm{p}}$); in other words,

$$W_{i,\mathrm{m}} = W_{i,\mathrm{p}} \tag{62}$$

Thermodynamic methods were developed based on the extended equation by Ugelstad et al. [169], and have been further dealt with by various researchers [170–181]. Maxwell et al. [170] worked on the partitioning of two monomers between the polymer particle, monomer droplet and aqueous phases in an

emulsion copolymerization system, and proposed a thermodynamic approach that could be easily extended to deal with systems of three or more solvents and/or monomers. They derived the following equations for *i* and *j* monomers by taking into account the partial molar free energy of mixing of the monomer with polymer, the contribution of monomer to the interfacial free energy, the partial molar free energy of the monomer in the monomer droplets and the partial molar free energy of the monomer in the aqueous phase, respectively.

$$\ln\varphi_{pi} + (1 - m_{ij})\varphi_{pj} + \varphi_p + \chi_{ij}\varphi_{pj}^2 + \chi_{ip}\varphi_p^2 + \varphi_{pj} + \varphi_p(\chi_{ij} + \chi_{ip} - \chi_{jp}m_{ij}) + \frac{2V_{mi}\gamma\varphi_p^{1/3}}{r_0RT} = \ln\varphi_{di} + (1 - m_{ij})\varphi_{dj} + \chi_{ij}\varphi_{dj}^2 = \ln\left(\frac{[M_i]_w}{[M_i]_{w,sat}}\right) \quad (63a)$$

$$\ln\varphi_{pj} + (1 - m_{ji})\varphi_{pi} + \varphi_p + \chi_{ij}\varphi_{pi}^2 + \chi_{jp}\varphi_p^2 + \varphi_{pi} + \varphi_p(\chi_{ij} + \chi_{jp} - \chi_{ip}m_{ji}) + \frac{2V_{mj}\gamma\varphi_p^{1/3}}{r_0RT} = \ln\varphi_{dj} + (1 - m_{ji})\varphi_{di} + \chi_{ij}\varphi_{di}^2 = \ln\left(\frac{[M_j]_w}{[M_j]_{w,sat}}\right) \quad (63b)$$

where φ_p is the volume fraction of polymer in the latex particles, φ_{pi}, φ_{di}, φ_{pj} and φ_{dj} respectively represent the volume fractions of monomers *i* and *j* in the polymer particles and monomer droplet phases, χ_{ij}, χ_{ip} and χ_{jp} are the Flory-Huggins interaction parameters between each of the respective monomers *i* and *j* and the polymer, m_{ij} is the ratio of the molar volumes of monomers *i* and *j* (so $m_{ij}=V_{mi}/V_{mj}$, where V_{mi} and V_{mj} are the molar volumes of monomers *i* and *j*, respectively), $[M_i]_w$ is the concentration of monomer *i* in the aqueous phase, and $[M_i]_{w,sat}$ is its saturation concentration value if there are no other monomers present. The derivations of Eq. 63a and Eq. 63b involve the reasonable assumption that m_{ip} and m_{jp}, the ratios of the respective molar volumes of monomers *i* and *j* and the molar volume of polymer are negligible compared to all other terms. Furthermore, they made the following three assumptions to simplify Eqs. 63a and 63b.

1. For many pairs of monomers, the differences between the molar volumes of the monomers is slight. If this is the case, the ratio of the molar volumes of monomer *i* and *j* is well approximated by unity, so $m_{ij}=m_{ji}=1$.
2. The contribution to the partial molar free energy arising from the residual (enthalpic and non-conformational entropic) partial molar free energy of mixing of the two monomers is small relative to all other terms in the monomer droplet phase.
3. The interaction parameters for each monomer with the same polymer are equal ($\chi_{ip}=\chi_{jp}$).

They finally obtained the following simple expressions for saturation swelling.

$$\frac{\varphi_{pi}}{\varphi_{pj}} = \frac{\varphi_{di}}{\varphi_{dj}} \quad (64)$$

$$f_{pi} = f_{di} \tag{65a}$$

$$f_{pj} = f_{dj} \tag{65b}$$

where f_{pi}, f_{di}, f_{pj} and f_{dj} represent the volume fractions of monomers *i* and *j* in the polymer particle and monomer droplet phases, respectively. This equation relates the ratios of the volume fractions (or concentrations) of monomers *i* and *j* in the monomer droplet and particle phases. Eq. 65 is basically the same as Eq. 62 derived empirically by Nomura et al. [122(a)]. The validity of Eq. 65 was experimentally demonstrated in the St-MA, St-BA and MA-BA systems using seed polymer particles with different copolymer compositions and diameters. Based on Eq. 65 and experimental results, they finally proposed the following simple empirical expressions that could predict the concentration of monomers *i* and *j* in the polymer particles.

$$C_i = f_{di}[(C_{i,m} - C_{j,m})f_{d,i} + C_{j,m}] \tag{66a}$$

$$C_j = f_{dj}[(C_{j,m} - C_{i,m})f_{d,j} + C_{i,m}] \tag{66b}$$

where C_i and C_j are the concentrations of monomers *i* and *j* in the polymer particles, and $C_{i,m}$ and $C_{j,m}$ the maximum saturations of monomers *i* and *j* in the polymer particles (the homo-monomer swelling concentrations in the particles). By comparing the predictions from Eqs. 64 and 65 with experimental data from the St-MA, St-BA, MA-BA systems, they demonstrated that Eqs. 64 and 65 could provide adequate predictions for the monomer concentrations in the polymer particles. In these discussions, the ratio of the molar volumes of monomers *i* and *j* (m_{ij}) was assumed to be unity. On the other hand, Schoonbrood et al. [171] examined the validity of the assumption m_{ij}=1, made by Maxwell et al. [170], and demonstrated that this assumption could be used with systems where m_{ij} deviated from 1, at least up to a value of 2.

Noël et al. [172] experimentally determined both the saturation and partial swelling of MA-VAc copolymer latex particles by MA-VAc monomer mixtures. Monomer partitioning at saturation swelling could be predicted using the simplified relationships developed by Maxwell et al. [170]. On the basis of the work by Maxwell et al. [166, 170], Noël et al. developed an extended thermodynamic model for monomer partitioning at the partial swelling of latex particles by two monomers with limited water solubility in order to predict the monomer concentrations and fractions within the different phases, and confirmed the validity of this model by showing that the model's predictions were in good agreement with the observed monomer partitioning.

On the other hand, Schoonbrood et al. [173] investigated multimonomer partitioning in latex particles and derived simple equations describing monomer partitioning among the latex particle, monomer droplet and aqueous phases during Intervals II and III in emulsion copolymerization with any number of low to moderately water-soluble monomers, by extending the approaches developed by Maxwell et al. [170] and Noël et al. [172]. They showed that it is mainly the conformational entropy from mixing the monomer and polymer

that governs the partitioning behavior, and that other contributions to the free energies of the monomers in the polymer particles are marginal. They confirmed that all of the assumptions made in this study were valid using experimental results for St, MMA and MA, and confirmed that the simple equations proposed describe the monomer partitioning with these three monomers in Intervals II and III very well. In this approach, the only parameters needed to calculate the monomer concentrations in all of the phases were the saturation concentrations of each monomer in the polymer particles, and the saturation concentrations of each monomer in the aqueous phase.

By combining thermodynamically-based monomer partitioning relationships for saturation [170] and partial swelling [172] with mass balance equations, Noël et al. [174] proposed a model for saturation and a model for partial swelling that could predict the mole fraction of a specific monomer *i* in the polymer particles. They showed that the batch emulsion copolymerization behavior predicted by the models presented in this article agreed adequately with experimental results for MA-VAc and MA-Inden (Ind) systems. Karlsson et al. [176] studied the monomer swelling kinetics at 80 °C in Interval III of the seeded emulsion polymerization of isoprene with carboxylated PSt latex particles as the seeds. The authors measured the variation of the isoprene sorption rate into the seed polymer particles with the volume fraction of polymer in the latex particles, and discussed the sorption process of isoprene into the seed polymer particles in Interval III in detail from a thermodynamic point of view.

These thermodynamic equations provide the most complete description of the swelling of polymer particles by monomers, but include a rather large number of parameters whose accurate estimation requires extensive work. Considering this, Gugliotta et al. [175] presented a criterion for choosing which monomer partitioning models developed so far in the mathematical modeling of emulsion copolymerization should be applied to a given system. In the mathematical simulations, the seeded emulsion copolymerization of four monomer systems with a wide variety of reactivity ratios and water-solubilities were considered: BA-St, VAc-MA, VAc-BA and St-MAA. They investigated the effect of the complexity of the monomer partitioning equations, the type of process, the solid contents, and the amount of seed on the time evolution of the conversion and copolymer composition, and tabulated a summary of recommended monomer partitioning models.

In the industrial production of structured AN-Bu-St (ABS) latex particles, the grafting copolymerization of AN and St on crosslinked polybutadiene (PB) seed latex is carried out in emulsion polymerization. Therefore, information on the effect of PB crosslinking density on the swelling of PB latex particles by a St-AN monomer mixture is very important for the production of ABS copolymers with desired properties. Mathew et al. [177] studied the effect of several thermodynamic parameters, such as the crosslinking density, particle size and monomer mixture composition on the swelling behavior of PB latex particles by pure St and AN, and St-AN mixtures of various compositions. They reported

that, in the case of mixtures, the higher the AN concentration in the mixture, the lower the maximum swelling by St, and the opposite effect was observed for AN swelling. The parameters describing the interaction between the two monomers were found to be functions of the composition in the initial mixture.

Liu and Nomura et al. [178–180] carried out a series of investigations on the swelling behaviors of St-AN (SAN) and ABS latex particles by St-AN monomer mixtures. In the first article, Nomura et al. [178] examined the effects of copolymer composition and its compositional inhomogeneity in SAN latex particles on their swelling behavior, and found that both the copolymer composition and the compositional inhomogeneity in SAN latex particles had little or no influence on the swellability of SAN latex particles with a St-AN monomer mixture, as long as the weight fraction of AN monomer units in SAN latex particles was less than a certain value (between 0.6 and 0.8). Based on the experimental data, they proposed semiempirical equations that could predict the saturation concentration of each monomer in the SAN latex particles as a function of the comonomer composition in the monomer droplets and the overall copolymer composition in the SAN latex particles. In the follow-on article, Liu et al. [179] investigated the possibility of a thermodynamic correlation between both the partial and saturation swelling of SAN latex particles by St-AN monomer mixtures. First, they determined the three unknown Flory-Huggins interaction parameters between each monomer and homopolymer, $\chi_{A,PA}$, $\chi_{A,PS}$, and $\chi_{S,PS}$ (S: styrene, PA: polyacrylonitrile, PS: polystyrene) by fitting the thermodynamic swelling equations to the experimentally observed monomer concentrations in SAN latex particles. Then, they showed that the AN concentrations predicted by using these interaction parameters agreed fairly well with those observed. However, agreement between the predicted and observed St concentrations was somewhat worse than that for the AN concentrations. On the basis of the preceding studies, Liu et al. [180] further studied the saturation swelling of ABS latex particles by a St-AN monomer mixture. In order to describe the observed saturation swelling behavior, they proposed a two-phase swelling model based on the assumptions that in ABS latex particles, St-AN (SAN) copolymer domains were randomly dispersed in a continuous PB matrix, and further that thermodynamic equilibrium was attained among the SAN copolymer domain, PB matrix and monomer droplet phases. By using the proposed model, the effects of various factors on the saturation concentrations of each monomer in the ABS latex particles were experimentally and theoretically discussed. The factors examined were the polymer crosslinking density $\overline{M}_C$, the interfacial tension between the PB latex particle and aqueous phases γ, the ratio of the molar volumes of the St and AN monomers m_{ab}, the weight fraction of AN units in the SAN copolymer domains H_A, and the weight fraction of PB in the ABS latex particles H_{PB}. It was found that the saturation concentration of each monomer in the SAN latex particles was insensitive to $\overline{M}_C$, γ, m_{AB} and H_A, but that H_{PB} had a large influence on the saturation concentration of the AN monomer but almost no influence on the saturation concentration of the St monomer. They finally concluded that the two-phase swelling model developed

in this study could predict the saturation concentrations of St and AN monomers in the ABS latex particles quite well.

On the other hand, Aerdts et al. [181] carried out partial and saturation swelling experiments in latex particles of St-MMA (SMMA) copolymers, polybutadiene (PB) and composite particles containing PB with St and MMA grafted on, and compared the results from them to predicted results from the semiempirical equations developed by Maxwell et al. [166, 170]. They showed that the partitioning of MMA was independent of the type of polymer/SMMA copolymers of different compositions and PB. Moreover, the partitioning of MMA in PB was independent of particle size, polymer crosslinking density and the presence of SMMA copolymer grafted onto PB. It was further shown that the swelling of latex particles by St and MMA monomer mixtures was also independent of the polymer type of the latex particles and that the saturation partitioning of monomers between the latex particle and monomer droplet phases could be predicted by the simplified equations of Maxwell et al. (Eq. 66).

Said et al. [182] studied the effects of adding inorganic electrolytes on the emulsion polymerization of St using three different ionic emulsifiers and potassium and sodium chlorides as the inorganic electrolytes. They observed a significant increase in the rate of polymerization in all cases as the concentration level of the added electrolyte was increased. At the same time, they carried out saturation swelling measurements and found a slight increase in the monomer concentration inside the polymer particles as the level of added electrolyte concentration was increased. They thought that one reason for an increase in the rate of polymerization was the increase in the monomer concentration inside the polymer particles as the level of added electrolyte concentration was increased.

Tognacci et al. [183] discussed various methods for measuring the monomer concentration in the polymer particles. The method proposed by the authors is a direct estimation of the solvent activity by the GC (gas chromatography) measurement of its partial pressure in the gas phase at equilibrium with the polymer particle, monomer droplet (if any) and aqueous phase in the latex. They proposed an original measuring technique and carried out measurements for different monomers (St, MMA, and VAc) and polymeric matrices (PSt and MMA-VAc copolymer), both above and below saturation conditions (corresponding to Intervals II and III). They compared the experimental data with that predicted by the monomer partitioning relationships derived by Maxwell et al. [166, 170] and Noël et al. [172].

3.3.5 Reaction Calorimetry

Reaction calorimetry has been widely explored in studies of the kinetics of heterophase polymerization in recent years [63, 82–84, 147, 184–191]. There are several advantages of using a reaction calorimeter: (1) the rate of polymerization is obtained directly, using the monomer conversion calculated from the

integral of the heat of reaction curve, and (2) nearly continuous information is obtained. Using this information, a more detailed examination of the polymerization kinetics can be made, allowing the observation of important features which cannot be seen using any other technique (such as gravimetry and gas chromatography). Therefore, reaction calorimetry provides a powerful tool for investigating heterophase polymerization [82]. Recently, many papers have been published on reaction calorimetry studies into the kinetics of emulsion polymerization. The kinetics of the emulsion polymerization of St was reinvestigated in detail [82–84, 184]. The effect of surface charge density on the kinetics of the seeded emulsion polymerization of St was studied [185]. The dependence of the reaction rate profiles on the water solubility of the monomers, on the presence of CTA, on the types and concentrations of the stabilizer and the initiator, and on the polymerization temperature was investigated [187]. The influence of oxygen on the kinetics of chemically initiated seeded emulsion homopolymerization of St and the seeded emulsion copolymerization of St and BA was investigated [188]. Reaction calorimetry has been used to estimate the parameters in emulsion copolymerization systems [63], to control monomer conversion and copolymer composition in semi-batch unseeded emulsion copolymerization on-line [186, 189–191], and to monitor the copolymer composition, the average molecular weight, and the average degree of branching in the semi-batch unseeded emulsion copolymerization of AN and Bu [147].

Most reaction calorimeters work according to heat-flow calorimetry principles. The heat of reaction Q_r evolved from a reaction mixture running at T_r under isothermal conditions is transferred to the fluid in the cooling jacket according to the equation

$$Q_r = R_p(-\Delta H_p) = UA_{const}(T_r - T_j) \tag{67}$$

where R_p is the reaction rate, ΔH_p is the heat of reaction per unit amount of reactant, U is the overall heat transfer coefficient, A_{const} is the constant heat transfer area, and T_j is the fluid temperature in the cooling jacket. The flow rate of the cooling fluid is so high that the cooling fluid temperature at any position in the jacket is considered to be, to a good approximation, equal to T_j. The temperature of the cooling fluid T_j is adjusted to keep the reaction temperature constant at T_r, and the heat of reaction Q_r is found by calculating the value of $UA_{const}(T_r - T_j)$. Here, the heat transfer area A_{const} and the value of U (determined by calibration before and after the reaction) are treated as constant during the reaction. However, the value of U is likely to change during the reaction wherever the viscosity of the reaction mixture varies and/or the deposition of scale on the heat transfer surface occurs during the reaction.

To avoid the drawbacks mentioned above, a novel calorimeter was developed [192], as shown in Fig. 6, which can accurately measure the heat of reaction independently of the variation of U during a reaction.

The working principle is as follows. A cooling fluid at temperature T_i at the inlet is fed into the cooling jacket at a constant mass flow rate F_{in}, and the wetted heat transfer area A_{var} in the jacket (which can be varied in this calorime-

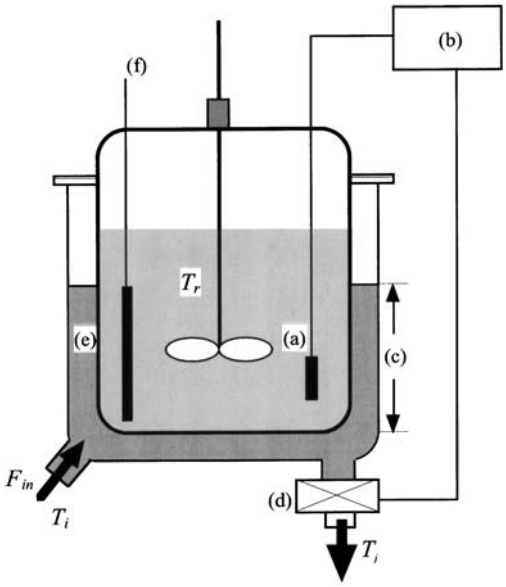

Fig. 6 Schematic diagram of a novel calorimeter with variable heat-transfer area

ter) is controlled to keep the temperature of the reaction mixture at the desired reaction temperature T_r by adjusting the fluid level (c) in the jacket, which is achieved by regulating the flow rate of the cooling fluid at the outlet with a computer-controlled throttle valve positioned there. The fluid temperature in the cooling jacket is considered to be T_j throughout the jacket because of satisfactory mixing due to the kinetic energy of the cooling fluid entering through a nozzle. Therefore, the temperature of the cooling fluid flowing through the outlet of the jacket is also T_j. To offset the heat loss from the reaction calorimeter Q_{loss}, a constant heat flux $Q_h (> Q_{loss})$ is passed into the reaction mixture through an immersed electrical heater (f) in order to maintain the reaction mixture at a constant temperature T_r even in the absence of the reaction. A reference run is carried out with no reaction before measuring the heat of reaction. Then, the steady-state heat balance for the reaction mixture in the calorimeter at temperature T_r is given by

$$Q_h = Q_{m0} + Q_{loss} \tag{68}$$

$$Q_{m0} = F_{in} C_p (T_i - T_j) = UA_{var} (T_r - T_j) \tag{69}$$

where Q_{m0} is the heat flux transferred to the cooling fluid across the reactor wall and T_j is the cooling fluid temperature at the outlet of the jacket. Since the values of F_{in}, T_i and T_j are measurable, the heat flux Q_{m0} is obtained by calculating the value of $F_{in} C_p (T_i - T_j)$, where C_p is the specific heat of the cooling fluid. Therefore, this calculated value of Q_{m0} gives a base-line reading and is constant

as long as Q_{loss} remains constant. On the other hand, when the reaction is allowed to take place at the constant temperature T_r, one gets the steady-state heat balances given by

$$Q_h + Q_r = Q_m + Q_{loss} \tag{70}$$

$$Q_m = F_{in}C_{pi}(T_i - T_j) = UA_{var}(T_r - T_j) \tag{71}$$

where Q_m is the heat flux corresponding to the new reading when the reaction is taking place. As long as the value of Q_{loss} is kept constant by maintaining the temperature around the region of the calorimeter constant, one gets the following expression from Eqs. 68 to 71.

$$Q_r = Q_m - Q_{m0} \tag{72}$$

Therefore, one can derive the heat of reaction Q_r independently of the value of U from the difference between the new and base-line readings.

3.4 Effect of Initiator Type

There are two types of chemical initiator that can be used to initiate emulsion polymerization. They are water-soluble initiators (such as KPS, hydrogen peroxide-iron (II) redox system) and oil-soluble initiators (like azobis-isobutyronitrile (AIBN), benzoil peroxide (BPO), benzoil peroxide-*N*,*N*-dialkylaniline redox system). Water-soluble initiators are more commonly used in emulsion polymerization than oil-soluble initiators. However, oil-soluble initiators are sometimes used when the fragments derived from ionic water-soluble initiators are not desirable either in the latex serum or on the surface of the polymer particles. Water-soluble initiators produce almost all of the free radicals in the water phase, because the amount of initiator partitioned into the organic phases is usually negligible. Contrary to water-soluble initiators, oil-soluble initiators distribute among the four phases: monomer-swollen micelles, monomer-swollen polymer particles, monomer droplets (if any), and the water phase. In the case of oil-soluble initiators, only a small fraction of radicals are produced in the water phase because the amount of initiator partitioned into the water is usally very small. Therefore, it is useful to find out whether the different principal initiator loci of polymerization systems with water-soluble and oil-soluble initiators brings about any differences in the kinetics and mechanisms of polymerization between both initiator systems.

Several researchers have carried out experimental and/or theoretical investigations on emulsion polymerizations initiated with oil-soluble initiators and reported that the kinetics of the emulsion polymerizations is basically similar to that initiated with water-soluble initiators [193–202]. Breitenbach et al. [193] carried out the emulsion polymerization of St initiated by BPO at 50 and 60 °C. The authors interpreted the experimental results by assuming a relatively rapid exchange of low molecular weight radicals between the micelle-polymer

particle and water phases. Van der Hoff [194] conducted the emulsion polymerization of St initiated by cumen hydroperoxide (CHP) and suggested three possible mechanisms. One possibility is the entry of single radicals generated from the fraction of the initiator dissolved in the water phase. A second possibility is that single radicals are formed by desorption of one of a pair radicals (that form within the particles or by a side reaction) into the water phase. Another possible mechanism is that pairs of radicals are produced in the emulsifier layer, and only the organic radical ($C_9H_{11}O\cdot$) enters the particle, while the inorganic initiator fragment ($OH\cdot$) remains in the water phase where it can undergo further reaction. The author stated that there was no direct evidence that any of these three mechanisms in fact came into play. Dunn et al. [195] carried out the emulsion polymerization of St at 60 °C using octadecyl sulfate as the emulsifier and AIBN as the initiator. They found that the number of polymer particles produced varied approximately with the 0.4^{th} power of the initially charged initiator concentration. This behavior is quite similar to that usually found in the emulsion polymerization of St initiated with KPS. They ascribed this kinetic similarity to desorption of either of the primary radicals that formed as a pair into the water phase, leaving a single radical inside the polymer particle for initiation. It was also found that only 4% of the whole initially charged initiator was effective in the emulsion polymerization in contrast with an efficiency of ~50% found in bulk or solution polymerizations. Barton et al. [196] investigated the effect of an oil-soluble initiator (AIBN) on the kinetics and mechanism of the emulsion polymerization of BMA at 60 °C in the presence of the anionic emulsifier disodium dodecylphenoxybenzene disulfonate. They compared the results obtained with the course of the emulsion polymerization of BMA initiated by KPS, and proposed that the radicals produced by decomposition in the aqueous phase determine the kinetics of the polymerization.

On the other hand, Il'menev et al. [197] carried out the emulsion polymerization of St at 50 °C using oil-soluble initiators such as AIBN, BPO and lauryl peroxide (LPO). The water-solubilities of AIBN, BPO and LPO at 20 °C are 3.6, 0.1 and 0.01 mol/dm^3-water, respectively. The rate of polymerization conducted at 50 °C with 0.025 mol/dm^3-St of each initiator was found to be (fastest to slowest): AIBN, BPO and LPO; in other words, in the order of decreasing water-solubility. They estimated the average times for a primary radical to terminate, propagate, and desorb into the aqueous phase, respectively, when a pair of radicals are generated in a micelle and a polymer particle. They concluded that the contribution to the polymerization (particle formation and growth) from the free radicals that are produced in pairs in the micelles and polymer particles is almost negligible, because they are very likely to cause rapid geminate termination, and that the free-radicals generated in the monomer droplets also play only a small part in the polymerization, because their desorption into the water phase can be ignored. This view was strongly supported later by the theoretical and experimental work of Nomura et al. [198–202]. Nomura et al. [198] proposed a theoretical approach by which the effects of various factors

on the average number of radicals per particle $\bar{n}$ could be predicted in seeded emulsion polymerizations initiated by oil-soluble initiators. In their approach, the following six kinetic events were considered, (i) the generation of a pair of radicals inside the particles, (ii) radical entry into the particles from the aqueous phase, (iii) overall radical desorption including both primary initiator radicals and single-unit monomeric radicals produced by chain transfer to monomer molecules, (iv) bimolecular termination of radicals in the particles, (v) bimolecular termination of radicals in the aqueous phase, and (vi) generation of radicals in the aqueous phase by decomposition of the initiator dissolved in the phase. Based on these events, they formulated a set of six differential equations describing the system in which particles containing more than six radicals per particle could be neglected. The authors introduced a new parameter $K=\rho_w/\rho_p$, where ρ_w is the rate of radical production per unit volume of water, and ρ_p is the rate of radical production inside the particles per unit volume of water. They solved a set of differential equations numerically and plotted the calculated values of $\bar{n}$ against $\alpha_p=(\rho_p \nu_p/k_{tp}N_T)$ for the range $0\leq K\leq\infty$. Here, the bimolecular termination of radicals in the water phase was assumed to be negligible ($Y=0$). An advantage of this approach is that the time evolution of the average number of radicals per particle can be evaluated. These plots were found to be quite similar to those obtained for the case of KPS, except for $K=0$. On the other hand, when $K=0$ (so the oil-soluble initiator employed is completely insoluble in water) no region of $\bar{n}=0.5$ was found regardless of the values of α_p and m (the parameter relating to the rate of radical desorption), and the polymerization proceeded according to suspension polymerization kinetics. Therefore, it was concluded that, kinetically, the similar behavior of emulsion polymerization initiated by oil-soluble initiators to that initiated by water-soluble initiators originated from the water-soluble portion of the oil-soluble initiator rather than from the desorption of the initiator radicals produced in the particles.

In order to delve deeper into the similarities and differences between the kinetic behaviors of emulsion polymerization initiated by oil-soluble initiators or water-soluble initiators, Nomura et al. [199–202] carried out extensive investigations into the kinetics and mechanisms of the unseeded and seeded emulsion polymerizations of St at 50 °C using sodium lauryl sulfate (NaLS) as the emulsifier and AIBN as the initiator, and obtained the following conclusions:

1. The latex (polymer) particles are generated from the emulsifier micelles and the number of latex particles produced is proportional to the 0.70^{th} power of the initial concentration of the emulsifier forming micelles and to the 0.30^{th} power of the concentration of initially charged AIBN. This behavior is very similar to that observed when the water-soluble initiator KPS is used.
2. The polymerization takes place both in the monomer droplets and in the latex particles produced. The polymerization inside the monomer droplets proceeds according to the kinetics of suspension polymerization until the

monomer droplets have disappeared from the reaction mixture due to complete absorption by the resultant latex particles. On the other hand, the polymerization in the latex particles proceeds according to emulsion polymerization kinetics, independently of the polymerization in the monomer droplets. The total amount of polymer produced inside the monomer droplets is only several percent of the whole polymer produced. Moreover, the molar mass of the polymer produced in the monomer droplets is the same as that produced by bulk polymerization under comparable conditions and is only about one-hundredth of that produced in the latex particles.

3. The free radicals produced from the fraction of initiator dissolved in the water phase are responsible for particle formation and growth in the emulsion polymerization of St initiated by AIBN. The free radicals produced in pairs in the polymer particles play almost no role in the polymerization inside the polymer particles because pairs of radicals produced within a volume as small as a monomer-swollen latex particle or a monomer-swollen micelle are very likely to recombine.
4. A kinetic model developed for unseeded emulsion polymerization based on the knowledge and conclusions obtained above could explain the progress of polymerization inside both the monomer droplets and the latex particles in the seeded emulsion polymerization of St initiated by AIBN at 50 °C.

Therefore, they showed both theoretically and experimentally that the kinetic behavior of the emulsion polymerization of St initiated by AIBN is basically similar to that initiated by KPS, and concluded that this similarity is mainly due to the radicals produced from the water-soluble fraction of the initiator, because the radicals produced pair-wise inside the small volume of a monomer-swollen latex particle or a monomer-swollen micelle are very likely to recombine.

Several researchers have also experimentally and theoretically investigated the reasons for this kinetic similarity [203–208]. Asua et al. [203] proposed a mathematical model that can predict the average number of radicals per particle $\bar{n}$ in seeded emulsion polymerization initiated by oil-soluble initiators. Their model includes the parameter f_w that denotes the fraction of the initiator dissolved in the aqueous phase, and the following various kinetic events: (i) generation of radicals inside the particles, (ii) desorption of primary initiator radicals from the polymer particles before reacting with a monomer molecule, (iii) termination of radicals by bimolecular reaction in the particles, (iv) desorption of single-unit monomeric radicals produced by chain transfer to monomer molecules, (v) absorption of radicals from the aqueous phase into the particles, (vi) termination of radicals in the aqueous phase, and (vii) generation of radicals in the aqueous phase by decomposition of the initiator dissolved in that phase. They calculated the average number of radicals per particle in a typical example of the seeded emulsion polymerization of St, using their model that distinguishes between desorption of primary initiator radicals and single-unit monomeric radicals. The effect of increasing the water-soluble fraction f_w of the initiator from 0 to 0.1 was calculated for various particle diameters in the range

23–231 nm. For a fixed particle size, the value of $\bar{n}$ was found to be essentially independent of the fraction f_w of the initiator present in the aqueous phase, even for f_w=0. Moreover, the plot of $\bar{n}$ versus the seed particle diameter was quite similar to that found for the emulsion polymerization initiated by KPS. The authors therefore concluded that the kinetic similarity mainly originated from desorption of the initiator radicals produced in the particles rather than from decomposition of the initiator present in the aqueous phase. Mørk et al. [208], however, pointed out that the almost identical values of $\bar{n}$ found for a completely water-insoluble initiator (f_w=0) appeared to contradict calculations performed by Mørk et al. [208] and Nomura et al. [198], and that calculations by Asua et al. [203] could not be taken as evidence that a desorption mechanism is the reason for the similarity. Alduncin et al. [204] studied the seeded emulsion polymerization and the miniemulsion polymerization of St using an oil-soluble initiator (AIBN) in an attempt to elucidate the main locus of radical formation in emulsion polymerization initiated by an oil-soluble initiator. The monomer/water weight ratio (M/W) was varied while keeping the monomer/initiator ratio constant. They found that the average number of radicals per particle ($\bar{n}$) increased as the M/W ratio increased. This was taken as evidence that the overall rate of radical entry into a particle increased when the M/W ratio increased. They claimed that this phenomenon could only be explained by assuming that the radicals responsible for emulsion polymerization initiated by oil-soluble initiators are mainly those produced from the initiator partitioned into the polymer particles, followed by desorption into the water phase. Mørk et al. [208] concluded, on the basis of their calculations, that the argument provided by Alduncin et al. [204] was not strong enough to resolve the issue of the similarities between the kinetic behaviors of emulsion polymerization with oil-soluble and water-soluble initiators.

Mørk et al. [206–208] recently published a series of theoretical works. In the first article of this series [206], the authors aimed to develop expressions that would allow easy and rapid calculation of the average number of radicals per particle in emulsion polymerizations with a constant number of reaction loci containing an oil-soluble initiator. Taking into account pairwise formation of radicals in the particles, desorption and reabsorption, water phase termination, solubility of the initiator in the water phase, and the possible formation of a single radical species, they derived the recurrence relation that determined the stationary state distribution of radicals in a particle. The calculation was based on a probabilistic analysis leading to a third-order recurrence relation solved using confluent, hypergeometric Kummer functions. The calculated results confirmed the previous finding of Nomura et al. [198] that the kinetics of emulsion polymerizations carried out with oil-soluble initiators are quite similar to those with water-soluble initiators, provided that the oil-soluble initiator is not completely insoluble in the water phase. The main intention of the second article [207] was to develop equations that make it relatively easy to assess the effects of the most common experimental variables on the stationary state average number of radicals per particle in a bidispersed seeded emulsion poly-

merization, and on the competitive growth of differently-sized seeded particles in this system. In the third article [208], the authors extended the third-order recurrence relation derived in the first article to the general case by including single radical formation in the particles; for example, by a redox reaction along with the formation of pairs of radicals by thermal decomposition. They carried out calculations for the case where single radicals are generated inside the particles by an oil-soluble initiator, with or without the simultaneous formation of pairs of radicals. The calculations showed that:

1. From a kinetic point of view, single radicals generated in the particles behaved quite similarly to radicals produced in the water phase.
2. However, at high rates of radical desorption, the effect of water phase termination on the average number of radicals per particle is much more prominent when the radicals are produced in the water phase.
3. In the system where an oil-soluble initiator generates both single radicals and pairs of radicals, the contribution of the latter to the average number of radicals per particle is almost negligible.
4. When an oil-soluble initiator distributes between phases, the single radicals that are responsible for the similar kinetic behavior observed with water-soluble and oil-soluble initiators originate from the water-soluble fraction of the initiator rather than from a desorption/reabsorption mechanism as claimed by Asua et al. [203] and Alducin et al. [204].

Consequently, the authors supported the conclusion of Nomura et al. [198, 199] that the reason for the similar kinetic behaviors observed for water-soluble and oil-soluble initiators originates from the water-soluble fraction of the initiator.

Unlike in conventional emulsion polymerization, no monomer droplets exist in a microemulsion polymerization system, and hence, oil-soluble initiators partition into the monomer-swollen micelles, the resultant polymer particles and the water phase. Therefore, in microemulsion polymerization, the polymerization only proceeds in the monomer-swollen micelles and the resultant polymer particles over the entire course of polymerization. Pairs of radicals produced in volumes as small as monomer-swollen micelles and polymer particles may terminate as soon as they are generated. If so, it is expected that the radicals responsible for the polymerization in the monomer-swollen micelles and the resultant polymer particles would usually be those generated from the fraction of the initiator dissolved in the water phase. In order to examine whether this expectation is correct, oil-in-water (O/W) microemulsion polymerizations of St were carried out using four kinds of oil-soluble azo-type initiators with widely different water-solubilities [209]. It was found that the rates of polymerization with these oil-soluble initiators were almost the same irrespective of their water-solubilities, when the polymerizations were carried out with the same rate of radical production for the whole system for all of the oil-soluble initiators used. Moreoever, the rate of polymerization with any of these oil-soluble initiators was only about 1/3 of that with KPS at the same rate of radical production. Considering that the rate of polymerization was pro-

portional to the 0.5^{th} power of the initiator concentration regardless of whether the initiator used was oil-soluble or water-soluble [210], the authors concluded that the apparent efficiencies of these oil-soluble azo-type initiators were all only 1/9 of that of KPS. This might suggest that although radicals were generated in the monomer-swollen micelles and polymer particles as well as the water phase, only 1/9 of the radicals generated were active in the microemulsion polymerization of St, while the rest were lost somewhere (possibly in the water phase) by bimolecular termination. These experimental results seem to support the desorption/reabsorption mechanism proposed by Asua et al. [203], although Candau et al. [205] also suggested that, in the case of AIBN, the radicals that initiate the polymerization are not those from the initiator localized within the monomer-swollen micelles, but from the initiator dissolved in the water phase. Therefore, the role of oil-soluble initiators in the kinetics of heterogeneous polymerizations such as emulsion and microemulsion polymerizations is still unanswered, and further studies are needed for its final elucidation. A recent review article [211] refers to the role of oil-soluble initiators in heterogeneous polymerizations including emulsion polymerization.

Conventional emulsion polymerizations are usually initiated by chemical initiators. However, there are some disadvantages in the use of chemical initiators. For example, some of the products produced by termination in the aqueous phase may undergo subsequent reactions, resulting in discoloration of the final latex, or any residual initiator present after the polymerization may act as an undesirable contaminant. To avoid these problems, alternative techniques for radical initiation that are safe and inexpensive have been explored. Ultrasound has been increasingly used to realize novel chemical reactions and enhance the reaction rate; this emerging field is called "sonochemistry". Relatively recently, several researchers have investigated the possibilities of using ultrasonic irradiation as a way to initiate free radical species in emulsion polymerizations of various monomers [212–219]. Biggs et al. [212] conducted pioneering work on the ultrasonically-initiated emulsion polymerization of St at 30 °C (±5 °C) using NaLS as the emulsifier and a 20 kHz horn sonifier as a ultrasound generator. From experiments carried out at a fixed ultrasound intensity, they concluded that: (1) radicals produced as a consequence of the cavitation process were sufficient to cause polymerization; (2) the rate of polymerization increased to a maximum at about 30% conversion before decreasing, showing no constant region; (3) the rate of polymerization increased with increasing concentration of initially charged NaLS (negligible polymerization without NaLS); (4) the diameters of final latex particles were very small (around 50 nm), and the PSt molecular weights were high ($>10^6$); (5) there was continuous formation of polymer particles, and; (6) the small particle sizes, high polymerization rates, and continuous nucleation of polymer particles were postulated to be due to the continuous formation of very small monomer droplets in the ultrasonic field, which could efficiently scavenge the radicals formed during the cavitation process. The authors concluded from these experimental results that this polymerization system had many similarities with microemulsion polymerization

but at a considerably reduced emulsifier level. They extended this study, mainly to clarify the effects of varying the input ultrasound intensity [213], and found that: (1) a marked increase in the rate of polymerization was seen as the input power was increased; (2) despite the increase in the rate of polymerization, the increasing intensity did not affect the resultant polymer particle sizes, which were in all cases 40–50 nm, and; (3) increases in both the concentration of NaLS and the reaction temperature resulted in an increased rate of polymerization at a fixed input intensity, but the particle sizes were invariant.

Cooper et al. [214] carried out the emulsion homopolymerization of BA and of VAc, and also the emulsion copolymerization of BA and VAc at 30 °C (±5 °C) using 20-kHz ultrasound as the initiator with SDS and Aerosol AT as the emulsifiers, respectively. The homopolymerization rate of VAc (10 wt%) was much lower than that of BA (10 wt%), and interestingly, lower rates of BA emulsion homopolymerization were observed at higher temperatures. The reason for such a large difference in the rate of polymerization between the BA and VAc systems was explained by the greater evaporation of the more volatile VAc monomer into the cavity, suppressing cavitation and thereby reducing the rate of radical production. The average particle sizes produced in the BA system and the copolymerization system with 50:50 wt% BA and VAc were very small; around 15–20 nm, respectively. But the average particle sizes produced in the emulsion homopolymerization of VAc were much larger, showing a size of around 300 nm. The reason for producing smaller polymer particles in both the BA homopolymer and BA-VAc copolymer systems than in the VAc homopolymer system even at low emulsifier concentrations was attributed to a high rate of particle formation due to a large number of very small monomer-emulsion droplets that were to be transformed into polymer particles.

Grieser et al. [215] investigated the kinetics and mechanisms of the emulsion polymerization of MMA and of BA at 30 °C (±5 °C) using ultrasonic irradiation (20-kHz horn sonifier) and a cationic emulsifier, dodecyltrimetylammonium chloride (DTAC). They observed the formation of stable dispersions with particle diameters in the range of 40–150 nm and with polymer molecular weights greater than 10^6 g mol^{-1}. In the case of MMA, the average particle size was found to be constant throughout the reaction time (sonication time) and independent of the initial DTAC concentration. The final particle size decreased as the initial DTAC concentration was decreased, but the rate of polymerization was approximately the same over the concentration range of DTAC examined. In the case of BA, the kinetic behavior was basically the same as that of MMA, except that the average particle size was constant (~30 nm) up to 50 min of sonication, after which a dramatic increase in size (100–140 nm) was observed when the initial TDAC concentration was comparatively low. Based on their experimental data, the authors proposed the kinetics and mechanisms of the ultrasonic (sonochemical) initiation in this polymerization process. When ultrasound is applied in a liquid medium, the cavitation event that occurs as ultrasound travels through the liquid medium, producing microbubbles in the solution. When the microbubbles rapidly collapse, this leads to high local temperatures

of the order of 4000–5000 K within the bubble and at least 1250 K in the liquid immediately surrounding the interfacial region. In an aqueous medium, such high temperatures lead to the homolysis of water, creating hydroxyl (·OH) and hydrogen (·H) radicals. The authors assumed that primary organic radicals produced from MMA and BA were unlikely to play a major role at 20 kHz even though MMA and BA are volatile and could enter cavitation bubbles to produce a variety of primary organic radicals by thermal decomposition. The hydroxyl and hydrogen radicals generated in the aqueous phase add several monomer units and then enter the miniemulsion droplets produced by ultrasonication, initiating polymerization. Therefore, the results obtained strongly support a polymerization process involving a miniemulsion polymerization system, where continuous formation of polymer particles takes place throughout the polymerization.

Chou and Stoffer [216, 217] carried out the ultrasonically-initiated free radical emulsion polymerization of MMA at ambient temperature using NaLS as the emulsifier, and published two articles on this topic. In the first article [216], the authors studied: (1) the nature and source of the free radicals for the initiation process; (2) the effects of different types of cavitations, and; (3) the dependence of the polymerization rate, the number of polymer particles generated, and the polymer molecular weight on the acoustic intensity, argon gas flow rate, surfactant concentration, and the initial monomer concentration. They found that, in the absence of argon gas flow, no polymerization took place, and that, contrary to Grieser et al. [215], the source of the free radicals for the initiation process came from the degradation of the NaLS, presumably in the aqueous phase. The molecular weight of the poly(MMA) obtained varied from $(2.5–3.5)\times10^6$ g mol^{-1}, and the monomer conversion was up to 70%. The rate of polymerization was found to be proportional to the acoustic intensity to the power of 0.98, to the argon gas flow to the power of 0.086, and to the emulsifier concentration to the power of 0.08 in the emulsifier concentration range of 0.035–0.139 M. The number of polymer particles was found to be proportional to the acoustic intensity to the power of 1.23, to the argon gas flow to the power of 0.16, and to the emulsifier concentration to the power of 0.3 in the emulsifier concentration range of 0.035–0.139 M. In the second article [217], the radical generation process was studied. Based on this experimental study, the authors tried to explain the kinetic data obtained in the previous work. In this study, radical trapping experiments were used to investigate the effects of acoustic intensity, argon gas flow rate, and NaLS concentration on the extent of free radical generation in aqueous NaSL solutions. Aqueous solutions of NaLS were ultrasonically irradiated in the presence of a radical scavenger. The NaLS molecules then decomposed by ultrasound to form free radicals in the aqueous phase. It was found that the extent of free radical generation increased as: (1) the 0.6^{th} power of the acoustic intensity, (2) the 0.44^{th} power of the argon gas flow rate, (3) the 0.35^{th} power of the emulsifier concentration in the emulsifier concentration range of 0.035–0.139 M. These experimental results were found to explain the effects of acoustic intensity, argon gas flow rate, surfactant con-

centration on the rate of polymerization and the number of polymer particles generated.

Recently, Wang et al. [218, 219] carried out the ultrasonically-initiated emulsion polymerization of MMA using a 20 kHz ultrasonic generator and NaLS as the emulsifier, respectively, in order to find a way to reach a high monomer conversion. It was found that, with increasing NaLS concentration, the monomer conversion increased significantly, but in the absence of NaLS, monomer conversion remained nearly zero. Therefore, the NaLS emulsifier played a key role and appeared to serve as an initiator. They observed that (1) an increase in the reaction temperature resulted in an increase in the monomer conversion, (2) an appropriate increase in the N_2 purging rate also increased the monomer conversion, and (3) the polymer particles prepared were nanosized, even with a small amount of emulsifier. Optimized reaction conditions were obtained using these experimental results, and so a high monomer conversion of about 67% and high molecular weight polymers of several million could be obtained in a period of about 30 min. They [219] also studied the ultrasonically-initiated emulsion polymerization of *n*-BA in order to investigate the factors that affect the induction period and the rate of polymerization, and proposed a mechanism for ultrasonically-initiated emulsion polymerization. Increasing the N_2 flow rate, temperature, NaLS concentration and power input, and decreasing the monomer concentration resulted in further decreases in the induction period and increased the rate of polymerization. Under optimized reaction conditions, the conversion of BA reached 92% in 11 min. In addition, they carried out a feasibility study on semicontinuous and continuous ultrasonically-initiated emulsion polymerization.

3.5 Effect of Additives and Impurities

Most kinetic studies on emulsion polymerization carried out in universities and industrial research laboratories have been done under extremely clean conditions. The polymerization is conducted in a high-purity nitrogen atmosphere with any remaining oxygen in the reaction system removed by degassing. High purity initiators and emulsifiers are used, and the commercially-available monomers are purified (by, say, distillation) to remove any inhibitors used during storage as well as any other reactive organic impurities that may act as radical scavengers or CTAs. In industry, however, it is usually impractical to purify the monomers, initiators, emulsifiers, water, and so on to remove reactive impurities from them. Moreover, the polymerization is usually carried out in an industrial-grade low-purity nitrogen atmosphere containing a trace of oxygen. The presence of inhibitors in the reaction mixture will affect both particle formation and growth processes. Therefore, it is very important to understand the effects of any impurities present in the starting materials when attempting the optimum design and operation of emulsion polymerization processes.

It has been recognized that the presence of oxygen during emulsion polymerization can have detrimental effects on the course of a reaction, causing inhibition periods and retarding the reaction rate. Relatively few publications have addressed the issue of the effects of oxygen in emulsion polymerization [126, 188, 220–223]. With the intention of clarifying the effect of stirring on emulsion polymerization, Nomura et al. [220] carried out St emulsion polymerization under three nitrogen atmospheres with different purities (containing a trace of oxygen) and at different stirring speeds. They observed that the faster the stirring speed, the longer the retardation period. They attributed the result to the diffusion limited transfer of oxygen from the headspace into the water phase through the liquid surface, which was controlled by stirring. Furthermore, they found that the polymerization rate following a long retardation period was often greater than that after a shorter retardation period, indicating that the final number of polymer particles produced with a long retardation period was higher than that with a shorter retardation period. The reason for this is discussed later. The same trend was also observed by other researchers [188, 222]. Cunningham et al. [222] examined the effects of oxygen on the induction period, conversion kinetics, molecular weight and particle size during the emulsion polymerization of St, by varying the initial dissolved oxygen concentration in the aqueous phase. They found that the length of the induction period did not vary linearly with the initial oxygen level, suggesting diffusion from the reactor headspace to the aqueous phase could have a significant impact on rates of particle formation and growth. Furthermore, the higher the initial dissolved oxygen level, the longer the induction period and the smaller the average diameter of polymer particles in the final latex product, which indicates that the longer the induction period, the greater the number of polymer particles produced. Their experimental results suggested that, during the induction and retardation period, the oxygen molecules in the reactor headspace were continuously transferred into the aqueous phase, and some of them are consumed by the radicals in the aqueous phase, but most of them diffuse further into both the monomer-swollen micelles and polymer particles. Therefore, the oxygen molecules that have diffused into the monomer-swollen micelles and polymer particles inhibit the growth of radicals within them, thereby reducing the volumetric growth rate per particle, μ and resulting in an increase in the number of polymer particles produced according to Eq. 29.

Arbina et al. [188] investigated the influence of oxygen on the kinetics of the chemically-initiated seeded emulsion homopolymerization of St and the seeded emulsion copolymerization of St and BA using reaction calorimetry. They discussed whether oxygen behaved kinetically as an ideal inhibitor. In the experiments, they observed that oxygen not only caused an inhibition period, but also behaved like a retarder by reducing the polymerization rate. Their explanation for this seemingly contradictory behavior was the existence of mass-transfer limitations from the reactor headspace to the latex, resulting in a gradual and continuous flow of oxygen into the aqueous phase. Their own experiments showed that this induction period decreased with increasing initiator concen-

tration. When the headspace to aqueous phase ratio was decreased, the induction period was reduced and the polymerization rate increased. The length of the retardation period caused by oxygen in the seeded emulsion polymerization is known to depend on the kind of monomer. In seeded emulsion polymerizations, the inhibition period may be followed by a retardation period during which the polymerization rate increases to a steady state value. The retardation period observed in the seeded emulsion polymerization of VAc is unusually long compared to that of St or MMA. Bruyn et al. [223] tried to quantitatively explain the reason for this unusually long retardation in terms of the initiator efficiency, f_{entry}, proposed by Maxwell et al. [11]. They argue that this unusually long retardation is due to the high radical entry efficiency of the aqueous phase oligomeric radicals, which allows latex particles to compete with dissolved oxygen for these initiating radicals. In the case of VAc, this is due to the high value of the product of the propagation rate constant and the water solubility. As oxygen is consumed, the competition increasingly favors the entry of initiating radicals into polymer particles and the rate of polymerization gradually increases. In another case, Kiparissides et al. [126] considered the different effects of the presence of oxygen on the kinetics and PSD in the emulsifier-free emulsion polymerization of VCl. Oxygen is capable of reacting with primary initiator radicals and the resulting oligomeric radicals in the aqueous phase to produce vinyl polyperoxides. Taking this into account, they developed a mathematical model into which the combined role of oxygen as an inhibitor and a radical generator, through the formation and subsequent decomposition of vinyl polyperoxides, was incorporated.

CTAs are used not only to reduce the molecular weight of the polymer produced, but also to limit the extent of the branching and crosslinking of the polymer produced in diene-polymerization. It is well known that an ideal CTA is able to reduce the molecular weight of the polymer produced in a homogeneous bulk or solution free radical polymerization, without affecting the overall rate of polymerization. For a long time it has been known that even an ideal CTA such as mercaptan could affect not only the molecular weight of the polymer produced in emulsion polymerization, but also the rate of the polymerization [224], but details about the effects of CTAs (including mercaptans) on the kinetics of heterophase radical polymerizations, like emulsion polymerizations, have only been revealed recently [225–229].

Whang et al. [225] observed that the rate of polymerization decreased in the seeded emulsion polymerization of St in the presence of carbon tetrabromide, which functions as an ideal CTA in the homogeneous bulk or solution free radical polymerization of St. They pointed out that this appeared to result from the enhanced rate of radical desorption of the free radicals from the polymer particles. Also, a substance which behaves as an ideal CTA in homogeneous polymerizations might apparently function as a retarder in heterogeneous free radical polymerization. Lichti et al. [227] advanced the discussion by Whang et al. [225] and argued that the increase in the rate of radical desorption which brought about the decrease in the rate of polymerization paralleled the increase

in the chain transfer constant for the additives: CBr_4>CCl_4>St. The efficiency of desorption of free radicals formed by chain transfer from the latex particles followed the inverse order CBr_4<CCl_4<St, and this reflected the reactivities of the low-molecular weight free radicals (formed by atom abstraction) with the monomer.

At almost the same time, Nomura et al. [226] carried out an extensive experimental study of the effect of typical CTAs such as CCl_4, CBr_4b, and four primary mercaptans (C_2, *n*-C_4, *n*-C_7 and *n*-C_{12}) on particle formation and growth processes in the unseeded emulsion polymerization of St. They found that these CTAs, which had almost no effect on the rate of bulk polymerization of St, decreased the rate of polymerization per particle μ and so increased the number of polymer particles produced (see Eq. 29). From a theoretical point of view, they suggested that these effects could be enhanced by increasing the rate of radical desorption from the polymer particles by adding a CTA with a higher value of the chain transfer constant and/or with higher water-solubility. Nomura et al. [20, 43] pointed out that the number of polymer particles produced N_T could be expressed as $N_T \propto S_0^z I_0^{1-z}$ in an emulsion polymerization system following micellar particle formation. They also showed that, by increasing the rate of radical desorption from the polymer particles in the interval of particle formation with the help of CTA, the emulsifier dependence exponent, z, would increase from about 0.6 to 1.0, thereby decreasing the initiator dependence exponent from about 0.4 to 0. This was also confirmed experimentally. Therefore, they demonstrated that the effect of CTA on particle formation and growth in the emulsion polymerization of St could be explained in terms of desorptions of chain-transferred radicals from the polymer particles.

Maxwell et al. [228] discussed the effect of CTA, such as mercaptan, on initiator efficiency and extended their quantitative model for initiator efficiency to take into account the effect of adding CTA. They assumed the following model. The effect of the CTA on the entry rate occurs by facilitating the production of aqueous-phase free radical species (CTA radicals) via transfer between species such as $\cdot M_nSO_4^-$ (where M is a monomer entity and n<z) and the CTA in the aqueous phase. The CTA radicals will be formed at a reasonable rate provided that the CTA is not too water-insoluble (as in $C_{12}H_{25}SH$) and the resultant CTA radical is able to enter the latex particles rapidly because of this relative insolubility in water. If the monomer-derived $\cdot M_nSO_4^-$ tends to suffer aqueous-phase termination rather than entry, the overall rate of entry (and hence initiator efficiency) will increase. They claimed that this mechanism could explain the accelerating (promoting) effect of intermediate molecular weight CTAs (C_{10}–C_{12}) on the emulsion polymerization of monomers such as Bu, where the z value is large and so initiator efficiency is very low in the absence of CTA, because most of the $\cdot M_nSO_4^-$ undergoes termination rather than entry into the latex particles. However, Weerts et al. [229] studied the "promoting effect" in the emulsion polymerization of Bu using SDS, potassium stearate and potassium oleate as the emulsifiers and sodium or potassium peroxodisulfate, 4,4′-azobis-(4-cyanopentanoic acid and AIBN as the initiators, and

concluded that the promoting effect appears to be related to impurities present in the emulsifier, because it was found to be completely absent in emulsifier-free polymerizations. They also demonstrated that a simple redox reaction between a sulfate radical anion and thiol could not provide a satisfactory explanation for the promoting effect. Therefore, the promoting effect of thiol in the emulsion polymerization of diene-hydrocarbons is still poorly understood.

Commercially-available monomers usually contain an inhibitor such as 4-*tert*-butylcatechol (TBC) or hydroquinone (HDQ) to prevent undesired autopolymerization before their use in polymerizations. In industry, however, distillation of the monomer to remove inhibitor is rarely carried out. Therefore, a good understanding of the effect of inhibitor on the kinetics of emulsion polymerization is important when designing and operating an industrial emulsion polymerization process. Huo et al. [230] investigated the effects of HDQ and TBC on the kinetics of the emulsion polymerization of St, where HDQ is a water-soluble inhibitor and TBC is an oil-soluble inhibitor, respectively. They found that HDQ produced an induction period proportional to the amount of HDQ present, but did not produce any significant difference in the rate of polymerization regardless of the different HDQ levels in the systems. Moreover, the final particle number, average particle diameter, molecular weights, and latex viscosities were identical to within experimental error for all four runs conducted. In contrast to HDQ, the monomer-soluble inhibitor TBC showed more complex effects. They found that the higher the level of TBC, the larger the number of polymer particles produced, and a longer induction time and an increased retardation of the initial rate of polymerization with increasing TBC level was evident, but the rate of polymerization at intermediate conversion increased for smaller TBC level runs because of the increased number of polymer particles produced. However, at higher TBC levels (200 ppm), TBC was never fully depleted before the polymerization was completed, and so in spite of the much larger number of polymer particles generated, the overall rate of polymerization never exceeded that for the purified monomer. The viscosity of the latex produced increased with the TBC level in the system, which was a direct consequence of the decrease in particle diameter. The average molecular weight of polymer formed decreased somewhat, and the polydispersity of the polymer produced increased from 1.5 to 2.0 with the TBC level, indicating that the dead polymer was predominantly formed by reactions with the impurity (TBC), which acted as a CTA as well as a retarder. These results were well predicted by the modification of an existing model for Case II emulsion polymerization which incorporated the effects of impurities. Penlidis et al. [221] also made necessary modifications to their Case I model for batch and continuous emulsion polymerization to account for the effects of reactive monomer-soluble impurities (TBC). A detailed mechanism was proposed through which TBC affected the emulsion polymerization of St [231]. TBC would oxidize into 4-*tert*-butyl-1,2-benzochinon (TBBC) during the storage of St and also during the sulfate-initiated emulsion polymerization of St. TBBC is soluble in St and is therefore readily absorbed by the polymer particles produced. TBBC is known to act

as a radical accepter, so radical transfer from a growing radical to TBBC may occur in the polymer particle. Because the TBBC radicals are relatively stable due to conjugation, probably most of the TBBC can be converted into TBBC radicals. Because of this radical transfer to TBBC, the chain growth in the particles stagnates and so the rate of polymerization per particle (μ) decreases, thereby increasing the number of polymer particles produced. The TBBC radicals, which desorb from the particles because of their charge, can react in different ways. The desorbed TBBC radicals react with persulfate radicals in the aqueous phase, converting the TBBC radicals back to TBBC and consuming persulfate radicals (the inhibition mechanism). These TBBC molecules may be taken up by the particles once more and transformed into TBBC radicals again, and so on. Of course, the desorbed TBBC radicals can also contribute to the emulsion polymerization in the usual way by reacting with monomer as initiating radicals.

Barton et al. [232] conducted the emulsion polymerization of the sparingly water-soluble monomer St and of the fairly water-soluble monomer MMA in the presence and absence of the water-soluble inhibitor, potassium nitrosodisulfonate (Fremy's salt). By using oil-soluble dibenzoyl peroxide (DBP) and water-soluble ammonium peroxodisulfate (APS) as the free-radical initiators, they examined the effect of the location of the initiator on the kinetics of these emulsion polymerizations with SDS as the emulsifier. Figure 7 shows an example of the experimental results.

When the emulsion polymerization of St was carried out in the presence of Fremy's salt and ammonium peroxodisulfate in the aqueous phase, a distinct

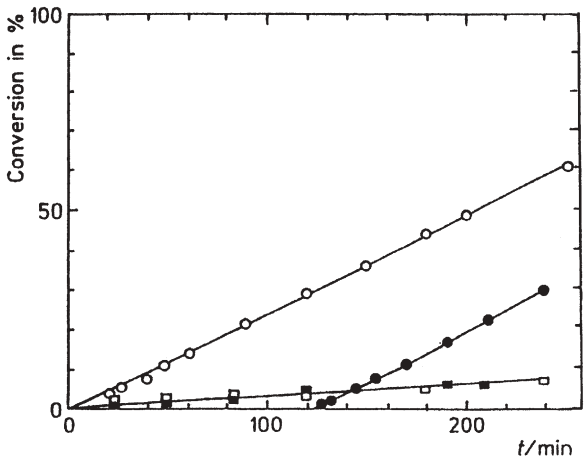

Fig. 7 A typical example of the effect of water-soluble (APS) and oil-soluble (DBP) initiators on the progress of the emulsion polymerization of St in the presence of a water-soluble radical inhibitor (Fremy's salt, FS); for [APS]=5×10^{-4} mol/dm^3, empty circles indicate [FS]=0, filled circles indicate [FS]=10^{-4} mol/dm^3; for [DBP]=5×10^{-4} mol/dm^3, empty squares indicate [FS]=0, filled squares indicate [FS]=10^{-4} mol/dm^3

inhibition period was observed, but after the end of the inhibition period the conversion versus time curve was almost the same as that encountered in the absence of Fremy's salt. On the other hand, when the emulsion polymerization of St was initiated by the oil soluble initiator DBP, the monomer conversion versus time curve observed in the presence of Fremy's salt was identical to that seen in the absence of Fremy's salt. In the case of MMA, the results were basically the same as those with St. Also, the rate of emulsion polymerization initiated by DBP was almost the same as the rate of bulk polymerization initiated by DBP. This indicated that in the emulsion polymerization initiated by DBP, the polymerization did not proceed in the monomer-swollen micelles and the resultant polymer particles according to emulsion polymerization kinetics, but in the monomer droplets according to bulk kinetics. This implies that neither member of a radical-pair generated in a monomer-swollen micelle initiates polymerization, either because geminate termination took place before either of the pair of radicals desorbs from the micelle into the aqueous phase, or because both of the radicals desorb as soon as they are generated and are scavenged in the aqueous phase. This finding is closely related to the claim [200] that in the emulsion polymerization of St initiated by oil-soluble initiators, the free radicals generated from the fraction of the initiator dissolved in the aqueous phase mainly participate in particle formation from the monomer-swollen micelles. Barton et al. claimed that, although many studies had been performed to clarify the effect of a variety of water-soluble and oil-soluble inhibitors on emulsion polymerization, no unequivocal results had been obtained for their effects on its kinetics, and specifically for their effect on particle formation, and that this problem is still open for discussion.

Ignoring their side effects, chain transfer agents (CTAs) were originally used in emulsion polymerization as additives to regulate the molecular weight distribution of the resultant polymers and to limit the extent of branching and crosslinking of the polymer produced in diene-polymerization. Recently, several investigations based on this point of view have been published [57, 125, 233–238]. Barudio et al. [57] studied the effect of CTAs (*tert*-butanethiol and *n*-dodecanethiol) on the microstructures of copolymers (the molecular weight distribution (MWD) and glass transition temperature (T_g)) and the diameters of polymer particles produced in the batch and semibatch emulsion copolymerizations of St and BA. The experimental results were interpreted in terms of enhanced radical desorption and diffusion limitations of CTA between the monomer droplet and particle phases. They proposed a kinetic model that was able to successfully compute the kinetic constants, the number of radicals per particle, the GPC/SEC diagram and the DSC thermogram related to the MWD and T_g, respectively. Salazar et al. [234] developed a mathematical model that included the effect of CTA (*tert*-nonyl mercaptan) on particle formation and the average molecular weights in the batch and monomer-starved emulsion polymerizations of St. Asua and co-workers [125, 233, 235–237] published several reports on the effects of CTAs on the kinetics and the microstructures of the resultant polymers in seeded and unseeded emulsion homo- and co-

polymerizations. Echevarria et al. [233] developed a closed-loop control strategy based on on-line gas chromatographic measurements of both monomer and CTA concentrations to obtain emulsion polymers of well-defined MWD. The control strategy was experimentally assessed, producing widely different MWDs in the emulsion polymerization of St using carbon tetrachloride (CCl_4) as CTA. Mendoza et al. [125] studied the effect of a CTA (*n*-dodecyl mercaptan) on the MWD in the emulsion polymerization of St. It was found that the CTA had no effect on the rate of polymerization but substantially affected the MWD of the resultant polymers, and that the efficiency of the CTA in reducing the MWD was lowered by mass-transfer limitations. The rate-controlling step for CTA mass-transfer was the diffusion of the CTA from the surface of monomer droplets to the aqueous phase, as already pointed out by Nomura et al. [239]. Mendoza et al. examined the process variables affecting CTA mass-transfer and developed a mathematical model that could predict monomer conversion, particle diameter, number of polymer particles, and number-average and weight-average molecular weights. Plessis et al. [237] investigated the effect of a CTA (dodecane-1-thiol) on the kinetics, gel fraction, level of branches and sol molecular weight distribution in the seeded semibatch emulsion polymerization of *n*-BA. They found that the gel fraction was strongly affected by the CTA concentration, and that the sol weight-average molecular weight decreased with increasing CTA concentration, whereas no effect on the kinetics and the level of branches was observed. Their proposed mathematical model was able to explain the effect of the process variables fairly well. Sayer et al. [235, 236] published two papers. One [236] discussed the effect of a CTA (dodecanethiol) on the kinetics and MWD of the semicontinuous emulsion copolymerization of MMA and BA. It was found that the CTA had only a slight effect on the reaction rate, but it significantly affected the secondary particle formation. Moreover, the effects of the CTA concentration on the gel formation and the mass-transfer limitations of the CTA were discussed. The other [235] dealt with the effects of different strategies for copolymer composition control on the MWD and gel fraction in the starved and semistarved seeded emulsion copolymerization of MMA and BA in the presence of dodecanethiol (CTA). It was shown that simultaneous control of the copolymer composition and the MWD was feasible. When the monomers were fed following the optimal semistarved strategy, the MWD was controlled by employing dodecanethiol as the CTA. Gugliotta et al. [238] studied the control of polymer molecular weight using *n*-nonyl mercaptan (*n*NM) as the CTA in the emulsion polymerization of St, with the aim of producing PSt latex particles of low molecular weight polydispersity at high conversion and in short reaction times. They claimed it was preferable to use *n*NM instead of other CTAs like *tert*-dodecyl mercaptan or CCl_4.

Okaya et al. [240] investigated the effect of additives such as alcohol (isopropyl alcohol) on the initial stage of the emulsion polymerization of MMA (1 wt%) initiated by APS in the presence of PVA (1%). They found that 90% of MMA and 60% PVA were grafted and that stable polymer particles with an

average diameter of 80 nm were produced. However, the addition of alcohols such as isopropyl alcohol to the system decreased the grafting to a great extent, resulting in an increase in particle size. This was attributed to decreased hydrogen abstraction from PVA by sulfate radicals, due to the competing hydrogen abstraction from the low molecular weight alcohol.

3.6 Effects of Other Important Factors

Batch, semi-batch and continuous emulsion polymerizations are usually carried out in stirred tank reactors, where agitation by a stirrer is necessary. The type of stirrer chosen and its stirring speed can often affect the rate of polymerization, the number of polymer particles and their size distribution (PSD), and the molecular weight of the polymer produced. However, the effect of stirring on emulsion polymerization has never been the main research parameter in research programs [241]. This is probably due to the conflicting results obtained so far by various researchers.

Shunmukham et al. [242] studied the effect of stirring on the emulsion polymerization of St, and concluded that violent agitation decreased the rate of polymerization, as shown in Fig. 8.

Schoot et al. [243], on the other hand, criticized Shunmukham's conclusion, stating that this strange effect of agitation observed by Shunmukham might have been due to the absorption of contaminant oxygen into the reaction mix-

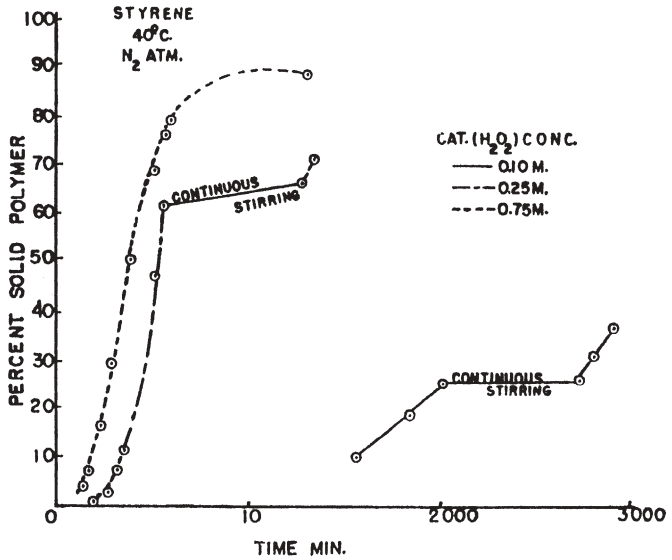

Fig. 8 A typical example of the effect of stirring on the progress of the emulsion polymerization of St in the presence of a typical inhibitor oxygen (40 °C, initiator: H_2O_2)

ture from nitrogen atmosphere in which the polymerization was carried out. Evans et al. [244] carried out the emulsion polymerization of VDC at 36±1 °C using NaLS as the emulsifier and APS as the initiator, and found that: (1) the first stage polymerization rate decreased with increasing stirring speed; (2) the second stage polymerization rate increased with increasing stirring speed, and; (3) the third stage polymerization rate was independent of stirring speed. To explain their results, they suggested two factors through which stirring affected the polymerization rate. The first factor was the reduced levels of effective emulsifier available for the formation of polymer particles, caused by the adsorption of emulsifier molecules onto monomer droplets finely dispersed by the stirring (in the first stage). The other factor was the effect of monomer-transport from the monomer droplets to the polymer particles where the polymerization proceeded (in the second stage) upon the rate. Omi et al. [245] came to the contrary conclusion that when the monomer used was St, stirring did not influence emulsion polymerization as long as initial emulsification conditions were not changed. They considered that stirring affected the polymerization only through the former of the two factors suggested by Evans et al. [244]. Later, Nomura et al. [75] carried out a kinetic study of the batch emulsion polymerization of VDC at 50 °C with KPS as the initiator and NaLS as the emulsifier, aiming to derive a quantitative explanation for the effect of stirring observed by Evans et al. [244]. Unfortunately, however, the polymerization proceeded very smoothly and the abnormal kinetic behavior caused by a change in the stirring speed was not observed. Therefore, they concluded that the effect of stirring observed by Evans et al. [244] in the VDC emulsion polymerization must be a very special case. Therefore, the reasons for such abnormal kinetic behavior remain a mystery.

These results illustrate that investigations into the effects of stirring on emulsion polymerization, have produced inconsistent results and conclusions. Further research was therefore needed to elucidate the effect of stirring in more detail. Nomura et al. [220] carried out an extensive investigation into the effect of stirring on the emulsion polymerization of St initiated by KPS at 50 °C with NaLS as the emulsifier, with the intention of explaining the effects of stirring quantitatively by showing how agitation affects emulsion polymerization, what steps of the polymerization are affected by stirring, and whether a suitable range of agitation exists in emulsion polymerization. The reactor used was a cylindrical glass vessel with a dished bottom, fitted with four baffle plates located at 90° intervals, and a four-bladed paddle type impeller. They concluded that the effect of stirring on emulsion polymerization appears through the following four factors:

1. When the polymerization is carried out in the presence of an imperfectly purified nitrogen atmosphere, the retardation period is prolonged with agitation due to an increase in the absorption rate of oxygen from the nitrogen atmosphere into the reaction mixture through the gas-liquid interface. It has often been observed that the polymerization rate after a longer

retardation period is higher than that after a shorter retardation period. The reason for this can be explained according to the S-E theory as follows. If the polymerization is retarded by oxygen during particle formation, the volumetric growth rate per particle (μ) decreases, and so the number of polymer particles produced (N_T) would increase according to Eq. 29. When the contaminant oxygen molecules in the nitrogen atmosphere are almost completely consumed and so the supply of them into the reaction mixture is not sufficient to restrain the polymerization appreciably, the polymerization rate increases in proportion to the increase in N_T.

2. In a pure nitrogen atmosphere, there is an optimum range of stirring speeds where emulsion polymerization is not affected by agitation. If the stirring speed is higher than the above-mentioned optimum range, the number of polymer particles decreases by coagulation during the course of polymerization, and so the polymerization rate also decreases.
3. At lower stirring speeds, on the other hand, stirring controls the rate of monomer transport from the monomer droplets to the polymer particles, thereby controlling the rate of polymerization. The rate-determining step is usually the monomer-transport step from the monomer droplets to the aqueous phase, because the monomer-transport step from the aqueous phase to the polymer particles is much faster than the former step due to the much greater total surface area of the polymer particles compared to that of the monomer droplets.
4. At low emulsifier concentrations near the CMC, an increase in the degree of agitation results in a reduction of the emulsifier used for the formation of polymer particles (like micelles). This is because the monomer droplets become smaller as the degree of agitation is increased, and so the amount of emulsifier adsorbed onto the surfaces of the monomer droplets increases in proportion to the increased surface area of the monomer droplets. This brings about a decrease in the number of polymer particles produced, and so a decrease in the rate of polymerization.

On the other hand, Weert et al. [246] investigated the effects of stirring on the kinetics of the emulsion polymerization of Bu at 60 °C using NaLS as the emulsifier. They carried out the polymerizations in a 2.3-liter reactor fitted with four baffle plates located at 90° intervals and a twelve-flat-bladed turbine impeller. In all of the experiments, the system was pre-emulsified by stirring for a few minutes at 400 rpm, before adjusting the stirring speed n to the desired level. The number of polymer particles produced, N_T, was found to remain constant within experimental error beyond a sufficiently high value of n, while a discontinuous increase in N_T became apparent towards lower values of n. The change in N_T was significant, especially at low n. They ascribed the reason for this change to the fact that the level of emulsifier available for particle formation and stabilization was influenced by the degree of agitation, as already pointed out by Nomura et al. [220]. They discussed the effect of stirring in connection with the flow conditions in the reactor, which are closely related to the stirring speed, and

finally arrived at the conclusions that the stirring speed influenced this polymerization system by reducing the effective emulsifier concentration available for particle formation and stabilization at higher n, and by limiting the diffusion of monomer to the polymer particles at low n. Arai et al. [247] studied the effect of agitation on the kinetics of the soapless emulsion polymerization of MMA in water at 65 °C. As expected, the stirring influenced the monomer conversion versus time history, the molecular weight of the polymer produced, and the number of polymer particles produced versus time. They found that agitation was an important factor that affected the rate of monomer-transport from the monomer droplets to the water phase. The authors proposed a quantitative kinetic model that could predict the effect of monomer transport on the rate of polymerization. Kostov et al. [158] also studied the effects of polymerization conditions, including stirring, on the emulsion copolymerization of tetrafluoroethlene (TFE) and propylene (P) with ammonium perfluorooctanoate, initiated by a redox initiator system containing *tert*-butylperbenzoate. They found that both the rate of copolymerization and the molecular weight of the copolymer produced increased as the stirring speed increased up to 450 rpm, but then became independent of the speed above 450 rpm. The explanation for this was that the stirring affected the rate of mass-transfer of TFE and P from the gaseous to aqueous phases, which was the rate-controlling step for speeds less than 450 rpm. Kim et al. [248] also reported the importance of agitation in the semi-batch emulsion polymerization of TFE carried out using a chemical initiator (APS) and a fluorinated surfactant (FC-143). The rate of polymerization was found to increase linearly with the stirring speed. Based on the experimental findings, they concluded that the diffusion or dissolution of TFE into the aqueous phase was the rate-determining step through which agitation affected the polymerization. Özdeğer et al. [249] investigated the effect of stirring speed and impeller type (axial and radial flow impellers) on the kinetics of the emulsion copolymerization of St and *n*-BA using Triton X-405 (octylphenoxy polyethoxy etanol) as the emulsifier. At low solids content (30%), the impeller type and speed did not have any significant effect on both the final number of polymer particles and the overall rate of polymerization. The PSDs were unimodal in all cases. For high solids content (50%), the rate of polymerization carried out with the axial flow impeller was slower, indicating that fewer polymer particles were produced. Bimodal PSDs were obtained for both cases. These differences were attributed to the partitioning of the emulsifier. The axial flow impeller created more shear than the radial flow impeller. This resulted in more monomer droplets being formed, leading to more of the emulsifier being associated with them. This also resulted in fewer emulsifier micelles being available for particle formation, thereby leading to the lower number of polymer particles produced.

In industrial emulsion polymerizations, CTAs like mercaptan are often used to regulate the molecular weight of the polymer produced. In some cases, other ingredients that directly participate in the polymerization reaction are used to modify the properties of the polymer latex produced. In these cases, these

reacting species must be transported from one phase, for example, the monomer droplets, via the aqueous phase, to the monomer-swollen polymer particles where the reaction takes place. Therefore, when designing a latex product to have particular properties, it is important to quantitatively elucidate the diffusional behavior of these reacting species when they move between the phases in an emulsion polymerization system. However, only a few researchers [125, 234, 239, 250–255] have presented quantitative discussions on the mass-transfer problem involved in emulsion polymerization. Brooks [250] discussed the monomer diffusion rate in an emulsion polymerization system. The author calculated the maximum diffusion rate from monomer droplets to a polymer particle via the water phase by using a simple diffusion equation and showed that this rate was usually far greater than the rate of polymerization per particle. He also suggested that an adsorbed emulsifier layer on the surface of the polymer particles would not impede monomer transfer to the particles. Finally, he concluded that in most systems the diffusional processes that occurred in the water phase would not affect the course of the polymerization. However, Nomura et al. [220] pointed out a possibility that the monomer-transport step from the monomer droplets to the water phase could control the polymerization rate when the intensity of agitation was comparatively low.

Nomura et al. [239] discussed the mass-transfer problem in more detail for the seeded emulsion polymerization of St initiated by KPS at 50 °C using NaLS as the emulsifier and CTAs as the diffusing species. They carried out the seeded emulsion polymerization of St using five normal aliphatic mercaptans with different molecular weights (*n*-C_7, *n*-C_8, *n*-C_9, *n*-C_{10}, and *n*-C_{12}) under the conditions of 400 rpm (stirring speed), N_T=1.4×10^{14} particles/cm^3-water (the number of seed polymer particles), d_{po}=48 nm (the average diameter of seed particles), and T_{mo}=8.44×10^{-6} mol/cm^3-water (the concentration of initially charged mercaptan per unit volume of water), and measured the consumption rate of each mercaptan. They found that the consumption rate decreased drastically with the molecular weight of mercaptan, although the consumption rate of *n*-C_8 was not so different from that of *n*-C_7. They analyzed these experimental data using a proposed diffusion model derived on the basis of the so-called two-films theory, and concluded that the concentration of the CTA in the polymer particles during the polymerization dropped to a value much lower than the one that would be attained if thermodynamic equilibrium for the CTA were reached between the monomer droplets and the polymer particles. This was due mainly to the CTA molecules' resistance to transfer across the diffusion film at the interface between the monomer droplet and water phases. The authors suggested that the proposed model can also be used to predict the rate of mass-transfer of any sparingly water-soluble reacting species from monomer droplets to the polymer particles where this species participate directly in the polymerization (this may include the monomer itself).

It is well known that emulsion polymerizations of highly water-insoluble monomers such as octadecyl methacrylate (OM), dodecyl methacrylate (DM), and stearyl acrylate (SA) are generally not feasible using traditional surfactant

systems. This is because monomer transport from the monomer droplets to the water phase is diffusion limited [239]. However, almost simultaneously, Rimmer et al. [256, 257], Leyer et al. [258] and Lau et al. [259] reported that these highly water-insoluble monomers could be emulsion polymerized in the presence of β-cyclodextrin (β-CD). These studies uncovered a very interesting phenomenon. Rimmer et al. [256, 257] successfully conducted the emulsion polymerization of OM and DM at 70 °C using KPS as the initiator and Dowfax 2A1 as the emulsifier. They claimed that the reason for this successful polymerization was that the use of β-CD appeared to aid monomer transport from the monomer droplets to the polymer particles across the aqueous phase by increasing the apparent water-solubility of these monomers, because the CDs apparently solubilize the hydrophobic compounds in aqueous media. On the other hand, Leyrer et al. [258] reported that they also succeeded in emulsion-polymerizing SA in the presence of methyl-β-CD, and claimed that in this case the CD served as a phase transfer agent, because the ability of the CD to form a water-soluble complex with hydrophobic molecules made it easier for the SA molecules to leave the monomer droplets and to be released from the complex after arriving at the surfaces of the growing polymer particles. The authors reported that only 5 wt% of CD was necessary to polymerize almost 100% of SA.

Recently, Soares and Hamielec [252] presented a review article on the study of transport phenomena in emulsion polymerization and introduced a case study on how to increase the amount of ethylene (E) content in the copolymer produced by the emulsion copolymerization of E and VAc under the conditions of a mass-transfer-controlled polymerization rate. Zubitur et al. [255] studied the effect of agitation on the batch and semicontinuous emulsion polymerizations of St in a reactor equipped with a four-paddle type stirrer and dodecyl mercaptan as the CTA. Here, the CTA mass-transfer from the monomer droplets to the aqueous phase was the rate-controlling step. They showed that the molecular weights of polymers decreased as the stirring speed was increased because of the improvement in the CTA mass transfer from the monomer droplets to the aqueous phase due to the improved emulsification of the monomer droplets. For semicontinuous polymerization, the instantaneous conversion increased as the stirring speed was increased for speeds less than 150 rpm because the system was monomer diffusion controlled, whereas at stirring speeds higher than 150 rpm, the agitation was strong enough for the polymerization rate to be kinetically controlled. They [251] further studied the effect of agitation on the monomer and CTA transport step from the monomer droplets to the polymer particles in the semicontinuous emulsion polymerization of St and BA with KPS as the initiator and NaLS as the emulsifier, respectively. Polymerizations were carried out in a 2 dm^3 glass reactor fitted with a stainless-steel anchor-type stirrer. It was found that when neat monomer addition was used, a mild degree of agitation (0.1 kW/m^3) was needed to overcome monomer mass transfer limitations. However, a moderate degree of agitation (0.3 kW/m^3) was not enough to avoid mass transfer limitations when dodecyl mercaptan (CTA) was present. Preemulsification of the feed was used to minimize the mass transfer

limitations of both the monomer and the CTA, even for a gentle degree of agitation (0.01 kW/m^3). The molecular weights of the polymers produced depended on the presence of the CTA. In the presence of the CTA, the molecular weights decreased with the stirring speed, whereas they increased in the absence of the CTA.

Salazar et al. [234] investigated how the molecular weight could be controlled in a starved emulsion polymerization of St using *tert*-dodecyl mercaptan and *tert*-nonyl mercaptan (more water-soluble) as the CTAs. The authors showed that in a starved polymerization with *tert*-dodecyl mercaptan, a mass-transfer resistance to the mercaptan was required to fit the observed PSt molecular weights to the model predictions, but this extra mass-transfer resistance could be neglected in the case of the more water-soluble *tert*-nonyl mercaptan. Cunningham et al. [253, 254] investigated the seeded emulsion polymerization of St in order to study the effects of *n*-dodecly mercaptan on the polymer molecular weight distribution. In the emulsion polymerization of St with *n*-dodecly mercaptan as the CTA, the transport of the CTA from the monomer droplets to the polymer particles is diffusion limited, meaning that it was difficult to calculate molecular weights, except perhaps by using empirical approaches. They developed a methodology that used the mass transfer model developed by Nomura et al. [239], which allowed the CTA concentration within the polymer particles to be determined, regardless of whether or not the CTA was at its equilibrium value, and validated the essential correctness of the approach by comparing experimental molecular weight distributions with the model's predictions. The authors further suggested that the methodology used might be amenable to online applications. Mendoza et al. [125] carried out a study of the kinetics of St emulsion polymerization using *n*-dodecly mercaptan as the CTA. In this study, it was found that the CTA had no effect on the polymerization rate, but had a substantial effect on the molecular weight distribution (MWD). The efficiency of the CTA in reducing the MWD was lowered by the mass transfer limitations. The process variables affecting the CTA mass-transfer were also investigated. For example, the average molecular weight of the polymers produced was found to decrease with increasing stirring speed. The authors developed a mathematical model to predict monomer conversion, the number of polymer particles, and the number-average molecular weights, and then validated the proposed model by fitting it to the experimental data.

During an emulsion polymerization, one often encounters the formation of coagulum, which is sometimes fatal for products such as paints. Moreover, it may prevent the scale-up of commercially-acceptable latex. Therefore, the formation of coagulum during an emulsion polymerization is an important industrial problem and may be closely related to agitation. Although some researchers [260–262] postulated that coagulum may form during emulsion polymerization due to tangential or shear stresses, which originate in the reaction mixture due to agitation, the literature has very little information on any quantitative experimental data in this field. Vanderhoff [260] discussed this problem and proposed two mechanisms for the formation of coagulum in

the emulsion polymerization process: (i) a failure of the stability of the latex, giving rise to flocculation and growth of the aggregates to macroscopic size (lumps), and (ii) a different mechanism of polymerization, for example polymerization in large monomer droplets or a separate monomer layer in the vapor space above the latex and on the reactor surfaces. Lowry et al. [261] studied the phenomenon of shear-induced coagulation in emulsion polymerization carried out in a stirred tank reactor. Here, the authors correlated the coagulum formation for different emulsion polymerizations to various agitation parameters. For a low Reynolds number, it was shown that the stirring speed is important, whereas, for a high Reynolds number, power consumption is the important parameter. Matejicek et al. [262] studied the influence of agitation on the creation of coagulum during the semicontinuous emulsion terpolymerization of St-BA-AA carried out in 25 dm^3 and 5 m^3 reactors, respectively, and gave the relationship between the amount of coagulum formed and the intensity of agitation. The authors found that the amount of coagulum formed (Y%) was correlated to the specific impeller power input ε_i introduced by agitation, showing that the dependence of the coagulum content in the dispersion on impeller speed passes through a minimum.

4
Kinetic Aspects in Polymer Structure Development

4.1
Molecular Weight Distribution (MWD)

4.1.1
Monte Carlo (MC) Simulation Method

Polymerization rate represents the instantaneous status of reaction locus, but the whole history of polymerization is engraved within the molecular weight distribution (MWD). Recently, a new simulation tool that uses the Monte Carlo (MC) method to estimate the whole reaction history, for both linear [263–265] and nonlinear polymerization [266–273], has been proposed. So far, this technique has been applied to investigate the kinetic behavior after the nucleation period, where the overall picture of the kinetics is well understood. However, the versatility of the MC method could be used to solve the complex problems of nucleation kinetics.

The MC method is a powerful technique for investigating complicated phenomena that are difficult to solve by the conventional differential equation approach. In the MC approach, all one needs are the individual probabilities of various kinetic events. It is easy to understand the advantages of applying the MC method to emulsion polymerization if we note that it is possible to simulate the formation processes of all polymer molecules in each polymer particle directly because the volume of the reaction locus is very small. One

unique characteristic of emulsion polymerization is that high molecular weight polymers are produced without decreasing the polymerization rate, and this is due to the compartmentalization of polymerization reactions inside the polymer particles, resulting in the isolation of macroradicals. Usually, the loci of polymerization is made up of 10^{16} to 10^{18} polymer particles per liter. As a consequence, the number of monomeric units in each reaction locus is limited to about 10^5 to 10^8. For example, suppose the diameter of a polymer particle at 100% conversion is 0.1 μm, the density of the polymer is 1 g/cm^3, and the molecular weight of a monomeric unit is 100. In this case, the total number of monomeric units in this polymer particle is 3×10^6. If the number average chain length is 10^4, which is not unusually large in emulsion polymers, each polymer particle consists of only 300 polymer molecules at 100% conversion. For such a small number of polymer molecules, one can readily simulate the formation processes of all polymer molecules using an MC method in a straightforward manner.

In this section we discuss unique MWDs formed via linear emulsion polymerization, while the kinetics of branched and crosslinked polymer formation are considered in Sect. 4.2.

Before the MC simulation method was proposed, theoretical analyses of the MWDs from linear emulsion polymerizations had been conducted on the basis of kinetic population balance equations [274–277] and Markovian statistics [278–280]. These approaches have clarified that the MWD of polymer molecules formed in emulsion polymerization is fundamentally different to that from corresponding bulk polymerization. However, due to the complex heterogeneous nature of the polymerization system, in which entry and desorption of oligomeric radicals are involved, applying these methods to real systems is not straightforward, and analytical solutions are limited to very special cases. Often, the effect of radical desorption on the MWD is taken into account using the first-order chain stoppage reaction [276–280], which does not reflect the real kinetics. Although some approximate methods have been proposed [277, 281], it appears to be a formidable task to correctly account for the chain-length dependence of radical desorption in the conventional approaches.

In MC simulation, any kinetic event can be accounted for, as long as the probability of each kinetic event is represented explicitly. Chain length dependent kinetics can be accounted for in a straightforward manner if the functional form is provided. In conventional MC simulations of molecular build-up processes, the monomeric units are added to each growing polymer molecule one-by-one; therefore, a multitude of random numbers and calculations are required to simulate the formation of each polymer molecule. To get around this problem, a new concept, the *competition technique*, was proposed in order to drastically reduce the amount of calculation required for the simulation [263, 264].

Figure 9 illustrates a case where two polymer radicals exist in a polymer particle.

In this technique, the *imaginary* time (or equivalently, the imaginary chain length, given by $P=k_p[M]_p t$) for a certain event to occur is calculated by using the appropriate probability distribution for each type of event. If the given process

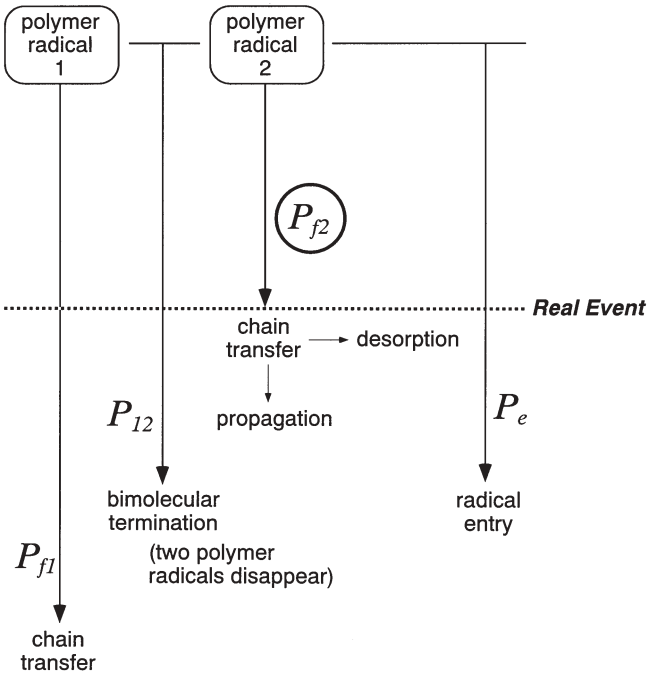

Fig. 9 Schematic drawing illustrating the simulation method based on the competition technique

is considered random and independent of chain-length, one can simply estimate the time for each event to occur by generating one random number that follows the most probable distribution [263, 264]. After calculating the imaginary chain lengths, a kind of event competition is considered, and the shortest "imaginary chain length" is chosen as the "real event". In the figure, P_{f2} is chosen as a real event. If this chain length is 1000, one can add 1000 monomeric units to both polymer radicals by using only four random numbers, not 2000 random numbers as in the conventional type of MC simulations. It is often claimed that MC methods are time-consuming, however, by using a well-designed method, the calculation time can be reduced significantly. In addition, virtually any type of information can be obtained from a set of MC simulations, and significant insights into the complex reaction system can be obtained in a straightforward manner. The MC method is useful for investigating emulsion polymerization kinetics that involve various types of simultaneous kinetic events.

4.1.2 Instantaneous Molecular Weight Distribution

In this part, the instantaneous MWD formed over a very small time interval is considered. This is equivalent to considering the distribution of polymer

chains formed in a certain fixed environment. Note that, because the polymer/monomer ratio is kept approximately constant during Interval II, the instantaneous MWD may be a reasonable approximation for the linear polymers formed during Interval II. This is not the case, however, for nonlinear polymer formation, as discussed later.

Assuming that the polymer particles have a uniform size, a single statistical polymer particle that is representative of the whole population of particles can be considered. This polymer particle is a kind of imaginary micro-reactor that does not modify either the volume or the polymer/monomer ratio, even after polymer chains are produced, so the reaction environment is kept constant except that the number and chain length distribution of the macroradicals are changed stochastically. By producing a large number of polymer molecules consecutively with this imaginary polymer particle, the instantaneous MWD can be determined.

After the nucleation period, three types of kinetic processes determine the kinetics of emulsion polymerization: radical entry, radical desorption, and polymer chain formation in the polymer particles. The kinetics of emulsion polymerization are fully described by the following five dimensionless parameters:

1. Radical entry

$$\varepsilon = \frac{\rho_e}{k_p[M]_p N_T} = \frac{1}{k_p[M]_p \bar{t}_e} \tag{73}$$

where ρ_e is the rate of radical entry into polymer particles, including the reentry of desorped radicals, N_T is the number of polymer particles, and $\bar{t}_e$ is the average time interval between radical entry.

Assuming a random entry of radicals to all polymer particles, the imaginary chain length P_e shown in Fig. 9 follows the most probable distribution, and can be determined by using a random number between 0 and 1, y, as follows [273]:

$$P_e = (1/\varepsilon)\ \ln(1/y) \tag{74}$$

2. Chain transfer

$$C_f = C_m + C_{fCTA}\frac{[CTA]_p}{[M]_p} \tag{75}$$

where C_m is the monomer transfer constant, and C_{fCTA} is the constant of transfer to chain transfer agents.

In the same way as in Eq. 74, the imaginary chain lengths P_{f1} and P_{f2} shown in Fig. 9 can be determined by using a random number between 0 and 1, y, as follows:

$$P_f = (1/C_f)\ \ln(1/y) \tag{76}$$

3. Bimolecular termination

$$\xi = \frac{2k_{tp}}{k_p[M]_p \nu_p N_A} \tag{77}$$

where k_{tp} is the bimolecular termination rate constant, in which the termination rate is represented by $R_t=2k_{tp}[R^*]^2$, not $R_t=k_{tp}[R^*]^2$ used in [263–273]. N_A is Avogadro's number, and ν_p is the volume of a swollen polymer particle. Note that the bimolecular termination rate depends on the particle size in emulsion polymerization, and is larger for smaller polymer particles.

Assuming that the bimolecular terminations are independent of chain-length, the imaginary chain length P_{12} shown in Fig. 9 can be determined by:

$$P_{12} = (1/\xi)\ln(1/y) \tag{78}$$

Note that Eq. 78 must be considered for all possible radical pairs.

4. Radical desorption

$$\delta = \frac{K_0}{k_p[M]_p} \tag{79}$$

where K_0 is the desorption rate coefficient for an oligomeric radical. Any chain-length-dependent radical desorption can be accounted for using the MC method, in principle. However, it is often reasonable to assume that only monomeric radicals can exit. For such cases, the average desorption rate coefficient for all radicals in polymer particles, k_f, which appears in the Smith-Ewart equation [4] can be approximated by [43, 44, 122] $k_f \cong K_0 C_f$. In this article, the simulated results for such simple cases are shown.

If a chain transfer reaction is the actual event, as shown in Fig. 9, a monomeric or a CTA radical is formed. Neglecting the difference between monomeric and CTA radicals, the probability of radical exit when the chain transfer reaction occurs is given by:

$$P_{des} = \frac{\delta}{1 + C_f + (n-1)\xi + \delta} \tag{80}$$

where n is the number of radicals in the polymer particle.

5. Type of bimolecular termination

$$\varphi_c = \frac{k_{tp,c}}{k_{tp,c} + k_{tp,d}} \tag{81}$$

where $k_{tp,c}$ and $k_{tp,d}$ are the bimolecular termination rate constants by combination and by disproportionation, respectively.

If bimolecular termination is the actual event, the probability that the termination is by combination is equal to φ_c.

The MC simulation was performed for 1×10^4 polymer molecules in each condition [264]. It was shown that both the average number of radicals $\bar{n}$ and the distribution of the number of radicals per polymer particle agree completely with the analytical solution derived by O'Toole [119], and it was confirmed that the present MC simulation can be conducted without significant statistical errors [264].

To clarify the unique characteristics of the MWD of emulsion polymers, one of the simplest and most common cases [264], where neither chain transfer (C_f=0) nor radical desorption (δ=0) occurs, is considered here. The magnitude of bimolecular termination (ξ) is changed with a constant radical entry frequency ($\varepsilon=2\times10^{-4}$). Figure 10 shows the calculated number- and weight-average chain lengths and the polydispersity index (PDI= $\bar{P}_w/\bar{P}_n$) as a function of $\bar{n}$.

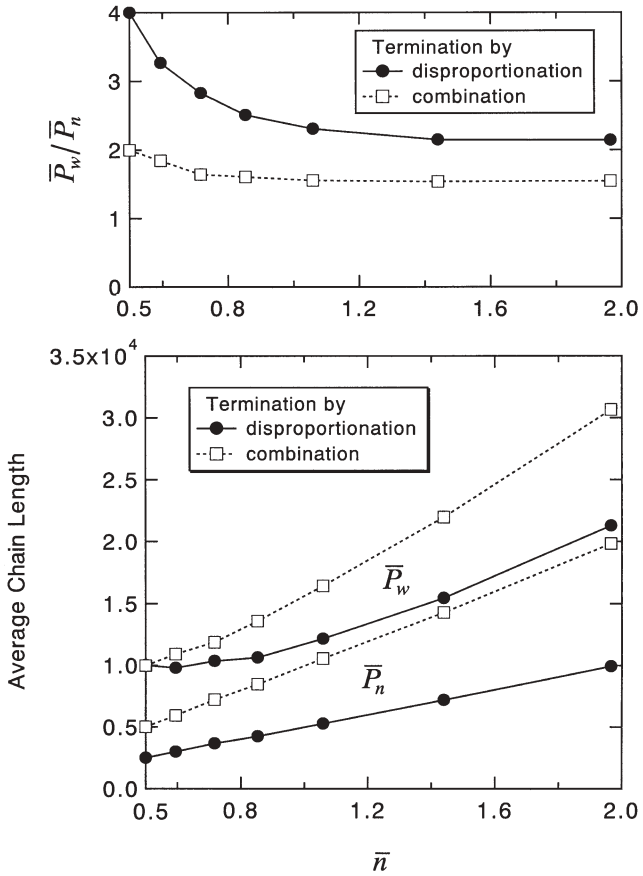

Fig. 10 Calculated number- and weight-average chain lengths as a function of the average number of radicals in a polymer particle, $\bar{n}$, with $\varepsilon=2\times10^{-4}$ and $C_f=\delta=0$

In the present investigation, because the value of $\bar{n}$ increases when the termination rate ξ is decreased, the average chain length becomes larger as $\bar{n}$ increases. As clarified in earlier theoretical investigations [276, 277], the PDI is the largest when $\bar{n}$ =0.5, which could be considered a typical example of emulsion polymerization. At $\bar{n}$ =0.5, PDI=4 if polymer chains are formed solely via bimolecular termination by disproportionation, and PDI=2 when formed by combination. In homogeneous polymerizations, it is well known that PDI=2 when polymer chains are entirely formed by disproportionation, and PDI=1.5 when they are formed solely by combination. Therefore, the PDI of the instantaneous MWD is larger for emulsion polymerization, and as the average number of radicals per polymer particle $\bar{n}$ increases, the PDI approaches that for homogeneous polymerization.

The reason for the broader distribution in a *typical* emulsion polymerization (the so-called zero-one system with $\bar{n}$ =0.5) can be rationalized from the point of view of a very fast termination reaction in a polymer particle. When an oligomeric radical (a monomeric radical is assumed in the present simulation) enters a polymer particle that contains a macroradical, the bimolecular termination occurs before the oligomeric radical grows to a sufficient chain length. An investigation of the MWD produced makes it easier to understand the origin of this behavior. Figure 11 shows the chain length distribution formed by disproportionation (solid curve) and by combination (broken curve).

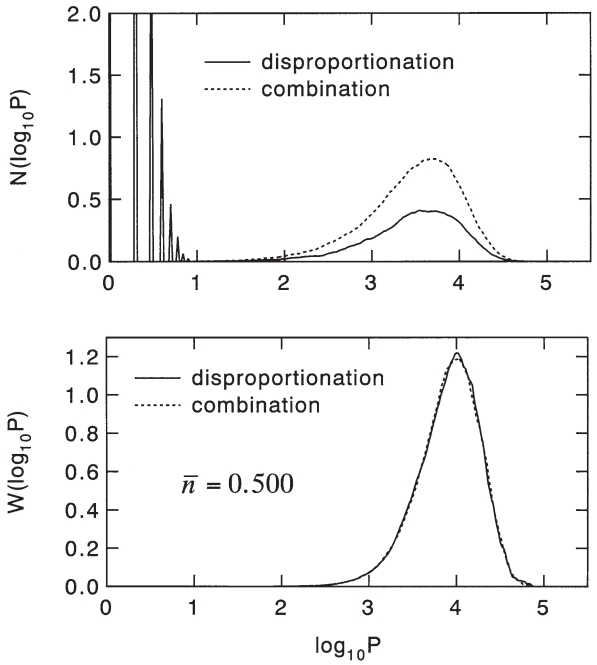

Fig. 11 Calculated chain length distribution on a number and weight basis, for $\bar{n}$=0.500

The independent variable is the logarithm of chain length ($\log_{10}P$), which is usually employed in size exclusion chromatography (SEC) analysis. The upper figure shows the chain length distribution on a number basis, while the lower figure shows that on a weight basis. The chain length distribution formed by disproportionation is the same as the distribution of radicals that cause bimolecular termination. When polymer chains are formed by bimolecular termination from disproportionation, very large peaks appear at smaller chain lengths in the number fraction distribution ($N(\log_{10}P)$). These discrete peaks correspond to integral numbers of monomer units in the chain lengths: 1, 2, 3, ... In the present case, half of the polymers formed by disproportionation are oligomeric chains from very fast bimolecular termination. When polymers are formed via bimolecular termination by combination, on the other hand, the chain length of the radical that has just entered is so small that the dead polymer distribution obtained is almost the same as the macroradical distribution in the polymer particles, which is given by the most probable distribution (PDI=2).

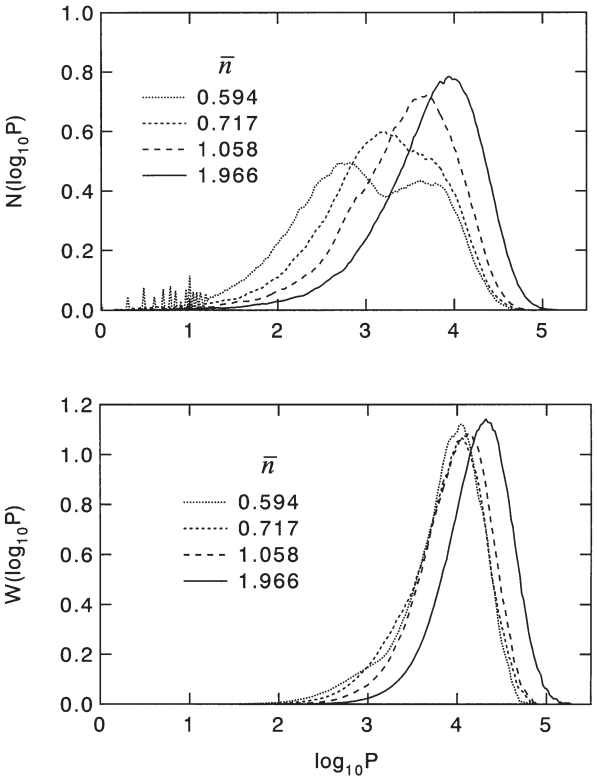

Fig. 12 Instantaneous chain length distribution on a number and weight basis, where dead chains are formed by disproportionation termination. The value of $\bar{n}$ is increased by decreasing the bimolecular termination rate

In addition, because the weight fraction of the oligomeric chains formed by disproportionation is very small, differences between the termination modes cannot be found in the weight fraction distributions obtained via usual SEC techniques, as shown in the lower figure of Fig. 11. Therefore, one needs to pay careful attention to the measurement of the MWD, especially when the effect of bimolecular termination by disproportionation cannot be neglected. If the oligomeric peaks cannot be determined accurately, the obtained PDI drops from 4 to 2, and it is expected that these oligomeric molecules are neglected in usual SEC analysis.

As $\bar{n}$ increases, the unique characteristics of the MWD formed in emulsion polymerization are lost, as shown in Fig. 12.

The smaller and larger peaks in the $N(\log_{10}P)$ formed via bimolecular termination by disproportionation merge as $\bar{n}$ increases. On the other hand, such drastic MWD change cannot be observed in the weight based distributions $W(\log_{10}P)$ that are usually measured by SEC. When $\bar{n}=2$, the MWD formed has already become very close to that for homogeneous polymerization, and in terms of the MWD, pseudobulk polymerization kinetics would be a reasonable approximation. Because $\bar{n}$ increases with particle size, the MWD changes with the particle size. This would be of special interest in cases with broad particle size distributions, as in the case of a continuous emulsion polymerization using a stirred tank reactor.

In our illustrative calculated results, chain transfer reactions are neglected in order to highlight unique characteristics of emulsion polymerization. However, the radical entry rate into a polymer particle is often much smaller than the chain transfer frequency; $\varepsilon \ll C_f$ in emulsion polymerization usually. In such cases, dead polymer chain formation is dominated by chain transfer reactions, and the instantaneous weight fraction distribution is given by the following most probable distribution:

$$N(P) = C_f \exp(-C_f P) \tag{82a}$$

$$W(P) = C_f^2 P \exp(-C_f P) \tag{82b}$$

4.1.3 Effect of Chain-Length-Dependent Bimolecular Termination

The bimolecular termination reaction in free-radical polymerization is a typical example of a diffusion controlled reaction, and is chain-length-dependent [282–288]. When pseudobulk kinetics applies, the MWD formed can be approximated by that resulting from bulk polymerization, and it can be solved numerically [289–291]. As in the other extreme case where no polymer particle contains more than one radical, the so-called zero-one system, the bimolecular termination reactions occur immediately after the entrance of second radical, so unique features of chain-length-dependence cannot be found. Assuming that the average time interval between radical entries is the same for all particles and that the weight contribution from oligomeric chains formed

via disproportionation termination can be neglected, the weight fraction distribution is given by the following most probable distribution:

$$W(P) = (C_f + \varepsilon)^2 P \exp\{-(C_f + \varepsilon)P\} \quad (83)$$

On the other hand, however, it is not straightforward to calculate the MWDs for intermediate cases using the conventional approach. A notable advantage of using an MC simulation technique is that it can be applied to virtually any type of emulsion polymerization, and can account for the chain-length-dependent bimolecular termination reactions in a straightforward manner [265]. Sample simulation results for instantaneous MWDs were shown [265] that were obtained using parameters for styrene polymerization that were reported by Russell [289].

When the bimolecular terminations are highly diffusion controlled, the termination reactions are dominated by interactions between radicals with short and long chain lengths even in bulk polymerization, and the MWD of the longer polymer radicals tends to follow the most probable distribution [287, 292]. Under such conditions, oligomeric chains that can be observed only in the number fraction distribution may be formed via disproportionation termination irrespective of particle size. Figure 13 shows the effect of particle size on the instantaneous chain length distribution where the bimolecular terminations are from disproportionation [265].

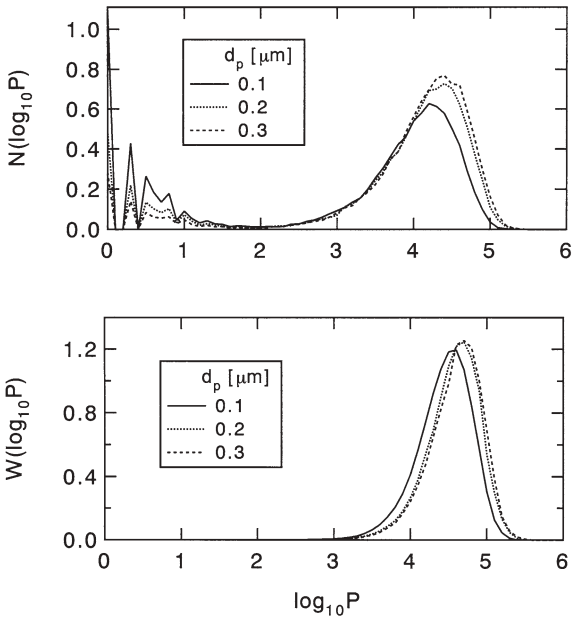

Fig. 13 Effect of particle size on the instantaneous chain length distribution, where bimolecular terminations are chain-length dependent and are by disproportionation

As the particle size increases, the bimolecular termination rate decreases. For cases with chain-length independent bimolecular termination, the oligomeric peak in the number fraction distribution moves toward larger chain length, as shown in Fig. 12. On the other hand, if the bimolecular terminations are highly diffusion controlled, the oligomeric peak location does not move, but the peak height becomes smaller due to an increased amount of dead polymer formation from chain transfer to the monomer, which is accounted for in this simulation. Note that we should not expect these oligomeric peaks to be detected via usual SEC analysis, represented on the basis of the weight fraction distribution, as shown in the lower panel of Fig. 13. The termination mode may not be distinguished from the SEC data.

The chain-length-dependence of bimolecular termination reactions needs to be taken into account in order to be able to accurately estimate the MWD formed, except when very small polymer particles are formed and/or chain transfer reactions dominate over dead polymer chain formation.

4.1.4 Accumulated Molecular Weight Distribution

In a deterministic approach, the instantaneous MWDs are calculated first, and then the accumulated MWD is obtained by integrating the instantaneous MWDs. However, in MC simulations, we can follow the reaction history of each polymer particle directly, and the full MWD is obtained by simulating a large number of polymer particles [263]. Therefore, highly complex reaction kinetics can be simulated directly in a straightforward manner.

During emulsion polymerization, the polymer concentration in the polymer particle that is the locus of polymer chain formation is larger than that in corresponding bulk polymerization. Therefore, the possibility of chain transfer reactions to the polymer occurring is higher, even when the monomer conversion to polymer is not very large. Besides these branching reactions (which will be discussed in Sect. 4.2), another accidental branching may occur during emulsion polymerization. In emulsion polymerization, the time interval between radical entries is usually large, and chain transfer to monomer tends to be the dominant chain termination mode, in the absence of other chain transfer agents. Depending on the mechanism of the chain transfer reaction, active terminal double bonds may be formed by the monomer transfer reaction, which may lead to terminal double bond polymerization (TDBP) [263]. Active terminal double bonds may not be formed during styrene polymerization [293]; however, in order to investigate the potential importance of the TDBP in general, a simulation that incorporates TDBP was conducted using kinetic parameters for the styrene polymerization.

Figure 14 shows the development of the weight fraction distribution with and without TDBP [263].

The parameter K shown in the figure represents the reactivity of the terminal double bonds, defined by $K=k'_p/k_p$, and k'_p is the rate constant of TDBP. The

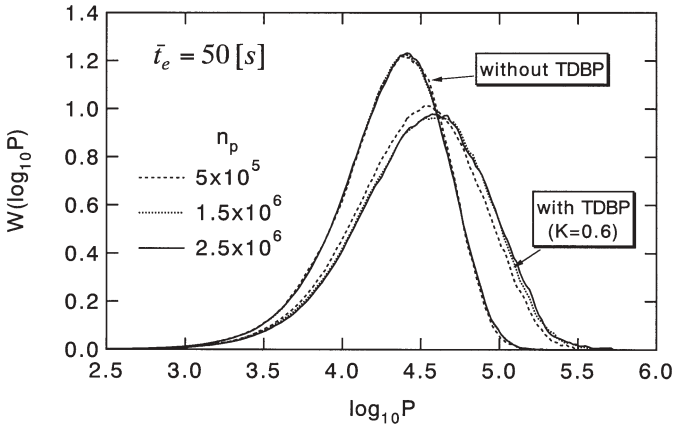

Fig. 14 Accumulated weight fraction distribution development with and without terminal double bond polymerization

average time interval between entries for radicals generated in the water phase (excluding reentry of desorped radicals) is 50 s. The value of n_p is the total number of monomeric units bound into polymer chains in a polymer particle, and therefore, n_p increases as the reaction proceeds. In the simulation, the polymer/monomer ratio in the polymer particle is kept constant. Both with and without TDBP, the MWD profiles do not change significantly during polymerization (as long as monomer droplets exist); however, much larger polymer molecules can be formed by the TDBP and this can change the MWD profile significantly. In emulsion polymerization, the enhanced accidental branching caused by a higher polymer concentration cannot be neglected, even for reaction systems in which the branching reactions are not significant in the bulk polymerization.

4.1.5 Determination of Monomer Transfer Constants from MWD

The traditional method of determining the monomer transfer constant C_m is the Mayo method [294, 295], where the inverse of the number average chain length $\bar{P}_n$ is extrapolated to zero polymerization rate. To obtain reliable C_m values, one needs to measure rather large $\bar{P}_n$ values to high precision that can then be extrapolated to zero polymerization rate. In addition, linear extrapolation is not guaranteed if bimolecular termination reactions are chain-length-dependent [296].

A simple alternative method was proposed by Gilbert et al. [296, 297] to determine the chain transfer constants based on the chain length distribution (CLD). If the dominant chain termination mechanism is chain transfer to monomer, the instantaneous numerical MWD (the number fraction distribution) is given by:

$$N(P) = C_m \exp(-C_m P) \tag{84}$$

In many emulsion polymerizations, the monomer/polymer ratio is kept constant during Interval II, and the accumulated MWD is approximately equal to the instantaneous distribution. Equation 84 shows that the C_m value can be determined from the slope of the $\ln N(P)$ versus P plot.

In a zero-one system in which a radical has just entered a polymer particle containing one polymer radical, and is terminated instantaneously, the number fraction distribution in the absence of a polymer transfer reaction is given by:

$$N(P) = (C_m + \varepsilon) \exp\{-(C_m + \varepsilon)P\} \tag{85}$$

where $\varepsilon = 1/(k_p[M]_p \bar{t}_e)$, as given by Eq. 73.

It is evident from Eq. 85 that the condition $\varepsilon = 1/(k_p[M]_p \bar{t}_e) \ll C_m$ is needed to apply the CLD method to emulsion polymerization. Note that the radical entry rate may be increased through the radical exit. Even when these conditions are satisfied, a higher polymer concentration than for the corresponding bulk polymerization may result in more occurrences of the polymer transfer reaction.

The effect of the polymer transfer reaction on the applicability of the CLD method can be examined by applying the MC simulation method [298]. Figure 15 shows the MC simulation results for the condition $C_m = 5\times10^{-5}$, $\varepsilon = 1/(k_p[M]_p \bar{t}_e) = 5\times10^{-7}$, and for the polymer transfer constant $C_{fp} = 5\times10^{-5}$, when the total number of monomeric units bound into polymer chains in a polymer particle $n_p = 1\times10^6$.

The upper panel of Fig. 15 shows the weight fraction distribution obtained by taking the logarithm of chain length as an independent variable, as in an SEC analysis. The distribution is clearly much broader than without the polymer transfer reactions, as shown in [298]. The lower panel shows the plot of $\ln(N(P))$ versus P, which is clearly curved although a straight regression line could be drawn around the peak region of the $W(\log P)$ curve. The slope obtained for this case is -5.102×10^{-5}, and therefore $\varepsilon + C_m = 5.102\times10^{-5}$. If we use $\varepsilon = 5\times10^{-7}$, we obtain $C_m = 5.052\times10^{-5}$, which is sufficiently close to the true monomer transfer constant, 5×10^{-5}. Note that the MC simulation inevitably involves a small amount of statistical error, and the slope changes slightly if the same simulation is repeated. However, an important conclusion from these kinds of simulations [298] is that, although the MWD is affected significantly by the polymer transfer reactions, the CLD method is still considered applicable as a reasonable approximation for many systems. The C_m value can be estimated reasonably well from the plot of $\ln(N(P))$ versus P, by taking the slope around the peak region of the $W(\log P)$ curve, as long as the polymer transfer constant is not too large.

The MC simulation method can be used to find the experimental conditions where the CLD method can be used to determine the monomer transfer constant.

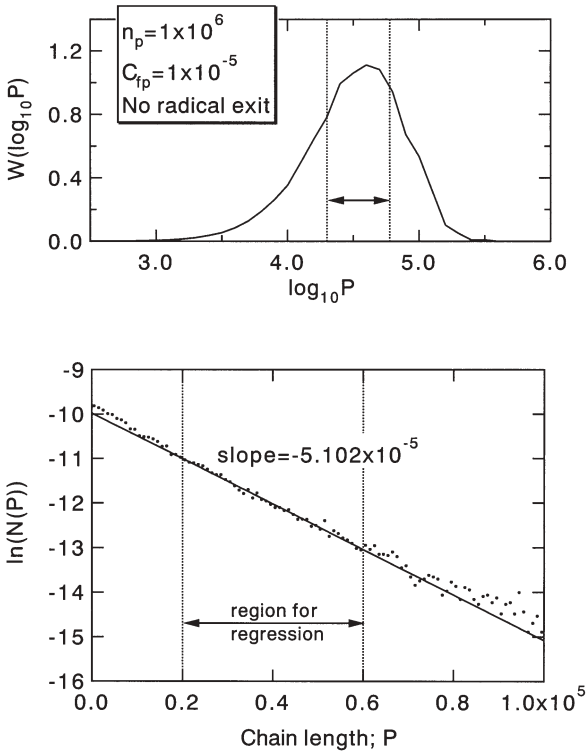

Fig. 15 Monte Carlo simulation results for emulsion polymerization that involves polymer transfer reactions, under the conditions C_m=5×10^{-5}, ε=5×10^{-7} and C_{fp}=5×10^{-5}, without radical desorption

4.2 Branched and Crosslinked Polymer Formation

4.2.1 Long-Chain Branched Polymers

Nonlinear polymer formation in emulsion polymerization is a challenging topic. Reaction mechanisms that form long-chain branching in free-radical polymerizations include chain transfer to the polymer and terminal double bond polymerization. Polymerization reactions that involve multifunctional monomers such as vinyl/divinyl copolymerization reactions are discussed separately in Sect. 4.2.2. For simplicity, in this section we assume that both the radicals and the polymer molecules that formed are distributed homogeneously inside the polymer particle.

In nonlinear emulsion polymerization, a comprehensive mathematical model must account for the following unique characteristics of emulsion polymeriza-

tion: (a) compartmentalization of radicals, (b) higher polymer concentration effects, and (c) limited space effects.

4.2.1.1 Compartmentalization of Radicals

Compartmentalization of radicals into polymer particles may yield a unique MWD for the linear chains, as discussed in Sect. 3.1, except when the dominant chain termination mode is the chain transfer reaction. Branched polymer molecules are assemblies of linear polymer chains (called primary chains), and compartmentalization effects on the primary chain length distribution must be properly accounted for.

The compartmentalization of radicals may produce another important effect when large-sized branched polymer molecules are formed by chain transfer to polymer plus combination termination. As clarified in Sect. 4.1, when the $\bar{n}$ value is small, the frequency of bimolecular termination reactions between large polymer radicals drops significantly compared to models that do not account for compartmentalization of radicals. From this fact, it is easy to see that the size of branched polymer molecule is smaller than that calculated without considering compartmentalization effects [281].

4.2.1.2 Higher Polymer Concentration Effects

The mechanism of emulsion polymerization ensures that the polymer concentration at the polymerization locus is semidilute or concentrated, which results in a greater probability of branch chain formation [299, 300]. This effect produces unique average branching densities and unique distributions of branching densities, that are significantly different from corresponding bulk polymerization [266, 301].

Figure 16a shows the development of average branching density in emulsion polymerization and in a corresponding bulk polymerization, both of which involve the polymer transfer reactions [301].

In bulk polymerization, the average branching density increases with the as the polymerization progresses, while it is fairly high even from a very early stage of the emulsion polymerization. This difference in behavior can be explained by the different polymer concentrations at the locus of each type of polymerization. In bulk polymerization, the polymer concentration at low conversions is very low. Because the branches are formed by the reaction between a polymer molecule and a polymer radical, a lower polymer concentration results in a lower frequency of branch formation and the branching density increases as the polymer concentration increases. On the other hand, in emulsion polymerization, the polymer concentration at the locus of polymerization (in the polymer particle) is high, even just after the formation of polymer particles. A higher polymer concentration results in a higher branching reaction rate. If

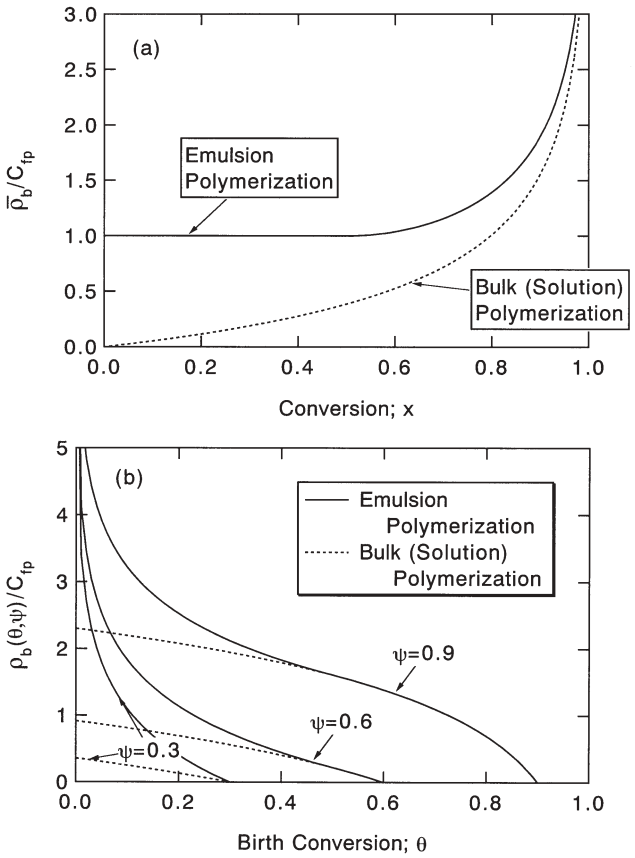

Fig. 16 Development of the average branching density **a** and the branching density distribution **b** for emulsion and bulk polymerizations. The conversion at which monomer droplets disappear in emulsion polymerization is x_c=0.5

the polymer concentration stays the same during the lifetimes of the monomer droplets, the ratio of the branching and propagation reaction rates is kept constant, resulting in a constant average branching density until the depletion of the monomer droplets, as shown in Fig. 16a. Emulsion polymerizations enhance the frequency of branching and crosslinking reactions due to the higher polymer concentration associated with the existence of monomer droplets.

Figure 16b shows the development of the branching density distribution, where $\rho_b(\theta,\psi)$ shows the expected branching density of the primary polymer molecule born at conversion $x=\theta$, when the conversion at the present time is $x=\psi$. The primary chains formed in the early stages of polymerization are subjected to branching reactions for a longer period of time, and therefore, the expected branching density is higher than those chains formed in the later

stages of polymerization. This is the reason that we obtain decreasing functions for both emulsion and bulk polymerization. However, the heterogeneity of the branched structure is more significant for emulsion polymers, as shown in Fig. 16b. Note that the fact that the average branching density does not change as long as monomer droplets exist, as shown in Fig. 16a, does not mean that a homogeneous branched structure is formed during that period.

4.2.1.3 Limited Space Effects

Considerations of "radical compartmentalization" and "higher polymer concentration effects" are not sufficient to describe the processes that build branched polymer molecules in emulsion polymerization, and the effects of limited space must be properly taken into account [266–269].

The locus of polymerization is confined to a very small space, which not only limits the highest molecular weight attainable but can also change the whole MWD profile significantly. The MC simulation technique [266–269] is the only method that can currently take the effects of limited space into account. If the effects of limited space are ignored, the calculated molecular weight may exceed the molecular weight of a whole polymer particle. For example, when the crosslinks – the bridges that connect chains – are formed, conventional deterministic models that do not account for the effects of limited space may predict that the second order moment of the MWD goes to infinity, which is clearly wrong, because the maximum molecular weight is limited by the particle size. In general, those models that do not include the particle size as a parameter when describing the formation of branched chains are illogical.

The limited space effects present rather difficult problems to account for in the conventional deterministic approach. The problem can be highlighted by considering the following hypothetical example. Suppose that there are three polymer chains and three radicals ($R^{\bullet}$), and that polymer transfer reactions are about to occur [269]. Within these polymer chains, suppose that one chain is much larger than the other two, as shown in Fig. 17.

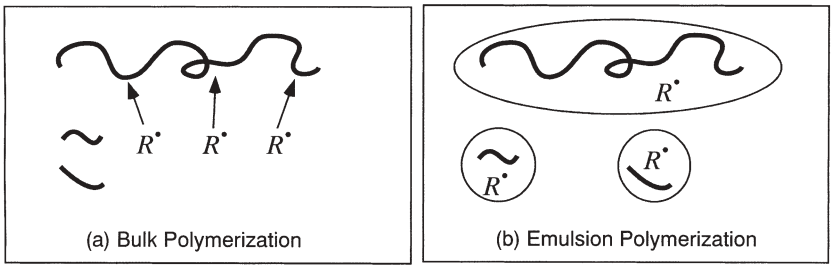

Fig. 17 Hypothetical example that illustrates the differences between the polymer transfer reactions that occur in bulk polymerization **a** and in emulsion polymerization **b**

If all of these species exist in the same reaction locus as in Fig. 17a, it would be highly probable that all of the radicals would attack the largest chain. In other words, the chain transfer rate of the polymer chain with chain length P, v_{fp,P_P}, is proportional to its chain length:

$$v_{fp,P_P} = k_{fp}[R^*]\, r[P_P] \tag{86}$$

where k_{fp} is the rate constant for chain transfer to polymer, $[R^\bullet]$ is the total radical concentration, and $[P_P]$ is the concentration of polymer molecules with chain length P in the whole reaction mixture.

On the other hand, suppose that each of these polymer molecules is isolated into different particles, and that each particle contains one radical, as shown in Fig. 17b. If the radical causes the polymer transfer reaction, the partner must be the polymer molecule that happens to exist in the same particle (so it cannot partner a larger polymer molecule that exists in a different polymer particle). As a consequence, the expected size of the polymer molecule attacked by a radical is smaller for emulsion systems than for the homogeneous model shown in Fig. 17a.

Equation 86 is commonly used for homogeneous reaction systems, but it is not exact in emulsion polymerization. The value of $[P_P]$ is different for each polymer particle, and the value obtained for $[P_P]$ when all of the particles are combined cannot be used either. Strictly, one needs to determine a discrete distribution function of polymer molecules in each polymer particle.

Figure 18 shows the simulated MWD profiles that clearly demonstrate the effects of limited space [273].

Because the total number of monomeric units bound into polymer molecules is $n_p=4\times10^5$ for the present calculation, the high molecular tail can never exceed 4×10^5. Figure 18 shows that the model that does not account for the effects of

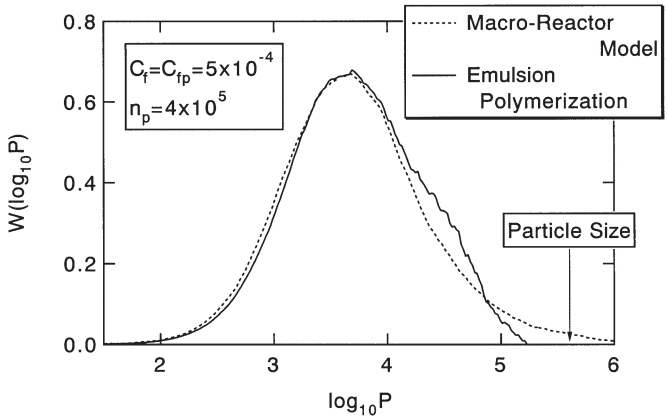

Fig. 18 Comparison of the calculated weight fraction distribution with $C_f=C_{fp}=5\times10^{-4}$ and $x_c=0.5$. For the emulsion polymerization model, the total number of polymerized monomeric units in a polymer particle $n_p=4\times10^5$, which is equal to the size of a dried polymer particle

limited space (the macro-reactor model) is incorrect, because the formation of polymer molecules that are too large to fit in a polymer particle is predicted. More details on the effects of limited space can be found in [268, 269].

The MC simulation method can account for the effects of limited space in a straightforward manner, because the kinetics of polymer formation inside each polymer particle is simulated directly in the MC method. The analytical solution for the development of the weight-average DP was also derived for a simpler case [268], but for more detailed information one needs to resort to the MC method. In MC simulations, one can investigate the structure of each polymer molecule directly, so that highly detailed information can be obtained. Figure 19 shows an example of the branched structure formed during emulsion polymerization that involves chain transfer to polymer, where the primary chains follow the most probable distribution with a number average of 1000.

As we can see, a rather large number of smaller branches exist, which is obviously not what we might expect from the term *long*-chain branches! The 3-D

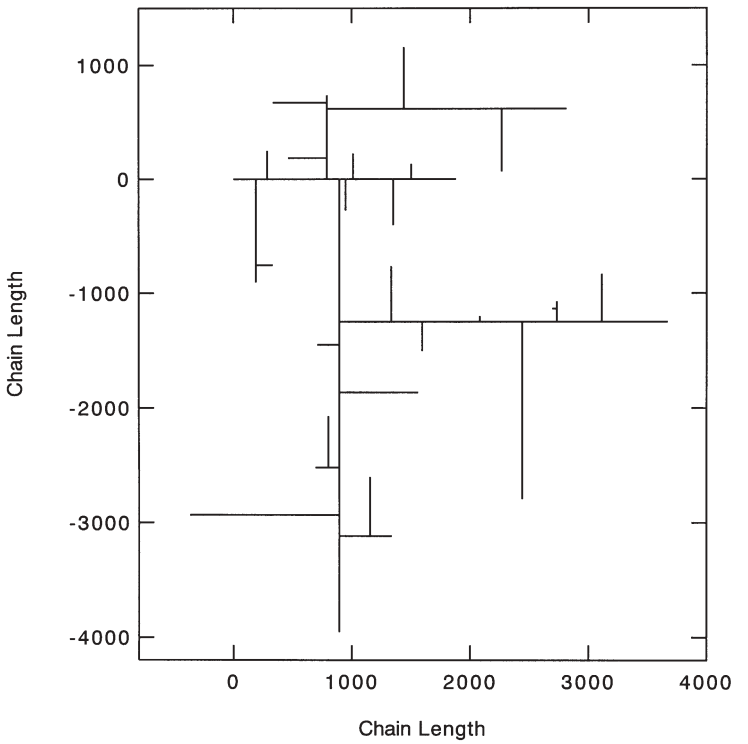

Fig. 19 Example of a branched polymer molecule formed in a model emulsion polymerization. The probability that the chain end is connected to a backbone chain is P_b=0.7. The primary chains follow the most probable distribution with a number-average chain length of 1000

structure of each nonlinear polymer molecule can be estimated, most simply in a θ solvent, using the structural information shown in Fig. 19. By determining the hydrodynamic size of each polymer molecule, we can also estimate the size exclusion chromatography (SEC) elution curve [302–306].

4.2.1.4 Formation of the Bimodal Molecular Weight Distribution

The bimodal MWDs of emulsion-polymerized polyethylenes, which are significantly different from those formed in bulk polymerization, have been reported experimentally [307–309]. An MC simulation was conducted for the experimental conditions reported in [307], and an example is shown in Fig. 20 [310].

The kinetic parameters used were mostly taken from the literature, and an important assumption made was that the particle diameter is about 80 nm (=1.4×10^8 g/mol in molecular weight, which is shown by an arrow in Fig. 20). In [307], it was reported that (1) the particle size is about 50 nm, and that (2) the weight of such a particle is close to the molecular weight of the high molecular weight, narrow distribution component. However, the weight of a low-density polyethylene particle 50 nm in diameter is 6×10^{-17} g, which is 3.6×10^7 g/mol in molecular weight. This molecular weight is too small to contain the polymers in the high molecular weight tail, whose molecular weight can be as large as 8×10^7 g/mol, and so the value of 1.4×10^8 g/mol (≈80 nm in diameter) was used in the MC simulation.

According to the MC simulation, the high molecular weight, narrow distribution component consists of the largest polymer molecule in each polymer particle, and the bimodal MWD is formed because of the limited space effects.

Assuming a simple zero-one system during Interval II, a model analysis was conducted to clarify the conditions needed to form bimodal MWD through the effects of limited space [311].

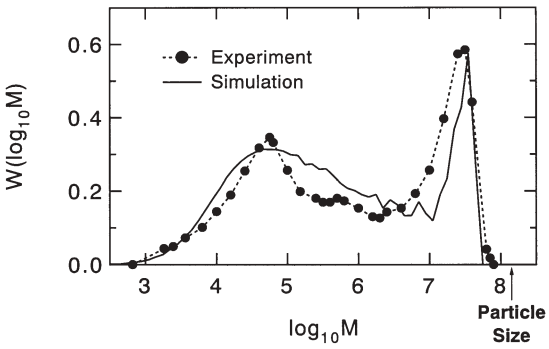

Fig. 20 MWD of emulsion-polymerized polyethylene. The experimental conditions are discussed in detail in [307], and the simulation method is described in [310]

The instantaneous MWD of the primary chains formed during Interval II in a zero-one system (assuming combination termination) is given by the most probable distribution, whose number fraction distribution is given by:

$$N_{pc}(P) = \tau \exp(-\tau P) \tag{87}$$

$$\tau = C_m + C_{fp}\frac{x_c}{(1-x_c)} + C_{fCTA} + \frac{[CTA]_p}{[M]_p} + \frac{1}{k_p[M]_p\bar{t}_e} \tag{88}$$

where x_c is the weight fraction of polymer in the polymer particle, which is kept approximately constant during Interval II, and is often equal to X_{Mc}.

The probability that a newly-formed primary chain starts growing from a radical center on a backbone chain (in other words, the probability that a primary chain end is connected to a backbone chain), P_b, is given by:

$$P_b = \frac{C_{fp}x_c/(1-x_c)}{C_m + C_{fp}x_c/(1-x_c) + C_{fCTA}[CTA]_p/[M]_p + 1/(k_p[M]_p\bar{t}_e)} \tag{89}$$

A model analysis was conducted, which assumed that (1) both τ and P_b do not change during polymerization, (2) all polymer particles are formed instantaneously, and (3) the number of primary chains in a polymer particle, n_{pc}, is the same for all particles. Important conclusions were that (i) bimodal MWDs (represented in terms of $W(\log P)$) are formed if P_b is larger than 0.5, and (ii) for $P_b>0.5$, the weight-average molecular weight increases without limits over the whole course of polymerization. Note that the second conclusion does not indicate that gelation occurs. Figure 21 shows the calculated development of the weight-average chain length [311].

For $P_b<0.5$, the weight-average chain length reaches a constant value that is given by $\bar{P}_w = \bar{P}_{wp}/(1-2P_b)$, where $\bar{P}_{wp}$ is the weight-average chain length of the primary chains. On the other hand, the weight-average molecular weight increases without limit for $P_b>0.5$, but it increases very gradually and it takes an infinitely long time to reach an infinitely large polymer molecule. It was found [313] that the formed MWD is a power-law distribution [312] that possesses fractal characteristics is formed.

For the emulsion-polymerized polyethylene shown in Fig. 20, which clearly shows a bimodal MWD, $P_b=0.813>0.5$. For another example investigated in [311], $P_b=0.711>0.5$, and the MWD is bimodal.

On the other hand, for the emulsion polymerization of vinyl acetate, Friis et al. reported that (i) the weight-average molecular weight does not increase significantly until the monomer droplets are depleted, and that (ii) the MWDs are unimodal [314, 315]. They considered the TDBP in addition to the polymer transfer reactions; however, the contribution of the TDBP is minor and a qualitative discussion on the MWD shape could be made without needing to involve the TDBP. The parameters they used are $C_m=2.32\times10^{-4}$, $C_{fp}=3.98\times10^{-4}$ and $x_c=0.2$, which gives $P_b=0.3$. With $P_b=0.3$, the theoretical analysis in [311] showed

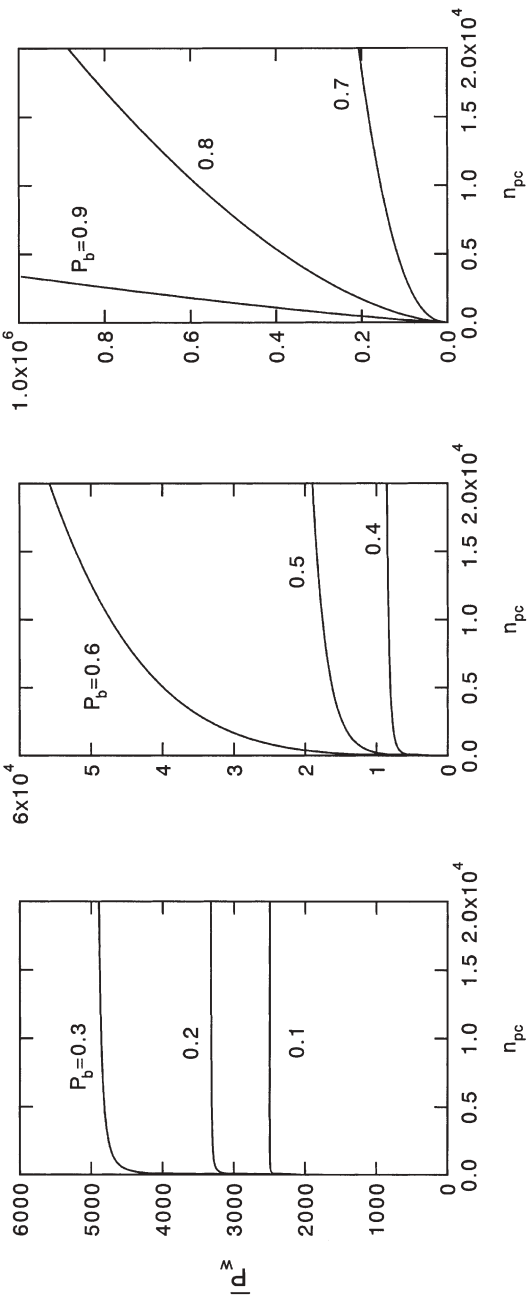

Fig. 21 Calculated development of the weight-average chain length during the model emulsion polymerization

that (i) the weight-average chain length reaches a steady state value rather quickly, and that (ii) the MWDs formed are unimodal, both of which agree with experimental observations.

Although the kinetic behavior during Interval III was not considered in [311], P_b=0.5 is an important consideration when we look at the possibility of forming bimodal MWDs in emulsion polymerization that involves chain transfer to polymer.

4.2.2 Crosslinked Polymers

4.2.2.1 Crosslinked Structure

Assuming that classical chemical kinetics are valid and that the crosslinking reaction rate is proportional to the concentrations of polymer radicals and pendant double bonds, it was shown theoretically that the crosslinked polymer formation in emulsion polymerization differs significantly from that in corresponding bulk systems [270, 316]. To simplify the discussion, it is assumed here that the comonomer composition in the polymer particles is the same as the overall composition in the reactor, and that the weight fraction of polymer in the polymer particle is constant as long as the monomer droplets exist. These conditions may be considered a reasonable approximation to many systems, as shown both theoretically [316] and experimentally [271, 317]. First, consider Flory's simplifying assumptions for vinyl/divinyl copolymerization [318]; that: (1) the reactivities of all types of double bonds are equal, (2) all double bonds

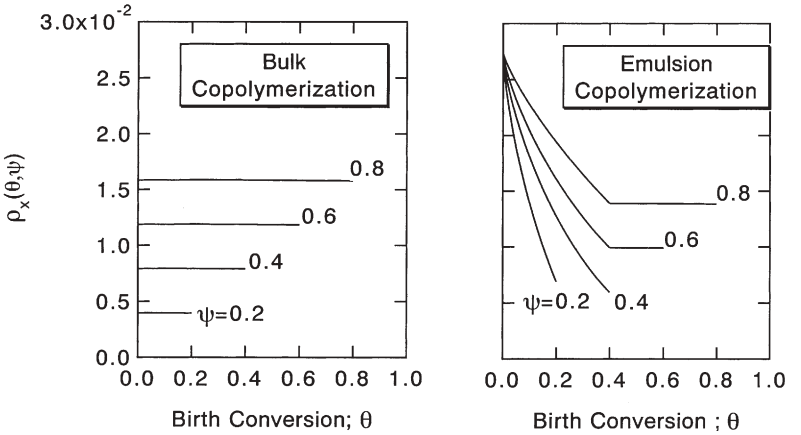

Fig. 22 Crosslinking density distribution development during bulk and emulsion polymerization under Flory's simplifying assumptions, where the initial mole fraction of divinyl monomer is 0.01, and x_c=0.4 for emulsion polymerization

react independently, and (3) there are no cyclization reactions in finite molecules. Under these simplifying assumptions, a completely homogeneous network is formed in homogeneous batch polymerization [319].

Figure 22 shows the calculated results for the expected crosslinking density of primary chains formed at conversion θ when the conversion at the present time is ψ, under Flory's simplifying assumptions for bulk and emulsion copolymerization.

The expected crosslinking density is the same for all primary chains at any stage of polymerization in a bulk system, indicating that a statistically homogeneous network is formed. On the other hand, the crosslinking density distribution is completely different in emulsion polymerization. In particular, the crosslinking densities of the primary chains formed in the earlier stages of polymerization are very high, and the variance of the crosslinking density distribution is significant in emulsion polymerization. The bending at θ=0.4 occurs because the conversion at which monomer droplets disappear is assumed to be 0.4 in these calculations. Homogeneous networks cannot be formed, even under Flory's simplifying assumptions in emulsion crosslinking copolymerization.

Figure 23 shows the average crosslinking density development under Flory's simplifying assumptions.

The average crosslinking density is higher for emulsion polymerization due to the higher polymer concentration effects inside the polymer particles, which are the loci of polymerization. The fact that the average crosslinking density is high even from a very early stage of polymerization has been confirmed experimentally, and this agrees with theoretical calculations adequately [271,

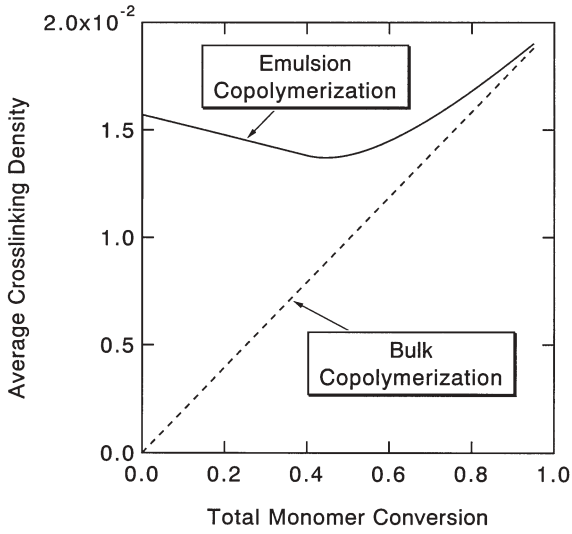

Fig. 23 Average crosslinking density development under Flory's simplifying assumptions

272, 317]. The fact that the average crosslinking densities in some emulsion polymerizations may not change much during emulsion polymerization, as shown in Fig. 23, is sometimes misunderstood as producing a homogeneous polymer network [320]. However, this argument may not be true, as shown in the crosslinking density distribution profile shown in Fig. 22.

4.2.2.2 Unique Molecular Weight Distributions

It has long been recognized that microgels formed in emulsion polymerization possess only supermolecular size and weight [321]. It is known that a reaction system with divinyl monomer makes the particle size smaller compared to the cases without crosslinker [97, 322]. Assuming that the final particle diameter is 50 nm, the molecular weight of this particle is about 4×10^7 g/mol. Such microgels could be soluble in a good solvent, and the MWD could be determined by

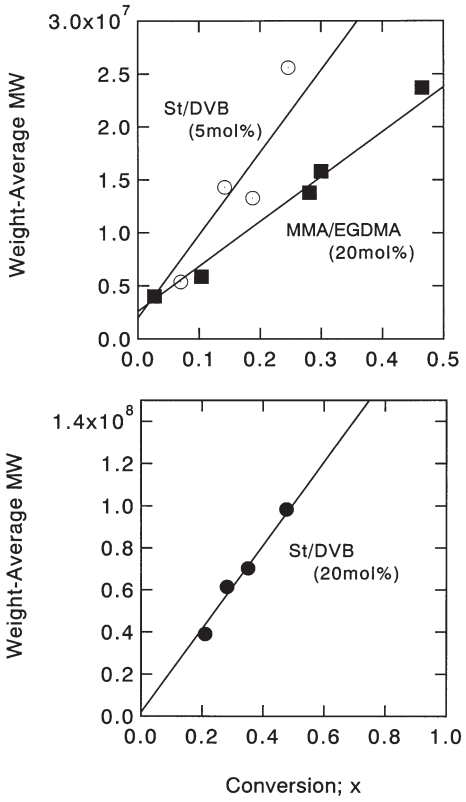

Fig. 24 Experimental results for the weight-average molecular weight development during the emulsion crosslinking copolymerization of styrene (St)/divinylbenzene (DVB) and methyl methacrylate (MMA)/ethylene glycol dimethacrylate (EGDMA). Data from [323]

using SEC even when each polymer particle forms a single crosslinked polymer molecule.

In a typical recipe for microgel formation, a sufficient amount of crosslinker is used. Because the crosslinking density tends to be high from a very early stage of polymerization, the MC simulation results showed [270, 271] that each polymer particle tends to consist of a single large crosslinked polymer molecule even from the early stage of polymerization. In such cases, it was shown [270, 271] that (1) the weight-average molecular weight grows linearly with conversion, and (2) the MWD formed is narrow and the distribution shifts to larger molecular weights, preserving the narrow profile, as polymerization proceeds.

Experimental data [323–325] in which the MWDs are measured by SEC with on-line multiangular laser light scattering (MALLS) show the above trend [326]. Figure 24 shows some examples of the weight-average molecular weight development, which show linear increases with respect to conversion.

The *y*-intercept might approximately correspond to the weight-average molecular weight of primary chains. It was further confirmed [326] that the MWD of polymer molecules and that of whole polymer particles are the same, showing that each polymer particle essentially consists of one crosslinked polymer molecule. Figure 25 shows such an example, and the MWD formed agrees reasonably well with the particle size distribution represented in terms of molecular weights.

On the basis of the MC simulation results [270], it is expected that if the amount of divinyl monomer is reduced to the level of, say, several crosslinkers per primary chain, a bimodal MWD (as shown in Fig. 26) may result.

The arrows indicate the molecular weight of a dried polymer particle, which gives an upper limit to the molecular weight of the polymers attainable. Qualitatively speaking, the high molecular weight peaks are formed because the crosslinked polymer molecules want to grow further due to the higher chain

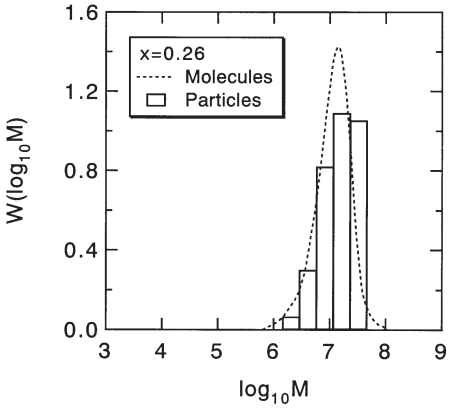

Fig. 25 MWD of polymer molecules and dried polymer particles in the emulsion copolymerization of St and DVB (20 mol%) [326]

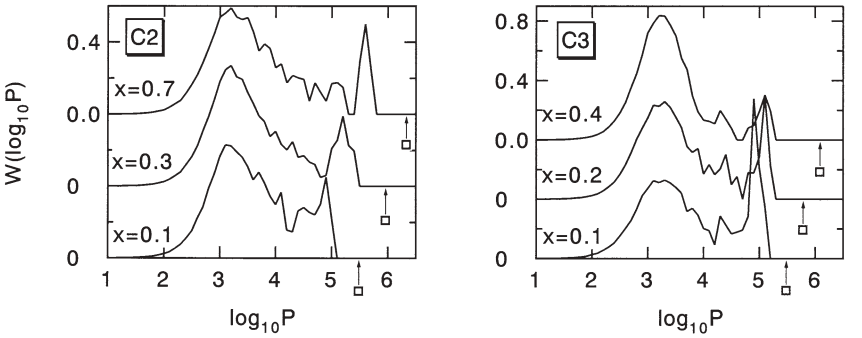

Fig. 26 MC simulation results that show bimodal MWDs in the emulsion copolymerization of vinyl/divinyl monomers [270]

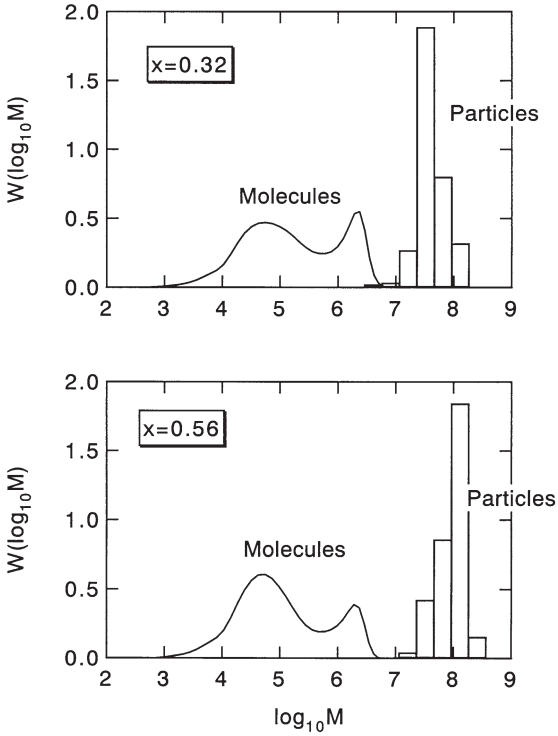

Fig. 27 Experimentally obtained MWD developments of polymer molecules and particles for the emulsion copolymerization of St and DVB [327]

connectivity, but they cannot because of the limitation of a small particle size. Experimentally, such unique bimodal distributions were obtained in the styrene/divinyl benzene system [327] by setting the number of divinylbenzene molecules per chain to ~5. An example of a bimodal MWD, together with the particle size distribution [327], is shown in Fig. 27.

It was found that the locations of these peaks can be controlled independently. The location of a high molecular weight peak is mainly controlled by the particle size, and the location of a low molecular weight peak is controlled by the chain lengths of the primary polymer molecules.

The MC simulation method is particularly suitable for investigating emulsion polymerization that involves various simultaneous kinetic events with a very small locus of polymerization. The MC simulation method will become a standard mathematical tool for the analysis of complex reaction kinetics, both for linear and nonlinear emulsion (co)polymerization.

5
Continuous Emulsion Polymerization

Continuous emulsion polymerization processes are industrially important for the large-scale production of synthetic polymer latexes, and have been used particularly where the solid polymer is to be recovered by coagulating the polymer latex. St-Bu rubber latex was one of the earliest latex products manufactured using continuous emulsion polymerization processes consisting of a number of stirred-tank reactors in series (CSTRs). Since the 1940s, continuous emulsion polymerization processes have been developed for a variety of products and with different reactor configurations [328]. This is because these continuous reactor systems have several advantages, such as [329]:

- Economical production of large-volume or closely-related products
- Uniform product quality
- Full utilization of heat transfer capability
- Fewer problems with wall polymer build-up and coagulation.

However, these systems have also potential disadvantages, such as [329]:

- Less flexibility in terms of the operation and control of product characteristics
- Possible production of off-specification material during start-up or product change-overs
- Difficulties with the direct development of continuous processes based on the information from batch and semi-batch R&D.

Reflecting the importance of continuous emulsion polymerization processes, numerous investigations have been carried out to date, which are categorized into three groups: (1) studies on the reactor configuration (stirred-tank reactors, tubular type reactors such as a simple tubular reactors, pulsed tubular reactors

and loop-tubular reactors, pulsed packed column reactors, Couett-Taylor vortex flow reactors and combinations of these reactors); (2) studies on operational techniques (pre-reactor concept [330] and split-feed operation [331–333]), and; (3) studies on the kinetics and mechanisms of particle formation and growth in a given reactor system. Research work carried out before ~1990 was introduced in a compact but excellent review article [328], which also included those cited in a review article published in 1977 [334]. The present review, therefore, mainly refers to the research work that has been published since ~1990, but also includes any historically important works reported before ~1990.

The stirred-tank reactor and the tubular reactor are two basic reactors used for continuous processes, so much of the experimental and theoretical studies published to date on continuous emulsion polymerization have been conducted using these reactors. The most important elements in the theory of continuous emulsion polymerization in a stirred-tank reactor or in stirred-tank reactor trains were presented by Gershberg and Longfield [330]. They started with the S-E theory for particle formation (Case B), employing the same assumptions as stated in Sect. 3.3, and proposed the balance equation describing the steady-state number of polymer particles produced as:

$$dN_T/dt = \rho_w[A_m/(A_m + A_p)] - N_T/\theta = 0 \tag{90}$$

where θ is the mean residence time of a single CSTR. Introducing the relation, $A_m+A_p=a_sS_0$ into Eq. 90 yields

$$N_T = \rho_w[1 - (A_p/a_sS_0)] \tag{91}$$

where S_0 is the emulsifier concentration in the feed. The residence time distribution for polymer particles in a perfectly mixed CSTR is given by $E(t)dt= dN_T/N_T=(1/\theta)\exp(-t/\theta)dt$. The total surface area of polymer particles per unit volume of water A_p is obtained by the integration

$$A_p = \int_0^{N_T} a_p dN_T = (36\pi)^{1/3} \int_0^{N_T} v_p^{2/3} dN_T = (36\pi)^{1/3} N_T \int_0^{\infty} (\mu t)^{2/3} E(t)\, dt \tag{92}$$

where a_p is the surface area of a polymer particle and $E(t)$ is the residence time distribution function. Combining Eqs. 91 and 92 gives

$$N_T = \frac{\rho_w \theta}{1 + (4.36 \rho_w \mu^{2/3} \theta^{5/3} a_s S_0)} \tag{93}$$

Thus, the rate of polymerization R_p can be predicted using Eqs. 1, 51 and 93.

Omi et al. [335] and Nomura et al. [163] pointed out that Eq. 93 suggests the existence of a maximum number of polymer particles $N_{T,max}$ at the optimum residence time θ_{max}, which is given by

$$\theta_{max} = 0.53(a_sS_0/\rho_w\mu^{2/3})^{3/5} \tag{94}$$

$$N_{T,max} = 0.21(\rho_w/\mu)^{0.4}(a_SS_0)^{0.6} \tag{95}$$

By comparing Eq. 31 with Eq. 95, they also pointed out that $N_{T,max}$ is only 58% of that produced in a batch operation with the same recipe and temperature, and also that

$$\theta_{max} = 0.83 t_c \tag{96}$$

where t_c is the time at which particle formation stops due to complete depletion of micelles in the water phase, in a batch operation with the same recipe as that used in a continuous operation.

Gershberg and Longfield [330] carried out the continuous emulsion polymerization of St at 70 and 100 °C in a train of three CSTRs, and compared the experimental results with theoretical predictions. They presented the following conclusions and suggestions;

1. The theoretical equation $N_T \propto R_p \propto \rho_w^0 S_0^{1.0} \theta^{-2/3}$, derived from Eqs. 1 and 93, correctly predicts the effect of the operating variables upon the rate of polymerization in the stirred-tank reactors at any stage at 70 °C for large θ values.
2. The number of polymer particles produced at 70 °C (and hence, the rate of polymerization) was higher than that at 100 °C, as Eq. 93 predicted.
3. The theory and the experimental data from this study demonstrates that in a train of CSTRs, essentially all of the particles form in the first reactor. Therefore, it is possible to maximize the monomer conversion in the latex leaving the first reactor by keeping the temperature and the residence time at the first reactor as low as possible in order to produce the maximum number of polymer particles and so increase the rate of polymerization in the succeeding stages. This is the so-called "*pre-reactor*" concept.
4. $N_{T,max}$ certainly occurs at low θ, as the theory predicts.
5. Sustained oscillation can take place in the monomer conversion.
6. The residence time in the first stage should be long enough to overcome the retarding effects of traces of oxygen and/or impurities in the feed-stream upon particle formation and growth.

Poehlein and Degraff [336] extended the derivation of Gershberg and Longfield [330] to the calculation of both molecular weight and particle size distribution in the continuous emulsion polymerization of St in a CSTR. On the other hand, Nomura et al. [163] carried out the continuous emulsion polymerization of St in a cascade of two CSTRs and developed a novel model for the system by incorporating their batch model [14], which introduced the concept that the radical capture efficiency of a micelle relative to a polymer particle was much lower than that predicted by the diffusion entry model ($\rho \propto d^{1.0}$). The assumptions employed were almost the same as those of Smith and Ewart (Sect. 3.3), except that the model did not assume a constant value of μ. The elementary reactions and their rate expressions employed in the first stage are as follows:

1. Particle formation by radical entry into a micelle (Eq. 32):

$$R^* + m_s \rightarrow N^*, k_{em} m_s [R_w^*] \tag{32}$$

2. Formation of dead particles by entry of a radical into an active particle containing a radical (Eq. 33):

$$R^* + N^* \rightarrow N_0, k_{ep} N^* [R_w^*] \tag{33}$$

3. Formation of active particles by entry of a radical into a dead particle containing no radical (Eq. 34):

$$R^* + N_0 \rightarrow N^*, k_{ep} N_0 [R_w^*] \tag{34}$$

where m_s is the concentration of monomer-swollen micelles, $[R_w^*]$ is the concentration of free radicals in the water phase, N^* is the concentration of active particles containing a radical, N_0 is the concentration of dead particles that contain no radicals, k_{em} is the rate constant for the entry of radicals into micelles, and k_{ep} is the rate constant for the entry of radicals into particles. If these rate expressions are used, then the balance equation describing the steady-state number of polymer particles produced becomes

$$dN_T/dt = \rho_w [k_1 m_s R^*/(k_1 m_s R^* + k_2 N_T R^*)] - N_T/\theta = 0 \tag{97}$$

where $N_T = N^* + N_0$. Then Eq. 97 is rearranged to give

$$N_T = \rho_w \theta/[1 + (k_2 N_T/k_1 m_s)] = \rho_w \theta/(1 + \varepsilon N_T/S_m) \tag{98}$$

where $\varepsilon = (k_2/k_1) M_m$; M_m is the aggregation number per micelle and S_m is the concentration of emulsifier forming micelles, given by $S_m = S_0 - (A_p/a_s)$. Rearranging Eq. 98 along with the steady-state balance equations for the monomer and the number of active particles finally yields

$$\varepsilon N_T^2/(\rho_w \theta - N_T) = S_0 - k_v (K M_0/2)[\rho_w \theta/(\rho_w \theta - N_T/2)]^{2/3} N_T \theta^{2/3} \tag{99}$$

where k_v and K are the constants associated with the adsorption area of the emulsifier on the particles' surface and the particle growth rate, respectively, and M_0 is the concentration of the monomer in the feed. Equation 99 can be used to calculate the relationship between N_T and θ, and that between $N_{T,max}$ and θ_{max}. A comparison of the experimental data and theoretical predictions for the dependence of N_T on θ is presented in Fig. 28 [163, 331].

The experimental data showed much better agreement with the results predicted using Eq. 99 than the results calculated using the Gershberg and Longfield model (Eq. 93), which gave a higher value of $N_{T,max}$ and a smaller value of θ_{max}. The reason for this may be that the rate of radical entry into a micelle must be less than that predicted by the collision entry model, given by $\rho_w [d_m^2/(d_m^2 + d_p^2)]$.

Gerrens and Kuchner [337] investigated the continuous emulsion polymerization kinetics in a cascade of three CSTRs, and with St and MA as monomers with different solubilities in water. They showed that the experimental results obtained with St agreed with the predictions from the Gershberg and Longfield

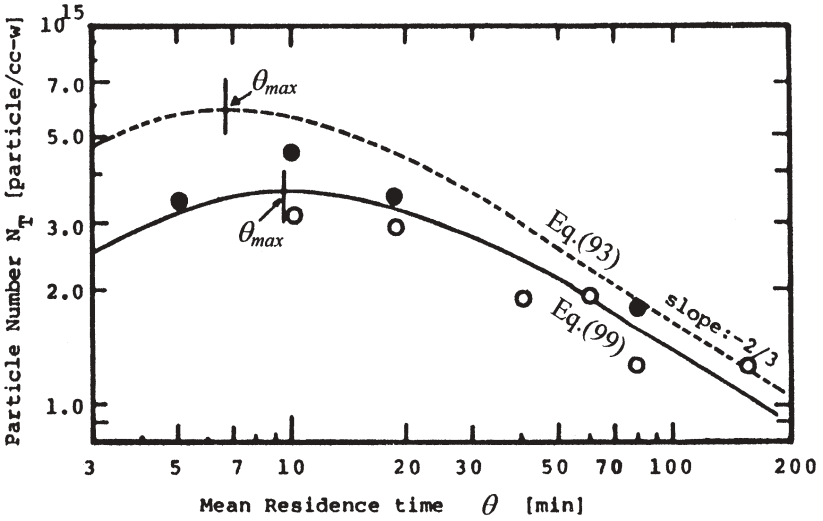

Fig. 28 Effect of the mean residence time in the first reactor θ on the number of polymer particles produced (S_0 (NaLS)=12.5 g/dm^3-water, I_0 (KPS)=1.25 g/dm^3-water, M_0 (St)= 500 g/dm^3-water; 50 °C. Experimental data: empty circles, first reactor; filled circles, second reactor

model, but for MA only the particle number varied in the manner predicted by the Gershberg and Longfield model. This showed that a relatively water-soluble monomer does not correlate with the model based on S-E theory. The existence of multiple steady-states for the isothermal operation of continuous emulsion polymerization in a CSTR was first demonstrated by Gerrens et al. [338, 339]. It is now well understood from a kinetic point of view that this phenomenon takes place as a consequence of the so-called "*gel-effect*" (the Trommsdorff-Norrish effect).

Oscillations in the number of polymer particles, the monomer conversion, and the molecular weight of the polymers produced, which are mainly observed in a CSTR, have attracted considerable interest. Therefore, many experimental and theoretical studies dealing with these oscillations have been published [328]. Recently, Nomura et al. [340] conducted an extensive experimental study on the oscillatory behavior of the continuous emulsion polymerization of VAc in a single CSTR. Several researchers have proposed mathematical models that quantitatively describe complete kinetics, including oscillatory behavior [341–343]. Tauer and Müller [344] proposed a simple mathematical model for the continuous emulsion polymerization of VCl to explain the sustained oscillations observed. Their numerical analysis showed that the oscillations depend on the rates of particle growth and coalescence. However, it still seems to be difficult to quantitatively describe the kinetic behavior (including oscillations) of the continuous emulsion polymerization of monomers, especially those with relatively high solubility in water. This is mainly because the kinetics and mech-

anisms of particle formation in systems containing such monomers are not completely understood yet. It is now known that oscillations in the monomer conversion and the molecular weight of the polymer produced occur due to oscillations in the number of polymer particles. Since oscillatory behavior is undesirable in practice from the standpoint of stable operation and product quality problems, a variety of techniques have been proposed to eliminate the oscillations in the number of polymer particles. The simplest but most effective technique among them would be to add a small continuous tubular type reactor – a pre-reactor with plug flow, operating as a seed generator (a seeding reactor), located upstream of the main CSTRs [331, 345].

To meet the growing demand for the large-scale production of latex with narrow PSD and consistent quality, it was initially recognized that continuous emulsion polymerization in a tubular reactor might be advantageous from the standpoint of higher performance (compared to a CSTR), greater heat transfer, better quality control and lower equipment costs [346]. Nevertheless, very little research work has been done with tubular reactors compared to CSTRs. Feldon et al. [346] successfully performed the continuous emulsion copolymerization of St and Bu in a continuous tubular reactor. It was originally thought that the polymerization needed to be conducted in the turbulent flow regime in order to obtain satisfactory heat transfer and mixing. However, it was found that this turbulent flow gave rise to the formation of a pre-coagulum, which resulted in an accumulation of polymer particles on the reactor wall which eventually plugged the reactor. Therefore, the stable and long-term operation of a continuous tubular reactor (CTR) is usually a very difficult task [346]. In addition, when the rate of polymerization is low, as it often is in such reactors, a very long tube is necessary to achieve high monomer conversion. This is not practical because it is difficult to transport a highly viscous latex product through a long tube.

In order to make full use of the advantages of a tubular reactor while avoiding its drawbacks, the use of a continuous loop-tubular reactor (CLTR) has been proposed. Background on this discovery, as well as a discussion of the main characteristics of the continuous loop-tubular reactor, was first provided by Geddes [347]. He studied the changes in properties during emulsion copolymerization in a continuous loop reactor, with particular reference to particle size distribution. Cycling of properties similar to that observed in CSTRs was found [348]. Bataille and co-workers [349, 350] carried out the emulsion homopolymerizations of St and VAc using a batch loop-tubular reactor. They found that a limiting conversion, lower than that obtained in a stirred-tank batch reactor, occurred for all cases, and that the value of the limiting conversion was a maximum at the laminar-turbulent transition point. Lee et al. [351–352] carried out the continuous emulsion polymerization of St in a continuous loop-tubular reactor with recycling. The effects of the emulsifier, initiator, and monomer concentrations, temperature, and mean residence time on the monomer conversion, average particle diameter, the number of polymer particles produced and, in some cases, the average molecular weight, were ex-

amined to clarify the characteristics of a CLTR. Overshoots in both monomer conversion and the number of polymer particles were observed, but these diminished at about three times the mean residence time. Neither oscillations nor multiple steady-states were observed. The steady-state number of polymer particles was independent of the mean residence time. Asua and co-workers [21, 353–356] carried out the redox-initiated emulsion copolymerization of VAc and Veoba 10 in a CLTR. They studied the effect of the flow rate on shear-induced coagulation and the effect of the start-up strategy on the smoothness of the operation and on the amount of off-specification product, as well as proposing a mathematical model for the process [353, 354]. They compared the performance of a CLTR with that of a CSTR operating under similar conditions, and concluded that, in most cases, both reactors showed a similar performance, but under exigent conditions, the CSTR was prone to thermal runaway, whereas the CLTR was much safer [355]. Moreover, the effects on the reactor performance of both macromixing (residence time distribution) and micromixing (the degree of monomer distribution in polymer particles) in the reaction mixture were examined and the macromixing was characterized by means of tracer response experiments [356]. They also showed that when the recycle ratio (the ratio of the flow rate inside the reactor to the feed flow rate) was increased, the behavior of the reactor approached that of a CSTR, and that when the feed was pre-emulsified, the state of micromixing was substantially improved because the rate of monomer diffusion from the monomer droplets into the polymer particles was enhanced. Araújo et al. [21] developed a detailed dynamic mathematical model that described the evolution of PSDs during the emulsion copolymerization of VAc and Veova 10 in a CLTR and compared the calculated results with their experimental data.

With the aim of improving the performance of a continuous tubular reactor by decreasing its backmixing, a pulsed tubular (PT) reactor [357], a pulsed packed column (PPC) reactor [358], and a pulsed sieve plate column (PSPC) reactor [19] have been proposed as continuous reactors with near-plug flow. These reactors are considered to be modified versions of a tubular reactor, but with less backmixing than a simple tubular reactor. Paquet and Ray [357] successfully conducted the continuous emulsion polymerization of MMA in a PT reactor. When they performed the first four runs without any pulsation, only one of the runs was successful; the other three plugged. They found, therefore, that the use of a pulsation source eliminated the reactor fouling and plugging problem that has frequently occurred in continuous tubular reactors. Also, no oscillatory behavior was observed. The exit conversion remained constant for three residence times and was close to that observed in a corresponding batch reactor. No clear dependence of the pulsation rate on monomer conversion was revealed.

Mayer et al. [358] investigated the performance of a PPC reactor in the continuous emulsion polymerization of St. They found that the number of polymer particles produced in the PPC reactor depended strongly on the residence time distribution (RTD) – in other words, on the pulsation conditions – and that it had a value between those recorded for the batch and the CSTR processes.

They developed a mathematical model based on a micellar nucleation hypothesis and plug flow with axial dispersion, and showed that there was a good agreement between the model predictions and the experimental results. On the other hand, Scholtens et al. [359] extended the Mayer model and predicted the effect of RTD on the intermolecular chemical composition distribution (CCD) of copolymers produced in the continuous emulsion polymerization of St and MA in a PPC reactor with side feed streams. They concluded that the PPC reactor was a good continuously operated alternative to a semi-batch process that produces latexes with a predicted CCD. Sayer et al. [19] utilized a PSPC reactor for the continuous emulsion polymerization of VAc and developed a dynamic mathematical model to simulate the experimental results, showing that the continuous PSPC reactor could be described by an axial dispersion model that covered the entire range between the plug flow and perfectly mixed stirred-tank reactors. Another possible way of producing a plug flow is to use a reactor system with a cascade of CSTR trains. Certainly, the larger the number of stages, the closer the flow pattern will approach plug flow. However, an increase in the number of stages is not necessarily desirable because of the probability of shear-induced latex coagulation, caused by the increased exposure of latex particles to stirring.

As an alternative to a cascade of CSTR trains, a novel continuous reactor with a Couette-Taylor vortex flow (CTVF) has been proposed, which can realize any flow pattern between plug and perfectly mixed flows [361–366]. A continuous Couette-Taylor vortex flow reactor (CCTVFR) consists of two concentric cylinders with the inner cylinder rotating and with the outer cylinder at rest. Figure 29 shows a typical flow pattern caused by the rotation of the inner cylinder.

Nomura et al. [360, 364] first utilized a Couette-Taylor vortex flow reactor (CTVFR) for the continuous emulsion polymerization of St to clarify its char-

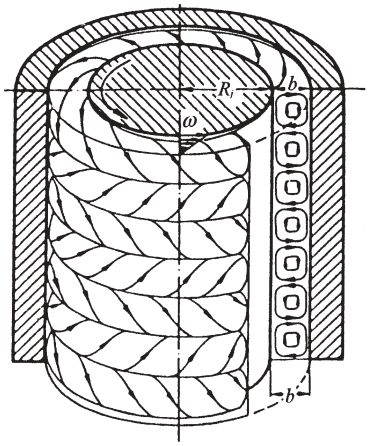

Fig. 29 Taylor vortices between two concentric cylinders (Couette-Taylor vortices): inner cylinder rotating, outer cylinder at rest

acteristics as a continuous emulsion polymerization reactor, and developed a model for the continuous emulsion polymerization of St in a single CCTVFR that incorporated their batch model. The flow pattern is governed by the dimensionless number called the Taylor number, T_a, defined by

$$T_a = \left(\frac{\omega b R_i}{\nu}\right)\left(\frac{b}{R_i}\right) \tag{100}$$

where R_i is the inner cylinder radius, b is the radial clearance between two concentric cylinders, ν is the kinematic viscosity, and ω is the angular velocity of the inner cylinder. When the Taylor number exceeds a certain value between 46 and 60, called the critical Taylor number, T_{ac}, a transition occurs from pure Couette flow to a flow regime in which toroidal vortices are regularly spaced along the cylinder axis, as shown in Fig. 29, which is the so-called "Couette-Taylor vortex flow". They adopted the tank-in-series model that has only one parameter, N, the number of tanks in series, to characterize the deviation of the flow in the CCTVFR from plug flow. The relationship between the number of tanks N and the Taylor number T_a was determined by using a stimulus-response method. Figure 30 shows an interesting example of the monomer con-

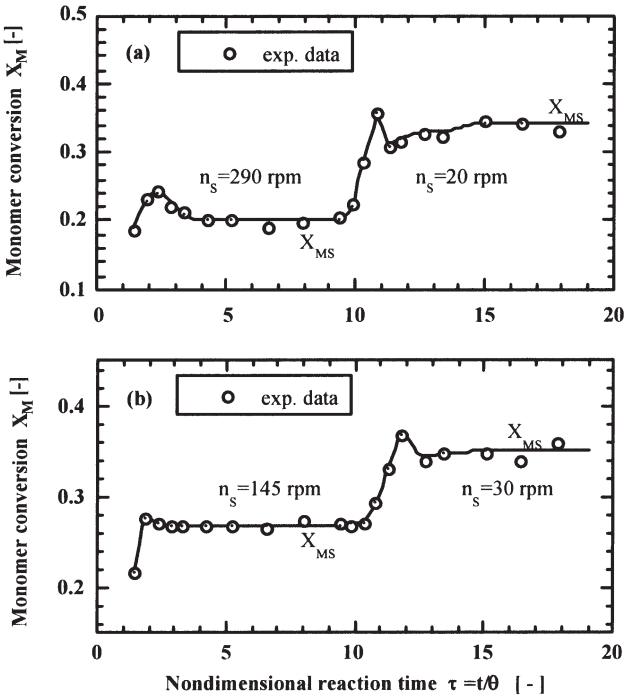

Fig. 30 Effect of rotational speed of inner cylinder on steady-state monomer conversion (S_0 (NaLS)=6.25 g/dm^3-water, I_0 (KPS)=1.25 g/dm^3-water, M_0 (St)=100 g/dm^3-water; 50 °C)

version versus reaction time, where the steady-state monomer conversion was increased from 27 to 35% simply by decreasing the rotational speed of the inner cylinder from 145 to 30 rpm.

This can be explained by the fact that the flow in the CCTVFR became closer to plug flow as the Taylor number was dropped closer to T_{ac}. Therefore, the steady-state particle number and the steady-state monomer conversion could be arbitrarily varied by simply varying the rotational speed of the inner cylinder. Moreover, no oscillations were observed, and the rotational speed of the inner cylinder could be kept low, so that the possibility of shear-induced coagulation could be decreased. Therefore, a CCTVFR with these characteristics is considered to be highly suitable as a pre-reactor for a continuous emulsion polymerization process. In the case of the continuous emulsion polymerization of VAc carried out with the same CCTVFR, however, the situation was quite different [365]. Oscillations in monomer conversion were observed, and almost no appreciable increase in steady-state monomer conversion occurred even when the rotational speed of the inner cylinder was decreased to a value close to T_{ac}. Why the kinetic behavior with VAc is so different to that with St cannot be explained at present.

Ohmura et al. [361, 362] carried out the continuous emulsion polymerization of St and of VAc in a single CCTVFR from the standpoint of controlling the particle size distribution of the latex produced. They also observed no oscillations in the monomer conversion for the St system, but did observe them in the system with VAc. They concluded that a self-sustained oscillation would be useful for controlling the size of latex particles and for raising the monomer conversion. On the other hand, Schmidt et al. [363] studied the continuous emulsion polymerization of *n*-BA in a single CCTVFR. The special flow pattern and residence time distributions of the reactor were investigated at different flow conditions. Both the hydrodynamics and the monomer conversion of the CCTVFR were modeled using computational fluid dynamics simulations. The model predictions were in good agreement with experimental results.

In order to increase the performance and the productivity of the whole continuous reactor system, it has been suggested that a pre-reactor operating as a seed generator (a seeding reactor) should be placed upstream of a reactor train. Even when it is optimized to have the mean residence time as θ_{max}, the steady-state number of polymer particles in a continuous stirred-tank pre-reactor, reaches only 58% of the number produced in an ideal plug flow reactor or in a batch reactor using the same recipe and temperature conditions [163, 335]. Therefore, it is generally desirable to place a pre-reactor with plug flow behavior (such as tubular, PSPC, PPC and CTVF reactors) upstream of the main reactors, because this can produce a similar number of polymer particles to that produced in a batch reactor if properly operated. Instead of incorporating a pre-reactor, Nomura et al. [331, 332] have devised an operational technique called "*split-feed operation*", by which the number of polymer particles produced could be increased to much higher than that in a batch reactor under

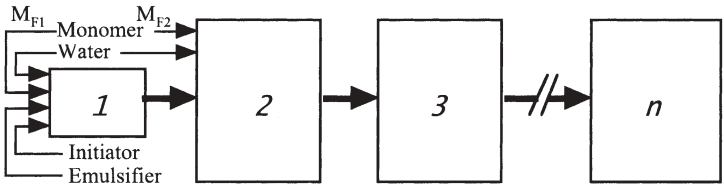

Fig. 31 Schematic diagram of split-feed operation in continuous emulsion polymerization

the same recipe conditions. Figure 31 indicates the general concept of the split-feed operation.

In a batch emulsion polymerization of St, they found that the number of polymer particles produced increased when the amount of initially charged monomer was decreased below a critical value, M_c, as shown in Fig. 32, where the solid line shows the values predicted by

$$N_T = (a_s^3 \rho_p^2 / 36\pi) S_0^3 M_0^{-2} I_0^0 \tag{101}$$

where ρ_p is the polymer density, and S_0, M_0 and I_0 are the emulsifier, monomer and initiator concentrations, respectively.

When a monomer split-feed operation based on the experimental result shown in Fig. 32 was applied, for example, to a continuous tubular pre-reactor with some backmixing, the number of polymer particles increased by about 30% at M_{F1}=0.02 g/cm^3-water, compared to the number produced in a batch reactor, as shown in Fig. 33.

The monomer split-feed operation was also shown to work in a continuous stirred-tank pre-reactor. When certain conditions are fulfilled, the split-feeds

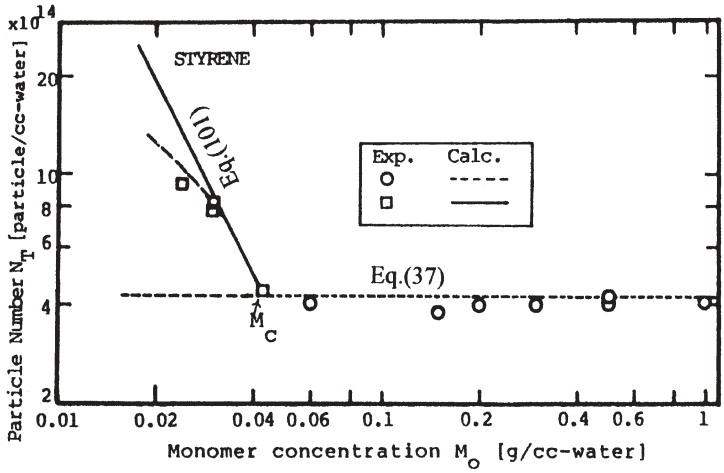

Fig. 32 Effect of lowering the initial monomer concentration on particle formation in the batch emulsion polymerization of St (S_0 (NaLS)=6.25 g/dm^3-water, I_0 (KPS)=1.25 g/dm^3-water, M_0 (St)=variable; 50 °C)

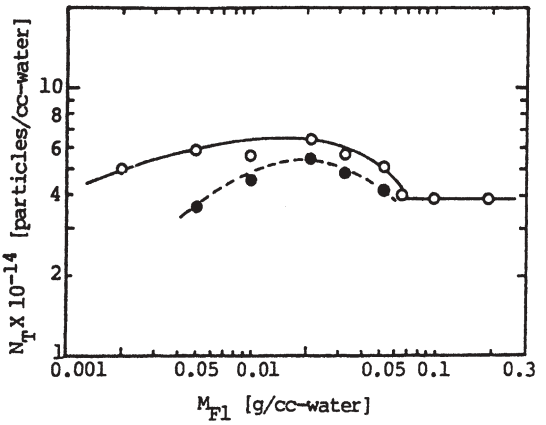

Fig. 33 Effect of monomer concentration M_{F1} fed to the first tubular seeding reactor with back mixing on the number of polymer particles produced (S_0 (NaLS)=6.25 g/dm^3-water, I_0 (KPS)=1.25 g/dm^3-water, M_{F1} (St)=variable; 50 °C. Experimental data: empty circles, particle number observed at t=40 min in a batch reactor; filled circles, steady-state particle number observed in the first tubular seeding reactor operated with mean residence time τ=40 min)

of emulsifier, initiator and water could effectively increase the number of polymer particles produced. The split-feed operation has additional advantages in that the volume of a pre-reactor can be made smaller, and oscillations can be eliminated when it is applied to a continuous stirred-tank pre-reactor. Penlides et al. [333] have also discussed the advantages of the split-feed operation.

Despite the industrial importance, very little work on the kinetics of continuous emulsion copolymerization has been reported. Poehlein et al. [366, 367] carried out the continuous emulsion copolymerization of St-AM and St-AN using a continuous reactor system comprised of a tubular reactor followed by one or two stirred-tank reactors, and developed a steady-state model by employing the kinetic model proposed by Nomura et al. [14] for batch emulsion copolymerization. Their model could predict the latex particle size distribution, average number of radicals per particle, rate of copolymerization, and copolymer composition. They also investigated the continuous emulsion copolymerization of a moderately water-soluble monomer, ethyl acrylate, with a completely water-soluble monomer, methacrylic acid. Several continuous processes involving a tubular reactor and/or a CSTR were designed and utilized so as to produce a latex product with properties similar to the batch product [368, 369]. Nomura et al. [370] carried out the continuous emulsion copolymerization of a sparingly water-soluble monomer, St, with a moderately water-soluble monomer, MMA, in a single CSTR, in order to experimentally elucidate how the kinetic behavior of the continuous emulsion homopolymerization of a sparingly water-soluble monomer changes when it is copolymerized with a moderately water-soluble monomer.

6 Concluding Remarks

The kinetics and mechanisms of particle growth and polymer structure development are comparatively well understood compared to those of particle nucleation. Therefore, the rate of polymerization and the properties of the polymer produced can be (roughly) estimated as long as the number of polymer particles produced is known (for example, in seeded emulsion polymerization). However, the prediction of the number of polymer particles produced is still far from being an established technique. Therefore, further efforts are needed to qualitatively and quantitatively clarify the effects of numerous factors that affect the process of particle formation in order to gain a more quantitative understanding of emulsion polymerization.

References

1. Gilbert RG (1995) Emulsion polymerization: A mechanistic approach. Academic, London
2. Lovell PA, El-Aasser MS (eds)(1997) Emulsion polymerization and emulsion polymers. Wiley, New York
3. Fitch RM (1997) Polymer colloids: A comprehensive introduction. Academic, London
4. Smith WV, Ewart RH (1948) J Chem Phys 16:592
5. Harkins WD (1947) J Am Chem Soc 69:1428
6. Leslie GL, Napper DH, Gilbert RG (1992) Aust J Chem 45:2057
7. Yeliseeva VI (1982) In: Piirma I (ed) Emulsion polymerization. Academic, New York, p 247
8. Gardon JL (1968) J Polym Sci A1 6:623
9. Ugelstad J, Hansen FK (1976) Rubber Chem Technol 49:536
10. Penboss IA, Napper DH, Gilbert RG (1983) J Chem Soc Farad T 1 79:1257
11. Maxwell IA, Morrison BR, Napper DH, Gilbert RG (1991) Macromolecules 24:1629
12. López de Arbina L, Barandiaran MJ, Gugliotta LM, Asua JM (1996) Polymer 37:5907
13. Gardon JL (1968) J Polym Sci A1 6:643
14. Harada M, Nomura M, Kojima H, Eguchi W, Nagata S (1972) J Appl Polym Sci 16:811
15. Hansen FK, Ugelstad J (1978) J Polym Sci Pol Chem 16:1953
16. Hansen FK (1992) ACS Sym Ser 492:12
17. Hansen FK (1993) Chem Eng Sci 48:437
18. Unzueta E, Forcada J (1997) J Appl Polym Sci 66:445
19. Sayer C, Palma M, Giudici R (2002) Ind Eng Chem Res 41:1733
20. Nomura M, Harada M, Eguchi W, Nagata S (1976) ACS Sym Ser 24:102
21. Araujo PHH, de la Cal JC, Asua JM, Pinto JC (2001) Macromol Theor Simul 10:769
22. Herrera-Ordóñez J, Olayo R (2000) J Polym Sci Pol Chem 38:2201
23. Dong Y, Sundberg DC (2002) Macromolecules 35:8185
24. Hawkett BS, Gilbert RG, Napper DH (1980) J Chem Soc Farad T 1 76:1323
25. Colombie D, Sudol ED, El-Aasser MS (2000) Macromolecules 33:4347
26. Marestin C, Guyot A, Claverie J (1998) Macromolecules 31:1686
27. Schoonbrood HAS, German AL, Gilbert RG (1995) Macromolecules 28:34
28. Liotta V, Georgakis C, Sudol ED, El-Aasser MS (1997) Ind Eng Chem Res 36:3252

29. Tauer K, Deckwer R (1998) Acta Polym 49:411
30. Adams ME, Trau M, Gilbert RG, Napper DH, Sangster DF (1988) Aust J Chem 41:1799
31. Penboss IA, Gilbert RG, Napper DH (1986) J Chem Soc Farad T 1 82:2247
32. Kusters JMH, Napper DH, Gilbert RG (1992) Macromolecules 25:7043
33. Wang X, Boya B, Sudol ED, El-Aasser MS (2001) Macromolecules 34:8907
34. Coen EM, Lyons RA, Gilbert RG (1996) Macromolecules 29:5128
35. Cheong IW, Kim JH (1997) Colloid Polym Sci 275:736
36. Vorwerg L, Gilbert RG (2000) Macromolecules 33:6693
37. Leemans L, Jerome R, Teyssie P (1998) Macromolecules 31:5565
38. Ohtsuka Y, Kawaguchi H, Sugi Y (1981) J Appl Polym Sci 26:1637
39. Nomura M, Ichikawa H, Fujita K, Okaya T (1997) J Polym Sci Pol Chem 35:2689
40. Nomura M, Suzuki K (2004) Prog Coll Pol Sci 124:7
41. Ugelstad J, Mørk PC, Dahl P, Rangnes P (1969) J Polym Sci C27:49
42. Nomura M, Harada M, Eguchi W, Nagata S (1971) J Chem Eng Jpn 4:54
43. Nomura M (1982) In: Piirma I (ed) Emulsion polymerization. Academic, New York, p 191
44. Nomura M, Harada M (1981) J Appl Polym Sci 26:17
45. Nomura M, Yamamoto K, Horie I, Fujita K, Harada M (1982) J Appl Polym Sci 27:2483
46. Casey BS, Morrison BR, Maxwell IA, Gilbert RG, Napper DH (1994) J Polym Sci Pol Chem 32:605
47. Nomura M, Kubo M, Fujita K (1983) J Appl Polym Sci 28:2767
48. Adams M, Napper DH, Gilbert RG, Sangster DF (1986) J Chem Soc Farad T 1 82:1979
49. Asua JM, Sudol ED, EL-Aasser MS (1989) J Polym Sci Pol Chem 27:3903
50. Barandiaran MJ, Asua JM (1996) J Polym Sci Pol Chem 34:309
51. Asua JM (1998) Polymer 39:2061
52. Morrison BR, Casey BS, Lacik I, Leslie GL, Sangster DF, Gilbert RG, Napper DH (1994) J Polym Sci Pol Chem 32:631
53. Kim JU, Lee HH (1996) Polymer 37:1941
54. Fang S-J, Wang K, Pan Z-R (2003) Polymer 44:1385
55. López de Arbina L, Barandiaran MJ, Gugliotta LM, Asua JM (1997) Polymer 38:143
56. Forcada J, Asua JM (1990) J Polym Sci Pol Chem 28:987
57. Barudio I, Guillot, Fevotte G (1998) J Polym Sci Pol Chem 36:157
58. Saldivar E, Dafniotis P, Ray WH (1998) J Macromol Sci R M C 38:207
59. Saldiver E, Araujo O, Giudici R, López-Barrón C (2001) J Appl Polym Sci 79:2380
60. Araujo O, Giudici R, Saldivar E, Ray WH (2001) J Appl Polym Sci 79:2360
61. Vega JR, Gugliotta LM, Bielsa RO, Brandolini MC, Meira GR (1997) Ind Eng Chem Res 36:1238
62. Gugliotta LM, Brandolini MC, Vega JR, Iturralde EO, Azum JL, Meira GR (1995) Polym React Eng 3:201
63. Barandiaran MJ, López de Arbina L, de la Cal JC, Gugliotta LM, Asua JM (1995) J Appl Polym Sci 55:231
64. Nomura M, Harada M, Nakagawara K, Eguchi W, Nagata S (1971) J Chem Eng Jpn 4:160
65. Hansen FK, Ugelstad J (1979) Makromol Chem 180:2423
66. Fitch RM (1981) ACS Sym Ser 165:1
67. Hansen FK, Ugelstad J (1982) In: Piirma I (ed) Emulsion polymerization. Academic, New York, p 51
68. Tauer K, Kuhn I (1995) Macromolecules 28:2236
69. Kuhn I, Tauer K (1995) Macromolecules 28:8122
70. Lichti G, Gilbert RG, Napper DH (1983) J Polym Sci Pol Chem 21:269
71. Feeney PJ, Napper DH, Gilbert RG (1984) Macromolecules 17:2520
72. Richards JR, Congalidis JP (1989) J Appl Polym Sci 37:2727

73. Sütterlin N (1980) In: Fitch RM (ed) Polymer colloids II. Plenum, New York, p 583
74. Nomura M, Fujita K (1994) Polym React Eng 2:317
75. Nomura M, Kodani T, Ojima J, Kihara Y, Fujita K (1998) J Polym Sci Pol Chem 36:1919
76. Morrison BR, Maxwell IA, Gilbert RG, Napper DH (1992) In: Daniels ES, Sudol ED, El-Aasser MS (eds) Polymer Latexes. ACS Symp Ser. 492. Am Chem Soc, Washington DC, p 28
77. Sajjadi S, Brooks BW (1999) J Polym Sci Pol Chem 37:3957
78. Nomura M, Sakai H, Kihara Y, Fujita K (2002) J Polym Sci 40:1275
79. Yuan X-Y, Dimonie VL, Sudol ED, Roberts JE, El-Aasser MS (2002) Macromolecules 35:8356
80. Herrera-Ordóñez J, Olayo R (2000) J Polym Sci Pol Chem 38:2219
81. Herrera-Ordóñez J, Olayo R (2001) J Polym Sci Pol Chem 39:2547
82. Varela de la Rosa L, Sudol ED, EL-Aasser MS, Klein A (1996) J Polym Sci Pol Chem 34:461
83. Varela de la Rosa L, Sudol ED, EI-Aasser MS, Klein A (1999) J Polym Sci Pol Chem 37:4066
84. Varela de la Rosa L, Sudol ED, EI-Aasser MS, Klein A (1999) J Polym Sci Pol Chem 37:4073
85. Nomura M, Satpathy US, Kouno Y, Fujita K (1988) J Polym Sci Pol Lett 26:385
86. Nomura M, Takahashi K, Fujita K (1990) Makromol Chem–M Symp 35/36:13
87. Chern C-S, Lin C-H (1998) Polymer 40:139
88. Chern C-S, Lin C-H (2000) Polymer 41:4473
89. Wang Z, Paine AJ, Rudin A (1995) J Polym Sci Pol Chem 33:1597
90. Morrison BR, Gilbert RG (1995) Macromol Symp 92:13
91. Coen EM, Gilbert RG, Morrison BR, Leube H, Peach S (1998) Polymer 39:7099
92. Prescott SW, Fellows CM, Gilbert RG (2002) Macromol Theor Simul 11:163
93. Butucea V, Sarbu A, Georgescu C (1998) Angew Makromol Chem 255:37
94. Cheong I-W, Kim J-H (1998) Macromol Theor Simul 7:49
95. Sajjadi S (2000) J Polym Sci Pol Chem 38:3612
96. Sajjadi S (2001) J Polym Sci Pol Chem 39:3940
97. Nomura M, Fujita K (1993) Polym Int 30:483
98. Sajjadi S (2002) J Polym Sci Pol Chem 40:1652
99. Ozdeger E, Sudol ED, El-Aasser MS, Klein A (1997) J Polym Sci Pol Chem 35:3813
100. Ozdeger E, Sudol ED, El-Aasser MS, Klein A (1997) J Polym Sci Pol Chem 35:3827
101. Ozdeger E, Sudol ED, El-Aasser MS, Klein A (1997) J Polym Sci Pol Chem 35:3837
102. Lin S-Y, Capek I, Hsu T-J, Chern C-S (1999) J Polym Sci Pol Chem 37:4422
103. Unzueta E, Forcada J (1995) Polymer 36:4301
104. Chen L-J, Lin S-Y, Chern C-S, Wu S-C (1997) Colloid Surface A 122:161
105. Lin S-Y, Capek I, Hsu T-J, Chern C-S (2000) Polym J 32:932
106. Colombie D, Sudol ED, El-Aasser MS (2000) Macromolecules 33:7283
107. Asua JM, Schoonbrood HAS (1998) Acta Polym 49:671
108. Amalvy JI, Unzue MJ, Schoonbrood HAS, Asua JM (1998) Macromolecules 31:5631
109. Wang X, Sudol ED, El-Aasser MS (2001) J Polym Sci Pol Chem 39:3093
110. Wang X, Sudol ED, El-Aasser MS (2001) Macromolecules 34:7715
111. Cochin D, Laschewsky A, Nallet F (1997) Macromolecules 30:2278
112. Ayoub MMH, Nasr HE, Rozik NN (1998) J Macromol Sci Pure 35:1415
113. Ayoub MMH (1998) J Elastom Plast 30:207
114. Wang X, Sudol ED, El-Aasser MS (2001) Langmuir 17:6865
115. Kato S, Nomura M (1999) Colloid Surface A 153:127
116. Cheong I-W, Nomura M, Kim J-H (2001) Macromol Chem Phys 202:2454

117. Piirma I (1993) Polymer surfactants (Surfactant Science Series No 42). Marcel Dekker, New York
118. Capek I (2002) Adv Colloid Interfac 99:77
119. O'Toole JT (1965) J Appl Polym Sci 9:1291
120. Ugelstad J, Mørk PC, Aasen JO (1967) J Polym Sci A1 5:2281
121. Stockmayer WH (1957) J Polym Sci 24:314
122. (a) Nomura M, Fujita K (1985) Makromol Chem Suppl 10/11:25, (b) Nomura M (1987) Kobunshi Kagaku 36:680
123. Sakai H, Kihara Y, Fujita K, Kodani T, Nomura M (2001) J Polym Sci Pol Chem 39:1005
124. Asua JM, Adams ME, Sudol ED (1990) J Appl Polym Sci 39:1183
125. Mendoza J, de la Cal JC, Asua JM (2000) J Polym Sci Pol Chem 38:4490
126. Kiparissides C, Achilias CDS, Frantzikinakis CE (2002) Ind Eng Chem Res 41:3097
127. de la Cal JC, Asua JM (2001) J Polym Sci Pol Chem l39:585
128. Gilmore CM, Poehlein GW, Schork FJ (1993) J Appl Polym Sci 48:1449
129. Gilmore CM, Poehlein GW, Schork FJ (1993) J Appl Polym Sci 48:1461
130. Budhlall BM, Sudol ED, Dimonie VL, Klein A, El-Aasser MS (2001) J Polym Sci Pol Chem 39:3633
131. Shaffie KA, Moustafa AB, Mohamed ES, Badran AS (1997) J Polym Sci Pol Chem 35:3141
132. Bruyn HD, Gilbert RG, Ballard MJ (1996) Macromolecules 29:8666
133. Chern C-S, Poehlein GW (1987) J Appl Polym Sci 33:2117
134. Bruyn HD, Miller CM, Bassett DR, Gilbert RG (2002) Macromolecules 35:8371
135. Matsumoto A, Kodama K, Aota H, Capek I (1999) Eur Polym J 35:1509
136. Ballard MJ, Napper DH, Gilbert RG (1981) J Polym Sci Pol Chem 19:939
137. Nomura M, Kubo M, Fujita K (1981) Mem Fac Eng Fukui Univ 29:167
138. Storti G, Carra S, Morbidelli M, Vita G (1989) J Appl Polym Sci 37:2443
139. Tobita H, Hamielec AE (1989) Macromolecules 22:3098
140. Nomura M, Horie I, Kubo M, Fujita K (1989) J Appl Polym Sci 37:1029
141. Chen S-A, Wu K-W (1988) J Polym Sci Pol Chem 26:1487
142. Giannetti E (1989) Macromolecules 22:2094
143. Saldivar E, Ray WH (1997) Ind Eng Chem Res 36:1322
144. Dube MA, Penlidis A, Mutha RK, Cluett WR (1996) Ind Eng Chem Res 35:4434
145. Martinet F, Guillot J (1999) J Appl Polym Sci 72:1627
146. Vicente M, Leiza JR, Asua JM (2001) AIChE J 47:1594
147. Vega JR, Gugliotta LM, Meira GR (2002) Polym React Eng 10:59
148. Shoaf GL, Poehlein GW (1991) J Appl Polym Sci 42:1213
149. Yang B-Z, Chen L-W, Chiu W-Y (1997) Polym J 29:744
150. Yang B-Z, Chen L-W, Chiu W-Y (1997) Polym J 29:737
151. Slawinski M, Schellekens MAJ, Meuldijk J, Herk AMV, German AL (2000) J Appl Polym Sci 76:1186
152. Wang PH, Pan C-Y (2001) Colloid Polym Sci 279:98
153. Santos AMD, Mckenna TF, Guillot J (1997) J Appl Polym Sci 65:2343
154. Yan C, Cheng S, Feng L (1999) J Polym Sci Pol Chem 37:2649
155. Henton DE, Powell C, Reim RE (1997) J Appl Polym Sci 64:591
156. Xu Z, Yi C, Cheng S, Zhang J (1997) J Appl Polym Sci 66:1
157. Fang S-J, Fujimoto K, Kondo S, Shiraki K, Kawaguchi H (2000) Colloid Polym Sci 278:864
158. Kostov GK, Petrov PC (1994) J Polym Sci Pol Chem 32:2229
159. Petrov PC, Kostov GK (1994) J Polym Sci Pol Chem 32:2235
160. Noel LFJ, Altveer JLV, Timmermans MDF, German AL (1996) J Polym Sci Pol Chem 34:1763

161. Urretabizkaia A, Asua JM (1994) J Polym Sci Pol Chem 32:1761
162. Ge X, Ye Q, Xu X, Chu G, Zhang Z (1998) J Appl Polym Sci 67:1005
163. Nomura M, Kojima H, Harada M, Eguchi W, Nagata S (1971) J Appl Polym Sci 15:675
164. Morton M, Kaizerman S, Altier MW (1954) J Colloid Sci 9:300
165. Gardon JL (1968) J Polym Sci A1 6:2859
166. Maxwell IA, Kurja J, Doremaele GHV, German AL, Morrison BR (1992) Makromol Chem 193:2049
167. Antonietti M, Kasper H, Tauer K (1996) Langmuir 12:6211
168. Vanzo E, Marchessault RH, Stannett V (1965) J Colloid Sci 20:62
169. Ugelstad J, Mørk PC, Mfutakamba HR, Soleimany E, Nordhuus I, Schmid R, Berge A, Ellingsen T, Aune O, Nustad K (1983) In: Pohelein GW, Ottewill RH, Goodwin JW (eds) Science and technology of polymer colloids, vol 1 (NATO ASI Ser E:67). Martinus Nijhoff, Boston, MA, p 51
170. Maxwell IA, Kurja J, van Doremaele GHJ, German AL (1992) Makromol Chem 193:2065
171. Schoonbrood HAS, German AL (1994) Macromol Rapid Commun 15:259
172. Noël LFJ, Maxwell IA, German AL (1993) Macromolecules 26:2911
173. Schoonbrood HAS, Boom MATVD, German AL, Hutovic J (1994) J Polym Sci Pol Chem 32:2311
174. Noël LFJ, van Zon JMAM, Maxwell IA, German AL (1994) J Polym Sci Pol Chem 32:1009
175. Gugliotta LM, Arzamendi G, Asua JM (1995) J Appl Polym Sci 55:1017
176. Karlsson O, Wesslen B (1998) J Appl Polym Sci 70:2041
177. Mathey P, Guillot J (1991) Polymer 32:934
178. Nomura M, Liu X, Ishitani K, Fujita K (1994) J Polym Sci Pol Phys 32:2491
179. Liu X, Nomura M, Fujita K (1997) J Appl Polym Sci 64:931
180. Liu X, Nomura M, Liu Y-H, Ishitani K, Fujita K (1997) Ind Eng Chem Res 36:1218
181. Aerdts AM, Boei MWA, German AL (1993) Polymer 34:574
182. Said ZFM, Fataftah ZA (1996) Polym Int 40:307
183. Tognacci R, Storti G, Bertucco A (1996) J Appl Polym Sci 62:2341
184. Varela de la Rosa L, Sudol ED, EI-Aasser MS, Klein A (1999) J Polym Sci Pol Chem 37:4054
185. Cheong I-W, Kim J-H (1999) Colloid Surface A 153:137
186. BenAmor S, Colombie D, McKenna T (2002) Ind Eng Chem Res 41:4233
187. Tauer K, Muller H, Schellenberg C, Rosengarten L (1999) Colloid Surfuce A 153:143
188. López de Arbina L, Gugliotta LM, Barandiaran MJ, Asua JM (1998) Polymer 39:4047
189. de Buruaga IS, Arotcarena M, Armitage PD, Gugliotta LM, Leiza JR, Asua JM (1996) Chem Eng Sci 51:781
190. de Buruaga IS, Echevarria A, Armitage PD, de la Cal JC, Leiza JR, Asua JM (1997) AIChE J 43:1069
191. Gugliotta LM, Leiza JR, Arotcarena M, Armitage PD, Asua JM (1995) Ind Eng Chem Res 34:3899
192. Nomura M, Ashizawa N (1998) US Patent 5 762 879, assigned to Todoroki Sangyo Co, Fukui, Japan
193. Breitenbach VJW, Edelhauser H (1961) Macromol Chem 44–47:196
194. van der Hoff BME (1960) J Polym Sci 48:175
195. Al-Shahib WAG, Dunn AS (1980) Polymer 21:429
196. Barton J, Karpatyova A (1987) Makromol Chem 188:693
197. Il'menev PY, Litvinenko GI, Kaminskii VA, Gritskova IA (1988) Polym Sci USSR 30:826
198. Nomura M, Fujita K (1989) Makromol Chem Rapid Commun 10:581
199. Nomura M, Yamada A, Fujita S, Sugimoto A, Ikoma J, Fujita K (1991) J Polym Sci Pol Chem 29:987

200. Nomura M, Ikoma J, Fujita K (1992) ACS Sym Ser 492:55
201. Nomura M, Fujita K (1992) DECHEMA Monogr 127:359
202. Nomura M, Ikoma J, Fujita K (1993) J Polym Sci Pol Chem 31:2103
203. Asua JM, Rodriguez VS, Sudol ED, El-Aasser MS (1989) J Polym Sci Pol Chem 27:3569
204. Alduncin JA, Forcada J, Barandiaran MJ, Asua JM (1991) J Polym Sci Pol Chem 29:1265
205. Vaskova V, Renoux D, Bernard M, Selb J, Candau F (1995) Polym Advan Technol 6:441
206. Mørk PC (1995) J Polym Sci Pol Chem 33:2305
207. Mørk PC, Ugelstad J, Aasen JO (1995) J Polym Sci Pol Chem 33:1759
208. Mørk PC, Makame Y (1997) J Polym Sci Pol Chem 35:2347
209. Suzuki K, Goto A, Takayama M, Muramatsu A, Nomura M (2000) Macromol Symp 155:99
210. Nomura M, Suzuki K (1997) Macromol Chem Phys 198:3025
211. Capek I (2001) Adv Colloid Interfac 91:295
212. Biggs S, Grieser F (1995) Macromolecules 28:4877
213. Ooi SK, Biggs S (2000) Ultrason Sonochem 7:125
214. Cooper C, Grieser F, Biggs S (1996) J Colloid Interf Sci 184:52
215. Bradley M, Grieser F (2002) J Colloid Interf Sci 251:78
216. Chou HCJ, Stoffer JO (1999) J Appl Polym Sci 72:797
217. Chou HCJ, Stoffer JO (1999) J Appl Polym Sci 72:827
218. Liao Y, Wang Q, Xia H, Xu X, Baxter SM, Slone RV, Wu S, Swift G, Westmoreland DG (2001) J Polym Sci Pol Chem 39:3356
219. Xia H, Wang Q, Liao Y, Xu X, Baxter SM, Slone RV, Wu S, Swift G, Westmoreland DG (2002) Ultrason Sonochem 9:151
220. Nomura M, Harada M, Eguchi W, Nagata S (1972) J Appl Polym Sci 16:835
221. Penlidis A, Macgegor JF, Hamielec AE (1988) J Appl Polym Sci 35:2023
222. Cunningham MF, Geramita K, Ma JW (2000) Polymer 41:5385
223. Bruyn HD, Gilbert RG, Hawkett BS (2000) Polymer 41:8633
224. Kokthoff IM, Harris WE (1947) J Polym Sci 2:49
225. Whang BCY, Lichti G, Gilbert RG, Napper DH (1980) J Polym Sci Pol Lett 18:711
226. Nomura M, Minamino Y, Fujita K, Harada M (1982) J Polym Sci Pol Chem 20:1261
227. Lichti G, Sangster DF (1982) J Chem Soc Farad T 1 78:2129
228. Maxwell IA, Morrison BR, Napper DH, Gilbert RG (1992) Makromol Chem 193:303
229. Weerts PA, van der Loos JLM, German AL (1991) Makromol Chem 192:2009
230. Huo BP, Campbell JD, Penlidis A, Macgregor JF, Hamielec AE (1987) J Appl Polym Sci 35:2009
231. Kemmere MF, Mayer MJJ, Meuldijk J, Drinkenburg AAH (1999) J Appl Polym Sci 71:2419
232. Barton J, Juranicova V (1991) Makromol Chem Rapid Commun 12:669
233. Echevarria A, Leiza JR, de la Cal JC, Asua JM (1998) AIChE J 44:1667
234. Salazar A, Gugliotta LM, Vega JR, Meira GR (1998) Ind Eng Chem Res 37:3582
235. Sayer C, Lim EL, Pinto JC, Arzamendi G, Asua LM (2000) J Polym Sci Pol Chem 38:1100
236. Sayer C, Lima EL, Pinto JC, Arzamendi G, Asua JM (2000) J Polym Sci Pol Chem 38:367
237. Plessis C, Arzamendi G, Leiza JR, Alberdi JM, Schoonbrood HAS, Charmot D, Asua JM (2001) J Polym Sci Pol Chem 39:1106
238. Gugliotta LM, Salazar A, Vega JR, Meira GR (2001) Polymer 42:2719
239. Nomura M, Suzuki H, Tokunaga H, Fujita K (1994) J Appl Polym Sci 51:21
240. Okaya T, Suzuki A, Kikuchi K (2000) Macromol Symp 150:143
241. Bataille P, Dalpe J-F, Dubuc F, Lamoureux L (1990) J Appl Polym Sci 39:1815
242. Shunmukham SR, Hallenbeck VL, Guile RL (1951) J Polym Sci 6:691
243. Schoot CJ, Bakker J, Klaassens KH (1951) J Polym Sci 7:657
244. Evans CP, Hay PM, Marker L, Murray RW, Sweeting OJ (1961) J Appl Polym Sci 5:39

245. Omi S, Shiraishi Y, Sato H, Kubota H (1969) J Chem Eng Jpn 2:64
246. Weerts PA, van der Loos JLM, German AL (1991) Makromol Chem 192:1993
247. Arai K, Arai M, Iwasaki S, Saito S (1981) J Polym Sci Pol Chem 19:1203
248. Kim CU, Lee JM, Ihm SK (1999) J Appl Polym Sci 73:777
249. Ozdeger E, Sudol ED, El-Aasser MS, Klein A (1998) J Appl Polym Sci 69:2277
250. Brooks BW (1971) Brit Polym J 3:269
251. Zubitur M, Asua JM (2001) J Appl Polym Sci 80:841
252. Soares JBP, Hamielec AE (1997) In: Asua JM (ed) Polymeric dispersions (NATO ASI Ser E:335). Kluwer Academic, London, p 289
253. Cunningham MF, Ma JW (2000) J Appl Polym Sci 78:217
254. Ma JW, Cunningham MF (2000) Macromol Symp 150:85
255. Zubitur M, Mendoza J, de la Cal JC, Asua JM (2000) Macromol Symp 150:13
256. Rimmer S, Tattersall P (1999) Polymer 40:5729
257. Rimmer S (2000) Macromol Symp 150:149
258. Leyrer RJ, Machtle W (2000) Macromol Chem Phys 201:1235
259. Lau W (1994) US Patent 5 521 266, assigned to Rohm and Haas Co, Philadelphia, PA, USA
260. Vanderhoff JW (1981) ACS Sym Ser 165:199
261. Lowry V, El-Aasser MS, Vanderhoff JW, Klein A (1984) J Appl Polym Sci 29:3925
262. Matejicek A, Ditl P, Pivonkova A, Kaska J, Formanek L (1988) J Appl Polym Sci 35:583
263. Tobita H, Takada Y, Nomura M (1994) Macromolecules 27:3804
264. Tobita H, Takada Y, Nomura M (1995) J Polym Sci Pol Phys 33:441
265. Tobita H (1995) Macromolecules 28:5128
266. Tobita H (1994) Polymer 35:3023
267. Tobita H (1994) Polymer 35:3032
268. Tobita H (1997) J Polym Sci Pol Phys 35:1515
269. Tobita H, Nomura M (1999) Colloid Surface A 153:119
270. Tobita H, Yamamoto K (1994) Macromolecules 27:3389
271. Tobita H, Uemura Y (1996) J Polym Sci Pol Phys 34:1403
272. Tobita H, Yoshihara Y (1996) J Polym Sci Pol Phys 34:1415
273. Tobita H (1995) Acta Polym 46:185
274. Min KW, Ray HW (1974) J Macromol Sci R M C 11:177
275. Lin CC, Chiu WY (1979) J Appl Polym Sci 23:2049
276. Lichti G, Gilbert RG, Napper DH (1980) J Polym Sci Pol Chem 18:1297
277. Lichti G, Gilbert RG, Napper DH (1982) In: Piirma I (ed) Emulsion polymerization. Academic, New York, p 93
278. Katz S, Shinnar R, Saidel GM (1969) Adv Chem Ser 91:145
279. Giannetti E, Storti G, Morbidelli M (1988) J Polym Sci Pol Chem 26:1985
280. Storti G, Polotti G, Cociani M, Morbidelli M (1992) J Polym Sci Pol Chem 30:731
281. Ghielmi A, Storti G, Morbidelli M (1998) Macromolecules 31:7172
282. Benson SW, North AM (1962) Am Chem Soc 84:935
283. Ito K (1974) J Polym Sci Pol Chem 12:1991
284. Mahabadi HK (1985) Macromolecules 18:1319
285. Olaj OF, Zifferer G, Gleizner G (1986) Makromol Chem 187:977
286. Russell GT, Gilbert RG, Napper DH (1992) Macromolecules 25:2459
287. O'Shaughnessy B, Yu J (1994) Macromolecules 27:5067
288. Buback M, Egorov M, Kaminsky V (1999) Macromol Theor Simul 8:520
289. Russell GT (1994) Macromol Theor Simul 3:439
290. Clay PA, Gilbert RG (1995) Macromolecules 28:552
291. Wulkow M (1996) Macromol Theor Simul 5:393

292. Tobita H (1995) Macromolecules 28:5119
293. Olaj OF, Kauffmann HF, Breitenbach JB (1977) Makromol Chem 178:2707
294. Mayo FR (1943) J Am Chem Soc 65:2324
295. Mayo FR, Gregg RA, Matheson MS (1951) J Am Chem Soc 73:1691
296. Christie DI, Gilbert RG (1996) Macromol Chem Phys 197:403
297. Buback M, Gilbert RG, Russell GT, Hill DJT, Moad G, O'Driscoll KF, Shen J, Winnik MA (1992) J Polym Sci Pol Chem 30:851
298. Tobita H, Shiozaki H (2001) Macromol Theor Simul 10:676
299. Morton M, Salatiello PP (1951) J Polym Sci 6:225
300. Britton D, Heatley F, Lovell PA (1998) Macromolecules 31:2828
301. Tobita H (1993) Polym React Eng 1:357
302. Tobita H, Saito S (1999) Macromol Theor Simul 8:513
303. Tobita H, Hamashima N (2000) J Polym Sci Pol Phys 38:2009
304. Tobita H, Hamashima N (2000) Macromol Theor Simul 9:453
305. Tobita H (2001) J Polym Sci Pol Phys 39:2960
306. Tobita H, Kawai H (2002) E-Polymers 048
307. Starkweather WH Jr, Han MC (1992) J Polym Sci Pol Chem 30:2709
308. Senrui S, Suwa T, Takehisa M (1974) J Polym Sci Pol Chem 12:93
309. Senrui S, Suwa T, Takehisa M (1974) J Polym Sci Pol Chem 12:105
310. Tobita H (2002) J Polym Sci Pol Chem 40:3426
311. Tobita H (2003) Bimodal molecular weight distribution formed in emulsion polymerization with long-chain branching. Polym React Eng 11:855
312. Barabasi A-L, Albert R (1999) Science 286:509
313. Tobita H (2004) Scale-free power-law distribution of emulsion-polymerized nonlinear polymers: Free-radical polymerization with chain transfer to polymer. Macromolecules 37:585
314. Friis N, Goosney D, Wright JD, Hamielec AE (1974) J Appl Polym Sci 18:1247
315. Friis N, Hamielec AE (1975) J Appl Polym Sci 19:97
316. Tobita H (1992) Macromolecules 25:2671
317. Tobita H, Kimura K, Fujita K, Nomura M (1993) Polymer 34:2569
318. Flory PJ (1953) Principles of polymer chemistry. Cornell University Press, Ithaca, NY
319. Tobita H, Hamielec AE (1989) In: Reichert K-H, Geiseler W (eds) Polymer reaction engineering. VCH, Weinheim, Germany, p 43
320. Ding ZY, Ma S, Kriz D, Aklonis JJ, Salovey R (1992) J Polym Sci Pol Phys 30:189
321. Baker WO (1949) Ind Eng Chem 41:511
322. Obrecht W, Seitz U, Funke W (1976) ACS Sym Ser 24:92
323. Nakamura K, Imoto A, Aota H, Matsumoto A (1994) The 8th Polymeric Microsphere Symposium, Fukui, Japan, p 37
324. Matsumoto A, Mori Y, Takahashi S, Aota H (1995) Netsukokasei-Jushi (J Thermoset Plast Jpn) 16:131
325. Matsumoto A, Kodama K, Mori Y, Aota H (1998) Pure Appl Chem A35:1459
326. Tobita H, Kumagai M, Aoyagi N (2000) Polymer 41:481
327. Tobita H, Aoyagi N, Takamura S (2001) Polymer 421:7583
328. Hamielec AE, Tobita H (1992) In: Ulmann's encyclopedia of industrial chemistry, vol A21. VCH, Weinheim, Germany, p 305
329. Pohelein G (1997) In: Lovell PA, El-Aasser MS (eds) Emulsion polymerization and emulsion polymers. Wiley, New York, p 277
330. Gershberg DB, Longfield JE (1961) Symp Polym Kinetics and Catalyst Systems, Preprint 10, 45th AIChE Meeting, New York
331. Nomura M (1981) ACS Sym Ser 165:121

332. Nomura M (1986) In: Reichert K-H, Geisler W (eds) Polymer eeaction engineering. Hüthig & Wepf, Basel, p 41
333. Penlidis A, MacGregor JF, Hamielec AE (1989) Chem Eng Sci 44:273
334. Poehlein GW, Dougherty DJ (1977) Rubber Chem Technol 50:601
335. Omi S, Ueda T, Kubota H (1969) J Chem Eng Jpn 2:193
336. Degraff AW, Poehlein GW (1971) J Polym Sci A2 9:1955
337. Gerrens H, Kuchner K (1970) Brit Polym J 2:18
338. Gerrens H, Kuchner K, Ley G (1971) Chem Ing Tech 43:693
339. Gregor L, Gerrens H (1974) Macromol Chem 175:563
340. Nomura M, Sasaki S, Xue W, Fujita K (2002) J Appl Polym Sci 86:2748
341. Kiparissides C, MacGregor JF, Hamielec AE (1979) J Appl Polym Sci 23:401
342. Rawlings JB, Ray WH (1988) Polym Eng Sci 28:237
343. Rawlings JB, Ray WH (1988) Polym Eng Sci 28:257
344. Tauer K, Muller I (1995) DECHEMA Monogr 131:95
345. Greens RK, Gonzalez RA, Poehlein GW (1976) ACS Sym Ser 24:341
346. Feldon M, McCann RF, Laundrie RW (1953) India Rubber World 128:51
347. Geddes K (1983) Chem Ind 21:223
348. Geddes KR (1989) Brit Polym J 21:443
349. Rollin AL, Patterson I, Huneault R, Bataille P (1977) Can J Chem Eng 55:565
350. Iabbadene A, Bataille P (1994) J Appl Polym Sci 51:503
351. Lee D-Y, Kuo J-F, Wang J-H, Chen C-Y (1990) Polym Eng Sci 30:187
352. Lee D-Y, Wang J-H, Kuo J-F (1992) Polym Eng Sci 32:198
353. Abad C, de la Cal JC, Asua JM (1995) Polymer 36:4293
354. Abad C, de la Cal JC, Asua JM (1994) Chem Eng Sci 49:5025
355. Abad C, de la Cal JC, Asua JM (1995) J Appl Polym Sci 56:419
356. Abad C, de la Cal JC, Asua JM (1995) DECHEMA Monogr 131:87
357. Paquet DA Jr, Ray WH (1994) AIChE J 40:73
358. Mayer MJJ, Meuldijk J, Thoenes D (1996) Chem Eng Sci 51:3441
359. Scholetens CA, Meuleijk J, Drinkenburg AAH (2001) Chem Eng Sci 56:955
360. Imamura T, Saito K, Ishikura S, Nomura M (1993) Polym Int 30:203
361. Kataoka K, Ohmura N, Kouzu M, Okubo Y (1995) Chem Eng Sci 50:1409
362. Ohmura N, Kataoka K, Watanabe S, Okubo M (1998) Chem Eng Sci 53:2129
363. Schmidt W, Kossak S, Langenbuch J, Moritz H-U, Herrmann C, Kremeskötter J (1998) DECHEMA Monogr 134:509
364. Wei X, Takahashi H, Sato S, Nomura M (2001) J Appl Polym Sci 80:1931
365. Xue W, Yoshikawa K, Oshima A, Nomura M (2002) J Appl Polym Sci 86:2755
366. Mead RN, Poehlein GW (1988) Ind Eng Chem Res 27:2283
367. Mead RN, Poehlein GW (1989) Ind Eng Chem Res 28:51
368. Shoaf GL, Poehlein GW (1989) Polym Plast Tech Eng 28:289
369. Poehlein GW (1995) Macromol Symp 92:179
370. Fang S-J, Xue W, Nomura M (2003) Polym React Eng 11:815

Received: February 2004

Adv Polym Sci (2005) 175: 129–255
DOI 10.1007/b100115

Miniemulsion Polymerization

F. Joseph Schork (✉)[1] · Yingwu Luo[2] · Wilfred Smulders[1] · James P. Russum[1] · Alessandro Butté[3] · Kevin Fontenot[4]

[1] School of Chemical and Biomolecular Engineering, Georgia Insitute of Technology, Atlanta Georgia30332–0100 USA
joseph.schork@chbe.gatech.edu, wilfred.smulders@chbe.gatech.edu, james.russum@chbe.gatech.edu

[2] The State Key Laboratory of Polymer Reaction Engineering, College of Material and Chemical Engineering, Zhejiang University, Hangzhou, 310027 P. R. China
yingwu.luo@cmsce.zju.edu.cn

[3] Prof. M. Morbidelli Group, ETH Zürich, Institute for Chemical- and Bioengineering, ETH Hönggerberg/HCI F 135, 8093 Zürich, Switzerland
butte@tech.chem.ethz.ch

[4] Eastman Chemical Company, P.O. Box 1972, Kingsport TN 37662, USA
fontenot@eastman.com

Abstract The subject of miniemulsion polymerization is reviewed. The approach taken is one that combines a review of the technology with historical and tutorial aspects. Rather than developing an absolutely exhaustive review, a tutorial approach has been taken, emphasizing the critical features and advantages of miniemulsion polymerization. In keeping with this tutorial approach, a discussion of conventional emulsion polymerization is included in order to be able to compare and contrast miniemulsion polymerization and conventional emulsion polymerization later in the review. Areas where miniemulsion polymerization has been adopted commercially, or where it is likely to be adopted are highlighted.

Keywords Miniemulsion · Polymerization · Emulsion · Free radical · Colloid

Abbreviations and Symbols

AMBN	2,2′-azobis(2-methylbutyronitrile)
ATRP	atom transfer radical polymerization
CA	cetyl alcohol
CMC	critical micelle concentration
CSA	camphorsulfonic acid
CSTR	continuous stirred tank reactor
CTA	chain transfer agent
CTAB	cetyltrimethylammonium bromide
DDM	dodecyl mertcaptan
DLS	dynamic light scattering
DOM	dioctyl maleate
DPPH	diphenylpicrylhydrazol
EHA	2-ethylhexyl acrylate
F_i	copolymer composition, monomer *i*
f_i	monomer composition, monomer *i*
GPC	gel permeation chromatography
HD	hexadecane
K_{eq}	equilibrium constant
k_p	propagation rate constant
KPS	potassium persulfate
LPO	lauroly peroxide
MAETAC	2-(methacryloyoxy)ethyl]tri-methyl ammonium chloride
M_{aq}	molarity, aqueous phase
m_{ij}	ratio of molar size, *i* to *j*
mM	millimolar
MMA	methyl methacrylate
$[M_p]$	concentration of monomer in the particle
MWD	molecular weight distribution
$\bar{n}$	average number of radicals per particle
N	number of particles per liter
N_A	Avogadro's number

nm	nanometer
NMA	*n*-methylol acrylamide
NMCRP	nitroxide-mediated controlled radical polymerization
NMR	nuclear magnetic resonance spectroscopy
PFR	plug flow reactor
pMS	paramethyl styrene
PS	polystyrene
PSD	particle size distribution
PST	polystyrene
PVA	polyvinyl alcohol
PVAc	polyvinyl acetate
QSSA	quasi-steady state approximation
r	radius
r_i	reactivity ratio
R	gas constant
RAFT	reversible addition-fragmentation chain transfer
R_p	rate of polymerization
RX	organic halide
SE	Smith Ewart
SPS	sodium persulfate
T	temperature
T_g	glass transition temperature
$\bar{V}_i$	partial molar volume of i
VAc	vinyl acetate
VD	vinyl *n*-decanoate
VEH	vinyl 2-ethylhexanoate
VEOVA	vinyl neo-decanoate (vinyl versatate)
VH	vinyl hexanoate
VS	vinyl stearate
W	Fuchs stability ratio
X	halogen
χ_{ij}	Flory Huggins interaction parameter
$\Delta\bar{G}_i$	partial molar free energy or phase i
γ	interfacial tension
φ_i	volume fraction of component i
μ	viscosity
μ_i	chemical potential of component i
µm	micron
%wt	percent by weight

1 Introduction

Over the past 25 years, miniemulsion polymerization has grown from being the subject of a single paper to being the focus of a great deal of academic and industrial research. During that time, some products have been commercialized based on this technology, and in the next few years a number of new

commercializations of the technology are expected to take place. This text attempts to trace the development of miniemulsion polymerization, the physics and chemistry behind it, its unique features, and its potential for future applications. It is not an exhaustive bibliography of published work, but it does cite significant and/or representative papers. Previous reviews of this field can be found in [1–3].

1.1 Dispersed-Phase Polymerization

Free radical polymerization may be carried out in various media. Bulk polymerization is the simplest, but while the reactants (monomers) are most often liquid, the product (polymer) is solid. This leads to problems when removing the polymer from the reactor. In addition, since most free radical polymerizations are highly exothermic, the high viscosity of the monomer/polymer mix inhibits the removal of the heat of reaction. Solution polymerization will reduce, to some extent, the viscosity of the polymerizing mass, but it brings with it the environmental and health issues of organic solvents. In addition, the solvent reduces the monomer concentration, and hence the rate of polymerization. Finally, recovery and recycling of the solvent can add substantially to the cost of the process. Nevertheless, solution polymerization of vinylic monomers is used in a number of commercial processes.

An alternative to solution polymerization is the whole realm of *dispersed-phase polymerization*. In this class of processes, the liquid monomer is dispersed in a second, continuous phase, usually water. As the monomer polymerizes, the viscosity of the dispersion remains low, aiding the removal of the heat of polymerization. If the dispersed phase is water, the high thermal conductivity provides a very effective heat transfer medium. The high specific heat and large latent heat of vaporization provide a large safety margin in the event of a runaway polymerization. In addition, water is plentiful, nontoxic, environmentally friendly, and inexpensive.

If an oil-soluble monomer is dispersed in a continuous aqueous phase without the use of surfactants, *suspension polymerization* results. The viscosity of the resulting suspension will remain essentially constant over the course of the polymerization. Oil-soluble free radical initiators are used to effect polymerization. The monomer is dispersed into beads by the action of an agitator. Since little or no surfactant is used, no emulsification takes place, and, if the agitation is stopped, the monomer will form a separate bulk phase, usually above the aqueous phase. The monomer is polymerized by the initiator within the droplets, forming polymer beads of approximately the same size as the monomer droplets (0.1–10 mm diameter). The product can be readily separated from the aqueous phase (via filtration or decantation) in the form of macroscopic particles or beads, which can be easily packaged and/or transported. Heat transfer is facilitated by the presence of the continuous aqueous phase. Blocking agents such as clays or talcs are used to prevent particle ag-

glomeration. Small quantities of nonionic surfactants (such as polyvinyl alcohol) may be used to impart particle stability and to disperse the blocking agent. Viscosity enhancers such as carboxymethylcellulose may be used to inhibit particle settling. The loci of polymerization are the monomer/polymer beads. Due to the large sizes of the beads, such systems are suspensions rather than emulsions or stable dispersions. The particles are kept suspended by agitation throughout the course of the polymerization. The suspension polymerization process is described in detail by Trommsdorff and Schildknecht [4].

Kinetically, each bead acts as a small independent reactor; there is little exchange of material between the beads. Since there is no solvent present at the locus of polymerization, the kinetics are those of bulk polymerization, with the molecular weight distribution (MWD) characteristics similar to those of bulk or solution polymerizations. If water-soluble initiator is used in a suspension polymerization, very little polymerization will occur, since few free radicals will reach the locus of polymerization in the monomer beads.

If surfactant is added to a suspension polymerization system, a number of phenomena may occur. If the surfactant is added in small amounts (below the critical micelle concentration or CMC), the reduction in interfacial tension between the organic and aqueous phases will result in smaller monomer droplets, but it has hardly any other effect. If surfactant is added above the CMC, and an oil-soluble initiator is used, the process is commonly termed a *microsuspension polymerization*. Due to the reduced interfacial tension, the droplet diameter (and hence bead diameter) is reduced to approximately 10–40 μm. Little polymerization takes place in the aqueous phase or in particles generated from surfactant micelles because of the hydrophobic nature of the initiator. However, some smaller particles initiated from surfactant micelles may be found. The kinetics are still essentially those of a bulk free radical polymerization. Microsuspension polymerization is used to produce pressure-sensitive adhesives for repositionable notes.

If a water-soluble initiator is used, both droplet nucleation (to form large particles) and micellar nucleation (to form submicron particles) may occur. The balance between these two mechanisms is a function of surfactant type and amount and monomer water solubility. In general, small particles derived from micellar nucleation will dominate, giving what is know as a *conventional emulsion polymerization* system. The kinetics of conventional emulsion polymerization are no longer those of bulk free radical polymerization, since the small sizes of the loci of polymerization introduce segregation effects, in which bimolecular termination of the growing polymer chains is suppressed by the small likelihood of two growing chains existing in the same particle. This results in higher molecular weight at constant polymerization rate. The particle diameter will range from 50 to 500 nm.

If the monomer droplet size in a conventional emulsion polymerization can be reduced sufficiently (see below), the loci of polymerization become the monomer droplets. This system is referred to as a *miniemulsion* polymerization and will be discussed in detail below. The particle diameter will range from 50 to 500 nm.

If the surfactant concentration in a macroemulsion is greatly increased, or if the monomer concentration is greatly reduced, a *microemulsion* results. Microemulsions are thermodynamically stable systems in which all of the monomer resides within the micelles. At high surfactant concentration, the micelles may form a bicontinuous network, rather than discrete micelles. Polymerization (with water- or oil-soluble initiator) of the monomer within a microemulsion is referred to as *microemulsion polymerization*. The particles produced in this way are extremely small, ranging from 10 to 100 nm.

1.2 The Concept of Miniemulsion Polymerization

The mechanisms of conventional emulsion and miniemulsion polymerizations are, in some ways, significantly different. A conventional unseeded (no small particles added at the beginning) batch emulsion polymerization reaction can be divided into three intervals. Particle nucleation occurs during Interval I and is usually completed at low monomer conversion (2–10%) when most of the monomer is located in relatively large (1–10 μm) droplets. Particle nucleation takes place when radicals formed in the aqueous phase grow via propagation and then enter into micelles or become large enough in the continuous phase to precipitate and form primary particles which may undergo limited flocculation until a stable particle population is obtained. Significant nucleation of particles from monomer droplets is discounted because of the small total surface area of the large droplets. Interval II involves polymerization within the monomer-swollen polymer particles, with the monomer supplied by diffusion from the droplets. Interval III begins when the droplets disappear – or at least reach a polymer fraction similar to that of the particles – and continues to the end of the reaction. Because the nucleation of particles can be irreproducible, commercial emulsion polymerizations are often "seeded" with polymer particles of known size and concentration, manufactured specifically for use as seed particles. In this paper, for the purpose of clearly distinguishing between conventional emulsions and miniemulsions, the term *macroemulsion* will be used for the former. In addition, a *latex* will be defined as a polymerized monomeric emulsion, while the term *emulsion* will refer to an unpolymerized monomeric emulsion.

Miniemulsion polymerization involves the use of an effective surfactant/costabilizer system to produce very small (0.01–0.5 μm) monomer droplets. The droplet surface area in these systems is very large, and most of the surfactant is adsorbed at the droplet surface. Particle nucleation is primarily via radical (primary or oligomeric) entry into monomer droplets, since little surfactant is present in the form of micelles, or as free surfactant available to stabilize particles formed in the continuous phase. Both oil- and water-soluble initiators may be used; the important feature is that the reaction proceeds by polymerization of the monomer in these small droplets, so there is no true Interval II. The mechanisms of macro- and miniemulsion polymerization are shown schematically in Fig. 1.

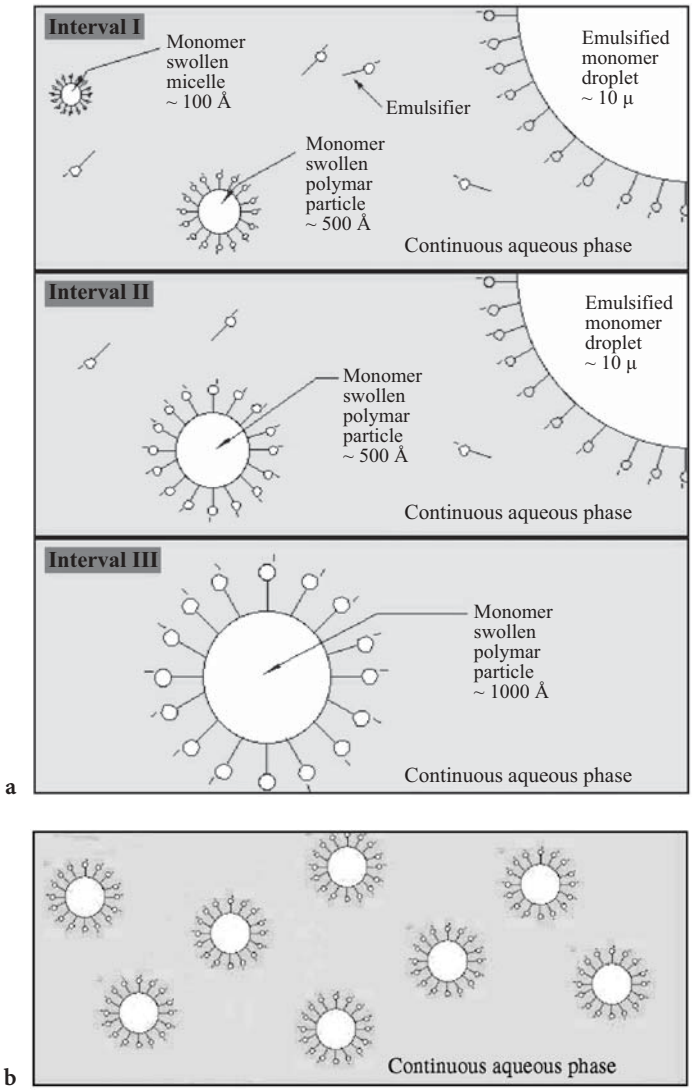

Fig. 1 Macroemulsion polymerization (**a**) versus miniemulsion polymerization (**b**)

1.3 Publication History

Miniemulsion polymerization began with a single paper [5]. Professor John Ugelstad of Norway was visiting John Vanderhoff in the Department of Chemistry at Lehigh University. Their discussions lead to speculation about the possibility of nucleation and polymerization in very fine monomer droplets during emulsion polymerization. Micellar nucleation is considered to be the

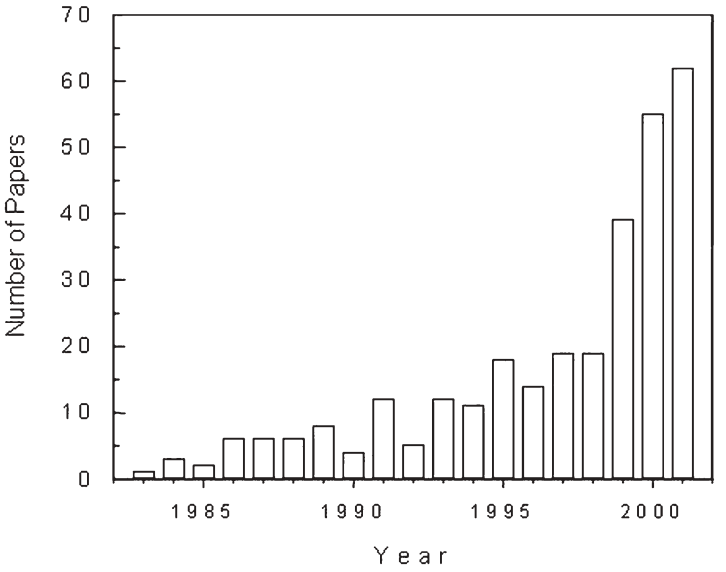

Fig. 2 Growth in the number of publications on miniemulsion polymerization. (Courtesy of Prof. M. S. El-Aasser)

dominant mechanism of particle nucleation in emulsion polymerization, but might nucleation in droplets occur if the droplets were sufficiently small? The task of investigating these ideas was given to a new postdoctoral fellow in Vanderhoff's lab, Dr. (now Provost) Mohamed S. El-Aasser. From this point, the field grew slowly. Figure 2 shows the total number of papers per year published on miniemulsion polymerization. It may be seen that, after a slow start, the number of contributions in the field has risen rapidly, as the scientific community made use of the basic research of the early years, and began to see the commercial utility of the process.

2
Miniemulsion Polymerization

In order to adequately discuss miniemulsion polymerization, it will be necessary to review the mechanism of macroemulsion polymerization.

2.1
The Mechanism of Macroemulsion Polymerization

Macroemulsion polymerization is a complex process. The literature contains extensive reviews of emulsion polymerization theory [6–11]. Only a brief review of the current state of the literature is given here. The theory of emul-

sion polymerization revolves around one equation (neglecting the aqueous phase),

$$R_p = k_p[M]_p N_p \bar{n}/N_A$$

where each of these terms is explained below.

The earliest qualitative theory of emulsion polymerization was developed by Harkins [12] and was quickly quantified by Smith and Ewart (SE) [13]. Although this theory only holds for the special case of water-insoluble monomers, it is the typical starting point for most other theories. This theory is based on the batch emulsion polymerization of styrene. It includes three intervals, as depicted in the left half of Fig. 1. The first interval begins with the initiation of the reaction and continues until all micelles become nucleated or are used up as surface stabilizing agents. At this point particle formation ceases. During Interval II, the particles grow at a constant rate in the presence of monomer droplets. Once the monomer droplets disappear, Interval III begins. The monomer concentration in the particle decreases and the reaction within the particles becomes diffusion-limited throughout the remainder of the polymerization.

Micellar nucleation may not be the only, or even primary process of nucleation and growth. Other mechanisms are discussed later. To provide a comprehensive model for emulsion polymerization, the applicability of each mechanism must be considered.

Equation 1 illustrates the concept of *radical segregation*, that is significant in macroemulsion, miniemulsion and microemulsion polymerization. In a bulk or solution free radical polymerization, the radical flux can be increased in order to increase the rate of polymerization, but only at the cost of reducing molecular weight. Equation 1 indicates that one might increase the rate of polymerization by increasing the surfactant level. This does not adversely impact the molecular weight of the product. The ability to decouple reaction rate and molecular weight come about because of the segregation of the free radicals in segregated disperse-phase polymerization. Since each radical is confined to a particle, bimolecular termination is suppressed, resulting in higher rates of polymerization and molecular weight. Segregation occurs only when $\bar{n}$ is reasonably close to unity, or lower than unity.

2.1.1 Interval I – Particle Nucleation

Nucleation mechanisms are generally divided into three types: micellar, homogeneous, and droplet. Statistically, all three types can occur simultaneously in every reaction. However it is the preponderance of one mechanism above the others in a given system that causes authors to consider only one in their studies. Numerous extensions have been made to the SE micellar nucleation theory in an effort to furnish explanations for experimental results observed

for monomers with slight water solubilities. Detailed reviews of these extensions are readily available [10, 11, 14, 15]. Monomer droplet nucleation is normally neglected, except when considering mini- and microemulsions, due to its insignificant contribution to the particle number and the size distribution.

2.1.1.1 Micellar Nucleation

All quantitative theories based on micellar nucleation can be developed from balances of the number concentrations of particles, and of the concentrations of aqueous radicals. Smith and Ewart solved these balances for two limiting cases: (i) all free radials generated in the aqueous phase assumed to be absorbed by surfactant micelles, and (ii) micelles and existing particles competing for aqueous phase radicals. In both cases, the number of particles at the end of Interval I in a batch macroemulsion polymerization is predicted to be proportional to the aqueous phase radical flux to the power of 0.4, and to the initial surfactant concentration to the power of 0.6. The Smith Ewart model predicts particle numbers accurately for styrene and other water-insoluble monomers. Deviations from the SE theory occur when there are substantial amounts of radical desorption, aqueous phase termination, or when the calculation of absorbance efficiency is in error.

Deviations with respect to order from the SE theory increase as the monomer water solubility increases.

2.1.1.2 Homogeneous Nucleation

Although the SE micellar nucleation theory explains data for certain systems, it fails for others. This has led some authors to propose a different mechanism for nucleation. In the homogeneous nucleation theory, aqueous phase radicals polymerize to form oligomers. These continue to grow until they reach a critical chain length, the size of a primary particle, and then precipitate. Throughout the growth process, the oligomers may also flocculate or coagulate. This theory is typically employed for relatively water-soluble monomers. Slight variations of this theory have also been postulated.

Prior to 1952, little evidence for homogeneous nucleation existed [16, 17]. In 1952, Priest [18] studied the polymerization of vinyl acetate and presented a qualitative theory for homogeneous nucleation. He concluded from experimental work that aqueous phase nucleation is important in systems with monomers that have a relatively high water solubility. Primary particle formation occurs throughout the course of the reaction. During later periods of the reaction, large monomer-swollen polymer particles act as sinks for these primary particles, encouraging coagulation.

In 1968, Roe [19] developed the SE limiting case equations for particle number from the homogeneous nucleation theory. He showed that the SE equation

for particle nucleation is not unique to micellar nucleation, but results from the SE assumptions. By assuming that (i) the nucleation stops upon depletion of micelles, (ii) the volumetric growth rate is constant, and (iii) the radical absorption is strictly a function of radical generation, he showed that the SE dependency on radical flux and surfactant concentration could be generated from homogeneous nucleation theory.

Fitch and Tsai [20, 21] developed a quantitative theory for homogeneous nucleation. By using the collision theory for radical capture, Fitch [22] has shown that the rate of radical capture is a function of radical production, particle number, particle size, and diffusion distance. Primary particles may coagulate with each other because of their small size and lower surface charge. As particles coagulate, the surface to volume ratio decreases, which causes an increase in surface potential. When particles become sufficiently large, coagulation ceases due to insufficient kinetic energy to overcome the biparticle surface repulsion. Fitch and Tsai have provided experimental support for this theory by polymerizing MMA with different initiators.

Ugelstad and Hansen [11] proposed that free radicals in the aqueous phase propagate with dissolved monomer. Primary particles form by precipitation when a critical chain length is reached. During growth from a monomer radical to a primary particle, each oligomer can (i) terminate with other radicals, (ii) precipitate if its length exceeds the critical chain length, or (iii) be captured by particle.

A fundamental extension to the homogeneous nucleation theory was proposed by Lichti et al. [23] and Feeney et al. [24]. Their theory is based on the positive skewness of the particle size distribution (PSD) as a function of volume during Interval II. This implies that the rate of nucleation during Interval I increases with time until it eventually drops off at the cessation of nucleation. Lichti and Feeney claim that micellar nucleation or one step homogeneous nucleation incorrectly predict either decreasing or constant nucleation rates.

This theory has been given the name coagulative nucleation. According to Lichti and Feeney's mechanism, precipitated "precursor particles" undergo coagulation to form "true" or "mature" latex particles. A precursor particle is unstable and said to be formed in either a micelle or the aqueous phase. Due to their small size and hydrophilic nature, the precursors have low swelling capacity and high radical desorption rates. Consequently, the propagation rate is low and these precursors tend to coagulate with other precursors or mature latex particles. These conclusions then rule out micellar nucleation as a possible mechanism for precursor formation.

More recently, Maxwell et al. [25] suggested that the values to be used for the critical chain length are much smaller than originally thought. They also suggested that oligomeric radical capture is independent of particle size and limited by the rate of propagation of the radical in the aqueous phase. However, this theory does not consider variations in other parameters with particle size.

2.1.1.3 Droplet Nucleation

Nucleation of monomer droplets has typically been neglected in emulsion polymerization. The large diameter (1–10 μm) and small number (~10^{13} versus 10^{21} micelles) of droplets in macroemulsions usually makes their consideration of no importance. Regardless of this, all droplets do get nucleated, because of their large size. These droplets show up in TEM photographs as abnormally large particles in very low concentrations. In 1973, Ugelstad et al. [5] showed how submicron styrene monomer drops can be made stable enough to become numerically significant in nucleation when a cosurfactant is used to enhance the stability of the smaller droplets. Table 1 shows how the micelle number varies with monomer droplet size at constant surfactant levels. Chamberlain et al. [26] have presented experimental evidence that the efficiency of radical capture by droplets is much lower than that for micelles or particles. This would affect the results in Table 1. Ugelstad et al. [27, 28] have shown how nucleation of monomer droplets can lead to latexes with large monodisperse particles. However, if insufficient shear or cosurfactant is used, the potential for production of bimodal PSD's exists [29, 130]. This could be desirable in certain instances.

The distinguishing feature of droplet nucleation as opposed to micellar or homogeneous nucleation is the nature of the particle at "birth". Droplets, which are nucleated into particles, begin as nearly 100% monomer. Micellar or homogeneous nucleated particles start out with much lower monomer concentrations and eventually swell to around 60% (for MMA) in the presence of monomer droplets. This fundamental difference may lead to large differences between miniemulsion and macroemulsion polymerizations in radical desorption and/or intraparticle termination during Intervals I and II.

Table 1 Variation of number of micelles with droplet size for MMA droplets and SLS surfactant in a basic emulsion recipe

Monomer droplet diameter (μm)	10.0	1.0	0.5	0.1
Volume of monomer droplet (liter)	5.2×10^{-13}	5.2×10^{-16}	6.5×10^{-17}	5.2×10^{-19}
Number of monomer droplets (#/1)	7.8×10^{11}	7.8×10^{14}	6.3×10^{15}	7.8×10^{17}
Total area of droplets (m^2/1)	247	2470	4930	24700
Surface area micelles (m^2/1)	5246	3027	562	0
Number of micelles (#/1)	1.5×10^{20}	8.6×10^{19}	1.6×10^{19}	0.0
Total number of preparticles (#/1)	1.5×10^{20}	8.6×10^{19}	1.6×10^{19}	7.8×10^{17}
Droplet percent area	4.5	45	90	100
Droplet percent number	5.3×10^{-7}	9.2×10^{-4}	0.040	100

Base case parameters: temperature=50 °C; monomer/water ratio=0.4 g/g; surfactant CMC=0.004 mol/L(aq); surfactant concentration=0.020 mol/L; surfactant surface area=0.57 nm^2/molecule; molecules per micelle=62; monomer watersaturation=0.137 mol/L(aq)

2.1.1.4 Competition for Radicals

As pointed out above, particle nucleation includes all three mechanisms – micellar, homogeneous, and droplet, since these mechanisms may compete and coexist in the same system. Often one will dominate. Therefore, any general model of emulsion polymerization should include all three mechanisms. Hansen and Ugelstad [31] and Song [10] have presented probabilities for each of these mechanisms in the presence of all three.

The competition for oligomeric radicals also includes particles that have been created. In miniemulsion polymerizations, the nucleation of one droplet results in the formation of one particle of equal surface area. Therefore, nucleation therein has little effect on competition for radicals. This is not so with macroemulsions, since both micellar and homogeneous nucleation result in a large shift in the surface area from micelles to particles as the particles are created and grow.

2.1.2 Interval II – Particle Growth

SE Interval II begins at the cessation of nucleation, or in light of the nucleation theory just reviewed, when the particle number becomes relatively constant. Most theories developed for this interval assume a constant particle number and use the quasi-steady-state approximation (QSSA) for average number of radicals per particle. The kinetics and mechanisms of Interval II have been some of the most studied aspects of macroemulsion polymerization. SE Interval II ends when the monomer droplets disappear and the monomer concentration in the particles begins to decrease.

The rate of polymerization during Interval II is usually considered constant for two reasons. The monomer concentration within the particle, as defined by equilibrium thermodynamics, is approximately constant in the presence of excess monomer. Mass transfer is assumed to be fast and particle size has little effect on this concentration. Secondly, emulsion polymerization kinetics tend to give a constant radical concentration within the particles during Interval II. Therefore, the rate of polymerization given by Eq. 1 is approximately constant until the end of Interval II, where $[M]_p$, $\bar{n}$, and k_p begin to change. These two assumptions have been substantiated by experimental observations and are considered reasonable. The challenge for Interval II is to determine the average number of radicals per particle. Particle monomer concentration can be determined as a function of particle radius by an equilibrium relationship such as the Morton [32] equation that considers both surface energy and mixing energy. Propagation rate coefficients have been widely studied and are readily available [33]. The particle number concentration is assumed constant.

Smith and Ewart developed three limiting cases for Interval II. Each of these cases can be generated through a balance of N_{pi} (the number of particles con-

taining i radicals), where the number of particles is considered constant (no nucleation). For Case 1, Smith and Ewart assume $N_{p0} \gg N_{p1} \gg N_{p2} \gg \ldots$. For this case $\bar{n}$ will be significantly less than 0.5. This case occurs when significant monomeric radical desorption occurs, and is more common with monomers of significant water solubility.

Case 2, assumes instantaneous termination of the existing radical with an entering radical. In this case, each particle will contain either zero or one radical, and $\bar{n}$ becomes 0.5. Styrene generally follows Case 2 kinetics. Smith and Ewart Case 3 assumes that both desorption from particles and aqueous phase termination may be neglected, and so $\bar{n} \gg 1.0$. This occurs with large particles, and in the limit results in bulk kinetics.

Coagulation of latex particles during Interval II is often neglected. If surfactant is available in great enough proportion, the particles will remain stable throughout the reaction.

2.1.3 Interval III – Gel and Glass Effects

Interval III begins when all monomer droplets have vanished and/or the aqueous phase becomes unsaturated. Since each droplet in a macroemulsion actually absorbs radicals, they cannot disappear but rather shrink to a point where they have no excess monomer. The monomer in the aqueous phase decreases corresponding to the decrease in the particles. The conversion at which Interval III begins varies for different monomers and systems, but is typically around 40 to 50%. However, it may not be as distinguishable in miniemulsions due to early initiation of the gel effect.

As the monomer within the particles is consumed by polymerization, the viscosity rises within the particles and the diffusion rate of the polymeric radicals decreases. This causes a reduction in the rate of termination, which corresponds to a dramatic increase in the radical concentration. A higher radical number within the particle results in an "auto acceleration" in the rate of polymerization. Common practice is to model this auto acceleration or gel effect by decreasing the termination rate constant byseveral orders of magnitude as a function of percent monomer in the particle. A free volume approach has been used by Sundberg et al. [34]. Gilbert and coworkers [35] suggest a completely empirical approach from precise experimental data. Empirical correlations used in modeling the gel effect in bulk or solution polymerization have also been modified for use in emulsion processes [36–38].

The problem with applying correlations derived from other systems to emulsion polymerization is twofold. First, normal macroemulsion particles are said to be created with 30 to 40% monomer in them and so the unbiased (zero conversion) termination rate is unknown. Secondly, the diffusional limitations in particles might be quite different from those observed in bulk or suspension polymerizations. It is for these reasons that an empirical approach is suggested.

If the reaction temperature is below the polymer glass transition temperature and the amount of monomer in the particle decreases far enough, the glass effect may become important. The polymerization rate virtually goes to zero because the particle becomes so internally viscous, essentially glasslike, that the diffusion of monomer to the radicals is limited. The glass transition point varies for different polymers. This effect has also been studied by several authors [34, 39, 40].

2.2 The Mechanism of Miniemulsion Polymerization

In the previous discussion of macroemulsion polymerization, all three forms of particle nucleation were discussed. In macroemulsion polymerization, micellar and homogenous nucleation dominate. This is because the large sizes of the monomer droplets, and their consequent low interfacial area, makes them ineffective in competing for water-borne free radicals. Droplet nucleation undoubtedly takes place in macroemulsion polymerization, but it is generally considered to be insignificant. If the monomer droplet size can be reduced to below 0.5 μm, two phenomena will occur. First, the droplets will be able to compete successfully for water-borne free radicals with any remaining micelles. Second, the huge increase in interfacial area caused by the reduction in droplet size will result in a huge increase in interfacial area. This new interface will require a monolayer of surfactant to remain stable. The surfactant necessary to support this large interfacial area will come from the break-up of surfactant micelles. In a properly formulated miniemulsion, all micelles will be sacrificed to support the droplet interfacial area. Therefore, not only do the small droplets compete effectively for micelles, their presence causes the destruction of the micelles, leaving droplet nucleation as the dominant particle nucleation process.

Miniemulsions are produced by the combination of a high shear to break up the emulsion into submicron monomer droplets, and a surfactant/costabilizer system to retard monomer diffusion from the submicron monomer droplets. Both are necessary to effect predominant droplet nucleation (nucleation in which a preponderance of the particles originate from droplets rather than from micelles or from homogeneous nucleation). High shear is provided by a sonicator or a mechanical homogenizer. The surfactant is necessary to retard droplet coalescence caused by Brownian motion, settling or Stokes law creaming or settling. The costabilizer (also referred to in earlier works as a *cosurfactant*) prevents Ostwald ripening [41]. When a liquid emulsion is subjected to high shear, small droplets will result. There will still be a statistical distribution of droplet sizes. If the monomer is even slightly soluble in the continuous aqueous phase (and most are, as evidenced by the fact that Interval II of macroemulsion polymerization takes place), the monomer will, over time, diffuse from the smaller monomer droplets into the larger ones. This results in a lower interfacial area (and interfacial energy), since the loss in interfacial area of the

smaller droplets is larger than the gain in interfacial area of the larger ones. The reduction in interfacial energy is the driving force for degradation of the small droplets.

If Ostwald ripening is allowed to continue unchecked, creaming of the monomer will occur as the droplet sizes become large enough for Stokes law creaming to occur. This will occur in a matter of seconds to minutes. If the system is initiated, bulk polymerization of the monomer layer will occur. If the emulsion is stirred, an emulsion of large monomer droplets (of the order of those of a macroemulsion) will result, and if the stirred emulsion is initiated, macroemulsion polymerization will take place. A costabilizer functions to prevent Ostwald ripening by retarding monomer diffusion from the smaller droplets to the larger. Costabilizers should be highly insoluble in the aqueous phase (so that they will not diffuse out of the droplets), and highly soluble in the monomer droplets. Under these conditions, diffusion of the monomer out of the smaller droplets results in an increase in the concentration of the costabilizer in those particles (since, by definition costabilizers are too insoluble in the aqueous phase to leave the droplet). The increase in free energy associated with the concentration of the costabilizer balances the decease from reduced interfacial area caused by Ostwald ripening, and, at some point, ripening stops. Since all costabilizers are somewhat water-soluble, Ostwald ripening will proceed, but on a timescale of months, which is unimportant since the timescale of polymerization is minutes to hours. This phenomenon is shown in Fig. 3 [42]. Here a macroemulsion and a miniemulsion of methyl methacrylate (same recipe, but with no costabilizer, and no high shear for the macroemulsion) are shown after three hours without mixing. The macroemulsion is completely creamed, since Stokes law creaming has taken place on the large monomer droplets. The miniemulsion has not creamed, since Brownian motion is sufficient to prevent creaming of the submicron monomer droplets. Similar miniemulsions have remained stable for six months or more.

Fig. 3 Macroemulsion and miniemulsion after three hours

In their original discovery of miniemulsion polymerization, Ugelstad and co-workers [5] used either cetyl alcohol (CA: water solubility estimated at 6×10^{-8} [43]) or hexadecane (HD: water solubility estimated at 1×10^{-9} [43]) to retard monomer diffusion from submicron monomer droplets. Both CA and HD, referred to here as costabilizers, are volatile organic components and are therefore not entirely desirable in the final product. Other researchers have used polymers, chain transfer agents, and comonomers as stabilizers, as will be discussed later.

Monomer droplet stability can be understood in terms of free energy. The partial molar free energy of adding a second component to a droplet is made up of two terms, the partial molar free energy of mixing and the interfacial partial molar free energy. The partial molar free energy of mixing (the Flory Huggins expression [44]) can be combined with the interfacial partial molar free energy to give

$$\frac{\Delta\bar{G}_i}{RT} = \ln\varphi_i = (1 + m_{ij})\varphi_j + \chi_{ij}\varphi_j^2 + \frac{2\bar{V}_i\gamma}{RTr} \tag{2}$$

Ugelstad et al. [45] have applied this equation to various monomers and surfactants. It is clear from this equation that the free energy increases as the phase diameter decreases. The smaller the monomer droplet, the less stable it is. Therefore, a driving force exists for the monomer to diffuse from a small droplet to a larger one. Over time, non-monodisperse systems of droplets of pure monomer will decrease in number as the smaller droplets swell the larger ones and then disappear. Jannson [46] has shown that this occurs in unagitated systems, and that the timescale for diffusional instability can be on the order of seconds.

Prior to 1962, droplets below 1 µm were considered too unstable to participate in the nucleation process. In 1962, Higuchi and Misra [47] proposed that the addition of a water insoluble compound to the monomer will enhance the stability of small droplets by prohibiting diffusion. In 1973, Ugelstad et al. [48] showed how submicron styrene droplets could be made stable enough to participate in the nucleation processes by adding small amounts of cetyl alcohol. Later, Ugelstad [48] used Eq. 2 to explain these experimental observations.

It can be shown [49] for two phases in equilibrium that the partial molar free energies must be equal. In an emulsion (or miniemulsion) there are three phases: monomer droplets, the aqueous phase and polymer particles. Since monomer is soluble in all of these phases, the equilibrium condition requires that the three phases have equal partial molar free energies. In the presence of monomer droplets, emulsion polymer particles contain 30–80% monomer in them. Therefore, they are said to be "swollen" with monomer. Ugelstad et al. [48] and Azad and Fitch [50] have shown that addition of a third water-insoluble component to a swollen polymer particle can increase the monomer to polymer ratio. They have shown that an optimum chain size for the additive exists since the solubility of the additive increases as the chain size decreases. They found

that the optimum hydrocarbon stabilizer is hexadecane. Others have found that if a fatty alcohol is used as the stabilizer, the minimum chain length required is 12 carbon atoms [51].

Ugelstad et al. [52] have shown how this theory may be used to devise a method to prepare large monodisperse particles of predetermined size. By using the appropriate amount of cosurfactant, polymer particles can be swollen with monomer to the desired size. Polymerization in conditions that prevent additional nucleation results in large monodisperse polymer particles of size 1–100 μm. This method has been criticized by other groups as being in error due to measurement selectivity.

If Ostwald ripening is retarded by using a costabilizer, predominant droplet nucleation can be achieved. This is the basis of miniemulsion polymerization. One of the first comprehesive studies of miniemulsion polymerization was done on styrene by Choi et al. [53].

2.3 Mathematical Modeling of Miniemulsion Polymerization

Various mathematical treatments of specific mechanisms within the miniemulsion polymerization reaction abound. This section will be limited to those papers that attempted to model the overall miniemulsion polymerization reaction. Perhaps the earliest (1981) serious attempt to model this system was that by Chamberlain, Napper and Gilbert [54]. Balances of the number of droplets, number of polymer particles and monomer conversion were constructed for batch miniemulsion polymerization. Droplets and particles were considered to be monodisperse. Comparison of the model with experimental data led to the conclusion that free radical entry into monomer droplets is substantially less than for ordinary macroemulsion particles. Chen, Gothjelpsen and Schork [55] published a model of approximately the same complexity for continuous stirred tank miniemulsion polymerization with an oil-soluble initiator. El-Aasser and coworkers [56–60] published a series of papers focusing on the modeling of miniemulsion copolymerization, particularly in relation to monomer transport. They described monomer transport in terms of a mass transfer coefficient and a driving force derived from an equilibrium concentration calculated from equating the partial molar free energies. This same group [61] modeled seeded miniemulsion polymerization (containing both polymeric seed particles and miniemulsion droplets) with oil-soluble initiator. Monomer transfer by collision of droplets with particles was found to be important. Fontenot and Schork [62, 63] published a very detailed model of batch macro- and miniemulsion polymerization, indicating the differences between the two mechanisms, and including both micellar and droplet nucleation mechanisms. Significant droplet coalescence was predicted. The model was in good agreement with data. Samer and Schork [64] published a mathematical model of continuous stirred tank (CSTR) and plug flow (PFR) miniemulsion polymerization reactors. They were able to explain why the rate of polymerization

for miniemulsion polymerization in a CSTR is substantially higher than for macroemulsion polymerization in the same reactor. All of the models discussed have been particle number models, containing no information about droplet size distribution or particle size distribution. None have attempted to model the formation of droplets during the miniemulsification stage.

Cunningham and coworkers [65–68] have completed detailed modeling of nitroxide mediated radical polymerization in miniemulsion. They found that issues of distribution of the control agent between the aqueous and organic phases can be critical to maintaining livingness.

3
Properties of Miniemulsion Polymerization

After having described the mechanism of miniemulsion polymerization and how it differs from macroemulsion polymerization in the previous section, this section will focus on the various mechanisms and properties of miniemulsion polymerization.

3.1
Shear Devices

Miniemulsions are produced by the combination of a high shear device to break up the emulsion into submicron monomer droplets with a water-insoluble, monomer-soluble component to retard monomer diffusion from the submicron monomer droplets. Both steps are necessary to effect predominant droplet nucleation. In the absence of a high-shear device, miniemulsion systems revert to macroemulsion polymerizations, indicating that the presence of a costabilizer alone is not sufficient to cause predominant droplet nucleation. The formation of submicron droplets is accomplished by placing a coarse emulsion (of monomer in water) in a high shear field. In general, it is best to form a coarse pre-emulsion before subjecting the system to high shear. This is because most devices that impart high shear are poor mixers, so unless a coarse emulsion is created first, the monomer and water phases may not be in close proximity when they enter the high shear field. A coarse pre-emulsion may be formed by vigorous stirring of the monomer, water, surfactant mix, as would be done to create a macroemulsion. For reasons of practicality, the costabilizer should be dissolved in the monomer before pre-emulsification.

For laboratory investigations of miniemulsions, a variety of high-shear devices have been used, although sonication has been the most popular. Sonication, however, may not be very practical for the large-scale production of commercial miniemulsion polymers. An effective alternative to sonication is also driven by the need to design an efficient miniemulsion polymerization process. A continuous process places greater demand on the shear device in terms of energy consumption and dissipation.

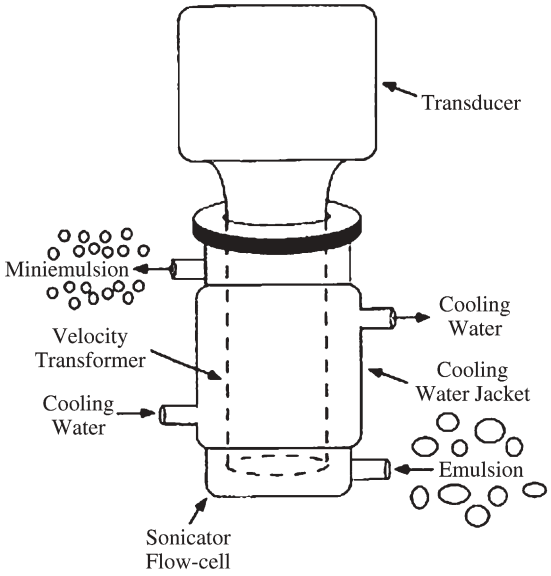

Fig. 4 Sonicator with cooling jacket (from [69])

The mechanism for ultrasonic emulsification is primarily that of cavitation. A typical sonicator for emulsification consists of a velocity transformer coupled to a transducer, capable of oscillating in a longitudinal mode, where the velocity transformer is immersed in the liquid. Figure 4 illustrates the basic parts of a sonicator with a continuous flow attachment, like the one used in this work. In this case, the flow cell is secured to the velocity transformer by a flange and a Teflon O-ring. The intensity of cavitation depends on the power delivered to the velocity transformer, which is relayed to the transducer from a variable transformer or some other control device not shown in Fig. 4.

The word homogenization is somewhat inconclusive and is typically defined as used in context. Two processes are considered here; the first is a fine clearance valve homogenizer, and the second is a rotor-stator-type mechanical homogenizer. Homogenization is similar to sonication and produces submicron droplets by a combination of mechanical shearing and cavitation.

The fine clearance valve homogenizer has been in use for nearly 100 years for the homogenization of milk and milk products. Raw milk is an emulsion of fat globules dispersed in a continuous skim milk phase. Without homogenization, the fat globules would rise to the top of the milk and form a cream layer. Homogenization reduces the average diameter of these fat globules and subsequently reduces their creaming rate, extending the shelf-life of the product. The MicroFluidizer used by many miniemulsion investigators is an example of this type of shear device.

The rotor-stator-type mechanical homogenizer generates submicron droplets by forcing the emulsion through small openings in the stationary

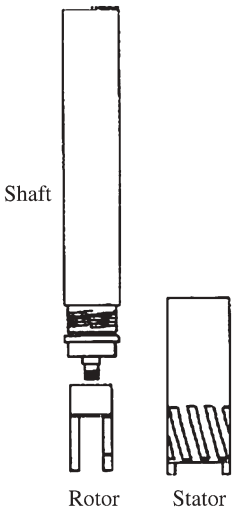

Fig. 5 Rotor-stator homogenizer (from [69])

stator at very high speeds, as illustrated in Fig. 5. The intensity of shearing depends on the rotor speed, which can be set anywhere from 5–35 krpm for most modern equipment. However, at higher speeds the shearing action generates a significant amount of heat, which may harm the sample being emulsified or the machine itself. This device has been used by Samer and Schork [69] and others, and has been shown to be effective. However, in general, the miniemulsion droplet size achievable with a rotor-stator device is larger than that achievable with sonication or valve homogenizers.

3.2 Choice of Surfactant

The vast majority of miniemulsion polymerizations reported in the literature have been stabilized with anionic surfactants, probably because of the widespread application of anionic surfactants in macroemulsion polymerization, and due to their compatibility with neutral or anionic (acid) monomers and anionic initiators. However, Landfester and coworkers [70, 71] have used the cationic surfactants cetyltrimethyl ammonium bromide (CTAB) and cetyltrimethyl ammonium tartrate for the production of styrene miniemulsions. They report that these surfactants produce similar particle sizes to anionic surfactants used at the same levels. Bradley and Grieser [72] report the use of dodecyltrimethyl ammonium chloride for the miniemulsion polymerization of MMA and BA.

Wang and Schork [73] miniemulsion polymerized vinyl acetate using the nonionic surfactant polyvinyl alcohol (PVA). They found that stable miniemulsions could be made with PVA and HD, but when the HD was removed, the PVA

alone was not capable of functioning as both surfactant and costabilizer. In general, the droplet diameter was greater with PVA than would be expected with an anionic surfactant. Chern and Chen [74, 75] used nonylphenol ethoxylate (40 ethylene oxides per molecule) with a monomeric costabilizer such as docecyl methacrylate or stearyl methacrylate to form stable miniemulsions of styrene. Wu and Schork [76] used polyoxyethylene-23 lauryl ether (BRIJ-35) as the surfactant with HD as the costabilizer to form stable miniemulsions of vinyl acetate. Landfester and coworkers [70, 71] also used polyethylene oxide for the miniemulsion polymerization of styrene. Luo and Schork used nonylphenyl ethoxylate (Triton X-405) and an interfacial initiation system to miniemulsion polymerize BA and BA copolymerized with cationic monomer. Graillat and Guyot [77] also used Triton X-405 to produce high solids vinyl acetate emulsions via miniemulsion polymerization.

Guyot and coworkers [78] have produced stable miniemulsions of styrene using the polymerizable surfactant, vinylbenzylsulfosuccinic acid sodium salt.

3.3 Choice of Costabilizer

Early work in miniemulsion polymerization [5, 48–50] used either cetyl alcohol (CA) or hexadecane (HD) to retard Ostwald ripening in submicron monomer droplets. Both CA and HD, referred to here as *costabilizers*, have the requisite properties for a costabilizer: high monomer solubility, low water solubility and low molecular weight. The need for these properties can be seen from Eq. 2. High monomer solubility will give a large Flory Huggins interaction parameter between the costabilizer and the monomer (χ_{ij}). Low water solubility will ensure a distribution coefficient for the costabilizer that very strongly favors the monomer drops, giving a higher volume fraction of costabilizer in the droplet. Low molecular weight will give a high ratio of costabilizer molecules to monomer molecules (m_{ij}) in the droplet. All of these factors will enhance swelling, or retard monomer loss via Ostwald ripening.

With cetyl alcohol, there is the complication that the polarity of the molecule may cause it to reside at the surface of the droplet, imparting additional colloidal stability. Here, the surfactant and costabilizer form an ordered structure at the monomer-water interface, which acts as a barrier to coalescence and mass transfer. Support for this theory lies in the method of preparation of the emulsion as well as experimental interfacial tension measurements [79]. It is well known that preparation of a stable emulsion with fatty alcohol costabilizers requires pre-emulsification of the surfactants within the aqueous phase prior to monomer addition. By mixing the fatty alcohol costabilizer in the water prior to monomer addition, it is believed that an ordered structure forms from the two surfactants. Upon addition of the monomer (oil) phase, the monomer diffuses through the aqueous phase to swell these ordered structures. For long chain alkanes that are strictly oil-soluble, homogenization of the oil phase is required to produce a stable emulsion. Although both costabilizers produce re-

latively stable emulsions, Azad et al. [80] have shown that the alkanes will produce emulsions of higher stability. A 1:3 molecular ratio of surfactant to costabilizer has been shown to provide optimal stability in emulsion systems where the costabilizer is a fatty alcohol. Shah [81] postulated that this ratio is due to an optimum alignment of surfactant and costabilizer molecules at the interface in microemulsions. Hallworth and Carless [82] have proposed that the stability of an emulsion containing long chain alkanes of fatty alcohols comes from a film at the interface which makes collisions at the interface more elastic.

Various researchers [83–88] have concluded from experimental data that liquid crystals of surfactants exist at the interface. These observations have been suggested through birefringence, interfacial tension, and viscosity measurements. Lack et al. [87] studied the formation of liquid crystals with fatty alcohol costabilizers as a function of concentration, chain length, and ratio of emulsifiers using birefringence measurements. Tertiary phase diagrams were presented which show two regions of normal micelle formation. There are also three regions of homogeneous anisotropic mesophases. These three mesophases, are (i) hexagonal rodlike aggregates of mixed micelles, (ii) lamellar double layers with overlapping tails, and (iii) lamellar double layers dispersed in the aqueous phase. The concentration of surfactants used in miniemulsions is found to fall within region (iii). These "liquid crystals" were shown to form more easily at higher emulsifier concentrations, with shorter chain alcohols, and with sonication.

Although evidence exists for liquid crystal formation with fatty alcohol costabilizers, it does not for systems with long chain alkanes. Delgado et al. [89] have presented evidence that the role of hexadecane costabilizer in miniemulsion polymerizations is one of diffusional control. Rodriguez [90] and Delgado [91] have reported that no optional ratio of hexadecane to SLS exists in the preparation of miniemulsions. This provides evidence for the lack of crystal formation. Ugelstad et al. [45] have presented evidence that alkanes are more likely to follow the diffusion mechanism.

3.3.1 Polymeric Costabilizers

The use of polymer as a costabilizer was first reported by Reimers et al. in 1995 [92]. Conventional thinking has been that effective costabilizers must be highly water-insoluble, highly monomer-soluble, and of low molecular weight, as required by Eq. 2. Polymer made from the same monomer from which the miniemulsion is to be made will be highly water-insoluble, and most polymers are quite soluble in their own monomers. The requirement that the costabilizer must be of low molecular weight is based on reported swelling experiments and theoretical swelling calculations [93]. Data from Schork and Reimers [94] demonstrate that it is possible to create miniemulsion latexes with a poor costabilizer (polymer). The inclusion of a small amount (~4%wt) of a monomer-

soluble polymer can significantly reduce the diffusional degradation of an emulsion. These emulsions are not *thermodynamically* stable, but they can be *kinetically* stable. This means that the droplets resist diffusional degradation long enough to allow nucleation to occur. The droplets are typically in the miniemulsion range of 100 to 500 nm in diameter. The polymeric costabilizer is thought to delay Ostwald ripening sufficiently to allow nucleation of the monomer droplets by water-phase radicals (primary or oligomeric). Once the droplets are nucleated, the polymer produced adds additional diffusional stability. It should be noted that the monomeric miniemulsions formed are not true miniemulsions in the sense that they are not stable over a period of months. However, Ostwald ripening can be reduced to permit the polymerization to be carried out. The latexes produced from polymer-stabilized emulsions have all the characteristics of miniemulsion latexes, and derive from droplet nucleation. The polymer has been shown to perform as well as hexadecane in stabilizing the droplets for the short periods necessary to ensure nucleation. It has the added advantages of being totally innocuous in the final product, very soluble in the monomer, and very water insoluble.

Reimers and Schork [94, 95] report the use of PMMA to stabilize MMA miniemulsions enough to effect predominant droplet nucleation. Emulsions stabilized against diffusional degradation by incorporating a polymeric costabilizer were produced and polymerized. The presence of large numbers of small droplets shifted the nucleation mechanism from micellar or homogeneous nucleation, to droplet nucleation. Droplet diameters were in the miniemulsion range and reasonably narrowly distributed. On-line conductance measurements were used to confirm predominant droplet nucleation. The observed reaction rates were dependent on the amount of polymeric costabilizer present. The latexes prepared with polymeric costabilizer had lower polydispersities (1.006) than either latexes prepared from macroemulsions (1.049) or from alkane-stabilized miniemulsions (1.037).

Wang and Schork [73] used PS, PMMA and PVAc as the costabilizers in miniemulsion polymerizations of VAc with PVOH as the surfactant. They found that, while PMMA and PS were effective kinetic costabilizers (at 2–4%wt on total monomer) for this system, PVAc was not. While the polymeric costabilizers did not give true miniemulsions, Ostwald ripening was retarded long enough for predominant droplet nucleation to take place.

Aizpurua et al. [96] have studied the kinetics of vinyl acetate miniemulsions stabilized with PS or PVAc. Guyot and coworkers [97] used PS as the costabilizer for the miniemulsion encapsulation of pigment. Samer [67] has used PMMA to stabilize MMA miniemulsions for continuous polymerization in a CSTR.

Various papers on hybrid miniemulsion polymerization have used alkyd [98, 99], polyester [100] or polyurethane [101] as both the costabilizer and a component of the hybrid particle. Since most of these materials were added far in excess of the levels normally used as costabilizers, it is not surprising that they are effective.

Polymeric materials are not costabilizers in the sense that costabilizers cause superswelling. Rather, they slow the onset of Ostwald ripening and preserve the number of monomer droplets, if not their size. However, this review will take a functional, rather than thermodynamic definition of a costabilizer, and include a discussion of the use of polymers as agents to enhance droplet nucleation under the heading of costabilizers.

3.3.2 Monomeric Costabilizers

Reimers and Schork [102] first used highly water-insoluble comonomers as costabilizers. Vinyl hexanoate, *p*-methyl styrene, vinyl 2-ethyl hexanoate, vinyl decanoate, and vinyl stearate were copolymerized with MMA at 10%wt on the total monomer. All formed stable miniemulsions with droplet diameters between 150 and 230 nm. All resulted in polymerization via predominant droplet nucleation (miniemulsion). Chern and coworkers [43, 74, 75,103] have used high molecular weight alkyl methacrylates at levels of 2–3%wt on the total monomer as both costabilizers and comonomers in the miniemulsion polymerization of styrene. The advantage, of course, is that, after polymerization, no low molecular weight costabilizer remains in the miniemulsion latex. Lauryl methacrylate and stearyl methacrylate have been used, since these high methacrylates have low water solubilities (10^{-8}–10^{-9} g/g) and high solubilities in styrene monomer. As might be expected, stearyl methacrylate is found to be better at retarding Ostwald ripening than lauryl methacrylate, but neither is found to be as effective as HD. Samer [104] found that 2-ethylhexyl acrylate (2EHA) as a comonomer was not an effective costabilizer in a continuous stirred tank (CSTR) copolymerization with MMA.

3.3.3 Other Costabilizers

The use of a chain transfer agent (CTA) as a costabilizer opens up new possibilities for molecular weight control. Macroemulsion polymerizations which utilize higher molecular weight mercaptan chain transfer agents exhibit retarded transport of the CTA from the monomer droplet into the growing polymer particles. This results in slower delivery of the mercaptan to the reaction sites over the course of the polymerization. (In some commercial recipes this retarded transport is used to "meter" the highly reactive CTA to the reaction site.) If the mercaptan were at the site of polymerization, as in a miniemulsion, new degrees of freedom in selecting chain transfer agents would exist. That is, the relative reactivities of chain transfer versus propagation can be used to select the CTA, without relying on retarded mass transfer. This may increase the efficiency of chain transfer (since CTA will not be "trapped" in the shrinking monomer droplets near the end of Interval II), or at least allow the chemist additional degrees of freedom in tailoring the molecular structure by manipulating the reaction conditions.

Mouran et al. [105] polymerized miniemulsions of methyl methacrylate with sodium lauryl sulfate as the surfactant and dodecyl mercaptan (DDM) as the costabilizer. The emulsions were of a droplet size range common to miniemulsions and exhibited long-term stability (of greater than three months). Results indicate that DDM retards Ostwald ripening and allows the production of stable miniemulsions. When these emulsions were initiated, particle formation occurred predominantly via monomer droplet nucleation. The rate of polymerization, monomer droplet size, polymer particle size, molecular weight of the polymer, and the effect of initiator concentration on the number of particles all varied systematically in ways that indicated predominant droplet nucleation.

For the MMA/DDM system, the value of the chain transfer constant (C_x) is 0.6–0.8, meaning that the chain transfer agent reacts slightly less rapidly than the monomer. Hence, the DDM will be present throughout the course of the reaction. In a system such as styrene/DDM, where C_x is 15–20, the rapid consumption of the DDM might leave the particles subject to Ostwald ripening before enough polymer is formed to stabilize the growing particles. In addition, the rapid consumption of CTA early in the course of the polymerization might give a clearly identifiable low molecular weight tail. Wang et al. [106] studied the miniemulsion polymerization of STY with DDM as the costabilizer. In this system, the chain transfer constant is at the other end of the kinetic spectrum.

The miniemulsion monomer droplets with dodecyl mercaptan as costabilizer were very stable. Shelf lives ranged from 17 hours to three months. The kinetics of miniemulsion polymerization were studied. Unlike other miniemulsion systems where the costabilizer does not act as a chain transfer agent, the polymerization rate fell with costabilizer level because the chain transfer agent enhances radical desorption from the particles. The polymerization rates in all of the miniemulsions were lower than those of the corresponding macroemulsions. Polymerized particles were larger than in the corresponding macroemulsions, but molecular weights were lower. Results indicate that DDM can serve as an effective costabilizer as well as a chain transfer agent, even when the chain transfer constant is quite high. The fact that the molecular weights were lower in the miniemulsion reactions indicates predominant droplet nucleation.

Reimers and Schork [107] used lauroyl peroxide (LPO) in the miniemulsion polymerization of MMA as a costabilizer as well as an initiator. They showed that lauroyl peroxide concentrations above 1 g/100 g of monomer are capable of stabilizing droplets against Ostwald ripening. The stable droplets produced were in the miniemulsion-size range and could then be nucleated. The ratio of the number of droplets to the number of particles was found to be close to unity. The overall rates of polymerization were high for the miniemulsions, as were the rates per particle. Once again, it was shown that components other than conventional costabilizers can stabilize small droplets against Ostwald ripening, causing droplet nucleation. Asua et al. [108] used LPO (in addition to the traditional costabilizer HD) to impart diffusional stability to styrene miniemulsions. They also evaluated a number of oil-soluble initiators (LPO, BPO, AIBN) as costabilizers, and concluded that only LPO was capable of acting as the sole costabilizer (without HD).

3.3.4 Enhanced Nucleation

Miller et al. [109–111] report that the addition of a small amount (as small as 0.05%wt) of polystyrene (PS) to the styrene phase of a miniemulsion polymerization of styrene causes an increase in both the rate of polymerization and the number of final polymer particles. This is not just a polymeric costabilizer effect, since these emulsions were also stabilized with what are known to be effective levels of HD or CA, although the effect was more pronounced with CA. With the addition of 1%wt styrene, the number of final particles was nearly the same as the original number of droplets, indicating 100% droplet nucleation. This was not the case for equivalent polymerizations without the PS. For polymerizations without the PS, the final particle number varied with the initial initiator concentration to the power of 0.31. With 1%wt PS, the particle number was independent of the initiator concentration, which is very clear evidence of 100% droplet nucleation. Miller hypothesized that miniemulsions prepared from polystyrene in styrene solutions resemble the polymer particles formed in normal (no polymer) miniemulsion polymerizations at early conversions. This being the case, these polymer-containing droplets would be able to effectively compete with growing polymer particles for free radicals, whereas their counterparts that contain no polymer are not, and as a result a greater fraction of the initial droplets become polymer particles. Based on this mechanism, Miller speculated that the presence of the polymer increases the capture efficiency of the droplets by modifying either their interior (by increasing the interior viscosity, thereby increasing the probability of a radical propagating rather than exiting) or the droplet/water interface (by disrupting the surfactant/CA interfacial barrier to radical entry). Experimental results were reported which support the latter explanation. (It should be noted that the effect was most pronounced with CA, and that other investigators have reported near 100% droplet nucleation with HD and without added polymer.)

In a follow-on set of papers, Blythe et al. [112–115] studied the effect on the polymerization kinetics of changing the properties of the polymer used to enhance nucleation. Miniemulsions were formed from CA with PS as the polymer additive, and CA as the costabilizer. Varying the molecular weight of the PS from 39,000 and 206,000 in systems containing 1% PS did not change the kinetics. Also, changing the end group of the polymer chain from a hydrophobic end group to a hydrophilic end group had no effect on the kinetics in 1% polymer systems. However, predissolving 1% PS in a miniemulsion always results in a significant enhancement in the kinetics compared to similar systems that do not contain predissolved polymer. The authors conclude that this enhancement in the kinetics is not due to either a change in the interior viscosity of the droplets or a disruption of the condensed phase formed by cetyl alcohol and sodium lauryl sulfate (since these effects would be altered by the variations in the PS above). Instead, it was suggested that the enhancement can primarily be attributed to a preservation of the droplet number due to the pre-

sence of polymer in each of the miniemulsion droplets formed during homogenization. The authors rightly point out that the polymer is a poor costabilizer, due to its high molecular weight, but that it does act to preserve the droplet due to the thermodynamic balance between monomer and polymer. Therefore, they conclude that the polymer is unable to preserve the size of the droplets produced during ripening, only the number produced during homogenization. They support this by using 1% PS with no other costabilizer, where they are able to show that particle formation occurs via droplet nucleation. In other experiments, they show that there is no enhancement unless the shear rate is high enough to bring the droplet size down into the range where it is susceptible to Ostwald ripening.

In another paper, Blythe et al. [116] studied enhanced droplet nucleation when HD is used as the costabilizer. The enhancement in this case is much less. The authors conclude that, since HD is a very effective costabilizer (much more so than CA), the effect of the polymer in preserving the droplet number, if not the droplet size distribution, is not pronounced. Therefore, this effect appears to occur primarily in systems with CA (perhaps due to its polar nature, and so, its probable interfacial activity). Multiple investigators have reported effective (near 100%) droplet nucleation with HD and other costabilizers.

Blythe et al. argue (with justification) that polymer should not be termed a costabilizer since it does not cause super-swelling; however, this review will take a functional, rather than thermodynamic definition of a costabilizer, and treat polymer-stabilized miniemulsions under the heading of costabilizers.

3.4 Choice of Initiator

Following the common practice in macroemulsion polymerization, most miniemulsion polymerizations have been run using water-soluble initiators. However, a number of researchers have looked at the possibility of using an oil-soluble initiator instead. As discussed previously, Schork and Reimers [107] and Asua et al. [108] have used LP as both the initiator and the costabilizer. In addition, Asua et al. used other oil-soluble initiators in conjunction with HD (as the costabilizer) to carry out miniemulsion polymerization of styrene.

Ghazaly et al. [117] used both water-soluble and oil-soluble initiators in the copolymerization of *n*-butyl methacrylate (BA) with crosslinking monomers. Variations in the particle morphologies were found between the water-soluble and oil-soluble initiators, depending on the hydrophobicity of the crosslinking monomer. It would seem that if the crosslinking monomer is quite hydrophobic, and therefore resides preferentially in the core of the particles (droplet), then the oil-soluble initiator is more effective at carrying out crosslinking, since the oil-soluble initiator will also reside preferentially in the core of the particle. Luo and Schork [118] carried out emulsion and miniemulsion polymerization using oil-soluble initiator in the presence of an aqueous phase free radical scavenger. They concluded that, for miniemulsion particles up to 100 nm in

diameter, even with an oil-soluble initiator, radicals originating in the aqueous phase play an important role in initiating polymerization. This is attributed to the fact that two radicals generated from the decomposition of an initiator molecular within the particle may recombine before initiating polymerization.

Choi et al. [53] have successfully used both water-soluble and oil-soluble initiators in the miniemulsion polymerization of styrene. Alducin and Asua [119] have studied the MWD of polystyrene miniemulsion polymerized with oil-soluble initiators. Rodriguez et al. [61] have developed a mathematical model of seeded miniemulsion polymerization with oil-soluble initiator. Blythe et al. [120] have successfully carried out miniemulsion polymerization of styrene with AMBN (oil-soluble). Ghazaly et al. [117] have used AIBN for the miniemulsion copolymerization of a hydrophobic bifunctional macromer. The polymerization progressed much faster when KPS was used than when AIBN was used. This may be due to the tendency of oil-soluble initiator radicals to recombine before initiating polymerization, as discussed by Luo.

Oil-soluble initiators have commonly been used in hybrid miniemulsion polymerization to improve monomer conversions. In most cases, the oil-soluble initiator was used as a *finishing initiator* to increase final monomer conversion, while a water-soluble initiator was used to carry out the majority of the polymerizations. These types of polymerizations will be discussed later.

3.5 Robust Nucleation

One of the problems with macroemulsion polymerization is the variability of the particle number with initiation rate, monomer quality, inhibition levels, and so on. This is a serious industrial problem, as shown by the fact that a great many industrial macroemulsion polymerizations are carried out as seeded polymerizations in which a known concentration of seed particles are added to the emulsion, and the polymerization is run under conditions that suppress nucleation of additional particles. The variance in particle number comes about because there is a competition for surfactant between the growth of existing particles (that need additional surfactant to stabilize their growing surface area), and the nucleation of new particles.

If a miniemulsion could be run at 100% droplet nucleation (or near to this), then a very robust nucleation system would result. The number of particles could be determined by the number of initial monomer droplets, and this can be controlled by adjusting surfactant, costabilizer and shear levels. In this case, the number of particles would be independent of radical flux. In fact, the most compelling evidence for droplet nucleation is experimental evidence that the number of polymer particles is independent of the initiator level. (Once the radical flux is high enough to nucleate all, or nearly all of the droplets, then changes in radical flux caused by inconsistent initiator or unknown inhibitors will not affect the final particle number.) We will discuss the results of such robust nucleation later.

3.6 Monomer Transport Effects

Macroemulsion polymerization relies on the transport of monomer from the monomer droplets to the polymer particles. This transport is driven by the equilibrium swelling of the polymer particles. This presumes rapid (relative to the rate of polymerization) transport of monomer. For most monomers, this is a good assumption. However, for monomers that are very water insoluble (VEOVA [vinyl versatatex] or DOM [dioctyl maleate]), this may not be true. In making this determination, the following assumptions can be made:

(i) The limiting resistance is the transport from the monomer droplets into the aqueous phase.
(ii) Transport across the aqueous phase is by forced convection (stirring) and it is not the rate-determining step.
(iii) Transport from the aqueous phase into the polymer particle may (or may not) have an overall mass transfer coefficient equal to that for exit from the monomer droplets, but the very large interfacial area of the particles (relative to the monomer droplets) will ensure that this is not the limiting step.
(iv) Transport out of the monomer droplet can be modeled with an overall mass transfer coefficient and a driving force based on the difference between the saturation concentration of monomer in the aqueous phase and the concentration in the aqueous phase in equilibrium with the particle.

For monomers that are highly water insoluble, the driving force in (iv) will be small, since the saturation value will be extremely small. Since accurate overall mass transfer coefficients are hard to determine accurately, the likelihood of transport limitation with highly water-insoluble monomers is an open question. Some data (which will be discussed later) indicate the presence of transport limitations in the copolymerization of highly water-insoluble monomers. These potential transport limitations can be avoided by using miniemulsion polymerization.

In the case of nanoencapsulations of solids, or the incorporation of high molecular weight, highly water-insoluble additives (such as polymers, oligomers, alkyds) into polymer particles, macroemulsion polymerization will not work, since the high molecular weight material will remain in the monomer droplet as the monomer is transported out. At the end of the reaction, the additive will remain in the depleted monomer droplets, rather than in the polymer particles. Clearly, these products can only be made via miniemulsion polymerization.

3.7 Droplet Stability

Different techniques are available to carry out a free radical polymerization in emulsion. In spite of the fact that their names (macro-, mini- and microemul-

sion) seem to indicate a correlation between process and final particle size of the polymer particle dispersion, this is usually not the case. On the contrary, these techniques should rather be distinguished by either their nucleation process or the stability of the initial oil (the monomer) dispersion. These two aspects of the emulsion polymerization processes, nucleation and stability, are strictly related and depend upon each other.

To clarify this point, let us first discuss the case of a conventional emulsion recipe, or macroemulsion. In this case, the monomer is initially dispersed in water under agitation in the presence of surfactants [121], resulting in a rather coarse oil dispersion. Droplet size typically depends upon rate of stirring, and the resulting droplet size is generally in the 1–10 μm range (the reason for the name "macroemulsion"). This dispersion is unstable and, if the stirring is stopped, the monomer phase separates very quickly. Because of the large sizes of the droplets, the total surface area of the dispersion is small (the surface-to-volume ratio for spherical droplets is proportional to the inverse of the droplet diameter) and most of the surfactant is not used to stabilize the droplets; it aggregates in water to form micelles. These micelles, and not the droplets, are the main loci for polymerization, while the droplets just act as monomer reservoirs. In other words, the final particles in the macroemulsion do not correspond to the initial droplets. The most important consequence is that, in order to have a successful process, the monomer, as well as all other possible comonomers and coreactants, must be water-soluble enough to diffuse from droplets to particles.

For historical reasons [122], a stable dispersion of sub-micron droplets is called a miniemulsion. Miniemulsions do not form spontaneously and require high shear devices to form. The resulting dispersion is usually quite fine, with the droplet size ranging from 50 to 500 nm [3], a large droplet surface area, with all of the surfactant used to stabilize the droplets and with no more micelles present in the system. As a result, the droplets become the predominant loci for nucleation and polymerization. That is, in an ideal miniemulsion, there is a 1:1 correspondence between initial monomer droplets and final polymer particles. (This 1:1 correspondence is not always attained, and remains a point of controversy [1].) This was experimentally demonstrated for the first time by Ugelstad and coworkers in 1973 [5]. The consequence of this virtual copying process from droplets to particles is twofold: (i) final particle size is given by the initial droplet dispersion, and both surfactant coverage and surface tension do not significantly change during the process; (ii) any kind of hydrophobic component can be conveniently included in the recipe, since we can be sure that it is going to participate to the polymerization process.

A third type of emulsion process is the so-called microemulsion [123]. In microemulsions, the polymerization starts in droplets as well. However, these are thermodynamically stable and, in contrast to miniemulsions, they form spontaneously by gentle stirring. They consist of large amounts of surfactants or mixtures of them, and they possess an interfacial tension close to zero at the water/oil interface, with droplet sizes usually ranging between 5 and 50 nm. In

contrast to miniemulsions, the high amount of surfactant needed to prepare the microemulsions leads to a complete coverage of the droplets surface. Given the huge number of droplets initially present in the system, nucleation cannot take place in all of the droplets, and a large number of empty micelles can still be found in the final product.

Besides the similarities between mini- and microemulsions, especially with respect to the nucleation process, microemulsions are characterized by very peculiar thermodynamics; in this respect, there are many similarities between a macro- and a miniemulsion. Accordingly, we should focus on the reason why monomer dispersions are unstable in macroemulsions, while they are stable in miniemulsions.

3.7.1 Stability of Monomer Dispersions

There are two ways by which a dispersion of monomer droplets can degrade: (i) by droplet coalescence, and (ii) by diffusion degradation (often referred to as Ostwald ripening). While the first mechanism of degradation can be avoided by adding enough surfactant to the system, when two monomer droplets of different sizes, and stabilized by a surfactant, are put in water, they will start exchanging monomer without even making direct contact – through monomer diffusion across the water (continuous) phase.

This process of molecular diffusion is governed by the difference in chemical potentials of the monomer in the two droplets. Morton's equation has been successfully used to describe the swelling of polymer particles with monomer [32]. According to this equation, the chemical potential of the monomer in a droplet of radius $r_p(\mu_m^{(d)})$ in the presence of polymer is given by:

$$\frac{\mu_m^{(d)}}{RT} = \ln(\varphi_m) + \left(1 - \frac{1}{m_{pm}}\right)\varphi_p + \chi_{m,p}\varphi_p^2 + \frac{2\gamma\bar{V}_m}{r_p RT} \tag{3}$$

where φ_m and φ_p represent the volume fraction of monomer and polymer, respectively, in the particle (so $\varphi_m+\varphi_p=1$); m_{pm} is the ratio of equivalent number of molecular segments between monomer and polymer; $\chi_{m,p}$ is the interaction parameter between monomer and polymer; γ is the interfacial tension at the water/oil interface; $\bar{V}_m$ is the molar volume of the monomer; R is the universal gas constant; T the temperature. In the case of pure monomer droplets, the partial molar free energy of mixing is zero, which is represented in Eq. 3 by the first two terms, accounting for the entropy of mixing, and by the third term, accounting for the enthalpy of mixing. Ugelstad and Hansen showed that this expression could be satisfactorily extended to the case where any other species, not necessarily a polymer, is involved [11]. Accordingly, we will use Eq. 3 to conveniently describe the monomer chemical potential in a miniemulsion droplet.

According to Eq. 3, in the case of a macroemulsion of pure monomer droplets, the monomer chemical potential is given by the last term with (φ_m=1),

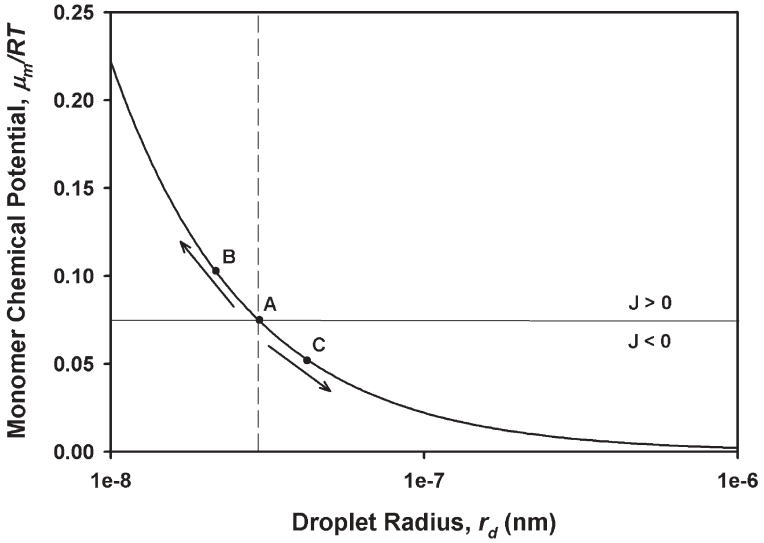

Fig. 6 Monomer chemical potential for a pure monomer droplet as a function of droplet radius (γ=25 Mn/M; $\bar{V}_m$=1.1·10^{-4} m^3 mol; T=298.15 K). Point A represents an unstable equilibrium

accounting for the contribution of the interfacial energy. Therefore, given two droplets with the same interfacial tension (we assume that surface tension is a function of the degree of coverage only, and that this is the same for the two droplets), their chemical potential is a function of the droplet radius only and it is only the same if the two droplets have the same size. Therefore, when two droplets of different radii $r_{d,1}$ and $r_{d,2}$ are put together, the difference in their chemical potential is given by:

$$\frac{\Delta\mu^{(d)}_{m,1-2}}{RT} = \frac{2\gamma\tilde{V}_m}{RT}\left(\frac{1}{r_{d,1}} - \frac{1}{r_{d,2}}\right) = \psi\left(\frac{1}{r_{d,1}} - \frac{1}{r_{d,2}}\right) \tag{4}$$

In other words, if $r_{d,2}>r_{d,1}$, the difference in chemical potential is positive and the monomer will diffuse from 1 to 2. This process is schematically represented in Fig. 6. Point A represents the initial size of the monomer droplets. Equilibrium exists only if all of the droplets have the same size. In the case where a smaller droplet is created (symbolized by point B), monomer will flow from B to A (positive flux to A, or $J>0$) as a result of the difference in chemical potential, making B smaller and smaller. The opposite happens for a bigger droplet (point C), which will become bigger and bigger. In other terms, point A is an unstable equilibrium. This process is usually referred to as monomer ripening.

The ripening process characteristic of oil dispersions is avoided in miniemulsions by introducing a so-called costabilizer in the oil phase (a species with no or very low water phase solubility). The mechanism that halts the

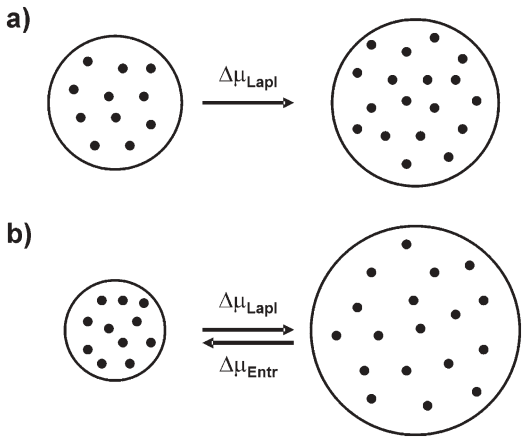

Fig. 7 Schematic representation of the role of the hydrophobe in halting the ripening process in a miniemulsion

ripening in a miniemulsion is sketched in Fig. 7. Let us suppose that the oil phase is initially comprised of the monomer and a perfectly water insoluble costabilizer. Let us also suppose that the system is initially made of two droplets with different sizes but the same compositions (or monomer volume fractions). Finally, let us suppose, for the sake of simplicity, that the mixture of monomer and costabilizer behaves like an ideal mixture, so that $\chi_{m,h}=0$. Under such hypotheses, the difference in chemical potential between the two droplets of Fig. 7a is given by the following equation:

$$\frac{\Delta\mu^{(d)}_{m,1-2}}{RT} = \ln\frac{\varphi_{m,1}}{\varphi_{m,2}} + (1-m_{m,h})(\varphi_{m,2}-\varphi_{m,1}) + \psi\left(\frac{1}{r_{d,1}}-\frac{1}{r_{d,2}}\right) \tag{5}$$

where the indexes 1 and 2 refer to the first and the second droplet, respectively, subscript *h* identifies the costabilizer, and ψ is defined as in Eq. 4. Knowing that $\ln\varphi_m \approx -(1-\varphi_m)$ for small volume fractions of the costabilizer, it is possible to simplify the previous equation as follows:

$$\frac{\Delta\mu^{(d)}_{m,1-2}}{RT} = m_{m,h}(\varphi_{m,1}-\varphi_{m,2}) + \psi\left(\frac{1}{r_{d,1}}-\frac{1}{r_{d,2}}\right) \tag{6}$$

Since the two droplets have the same initial composition ($\varphi_{m,1}=\varphi_{m,2}$), it follows from this equation that the difference in chemical potential is given by the difference in size only, and (as in a macroemulsion) monomer will flow from the smaller to the bigger droplet. The main consequence of this process is that the costabilizer is concentrated in the smaller droplet, while the big droplet becomes more and more dilute. This creates a gradient in composition (see Fig. 7b), which is represented by the first term on the right hand side of Eq. 6.

Therefore, an opposite flow of monomer is generated, which eventually leads to an equilibrium between the two terms of Eq. 6 (to a stable situation).

Just for completeness, these two contributions to the monomer equilibrium in a miniemulsion are often expressed in terms of pressures in the literature. The droplet composition gives rise to a so-called osmotic pressure:

$$\Pi_{osm} = RTc_m \tag{7}$$

while the presence of an interface generates a so-called Laplace pressure inside the droplet, defined as follows:

$$\Pi_{Lapl} = \frac{3\gamma}{r_d} \tag{8}$$

Note that, when accounting for the differences in osmotic and Laplace pressures between the two droplets, one obtains the same equation as Eq. 6, with $m_{m,h}$=8/3.

This same process is described in Fig. 8 in terms of the different contributions to the monomer chemical potential. In this figure, the initial droplet size (r_d) and monomer volume fraction (φ_m) have been fixed, and the corresponding volume of costabilizer inside the droplet has been computed ($V_h = 4/3\pi r_d^3$ ($1-\varphi_m$). Assuming that the costabilizer cannot diffuse out of the particle, in Fig. 8 it is possible to observe how chemical potential of the monomer changes by increasing or decreasing the monomer volume fraction in the droplet. In particular, two contributions to the global potential (entropy of mixing and surface tension) have been reported. It is clear that if a second droplet is inserted into the system, these two terms will act in opposite ways until the difference in chemical potential between the droplets is compensated for.

Even though two droplets are always able to find an equilibrium when put together, because of the presence of the costabilizer, it is useful to check whether this equilibrium is stable or not. Going back to the case of the macroemulsion depicted in Fig. 6, point A is an unstable point because, if the system is perturbed and a new droplet is formed, it will diverge from the equilibrium point. Clearly, the necessarily condition to have a stable equilibrium is that the slope of the chemical potential versus radius is positive at the point of equilibrium [122, 124]. For a macroemulsion, this condition leads to the following expression:

$$\frac{\partial}{\partial r_d}\left(\frac{\mu_m^{(9)}}{RT}\right) = -\frac{\psi}{r_d^2} \tag{9}$$

which is always a negative function. This is not true for a miniemulsion. Referring to Fig. 8, we observe that the equilibrium point of the system is stable. In fact, if a larger droplet is generated by perturbing the equilibrium, this has a larger chemical potential and the monomer will flow back, bringing the droplet back to the original equilibrium point. The opposite happens when producing a smaller droplet.

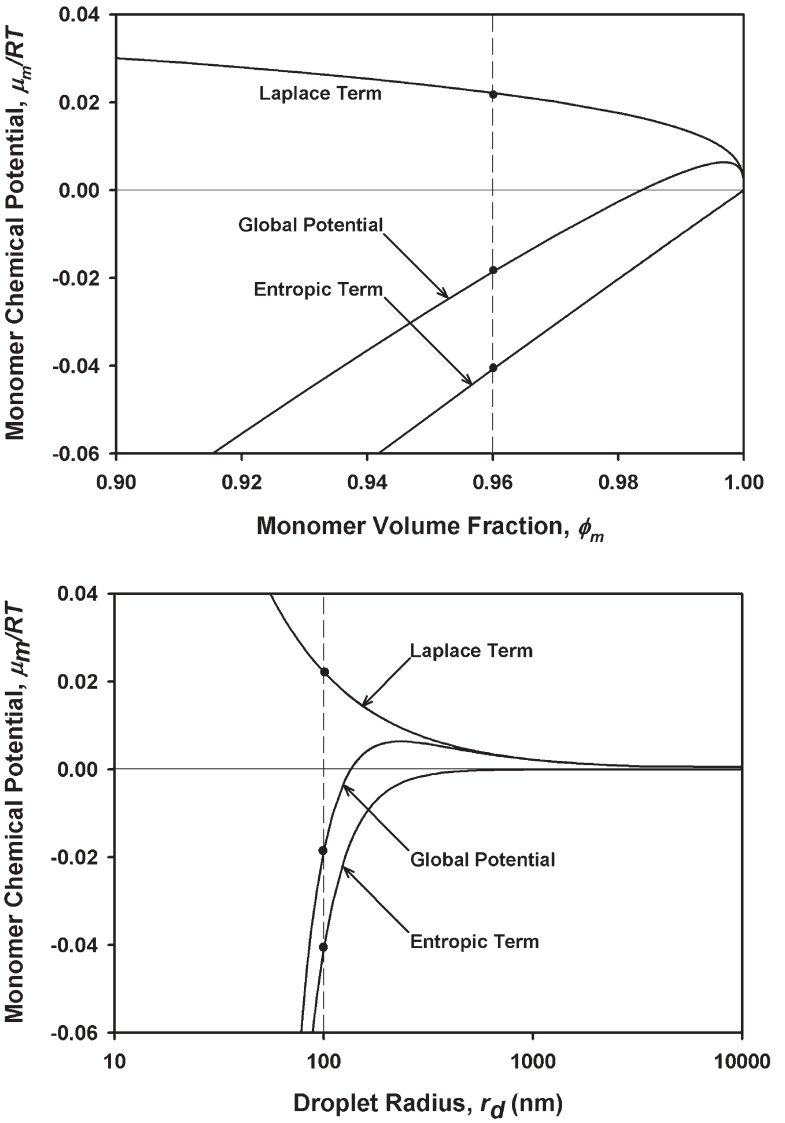

Fig. 8 Monomer chemical potential in a droplet comprising monomer and hydrophobe as a function of the monomer volume fraction (top) and droplet radius (bottom). The global potential (as given by Ugelstad's equation) is given, as well as the entropic term due to mixing and the Laplace term due to surface tension. Parameters: $m_{m,h}$=1; $\chi_{m,h}$=0; γ=25 mN/m; $\tilde{V}_m$=1.1 · 10^4 m^3 mol; T=298.15 K; φ_m=0.96; r_d=100 nm

Let us check the conditions under which the derivative of the chemical potential is positive in a miniemulsion. Under the hypothesis of small concentrations of costabilizer in the droplet ($\varphi_m \rightarrow 1$), and of ideal behavior of the mixture ($\chi_{m,h}=0$), the condition of local stability leads to the following expression:

$$\frac{\partial}{\partial r_d}\left(\frac{\mu_m^{(9)}}{RT}\right) = \frac{9 m_{m,h} V_h}{4\pi r_d^4} - \frac{\psi}{r_d^2} \tag{10}$$

and in turn to:

$$r_d < \bar{r}_d = \left(\frac{9 m_{m,h} V_h}{4\pi\psi}\right) \tag{11}$$

The previous expression returns the value of the droplet radius corresponding to the maximum of the monomer chemical potential curve ($\bar{r}_d$), and says that, for a given amount of costabilizer in the particle (V_h), the droplet radius must be smaller than $\bar{r}_d$ in order to be locally stable. The same equation can be expressed in terms of the critical costabilizer volume fraction, $\bar{\varphi}_h$, as follows:

$$\varphi_h > \bar{\varphi}_h = \left(\frac{\psi}{3 m r_h}\right)^{3/2} \tag{12}$$

where $r_h=(3V_h/4\pi)^{1/3}$. Both these two critical quantities, $\bar{r}_d$ and $\bar{\varphi}_h$, are functions of costabilizer concentration, costabilizer type and surface tension, as well as the corresponding value of the monomer chemical potential, which is given by the following simple expression:

$$\left.\frac{\mu_m^{(d)}}{RT}\right|_{r_d=\bar{r}_d} = 2\left(\frac{\psi}{3}\right)^{3/2}\left(\frac{1}{m_{m,h} r_h}\right)^{1/2} \tag{13}$$

Therefore, it is important to show how these quantities depend upon the parameters involved, and what their effects are, in order to understand the stability of the droplet.

This analysis is shown in Fig. 9, where the parameters ψ, $m_{m,h}$, r_d and φ_m have been varied systematically. Let us start with the analysis of Fig. 9a. In this figure, the volume of the droplet has been varied while the volume fraction of the costabilizer is kept constant (the vertical dashed line represents the corresponding monomer volume fraction). This, in turn, changes the volume of the costabilizer inside the droplet, and the monomer chemical potential curve changes accordingly. As predicted by Eq. 12, when the droplet size is decreased, the maximum of the chemical potential curve shifts to smaller monomer volume fractions, and the height of the maximum increases. In other terms, as droplet size decreases (or costabilizer volume fraction decreases) the system approaches the unstable region. Figure 9b is conceptually identical to Fig. 9a,

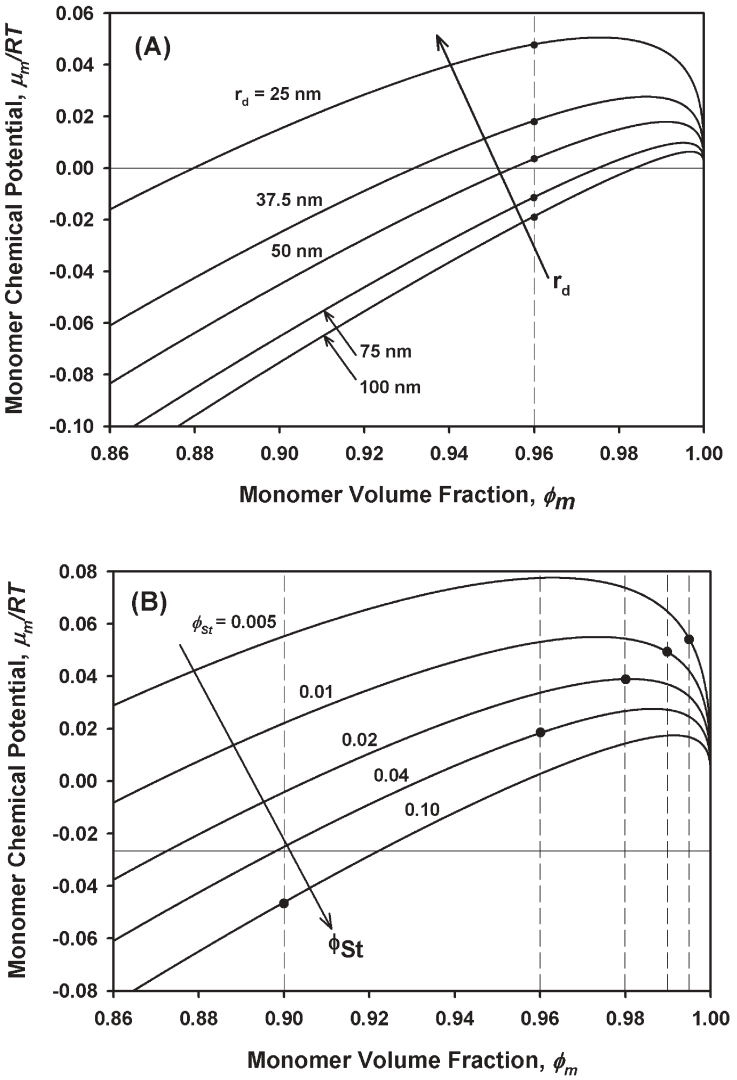

Fig. 9 Monomer chemical potential in a droplet comprising monomer and hydrophobe as a function of the monomer volume fraction. (A) Effect of droplet size (r_d=25, 37.5, 50, 75 and 150 nm); (B) effect of hydrophobe volume fraction (φ_h=0.005, 0.01, 0.02, 0.04 and 0.1)

but the amount of costabilizer in the droplets is varied while the droplet radius is kept constant and the costabilizer volume fraction varies. Again, as the costabilizer concentration decreases, the system moves from a region of complete stability to a region of instability. By observing Fig. 9b, it is also possible to distinguish between local and global equilibrium stability. The curve corresponding to φ_h=0.04 clearly satisfies the requirements of local equilibrium stability. In fact, if the system is slightly perturbed, the equilibrium point is always

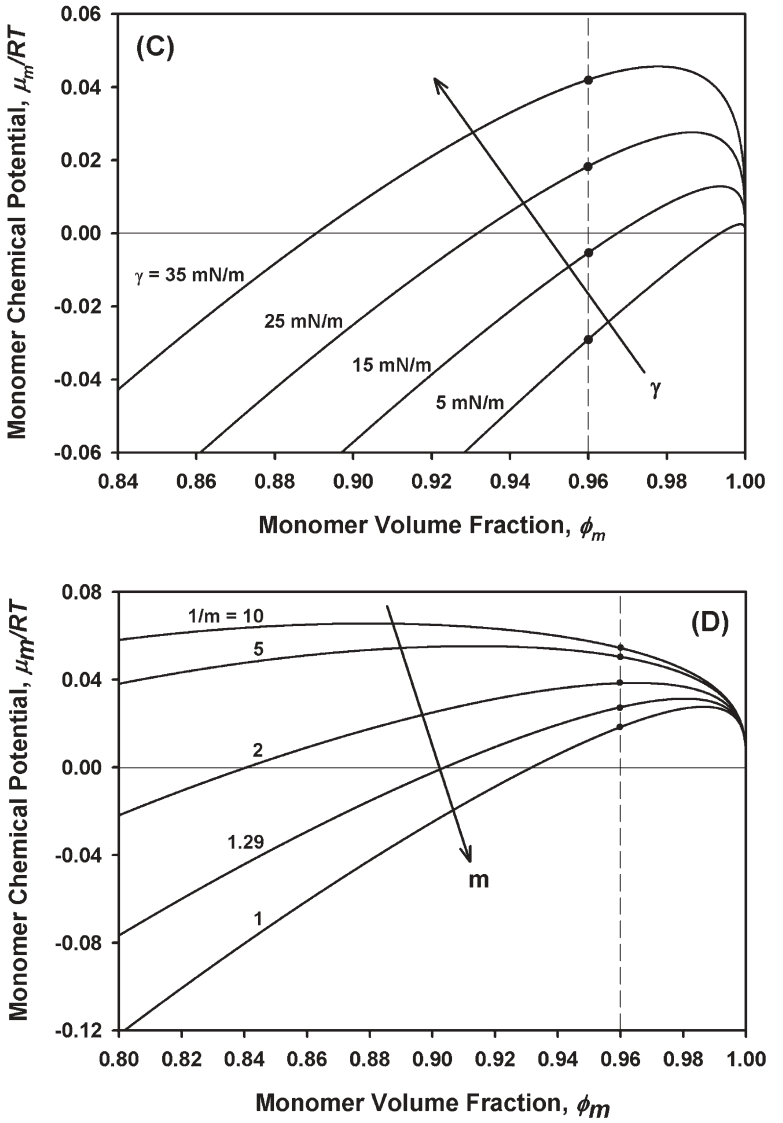

Fig. 9c,d (C) effect of surface tension (γ=5, 15, 25 and 35 mN/m); and (D) effect of hydrophobe to monomer segment ratio ($1/m_{m,h}$=1, 1.29, 2, 5 and 10). Other parameters (otherwise differently indicated): $m_{m,h}$=1; $\chi_{m,h}$=0; γ=25 mN/m; $\tilde{V}_m=1.1\cdot10^4$ m^3 mol; T=298.15 K; φ_h=0.04; r_d=100 nm

convergent. However, in the case of large perturbations, it is possible to create droplets large enough to fall to the right of the maximum of the monomer chemical potential curve; these droplets have chemical potentials lower than that corresponding to equilibrium. Such a droplet will receive monomer from the droplets at the equilibrium point and will grow indefinitely. On the other hand, the same cannot happen for the equilibrium point corresponding to the curve for φ_h=0.10. In fact, in this case, all of the droplets that are larger than those at the equilibrium point also have larger monomer chemical potentials. Therefore, these droplets will always shrink back to the equilibrium point.

In Fig. 9c, the effects of different surface tension values on the equilibrium are examined. By decreasing the interfacial tension, the Laplace term becomes less significant than the contribution given by the entropy of mixing, and therefore ripening is decreased and stability is enhanced. Theoretically, in a system with zero surface tension at the oil/water interface, the total monomer chemical potential is given solely by the entropic terms, and it is always stable.

Finally, in Fig. 9d, the influence of the ratio of the equivalent number of molecular segments in the costabilizer to that of the monomer, $m_{m,h}$ is shown. This value can be thought of as the ratio between the molecular weights of the two components, and for oligomers and polymers this can be replaced by the average chain length. If we look closely at this figure, as well as Eqs. 12 and 13, we can see that the maximum of the chemical potential curve becomes smaller and shifts to larger droplet sizes as $m_{m,h}$ approaches unity, which facilitates the formation of a stable equilibrium. When dealing with very bulky costabilizers (such as a polymer), the maximum increases and shifts to low droplet sizes, making the equilibrium unstable.

There are two issues we should remark upon at this point. First, even though we have shown that the presence of a costabilizer in the system can lead to complete thermodynamic stability, we have also shown that costabilizers with smaller molecular weights are more effective. Therefore, even though these species are hydrophobic, they always have a small but finite solubility in water. As a result, the differences in costabilizer chemical potentials among the droplets will lead to a very slow diffusion of the costabilizer and eventually to the destabilization of the system. Second, Eqs. 11 and 12 do not contradict those reported by (for example) Sood and Awasthi, that point to a minimum droplet diameter below which there is no stability [124]. In our analysis, we set the equilibrium and the corresponding volume of costabilizer, and then we perturbed the system by changing the monomer concentration, and observed what happened. In their work, they computed the corresponding equilibrium point as a function of droplet radius for a given costabilizer concentration, and they checked the conditions at which this point corresponds to a stable equilibrium. As in our analysis, they conclude that decreasing droplet radius sufficiently eventually pushes the system into the region of instability.

3.7.2 Experimental Validation

Our understanding of miniemulsion stability is limited by the practical difficulties encountered when attempting to measure and characterize a distribution of droplets. In fact, most of the well-known, established techniques used in the literature to characterize distributions of polymer particles in water are quite invasive and generally rely upon sample dilution (as in dynamic and static laser light scattering), and/or shear (as in capillary hydrodynamic fractionation), both of which are very likely to alter or destroy the sensitive equilibrium upon which a miniemulsion is based. Good results have been obtained by indirect techniques that do not need dilution, such as soap titration [125], SANS measurements[126] or turbidity and surface tension measurements [127]. Nevertheless, a substantial amount of experimental evidence has been collected, that has enabled us to establish the effects of different amounts of surfactant and costabilizer, or different costabilizer structures, on stability.

This work has been summarized very effectively by Landfester and coworkers [127]. They showed that many costabilizers act as osmotic agents, blocking monomer ripening. All of these costabilizers have relatively low molecular weights and, according to the analysis above, the polymers can barely be used to prevent ripening, even though the resulting miniemulsion can be stable for enough time to run the polymerization.

However, the most significant result of their work was that they clearly demonstrated the role of surfactant in the formation of miniemulsions. They showed that it is possible to effectively control droplet size by tuning the surfactant concentration. The more surfactant, the smaller the droplets one can obtain. They also showed that, apart from the case where extremely large amounts of surfactant are used, the surfactant coverage of the droplets is always incomplete. In particular, larger droplets exhibit very low coverage and, therefore, large interfacial tensions at the oil/water interface. On the other hand, small droplets need large surfactant coverage in order to be stable.

In the same work, it is also supposed that colloidal stability, rather than monomer ripening, plays an effective role in determining the final droplet size. Such a conclusion was supported by two different experimental results. First, it was noticed that droplet size increases right after the emulsification process stops, and a stable situation is typically achieved after just a few hours. However, if surfactant is added immediately after, this growth in size does not occur. Second, it is shown that there is a clear correlation between final droplet size and amount of oil phase used in the recipe. In particular, when the oil fraction in the system increases, droplet size also increases.

These results can be effectively explained by supposing that colloidal stability plays a major role in determining miniemulsion stability. In fact, it is clear that addition of surfactant stops the droplet growth, which is explained by the enhanced colloidal stability. Moreover, in more concentrated systems, where the rate of droplet coalescence is larger, one obtains larger droplets, as

expected. However, some droplet flocculation or the formation of a limited layer of monomer at the water/air interface is commonly observed in many miniemulsion recipes. Moreover, there are well documented cases in the literature where either a bimodal distribution has been obtained at the end of the polymerization [124], or instability problems are evident at the beginning of the polymerization [128].

When speculating about the colloidal stability of a monomer droplet dispersion in water, one could use the Deryaguin-Landau-Verwey-Overbeek theory, also known as DLVO theory, to analyze the stability of the system. This has been done in Fig. 10a, where we show the effect of different surface potentials upon the rate of coagulation, β, defined in the case of two droplets of the same size as:

$$\beta = \frac{8\, k_b T}{3 \mu W} \tag{14}$$

where μ represents the water viscosity and W is Fuch's stability ratio (see [129] for a further explanation of how this value has been computed). In Fig. 10b, the quantity $1/\beta N_d$ is reported, which expresses the characteristic time for coalescence. We can see that even small surface potentials are enough to give great colloidal stability. These values correspond to rather low surfactant coverage (around 5%) [124, 129], which is well below the typical coverage measured experimentally for miniemulsions [127]. It is therefore apparent that colloidal stability is a very strong function of droplet size, and it is quite difficult to explain the formation of bimodalities or monomer separation by colloidal stability only.

On the other hand, previous analyses of the monomer chemical potential in miniemulsions may justify some of the previous results. In Fig. 8, it is shown that miniemulsion formulations are often very close to instability, with positive monomer chemical potentials (which corresponds to conditions of monomer oversaturation, or superswelling). Experimental proof of this was reported by Landfester et al. [127], who said that the Laplace pressure is much larger than the osmotic pressure at equilibrium. We must also consider that, in reality, we are never dealing with perfectly monodispersed distributions of droplets, as the previous analysis supposed. Therefore, it is realistic to suppose that in the presence of a droplet size distribution, a fraction of the droplets lie in the unstable region and can lead to the formation of either pronounced bimodalities, monomer phase separation, or droplet flocculation [124]. Moreover, from the analysis of Fig. 9a to d, we observe that critical stability is almost reached when small droplets are formed. Therefore, it is not surprising to observe that smaller droplets require larger surfactant coverage to be stable, since lower surface tension helps the droplets to move away from the instability region. The same influence of surface tension on the chemical potential of the monomer could also explain why, on the addition of surfactant, the sizes of the droplets do not change significantly after emulsification. In fact, by adding surfactant, one decreases the interfacial tension and stabilizes the miniemulsion ripening.

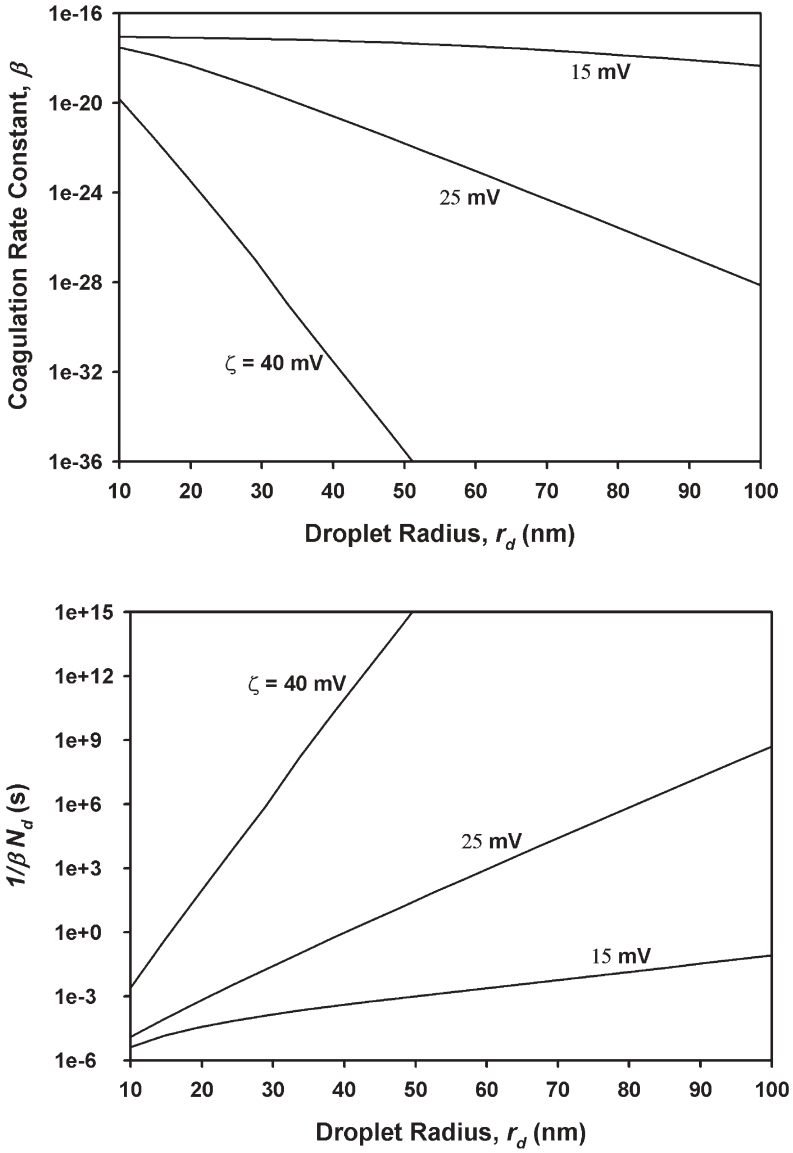

Fig. 10 Coagulation rate constant (β) and characteristic time for coagulation ($1/\beta N_d$) as a function of droplet size for various droplet surface potential values (ζ=15, 25 and 40 Mv), as computed by DLVO theory. In order to compute N_d, a system with 20% oil fraction was supposed

It is certain that we do not know what the leading effect in determining droplet stability and droplet distribution in miniemulsion is at this point; both colloidal and ripening effects probably play a role. Future work is therefore needed to clarify these problems.

3.8 Semibatch and Plug Flow Reactors

Semibatch (also known as *semicontinuous*) reactors are used commercially for two primary reasons: to limit the rate of polymerization by effecting some level of monomer starvation, or to correct for copolymer composition drift in copolymerization. Since the use of semibatch reactors for miniemulsion copolymerization involves important concepts (relative rates of mass transfer and reactivity ratios), a discussion of semibatch copolymerization reactions will be deferred until the section on copolymerization. In the area of semibatch homopolymerization, Tang et al. [116] studied seeded semibatch polymerization of BA. They found that when the monomer was added neat, a small number of new particles were formed. However, when the semibatch feed was a miniemulsion, a large number of new particles were formed, presumably by droplet nucleation. Monomer droplet nucleation decreased with increasing seed concentration, presumably because of monomer transport to the existing particles. Leiza, Sudol and El-Aasser [130] used semibatch miniemulsion polymerization (starting from a seed latex) to prepare high solids (>60%) lattices of BA. It is well-known that semibatch polymerization can be an effective method for making high solids latex. Part of the advantage of semibatch when making high solids is the broad PSD brought on by nucleation of particles over most of the reaction time. Miniemulsion can be effective in this regard, since a miniemulsion feed is likely to produce additional polymer particles, as shown by Tang et al. [131].

Sajjadi and Jahanzad [132] have used semibatching to study the effects of monomer-starved and monomer-flooded conditions on the seeded polymerization of styrene. Seed particles were grown via macroemulsion polymerization and added to the initial charge of the reactor. Feeds of styrene miniemulsion (using HD as the costabilizer) were then added, either batch-wise or in a semibatch mode. Under starved conditions, the miniemulsion droplets were depleted of their monomer by transport into the growing particles. (Even though HD prevents the loss of monomer to droplets of a larger size, it cannot prevent monomer depletion to polymer particles with a low degree of monomer saturation, as would be found in a starved reactor; this same effect will be seen later in experiments where fresh miniemulsion droplets are introduced into a CSTR at high monomer conversion.) When the miniemulsion was added batch-wise (flooded conditions) the final particle number was greater, since a greater portion of the miniemulsion droplets were nucleated before being depleted of monomer. When polymer was predissolved in the monomer prior to miniemulsion formation, the final number of particles was indepen-

dent of the method of addition, and was equal to the seed particles plus the number of miniemulsion droplets added. Therefore, with predissolved polymer, the droplet number (but not the droplet size distribution as inferred from the final PSD) was preserved. This result reinforces the idea of polymer as an agent for preserving droplet number.

Macro- and miniemulsion polymerization in a PFR/CSTR train was modeled by Samer and Schork [64]. Since particle nucleation and growth are coupled for macroemulsion polymerization in a CSTR, the number of particles formed in a CSTR only is a fraction of the number of particles generated in a batch reactor. For this reason, their results showed that a PFR upstream of a CSTR has a dramatic effect on the number of particles and the rate of polymerization in the CSTR. In fact, the CSTR was found to produce only 20% of the number of particles generated in a PFR/CSTR train with the same total residence time as the CSTR alone. By contrast, since miniemulsions are dominated by droplet nucleation, the use of a PFR "prereactor" had a negligible effect on the rate of polymerization in the CSTR. The number of particles generated in the CSTR was 100% of the number of particles generated in a PFR/CSTR train with the same total residence time as the CSTR alone.

Durant [133] has used a PFR to achieve a miniemulsion with a solids content in the industrially relevant range. Ouzineb and McKenna [134] have used a PFR to obtain miniemulsion latexes with high solids contents.

3.9
Continuous Stirred Tank Reactors

The first work on continuous miniemulsion polymerization was by Chen,Gothjelpsen and Schork [55]. Theirs was a very simple model of CSTR miniemulsion polymerization using an oil-soluble initiator. The first experimental work was that of Barnette [35, 135]. This work showed two significant facts:

(i) Miniemulsion polymerization in a CSTR is not subject to the sustained or decaying oscillations very often found in CSTR macroemulsion polymerization. The sustained oscillations in macroemulsion take place at low surfactant concentration due to the competition for micellar surfactant between existing particles requiring additional surfactant to stabilize the increased interfacial area produced by particle growth, and nucleation of new particles from micelles. Since, in miniemulsion polymerization, the nucleation occurs from monomer droplets, and micelles do not exist, no such competition exists, and the monomer conversion climbs monotonically on start-up to its steady-state value.
(ii) In miniemulsion polymerization, the steady-state monomer conversion is approximately twice that found in macroemulsion polymerization (after the oscillations have died away). This means that a single CSTR will yield approximately twice as much polymer as the same reactor carrying out a macroemulsion polymerization.

Observation (i) above can be understood in terms of droplet nucleation and the lack of competition between nucleation and growth. A mechanistic understanding of observation (ii) above was provided by Samer and Schork [64]. Nomura and Harada [136] quantified the differences in particle nucleation behavior for macroemulsion polymerization between a CSTR and a batch reactor. They started with the rate of particle formation in a CSTR and included an expression for the rate of particle nucleation based on Smith Ewart theory. In macroemulsion, a surfactant balance is used to constrain the micelle concentration, given the surfactant concentration and surface area of existing particles. Therefore, they found a relation between the number of polymer particles and the residence time (reactor volume divided by volumetric flowrate). They compared this relation to a similar equation for particle formation in a batch reactor, and concluded that a CSTR will produce no more than 57% of the number of particles produced in a batch reactor. This is due mainly to the fact that particle formation and growth occur simultaneously in a CSTR, as suggested earlier.

An approach similar to that taken by Nomura and Harada was used by Samer to quantify the effects of droplet nucleation on emulsion polymerization kinetics in a CSTR. In their simplified analysis, it was assumed that radical capture by particles and droplets is proportional to the ratio of particle and droplet diameters. This assumption is reliable at low to moderate residence times, when polymer particles still closely resemble monomer droplets with respect to composition and surface characteristics. For predominant droplet nucleation, the maximum particle generation is limited by the concentration of monomer droplets in the feed. In Fig. 11 the steady state particle generation is given as a function of the residence time and temperature. Nucleation efficiency is defined as the number of particles divided by the number of droplets in the

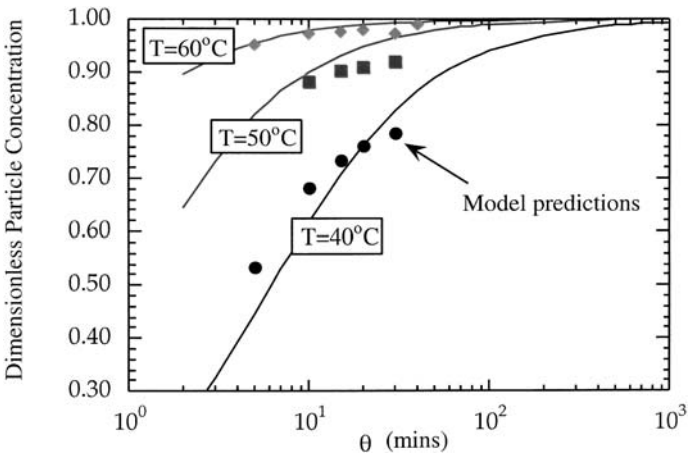

Fig. 11 Model predictions for the number of particles in CSTR miniemulsion polymerization expressed as the number of particles divided by the number of droplets in the feed (from [64])

feed and is shown to increase with increasing temperature. It can be seen in this figure that the nucleation efficiency approaches unity for residence times greater than 30 minutes. Therefore, whereas the particle number is limited by surfactant in macroemulsion emulsion polymerization in a CSTR, in miniemulsion polymerization, the particle number is limited by monomer droplet concentration, *but to a much smaller extent*. Therefore, since nucleation efficiencies in miniemulsion polymerization approach 100%, rather than the 57% predicted for macroemulsion polymerization, the steady-state conversion in a miniemulsion (proportional to particle number) found by Barnette [36] is approximately twice that in a macroemulsion.

Samer and Schork [69, 137] confirmed Barnette's findings on the lack of oscillations in the CSTR miniemulsion polymerization of MMA. Aizpurua and Barandiaran [138] confirmed the lack of oscillations in CSTR miniemulsion polymerization over a wide range of surfactant and initiator concentrations for VAc. They also observed near-identical MWD for macroemulsion and miniemulsion polymerizations under the same conditions. This is understandable, since MWD should be determined by particle size (and number of radicals per particle) rather than by particle nucleation mechanism. Aizpurua et al. [139] successfully used polymeric costabilizers in the CSTR miniemulsion polymerization of VAc at high solids levels. Neither sonication alone, nor the presence of costabilizer alone, was able to eliminate the oscillations found in macroemulsion polymerization. However, sonication and costabilizer together were capable of eliminating oscillations, indicating droplet nucleation. The results cited above are particularly significant, since, as fresh miniemulsion droplets are introduced into a CSTR, they must compete to retain their monomer with existing particles that may contain more than 50% polymer (50% conversion). Therefore, for instance, miniemulsion droplets stabilized with 5% polymer would need to compete with existing particles containing 50% polymer. The fact that the particle number approaches the droplet number in the feed suggests that the droplet number (if not droplet size distribution) is conserved.

Samer also demonstrates the existence of multiple steady states in isothermal miniemulsion polymerization in a CSTR. This is not surprising, since multiplicity is a function of gel or Trommsdorf effect, and not of nucleation mechanism.

Miniemulsion copolymerization in a CSTR involves some very interesting features. However, in the interest of clarity, these systems will be discussed along with results for batch copolymerization.

4 Applications

It should be apparent by now that miniemulsion polymerization systems have some properties that ought to be exploitable when making polymer colloidal products with unique or improved properties. This section will discuss some of these documented and potential applications.

Overall, there are two areas in which miniemulsion polymerization differs significantly from macroemulsion polymerization. First, miniemulsions exhibit a significant robustness of nucleation. Macroemulsion polymerization relies heavily on micellar nucleation. Micellar nucleation is notoriously nonrobust. It has been called "near-chaotic", because final particle number depends on the operating variables (temperature, initiator concentration and addition method, mixing, and so on) and on the quality of the reagents (including initiator purity and level of inhibitor in the monomer). As stated above, this is due to the competition for surfactant between the nucleation of new particles from micelles and the adsorption of surfactant onto the surface of growing polymer particles. In fact, the sensitivity to inhibitor levels has actually been used to manipulate particle size: addition of an oil-soluble initiator is known to result in the nucleation of more particles, and hence smaller particles. The introduction of a water-phase inhibitor is known to extend Interval I, allowing particle growth to occur simultaneously with particle nucleation, producing fewer and hence smaller particles. Finally, the use of seeded systems to control particle number and size in commercial macroemulsion polymerization highlights the poor robustness of particle nucleation in macroemulsion polymerization. This should be contrasted with miniemulsion polymerization where, *if* droplet nucleation efficiency can be driven close to unity, the number of particles is determined by the levels of surfactant and costabilizer, and so should be controllable independent of the initiation system. While the number of particles is often preserved during miniemulsion polymerization, we have seen before that the PSD may not be. We have also seen the effect of robustness on CSTR polymerization, in that CSTR miniemulsion polymerization exhibits a substantially higher rate of particle nucleation *and* a lack of oscillations. This section will explore the ramifications of robust nucleation in miniemulsions.

The second property of miniemulsions that makes them unique when compared to macroemulsions is the virtual lack of monomer transport. Recall that, during Interval II of a macroemulsion polymerization, monomer must diffuse from the monomer droplets, across the aqueous phase, and into the growing polymer particles. Most macroemulsions are presumed to be reaction-limited. In other words, the rate of monomer diffusion is rapid in comparison with the rate of propagation, so that polymerization is reaction-limited. This is certainly true for monomers with water solubilities as low as that of styrene, but for monomers of much lower water solubility, this assumption may be questioned. Also, if any sort of non-monomeric materials are to be incorporated into the polymer particles, these are not likely to be transported easily across the aqueous phase. Examples of such systems would be preformed polymers or oligomers in hybrid miniemulsion polymerization, or solid particles in the case of nanoencapsulation. Certainly high molecular weight prepolymers or solid particles will not traverse the aqueous phase, and so, if introduced into a macroemulsion system, they will remain outside the loci of polymerization. In addition, in living radical polymerization, the molecular weight control agents are often only sparingly soluble in water. If the control agent is not at the locus

of polymerization, the polymerization will proceed by uncontrolled free radical polymerization, and any advantages of livingness are lost. This section will explore areas where miniemulsion polymerization may be superior to macroemulsion polymerization because of its virtual lack of interphase mass transfer.

4.1 Robust Nucleation

4.1.1 Effect of Initiation and Inhibition

Reimers [95] used polymeric costabilizer to carry out miniemulsion polymerization of MMA. Droplet nucleation was found to be the dominant nucleation mechanism in the polymerization. As a result, the nucleation was more robust, and the polymerizations were less sensitive to variations in the recipe or contaminant levels. This was evident in the rates of polymerization and in the particle numbers. The miniemulsion polymerizations were subjected to changes in initiator concentration, water-phase retarder, and oil-phase inhibitor, and were shown to be significantly more robust.

Batch miniemulsion polymerization of MMA using PMMA as the costabilizer was carried out with SLS as the surfactant and KPS as the initiator. Solids content was kept at ~30%. A low surfactant level was used with the miniemulsions to ensure droplet nucleation. The initiator concentration of the polymer-stabilized miniemulsion polymerizations was varied from 0.0005 to 0.02 M_{aq}, based on the total water content. An aqueous phase retarder, (sodium nitrite) or an oil-phase inhibitor (diphenylpicrylhydrazol [DPPH]), was added to both the miniemulsions and the macroemulsions prior to initiation. Particle numbers and rates of polymerization for both systems were determined.

4.1.1.1 Results

Results from the polymer-costabilized miniemulsion polymerizations are shown in Table 2. Droplet sizes were found to vary between 115.1 and 121.0 nm. These are in accord with measurements made by Fontenot [140] for MMA miniemulsions stabilized with hexadecane. The sizes of the particles in the final products were close to the sizes of the droplets, ranging from 102.6 to 108.1 nm, with polydispersities ranging from 1.011 to 1.027. The ratio of the number of particles to the number of droplets (N_p/N_d) was found to be between 0.95 and 1.08. Therefore, the majority of the droplets were nucleated to form polymer particles. Droplet nucleation led to polymerization rates comparable to those for the corresponding macroemulsions. For equal concentrations of initiator, 0.01 M_{aq}, the rates are 0.199 and 0.233 gmol/min L_{aq} for the mini- and the macroemulsion polymerizations, respectively.

Table 2 Results from polymer-stabilized miniemulsion polymerizations (from [95])

		D_d (nm)	D_p (nm)	PDI_p	$N_p \times 10^{-17}$ (L^{-1})	N_p/N_d	R_p (mol/min L_{aq})
[I]=	0.0005	118.1	105.1	1.013	4.452	0.99	0.096
	0.001	117.5	104.3	1.015	4.508	1.00	0.102
	0.002	116.8	105.1	1.018	4.428	0.98	0.151
	0.005	120.2	103.1	1.017	4.328	1.04	0.263
	0.01	117.4	105.1	1.016	4.548	1.01	0.199
	0.02	–	–	–	–	–	0.176
[$NaNO_2$]=	0.0	117.4	105.1	1.016	4.548	1.01	0.199
	0.0001	115.1	103.3	1.027	4.432	0.99	0.253
	0.0005	117.3	104.1	1.016	4.780	1.06	0.203
	0.001	118.7	102.7	1.011	4.840	1.08	0.201
	0.002	117.1	102.9	1.017	4.640	1.03	0.180
	0.005	118.2	118.4	1.014	3.304	0.47	0.016
[DPPH]=	0.0	117.4	105.1	1.016	4.548	1.01	0.199
	0.00005	118.2	103.2	1.013	4.704	1.05	0.155
	0.0001	118.4	103.3	1.012	4.720	1.05	0.149
	0.0005	117.8	102.6	1.014	4.732	1.05	0.146
	0.001	117.3	102.1	1.017	4.752	1.06	0.090
RPM=	100	119.2	107.0	1.012	4.328	0.95	0.086
	200	120.2	103.1	1.017	4.096	1.04	0.111
	300	120.8	108.1	1.012	4.096	0.97	0.138
	400	120.8	107.9	1.015	4.072	0.98	0.144
	500	121.0	107.4	1.012	3.996	0.95	0.143

The effects of the (water-soluble) initiator concentration on the polymerization of polymer-stabilized miniemulsion are shown in Table 2. An increase in the initiator concentration does not change the number of particles, but does increase the rate of polymerization. This is due to an increase in the number of radicals per particle. However, the number of radicals per particle ranged from just 0.5 to 0.8, indicating that the kinetics (after nucleation) are still essentially Smith Ewart Case II. The number of particles was found to be proportional to the initiator concentration raised to the power of 0.002±0.001. Macroemulsion polymerizations, in contrast, show a dependence of 0.2 and 0.4 for methyl methacrylate and styrene, respectively [141]. The fact that the exponent approaches zero indicates that all or nearly all of the droplets are being nucleated.

A water-phase retarder (sodium nitrite) was added to both the mini- and macroemulsion polymerizations. The rate of polymerization was reduced with increasing level of retarder, as would be expected. However, the number of particles *increased* with increasing retarder concentration. This result would only be expected with an *oil-soluble* retarder. The reason for this anomaly is

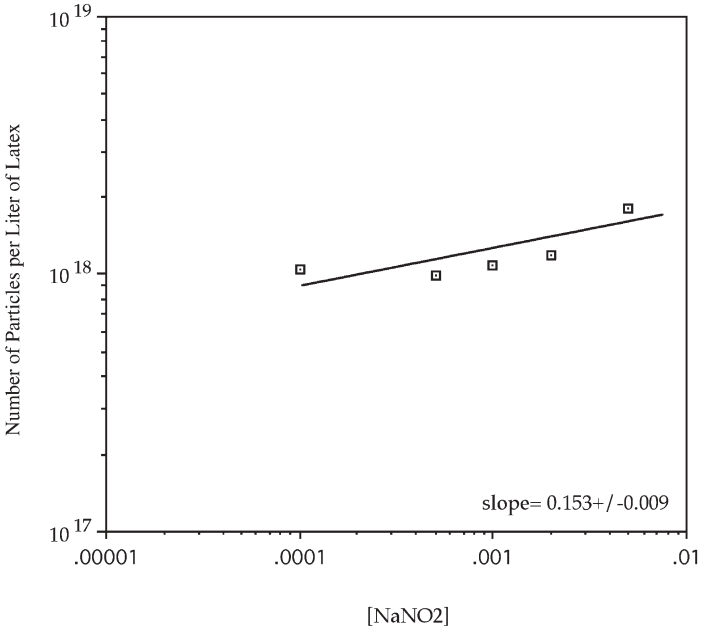

Fig. 12 The effect of a water-phase retarder on the number of particles in macroemulsion polymerization (from [95])

unknown. If we plot the log of the nitrite concentration against the log of the number of particles, we find a linear relationship between them, as depicted by Fig. 12. The slope of this line is 0.153±0.009. This value is close to the value of 0.2 reported for the initiator dependence, perhaps implying that the function of the water-phase retarder is simply to reduce the effective radical flux to the particles. The polymer-stabilized miniemulsions are far less sensitive to the presence of the retarder than are the macroemulsions. The retarder has little effect on the particle number. Particle numbers remained fairly constant up to a concentration of 5 mM_{aq}. Up to this amount, the dependence of the retarder concentration on the number of particles was calculated to be 0.020±0.007 (Fig. 13). This is significantly less than the value found for macroemulsions. (It is presumed that the highest level of retarder prevents a large fraction of the droplets from ever being nucleated.) Monomer conversions exhibit prolonged nucleation periods, but the rates are not significantly affected. Again the nitrite is acting as a retarder, since no induction period is observed.

Macroemulsion polymerizations carried out in the presence of an oil-phase inhibitor (DPPH) resulted in an increase in the number of particles. Presumably initiator radicals that enter droplets are terminated by the inhibitor, resulting in dead particles. These particles do not grow, and hence do not consume surfactant to stabilize their increasing surface area, until they absorb another radical. The surfactant not adsorbed by dead particles is available to

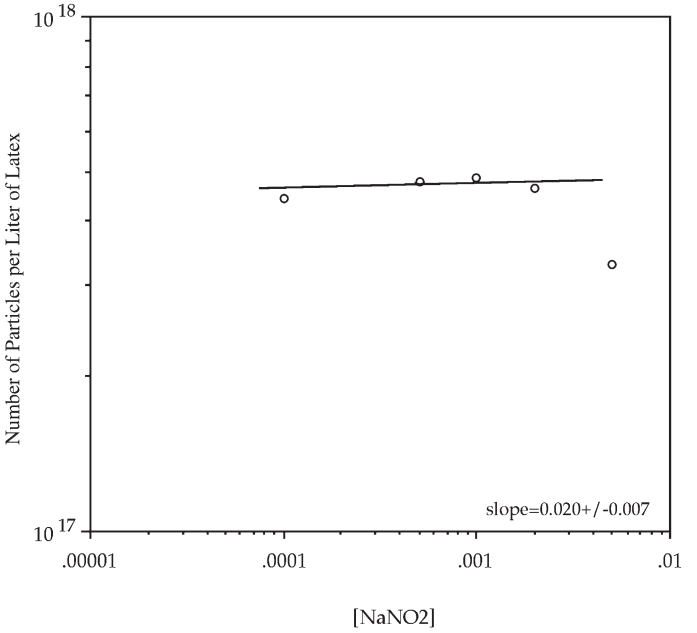

Fig. 13 The effect of a water-phase retarder on the number of particles in a polymer-stabilized miniemulsion polymerization (from [95])

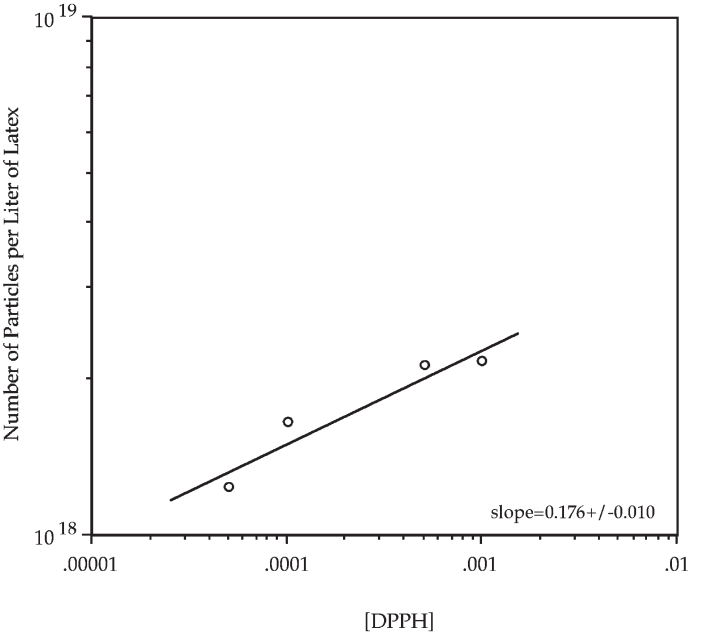

Fig. 14 The effect of an oil-phase inhibitor on the number of particles in macroemulsion polymerization (from [95])

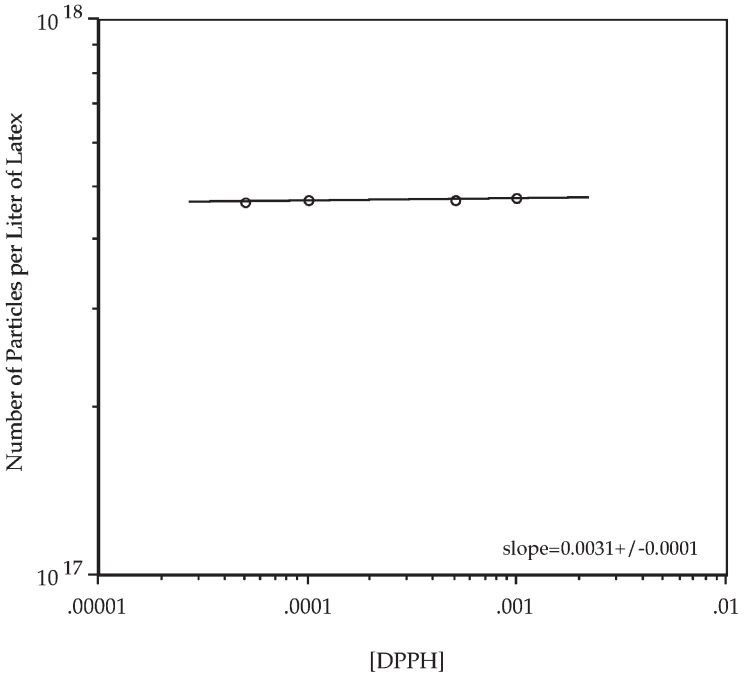

Fig. 15 The effect of an oil-phase inhibitor on the number of particles in miniemulsion polymerization (from [95])

stabilize new particles, thereby increasing the total number of particles. Since the nucleation period is lengthened, the polydispersity increases. Figure 14 shows that the dependence of the inhibitor concentration on the number of particles is 0.176±0.010. Conversion time curves indicate that an induction period results from the presence of the inhibitor. Since polymer-stabilized miniemulsion polymerization occurs via droplet nucleation, it should be less sensitive to oil-phase inhibition. Initiator radicals will enter the droplet one after the other until all of the inhibitor is used up, and the monomer polymerizes. This does not affect the number of droplets or particles. As seen in Fig. 15, the number of particles is proportional to the DPPH concentration raised to the power of 0.0031±0.0001. Therefore, the number of particles is essentially independent of the presence of inhibitor.

4.1.1.2 Summary

Shifting the site of nucleation to the droplets greatly enhances the robustness of the nucleation process to recipe variations, inhibition levels, and changes in operating procedure (initiation rate and/or agitation rate). As a result of droplet nucleation, polymer-stabilized miniemulsion polymerizations are far less sen-

Table 3 Summary of dependence of particle number on impurities and operational variations ([95])

X	*a* (macroemulsion)	*a* (miniemulsion)
[I][a]	0.2[3]	0.002±0.001
[$NaNO_2$]	0.153±0.009	0.020±0.007
[DPPH][b]	0.176±0.010	0.0031±0.0001
RPM	–	–0.026±0.001

[a] [I] and [$NaNO_2$] in gmol/L_{aq}.
[b] [DPPH] in gmol/L_{mon}.

sitive to these variations in operation. The dependence of the particle number on the concentration of initiator, water-phase retarder, oil-phase inhibitor, and agitation are shown in Table 3. The exponents for the variation of particle number with each of these variations were 0.002, 0.02, 0.0031, and –0.026, respectively. The corresponding values for the macroemulsions were one to two orders of magnitude larger. Therefore, nucleation in polymer-stabilized miniemulsion polymerizations was found to be more robust than in macroemulsion polymerizations.

An enhanced robustness can benefit a process in a number of ways. Since the polymer-stabilized miniemulsions are less susceptible to disturbances, their polymerization is less likely to be affected by operator error, fluctuations in feed stream concentrations and residual contaminants in the reaction vessel. Many monomers contain species that can act as inhibitors or retarders as a result of monomer production, storage, or processing. These contaminants also cause batch-to-batch variability in particle number in macroemulsions. Therefore, miniemulsion polymerization may be an alternative to seeded polymerization as a way of maintaining robust control of particle number.

4.1.2 Particle Size Distribution

There has been a belief that, due to the fact that the original miniemulsion droplets are formed by a shear process, the droplet size distribution will be broad, and so the resulting PSD will have a large polydispersity (as measured by the *polydispersity index*, defined as the mass average over the number average particle radius). In a recent note [142] Landfester et al. discuss particle size polydispersity in miniemulsions and attempt to dispel the idea that miniemulsions necessarily have broader PSD than the equivalent macroemulsions. Rather, they argue that the PSD of a miniemulsion can be either broader or narrower than its macroemulsion counterpart, and that, in most cases, the miniemulsion will have a polydispersity equal to, or only very slightly greater than, the equivalent macroemulsion.

4.1.2.1 Hexadecane as Costabilizer

Fontenot and Schork [140] studied the miniemulsion polymerization of methyl methacrylate using hexadecane as the costabilizer. A portion of their results are shown in Table 4. Polydispersities are listed for macroemulsion, and miniemulsions subjected to varying durations of sonication, at two levels of initiator. In this and all cases following, the macroemulsions and miniemulsions were made from the same recipe, but with the costabilizer left out of the macroemulsion. The miniemulsions and macroemulsions were polymerized by the same procedure except that the sonication was eliminated for the macroemulsions. It may be seen that at both initiator levels, the macroemulsion is slightly more narrow than some of the miniemulsions, but broader than others. An estimate of the standard deviation of the polydispersity measurement is given as ±0.01–0.02, and may be applied to all of the polydispersity data reported. With this standard deviation estimate, it may be seen that the differences in polydispersity between the macro- and miniemulsions are not likely to be significant.

Landfester et al. [143] studied the miniemulsion polymerization of styrene using hexadecane as the costabilizer. When styrene miniemulsions were subjected to varying sonication times (see Table 5), very similar trends are seen as for the MMA miniemulsions. The particle size and the polydispersity of miniemulsion droplets rapidly polymerized after sonication either do not depend on the amount of the costabilizer, or are very weak functions of the amount of costabilizer (see Table 6). It was found that doubling the amount of costabilizer does not decrease the radius nor have any effect on the polydis-

Table 4 Polydispersity index as a function of initiator concentration and sonication time, with hexadecane as costabilizer and MMA as monomer ([140])

Sonication time	Polydispersity index
[I] 0.005 mol/L(aq)	
Macroemulsion	1.05
2 min	1.08
4 min	1.06
6 min	1.04
12 min	1.05
[I] 0.01 mol/L(aq)	
Macroemulsion	1.05
2 min	1.07
4 min	1.06
6 min	1.05
8 min	1.07
12 min	1.04

Table 5 Polydispersity index as a function of sonication time, with hexadecane as costabilizer, styrene as monomer, and [I]=0.3 mol/L (aq) (from [143])

Sonication time	Diameter d_i (nm)	Polydispersity index
Macroemulsion	–	1.04
0.5 min	135	1.01
1 min	112	1.03
2 min	96	1.00
5 min	87	1.03
10 min	84	1.02
20 min	83	1.01

Table 6 Hexadecane as costabilizer, with styrene monomer (from [143])

Hexadecane level (gm)	Particle diameter d_i (nm)	Polydispersity index
Macroemulsion	98	1.04
0.33	109	1.03
0.66	108	1.01
1.66	108	1.01
3.33	102	1.04
5	100	1.03
6.66	99	1.05
8.33	95	1.01

persity. It was also found that the droplet size is initially a function of the amount of mechanical agitation. The droplets are rapidly reduced in size throughout sonication in order to approach a pseudo-steady state [143]. Once this state is reached, the size of the droplet does not change. Higher sonication time causes a slight reduction in polydispersity.

After halting sonication, a rather rapid equilibration process must occur. Since the droplet number after sonication is fixed, this process does not influence the average size, but the droplet size distribution usually undergoes very rapid change. It was found that steady-state miniemulsification results in a system "with critical stability"; in other words the droplet size is the product of a rate equation of fission by ultrasound and fusion by collisions, and the droplets are as small as possible for the timescales involved. The equality of droplet pressures makes such systems insensitive against net mass exchange by diffusion processes (after the very fast equilibrium process at the beginning), but the net positive character of the pressure makes them sensitive to all changes in the droplet size. Steady-state homogenized miniemulsions, which are critically stabilized, undergo droplet growth on a timescale of hundreds of hours, presumably by collisions or by costabilizer exchange. As can be seen from Table 7, during this growth, the polydispersity does not change significantly.

Table 7 Influence of time delay between the ultrasonication and the polymerization (from [143])

Time delay between start of polymerization and sonication (h)	Particle diameter d_i (nm)	Polydispersity index
0	82	1.01
1	87	1.05
6	108	1.03
48	152	1.03
96	164	1.04

Therefore, we may conclude that there is indeed no significant difference in polydispersity between the miniemulsion and the equivalent macroemulsion.

4.1.2.2 Dodecyl Mercaptan as Costabilizer

Mouron et al. [105] and Wang et al. [106] have used dodecyl mercaptan (DDM) as the costabilizer in styrene and MMA miniemulsion polymerizations, respectively. Some of the results are shown in Table 8 and Table 9. For styrene (Table 8), the macroemulsion is compared with miniemulsions containing varying levels of DDM (costabilizer). In this case, the macroemulsion has a broader particle size distribution than all but one of the miniemulsions. For MMA (Table 9), miniemulsions and the equivalent macroemulsions have been compared at varying initiator concentrations. In this case, the macroemulsions

Table 8 Dodecyl mercaptan as costabilizer with styrene monomer (from [106])

DDM level (gm)	Polydispersity index
Macroemulsion	1.02
1	1.01
2	1.01
3	1.02
4	1.04

Table 9 Dodecyl mercaptan as costabilizer with methyl methacrylate monomer (from [105])

Initiator (mol/L(aq))	Macroemulsion PDI	Miniemulsion PDI
0.005	1.02	1.02
0.01	1.01	1.02
0.02	1.01	1.02

all have narrower particle size distributions, although the difference is hardly significant.

4.1.2.3 Polymethyl Methacrylate as Costabilizer

Reimers and Schork [144] have used polymethyl methacrylate as the costabilizer for methyl methacrylate miniemulsion polymerization. A portion of the results are shown in Table 10. In this case, the miniemulsion has a narrower particle size distribution than the equivalent macroemulsion.

4.1.2.4 Influence of the Amount of the Surfactant

Colloidal stability is usually controlled by the type and amount of surfactant employed. In miniemulsions, the fusion-fission rate equilibrium during sonication, and therefore the size of the droplets directly after primary equilibration, depends on the amount of surfactant. For styrene miniemulsions that use SLS as surfactant, droplet sizes between 180 nm down to 32 nm can be obtained. The polydispersity slightly increases with decreasing size, but is still quite low (see Table 11). Using similar molar amounts of the simple cationic surfac-

Table 10 Polymethyl methacrylate as costabilizer with methylmethacrylate monomer (from [144])

	Polydispersity index
Macroemulsion	1.02
Miniemulsion	1.01

Table 11 Polydispersity index as a function of SDS concentration (from [105])

SDS concentration (% compared to monomer)	Particle diameter d_i (nm)	Polydispersity index
0.3	180	1.03
0.5	134	1.07
1.0	108	1.02
1.5	94	1.02
2.1	89	1.08
3.5	82	1.08
4.9	82	1.03
6.8	65	1.03
10.3	55	1.05
17.0	46	1.06
25.2	42	1.07

Table 12 Polydispersity index as a function of CTAB concentration (from [70])

CTAB concentration (% compared to monomer)	Particle diameter d_i (nm)	Polydispersity index
0.4	347	1.01
0.7	159	1.05
1.2	125	1.05
2.4	102	1.04
3.6	86	1.01
10.0	59	1.09
16.7	59	1.13

tant cetyltrimethylammonium bromide (CTAB) or the anionic surfactant SLS results in similar particle sizes, showing that the particle size is essentially controlled by the limit of the surfactant coverage of the latex particles [71, 145]. Again, the polydispersity increases with decreasing size (see Table 12), but is only slightly higher than in the SDS miniemulsions.

4.1.2.5 Summary

Based on the data above, it would appear that it is possible, via miniemulsion polymerization, to make a polymer latex with a particle size distribution that approaches that made by macroemulsion polymerization. In some cases, the miniemulsion product may be even narrower than the macroemulsion. There are two significant mechanisms leading to this narrowness. First, the monomer droplet size distribution is to some extent determined by the thermodynamics of swelling, and not solely by the droplet size distribution induced by the sonicator or homogenizer. For this to be true, the process should include a *ripening time* between sonication and polymerization. During this ripening time, the droplets will come to swelling equilibrium. Studies show that the ripening time is of the order of seconds to minutes, and is naturally included in the preparation of batch polymerizations. Second, the narrowness of the particle size distributions depends on the ability to nucleate nearly all of the droplets over a short period of time. If droplet nucleation takes place over a longer period of time, some particles will have polymerized for a longer time, and some droplets will lose monomer by mass transfer to growing particles before the droplets begin to polymerize. Using hexadecane or polymer as a costabilizer will facilitate one hundred percent droplet nucleation, while the use of cetyl alcohol does not. Miller et al. [109] have shown that a small amount of polymer dissolved in the monomer droplets enhances droplet nucleation. Also, the initiator flux must be high enough to nucleate all of the droplets within a short time interval.

In summary, the miniemulsion route to polymer latexes should not be dismissed solely due to a requirement for narrow particle size distribution, par-

ticularly when the unique properties of the miniemulsion process may be of particular advantage.

4.1.3 Shear Stability

The shear stabilities of mini- and macroemulsion latexes were compared and quantitatively evaluated with respect to their particle size distributions by Rodrigues and Schork [146]. Although miniemulsion latexes exhibit many of the properties of macroemulsion latexes, there may be subtle differences in particle size distribution and surface characteristics due to differences in their polymerization mechanisms. To study the effects of these differences on the shear stabilities of the miniemulsions, a quantitative approach was developed where changes in the average diameter and total number of particles have been related to the particle size distribution before and after shearing.

Two pairs of MMA mini- and macroemulsion latexes were polymerized for this study. HD was used as the costabilizer for the miniemulsions, and the polymerizations were carried out at 60 °C. Efforts were made to make the main- and macroemulsion in each pair as similar as possible. The two pairs were:

Pair I

Macroemulsion (Sample A)
0.02 mol. SLS/L_{aq}; 0.0115 mol. KPS/L_{aq}; 2 g DDM;
PSD range: 141–188 nm (diameter)

Miniemulsion (Sample E)
0.02 mol. SLS/L_{aq}; 0.0115 mol. KPS/L_{aq}; 2 g DDM;
PSD range: 96–123 nm (diameter)

Pair II

Macroemulsion (Sample H)
0.01 mol. SLS/L_{aq}; 0.0115 mol. KPS/L_{aq}; 4 g DDM
PSD range: 167–241 nm (diameter)

Miniemulsion (Sample D)
0.01 mol. SLS/L_{aq}; 0.0115 mol. KPS/L_{aq}; 4 g DDM
PSD range: 145–209 nm (diameter)

The samples were sheared using a rotational viscometer with a coaxial cylinder system, based on the Searle-type, where the inner cylinder (connected to a sensor system) rotates while the outer cylinder remains stationary. The outer cylinder surrounding the inner one was jacketed, allowing good temperature control, and the annular gap was of constant width. The sensor system used was the NV type, with a rotor with a recommended viscosity range of 2×10^3 mPa, a maximum recommended shear stress of 178 Pa, and a maximum recommended shear strain rate of 2700 s^{-1}; this rotor could work with volumes from 10–50 ml. Flow was laminar.

The optimum shear rate for each pair was arrived at by trial and error, such that the shearing produced aggregation, but not massive coagulation. That is, the shear rate was not increased beyond the point at which the particle diameters stopped increasing (and maybe even started decreasing again). All the tests were conducted at 25 °C; each miniemulsion latex within a pair was sheared for the same time interval as its macroemulsion latex counterpart. Only changes in particle sizes were followed during these series of experiments, with the particle size distribution (analyzed by dynamic light scattering, DLS) recorded before and after shearing for each of the shear experiments.

The ratio of total number of particles initially present to the total number of particles after shearing (N_i/N_f) was computed and used both to compare the two types of latexes, and to determine the extent of aggregation and the nature of the aggregates formed.

4.1.3.1 Relative Shear Stability of Miniemulsion and Macroemulsion Latexes

The particle size range and average particle diameter before and after shearing, and the shear rate and time of shear used for each of the sample pairs is shown in Table 13. For both pairs, the shifts in the particle size range and in the average diameter are substantially greater for the macroemulsion latex than the corresponding miniemulsion latex. In all cases, the particle size distribution broadened after shearing. The percentage change in average diameter is greater for the macroemulsions as well.

The ratio of the initial total number of particles to the final total number of particles after shearing (N_0/N_f) is shown in Table 14. It is clear that the macroemulsion latexes showed greater shear instability. The ratio N_o/N_f gives an indication of the extent of aggregation in each of the latexes; a N_o/N_f ratio of two would indicate that average aggregation up to doublet formation has taken place, and so on. It can be seen from Table 14 that aggregation has taken place in all the latexes essentially up to doublet formation, with slightly higher

Table 13 Particle size ranges and average particle diameters before and after shearing, and the shear rates and times of shear for samples A, E, H, and D (from [146])

Sample	Shear rate (s^{-1})	Time of shear (s)	Initial PSD range (diameter) (nm)	Average diameter before shearing (nm)	PSD range after shearing (nm)	Average diameter after shearing (nm)	% Change in average diameter (nm)
A (macro)	200	1260	141–188	155	181–244	204	31.61
E (mini)	200	1260	96–123	108	106–143	121	12.04
H (macro)	200	1260	167–241	195	218–319	264	35.38
D (mini)	200	1260	145–209	168	170–223	195	16.07

Table 14 Ratio of the initial total number of particles to the final number of particles after shearing for samples A, E, H, and D (from [146])

Sample	% Solids	N_i/N_f
A (macro)	27.2	2.28
E (mini)	25.9	1.41
H (macro)	20.9	2.87
D (mini)	24.8	2.43

aggregate formation in the macroemulsion latexes than in the miniemulsion latexes, as evidenced by their correspondingly higher N_o/N_f values.

4.1.3.2 Effect of Large Particles

The effects of a few externally-added large particles on the shear stabilities of miniemulsion- and macroemulsion latexes were also investigated. This was done to determine if the greater shear instability of the macroemulsion latex was due to the presence of a few large particles, possibly formed by droplet nucleation during the synthesis of the latex itself. To test this, portions of a larger particle size macroemulsion (Sample C) were added to the two macroemulsion latexes (Samples A and H), and portions of a larger miniemulsion (Sample G) were added to the two miniemulsion latexes (Samples E and D) used in the first part of this analysis. The large particles were as follows:

Macroemulsion Seed Latex (Sample C)

PSD range: 252–298 nm (diameter)
Average diameter: 276 nm

Miniemulsion Seed Latex (Sample G)

PSD range: 320–380 nm (diameter)
Average diameter: 344 nm

The percentages by weight of the larger particle size latexes used were 2, 5, 10 and 25% of total sample weight. The latexes were then sheared, and the shift in the particle size distribution range and average particle diameter, the percent change in this average diameter after shearing, and the N_o/N_f values were determined for both sets of samples. These results are shown in Tables 15 and 16.

Table 15 shows that, for all four samples analyzed, the percent change in average diameter increases with the fraction of larger particles, reaches a maximum, and then decreases. In all cases, the maximum shear aggregation occurs at approximately 5–10% large particles. This supports (but by no means proves) the hypothesis that macroemulsion latexes are more susceptible to shear coagulation than miniemulsion latexes due to the presence of a small fraction of large particles originating from droplet nucleation. It is important to remember

Table 15 Particle size ranges and average particle diameters before and after shearing, and the shear rates and times of shear for samples A, E, H, and D with large particles added (from [146])

Sample	Shear rate (s^{-1})	Time of shear (s)	Initial PSD range (diameter) (nm)	Average diameter before shearing (nm)	PSD range after shearing (nm)	Average diameter after shearing (nm)	% Change in average diameter (nm)
A (original-macro)	200	1260	141–188	155	181–244	204	31.61
A (2% big C)	200	1260	143–310	170	194–334	228	34.12
A (5% big C)	200	1260	144–317	176	208–358	249	41.48
A (10% big C)	200	1260	143–312	182	202–344	246	35.16
A (25% big C)	200	1260	143–308	199	196–333	250	25.63
E (original-mini)	200	1260	96–123	108	106–143	121	12.04
E (2% big G)	200	1260	102–372	118	114–380	153	29.66
E (5% big G)	200	1260	103–379	124	124–389	168	35.48
E (10% big G)	200	1260	106–384	131	130–397	177	35.11
E (25% big G)	200	1260	105–377	140	123–394	186	32.86
H (original-macro)	250	1740	167–241	195	233–348	277	42.05
H (2% big C)	250	1740	169–323	199	236–352	290	45.73
H (5% big C)	250	1740	171–338	207	264–388	324	56.52
H (10% big C)	250	1740	170–333	212	253–369	305	43.87
H (25% big C)	250	1740	170–312	222	242–355	297	33.78
D (original-mini)	250	1740	145–209	168	197–281	226.00	34.52
D (2% big G)	250	1740	149–370	179	224–377	247.00	37.99
D (5% big G)	250	1740	151–374	193	233–381	266	37.82
D (10% big G)	250	1740	154–373	208	242–399	284	36.54
D (25% big G)	250	1740	155–375	226	237–389	305	34.96

that in all four latexes used here, the size differential between these latexes and the two latexes used as large particles (Samples C and G) is not very large. Therefore, the particles that qualify as large particles by definition lie at the upper end of the particle size distribution of samples C and G; in other words, only a small fraction of the externally-added larger latex actually functions as large particles in terms of influencing shear stability.

The results shown in Table 16 support the observations drawn from Table 15. For all of the latexes, there is an increase in N_o/N_f value as the percentage of externally added large particles increases, up to approximately 5–10%wt of large particles. Any further addition of large particles decreases the N_o/N_f value.

Table 16 Ratio of the initial total number of particles to the final number of particles after shearing for samples A, E, H, and D with large particles added (from [146])

Sample	% Solids	N_i/N_f
A (original-macro)	27.2	2.28
A (2% big C)	27.1	2.41
A (5% big C)	26.9	2.83
A (10% big C)	26.7	2.47
A (25% big C)	26.2	1.98
E (original-mini)	25.9	1.41
E (2% big G)	25.7	2.18
E (5% big G)	25.6	2.49
E (10% big G)	25.3	2.47
E (25% big G)	25.2	2.34
H (original-macro)	20.9	2.87
H (2% big C)	21.1	3.09
H (5% big C)	21.2	3.83
H (10% big C)	21.2	2.98
H (25% big C)	21.3	2.39
D (original-mini)	24.8	2.43
D (2% big G)	24.9	2.63
D (5% big G)	25.3	2.62
D (10% big G)	25.5	2.55
D (25% big G)	25.6	2.46

4.1.3.3 Summary

Under controlled shearing conditions, miniemulsions were shown to be more shear stable than similar conventional or macroemulsions. This *may* be due to macroemulsion shear instability resulting from the presence of a small number of large particles (derived from droplet polymerization) that act as seeds for aggregation. Intentional seeding of mini- and macroemulsions with larger particles induced increased shear instability, supporting this hypothesis. However, it may be that miniemulsion polymerization avoids the burying of some of the initiator end groups. For KPS initiation, these end groups, if on the surface of the particle, will add substantially to the colloidal stability of the particles. Due to the nature of macroemulsion polymerization (particle growth at the expense of monomer droplets), end groups tend to become buried in the particle where they contribute nothing to colloidal stability. Since there is less particle growth (none in the ideal case) for miniemulsion polymerization, most of the initiator end groups should remain on particle surfaces.

While the mechanism is an open question, there clearly seems to be a difference in shear stability between miniemulsions and macroemulsions.

4.2 Monomer Transport Effects

One of the most unique properties of miniemulsion polymerization is the lack of monomer transport. Recall from Fig. 1 that with macroemulsion polymerization, the monomer must diffuse from the monomer droplets, across the aqueous phase, and into the growing polymer particles. In contrast, in an ideal miniemulsion (nucleation of 100% of the droplets), there is no monomer transport, since the monomer is polymerized within the nucleated droplets. This lack of monomer transport leads to some of the most interesting properties of miniemulsions. For most monomers, macroemulsion polymerization is considered to be reaction, rather than diffusion limited. However, for extremely water insoluble monomers, this might not be the case. In this instance, polymerization in a miniemulsion might be substantially faster than polymerization in an equivalent macroemulsion. For copolymerization in a macroemulsion, where one of the comonomers is highly water insoluble, the comonomer composition at the locus of polymerization might be quite different from the overall comonomer composition, resulting in copolymer compositions other than those predicted by the reactivity ratios.

4.2.1 Polymerization of Highly Water-Insoluble Monomers

Balic [147] has made a complete study of the macroemulsion polymerization of vinyl neo-decanoate (vinyl versatate or VEOVA). This monomer is highly water-insoluble (4×10^{-5} mol/L at 25 °C). Balic reports low rates of polymerization and long inhibition periods in macroemulsions. He asserts that this is not due to monomer transport limitations, and provides calculations to support this. He attributes the low rates to impurities in the monomer, although he could not remove these. It could be that the extremely low solubility of the monomer in the aqueous phase retards the formation of oligomeric radicals of sufficient length (hydrophobicity) to enter the polymer particles. Under these conditions of very slow aqueous phase polymerization, the oligomers might be particularly susceptible to low levels of aqueous phase inhibitor. With the resultant low radical flux into the particles, the rate of polymerization would be low. It could also be that the rate of monomer diffusion is not sufficient to allow the polymerization to be reaction limited, since Balic's arguments do not necessarily rule out this possibility. It would be interesting to see the same polymerizations run in miniemulsion, since this would rule out the monomer transport effect.

Kitzmiller et al. [148] have found the rate of copolymerization for VAc and vinyl 2-ethylhexanoate to be much slower in macroemulsion than in miniemulsion. They attribute this to monomer transport effects for the less water-soluble monomer.

4.2.2 Copolymer Composition Distribution

While the rate of monomer transport in macroemulsions may or may not limit the rate of polymerization, it is quite possible that unequal rates of diffusions for comonomers may make the comonomer composition at the locus different (richer in the more water-soluble monomer) from the overall composition.

Copolymerization refers to the process by which two monomers (M_1 and M_2) are simultaneously polymerized. Mayo and Lewis [149] developed the following equation to describe copolymerization kinetics

$$\frac{d\mathrm{M}_1}{d\mathrm{M}_2} = \frac{\mathrm{M}_1(r_1\mathrm{M}_1 + \mathrm{M}_2)}{\mathrm{M}_2(\mathrm{M}_1 + r_2\mathrm{M}_2)} \tag{15}$$

where M_i is the molar concentration of monomer i at the site of propagation. The reactivity ratios, r_1 and r_2, are the homopropagation rate constants divided by the cross propagation rate constants, such that

$$r_1 = \frac{k_{\mathrm{p11}}}{k_{\mathrm{p12}}} \qquad r_2 = \frac{k_{\mathrm{p22}}}{k_{\mathrm{p21}}} \tag{16}$$

where r_1 and r_2 are determined experimentally, typically from bulk or solution polymerization experiments. Different types of copolymerization behavior are observed, depending on the values of r_1 and r_2. Equation 15 is rewritten in a more useful form, where the comonomer compositions (f_1 and f_2) are related to the instantaneous copolymer compositions (F_1 and F_2):

$$\frac{d\mathrm{M}_1}{d\mathrm{M}_2} = \frac{F_1}{F_2} = \frac{\dfrac{r_1 f_1}{f_2} + 1}{\dfrac{r_2 f_2}{f_1} + 1} \tag{17}$$

Equation 17 is known as the *copolymerization or Mayo Lewis equation*.

Schuller [150] and Guillot [98] both observed that the copolymer compositions obtained from emulsion polymerization reactions did not agree with the Mayo Lewis equation, where the reactivity ratios were obtained from homogeneous polymerization experiments. They concluded that this is due to the fact that the copolymerization equation can be used only for the exact monomer concentrations at the site of polymerization. Therefore, Schuller defined new reactivity ratios, $r'1$ and $r'2$, to account for the fact that the monomer concentrations in a latex particle are dependent on the monomer partition coefficients (K_1 and K_2) and the monomer-to-water ratio (ψ):

$$r'1 = r_1 \frac{1 + \frac{1}{K_2\psi}}{1 + \frac{1}{K_1\psi}} \qquad r'2 = r_2 \frac{1 + \frac{1}{K_1\psi}}{1 + \frac{1}{K_2\psi}} \tag{18}$$

The Mayo Lewis equation, using reactivity ratios computed from Eq. 18, will give very different results from the homogenous Mayo Lewis equation for mini- or macroemulsion polymerization when one of the comonomers is substantially water-soluble. Guillot [151] observed this behavior experimentally for the common comonomer pairs of styrene/acrylonitrile and butyl acrylate/vinyl acetate. Both acrylonitrile and vinyl acetate are relatively water-soluble (8.5 and 2.5%wt, respectively) whereas styrene and butyl acrylate are relatively water-insoluble (0.1 and 0.14%wt, respectively). However, in spite of the fact that styrene and butyl acrylate are relatively water-insoluble, monomer transport across the aqueous phase is normally fast enough to maintain equilibrium swelling in the growing polymer particle, and so we can use the monomer partition coefficient.

Schuller's equation is appropriate when one of the monomers has significant water solubility and the other does not. In the case where one monomer is water insoluble, and the other is *extremely* water insoluble, Schuller's equation does not hold. For the comonomer pair of MMA/VS (vinyl stearate), $K_1 \ll K_2$, so Schuller's equation predicts that, for macroemulsion polymerization, the polymer formed early in a batch reaction will be richer in vinyl acetate (VA) than in the homogenous case. The opposite was found by Reimers [102]. It has long been accepted that monomer transport is not a rate-limiting step in the conventional emulsion polymerization of *relatively water-insoluble* monomers, such as MMA, styrene, and butyl acrylate (BA). However, the water solubility of VS is as much as three orders of magnitude smaller than these typical emulsion polymerization monomers. In this case, VS cannot readily cross the aqueous phase to saturate the growing polymer particles. (The major transport resistance is actually from the monomer droplets into the aqueous phase.) Therefore, Schuller's partition coefficient model cannot be used here, since it assumes that the particles are saturated with both monomers. The homogeneous polymerization model is not useful either since the monomer concentration in the particles is not identical to the bulk monomer concentration. Therefore, a pseudo-partition coefficient κ_2 was proposed by Samer [137] for *extremely water-insoluble* comonomers in order to interpret the experimental data. κ_2 is not a partition coefficient and does not have any physical significance. As defined by Samer, it is simply an adjustable parameter that replaces K_2 in Eq. 18. If K_1 is set to infinity and κ_2 is set to unity, Eq. 17 and Eq. 18 can be used to correlate the copolymer composition with the total monomer conversion data in the MMA/VS (and other) systems.

Extremely water insoluble comonomers are only selectively used in emulsion polymerization because of concerns about monomer transport limitations.

Typically, copolymer composition can be manually adjusted by slowly feeding the more reactive monomer in throughout the reaction; but this may not be helpful when trying to overcome monomer transport limitations. Therefore, Reimers and Schork [102] performed identical copolymerization experiments in miniemulsions, where monomer transport is less significant, in order to determine what effect this would have on the evolution of the copolymer composition. Data on the MMA/VS (and other) copolymerizations indicate that the Schuller equation (and not the Samer adaptation) fits the copolymer composition data. This points to the effect of extremely low monomer water solubility on copolymer composition in macroemulsion polymerization, and the relative insensitivity of miniemulsion polymerization to this effect.

We will now look at the type of reactor system (batch, semibatch or CSTR) from the point of view of miniemulsion copolymerization.

4.2.2.1 Batch Copolymerization

Reimers [102] carried out batch copolymerizations in both macro- and equivalent miniemulsions. MMA was used as the main monomer. The MMA was copolymerized in macroemulsion- or miniemulsion with *p*-methylstyrene (pMS), vinyl hexanoate (VH), vinyl 2-ethylhexanoate (VEH), vinyl *n*-decanoate (VD) or vinyl stearate (VS). The comonomers were copolymerized at 10%wt comonomer, 90%wt MMA. SLS was used as the surfactant and KPS as the initiator. The comonomers (all highly water insoluble) were used as the co-stabilizer. Miniemulsions were sonicated, while equivalent macroemulsions were only subjected to vigorous mixing. Polymerizations were carried out at 60 °C.

Copolymer composition was obtained by integrating characteristic peaks in the ^{1}H NMR spectra. The integrated peaks correspond to signals produced by the methyl ester protons (three) of MMA, 3.56 ppm, the aromatic protons (four) of pMS, 6.7 ppm, and the α-proton of the vinyl esters at 4.8 to 5.6 ppm. The relative ratios of the peaks allowed the mole fraction of each comonomer in the copolymer to be assessed. Samples were taken throughout the reaction at different times to monitor the incorporation of comonomer as a function of the extent of total monomer conversion. These results were then compared with the results for average comonomer fraction given by an integrated copolymer (Mayo Lewis) equation [149], using r_1 and r_2 from bulk polymerization. The mole fractions used were based on the total moles of monomer in the droplets and were corrected for the water solubility.

Both the mini- and macroemulsion copolymerizations of pMS/MMA tend to follow bulk polymerization kinetics, as described by the integrated copolymer equation. MMA is only slightly more soluble in the aqueous phase, and the reactivity ratios would tend to produce an alternating copolymer. The miniemulsion polymerization showed a slight tendency to form copolymer that is richer in the more water-insoluble monomer. The macroemulsion formed a copolymer that is slightly richer in the methyl methacrylate than the co-

polymer equation would predict. This may be explained by different nucleation mechanisms operating in each polymerization. Droplets would have a higher concentration of the less water-soluble comonomer throughout the reaction. Therefore their nucleation should yield a copolymer with a higher pMS fraction. In contrast, micellar nucleation should lead to a copolymer with a higher methyl methacrylate content, because it can cross the aqueous phase more readily.

As the water solubility of the comonomer decreases, the difference in incorporation of the hydrophobic monomer between the mini- and macroemulsion polymerization becomes more pronounced. This was seen in the copolymerization of VH/MMA. The fraction of the hexanoate in the copolymer formed in the miniemulsion polymerization was substantially higher than that found with the macroemulsion. This incorporation closely follows the copolymer equation. The VEH/MMA miniemulsion copolymerization also followed the copolymer equation. Differences between the mini- and macroemulsion polymerization are not as pronounced in this system. For the VD/MMA and VS/MMA systems there were large differences between the two copolymerizations. In addition, none of the mini- or macroemulsion copolymerizations of vinyl decanoate or vinyl stearate are predicted by the copolymer equation. The miniemulsion copolymerizations fall above the prediction curve (more hydrophobic monomer incorporation than predicted), and the macroemulsions fall below. In these cases, both micellar and droplet nucleation took place in the miniemulsion polymerizations, and the presence of micelles tended to enrich the concentration of the hydrophobic monomer in the droplets, since the micelles would likely be richer in the more water-soluble MMA.

Samer [104] carried out similar copolymerizations with similar results. An example of his data is given in Fig. 16. Here 2-ethylhexyl acrylate (EHA) was copolymerized with MMA in batch. The miniemulsion polymerizations (two are shown) follow the copolymer equation, while the macroemulsion polymerization gives EHA incorporation that is lower than predicted by the copolymer equation, presumably due to the low concentration of EHA at the locus of polymerization. The dotted line in Fig. 16 is for a model derived by Samer that accurately predicts the copolymer composition. Samer derived this model by adapting the work of Schuller [149]. Schuller modified the reactivity ratios for the macroemulsion polymerization of *water-soluble* monomers to take into account that the comonomer concentration at the locus of polymerization is different from the comonomer composition in the reactor due to the water solubilities of the monomers. Samer used the same approach to account for the fact that the comonomer concentration at the locus of polymerization might be different from that of the reactor due to transport limitations of *water insoluble* comonomers.

Delgado et al. published a series of papers [56, 58, 91, 153–157] on the miniemulsion copolymerization of vinyl acetate and butyl acrylate. A very comprehensive mathematical model of the polymerization system was developed. Equilibrium swelling was accounted for, since the model did not presume complete droplet nucleation, and so monomer transport from unnucleated mini-

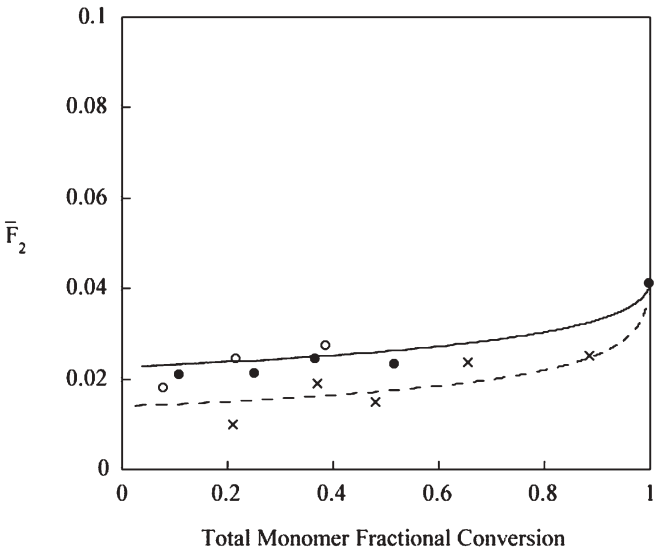

Fig. 16 Copolymer composition during the batch miniemulsion copolymerization of methyl methacrylate with 2-ethylhexyl acrylate (from [104])

emulsion droplets to polymer particles occurred. Monomer transport limitations were minor, but with these two monomers, that is not surprising. Delgado did report [91] a higher BA content (up to 70% conversion) for miniemulsion-polymerized copolymers relative to those polymerized in an equivalent macroemulsion. Since BA is significantly less water-soluble than VAc, this result is in agreement with Reimers. Rodriguez et al. [60, 61] developed a comprehensive model of the miniemulsion copolymerization of styrene and MMA. This system presumes significantly less than 100% nucleation of monomer droplets, and so there was significant monomer transport from the monomer droplets to the polymer particles. However, since neither of these monomers are extremely water insoluble, no effects on copolymer composition were observed. Ghazaly et al. [117] studied the miniemulsion copolymerization of *n*-butyl methacrylate with crosslinking macromonomers (two double bonds per molecule). Since the comonomers were macromers, presumably, it was important to use a miniemulsion to avoid common transport issues. Wu and Schork [152] studied the batch and semibatch miniemulsion copolymerization of VAc with BA. They found the copolymer composition for batch miniemulsion polymerization to be in good agreement with the copolymer equation. However, there was significant deviation for batch macroemulsion polymerization, especially at low conversion. Delgado [157] attributed this effect to the small amount of water that exists in the monomer-swollen polymer particles. Because of the high water solubility of VAc, the particles then contain a higher level of VAc, and so BA incorporation is suppressed.

4.2.2.2 Semibatch Copolymerization

Controlling copolymer composition has long been of prime interest in polymer reaction engineering. Because of possible differences in reactivity ratios, the copolymer composition distribution may be broad, and only the overall (average) copolymer composition at full conversion need be at the ratio of monomer feeds. As noted above, Mayo and Lewis [149] studied the kinetics of copolymerization and developed an equation to describe the relationship between the molar concentrations at the site of propagation and reactivity ratios of monomers for homogeneous copolymerization, such as bulk or solution polymerization. Semibatch polymerization (both solution and macroemulsion) has long been used to produce copolymers of desired copolymer composition distribution. This may be done on one of two ways. First, in a binary polymerization the more reactive monomer may be fed in a semibatch manner. This will result in a high concentration of the less reactive monomer at the locus of polymerization, and the formation of polymer that is higher in the less reactive monomer than would be the case for batch polymerization. Alternatively, the reaction may be run monomer-starved. In this case, the monomers are fed into the system in the desired ratio, but at a slow rate. The rate of polymerization is then controlled by the rate of monomer feed. Since polymerization occurs under monomer-starved conditions, the copolymer composition will be that of the comonomer feed. Obviously, monomer-starved conditions will result in low rates of polymerization. If either policy for semibatch monomer feeding is to be used, issues of relative transport of the monomers must be considered. Also, the decision must be made as to whether to feed in neat monomer, a macroemulsion of monomer droplets, or a miniemulsion of monomer droplets. In general, neat monomer feed will result in the least nucleation, while miniemulsion feed will result in the most. Depending on the goals of the polymerization, nucleation of new particles during the semibatch feeding may be desirable or undesirable.

In 1993, Unzue and Asua [158] studied the semibatch miniemulsion terpolymerization of BA, MMA and VAc. The aim was to produce a miniemulsion of 65% solids. It is well known that semibatch polymerization can be an effective method of making high solids latex. Part of the advantage of semibatch in making high solids is the broad PSD brought on by nucleation of particles over most of the reaction time. Miniemulsion can be effective in this regard, since a miniemulsion feed is likely to produce additional polymer particles, as shown by Tang et al. [131].

Wu and Schork [152] compared batch and semibatch and mini- and macroemulsion polymerization for three monomer systems, VAc/BA, VAc/dioctyl maleate (DOM) and VAc/*n*-methylol acrylamide (NMA), with large differences in reactivity ratios and water solubilities. HD was used as the costabilizer. (It should be noted that DOM could function as a costabilizer itself, but for the sake of consistency, HD was added to the DOM polymerizations.) KPS and the

emulsifier SLS was used as the initiator. The semibatch miniemulsion polymerization involved two stages, a miniemulsion batch stage and semibatch stage. The miniemulsion batch stage was performed as above. When the monomer conversion was estimated to be about 80%, the feeding stage was initiated by pumping monomer emulsion (miniemulsion or macroemulsion, which was continuously formed while feeding) and initiator solution at set flow rates simultaneously into the reactor. The composition of the monomer feed was identical to the composition of the monomer in the batch stage. Copolymer composition was determined by NMR, MWD by GPC and PSD by dynamic light scattering.

Miniemulsion and macroemulsion copolymerizations of VAc and comonomers with extremely different physical and kinetic properties (BA, NMA and DOM), were investigated in batch and semibatch systems. The results for polymer particle size and number, monomer conversion, composition and molecular weights of copolymers indicated that there was an obvious divergence between macroemulsion and miniemulsion copolymerization. In all cases, the particle size was smaller and the particle number was higher in macroemulsion copolymerization than in miniemulsion copolymerization. For the systems VAc/BA and VAc/DOM, the particle number increased with increasing conversion throughout the reaction for both batch macroemulsion and miniemulsion runs. This was taken to indicate that the nucleation of new particles takes place via homogeneous nucleation throughout these reactions. For the batch runs, the rate of polymerization of the macroemulsion polymerization runs was faster than that of the miniemulsion.

An investigation of the copolymer composition demonstrated the important effect of monomer transport on the copolymerization. The droplets in the macroemulsion act as monomer reservoirs. In this system, the effect of monomer transport will be predominant when an extremely water-insoluble comonomer, such as DOM, is used. In contrast with the macroemulsion system, the miniemulsion system tends to follow the integrated Mayo Lewis equation more closely, indicating less influence from mass transfer.

Likewise, for the semibatch operation, the influence of monomer was seen in the differences between macro- and miniemulsion feeds. For extremely water-insoluble monomers, the miniemulsion-feed mode lessens the departure of the copolymer composition from the feed composition during semi-starved semibatch polymerization. However, this is accomplished by simultaneously broadening the PSD. Results from the GPC analysis indicated that the polymers with lower molecular weight and broader distribution were formed in the semibatch process, in contrast to the batch run.

Wu [159] also investigated the miniemulsion and macroemulsion copolymerization of VAc and vinyl versitate (VEOVA). At room temperature, the water solubility of VAc is 2.58%wt, and vinyl versitate (also known as neodecanoate, one of the isomers in VEOVA-10) is 7.5×10^{-4}%wt. The extreme difference in water solubility between the two comonomers may impact on copolymer composition and the properties of the final polymer, due to the mass

transfer of monomer.In this work, mini- and macroemulsion polymerizations of VAc/vinyl versatate were designed to investigate the effects of monomer transport and feeding strategies (for semibatch runs) on the reaction rate, particle size distribution, molecular weight distribution, copolymer composition, and glass transition temperature (T_g) of the resultant polymer. Polymerizations were run at 55 °C. HD was used as the costabilizer, and SLS as the surfactant. The initiator was KPS. VEOVA was added either as an emulsion with the vinyl acetate, or as a neat liquid stream. In the polymerization of VAc miniemulsion (or macroemulsion) plus neat vinyl versatate, the VAc miniemulsion (or macroemulsion) was pre-formed. The neat vinyl versatate was then injected into the polymerization system at the same time as the injection of initiator solution. For the semibatch processes, 20%wt of the polymer solids was in the form of seed and the remaining 80% was fresh monomer emulsion. The seed latex was prepared as a miniemulsion polymerization. The miniemulsion was made (sonicated) in-line, immediately prior to feeding into the reactor. The first shot of initiator solution was introduced when the feed of monomer emulsion started. A subsequent shot followed the removal of each latex sample for analysis.

In the semibatch runs of VAc miniemulsion (or macroemulsion) plus neat VEOVA, with simultaneous feeding of VAc miniemulsion (or macroemulsion), the neat vinyl versatate was injected into the polymerization system two (for the feedrate of 0.6 ml/min) or three (for 0.3 ml/min) times during each sampling interval. Copolymer composition was determined by NMR, MWD by GPC, T_g by DSC, and PSD by dynamic light scattering.

The effect of mass transfer of vinyl versatate on the mini/macroemulsion polymerization of VAc/VEOVA in batch and semibatch systems was explored. For the batch experiments, the addition of neat VEOVA formed poor dispersions of VEOVA, which resulted in smaller particles, lower polymerization rates and different polymer composition tracks compared to normal mini/macroemulsion polymerization of VAc/VEOVA. The well-dispersed VEOVA seemed to help the monomer-swollen particle to gain more radicals in the nucleation period.

In the semibatch experiments, the particle size distributions of the final latexes were affected by the residual surfactant in the seed latex, which tended to facilitate homogeneous nucleation during the entire feed period. The monomer feedrate determined the polymerization rate and had little effect on copolymer composition. The polymer compositions for the runs with different monomer feeding modes tended to be identical at very low feedrate.

For all runs, thermal analysis of the resulting polymers showed that only one glass transition temperature could be found. This corresponded to the T_g of the VAc/VEOVA copolymer. Lower glass transition temperatures were found for the semibatch runs, perhaps due to slightly improved VEOVA incorporation.

In summary, the semibatch feeding of neat monomer or a macroemulsion of monomer to a miniemulsion does not differ substantially from the equivalent semibatch feeding into a macroemulsion. The semibatch feeding of a

miniemulsion tends to cause an increase in the particle number (due to partial nucleation of the monomer droplets in the feed) and copolymer compositions that more closely follow the Mayo Lewis Equation (due to the ability of the miniemulsion droplets to, at least partially, retain their monomer, rather than being depleted of monomer to feed the existing higher conversion polymer particles).

4.2.2.3 Copolymerization in a Continuous Stirred Tank Reactor

Samer [137] studied miniemulsion copolymerization in a single CSTR. Two separate feed streams, miniemulsion (or macroemulsion for comparative studies) and initiator were fed at constant rates into the reactor. SLS was used as the surfactant, HD as the costabilizer, and KPS was the initiator. In the miniemulsion configuration (costabilizer included in recipe), the emulsion stream was continuous. Constant volume was provided by an overflow outlet. Salt tracer experiments were used to validate the ideal mixing model assumed for a CSTR. Total monomer conversion was measured via in-line densitometry, and copolymer composition via offline NMR.

Continuous macroemulsion copolymerization of MMA with 0.033–0.05mol% 2-ethylhexyl acrylate (EHA): On the basis of the batch copolymerization experiments for this system, one would expect the average compositions to follow the relation $F_{2\,\mathrm{Mini}} > F_{2\,\mathrm{Macro}}$. (The subscript 2 refers to the EHA.) However, this behavior was not observed in a CSTR. Although the steady-state conversion was significantly greater (as expected) for miniemulsions than for macroemulsions, the copolymer composition is nearly identical for both reactions. In this case, it does not appear that droplet nucleation leads to an increase in the amount of the *extremely water-insoluble* comonomer incorporated into the copolymer, as observed in batch reactors. The experimental copolymer compositions were compared with the predicted copolymer compositions calculated from the Mayo Lewis equation where the reactivity ratios were obtained from homogeneous copolymerization experiments and where the pseudo-partition coefficient κ_2 was adjusted to fit the data. Surprisingly, both the macroemulsion and miniemulsion data showed good agreement with Samer's modification of Schuller's modified reactivity ratio model. This included both mini- and macroemulsion copolymer compositions at different initial comonomer compositions. Since the water solubility cannot change, it was suggested that monomer transport, or at least the relative difference in monomer transport between MMA and EHA, changes between batch and continuous miniemulsion copolymerization reactions.

The difference in copolymer composition between miniemulsion and macroemulsion copolymerization in a batch reactor was not observed in a CSTR. In this case, the copolymer composition for the *extremely water insoluble* comonomer in a miniemulsion recipe decreases from a batch reactor to a CSTR. This difference can be attributed to the fact that monomer transport is

enhanced in the steady-state CSTR where fresh monomer droplets are in contact with "monomer-starved" particles. The comonomers cannot cross the aqueous phase at similar rates because of their water-solubility differences, which favors incorporation of the more water-soluble comonomer. All of the droplets are nucleated at roughly the same time in a batch reactor, so little monomer is available to quench monomer-starved particles.

However, this does not preclude miniemulsion copolymerization in a CSTR for *extremely water-insoluble* comonomers. In spite of the fact that the copolymer composition in the continuous miniemulsion is less than that predicted using the homogeneous copolymerization reactivity ratios, the miniemulsion copolymer might be more uniform than the macroemulsion copolymer, where the possibility of significant droplet nucleation could lead to two separate homopolymers or, at the very best, copolymers of various composition. Therefore, it is very important to use CSTR data to scale up a continuous miniemulsion copolymerization product to take into account the different particle growth kinetics for batch and continuous reactors.

4.2.3 Interfacial Polymerization

Interest in the design and controlled fabrication of composite nanoparticles consisting of hydrophobic polymer cores coated with hydrophilic polymer shells continues to increase. These particles have potential technological applications in diagnostic testing, bioseparations, controlled release of drugs, gene therapy, catalysis, and water-borne coatings and adhesives [160–170]. Emulsion copolymerization of hydrophobic and hydrophilic monomers seems to be a straightforward approach to fabricating such nanoparticles. However, this kind of emulsion copolymerization presents a big challenge, because the hydrophilic monomer resides almost exclusively in the aqueous phase while the hydrophobic monomer resides almost exclusively in the organic phase. AIndeed, most of the studies made so far have been limited to a very low hydrophilic monomer level. In all cases, the incorporation of water-soluble monomer was very limited, regardless of the initial amount of water-soluble monomer loaded into the system [171]. It was proposed that interfacial graft-polymerization of hydrophilic monomer onto hydrophobic polymer should be possible in an emulsion process by selecting an appropriate initiator system [172]. In the work of Luo et al. [170], the idea of interfacial polymerization was used to develop a novel repulpable pressure-sensitive adhesive. In order to maximize the incorporation of cationic monomer (hydrophilic monomer), an interfacial redox initiator system was used. In this initiator system, oil-soluble cumene hydroperoxide (CHP) was used as the oxidizer while hydrophilic tetraethylenepentamine was employed as the reducer. It was hoped that by using CHP/TEPA, the hydrophobic CHP would meet the hydrophilic TEPA at the particle-water interface, where hydrophobic and hydrophilic monomer are both present. In the meanwhile, non-ionic surfactant (Triton X-405) was used to facilitate the adsorption of cationiccomonomer at the interface.

In order to gain evidence for interfacial initiation, the redox initiator system was compared with a water-soluble initiator (VA-044) in terms of the emulsion polymerization behavior of butyl acrylate (BA)/[2-(methacryloyoxy)ethyl]trimethyl ammonium chloride (MAETAC). It was found that for the water-soluble initiator system, only homopoly(MAETAC) was formed and BA did not polymerize at all. In the case of VA-044, it was suggested that it may be difficult for polymeric free radicals in the aqueous phase to penetrate the viscous surfactant layer to initiate the polymerization of the BA monomer. On the other hand, it has also been found that BA could be rapidly polymerized under the same conditions if VA-044 is replaced with CHP/TEPA, indicating that radicals are formed in the interface, where they do not need to penetrate through viscous surfactant layer.

The polymerization kinetics of BA/MAETAC macroemulsion and miniemulsion copolymerization was investigated with the interfacial redox initiator system. It was found that adding MAETAC had a complex effect on the polymerization kinetics of BA, as shown in Figs. 17 and 18 [170].

In comparison with the homopolymerization of BA, adding 5%wt MAETAC greatly increases the BA polymerization rate for both macroemulsion and miniemulsion polymerization. However, when the MAETAC level is increased further, the polymerization rate begins to decrease. At higher MAETAC levels, the effect of MAETAC is different for macroemulsion and miniemulsion polymerizations. For macroemulsion polymerization at high MAETAC level, there seems to be an induction period before polymerization begins. At higher MAETAC levels, the length of the induction period increases. For miniemulsion polymerization, there is no induction period; instead, the BA polymerization rate decreases to zero at less than full conversion. BA homopolymerization with CHP/TEPA levels off at ~30% conversion. At higher MAETAC levels, the BA conversions levels off at substantially higher conversion. The leveling-off has

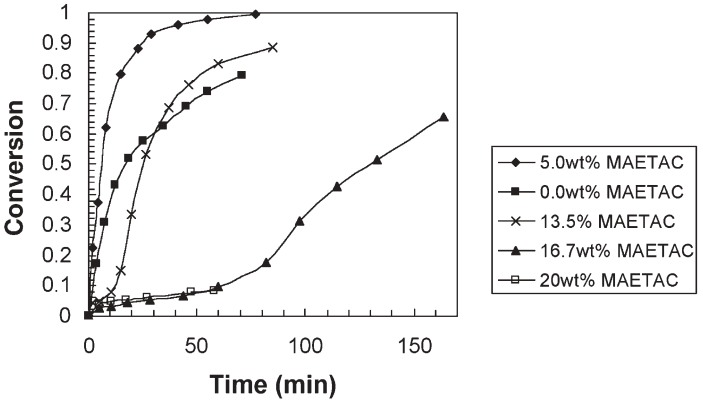

Fig. 17 BA monomer conversion for macroemulsion copolymerization with varying levels of MAETAC (from [170])

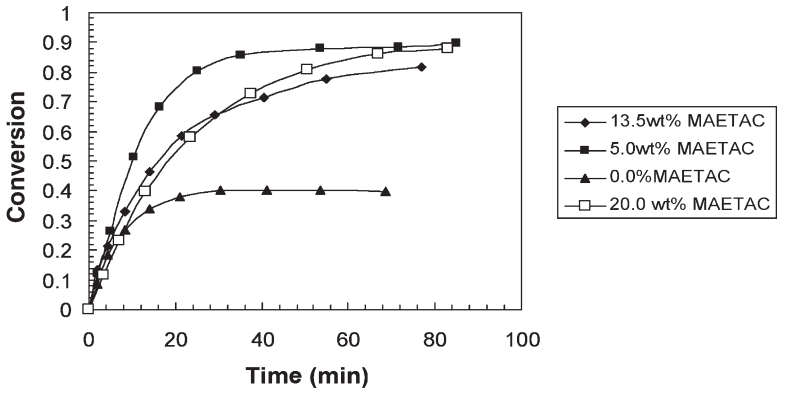

Fig. 18 BA monomer conversion for miniemulsion copolymerization with varying levels of MAETAC (from [170])

been ascribed to the depletion of TEPA. Comparing Fig. 17 with Fig. 18, it is clear that the influence of MAETAC levels on macroemulsion polymerization is much greater than on miniemulsion polymerization, especially in the early stage of polymerization. With increasing MAETAC levels, the polymerization rate of BA, especially in the early stage of polymerization, rapidly drops off in the macroemulsion polymerization. It is suggested that adding MAETAC would interfere with the nucleation of macroemulsion polymerization. At low MAETAC levels, introducing MAETAC leads to homogeneous nucleation, so the polymerization rate increases. However, at high MAETAC level, adding MAETAC did not result in homogeneous nucleation but suppressed micellar nucleation. It has been suggested that polymer formed in the aqueous phase is too hydrophilic to lead to homogeneous nucleation at high MAETAC. The suppression of micelle nucleation can be illustrated by Fig. 19. The hydrophobic molecules such as BA and CHP will be present in the micelles at the beginning of the polymerization. When TEPA was added to the reactor, many of the free radicals will be formed by the following mechanism in the surface of a micelle, where CHP and TEPA meet each other [173].

Because of their different hydrophilicities, the two free radicals formed at the same time can separate from each other quickly which can eliminate the cage effect. In a micelle, the local BA concentration may be quite high. Once a micelle is initiated, a number of BA molecules may be added quickly. As a result, some short BA blocks would be incorporated into a poly(MAETAC) chain to form something like multi-block copoly(MAETAC-BA), as shown in Fig. 19 [170]. Surfactant should stabilize the BA blocks so that the block copolymer remains in the aqueous phase.

The BA blocks in the copolymer, which is surrounded by surfactant, swell with BA monomer, which polymerizes there until particles form. Therefore, micellar nucleation is diminished or even eliminated. As a result, micellar nucleation is retarded, and N_p decreases. It is clear that the nucleation is very

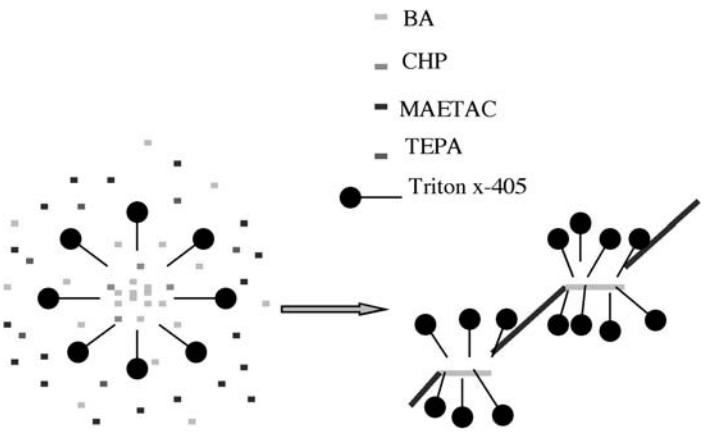

Fig. 19 Schematic of the formation of multi-block poly(MAETAC-BA) (from [170])

sensitive to the level of hydrophilic monomer for macroemulsion polymerization. As a result, the polymerization rate and particle size change dramatically with changes of hydrophilic monomer level. For miniemulsion polymerization, the monomer is dispersed into droplets of 50–500 nm prior to polymerization and no micelles exist. Therefore, TEPA comes into contact with CHP at the droplet-water interface. MAETAC and BA copolymerize at the interface. The number of BA molecules in a monomer droplet is far larger than that in a micelle, so the resultant copolymer has a much higher composition of BA and is anchored at the interface. Therefore, droplet nucleation during miniemulsion polymerization is hardly affected, although it was found that when the hydrophilic monomer was low, homogeneous nucleation could occur in the miniemulsion polymerization, as shown in Fig. 20 [170]. As a result, there is little initial dependence of the polymerization rate on the hydrophilic monomer level

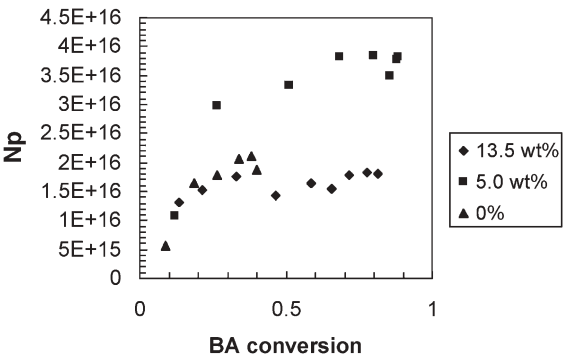

Fig. 20 Particle number development for miniemulsion copolymerization with varying levels of MAETAC (from [170])

during miniemulsion polymerization, in sharp contrast to macroemulsion polymerization, as shown in Figs. 17 and 18. Clearly, nucleation during miniemulsion polymerization is highly robust to the level of hydrophilic comonomer.

4.3 Multiphase Particles

4.3.1 Hybrid Miniemulsion Polymerization

It would often be desirable to create submicron particles containing two or more polymers. These could be in the form of a blend or in the form of a graft copolymer. In a simple blend, the two polymers may or may not be compatible. If they are compatible, the particle will be homogenous. If the polymers are not compatible, then microphase separation is likely. However, if the phase separation occurs in submicron particles, the phase domains will be small, and decent dispersion of the two polymers will occur. Homogenous, grafted, or phase-separated morphologies might conceivably be of practical value.

One method of creating such polymer blends or grafts in submicron particles is through *hybrid miniemulsion polymerization*. In this technology, a preformed polymer (or oligomer) is dissolved into a monomer (or monomer solution). A miniemulsion is then created from the monomer-polymer solution, and this miniemulsion is polymerized via standard techniques. Care must be taken in creating the miniemulsion, because the polymer solution will likely have a high viscosity (higher than for a simple monomer miniemulsion) and so the droplet break-up by the shear device may be more difficult. On the other hand, the preformed polymer may act as the costabilizer, eliminating the need for HD or other costabilizers. For some chemistries, grafting will take place during the polymerization of the monomer, and for some polymers phase separation will occur. In any case, the product is a submicron dispersion of one polymer in another, and may well have practical value. Since most of the oligomers or prepolymers are polymeric and probably highly water-insoluble, macroemulsion polymerization will not result in a graft copolymer or an intimate blend. Since the prepolymer is not transported from the monomer droplets to the polymer particles, the prepolymer does not reach the locus of polymerization. Macroscopic phase separation and colloidal instability often result.

Details of the chemistry and process (and the product) are very specific to the choice of prepolymer and monomer; for this reason, each system will be discussed separately here.

4.3.1.1 Alkyds

Water-based coatings have become more widely used over the past few decades because they are environmentally friendly, offer easy clean-up, and their properties and application performance characteristics have improved. Solvent-based systems such as alkyd resins and polyurethanes have remained important for some applications because of superior properties, such as gloss and hardness. This is due to the curing mechanism of oil-based coatings in which the oils react with atmospheric oxygen to form very hard crosslinked materials. This mechanism is generally lacking in water-based coatings, which tend to be soft and pliable, due to the fact that the coatings are made soft to allow film formation, and since there is no curing chemistry available, remain soft on drying. Several researchers have focused on the use of the hybrid miniemulsion polymerization of acrylic monomers in the presence of alkyd and polyurethane resins to develop alternative coatings which have the advantages of water-based systems (like low VOC) with the drying (air cure) properties of solvent-based systems. Alkyd/acrylate coatings are targeted as replacements for solvent-based architectural coatings, and oil-modified polyurethane (OMPU)/acrylate coatings may provide a low VOC alternative to solvent-based clear coats. Since U.S. architectural coating sales in 1995 amounted to 625 million gallons [174], a conservative estimate of the VOC reduction if all of these coatings were water-based is approximately 500 million pounds of solvent that would not be released into the air.

Nabuurs and German [175] developed an alkyd-acrylic hybrid system via emulsion polymerization. They were able to produce a stable product using MMA as the acrylic. When the alkyds were functionalized by sulfonation, there was no evidence of heterogeneity in the particles. When unfunctionalized alkyd was used, the MMA appeared as microdomains within the particles. Grafting of acrylic to alkyd was low. The presence of the alkyd led to low rates of polymerization and limited conversion that were both attributed to retardation through radical delocalization following radical transfer to the unsaturated groups in the fatty acids of the alkyd. Although this work was not reported to be miniemulsion polymerization, the emulsions were subjected to high shear prior to polymerization. No costabilizer was added, but the alkyd presumably functioned as such. Since the alkyd-acrylic droplet size was probably quite small, droplet nucleation was probably the dominant nucleation mechanism. This would explain the good colloidal stability of the resulting system, and the fact that both alkyd and acrylic domains were found in the same particles.

Wang et al. [98] carried out macroemulsion and miniemulsion polymerization of acrylic monomers in the presence of alkyd resins. Miniemulsion and macroemulsion polymers were produced using a commercial medium soya-linseed alkyd and a mix of acrylic monomers consisting of 50% BA, 49% MMA, and 1% acrylic acid (AA). PMMA polymer with a weight average molecular weight of 100,000 was used as the costabilizer. Alkyd levels were 5, 30, 60 or

100% based on total acrylic monomer. SLS was used as the surfactant, and sodium persulfate (SPS) was used as the initiator. The miniemulsions were prepared by dispersing the desired amount of monomer-PMMA-alkyd solution in the aqueous SLS solution by mixing with stirring at room temperature. The resulting emulsion was sheared further by sonication. Polymerization was carried out at 60–80 °C. The reaction was followed by gravimetric conversion analysis. Macroemulsion polymerizations were carried out in the same manner except that no sonication process was used and the PMMA costabilizer was not employed. Droplet and particles sizes were determined by dynamic light scattering, and double bond content of the alkyd by NMR. Grafting was determined by extraction, and degree of crosslinking by exhaustive extraction.

The monomer miniemulsions with PMMA as costabilizer were prepared with different amounts of alkyd resin. The PMMA costabilizer was effective in the preparation of stable miniemulsions, especially in conjunction with the alkyd. The size of monomer droplets was below 300 nm. After five days, the unpolymerized macroemulsions with alkyd separated into three phases, monomer on the top, clear water in the middle, and alkyd resin on the bottom. The miniemulsion without alkyd showed two phases, monomer and water. All miniemulsions with alkyd resin appear to remain uniform. Very stable miniemulsions were obtained when the alkyd content was higher than 30%. The shelf life of macroemulsions was only 2–8 minutes.

The polymerization rate in the presence of alkyd was slower than that without alkyd. Doubling the initiator and emulsifier concentration increased the reaction rate, but not to the level achieved with the miniemulsion polymerization without alkyd. This retardation (as reported also by Nabuurs) increased with increasing alkyd level. The latexes obtained from the miniemulsion polymerization of the alkyd-acrylate mixtures were uniform emulsions, and no coagulation occurred during polymerization. Macroemulsion polymerization with alkyd resulted in colloidal instability, probably due the inability of the alkyd to reach the locus of polymerization.

NMR analysis indicated that approximately 30% of the alkyd double bonds had been consumed in the polymerization process. This is important in that it indicates that a substantial fraction of the double bonds remain for oxidative crosslinking while a coating made from this material is dried. Selective extraction indicated that approximately 60% of the acrylate was grafted to alkyd. Exhaustive extraction indicated less than 5% crosslinked material. The polymerized latex formed good films with acceptable hardness.

On the whole, the miniemulsion polymerization process proved to be effective for incorporating an alkyd resin into acrylic coated copolymers. The reaction produced stable, small particle size latexes that contain graft copolymer of the acrylic and alkyd components. Attempts at macroemulsion hybrid polymerization were unsuccessful.

Van Hamersveld et al. [176, 177] carried out hybrid miniemulsion polymerization of MMA, using HD as the costabilizer. In an attempt to encourage grafting, oxidized triglycerides (such as sunflower oil) were used as initiators.

This produced homogenous particles (presumably due to higher levels of grafting), whereas the use of conventional initiators resulted in particle inhomogeneity due to phase separation of the alkyd and acrylic.

Wu et al. [99, 174] further investigated the hybrid miniemulsion polymerization of alkyd-acrylic systems, using the same monomer mix as Wang [98]. Retardation by the alkyd was reported; high polymerization temperature and mixed (oil and water-soluble) initiators were used to improve monomer conversion. The polymers obtained had a very wide molecular weight distribution, with polydispersities of more than 19 and a number average molecular weight slightly larger than alkyd. This indicates that a fraction of the alkyd remains in the ungrafted form. On the other hand, extraction results indicate that a large fraction of polyacrylate chains contain at least some grafted alkyd. Approximately 20% of the double bonds in the alkyd are consumed in grafting reactions. Two glass transition temperatures were observed, indicating the presence of at least two forms of polymer. The two glass transition temperatures correspond to those of poly(acrylate-graft-alkyd) and polyacrylate respectively. The proportion of the two kinds of polymers in the samples was determined by extraction, and this indicated that poly(acrylate-graft-alkyd) is the predominant form.

Tsavalas et al. [178] studied the limiting conversion phenomenon brought on by alkyd retardation. He concluded that retardive chain transfer to the alkyd double bonds was not adequate, especially for systems that graft through addition through double bonds (acrylates, but not methacrylates) as well as through chain transfer via hydrogen abstraction at alkyd double bonds (acrylates and methacrylates). Without transfer, no radicals of low activity would be created, and so the dramatic reduction in polymerization rate would have to be attributed to another cause. He concluded that there are two mechanisms for limiting conversion, one kinetic, and one physical. MMA, which has a high T_g, and grafts primarily through chain transfer, was found to produce a plateau in the kinetic profile of monomer conversion when the monomer glass transition temperature was near the reaction temperature. However, simple calculations suggest that transfer alone could not produce such a dramatic change in kinetics. The physical mechanism is thought to play a significant role, particularly since MMA/alkyd particles display core shell morphology, with the possibility of residual monomer trapped in the alkyd-rich core.

Butyl acrylate has a low T_g and no steric hindrance to prevent direct addition to alkyd double bonds. In this case, the limiting conversion is not absolute, but more of a very significant reduction in the rate of polymerization at high conversion. Again, simple calculations suggest that retardive chain transfer alone could not produce such a dramatic change in kinetics. Instead, the physical mechanism was found to be significant as well. PBA and alkyd both have glass transitions well below the reaction temperature, so a barrier to entry is never formed in that type of system. However, a viscous environment forms after appreciable conversion that slows the mobility of both monomer and initiator. BA monomer is thought to be dissolved in small alkyd domains dis-

tributed throughout a continuous BA particle phase. These islands eventually act as reservoirs diffusing monomer to the polymerization of BA in the continuous particle phase. The viscosity and diffusion rate are then what retard the rate in this type of hybrid system. This is evidenced by the fact that although there is a point of dramatic rate change, afterwards the new rate continues to complete conversion. That point of rate change likely corresponds to a morphology transformation to those alkyd island domains. Butyl methacrylate exhibits a reduced rate of polymerization like that of BA, rather than a true limiting conversion like that of MMA. The grafting kinetics of BMA are similar to those of MMA, but its limiting conversion behavior is similar to that of BA. Therefore it was concluded that the physical mechanism (based on T_g) is dominant over the kinetic mechanism (retardive chain transfer) for all three monomers.

Tsavalas [179] also studied the grafting of alkyd-acrylic hybrid systems. He attributed differences in levels of grafting for different monomers to differences in grafting mechanism. Grafting was observed between methacrylates and typical alkyds, but steric hindrance at the methacrylate reactive center directs addition to an alkyd double bond. This method was shown to give optimal grafting efficiency. Instead, methacrylates tend towards allylic hydrogen abstraction, a process that creates a relatively stable and unreactive radical on the resin along with terminating the abstracting methacrylate chain. These effects degrade both the grafting efficiency and the rate of polymerization. Acrylate monomers were found to produce high levels of grafting. Direct addition to resin double bonds is facilitated and virtually complete grafting of the component is observed. This was attributed to the lack of steric hindrance of the acrylate reactive center. The double bond content of the resin was shown to be important to grafting. Double bonds are needed, even in systems where abstraction is the dominant route of attack, since hydrogens allylic to them are good leaving groups. The double bond density correlates directly with the concentration of possible grafting sites and was shown to lead to higher levels of grafting. Tsavalas showed that the choice of monomer(s) is the most important variable in determining the level of grafting. Chain transfer dominates the interaction of methacrylate with resin, and so there is less opportunity for grafting. Conversely, the interaction of acrylate with resin is dominated by direct addition to a resin double bond, a highly efficient mode of grafting. In a third paper, Tsavalas [180] confirmed the differences in particle morphologies between acrylates and the methacrylates described above.

Shoaf and Stockl [181] optimized the formulations for hybrid miniemulsion polymerization. By adjusting the T_g of the polymer phase (acrylate-styrene), they were able to create latex that gave good film formation with little coalescing aid, and hence, very low VOC. By adding a latent oxidative functional monomer, they were able to get very hard film. Latexes containing up to approximately 50% alkyd (based on total solids) were produced. The coatings exhibited high gloss, which is sometimes unattainable with water-based systems. No information on the heterogeneity of the particles was provided.

4.3.1.2 Polyester

Tsavalas et al. [100] carried out hybrid miniemulsion polymerization with a three component acrylic system of methyl methacrylate, butyl acrylate, and acrylic acid in the presence of a Bayer Roskydal TPLS2190 unsaturated polyester resin. Latexes were obtained in which the polyester resin was grafted to the acrylic polymer, forming a water-based crosslinkable coating. Both emulsions and latexes were shelf stable for over six months, shear stable, and resistant to at least one freeze/thaw cycle. Resin to monomer ratios as high as 1:1 (wt:wt) and total emulsion solids as high as 45% were studied. The sizes of the monomer droplets and latex particles were similar, suggesting predominant droplet nucleation. A high level of crosslinking (>70%) during polymerization was observed in this particular hybrid system in contrast to those involving alkyd, as reported above. Homogeneous and hard films were achieved with exceptional adhesion. Electron microscopy showed the hybrid particle morphology to have internal domains of polyester resin in an acrylic matrix. Kinetic studies showed that as resin content increased in comparison to monomer content, the polymerization rate decreased, suggesting retardive chain transfer as found with the alkyds.

4.3.1.3 Polyurethane

Oil-modified polyurethanes (OMPU) are, in terms of volume produced and sold, the most important polyurethane coatings, with superior properties such as gloss, chemical resistance and film formation. Most urethane coatings are solvent-based, and solvent-based coatings are less than desirable due to the environmental impact of their high VOC. To meet the increasing concern for health, safety and the environment, there has been a strong preference in recent years for water-borne coatings. Dong et al. [101] carried out hybrid miniemulsion polymerization with acrylic monomers (methyl methacrylate, butyl acrylate and acrylic acid) in the presence of oil-modified polyurethane resin. The OMPU served as the costabilizer. Latexes with different ratios of resin to acrylic monomer were synthesized. The monomer emulsions prepared for hybrid miniemulsion polymerization showed excellent shelf-life stability (more than five months) and the polymerization was run free of coagulation. Solvent extraction indicated that the grafting efficiency of polyacrylates was greater than 29% for all of the samples produced. The ^{13}C solution NMR spectrum showed that a substantial fraction of the original carbon double bonds (>61%) in oil-modified polyurethane remained after polymerization for film curing. Films obtained from the latexes presented good adhesion properties and fair hardness properties.

Li et al. [182] used hybrid miniemulsion polymerization to prepare urethane/BMA latexes with particle sizes of about 50 nm. Hexadecane was used as the

costabilizer. In this case, the presence of the prepolymer (polyurethane, MW <10,000) resulted in an increase, rather than a decrease, in the rate of polymerization due to the fact that the presence of the polyurethane prepolymer resulted in smaller initial droplet sizes. (Presumably there was no retardive chain transfer, since there was no significant unsaturation in the polyurethane.) Free isocyanate groups remaining on the polyurethane reacted with the aqueous phase, causing an increase in particle size over several days due to flocculation.

Wang et al. [183] carried out hybrid miniemulsion polymerization of acrylates in the presence of polyurethane. The polyurethane was used as the costabilizer, and SLS as the surfactant. When MMA was used as the monomer, some homogenous nucleation was observed. This is in agreement with Tsavalas [179] who reported evidence of homogenous nucleation in the hybrid miniemulsion of MMA in the presence of alkyd.

Barrere and Landfester [184] prepared a hybrid miniemulsion in which isophorone diisocyanate was condensation polymerized with dodecanediol to form polyurethane at the same time that the polystyrene or polyBA was free radical polymerized. Unlike previous work, the polyurethane was not prepared in organic solvent in advance. Therefore, in this one-pot synthesis, polyaddition and free radical polymerization both take place in the same particle. HD was used as the costabilizer. After miniemulsification, the polycondensation was allowed to take place, and then a free radical initiator was added to polymerize the styrenic or acrylic monomer. Molecular weight distributions were bimodal; the PU had a substantially lower molecular weight than the polyacrylate. Neither intra- nor interparticle phase separation could be detected by TEM; the particles appeared to be homogeneous. No measurements of grafting were made, but since there was no unsaturation in the PU, none was expected.

4.3.1.4 Other Hybrids

El-Aasser and coworkers [185, 186] have carried out miniemulsion polymerization of styrene monomer in the presence of Kraton D1102 thermoplastic elastomer, to form hybrid composite latexes approximately 100–150 nm in size. A costabilizer other than the rubber was used. The miniemulsification was carried out via homogenization, and resulted in a very broad droplet size distribution. This resulted in the formation of inhomogeneous hybrid composite particles due to monomer diffusion during polymerization. When an oil-soluble initiator was used, an induction period was observed, resulting from the presence of radical scavengers such as antioxidants and UV stabilizers within the Kraton-styrene droplets. This also lead to inhomogeneous particles, but was eliminated with a water-soluble initiator. TEM showed domains of polystyrene within the rubber particles. Some evidence of homogeneous (or micellar) nucleation was found.

Kawahara et al. [187] prepared acrylic/epoxy composite latexes via hybrid miniemulsion polymerization. Landfester et al. [188] have incorporated PMMA

macromer as a phase capatibilizing agent in the core shell polymerization of styrene and MMA. Roberts et al. [189, 190] copolymerized vinyltriethoxysilane with various acrylates. Phase separation resulted. Hydrolysis of the triethoxysilane and subsquent condensation resulted in a crosslinked siloxane phase, separate from the polyacrylate.

4.3.1.5 Artificial Miniemulsions

El-Aasser and coworkers [191–193] have used the miniemulsification process to create water dispersions of preformed polymers. In this technique, a polymer is dissolved in a volatile organic solvent. The polymer-solvent solution is then miniemulsified and the solvent is evaporated off. This leaves a submicron water dispersion of the polymer. This technology has some distinct advantages. First, it can be applied to any polymer that is insoluble in water, but soluble in an organic solvent. Second, the polymerization need not be via free radical polymerization, since it is accomplished previous to miniemulsification. For this reason, polymerizations that are not water-tolerant may be used to form the polymer. This technique has been applied to a number of commercial applications.

4.3.2 Nanoencapsulation

Nanoencapsulation, or the encapsulation of solids within submicron particles, has been the subject of considerable work in recent years. Most have attempted nanoencapsulation via emulsion and miniemulsion polymerization techniques. Lee and coworkers [194, 195] have carried out emulsion polymerization in the presence of layered silicate. The term emulsion polymerization is unfortunate, since the polymerization takes place between the layers of silicate rather than in latex particles, forming an intercalated silica nanocomposite. Garcés et al. [196] and many others have reported marked improvement in mechanical properties if the inorganic reinforcing material (such as silica) is dispersed on the nano-scale. None of these applications are truly nanoencapsulation, since the polymer resides in the interstices of large inorganic particles, rather than having the inorganic fully encapsulated within a polymer particle.

Van Herk and German [197] have surveyed the true nano (micro) encapsulation of inorganic and organic pigments and fillers via emulsion polymerization. In this technique, small inorganic particles are used as nuclei for the formation of polymer particles. A number of materials have been encapsulated in this way, including clays, limestone, alumina, silica, carbon black, and magnetic materials. The practical challenges associated with these encapsulations include stabilizing the inorganic colloids, and controlling particle nucleation.

A more direct and reproducible route to nanoencapsulation is that of miniemulsion polymerization. If an organic or inorganic solid is contained

within the monomer droplets, nanoencapsulation can be accomplished; unlike in macroemulsion polymerization, no transport of solids from the monomer droplets to the locus of polymerization is required. Erdem et al. [198–200] have published a series of papers on the nanoencapsulation of titanium dioxide (TiO_2) particles in styrene. The challenges in this work involved getting the hydrophilic TiO_2 particles to reside in the hydrophobic environment of the interior of the miniemulsion monomer droplet, rather than in the hydrophilic environment of the continuous aqueous phase. This was accomplished through the use of specific surfactant systems. Landfester et al. [3, 201–204] studied the nanoencapsulation of solid materials via miniemulsion polymerization. They successfully encapsulated a wide variety of materials. For hydrophobic solids (like carbon black) that will easily transport into the monomer droplets, the technique is straightforward. For hydrophilic solids (like TiO_2) that prefer the aqueous phase, the authors used a combination of oil-in-water and water-in-oil surfactants to move the solids into the miniemulsion monomer droplets.

While the literature has demonstrated the viability of nanoencapsulation via miniemulsion technology, a great many issues remain. These include the use of surfactant systems to stabilize the solid colloidal particles and bring them into the monomer droplets, uniformity of encapsulation (a uniform [small] number of solid particles per polymer particle for a minimum number of polymer particles, not including the encapsulated solid), and complete coverage of the solids by the resultant polymer coating.

4.4 Controlled Free Radical Polymerization

4.4.1 Nitroxide-Mediated Polymerization

Nitroxide-Mediated Controlled Radical Polymerization (NMCRP) was first discovered by Solomon et al., who patented their discovery in 1985 [205]. This opened up new pathways in the field of free-radical polymerization. Polymer architectures, which were the domain of the anionic polymer chemist, became accessible to the free-radical polymer chemist. However, it was not until the work of Georges et al. [206] was published in 1993, that the world of polymer chemistry became aware of the possibilities of this new class of free-radical polymerization. This was the beginning of what is today one of the leading topics in free-radical polymer chemistry: Controlled or "Living" Free Radical Polymerization. This initiated the search for new Controlled or "Living" Free Radical Polymerization techniques, and soon afterwards other methods (which will be discussed later) were developed.

4.4.1.1 Mechanism

In processes based on reversible termination, like NMCRP and ATRP (Sect. 4.4.2), a species is added which minimizes bimolecular termination by reversible coupling. In NMCRP this species is a nitroxide. The mechanism of nitroxide-mediated CRP is based on the reversible activation of dormant polymer chains (P_n-T) as shown in Scheme 1. This additional reaction step in the free-radical polymerization provides the living character and controls the molecular weight distribution.

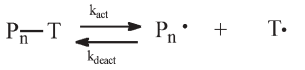

Scheme 1 Reversible activation of dormant polymer chains

When a dormant species or alkoxyamine dissociates homolytically, a carbon-centered radical and a stable nitroxide radical are formed (Scheme 2). This is a reversible process and the reversible reaction is very fast – close to diffusion-controlled rates. With increasing temperature, the dissociation rate will increase, which will increase the concentration of the polymeric radicals ($P_n^{\bullet}$). These will have a chance to add to monomer before being trapped again, which allows growth of the polymer chains. The nitroxide is an ideal candidate for this process since it only reacts with carbon-centered radicals, is stable and does not dimerize, and in general couples nonspecifically with all types of carbon-centered radicals (at close to diffusion-controlled rates).

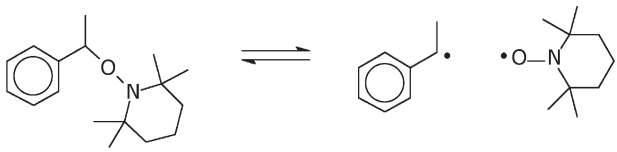

Scheme 2 Dissociation of a typical alkoxyamine into a carbon-centered radical (ethylbenzene radical) and a nitroxide (TEMPO)

Polymerization can be started using an alkoxyamine as initiator such that, ideally, no reactions other than the reversible activation of dormant species and the addition of monomer to carbon-centered radicals take place. The alkoxyamine consists of a small radical species, capable of reacting with monomer, trapped by a nitroxide. Upon decomposition of the alkoxyamine in the presence of monomer, polymeric dormant species will form and grow in chain length over time. Otherwise, polymerization can be started using a conventional free-radical initiator and a nitroxide. The alkoxyamine will then be formed in situ when an initiator molecule decomposes, and, after adding a monomer unit or two, is trapped by a nitroxide.

Since the nitroxide and the carbon-centered radical diffuse away from each other, termination by combination or disproportionation of two carbon-centered radicals cannot be excluded. This will lead to the formation of "dead" polymer chains and an excess of free nitroxide. The build-up of free nitroxide is referred to as the Persistent Radical Effect [207] and slows down the polymerization, since it will favor trapping (radical-radical coupling) over propagation. Besides termination, other side reactions play an important role in nitroxide-mediated CRP. One of the important side reactions is the decomposition of dormant chains [208], yielding polymer chains with an unsaturated end-group and a hydroxyamine, TH (Scheme 3, reaction 6). Another side reaction is thermal self-initiation [209], which is observed in styrene polymerizations at high temperatures. Here two styrene monomers can form a dimer, which, after reaction with another styrene monomer, results in the formation of two radicals (Scheme 3, reaction 7). This additional radical flux can compensate for the loss of radicals due to irreversible termination and allows the poly-

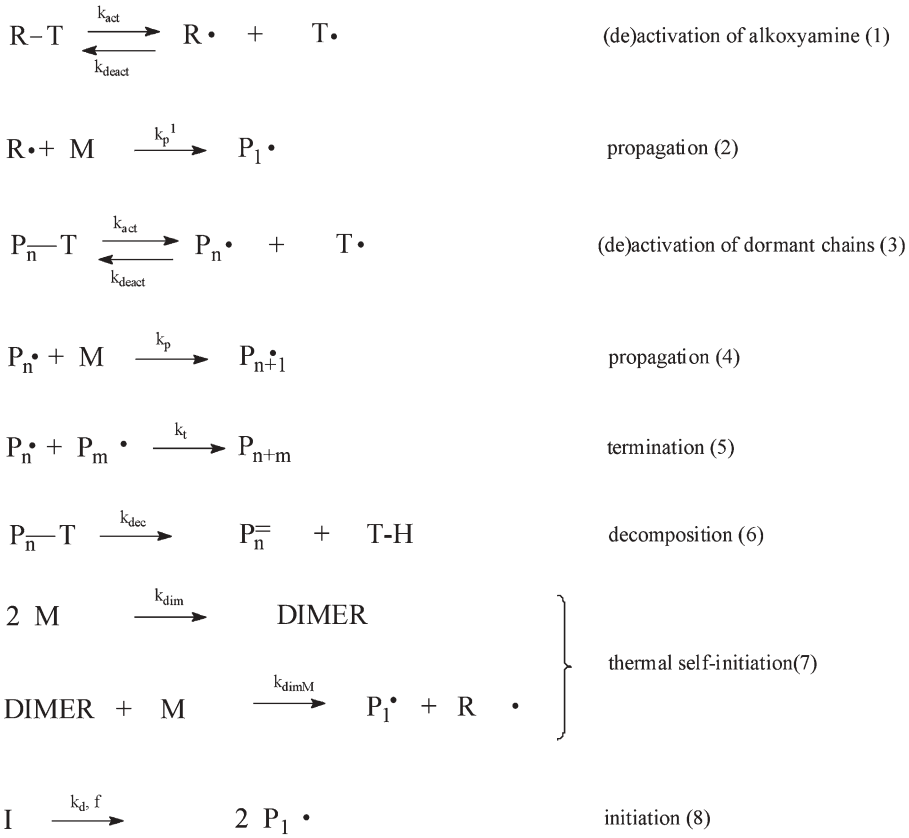

Scheme 3 Mechanism of nitroxide-mediated CRP. R-T represents an alkoxyamine, T· represents a nitroxide

merization to proceed successfully, providing that the number of initiating radicals is small compared to the number of nitroxide-trapped polymer chains [210]. Systems that do not show thermal self-initiation can also be controlled by using an additional initiator, which will provide the additional radical flux [210]. In addition, the dimer formed (Scheme 3, reaction 7) can react with a nitroxide molecule to provide the dimer radical and a hydroxyamine. The most important reactions in nitroxide-mediated CRP are shown in Scheme 3. An excellent overview of the kinetics and mechanism, supported by simulations, is given by Fukuda [211].

4.4.1.2 Effects Of Segregation And Heterogeneity

Similar to conventional free radical polymerization, heterogeneity and segregation effects make the kinetics of NMCRP more complex when applied in miniemulsions. This issue has also been discussed in a review article by Qiu et al. [212], which covers controlled free-radical polymerization in heterogeneous media up to 2001 (and so also covers miniemulsion polymerization). Butté et al. [213, 214] and Charleux [215] both discussed compartmentalization effects. Butté et al. came to the conclusion that the effects of segregation in NMCRP miniemulsions are very small, while Charleux predicted an increased polymerization rate for small (50–100 nm) particles. Both groups come to different conclusions, because Butté et al. did not account for the possibility that a nitroxide molecule exits a particle, while Charleux did. In summary, the segregation effect in NMCRP miniemulsions is not large unless the particles are small or a lot of the nitroxide partitions to the aqueous phase. This is nicely illustrated by work of Pan et al. [216], who performed NMCRP miniemulsions with varying surfactant concentrations. Although the surfactant concentration had a large effect on particle size, it hardly affected the polymerization rate.

Since both NMCRP and ATRP (Sect. 4.4.2) are based on reversible termination, the effects observed for these will be similar and are further discussed later.

4.4.1.3 Results

A review article by Qiu et al. [212] and references herein [217–226] covers NMCRP in miniemulsions up to 2001. Cunningham wrote a related review in 2002, also covering controlled radical polymerization in dispersed phase systems [227]. Here, the main results reported in the Qiu review will be summarized, and new developments in the field since then will be reviewed.

For several reasons, miniemulsion polymerization is the preferred technique for NMCRP in aqueous dispersed systems. Since NMCRP in general requires high reaction temperatures (above 100 °C) for the thermal polymerization of

styrene, the presence of a monomer phase is not desired. This would lead to colloidal instability. Furthermore, the presence of a large monomer reservoir makes the nitroxide partition out of the loci of polymerization, which will reduce control of the polymerization. Another reason for using miniemulsion polymerization is the fact that pre-formed alkoxyamines or nitroxide-terminated oligomers are often used. Generally, these are too water-insoluble to be transported through the aqueous phase, which excludes the use of conventional or seeded emulsion polymerization. Finally, the poorly understood and complex particle nucleation step is avoided in miniemulsion polymerization, which allows the use of oil-soluble initiators and makes results easier to understand.

The first results for NMCRP in miniemulsion were reported by Propdan et al. [218, 221] and Macleod et al. [219]. Both groups performed miniemulsion polymerizations of styrene at high temperatures (above the boiling point of water) using high pressure reactors. Propdan et al. used oil-soluble benzoyl peroxide (BPO) free-radical initiator and TEMPO, **1** (see Scheme 4), in a Dowfax 8390 surfactant system at 125 °C, while Macleod et al. used water-soluble potassium persulfate (KPS) initiator and sodium dodecylbenzene sulfonate (SDBS) surfactant at 135 °C. The Propdan system resulted in stable latexes and 90% conversion was reached in 12 hours. The polydispersity was 1.15–1.60 and molecular weights were up to 40 kg/mol. The Macleod system, if a proper nitroxide/initiator ratio was chosen, also gave stable latexes with good control, with polydispersities in the range of 1.1–1.2. Conversion reached 87% in six hours, although a later publication [225] showed that this relatively fast polymerization also resulted in a large proportion of dead chains.

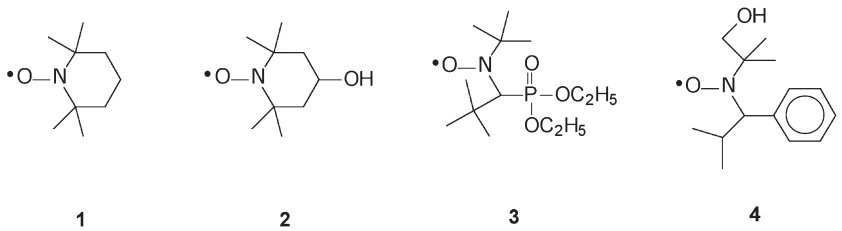

Scheme 4 Nitroxides used for NMCRP in miniemulsion

Later on, these same research groups started using pre-formed TEMPO-terminated polystyrene as a one component initiator system instead of a bi-component nitroxide/initiator system. Pan et al. [224] prepared TEMPO-terminated polystyrene in bulk and isolated this to use it as the initiator in their miniemulsions. This led to slower polymerization rates, molecular weights lower than predicted and relatively broad molecular weight distributions. Keoshkerian et al. [225], on the other hand, reported very high conversions in six hours (99.6%) and narrow polydispersities (1.15) by preparing TEMPO-terminated polystyrene in bulk up to a conversion of about 5% and applying

the mixture directly in miniemulsion without purification. As a proof of livingness, they were able to extend the chains with styrene in bulk and to produce block copolymers with butyl acrylate (BA) by directly adding the BA to the miniemulsion, yielding a block copolymer with a polydispersity of 1.18.

A disadvantage of TEMPO mediated systems is that a high temperature (above the boiling point of water) is required and so conventional emulsion polymerization reactors cannot be used. Another disadvantage of TEMPO is the limited monomer choice. The use of the so-called SG1 nitroxide, **3** (see Scheme 4), partially overcomes these problems, since it has been reported to work at 90 °C and to work with both styrene and BA [217, 220, 223, 226, 228, 229, 230]. When AIBN, an oil-soluble initiator, was used, poor results were obtained in styrene miniemulsion polymerizations [217, 220]. Conversion was low and the polydisperity was around 1.6. On the other hand, the use of a water-soluble initiator was more successful [223, 226, 228]. Conversion reached 90% within eight hours. Another important observation was that the pH was a very important parameter in the SG1-mediated polymerizations. This was assigned to side-reaction of the SG1 nitroxide. The best results were obtained when the pH was close to 7. Also, the monomer/water ratio appeared to have an important effect on the controllability of the polymerizations. Increasing the monomer/water ratio led to better-controlled (lower polydispersity) reactions. This was assigned to the fact than at a higher monomer/water ratio, less nitroxide partitions to the aqueous phase.

As already mentioned, the SG1 nitroxide is also capable of controlling polymerizations other than styrene [226, 229, 230]. Farcet et al. showed that it also worked with BA, although it required higher reaction temperatures (above 100 °C) because of the lower activation rate constant of SG1-terminated polybutyl acrylate compared to polystyrene. Polydispersities as low as 1.19 were obtained for BA miniemulsion homopolymerizations, while M_n increased linearly with conversion. Addition of styrene, after the majority of BA had reacted, resulted in the formation of block copolymers with a narrow polydispersity of 1.27. Additional evidence for the livingness of the polybutyl acrylate chains was given by thorough analyses of the materials formed via ^{1}H NMR, ^{13}C NMR, SEC and MALDI-TOF [230]. These analyses showed that the majority of chains consisted of polybutyl acrylate with one initiator-derived and one SG1 chain-end. Besides block copolymers, gradient copolymers of styrene and BA were also synthesized [230] using miniemulsion copolymerization of styrene and BA. Due to the composition drift and the livingness of the chains, this gives gradient block copolymers that contain relatively more styrene in the beginning of the chain and relatively more BA closer to the chain end.

Keoshkerian et al. used another nitroxide, **4** (see Scheme 4), to perform miniemulsion polymerizations with acrylates [231]. First the nitroxide was reacted with styrene and BPO in bulk to form nitroxide-terminated oligomers. These oligomers were used in a miniemulsion polymerization of BA at 135 °C. 86% conversion was reached after three hours, and at this point the polymer

had a M_n of 12 kg/mol with a polydispersity of 1.27. When the same procedure was followed with TEMPO as the nitroxide, conversion was less than 8% and did not proceed any further. The addition of a small amount of ascorbic acid, which destroys free nitroxide, led to conversions close to 65% after three hours, although the polydispersity of 1.62 was broader than with **4**.

Tortosa et al. [228] tried to synthesize styrene/BA block copolymers using both TEMPO and OH-TEMPO, **2** (see Scheme 4). OH-TEMPO was used because of the aqueous phase partitioning of this nitroxide, which would reduce the nitroxide concentration in the particles and so result in higher polymerization rates. It was indeed found that the conversion in the OH-TEMPO-mediated polymerizations was much higher. However, it was also found that the TEMPO-mediated polymerizations showed a greater living character and that the OH-TEMPO-mediated polymerizations also gave pBA homopolymer. In a later publication, Cunningham et al. [232] studied the effects of camphorsulfonic acid (CSA), a nitroxide destroyer known to accelerate bulk polymerizations, on styrene miniemulsion polymerizations with TEMPO and OH-TEMPO. It was found that the CSA effectively accelerates the polymerization rate, especially at high nitroxide/initiator ratios, although the effects were not as large as seen in bulk experiments. This was ascribed to the aqueous phase partitioning of the CSA, which reduces the CSA concentration in the particles. Unlike the large differences in polymerization rate seen in the BA polymerizations with TEMPO and OH-TEMPO [228], the experiments with styrene showed about equal polymerization rates for both the TEMPO and OH-TEMPO-mediated systems. Also, the increase in rate caused by the addition of CSA was equal in both systems, despite the large difference in water-solubilities between TEMPO and OH-TEMPO.

In another publication, Cunningham et al. [233] studied the effects of the KPS concentration and the TEMPO/KPS ratio on conversion, molecular weight and particle size in styrene miniemulsion polymerizations. It was found that most characteristics were similar to those for bulk polymerizations, although some unique features for heterogeneous systems were identified. A much higher initiator efficiency (approaching 100% at TEMPO/KPS=4) compared to conventional emulsion and miniemulsion polymerization was also observed, which emphasized the role of aqueous phase TEMPO in deactivating aqueous phase radicals. These results inspired the authors to model these systems in order to gain an even better understanding and to identify the operating conditions for optimal process performance [234, 235]. Ma et al. were the first to model the interfacial mass transfer of TEMPO and they found that phase equilibrium is achieved before TEMPO has an opportunity to react with active polymer radicals, and this is fast enough to maintain phase equilibrium throughout the polymerization [234]. In a second publication [235], they modeled the whole system, and by varying the KPS and TEMPO concentration they were able to find operating conditions at which the polydispersity was minimized and the degree of polymer livingness was maximized. In addition, it was found that the polymerization rate and the degree of livingness could be further im-

Table 17 Different NMCRP miniemulsion systems, with associated references

Nitroxide	*T*	Monomers	Initiators	Surfactants	Reference
1	125	Sty	BPO	Dowfax 8390	[219, 222]
1	125	Sty	pSty-**1**	Dowfax 8390	[225]
1	135	Sty	KPS	SDBS	[220, 223, 234]
1	135	Sty, BA	pSty-**1**	SDBS	[226]
3	90	Sty	AIBN	SDS	[218, 221]
3	90	Sty	KPS/SPS	SDS	[218, 221, 224]
3	112–120	BA, Sty	**3**-alkoxyamine	SDS/Forafac Dowfax 8390	[227, 229, 230, 231]
1, 2	135	Sty, BA	BPO, KPS	SDBS	[229, 233]
1,4	135	BA	pSty-**1** pSty-**4**	SDBS	[232]
1	125	Sty	pSty-**1**	Dowfax 8390	[217]

proved by increasing the volume fraction of water, although from an industrial point of view this might not be desirable.

The final paper that will be discussed in this section is a kinetic investigation by Pan et al. [216]. They created a series of styrene miniemulsions, using TEMPO-terminated polystyrene, in which they varied the Dowfax 8390 surfactant concentration from 1.25 to 25 mM. Although this had a large effect on the particle size, the effect on molecular weight and polymerization rate was small, while for conventional miniemulsion polymerization the effect of the particle size on polymerization rate is generally very significant. This was explained by the low average number of radicals per particle as a result of the coupling between TEMPO and active radicals, which overwhelms the compartmentalization effect in this case.

All systems discussed are summarized in Table 17.

4.4.2 Atom Transfer Radical Polymerization

4.4.2.1 Mechanism

Atom Transfer Radical Polymerization (ATRP) was first reported in 1995 by Matyjaszewski et al. [236–238] who investigated its potential for copper complexes, and Sawamoto et al. [239–241] who utilized ruthenium complexes. ATRP belongs to a class of living polymerizations known as reversible termination, that includes nitroxide-mediated radical polymerizations (NMRP). They are so named because the growth of the chain is controlled by a reversible termination event where the chain-end is exchanged between an active and dormant species. The lifetime of the active species is very short, such that only a few monomer units are added during each active cycle, giving the reaction its living character.

To induce this reversible termination, ATRP employs a transition metal complex with sufficient redox potential to deactivate propagating radicals. A halide atom, typically Cl or Br, is transferred reversibly (hence the name "atom transfer") to the metal complex. In the process the metal alternates between a lower and higher oxidation state. A general mechanism is shown in Scheme 5.

$$\text{P-X} + \text{M}_\text{t}^\text{n}/\text{L} \underset{k_d}{\overset{k_a}{\rightleftharpoons}} \text{P}^\bullet + \text{X-M}_\text{t}^{\text{n+1}}/\text{L}$$

Scheme 5 General ATRP mechanism

The metal undergoes a one-electron oxidation with the simultaneous abstraction of the halogen, generating radicals via a reversible redox process. The success of the process depends upon the fact that the equilibrium is shifted heavily in the direction of the dormant species. While complexes of copper and ruthenium have been most widely studied, complexes of nickel, palladium and iron can also be used [242–244]. Molybdenum, rhenium and rhodium ATRP have also been reported [245–247]. ATRP reactions are very well behaved and can easily produce polymers of controlled molecular weight and narrow polydispersity. Most classes of monomers have been successfully polymerized via ATRP. These include styrenes, (meth)acrylates, (meth)acrylamides, dienes, acrylonitrile and other monomers containing radical stabilizing substituents [248, 249]. Ring-opening polymerizations are also possible with ATRP [250, 251]. The initiators used are typically alkyl halides, but any compound with a weak halogen-heteroatom bond will suffice. The halogen end-group has the advantage of offering the ability to add functionality to the polymer.

In general, reaction rates in ATRP are slower than conventional free radical polymerizations. The unique nature of the ATRP equilibrium, which is shifted strongly towards the dormant species, effectively lowering the active, propagating radical concentration as compared to the conventional analog, is the source of the lower rates. This can be overcome to a certain degree by adjusting the metal/ligand ratio or through the use of additives [252–254]. Another factor contributing to the rate is that each bimolecular termination event releases two metal complexes in the higher oxidation state. As such, a shift in equilibrium in order to increase the propagation rate results in increased termination and an increase in the concentration of the complex in the higher oxidation state. The system tends to self-regulate and maintain the rate of polymerization. ATRP with transition metal complexes is extremely sensitive to oxygen owing to its reliance on the redox reaction between the halide and the metal complex. Reactions must be conducted in an inert environment or the metal will oxidize, effectively killing the polymerization. Because the quantity of metal complex required is relatively large and much of it will remain in the polymer, its residue must be removed for both environmental and economic reasons.

Although ATRP behaves differently from conventional free radical polymerization, the fundamental reactions involved are very similar and include initiation, propagation, transfer and termination (see Scheme 6). Since chain termination does not occur in a truly living polymerization, the "living" character of the chains in ATRP derives from the fact that chain propagation is first order with respect to radical concentration and irreversible bi-molecular termination is second order. As such, the concentration of the radicals is kept very low, the rate of bi-molecular termination is greatly reduced, and typically less than 10% of all of the chains will terminate. Unlike conventional free radical polymerization, where the rate is dictated by a steady state between the initiation and termination rates, the rate and concentration of propagating radicals in ATRP is controlled entirely by the equilibrium between activation and deactivation [255].

Initiation

$$R\text{-}X + M_t^n/L \underset{k_d^0}{\overset{k_a^0}{\rightleftarrows}} R^\bullet + X\text{-}M_t^{n+1}/L$$

$$R^\bullet + M \xrightarrow{k_i} P_1^\bullet$$

Propagation

$$P_n\text{-}X + M_t^n/L \underset{k_d}{\overset{k_a}{\rightleftarrows}} P_n^\bullet + X\text{-}M_t^{n+1}/L$$

$$P_n^\bullet + M \xrightarrow{k_p} P_{n+1}^\bullet$$

Termination

$$P_n^\bullet + P_m^\bullet \xrightarrow{k_t} P_{n+m} \quad \left(\text{or } P_n^= + P_m^H\right)$$

Scheme 6 Fundamental ATRP reactions

The initiators used are typically alkyl halides with similar structures to that of the monomer being employed. Of the halogens, chlorine and bromine have been shown to produce the best overall results with respect to molecular weight control [256]. However, iodine works well in certain cases, for example, rhenium-mediated styrene polymerizations [246] and copper-mediated acrylate polymerizations [257]. The C–F bond with fluorine is too strong to cleave homolytically, ruling out its use as an effective initiator. In general, any alkyl halide with activating substituents on the α-carbon (aryl, carbonyl or allyl groups) can act as an ATRP initiator. In addition, polyhalogenated compounds (like CCl_4 or $CHCI_3$) and compounds with a weak R–X bond (like N–X, S–X) can also be used.

There are several requirements that are generally recognized as essential to an effective ATRP catalyst [256, 258, 259, 260]. The metal center should be able to assume at least two oxidation states, separated by one electron, like Cu(I) and Cu(II). It should also be attractive to halogens, it should possess an expandable

coordination sphere such that when oxidized it can contain the halogen, and it should have a low affinity for alkyl radicals and the hydrogen atoms on alkyl groups.

Conventional free radical polymerizations in miniemulsions benefit kinetically from the effects of radical segregation. In solution, any radical could terminate with another theoretically. However, when the radicals are segregated into isolated reaction loci (such as miniemulsion droplets or particles) termination is no longer possible. Because the total concentration of radicals is distributed throughout the particles, the probability that any two radicals will terminate bi-molecularly is greatly reduced. The ideal situation is one in which a lone radical in a particle can terminate only with a radical that enters the particle. This is known as the "zero-one" limit [121], and in this case the rate of bimolecular termination is controlled by radical entry alone. In the absence of other effects, this lowering of the incidence of bi-molecular termination events tends to increase the overall rate of polymerization while simultaneously narrowing the molecular weight distribution. However, because of the mechanism involved, the same benefit is not seen with ATRP in miniemulsion. With ATRP, the dominating rate-controlling factor is the equilibrium between the dormant and active species. Since the equilibrium heavily favors the dormant species, the lifetime of the active species is extremely short. As such, the concentrations of these active radicals are always minute [261]. Therefore, the probability that a water phase radical will enter a particle containing another radical and terminate is exceedingly low. Any kinetic benefit that might otherwise be gained from segregation is overshadowed by this low radical concentration. It should also be noted that, because of the ATRP mechanism, increases in reaction rate, whatever their origin, will come at the expense of the deactivator species. The resulting decrease in the concentration of deactivator tends to produce broader polydispersities.

4.4.2.2 Results

There are few reported instances of ATRP in miniemulsion in the current literature. Matyjaszewski [262] and co-workers employed both forward (direct) and reverse-ATRP of *n*-butyl methacrylate in miniemulsion stabilized with a non-ionic surfactant, polyoxyethylene(20) oleyl ether (Brij 98), and using 4,4′-di(5-nonyl)-4,4′-bipyridine (dNbpy) with either CuBr or $CuBr_2$. They looked at the effects of using both oil and water-soluble initiators (AIBN and 2,2′-azobis(2-methylpropionamidine) dihydrochloride, or V-50) with the reverse process. With AIBN, the final polydispersity was relatively narrow (~1.4) but increased with conversion. Also, the number average molecular weight began higher than predicted and exhibited some curvature. This was attributed to slow decomposition of the AIBN, causing a slow and less quantitative formation of chains. Polydispersities were slightly lower with the V-50 and the number average weight progressed linearly with conversion, although the over-

all rate was much slower than with AIBN. Additionally, the progression of M_n, though linear, was much higher than found theoretically. In this case, the initiator decomposed faster but the radicals formed tended to terminate in the aqueous phase, contributing both to the slower overall rate and the higher than predicted actual molecular weights. The authors performed direct ATRP with an oil-soluble initiator, ethyl 2-bromoisobutyrate (EB*i*B). At a lower temperature than the reverse process, 70 °C vs 90 °C, the polymerization rate of the direct process was significantly faster. The polydispersity remained relatively flat throughout the experiment, with a final value of approximately 1.3. The molecular weight evolution, though roughly linear, was higher than predicted. Additionally, a semilog plot of the conversion data revealed some curvature, indicating a larger than expected number of chain termination events. It was postulated that the cause lay in the partitioning of the Cu(II) species into the aqueous phase. Recent studies with ATRP in aqueous dispersions lend credence to this argument [263]. They observed that the polymerization rate was insensitive to the size and number of particles and controlled entirely by the atom transfer equilibrium. The researchers also studied the effect of removing the costabilizer, hexadecane, from the recipe in order to determine if the hydrophobic dNbpy ligand alone would act as a sufficient droplet stabilizer. However, it was noted that the droplet size increased dramatically in the absence of hexadecane, indicating that the osmotic pressure would be insufficient to prevent Ostwald ripening.

Li and Matyjaszewski [264], building on the earlier work mentioned here [262], conducted reverse ATRP in miniemulsions using *n*-butyl methacrylate (BMA) with a more active catalyst system and a faster initiator. The solids content was roughly double that of the previous effort, jumping from approximately 13% to over 20%. More importantly, the surfactant (Brij 98) concentration was reduced from 13.5%wt to 2.3%wt based on monomer, decreasing the likelihood of micellar nucleation. Because of their high activities in bulk and solution ATRP, complexes of hexasubstituted tris(2-aminoethyl)amine (TREN) with Cu/Br_2 were utilized as the metal activator/deactivator. The water-soluble initiator used was 2,2′-azobis[2-(2-imidazolin-2-yl)propane] dihydrochloride (VA-044). The VA-044 was chosen for its fast decomposition rate, which facilitates a well-controlled ATRP and contributes to colloidal stability. The authors looked at the effect of the ligand and noted that there was no induction period with the TREN ligand as compared to dNbpy. While linear progressions of M_n with conversion were seen, the authors found that the molecular weight was not quantitative in initiator concentration. Instead M_n tended to be much higher than that calculated based on the initiator concentration and more closely followed a trajectory calculated from the initial concentration of deactivator, Cu(II). Assuming 100% initiator efficiency, the authors explain the deviation in terms of an excess radical concentration over the concentration of Cu(II), leading to the generation and subsequent termination of some of the oligomeric chains. Since a 1:1 molar ratio of $[Cu(II)]_0/[I]_0$ was used in most of the experiments, in theory there would be two initiator radicals for every

molecule of Cu(II) deactivator very early on in the polymerization. Many of the radicals would indeed quickly terminate until their concentration reached low enough levels that bi-molecular termination was insignificant compared to deactivation and they no longer competed for Cu(II). When a 2:1 ratio of $[Cu(II)]_0/[I]_0$ was employed, marginally better control of M_n was observed and the progression still tended to follow that calculated based upon $[Cu(II)]_0$, leading the authors to conclude that higher levels of Cu(II) would be needed for polymerizations that provide better control of M_n and relatively low polydispersities. The effect of surfactant concentration was studied using several nonionic surfactants in addition to Brij 98. The principal finding was that at higher surfactant concentrations (>13 wt% based on monomer), bi-modal molecular weight distributions and bi-modal particle size distributions of the latex were observed, indicating micellar and droplet nucleation. By increasing the initiator concentration and lowering the deactivator concentration, the authors also demonstrated that the kinetics of the polymerization are controlled primarily by the atom transfer equilibrium.

4.4.3 Reversible Addition Fragmentation Polymerization

4.4.3.1 Mechanism

The third (and also the most recently developed) controlled free radical technique discussed in this review is RAFT. In 1998 Rizzardo et al. published a novel "controlled" free-radical polymerization technique, which they designated the RAFT process [265–267] because the mechanism involves Reversible Addition-Fragmentation chain Transfer. This technique allowed the production of polymer with a narrow molecular weight distribution. In fact, this concept was not entirely new, and stemmed from the same researchers' previously published work to produce block copolymers using methacrylate macromonomers as reversible addition-fragmentation chain transfer agents in 1995 [268]. However, these macromonomers were not very effective RAFT agents. The breakthrough came with the discovery of a more reactive double bond species, S=C(Z)SR. During styrene polymerization, the propagating radicals were very reactive to the dithioesters and to a much lesser extent to the xanthates [269]. A brief description of the RAFT process is given below, and a schematic representation is given in Scheme 7.

A conventional free-radical initiator is added (contrary to some other controlled free-radical polymerization techniques) that generates radicals, which can add either to the monomer or the S=C moiety of the RAFT agent (step 1). In most cases the addition of small carbon-centered radicals to the RAFT agent is rapid and is not rate determining. Therefore, step (1) involves polymeric radical addition to **1** to form an intermediate radical species **2** that will fragment back to the original polymeric radical species or fragment to a dormant species **3**

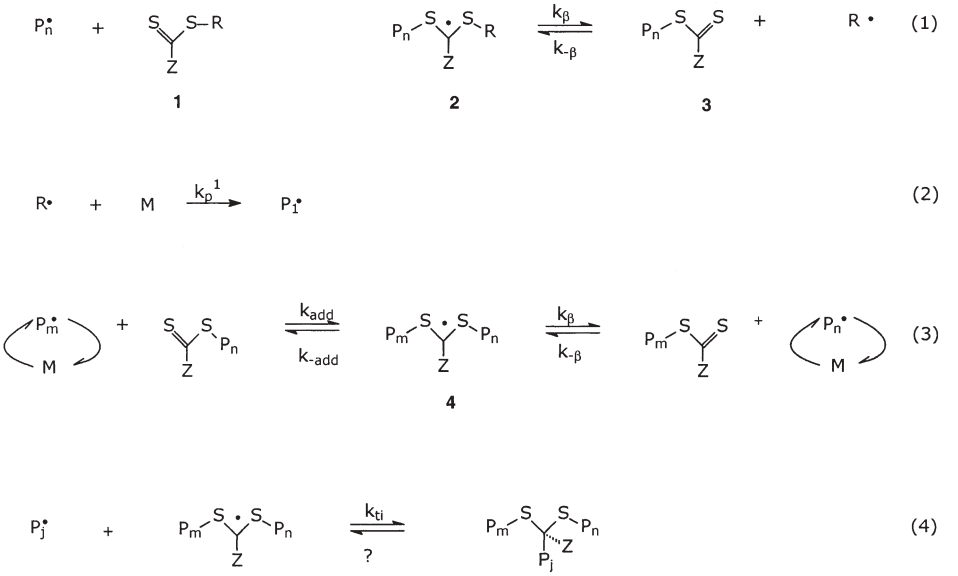

Scheme 7 Schematic representation of the proposed RAFT mechanism. It should be noted that in these equilibria any radical can react with any dormant species or RAFT agent. (1) Addition of a propagating polymeric radical to the initial RAFT agent **1**, forming the intermediate radical **2**. The intermediate radical can either fragment into the two species it was formed from or into a dormant polymeric RAFT agent **3** and a small radical R•. (2) The small radical initiates polymerization, forming a polymeric radical, rather than reacting with **3** (reforming **1**). Therefore R should be a good leaving group and should have the ability to be added to the monomer. (3) Equilibrium between propagation polymeric radicals and dormant polymeric RAFT agents. (4) Intermediate radical termination

and a small radical, R•. R• can then further propagate to form a polymeric radical (step 2 in Scheme 7), rather than adding to **3**. The dormant polymeric RAFT agent acts in a similar way to a RAFT agent, so growing polymeric radicals can also add to the dithiocarbonyl double bond of the polymeric RAFT agent, thereby forming an intermediate radical **4**. This intermediate has an equal probability of fragmenting back into its starting species or into a dormant polymeric RAFT agent and a polymeric radical, in which the dithiocarbonate moiety has been exchanged between the active and dormant polymer chains of the starting species. This equal probability of fragmenting to either side of the equilibrium is a result of the symmetry of **4**. There might be a difference in the chain length of both sides, but this will not have an effect, unless one of the two sides is extremely short. This mechanism of addition of radicals to the dithiocarbonyl double bond and fragmentation of the intermediate was shown by Moad et al. [270], who observed the intermediate radical directly by ESR.

Overall, polymer chains with a dithiocarbonate end-group are formed. If addition to the dithiocarbonyl double bond is fast compared to propagation,

and termination is suppressed by keeping the radical concentration low, all of the chains will grow in a sequential process, leading to a low polydispersity. The number of chains is determined by the amount of RAFT agent and initiator that has been consumed. Assuming termination by combination, the number of dead chains will be equal to the amount of initiator that is consumed. The number of chains with a dithiocarbonate end-group, the dormant chains, is equal to the amount of consumed RAFT agent. One should therefore keep the initiator to RAFT agent ratio low in order to obtain a high percentage of dormant chains. This criterion is especially important in the preparation of block copolymers [271–273].

In fact, the RAFT process resembles the degenerative transfer (DT) process [274]. In a polymerization in which an alkyl iodide is used as the degenerative transfer agent, the iodine atom is exchanged between a polymeric radical and a dormant chain, similar to the dithiocarbonate exchange in RAFT. However, in the case of degenerative transfer there is a direct equilibrium between the dormant and growing chains, without formation of an intermediate radical.

If reactions 1 to 3 in Scheme 7 are considered, there is no reason to assume that addition of a RAFT agent to a conventional free radical polymerization will have an effect on the polymerization rate, since the equilibrium concentration of propagating radicals will not be affected. However, it has been found that considerable retardation does take place in RAFT polymerization [275–281]. The intermediate radical was postulated to be the reason for the significant retardation of the polymerization rate. Two explanations for retardation have been put forward:

(i) slow fragmentation of the intermediate radical [277–280]
(ii) termination of the intermediate radical (reaction 4 in Scheme 7) [275, 276, 281]

The key variable in both explanations is the fragmentation rate constant. There is a difference of six orders of magnitude between the fragmentation rate constants obtained via explanations (i) and (ii). The question of which explanation is correct has been hotly debated for over three years, but is still unresolved.

4.4.3.2
Effects of RAFT and Transfer Agents on Emulsion Polymerization Kinetics

As far back as 1948, Smith and Ewart [13] included the effects of radical desorption in emulsion polymerization kinetics, and in 1965 Romatowski et al. [282–284] showed that radicals resulting from chain transfer to monomer indeed escape from the particles.

Nomura et al. [285] and Lichti et al. [286] studied the effects of transfer agents on the kinetics of ab initio and seeded emulsion polymerization of styrene, respectively. Nomura et al. found that the polymerization rate per particle decreased with increasing amounts of carbon tetrachloride, carbon tetrabromide and primary mercaptans, and that the effects were stronger when

the transfer constant or the water-solubility was higher. Lichti et al. observed the same in seeded experiments with carbon tetrachloride and carbon tetrabromide as chain transfer agents. They were the first to actually measure the exit rate coefficient, using γ-radiolysis relaxation data. They found an increasing exit rate coefficient with increasing amounts of transfer agents and a higher exit rate coefficient when the transfer constant was higher. They also found that the entry rate coefficient increased with increasing amounts of carbon tetrabromide. Due to the counterbalancing effects of an increased exit rate and an increased entry rate the polymerization rate passed through a minimum.

Maxwell et al. [287] extended their own model for entry by taking the effect of transfer agent into account and used this model to explain the increase observed in emulsion polymerizations with monomers with a high critical chain length z and thiols of intermediate chain length. They also used this model to show that longer chain thiols are too water-insoluble to have an effect and that short chain thiols might suffer aqueous phase termination and increase the exit rate, and so they can reduce the polymerization rate instead of increasing it. No effect was expected for styrene from Maxwell's model, which was confirmed by the work of Asua et al. [288]. They found that *n*-dodecyl mercaptan had no effect on the polymerization rate.

The work of Monteiro et al. [289] showed that when RAFT agents are applied in emulsion, the rate of polymerization is significantly retarded. This effect is stronger when a RAFT agent with a more water-soluble leaving group is used. Exit from the particles after fragmentation was proposed to be the main reason for the observed retardation. Because of the high reactivity of the RAFT agents used, it is expected that all of the RAFT agent is consumed after a few percent conversion, and so it should no longer should have an effect. However, it was observed that the rate of polymerization decreased with increasing RAFT in interval II. Monteiro et al. claimed that this was due to transport limitation of RAFT from the monomer droplets to the particles, meaning that there is a constant flux of RAFT agent to the particles, even if all of the RAFT agent has been consumed in the particles. Therefore, not all of the chains start to grow simultaneously, resulting in broad polydispersities. However, retardation was also observed in Interval III, and this could not be ascribed to exit and transport limitations. When this work was published, intermediate radical termination [275, 276] had not yet been put forward by Monteiro et al. as a source of retardation. However, since the system might not be under zero-one conditions in Interval III due to the increased particle size, intermediate radical termination might explain these results.

Another observation Monteiro et al. made was that a red layer was observed during Interval II, consisting of low molecular weight dormant chains, swollen with monomer. At the crossover to Interval III, this red layer coalesced, forming red coagulant. The same red layer was also observed by De Brouwer et al. [290] in miniemulsions stabilized with ionic surfactants. When polymer was used as the so-called cosurfactant, this polymer was not present in the red layer, indicating that this layer was not due to droplet coalescence. Also, the use of an

oil-soluble initiator did not reduce the formation of the red layer. Using a higher radical flux (to enhance droplet nucleation) did not have an effect. Indeed, the formation of the red layer was correlated to the polymerization rate, which indicates that the product formed during the polymerization plays a crucial role in the destabilization. However, when nonionic surfactants were used, destabilization did not occur, and controlled miniemulsion polymerizations could be performed without destabilization. Later, Luo et al. suggested that the instabilities are the result of the large number of oligomers formed in the early stages of RAFT miniemulsions, causing a superswelling state [128], which could be prevented by increasing the amount of cosurfactant.

Moad et al. [291] showed that the type of RAFT agent is important. Using a very reactive RAFT agent (with a transfer constant of about 6000), similar to that used in the work of De Brouwer and Monteiro, resulted in a broad polydispersity in ab initio styrene polymerizations with ionic surfactant, which was ascribed to the fact that the RAFT agent was not uniformly dispersed in the polymerization medium. The use of less reactive RAFT agents (with transfer constants of 10–30) did not result in destabilization and the final polymer had a polydispersity close to 1.4.

Prescott et al. [292] used acetone to transport a water insoluble RAFT agent to the seed particles. The polymerization was initiated in Interval III after removing the acetone. No destabilization was observed, which according to our previous discussion might indicate that the transfer constant of the RAFT agent used was not extremely high. However, it was high enough to result in a linear increase in molecular weight, and polydispersities between 1.2 and 1.4. Although the RAFT agent is consumed at the beginning of the reaction (the molecular weight follows the theoretical linear increase), a reduction in rate is observed throughout the reaction. In these experiments, a small seed was used and the amount of monomer was such that the particle size does not increase much, which means that the system is likely to be under zero-one conditions throughout the polymerization and so intermediate radical termination cannot explain the retardation observed.

Monteiro et al. [293] also studied the effect of xanthates (RAFT agents with low transfer constants) with styrene, in ab initio styrene polymerizations. Again rate retardation was observed throughout the polymerization. This is not surprising, since the low transfer constants of these RAFT agents mean that they are present during the whole polymerization, which results in an increased exit rate throughout the reaction.

This was later confirmed by Smulders et al. [294], who experimentally determined the exit rate in similar systems using γ-relaxation experiments. The exit rate was found to increase linearly with the RAFT concentration, although the decrease in rate could not be ascribed to the increase in exit rate alone.

Summarizing, we know that RAFT can be applied in emulsion, although the mechanism for this is not yet fully understood. Highly reactive RAFT agents can lead to destabilization, although the use of nonionic surfactants seems to prevent this destabilization.Rate retardation is observed in all cases. This can

be partly ascribed to the increased exit rate, although the retardation is still observed even when all of the RAFT agent has been consumed. In that case, intermediate radical termination might explain the reduction in rate. However, even when the system is under zero-one conditions and all RAFT is consumed, retardation still occurs. This cannot be ascribed to intermediate radical termination or to exit. In fact, an explanation for this might be quite simple, as shown by Smulders [295]. Retardation with RAFT in zero-one systems in which all of the RAFT has been consumed cannot be ascribed to increased exit rate anymore, since the leaving groups of the dormant polymer chains cannot exit. Intermediate radical termination is also not a dominant mechanism, since each particle contains only one radical. However, the fact that each particle contains only one radical explains why retardation is observed in these systems. This one radical is either present as a "normal" radical, $R^{\bullet}$, capable of propagating and so consuming monomer, or as a "intermediate" radical, $I^{\bullet}$. While the radical is in the intermediate state it does not consume monomer, which in turn leads to retardation. Since the system is under zero-one conditions, the system does not reach steady state at the microscopic level (inside a particle), because a particle contains either no radical, one "normal" radical, or one "intermediate" radical. The lifetimes of $R^{\bullet}$ and $I^{\bullet}$ are given by:

$$\tau_{R^{\bullet}} = \frac{1}{k_{add}[dormant\ chains]} \quad \tau_{I^{\bullet}} = \frac{1}{2k_{-add}} \tag{19}$$

Using the rate parameters for dithiobenzoate RAFT polymerization of styrene at 70 °C, as reported by Monteiro et al. [275] (k_{add}=4×10^6 dm^{3}mol^{-1}s^{-1}, k_{-add}= 1×10^5 s^{-1}), and a dormant chain concentration of 0.06 M, this results in a lifetime of 4.2×10^{-6} s for a "normal" radical, and a lifetime of 5.0×10^{-6} s for an intermediate radical. This means that the fraction of time that a radical is present as a propagating radical in this system is 4.2×10^{-6}/(4.2×10^{-6}+5.0× 10^{-6})= 0.46. This also means that the polymerization rate in this example would only be 46% of the polymerization rate without RAFT. The mechanism proposed by Monteiro et al., which included intermediate radical termination, was supported by Fukuda et al. [281, 296]. However, the latter authors proposed a value of k_{dd} on the order of 10^4 s^{-1}. Following the same pathway, this value means that the polymerization rate with RAFT is only 7.7% of the rate without RAFT in a zero-one system. Since no good experimental data is currently available for zero-one emulsion systems with dithiobenzoate RAFT agents, at the moment no definitive statement can be made about which value of the fragmentation rate constant best describes a zero-one system. However, these results indicate that zero-one experiments can be a useful tool for determining this rate parameter, and they provide data useful as we attempt to pinpoint the correct value for the fragmentation rate constant (see previous section). Davis et al. fitted conversion-time data for a styrene polymerization with RAFT at 60 °C using k_{add}=5.4×10^5 dm^3 mol^{-1} s^{-1} and k_{-add}=3.3×10^{-2} s^{-1}. For a zero-one system with 1 mol% RAFT, these values would lead to $t_{R^{\bullet}}$=3.1×10^{-5} s and

$t_{I\cdot}$=15.2 s. This means that zero-one polymerization should not proceed, because the radicals are present as intermediate radicals for more than 99.99% of time. Since we have experimental evidence that RAFT systems do proceed under zero-one conditions [292], these rate parameters seem highly unlikely, although it should be noted that Prescott et al. used a RAFT agent with a less stable intermediate. Zero-one experiments with dithiobenzoate RAFT agents might be the key to closing the "six-orders-of-magnitude-gap" for the fragmentation rate constant.

4.4.3.3 Application of RAFT in Miniemulsion

As with nitroxide-mediated polymerizations and ATRP, and with RAFT, miniemulsion systems are often preferred over conventional emulsion systems, although not as exclusively as with NMCRP and ATRP. In this section we will discuss some applications of RAFT in miniemulsions.

In 2000, Moad et al. reported the synthesis of controlled polystyrene using RAFT in miniemulsion [291]. Using phenyl ethyl dithiobenzoate in a SDS/cetyl alcohol stabilized system at 70 °C, 25% conversion was obtained in four hours, while a control experiment without RAFT reached 82% conversion in one hour. Molecular weight increased with conversion and the polydispersity went down to 1.18. No problems with stability were reported. On the other hand, De Brouwer et al. [290] and Tsavalas et al. [296] were unable to obtain stable latexes using dithiobenzoate RAFT agent in either anionic- or cationic-stabilized miniemulsions. They reported the formation of a red organic layer on top of the miniemulsion as soon as the polymerization started. This layer consisted of low molecular weight polymer and monomer. Luo et al. later ascribed the observed phenomena to a superswelling state, caused by the large number of oligomers formed at the beginning of the polymerization [128]. However, when nonionic surfactants like Igepal 890 and Brij 98 were used by Brouwer et al. [290], they could perform stable RAFT miniemulsion polymerizations. Miniemulsion polymerizations of EHMA, STY, MMA, BMA, and MA all resulted in stable latexes with polydispersities below 1.4, and sometimes as low as 1.1, at very high conversions. When the miniemulsions formed were used as seed latexes in either batch or semi-batch polymerization with a second monomer, block copolymers with a low polydispersity and a high level of block purity were obtained.

Butté et al. [261] were able to perform miniemulsion polymerizations stabilized with SDS and hexadecane using dithiobenzoate and "pyrrole" RAFT agents. In most cases oligomerized RAFT agents were used, but "monomeric" RAFT agents were also applied successfully. Although they used basically the same systems, Butté et al. did not observe the red layer formation reported earlier by De Brouwer and Tsavalas. Linear molecular weight growth and relatively narrow polydispersities were reported, although they were broader than for bulk polymerizations. This was ascribed to the presence of dead chains in the oligomers and differences in miniemulsion droplet sizes, leading to dif-

ferences in monomer-to-RAFT ratios. Smaller particles have a larger surface/volume ratio and are therefore preferentially entered by z-mers, leading to monomer consumption in these particles which is replaced by monomer from the larger particles.

Butté found that the polymerization rate decreased with RAFT. This was supposed to be the result of an increasing exit rate. However, even when oligomeric RAFT agents were used, which should not lead to an increased exit rate, a decrease in rate was observed, which was ascribed to the presence of "monomeric" RAFT agent in the oligomer mixture. Finally, Butté reported the synthesis of block copolymers in miniemulsion by adding styrene to a fully polymerized MMA miniemulsion and by adding BA to a 63% polymerized styrene miniemulsion. In both cases it was shown that block copolymer was formed, although polydispersities were relatively high.

In order to prevent the formation of the red layer observed by De Brouwer and Tsavalas, Vosloo et al. performed SDS-stabilized miniemulsion polymerizations of styrene using pre-formed dithiobenzoate-end-capped styrene oligomers, formed in bulk [297]. Two types of cosurfactant (hexadecane and cetyl alcohol) and two oligomers with different molecular weights were used. Red layer formation was not observed in any of the miniemulsion polymerizations, and the results were better – lower polydispersities, and molecular weights that were closer to the theoretical values – when hexadecane and the lower molecular weight oligomers were used.

Lansalot et al. studied the influence of the structure of the RAFT agent on styrene miniemulsion polymerization [298]. The use of 1-phenylethyl phenyldithioacetate (PEPDTA) was compared to cumyl dithiobenzoate (CDB) and 1-phenylethyl dithiobenzoate (PEDB). It was shown that PEPDTA did not show retardation in bulk experiments, while CDB and PEDB show a large decrease in rate with increasing RAFT concentration. This was ascribed to the less stable PEPDTA macroRAFT radical. When the same RAFT agents were used in styrene miniemulsion polymerizations, stabilized by SDS/hexadecane, again the PEPDTA showed much higher polymerization rates than CDB and PEDB. However, in contrast to the bulk experiments with PEPDTA, a decrease in rate with an increase in RAFT was observed in the miniemulsion. This was ascribed to the exiting of radicals formed after addition and the fragmentation of the initial RAFT agent. This was confirmed by miniemulsion polymerization experiments performed using oligomerized PEPDTA, where the leaving radical cannot exit to the aqueous phase. In that case, using the same concentration as in the experiment with "monomeric" PEPDTA, the polymerization rate dramatically increased to almost the same polymerization rate as without RAFT.

4.4.4 Colloidal Stability

After being frustrated by poor colloidal stability (phase separation or coagulation) in controlled macroemulsion polymerization (NMP, ATRP, RAFT), re-

searchers turned to living miniemulsion polymerization [299–304]. It was expected that the colloidal stability should be improved in living miniemulsion polymerization on the premise that molecular weight controlling agents (RAFT agent, nitroxide, and ATRP catalyst) do not need to be transferred from the monomer reservoir to the polymerization loci. However, this strategy only gave limited success. Problems included loss of colloidal stability, large particle size, broad particle size distributions, and irreproducible particle sizes were observed [221, 222, 226, 296, 305–307]. It is evident the stabilization of colloids during living polymerization is more difficult than during regular miniemulsion polymerization. The stability of latex seems to be sensitive to the recipe. Georges and co-workers [222, 307] reported that, for the styrene miniemulsion polymerization of TEMPO-mediated living polymerization, when the surfactant concentration was reduced from 1.4%wt to 0.7%wt but the HD was kept constant at 3 wt%, the system could be made stable. In an effort to commercialize nitroxide-mediated miniemulsion polymerization, Georges [226] proposed a modified miniemulsion SFRP process in which TEMPO-terminated polystyrene oligomers were used to initiate the polymerization with 10 wt% HD and 6.7 wt% sodium dodecylbenzenesulfonate (surfactant), yielding polymers that have a high degree of livingness and stable latex. Charleux [223] found that about 5 wt% hexadecane is needed for ST miniemulsion SFRP to get stable latex, but with *n*-butyl acrylate, the proportion of HD must be decreased to less than 1 wt%. For butyl acrylate SFRP in miniemulsion, it has been reported that the particle size is not reproducible [226]. The El-Aasser group reported successful miniemulsion polymerization that employed nitroxides with controlled molecular growth and good miniemulsion stability [221]. It is interesting to note that the level of costabilizer was more than 5%wt, far more than the typical 2%wt. Even so, El-Aasser's particle size is much larger than the non-living counterpart, and the particle size distribution is much broader. In the next paper of the El-Aasser group [308], TEMPO-terminated oligomers of polystyrene were prepared via bulk polymerization of styrene, and they were used as initiator in miniemulsion polymerization. The stable latexes were obtained with 3 wt% HD and smaller particles. The Matyjaszewski group [309] studied ATRP-controlled free radical miniemulsion polymerization and found that using either anionic (SLS) or cationic (dodecyltrimethylamomonium bromide) surfactant led to instability.It was argued that the catalyst may interfere with SLS, while no reason was given for the instability of dodecyltrimethylamomonium bromide. The final particle size was more than 1 μm in the normal ATRP polymerization of butyl methacrylate, and more than 250 nm in reverse ATRP. It has been reported that the use of nonionic polymeric surfactant improved the stability. Also, the longer the PEO segment in the surfactant, the better the stability. In the case of Tween 20, a portion of the monomer phase separated, forming small pools in the reaction mixture, but these would dissipate as the polymerization progressed, and there was no coagulation of polymer at higher conversion. In another ATRP paper by Matyjaszewski et al. [262], dNbpy, nonionic Brij 98, hexadecane, and the water-soluble azo com-

pound 2,2′-azobis (2-methylpropinonamide) dihydrocholoride (VA-50), were used as ligand, surfactant, costabilizer, and initiator, respectively. The resulting latexes showed improved stability. It is worth noting that a large amount of surfactant (5.0%wt, 13.5%wt based on monomer) and HD (1/10 [v/v monomer]) was used but particle sizes are large too (around 300 nm). In the most recent paper by the same group [264], it was reported that the amount of Brij 98 and HD can be reduced to 2.3%wt and 3.6%wt, respectively, by replacing VA-50 by the more reactive VA-44, and replacing dNbpy by hydrophobic hexa-substituted TREN with high catalytic activity, which gives polymerization with good colloidal stability and particle sizes of 200–250 nm. De Brouwer et al. [296, 305] reported stability problems in controlled free radical miniemulsion polymerization using RAFT. It was reported that when an ionic surfactant (either cationic or anionic) was used, a monomer bulk phase constituting up to 35% of the total organic material in the system could be observed at low monomer conversion. The phenomenon can be seen with various different monomers, different initiator systems, and different costabilizers. Sanderson [310] also reported these instability issues at less than 5 wt% SDS. De Brouwer et al. [305] found that when nonionic surfactant is used, the polymerization is well controlled in terms of molecular weight, and the colloidal stability is good. However, both Butté et al. [261] and Lansalot et al. [298] did not report any instability issues in RAFT miniemulsion polymerization. In Butté's work, 3.3%wt HD and 1.67%wt SDS was employed. The miniemulsion were prepared by a three-step approach: after mechanical preemulsification for 10 minutes and sonication for 20 minutes, the mixture was passed into a microfluidizer ten times. No colloidal characteristics were reported. In Lansalot's work, 2%wt hexadecane, 1%wt PST, and 0.01 mol/L water SLS were used. The miniemulsion was prepared by ultrasonication for a period of 7 minutes at 35% amplitude, 30–35 W power, in a Branson 450 sonicator. In Lansalot's work, although stable latex was obtained, the particle size was much bigger than the corresponding non-living system (except when oligomeric RAFT agent was used), and particle size distribution was broad. This seems to indicate that miniemulsification procedure plays some role in obtaining stable latex. To avoid colloidal instability, Sanderson [310, 311] successfully developed two approaches based on the predictions of Luo's theory [128]:

a. Form RAFT-endcapped oligomers in bulk, dissolve the RAFT agent into the monomer, then disperse the monomer into water under shear with surfactant and costabilizer, and recommence polymerization.
b. Use high surfactant concentrations (10%wt with respect to monomer), and high costabilizer (*n*-HD) concentration (>4%wt with respect to monomer).

From the above summary of experimental investigations into living miniemulsion polymerization, we can see that controlled miniemulsion polymerization (SFRP, ATRP, and RAFT) is less colloidal-stable during polymerization than its non-living counterpart. Colloidal instability leads to phase separation in the worst cases. In improved cases, the latex that results from the controlled mini-

emulsion polymerization has much bigger particle size and much broader particle size distribution than that obtained using regular miniemulsion polymerization. One can also see that colloidal instability is very sensitive to the polymerization recipe. Monomer, surfactant, dormant agent, and levels of surfactant and costabilizer all have large influences on the stability. High levels of surfactant and costabilizer, and use of a nonionic surfactant and an oligomeric control agent all proved to aid stability, although larger particle sizes and broader particle size distributions were still seen. On the other hand, the literature indicates that instability is a general problem in controlled free radical miniemulsion polymerization, regardless of the living control mechanism, monomer, surfactant system (except for polymeric surfactant), or initiator system. It seems reasonable to assume that the instability is caused by the "living" nature of the systems. In a controlled free radical polymerization system, the kinetics of polymer chain formation is totally different from that for classical free radical polymerization. In classical free radical polymerization, a polymer chain is fully polymerized in about 1 s. At the very beginning of polymerization, a few polymer chains of high molecular weight are formed. During polymerization, monomer is consumed to form more and more large polymer chains. However, in controlled free radical polymerization, a large number of oligomers are formed at the beginning of polymerization. During polymerization, the oligomers gradually grow into large polymers. The feature common to all of the controlled free radical systems is the presence of large concentrations of oligomers early in the polymerization. In miniemulsion polymerization, polymerization occurs in the particles (around 100 nm in size). Ugelstad et al. [40] showed that oligomers are very efficient swelling agents, and hence the existence of oligomers may dramatically modify the state of the miniemulsion. A theoretical model has been developed by Luo et al. [128] to simulate the swelling of oligomers formed in the controlled miniemulsion polymerization.

The chemical potential of monomer droplets is determined by [128]

$$\mu_d = RT\left(\ln \varphi_{d1} + \left(1 - \frac{1}{m_2}\right)\varphi_{d2} + \varphi_{d2}^2 \chi_{12} + \frac{2\bar{V}_1}{\gamma r_d} RT\right) \tag{20}$$

Before the start of polymerization, the monomer chemical potentials in all droplets can be assumed to equal because the monomer has at least limited solubility in the aqueous phase. However, once a monomer droplet is initiated, a part of the monomer will polymerize into oligomers, and the droplet is converted into a particle. The particle chemical potential is described by [312]

$$\mu_d = RT\left(\ln \varphi_{d1} + \left(1 - \frac{1}{m_2}\right)\varphi_{d2} + \left(1 - \frac{1}{m_3}\right)\varphi_{p3} + \varphi_{p2}^2 \chi_{12} + \varphi_{p3}^2 \chi_{13} + \varphi_{p2}\varphi_{p3}\left(\chi_{12} + \chi_{13} - \frac{\chi_{13}}{m_2}\right) + \frac{2\bar{V}_1}{\gamma r_d} RT\right)\right) \tag{21}$$

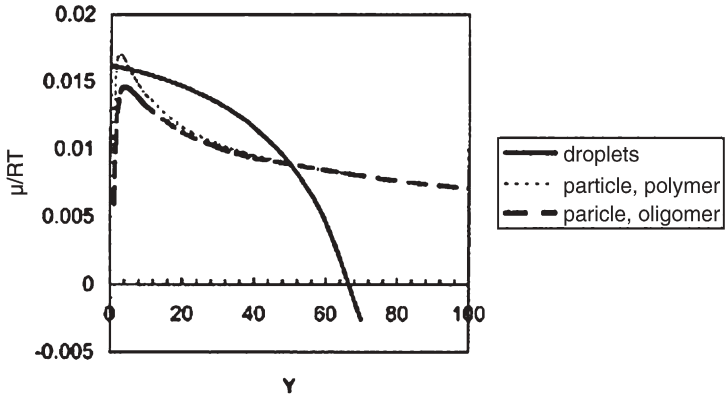

Fig. 21 Variation in the droplet chemical potential (top) and particle chemical potential (bottom) during particle swelling (from [170])

The monomer chemical potential in the particles is lower than that in the droplets, so that the monomer in the droplets will diffuse across the aqueous phase and into the particles, leading to changes in the monomer chemical potentials of the the particles and droplets. The change in the monomer chemical potential is illustrated in Fig. 21, where *Y* is defined as the swelling capacity: the ratio of the weight of a swollen particle to its weight before it is swollen.

As shown in Fig. 21, the particles swell with monomer diffusion (increase in *Y*). During swelling, the monomer chemical potential in the particles first rapidly increases and then decreases gradually down to zero with more and more monomer swelling. On the other hand, the droplets shrink and the co-stabilizer is concentrated since it cannot (by definition) diffuse out with the monomer. The monomer chemical potential decreases monotonically. During the process of monomer diffusion, if the monomer chemical potential in the droplets is equal to that of the particles, equilibrium is established and monomer diffusion ceases. In Fig. 21, the formation of high MW polymer is shown for contrast. Three intersections of the droplet and particle chemical potential curves can be seen. Two of these occur at low *Y* and the third at a much higher *Y*. As is often the case with three equilibrium points, the middle point is unstable. When the system arrives at the first intersection during swelling (lowest *Y*), monomer transfer stops and the system reaches an equilibrium state that is called the *normal swelling state*. In this case, the other two equilibrium points will never be reached. However, in the case of controlled polymerization, the formation of oligomers rather than high molecular weight polymer leads to a lower mixing free energy so that the monomer in the particles has a lower chemical potential. If the effect is large enough so that the chemical potential of the droplets remains higher than that of the particles at the peak of the particle chemical potential curve, the system will move to the right-most equilibrium point. This will be denoted as the *super-swelling state*. In this case, a large amount of monomer will transfer from the droplets to the particles.

Super-swelling may be the cause of the stability problems encountered in controlled miniemulsion polymerization. As the super-swelling equilibrium point is approached, a large amount of monomer would transfer from a large number of droplets to a small number of particles, which would cause the monomer droplets to shrink and the particles to swell. This would broaden the particle size distribution, or even destroy the miniemulsion. In the worst case, the super-swelling would lead to a very large size difference between the droplets and particles. The particles may be swollen to around 1 μm, a critical size where the system becomes shear-sensitive and buoyant forces dominate. Because shear is low in a miniemulsion polymerization reactor, the particles would rapidly approach a breaking-coagulating dynamically balanced particle size, as in suspension polymerization. In this case, particle size could be more than 10 μm, or they may even form a bulk phase, depending on the shear field. Alternatively, it is possible to destroy the miniemulsion using so-called hetero-coagulation (small particles/droplets coagulating onto large ones) when the size difference becomes large. The hypothesis that super-swelling causes the instability is also supported by two other papers on controlled free radical miniemulsion polymerization that used a degenerative transfer agent (C6F13I) to control molecular weight. It was reported that the final latex morphology was well controlled. C6F13I is a relatively inefficient transfer agent (C_{tr}=1.4 at 70 °C), so the degree of polymerization of the product was rather high at the beginning of polymerization. Super-swelling is less likely to occur in such a case.

Based on Luo's simulations [128], it has been found that the super-swelling state is rather sensitive to recipe variations. Simply increasing the costabilizer level and/or using a nonionic polymeric surfactant would probably eliminate super-swelling, and hence, the instability. More recently, Sanderson [310] reported that two strategies could successfully form stable latex from RAFT miniemulsion polymerization:

a. Replace common RAFT by RAFT-endcapped oligomers
b. Use high levels of SDS and HD

The fact that these two quite different approaches are both successful can largely be reconciled using Luo's theory. Replacing common RAFT by RAFT-endcapped oligomers can avoid the super-swelling because the dangerous stage of oligomer formation is avoided. Using oligomers of a molecular weight controlling agent has also proved very helpful with SFRP in miniemulsion [226, 232]. High levels of SDS would lead to low interfacial tension, which helps to suppress the super-swelling, and high HD levels would also suppress the super-swelling. The super-swelling could also explain the instability or broad particle size distribution in most cases, as discussed in the literature [128].

Super-swelling was postulated as a cause of instability in controlled free radical miniemulsion polymerization. Asua [312] thought that the interfacial tension used in the simulations was too high and the droplet size was too small. However, it is turned out that the question about droplet size is due to a misunderstanding. It is well accepted that a well-performed miniemulsion has

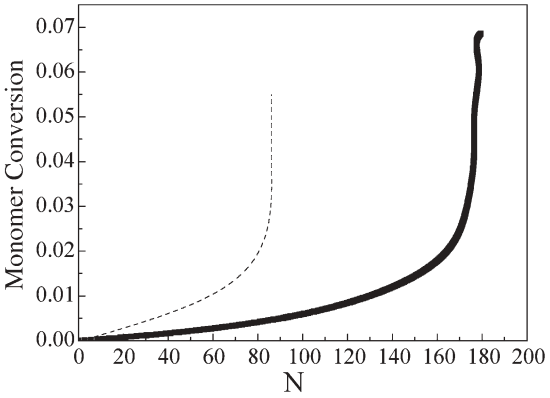

Fig. 22 Plot of monomer conversion versus the number of input free radicals in a droplet (dotted: D=50 nm; solid: D=100 nm) (from [170])

increased interfacial tension. Actually, the interfacial tension used in the simulations was cited from Landfester's work on miniemulsions [313]. Another controversy is about the view of the nucleation process in controlled free radical miniemulsion polymerization. In Luo's work [312], it was found that superswelling happens only in the presence of a small fraction of particles with rather high conversion (10%); the majority of droplets have zero conversion. It is difficult to understand what would lead to such scenarios. However, Luo's simulations [179] showed that the nucleation process of RAFT miniemulsion polymerization could be very different to that of regular miniemulsion polymerization. As shown in Fig. 22, the simulations suggest that, by introducing a highly reactive RAFT agent, a large number of free radicals (N_c) need to be captured by a droplet before rapid polymerization in the droplet can take place, which is totally different from the situation in regular miniemulsion polymerization. More interestingly, it was found that droplet size had a significant influence on N_c. In Fig. 23, droplets larger than 150 nm (about 8.24% of all droplets) have been nucleated. Interestingly, monomer conversion for droplets less than 130 nm in size (unnucleated) is less than 2.5%, while conversion for droplets larger than 150 nm in size (nucleated particles) is much higher, depending the radical flux. The nucleation process for ATRP or SFRP in miniemulsion has not been reported yet, though it is very important. However, Charleux [215] has theoretically studied the segregation effect of the emulsion for SFRP. The results showed that segregation is only effective for particles far smaller than 130 nm (for example 50 nm). The polymerization rate in miniemulsion, in most cases, is similar to that in homogeneous polymerization because the droplet size miniemulsion polymerization usually is around 100 nm. However, in reality, droplet size is polydispersed, so we cannot exclude the existence of very small droplets, where the segregation is effective. In such a case, it is possible that a minor fraction of the very small particles has a much higher polymerization rate than the majority of particles with larger particle

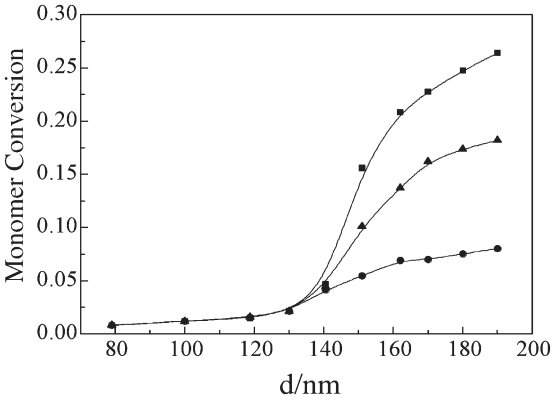

Fig. 23 The monomer conversion in particles with different initial droplet sizes at various average free radical fluxes (average of ten runs, in s^{-1}). Filled squares: 0.02; filled triangles: 0.05; filled circles: 0.1 (from [107])

sizes where segregation is not effective. The same argument is suitable for ATRP in miniemulsion. Additionally, it is well-known that it takes some time for SFRP and ATRP to set up the propagation/dormant equilibrium. It is likely that the time required to build up the equilibrium is droplet-size dependent. In such cases, the scenarios above might also occur. In fact, it has been reported that the reverse ATRP in miniemulsion has a higher colloidal stability than the direct ATRP in miniemulsion [264].

The above argument suggests that the initial droplet size distribution may play an important role in super-swelling or colloidal instability. This indicates that one should monitor the emulsification procedure for controlled free radical emulsion polymerization closely.

4.5 Other Applications and Future Directions

Recently, many new reactions have been carried out in miniemulsions. Most of these are polymerizations, but a number of nonpolymerization reactions have been proposed. This section will survey these applications, and close with some speculation on the future of miniemulsions.

4.5.1 Anionic/Cationic Polymerization in Miniemulsions

Maitre et al. [314] carried out anionic polymerization of phenyl glycidyl ether (PGE) in miniemulsion using didodecyldimethylamonium hydroxide as an *inisurf* (combination initiator and surfactant). Long chain alcohols were used as the costabilizer and stable miniemulsions were created by sonication. Monomer conversion was low, as was the degree of polymerization, which only

reached eight. The degree of polymerization was dependent on the initiator concentration, the type of alcohol, and its concentration. Comparison with bulk polymerization suggests that polymerization takes place near the droplet surface, since no high molecular weight material (expected from bulk polymerization in the droplet core) is formed. The authors postulate that initiation and propagation take place near the droplet-water interface, initiated by the inisurf. Termination with water takes place after a few propagations. However, the oligomers formed would be surface active and are thought to adsorb at the interface and increase the solubility of PGE in the locus of interfacial polymerization, enhancing subsequent propagation reactions. One might conjecture that with a hydrophobic initiator, polymerization in the droplet core might be encouraged, resulting in higher degrees of polymerization.

The same researchers [315, 316] reported the anionic ring opening polymerization of 1,3,5-tris(trifluoropropylmethyl)cyclotrisiloxane in miniemulsion using didodecyldimethylammonium bromide as the surfactant and sodium hydroxide as the initiator. Molecular weights were 2000–30,000. A two state mechanism was put forward, consisting of anionic kinetically-controlled ring opening polymerization continuing to complete conversion, followed by condensation and backbiting reactions. The delay between the two stages was long enough to allow high polymer yield.

These same researchers [317] reported the anionic polymerization of *n*-butyl cyanoacrylate in macroemulsion and miniemulsion. Dodecylbenzenesulfonic acid (DBSA) was used as the surfactant. The DBSA slows the rate of interfacial anionic polymerization through reversible termination, preventing an undesirably high degree of polymerization. Polymerization in macroemulsion resulted in a much higher degree of polymerization, perhaps due to droplet polymerization where the interface is less significant.

This same research group also reported [318] the cationic polymerization of *p*-methoxystyrene in miniemulsion. DBSA was used as both a protonic initiator and surfactant. A monomer conversion of 100% was achieved in eight hours at 60 °C. Molecular weights were low (approximately 1,000) and solids of up to 40% could be achieved with good colloidal stability. Polymerization takes place at the interface, initiated by the proton, and terminated by water. Molecular weight increased with conversion, suggesting either reversible termination or decreasing termination.

While all of these results are far from providing commercial products, they highlight the possibilities for alternative polymerization chemistries in miniemulsions.

4.5.2 Polycondensation in Miniemulsions

Barrère and Landfester [319] reported the synthesis of polyester in miniemulsions. Hydrophobic polyesters were synthesized in miniemulsion. DBSA was used as a *catsurf* (catalyst and surfactant) and HD was used as the co-

stabilizer. The pH was kept below 4 in order to prevent deprotonation of the acid monomers. Molecular weights of approximately 1000–2000 were found, with yields generally 70–80%. Both molecular weights and yields varied with monomer choice. Most interestingly, the presence of the particle-water interface did not change the polymerization-depolymerization equilibrium; the yield was the same in 100 nm particles as in very large droplets. However, the water concentration within the particle was found to be critical. Highly hydrophobic monomers reduced the monomer concentration in the particles, pushing the equilibriums toward esterification, and increasing yield. Alcohols bearing electron-donating groups were found to displace the equilibrium toward ester formation. They also report the formation of polyester-polystyrene hybrid particles using a one-pot procedure. In a separate paper [319] the same authors report one-pot polymerizations of polyurethane/acrylic hybrids. The procedures for both the polyester/polystyrene and the polyurethane/polyacrylate polymerizations were similar. First, the entire system was miniemulsified; then the polycondensation took place. After the polycondensation, a free radical initiator was added and the addition monomers were polymerized. Two molecular weight peaks were found for the polyurethane/polyacrylate system, a low one for the polyurethane, and a much higher MW peak for the polyacrylate. Hydroxybutyl acrylate, when added, was found to be a crosslinking agent, since it can undergo polycondensation and polyaddition.

4.5.3 Other Polymerizations in Miniemulsions

Extremely hydrophobic monomers do not polymerize well via macroemulsion polymerization due to their very low rates of monomer transport across the aqueous phase. Obviously, these monomers can be polymerized much more effectively in a miniemulsion system. One example of this is provided by Landfester et al. [320]. In this paper, fluoroalkyl acrylates are polymerized in a miniemulsion with low levels of a protonated surfactant. When fluorinated monomers were copolymerized with standard hydrophobic and hydrophilic monomers, either core-shell structures or statistical copolymers were formed.

A similar situation occurs with vinyl chloride (VC) for a very different reason. Vinyl chloride is very soluble in water, but polyvinyl chloride (PVC) is not soluble in its own monomer. VC does swell PVC, and for that reason, there is a driving force for VC transport across the aqueous phase in macroemulsion polymerization. This transport is aided by the fact that VS is very soluble in water. However, this is one macroemulsion system that might greatly benefit from the miniemulsion synthesis route.

Willert and Landfester [321] have polymerized amphiphilic copolymers from miniemulsion systems. The hydrophobic monomer was miniemulsified, while the hydrophilic monomer resides in the continuous phase. Polymerization was found to take place in the droplet phase, at the interface, or in the continuous phase; the quality of the product depended strongly on the primary

locus of polymerization. Inverse miniemulsions (oil as the continuous phase, with water-soluble monomer dissolved in water droplets) was also used.

Marie et al. [322] have reported the synthesis of polyaniline particles via inverse and direct miniemulsion. Inverse miniemulsions of anilinium hydrochloride were oxidized by hydrogen peroxide, resulting in highly crystalline polyaniline. Oxidation of aniline miniemulsions in water also leads to highly crystalline polyaniline. The same research group reports the use of chitosan as a surfactant for miniemulsions [338], resulting in latex particles with functional biopolymer surfaces for grafting in biological applications. Taden et al. [324] report the enzymatic polymerization of lactone to form biodegradable nanoparticles.

Claverie et al. [325] have polymerized norbornene via ROMP using a conventional emulsion polymerization route. In this case the catalyst was water-soluble. Particle nucleation was found to be primarily via homogenous nucleation, and each particle in the final latex was made up of an agglomeration of smaller particles. This is probably due to the fact that, unlike in free radical polymerization with water-soluble initiators, the catalyst never entered the polymer particle. Homogeneous nucleation can lead to a less controllable process than droplet nucleation (miniemulsion polymerization). This system would not work for less strained monomers, and so, in order to use a more active (and strongly hydrophobic) catalyst, Claverie employed a modified miniemulsion process. The hydrophobic catalyst was dissolved in toluene, and subsequently, a miniemulsion was created. Monomer was added to swell the toluene droplets. Reaction rates and monomer conversion were low, presumably because of the proximity of the catalyst to the aqueous phase due to the small droplet size.

4.5.4 Other Miniemulsion Applications

The miniemulsification technique can also be applied to nonpolymerization systems. The number of nonpolymerization applications of miniemulsions is small, but seems to be growing. Landfester [326] has reviewed the generation of nanoparticles in miniemulsions. Revelino et al. [327] has studied crystallization from direct and inverse miniemulsions. It was found that, since each droplet must be nucleated separately, the undercooling necessary to effect crystallization increases dramatically. The crystallization rate was higher in miniemulsions and proportional to droplet size. Taden et al. [328] studied the crystallization of polyethylene oxide from miniemulsions. Crystallization only occurred at large supercooling. Drying of the crystallized dispersion resulted in a highly ordered arrangement of polyethylene oxide platelets. Montenegro et al. [329] studied crystallization of alkanes from miniemulsions. Wegner et al. [330] have used polymeric nanospheres produced via miniemulsion polymerization to control nucleation and growth of inorganic crystals from aqueous media.

Vaihinger et al. [331] have molecularly imprinted polymer nanospheres as synthetic affinity receptors via miniemulsion techniques. Landfester et al. [332] have created semiconducting polymer nanospheres in aqueous dispersions via the synthetic miniemulsion technique. That is, conducting polymers were dissolved in solvent and then miniemulsified. Films produced by spin coating retained the nanosphere character until they were annealed above the glass transition temperature. In similar work, Piok et al. [333–335] formed organic light-emitting devices fabricated from semiconducting nanospheres created by the miniemulsification process. Willert et al. [336] created inorganic and metallic nanoparticles by the miniemulsification of molten salts and metals. Zu Putlitz et al. [337] created "armored latexes" and hollow inorganic shells made of clay sheets by templating cationic miniemulsions and latexes.

4.5.5 Future Directions

It would seem that miniemulsions have finally moved from being a laboratory curiosity to being a viable commercial process and a useful synthetic technique for producing interesting materials with nano-scale structure. It would appear that polymer-polymer hybrids and polymer-inorganic hybrids achieved via miniemulsion polymerization will result in new classes of water-borne materials. Other, traditionally solvent-based, polymerization chemistries may soon be carried out routinely via the miniemulsion route due to improvements in polymerization catalysts. The use of miniemulsions in ROMP has been cited above. Metallocene polymerization of ethylenic monomers has been carried out in macroemulsion. A short review and discussion of this work is given in [338]. If these water-tolerant polymerization chemistries are successful, it cannot be long before they are ported into miniemulsions. Controlled radical polymerization, particularly using RAFT chemistry, is a natural application for miniemulsion technology. Perhaps most importantly, miniemulsion techniques will be used in a variety of nonpolymerization technologies to produce nano-scale, highly structured materials.

References

1. Asua JM (2002) Prog Polym Sci 27:1283
2. Guyot A (2001) Curr Trends Polym Sci 6:47
3. Antonietti M, Landfester K (2002) Prog Polym Sci 27:689
4. Trommsdorf E, Schlidknecht E (1956) Suspension polymerization in polymer processes. Interscience, New York
5. Ugelstad J, El-Aasser MS, Vanderhoff JW (1973) J Polym Sci Pol Lett 11:503
6. Gardon JL (1970) Brit Polym J 2:1
7. Poehlein GW (1982) In: Piirma I (ed) Emulsion polymerization. Academic, New York, p 357
8. Poehlein GW (1985) ACS Sym Ser 285:131–150

9. Poehlein GW, Dougherty DJ (1976) Rubber chemistry and technology 50:601
10. Song Z (1988) PhD Thesis, Georgia Institute of Technology, Atlanta, GA
11. Ugelstad J, Hansen FK (1976) Rubber Chem Technol 49:536
12. Harkins WD (1947) J Am Chem Soc 69:1428
13. Smith WV, Ewart RH (1948) J Chem Physics 16:592
14. Alexander AE, Napper DH (1971) Prog Polym Sci 3:145
15. Blackley DC (1982) Emulsion polymerization. Academic, New York
16. Baxendale JH, Bywater S, Evans MG (1946) T Faraday Soc 42:675
17. Baxendale JH, Evans MG, Kilham JK (1946) T Faraday Soc 42:668
18. Priest WJ (1952) Phys Chem J 56:1077
19. Roe CP (1968) Ind Eng Chem 60:20
20. Fitch RM, Tsai CH (1971) In: Fitch RM (ed) Polymer colloids. Plenum, New York, p 73
21. Fitch RM, Tsai CH (1971) In: Fitch RM (ed) Polymer colloids. Plenum, New York, p 103
22. Fitch RM (1973) Brit Polym J 5:467
23. Lichti G, Gilbert RG, Napper DH (1983) J Polym Sci Pol Chem 21:269
24. Feeney PJ, Napper DH, Gilbert RG (1984) Macromolecules 17:2520
25. Maxwell IA, Morrison BR, Napper DH, Gilbert RG (1991) Macromolecules 24:1629
26. Chamberlain BJ, Napper DH, Gilbert RG (1982) J Chem Soc Farad T I 78:591
27. Ugelstad J, Kaggerud KH, Hansen FK, Berge A (1979) Makromol Chem 180:737
28. Ugelstad J, Mfutakamba HR, Mork PC, Ellingsen, Berge A, Schmidt R, Holm L, Jorgedel A, Hansen FK, Nustad K (1985) J Polym Sci Pol Sym 72:225
29. Hansen FK, Ofstad EB, Ugelstad J (1976) Theory and practice of emulsion technology. Academic, New York
30. Ugelstad J, Flagstad H, Hansen FK, Ellingsen T (1973) J Polym Sci 42:473
31. Hansen FK, Ugelstad J (1979) J Polym Sci 17:3047
32. Morton M, Kaizermann S, Altier MW (1954) J Colloid Interf Sci 9:300
33. Beuermann S, Buback M (2002) Prog Polym Sci 27:191
34. Sundberg DC, Hsieh JY, Soh SK, Baldus RF (1982) ACS Sym Ser 165:327
35. Buback M, Garcia-Rubio LH, Gilbert RG, Napper DH, Gulliot J, Hamielec AE, Hill D, O'Driscoll KF, Olaj OF, Shen J, Solomon D, Moad G, Stickler M, Tirrell M, Winnick MA (1988) J Polym Sci Pol Phys 26:293
36. Barnette DT, Schork FJ (1987) Chem Eng Prog 83:25
37. Fris N, Hamielec AE (1973) J Polym Sci Pol Chem 11 3321
38. Rawlings JB, Ray WH (1988) Polym Eng Sci 28:257
39. Ballard MJ, Gilbert RG, Napper DH, Pomery PJ, O'Sullivan PW, O'Donnell JH (1986) Macromolecules 19:1303
40. Soh SK, Sundberg DC (1982) J Polym Sci Pol Chem 20:1331
41. Ostwald WZ (1901) Z F Phys Chem 37:495
42. Fontenot K, Schork FJ (1993) Ind Eng Res 32:373
43. Chern CS, Chen TJ (1998) Colloids Surface A 138:65
44. Flory PJ (1953) Principles of polymer chemistry. Cornell Univ Press, Ithaca, NY
45. Ugelstad J, Mork PC, Kaggerud KH, Ellingsen T, Berge A (1980) Adv Colloid Interfac 13:101
46. Jansson LH, Wellons MC, Poehlein GW (1983) J Polym Sci Pol Lett 21:937
47. Higuchi WI, Misra J (1962) J Pharm Sci 51:459
48. Ugelstad J (1978) Makromol Chem 179:815
49. Fontenot K (1991) PhD Thesis, Georgia Institute of Technology, Atlanta, GA
50. Azad ARM, Fitch RM (1980) In: Polymer colloids II. Plenum, New York, p 95

51. El-Aasser MS, Lack CD, Choi YT, Min TI, Vanderhoff JW, Fowkes FM (1984) Colloids Surface 12:79
52. Ugelstad J, Kaggerud KH, Fitch RM (1980) In: Fitch RM (ed) Polymer colloids II. Plenum, New York, p 83
53. Choi YT, El-Aasser MS, Sudol ED, Vanderhoff JW (1985) J Polym Sci Pol Chem 23: 2973
54. Chamberlain BJ, Napper DH, Gilbert RG (1982) J Chem Soc Farad T 1 78:591
55. Chen CM, Gothjelpsen L, Schork FJ (1986) Polym Proc Eng 4:1
56. Delgado J, El-Aasser MS, Silebi CA, Vanderhoff JW (1986) Polym Mat Sci Eng 54:444
57. Rodriguez VS, Delgado J, Silebi CA, El-Aasser MS (1988) Polym Mat Sci Eng 58:761
58. Delgado J, El-Aasser MS, Vanderhoff JW (1986) J Polym Sci Pol Chem 24:861
59. Asua JM, Rodriguez VS, Silebi CA, El-Aasser MS (1990) Makromol Chem M Symp 35–36:59
60. Rodriguez VS, Delgado J, Silebi CA, El-Aasser MS (1989) Ind Eng Chem Res 28:65
61. Rodriguez VS, Asua JM, El-Aasser MS, Silebi CA (1991) J Polym Sci Pol Physics 29:483
62. Fontenot K, Schork FJ (1992) Polym Reaction Engineering 1:75
63. Fontenot K, Schork FJ (1993) Polym React Eng 1:289
64. Samer CJ, Schork FJ (1997) Polym React Eng 5:85
65. Ma JW, Cunningham MF, McAuley KB, Keoshkerian B, Georges MK (2003) Macromol Theor Simul 12:72
66. Ma JW, Cunningham MF, McAuley KB, Keoshkerian B, Georges M (2003) Chem Eng Sci 58:1177
67. Ma JW, Smith JA, McAuley KB, Cunningham MF, Keoshkerian B, Georges MK (2003) Chem Eng Sci 58:1163
68. Ma JW, Cunningham MF, McAuley KB, Keoshkerian B, Georges MK (2002) Macromol Theor Simul 11:953
69. Samer CJ, Schork FJ (1999) Ind Eng Res 38:1801
70. Landfester K, Bechthold N, Tiarks F, Antonietti M (1999) Macromolecules 32:2679
71. Bechthold N, Tiarks F, Willert M, Landfester K, Antonietti M (2000) Macromol Symp 151:549
72. Bradley M, Grieser F (2002) J Colloid Interf Sci 251:1
73. Wang S, Schork FJ (1994) J Appl Polym Sci 54:2157
74. Chern CS, Chen TJ (1997) Colloid Polym Sci 275:1060
75. Chern CS, Liou YC (1999) Polymer 40:3763
76. Wu XQ, Schork FJ (2001) J Appl Polym Sci 81:1691
77. Graillat C, Guyot A (2003) Macromolecules 36:6371
78. Boisson F, Uzulina I, Guyot A (2001) Macromol Rapid Comm 22:1135
79. Lack CD, El-Aasser MS, Vanderhoff JW, Fowkes FM (1985) ACS Sym Ser 272:345
80. Azad ARM, Ugelstad J, Hansen FK (1976) ACS Sym Ser 24:1
81. Hawkett BS, Napper DH, Gilbert RG (1980) J Chem Soc Farad T I 76:1323
82. Hallworth GW, Carless JE (1974) Theory and practice of emulsion technology. Academic, New York, p 305
83. Choi YT, El-Asser MS, Sudol ED, Vanderhoff JW (1985) J Appl Polym Sci 23:2973
84. Choi YT (1986) PhD Thesis, Lehigh University, Bethlehem, PA
85. Friberg SE, Neogi P (1986) Disp Sci Tech J 7:50
86. Kislalioglu S, Friberg S (1976) Theory and practice of emulsion technology. Academic, New York, p 257
87. Lack CD, El-Aasser MS, Silebi CA, Vanderhoff JW, Fowkes FM (1987) Langmuir 3:1155
88. Shah DO, Schechter RS (1977) Improved oil recovery by surfactant and polymer flooding. Academic, New York

89. El-Aasser MS, Lack CD, Choi YT, Min TI, Vanderhoff JW, Fowkes FM (1984) Colloids Surface 12:79
90. Rodriguez VS (1988) PhD Thesis, Lehigh University, Bethlehem, PA
91. Delgado J, El-Aasser MS, Vanderhoff JW (1986) J Polym Sci Pol Chem 24:861
92. Reimers JL, Skelland AHP, Schork FJ (1995) Polym React Eng 3:235
93. Ugelstad J (1980) Adv Colloid Interfac 13:101
94. Reimers JL, Schork FJ (1996) J Appl Polym Sci 60:251
95. Reimers JL, Schork FJ (1996) J Appl Polym Sci 59:1833
96. Aizpurua I, Amalvy JI, Barandiaran MJ (2000) Colloids Surface A 166:59
97. Lelu S, Novat C, Graillat C, Guyot A, Bourgeat-Lami E (2003) Polym Int 52:542
98. Wang ST, Schork FJ, Poehlein GW, Gooch JW (1996) J Appl Polym Sci 60 2069
99. Wu XQ, Schork FJ, Gooch JW (1999) J Polym Sci Pol Chem 37:4159
100. Tsavalas JG, Gooch JW, Schork FJ (2000) J Appl Polym Sci 75:916
101. Dong H, Gooch JW, Schork FJ (2000) J Appl Polym Sci 76:105
102. Reimers JL, Schork FJ (1996) Polym React Eng 4:135
103. Chern C-S, Sheu J-C (2000) J Polym Sci Pol Chem 38:3188
104. Samer CJ, Schork FJ (1999) Ind Eng Res 38:1792
105. Mouron D, Reimers J, Schork FJ (1996) J Polym Sci Pol Chem 34:1073
106. Wang S, Poehlein GW, Schork FJ (1997) J Polym Sci Pol Chem 35:595
107. Reimers JL, Schork FJ (1997) Ind Eng Resh 36:1085
108. Asua J, Alduncin J, Forcada J (1994) Macromolecules 27:2256
109. Miller CM, Blythe PJ, Sudol ED, Silebi CA, El-Aasser MS (1994) J Polym Sci Pol Chem 32:2365
110. Miller CM, Sudol ED, Silebi CA, El-Aasser MS (1995) Macromolecules 28:2754
111. Miller CM, Sudol ED, Silebi CA, El-Aasser MS (1995) Macromolecules 28:2765
112. Miller CM, Sudol ED, Silebi CA, El-Aasser MS (1995) Macromolecules 28:2772
113. Blythe PJ, Morrison BR, Mathauer KA, Sudol ED, El-Aasser MS (1999) Macromolecules 32:6944
114. Blythe PJ, Klein A, Sudol ED, El-Aasser MS (1999) Macromolecules 32:6952
115. Blythe PJ, Klein A, Sudol ED, El-Aasser MS (1999) Macromolecules 32:4225
116. Blythe PJ, Morrison BR, Mathauer KA, Sudol ED, El-Aasser MS (2000) Langmuir 16:898
117. Ghazaly HM, Daniels ES, Dimonie VL, Klein A, El-Aasser MS (2001) J Appl Polym Sci 81:1721
118. Luo Y, Schork FJ (2002) J Polym Sci Pol Chem 40:3200
119. Alduncin JA, Asua JM (1994) Polymer 35:3758
120. Blythe PJ, Klein A, Phillips JA, Sudol ED, El-Aasser MS (1999) J Polym Sci Pol Chem 37:4449
121. Gilbert RG (1995) Emulsion polymerization: A mechanistic approach. Academic, London
122. Kabalnov AS, Pertzov AV, Shchukin ED (1987) J Colloid Interf Sci 118:590
123. Candau F, Pabon M, Anquetil J-Y (1999) Colloid Surface A 153:47
124. Sood A, Awasthi KJ (2003) Appl Polym Sci 88:3058
125. Erdem B, Sully Y, Sudol ED, Dimonie VL, El-Aasser MS (2000) Langmuir 16:4890
126. Landfester K, Bechthold N, Föster S, Antonietti M (1999) Macromol Rapid Comm 20:81
127. Landfester K, Bechthold N, Tiarks F, Antonietti M (2000) Macromolecules 32:5222
128. Luo Y, Tsavalas JG, Schork FJ (2001) Macromolecules 34:5501
129. Melis S, Kemmere M, Meuldijk J, Storti G, Morbidelli M (2000) Chem Eng Sci 55:3101
130. Leiza JR, Sudol ED, El-Aasser MS (1997) J Appl Polym Sci 64:1797
131. Tang PL, Sudol ED, Adams M, El-Aasser MS, Asua JM (1991) J Appl Polym Sci 42: 2019

132. Sajjadi S, Jahanzad F (2003) Euro Polym J 39:785
133. Durant YG (1999) Book of Abstracts 217th ACS National Meeting (PMSE-326), Anaheim, CA, 21–25 March 1999, American Chemical Society, Washington, DC
134. Ouzineb K, Graillat C, McKenna TF (2001) DECHEMA Monographien (7th Int Workshop on Polymer Reaction Eng), Hamburg, Germany, 8–10 October 2001, 137: 293
135. Barnette DT, Schork FJ (1989) Chem Eng Commun 80:113
136. Nomura M, Harada M (1981) ACS Sym Ser 165:121
137. Samer CJ, Schork FJ (1999) Ind Eng Res 38:1792
138. Aizpurua I, Barandiaran M (1999) Polymer 40:4105
139. Aizpurua I, Amalvy JI, de la Cal JC, Barandiaran MJ (2000) Polymer 42:1417
140. Fontenot K, Schork FJ (1993) J Appl Polym Sci 49:633
141. Odian G (1988) Principles of polymerization, 3rd edn. Wiley-Interscience, New York
142. Landfester K, Schork FJ, Kusuma VA (2003) CR Acad Sci 6(11–12):1337–1342
143. Landfester K, Bechthold N, Tiarks F, Antonietti M (1999) Macromolecules 32:5222
144. Reimers JL, Schork FJ (1996) J Appl Polym Sci 59:1833
145. Landfester K, Bechthold N, Tiarks F, Antonietti M (1999) Macromolecules 32:2679
146. Rodrigues JC, Schork FJ (1997) J Appl Polym Sci 66:317
147. Balic R (2000) PhD Thesis, University of Sydney, Sydney, Australia
148. Kitzmiller EL, Miller CM, Sudol ED, El-Aasser MS (1995) Macromol Symp 92:157
149. Mayo VF, Lewis FM (1944) J Am Chem Soc 66:1594
150. Schuller H (1986) In: Reichert K, Geisler W (eds) Polymer reaction engineering. Hüthig and Wepf, Heidelberg, Germany, p 137
151. Guillot J (1986) In: Reichert K, Geisler W (eds) Polymer reaction engineering. Hüthig and Wepf, Heidelberg, Germany, p 147
152. Wu XQ, Schork FJ (2000) Ind Eng Chem Res 39:2855
153. Delgado J, El-Aasser MS, Silebi CA, Vanderhoff JW (1987) Polym Mat Sci Eng 57:976
154. Delgado J, El-Aasser MS, Silebi CA, Vanderhoff JW, Guillot J (1987) In: El-Aasser MS, Fitch RM (eds) NATO ASI Ser E: Appl Sci 138:79
155. Delgado J, El-Aasser MS, Silebi CA, Vanderhoff JW (1988) Makromol Chem M Symp 20/21:545
156. Delgado J, El-Aaser MS, Silebi CA, Vanderhoff JW (1989) J Polym Sci Pol Chem 27:193
157. Delgado J, El-Aasser MS, Silebi CA, Vanderhoff JW (1990) J Polym Sci Pol Chem 28:777
158. Unzue MJ, Asua JM (1993) J Appl Polym Sci 49:81
159. Wu XQ, Hong XM, Schork FJ (2002) J Appl Polym Sci 85:2219
160. Caruso F, Caruso RA, Mohwald H (1998) Science 282:1111
161. Caruso F (2001) Adv Mater 13:11
162. Numo-Donlunas S, Rhoton AI, Corona-Galvan S, Puig JE, Kaler JE (1993) Polym Bull 30:207
163. Antonova LF, Leplyanin GV, Zayev YY, Rafikov SR (1978) Polym Sci USSR 20:778
164. Turner SR, Weiss RA, Lundberg RD (1985) J Polym Sci Pol Chem 37:535
165. Kim JH, Chainey M, El Aasser MS, Vanderhoff JW (1992) J Polym Sci Pol Chem 30:535
166. Emelie B, Pichot D, Guillot J (1988) Makromol Chem 189:1879
167. Shoaf GL, Poehlein GW (1992) Polym React Eng 9:1
168. Charmot D, D'Allest JF, Dobler F (1996) Polymer 37:5237
169. Ganachaud F, Sauzedde F, Elaissari A, Pichot C (1997) J Appl Polym Sci 65:2315
170. Luo YW, Schork FJ (2001) J Polym Sci Pol Chem 39:2696
171. Kim JH, Chainey M, El Aasser MS, Vanderhoff JW (1990) J Polym Sci Pol Chem 28:3188

172. Gilbert RG, Anstey JF, Subramaniam N, Monteiro MJ (1999) ACS Polym Prepr Div Polym Chem 40:102
173. Blackley DC (1975) Emulsion polymerization. Wiley, New York, p 244
174. Dong H, Gooch JW, Poehlein GW, Wang ST, Wu X, Schork FJ (2001) ACS Sym Ser 766:8–17
175. Nabuurs T, Baijards RA, German AL (1996) Prog Org Coat 27:163
176. Van Hamersveld EMS, van Es GS, Cuperus FP (1999) Colloids Surface A 153:285
177. Van Hamersveld EMS, Van Es GS, German AL, Cuperus FP, Weissenborn P, Hellgren AC (1999) Prog Org Coat 35:235
178. Tsavalas JG, Luo Y, Hudda L, Schork FJ (2003) Polym React Eng 11:277
179. Tsavalas JG, Luo Y, Schork FJ (2003) J Appl Polym Sci 87:1825
180. Tsavalas JG, Schork FJ, Landfester K (2003) J Coating Technol (in press)
181. Shoaf GL, Stockl RR (2003) Polym React Eng 11:319
182. Li, Daniels ES, Dimonie VL, Sudol ED, El-Aasser MS (2001) Polym Mat Sci Eng 85:258
183. Wang C, Chu F, Graillat C, Guyot A (2003) Polym React Eng 11:541
184. Barrere M, Landfester K (2003) Macromolecules 36:5119
185. El-Aasser MS, Li M, Jeong P, Daniels ES, Dimonie VL, Sudol ED (2001) DECHEMA Monographien (7th Int Workshop on Polymer Reaction Engineering), Hamburg, Germany, 8–10 October 2001, 137:1
186. Jeong P, Dimonie VL, Daniels ES, El-Aasser MS (2002) ACS Sym Ser 801:357
187. Kawahara H, Goto T, Okamoto Y, Kage H, Ogura H, Matsuno Y (2002) Kagaku Kogaku Ronbun 28:175
188. Landfester K, Dimonie VL, El-Aasser MS (1998) DECHEMA Monographien 134 (6th Int Workshop on Polymer Reaction Engineering 1998), Berlin, 5–7 October 1998, 134:469
189. Roberts JE, Marcu I, Dimonie V, Daniels E, El-Aasser MS (2003) ACS Polym Prepr Div Polym Chem 44:277
190. Marcu I, Daniels ES, Dimonie VL, Hagiopol C, Roberts JE, El-Aasser MS (2003) Macromolecules 36:328
191. El-Aasser MS, Vanderhoff JW, Poehlein GW (1977) Coating Plastic Prepr 37:92
192. El-Aasser MS, Hoffman JD, Manson JA, Vanderhoff JW (1980) Org Coating Plast Chem 43:136
193. Vanderhoff JW, El-Aasser MS, Hoffman JD (1978) US Patent 4070323
194. Noh MH, Jang LW, Lee DC (1999) J Appl Polym Sci 74:179
195. Noh MH, Lee DC (1999) J Appl Polym Sci 74:2811
196. Garcés JM, Moll DJ, Bicerano J, Fibinger R, McLeod DG (2000) Adv Mater 12:1835
197. Van Herk AM, German AL (1999) Microsph Microcaps Lipos 1:457
198. Erdem B, Sudol ED, Dimonie VL, El-Aasser MS (2000) J Polym Sci Pol Chem 38:4419
199. Erdem B, Sudol ED, Dimonie VL, El-Aasser MS (2000) J Polym Sci Pol Chem 38:4431
200. Erdem B, Sudol ED, Dimonie VL, El-Aasser MS (2000) J Polym Sci Pol Chem 38:4441
201. Tiarks F, Landfester K, Antonietti M (2001) Langmuir 17:5775
202. Antonietti M, Landfester K (2002) Chem Ing Tech 74:543
203. Landfester K, Montenegro R, Scherf U, Guntner R, Asawapirom U, Patil S, Neher D, Kietzke T (2002) Adv Mater 14:651
204. Ramirez LP, Landfester K (2003) Macromol Chem Phys 204:22
205. Solomon DH, Rizzardo E, Cacioli P (1985) Eur Pat Appl EP 135280
206. Georges MK, Moffat KA, Veregin RPN, Kazmaier PM, Hamer GK (1993) Polym Mater Sci Eng 69:305
207. Fischer H (1997) Macromolecules 30:5666
208. Gridnev AA (1997) Macromolecules 30:7651

209. Moad G, Solomon DH (1995) The chemistry of free radical polymerization, 1st edn. Elsevier, Amsterdam
210. Fukuda T, Terauchi T, Goto A, Ohno K, Tsujii Y, Miyamoto T, Kobatake S, Yamada B (1996) Macromolecules 29:6393
211. Fukuda T (2002) Handbook of radical polymerization. Wiley, New York, Ch 9
212. Qiu J, Charleux B, Matyjaszewski K (2001) Prog Polym Sci 26:2083
213. Butte A, Storti G, Morbidelli M (1998) In: Reicher KH, Moritz HU (eds) 6th Int Workshop on Polymer Reaction Engineering. DECHEMA Monographien, Berlin, 5–7 October 1998, 134:497
214. Butte A, Storti G, Morbidelli M (2000) Macromolecules 33:3485
215. Charleux B (2000) Macromolecules 33:5358
216. Pan G, Sudol ED, Dimonie VL, El-Aasser MS (2002) Macromolecules 35:6915
217. Lansalot M, Farcet C, Charleux B, Vairon J-P, Pirri R, Tordo P (2000) ACS Sym Ser 768:138
218. Prodpan T, Dimonie VL, Sudol ED, El-Aasser M (1999) Polym Mater Sci Eng 80:534
219. MacLeod PJ, Keoshkerian B, Odell P, Georges MK (1999) Polym Mater Sci Eng 80:539
220. Lansalot M, Charleux B, Vairon J-P, Pirri R, Tordo P (1999) ACS Polym Prepr 40:317
221. Prodpan T, Dimonie VL, Sudol ED, El-Aasser M (2000) Macromol Symp 155:1
222. MacLeod PJ, Barber R, Odell P, Keoshkerian B, Georges MK (2000) Macromol Symp 155:31
223. Farcet C, Lansalot M, Charleux B, Pirri R, Vairon JP (2000) Macromolecules 33:8559
224. Pan G, Sudol ED, Dimonie VL, El-Aasser MS (2001) Macromolecules 34:481
225. Keoshkerian B, MacLeod PJ, Georges MK (2001) Macromolecules 34:3594
226. Farcet C, Charleux B, Pirri R (2001) Macromolecules 34:3823
227. Cunningham MF (2002) Prog Polym Sci 27:1039
228. Tortosa K, Smith JA, Cunningham MF (2001) Macromol Rapid Comm 22:957
229. Farcet C, Belleney J, Charleux B, Pirri R (2002) Macromolecules 35:4912
230. Farcet C, Charleux B, Pirri R (2002) Macromol Symp 182:249
231. Keoshkerian B, Szkurham AR, Georges MK (2001) Macromolecules 34:6531
232. Cunningham MF, Tortosa K, Lin M, Keoshkerian B, Georges MK (2002) J Polym Sci Pol Chem 40:2828
233. Cunningham MF, Xie M, McAuley KB, Keoshkerian B, Georges MK (2002) Macromolecules 35:59
234. Ma JW, Cunningham MF, McAuley KB, Keoshkerian B, Georges MK (2002) Macromol Theor Simul 11:953
235. Ma JW, Cunningham MF, McAuley KB, Keoshkerian B, Georges MK (2003) Macromol Theor Simul 12:72
236. Matyjaszewski K, Wang J (1995) J Am Chem Soc 117:5614
237. Matyjaszewski K, Wang J (1995) Macromolecules 28:7901
238. Matyjaszewski K, Xia J, Patten T, Abernathy T (1996) Science 272:866
239. Sawamoto M, Kamigaito M, Higashimura T, Kato M (1995) Macromolecules 28:1721
240. Sawamoto M, Kamigaito M, Ando T, Kato M (1996) Macromolecules 29:1070
241. Sawamoto M, Kamigaito M, Kotani Y, Kato M (1996) Macromolecules 29:6979
242. Uegaki H, Kotani Y, Kamigato M, Sawamoto M (1998) Macromolecules 31:6756
243. Moineau G, Minet M, Dubois P, Teyssié P, Sennenger T, Jérôme R (1999) Macromolecules 32:27
244. Lecomte P, Drapier I, Dubois P, Teyssié P, Jérôme R (1997) Macromolecules 30:7631
245. Brandts JAM, van de Geijn P, van Faassen EE, Boersma J, van Koten G (1999) J Organomet Chem 584:246
246. Kotani Y, Kamigaito M, Sawamoto M (1999) Macromolecules 32:2420

247. Percec V, Barboiu B, Neumann A (1996) Macromolecules 29:3665
248. Patten TE, Matyjazsweski K (1998) Adv Mater 10:901
249. Matyjaszewski K (1999) Chem Eur J 5:3095
250. Pan CY, Lou XD (2000) Macromol Chem Phys 201:1115
251. Chen XP, Padias AB, Hall HK (2001) Macromolecules 34:3514
252. Matyjaszewski K, Wei M, Xia J, Gaynor S (1998) Macromol Chem Phys 199:2289
253. Hamasaki S, Kamigaito M, Sawamoto M (2002) Macromolecules 35:2934
254. Hamasaki S, Sawauchi C, Kamigaito M, Sawamoto M (2002) J Polym Sci Pol Chem 40:617
255. Fischer H (1999) J Polym Sci Pol Chem 37:1885
256. Sawamoto M, Kamigaito M (2000) Macromol Symp 161:11
257. Davis K, O'Malley J, Paik H, Matyjaszewski K (1997) ACS Polym Prepr 38:687
258. Matyjaszweski K, Xia J (2001) Chem Rev 101:2921
259. Takhashi H, Ando T, Kamigaito M, Sawamoto M (1999) Macromolecules 32:3820
260. Matyjaszewski K (1996) Macromol Symp 111:47
261. Butté A, Storti G, Morbidelli M (2001) Macromolecules 34:5885
262. Matyjaszewski K, Qiu J, Tsarevsky NV, Charleux B (2000) J Polym Sci Pol Chem 38: 4724
263. Zhang B, Zhang ZB, Xan XL, Hu CP, Ying SK (2002) Chinese J Polym Sci 20:445
264. Li M, Matyjaszewski K (2003) Macromolecules 36:6028
265. Chiefari J, Chong YK, Ercole F, Krstina J, Jeffery J, Le TPT, Mayadunne RTA, Meijs GF, Moad CL, Moad G, Rizzardo E, Thang SH (1998) Macromolecules 31:5559
266. Le TP, Moad G, Rizzardo E, Thang SH (1998) PCT Int Appl, p 88
267. Rizzardo E, Thang SH, Moad G (1999) PCT Int Appl, p 40
268. Krstina J, Moad G, Rizzardo E, Winzor CL, Berge CT, Fryd M (1995) Macromolecules 28:5381
269. Corpart P, Charmot D, Biadatti T, Zard S, Michelet D (1998) PCT Int Appl, p 70
270. Hawthorne DG, Moad G, Rizzardo E, Thang SH (1999) Macromolecules 32:5457
271. Chong YK, Le TPT, Moad G, Rizzardo E, Thang SH (1999) Macromolecules 32:2071
272. De Brouwer H, Schellekens MAJ, Klumperman B, Monteiro MJ, German A (2000) J Polym Sci Pol Chem 38:3596
273. Monteiro MJ, Sjoberg M, Van der Vlist J, Gottgens CM (2000) J Polym Sci Pol Chem 38:4206
274. Matyjaszewski K, Gaynor S, Wang JS (1995) Macromolecules 28:2093
275. Monteiro MJ, De Brouwer H (2001) Macromolecules 34:349
276. Kwak Y, Goto A, Tsujii Y, Murata Y, Komatsu K, Fukuda T (2002) Macromolecules 35:3026
277. Barner-Kowollik C, Quinn JF, Morsley DR, Davis TP (2001) J Polym Sci Pol Chem 39:1353
278. Barner-Kowollik C, Quinn JF, Nguyen TLU, Heuts JPA, Davis TP (2001) Macromolecules 34:7849
279. Barner-Kowollik C, Vana P, Quinn JF, Davis TPJ (2002) J Polym Sci Pol Chem 40:1058
280. Barner-Kowollik C, Coote ML, Davis TP, Radom L, Vana P (2003) J Polym Sci Pol Chem 41:2828
281. Wang AR, Zhu S, Kwak Y, Goto A, Fukuda T, Monteiro MJ (2003) J Polym Sci Pol Chem 41:2833
282. Jovanovic S, Romatowski J, Schulz GV (1965) Makromol Chem 85:187
283. Schulz GV, Romatowski J (1965) Makromol Chem 85:195
284. Romatowski J, Schulz GV (1965) Makromol Chem 85:227
285. Nomura M, Minamino Y, Fujita K, Harada M (1982) J Polym Sci Pol Chem 20:1261

286. Lichti G, Sangster DF, Whang BCY, Napper DH, Gilbert RG (1982) J Chem Soc Farad T 1 78:2129
287. Maxwell IA, Morrison BR, Napper DH, Gilbert RG (1992) Makromol Chem 193:303
288. Mendoza J, De La Cal JC, Asua JM (2000) J Polym Sci Pol Chem 38:4490
289. Monteiro MJ, Hodgson M, De Brouwer HJ (2000) Polym Sci Pol Chem 38:3864
290. de Brouwer H, Tsavalas JG, Schork FJ, Monteiro MJ (2000) Macromolecules 33:9239
291. Moad G, Chiefari J, Chong YK, Krstina J, Mayadunne RTA, Postma A, Rizzardo E, Thang SH (2000) Polym Int 49:993
292. Prescott SW, Ballard MJ, Rizzardo E, Gilbert RG (2002) Macromolecules 35:5417
293. Monteiro MJ, de Barbeyrac J (2001) Macromolecules 34:4416
294. Smulders WW, Gilbert RG, Monteiro MJ (2003) Macromolecules 36:4309
295. Smulders WW (2002) PhD Thesis, Technische Universiteit Eindhoven, The Netherlands
296. Tsavalas JG, Schork FJ, de Brouwer H, Monteiro MJ (2001) Macromolecules 34:3938
297. Vosloo JJ, De Wet-Roos D, Tonge MP, Sanderson RD (2002) Macromolecules 35:4894
298. Lansalot M, Davis TP, Heuts JPA (2002) Macromolecules 35:7582
299. Uzulina I, Kanagasbapathy S, Claverie J (2000) Macromol Symp 150:33
300. Monteiro MJ, Hodgson M, de Brouwer H (2000) J Polym Sci Pol Chem 38:3864
301. Bon SAF, Bosveld M, Klumperman B, German AL (1997) Macromolecules 30:324
302. Marestin C, Noel C, Claverie J (1998) Macromolecules 31:4041
303. Lansalot M, Farcet C, Charleux B, Vairon JP, Pirri R, Tordo O (2000) ACS Sym Ser 768:138
304. Jousset S, Qiu J, Matyjaszewski K, Granel C (2001) Macromolecules 34:6641
305. De Brouwer H, Tsavalas JG, Schork FJ, Monteiro MJ (2000) Macromolecules 33:9239
306. Prodpan T, Dimonie VL, Sudol ED, El-Aasser M (1999) Polym Mater Sci Eng 80:534
307. MacLeod PJ, Keoshkerian B, Odell P, Georges MK (1999) Polym Mater Sci Eng 80:539
308. Pan GF, Sudol ED, Dimonie VL, El-Aasser MS (2002) Macromolecules 35:6915
309. Matyjaszewski K, Qui J, Shipp DA, Gaynor SG (2000) Macromol Symp 155:15
310. Tonge MP, McLeary JB, Vosloo JJ, Sanderson RD (2003) Macromol Symp 193:289
311. Vosloo JJ, Roos DW, Tonge MP, Sanderson RD (2002) Macromolecules 35:4894
312. Ausa JM (2002) Prog Polym Sci 27:1283
313. Landfester K, Bechthold N, Tiarks F, Antonietti M (1999) Macromolecules 32:5222
314. Maitre C, Ganachaud F, Ferreira O, Lutz JF, Paintoux Y, Hemery P (2000) Macromolecules 33:7730
315. Barrere M, Maitre C, Dourges MA, Hemery P (2001) Macromolecules 34:7276
316. Barrere M, Ganachaud F, Bendejacq D, Dourges MA, Maitre C, Hemery P (2001) Polymer 42:7239
317. Limouzin C, Caviggia A, Ganachaud F, Hemery P (2003) Macromolecules 36:667
318. Cauvin S, Sadoun A, Santos R, Belleney J, Ganachaud F, Hemery P (2002) Macromolecules 35:7919
319. Barrere M, Landfester K (2003) Polymer 44:2833
320. Landfester K, Rothe R, Antonietti M (2002) Macromolecules 35:1658
321. Willert M, Landfester K (2002) Macromol Chem Phys 203:825
322. Marie E, Rothe R, Antonietti M, Landfester K (2003) Macromolecules 36:3967
323. Marie E, Landfester K, Antonietti M (2002) Biomacromolecules 3:475
324. Taden A, Antonietti M, Landfester K (2003) Macromol Rapid Comm 24:512
325. Claverie JP, Viala S, Maurel V, Novat C (2001) Macromolecules 34:382
326. Landfester K (2001) Adv Mater 13:765
327. Montenegro R, Antonietti M, Mastai Y, Landfester K (2003) J Phys Chem B 107:5088
328. Taden A, Landfester K (2003) Macromolecules 36:4037

329. Montenegro R, Landfester K (2003) Langmuir 19:5996
330. Wegner G, Baum P, Muller M, Norwig J, Landfester K (2001) Macromol Symp 175: 349
331. Vaihinger D, Landfester K, Krauter I, Brunner H, Tovar GEM (2002) Macromol Chem Phys 203:1965
332. Landfester K, Montenegro R, Scherf U, Guntner R, Asawapirom U, Patil S, Neher D, Kietzke T (2002) Adv Mater 14:651
333. Piok T, Wenzl FP, Gamerith S, Gadermaier C, Patil S, Montenegro R, Kietzke T, Neher D, Scherf U, Landfester K, List EJW (2003) Mater Res Soc Symp Proc 738:245
334. Piok T, Romaner L, Gadermaier C, Wenzl FP, Patil S, Montenegro R, Landfester K, Lanzani G, Cerullo G, Scherf U, List EJW (2003) Synthetic Met 139:609
335. Piok T, Gamerith S, Gadermaier C, Plank H, Wenzl FP, Patil S, Montenegro R, Kietzke T, Neher D, Scherf U, Landfester K, List EJW (2003) Adv Mater 15:800
336. Willert M, Rothe R, Landfester K, Antonietti M (2001) Chem Mater 13:4681
337. zu Putlitz B, Landfester K, Fischer H, Antonietti M (2001) Adv Mater 13:500
338. Manders B, Sciandrone L, Hauck G, Kristen M (2001) Angew Chem Int Edit 40:4006

Received: June 2004

Adv Polym Sci (2005) 175: 257–298
DOI 10.1007/b100117

Microemulsion Polymerizations and Reactions

Pei Yong Chow (✉)[1] · Leong Ming Gan[2]

[1] Institute of Bioengineering and Nanotechnology, 31 Biopolis Way, The Nanos, #04–01, 138669 Singapore
echow@ibn.a-star.edu.sg
[2] Institute of Materials Research & Engineering, 3 Research Link, 117602 Singapore
lm-gan@imre.a-star.edu.sg

Abstract This review describes how the unique nanostructures of water-in-oil (W/O), oil-in-water (O/W) and bicontinuous microemulsions have been used for the syntheses of some organic and inorganic nanomaterials. Polymer nanoparticles of diameter approximately 10–50 nm can easily be obtained, not only from the polymerization of monomers in all three types of microemulsions, but also from a Winsor I-like system. A Winsor I-like system with a semi-continuous process can be used to produce microlatexes with high weight ratios of polymer to surfactant (up to 25). On the other hand, to form inorganic nanoparticles, it is best to carry out the appropriate chemical reactions in W/O- and bicontinuous microemulsions.

Recent developments in the cross-polymerization of the organic components used in bicontinuous microemulsions ensure the successful formation of transparent nanostructured materials. Current research into using polymerizable bicontinuous microemulsions as a one-pot process for producing functional membranes and inorganic/polymer nanocomposites is highlighted with examples.

Keywords Microemulsion polymerization · Microemulsion reaction · Water-in-Oil (W/O) microemulsion · Oil-in-Water (O/W) microemulsion · Bicontinuous microemulsion · Functional membranes and inorganic/polymer nanocomposites

Abbreviations

AN	Acrylonitrile
AA	Acrylic acid
AM	Acrylamide
APTAC	2-acrylamido-2-propane trimethylammonium chloride
AUTMAB	(Acryloyloxy)-undecyltrimethylammonium bromide
AUDMAA	(Acryloyloxy)-undecyldimethylammonioacetate
AIBN	Azobisisobutyronitrile
AOT	1,4-Bis(2-ethylhexyl)sulfosuccinate sodium salt
APS	Ammonium persulfate
BL	γ-butyrolactone
BUA	Butylacrylate
C_1-PEO-C_{11}-MA-40	ω-methoxypoly(ethylene oxide)$_{40}$-undecyl-α-methacrylate
CTAB	Cetyltrimethylammonium bromide
DMC	Dimethyl carbonate
DTAB	Dodecyltrimethylammonium bromide
EGDMA	ethyleneglycol dimethacrylate
EC	Ethylene carbonate
HC	Hydrocarbon
HA	Hydroxyapetite
HEMA	2-hydroxylethylmethacrylate
MADQUAT	2-Methacryloyloxyethyltrimethyl ammonium chloride
MMA	Methyl methacrylate
NaA	Sodium acrylate
NaAMPS	Sodium-2-acrylamido-2–2-methylpropane sulfonate
NaSS	Sodium styrenesulfonate
NIPAM	*N*-isopropylacrylamide
NP	Poly(oxyethylated alkylphenyl ether)
OTAC	Octyldecyltrimethylammonium chloride
PC	Propylene carbonate
PMMA	Poly(methyl methacrylate)
PNIPAM	Poly(*N*-isopropylacrylamide)

PS	Poly(styrene)
SDS	sodium dodecyl sulfate
SEAAU	Sodium 11-(*N*-ethylacrylamido)-undecanoate
St	Styrene
TEM	Transmission electron microscope
THFM	Tetrahydrofurfuryl methacrylate
TTAB	Tetradecyltrimethylammonium bromide
VA	Vinyl acetate
VBSLi	4-Vinylbenzene sulfonate, lithium salt

1 Introduction

Microemulsions are transparent liquid systems consisting of at least ternary mixtures of oil, water and surfactant. Sometimes a cosurfactant is needed for the formation of a thermodynamically-stable microemulsion. A transparent microemulsion is, in fact, heterogeneous (nanostructured) on a molecular scale. Microemulsion domains fluctuate in size and shape and undergo spontaneous coalescence and break-up [1]. They can exhibit water continuous and bicontinuous structures, with typical equilibrium domain sizes ranging from about 10 to 100 nm [2]. The transparent microemulsions can be in the form of nano-globules of oil-swollen micelles dispersed in the water continuous phase as oil-in-water (O/W) microemulsions, or water-swollen micellar globules dispersed in oil as water-in-oil (W/O) microemulsions. In between the regions of O/W and W/O microemulsions, there may also exist a composition region of bicontinuous (sponge-like structure) microemulsions [3], whose oil and water domains are randomly dispersed in two phases, as can be seen from the sketched phase diagram of Fig. 1.

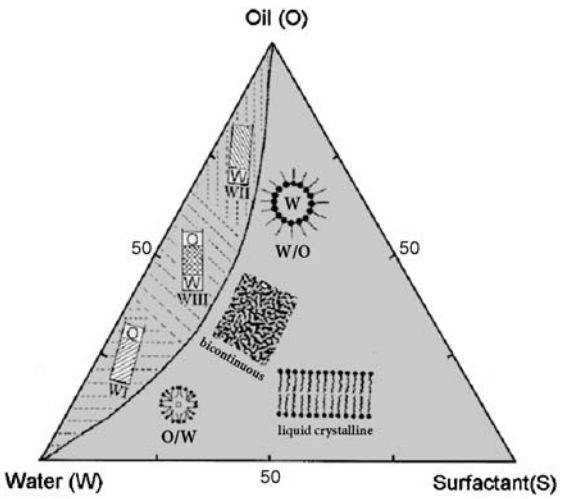

Fig. 1 Illustration of some phase equilibria encountered in multicomponent systems

In addition to single phase microemulsions, several phase equilibria known as Winsor systems [4] are also shown at low surfactant concentrations. A Winsor I (WI) system consists of an O/W microemulsion that is in equilibrium with an oil phase, while a Winsor II (WII) system is a W/O microemulsion in equilibrium with an aqueous phase. A WIII system has a middle phase (bicontinuous) microemulsion that coexists with both oil and aqueous phases.

When a single chain anionic surfactant (such as sodium dodecyl sulfate, SDS) is used, it generally requires a cosurfactant for the formation of a microemulsion. A cosurfactant may not be needed to form a microemulsion if nonionic surfactant(s), certain types of cationic surfactants, or double-chain surfactants such as sodium 1,4-bis(2-ethylhexyl)sulfosuccinate (Aerosol OT or simply AOT) are used.

Due to the enormous inner surfaces of the nanostructures of W/O and O/W globular microemulsions, they can provide novel reaction sites for some inorganic/organic reactions and polymerizations. Nano-sized particles of inorganic materials are generally prepared in W/O microemulsion, and microlatexes (d<50 nm) of polymers from both O/W- and W/O-microemulsion polymerizations. The recently developed approach of using polymerizable surfactants in bicontinuous microemulsions also enables the syntheses of transparent nanoporous polymeric materials and nanocomposites. Hence, microemulsions have been used as novel chemical nanoreactors for producing nanophase materials such as polymer latexes [5, 6], inorganic particles [7], and industrially useful materials [8]. This review relates the development of microemulsion polymerizations and reactions to the formation of nanostructured materials.

2
Polymerizations in Globular and Bicontinuous Microemulsions for Producing Microlatexes

Over the past two decades, free radical polymerization studies have mainly been carried out in globular microemulsions (both O/W microemulsions and W/O microemulsions, also known as inverse microemulsions). Each milliliter of the globular microemulsion usually contains 10^{15}–10^{17} W/O- or O/W nanosized (5–10 nm in diameter) droplets (globules). The enormous number of nano-globules are potential loci for fast polymerization, producing microlatex particles much less than 50 nm in diameter. Though small polymer particles, molecular weights exceeding one million can easily be obtained from these polymerization systems. Most of the microemulsion polymerization studies [5] have dealt with hydrophobic monomers, such as styrene (St) or methyl methacrylate (MMA), within oil cores of O/W microemulsions [9] and with the polymerization of water-soluble monomers, such as acrylamide (AM), within aqueous cores of inverse microemulsions [10, 11]. For both O/W and inverse microemulsion systems, the amount of monomer was usually restricted to less than 10 wt% with respect to the total weight of microemulsion. Moreover,

higher amounts of surfactant (5–15 wt%) were normally needed for the stability of the polymerization. For those microemulsions requiring a cosurfactant, the compatibility between the cosurfactant and the polymers formed becomes an issue. For instance, if styrene is polymerized within an O/W microemulsion that contains an alcohol cosurfactant, this alcohol will not dissolve polystyrene. However, this is not the case for the polymerization of acrylamide (AM) in alcohol-free inverse microemulsion.

2.1 Inverse Microemulsion Polymerization

The polymerization of a water-soluble monomer such as AM, acrylic acid (AA), sodium acrylate (NaA), or 2-hydroxyethylmethacrylate (HEMA), can be carried out easily in inverse microemulsion or/and bicontinuous microemulsion. These water-soluble monomers also act as cosurfactants, increasing the flexibility and the fluidity of the interfaces, which enhances the solubilization of the monomer. A cosurfactant effect during the polymerization of vinyl acetate in anionic microemulsions has also been reported [12].

Candau and co-workers were the first to address the issue of particle nucleation for the polymerization of AM [13, 14] in an inverse microemulsion stabilized by AOT. They found that the particle size of the final microlatex (d~20–40 nm) was much larger than that of the initial monomer-swollen droplets (d~5–10 nm). Moreover, each latex particle formed contained only one polymer chain on average. It is believed that nucleation of the polymer particle occurs for only a small fraction of the final nucleated droplets. The non-nucleated droplets also serve as monomer for the growing particles either by diffusion through the continuous phase and/or by collisions between droplets. But the enormous number of non-nucleated droplets means that some of the primary free radicals continuously generated in the system will still be captured by non-nucleated droplets. This means that polymer particle nucleation is a continuous process [14]. Consequently, each latex particle receives only one free radical, resulting in the formation of only one polymer chain. This is in contrast to the large number of polymer chains formed in each latex particle in conventional emulsion polymerization, which needs a much smaller amount of surfactant compared to microemulsion polymerization.

The polymerization of acrylamide (AM) and the copolymerization of acrylamide-sodium acrylate in inverse microemulsions have been studied extensively by Candau [10, 11, 13–15], Barton [16, 17], and Capek [18–20]. One of the major uses for these inverse microlatexes is in enhanced oil recovery processes [21]. Water-soluble polymers for high molecular weights are also used as flocculants in water treatments, as thickeners in paints, and retention aids in papermaking.

2.2 Bicontinuous Microemulsion Polymerization

The polymerization of AM in inverse microemulsions originally required a high weight ratio of surfactant/monomer. This high ratio was subsequently drastically reduced by polymerizing water-soluble monomers in nonionic bicontinuous microemulsions [10, 22]. Besides AM, other water-soluble monomers investigated were sodium acrylate [23], sodium 2-acrylamido-2–2-methylpropane sulfonate [24] (NaAMPS, CH_2=CHCONHC$(CH_3)_2CH_2SO_3Na$) and 2-methacryloyloxyethyltrimethylammonium chloride [25] (MADQUAT, CH_2=C(CH_3)COO$CH_2CH_2H(CH_3)_3Cl$). This type of polymerization has been extended to syntheses of copolymers that possess both positively and negatively charged moieties along the macromolecular backbone (polyampholytes). High charge density polyampholytes can be formed from the microemulsion copolymerization [25] of NaAMPS and MADQUAT. Polymerization of water-soluble monomers in bicontinuous microemulsions produced transparent microlatexes [26] with particle sizes (50–100 nm) that remain unchanged for years.

Microemulsion formulation was further optimized by Candau [27] using cohesive energy ratio (CER) and hydrophile-lipophile balance (HLB) concepts. The best formulation was obtained for high HLB values (8–11) using a blend of nonionic surfactants. This favors microemulsions with bicontinuous structures in the presence of AM and NaAMPS or AM and NaA. The process yielded clear, stable microlatexes of moderate particle size (d<100 nm) for high molecular weight copolymers up to 25 wt% solids. High-solid content (~30 wt%) of water-soluble poly(vinyl acetate) latexes [28] could also be obtained by the multi-stage addition of monomer to a latex pre-produced by the polymerization of 3 wt% vinyl acetate in three-component microemulsions stabilized by low concentration of AOT (<1 wt%). These microemulsion-made latexes contained latex particles two to three times smaller than those obtained by emulsion polymerization.

Syntheses of thermosensitive polyampholytes by polymerization in bicontinuous microemulsions have also been studied by Candau's group [29, 30] recently. Poly(*N*-isopropylacrylamide) (PNIPAM) exhibits a well-defined lower critical solution temperature (LCST) in water around 32 °C, and it is the most extensively studied temperature-responsive polymer. The microemulsion contained three-monomer-mixtures, namely, *N*-isopropylacrylamide (NIPM, neutral), NaAMPS (anionic), and 2-acrylamido-2-propanetrimethylammonium chloride (APTAC, cationic). Bicontinuous microemulsions were produced in an HLB domain ranging between around 10.6 and 11.3 using a blend of nonionic surfactants. After polymerization, it formed thermosensitive polymers, namely NIPAM-based polyelectrolytes and polyampholytes. The final products consisted of stable and clear microlatexes of small particle size containing up to 20 wt% high molecular weight copolymers. In order to overcome the high surfactant-to-monomer ratio used, they performed the polymerization by a

semi-continuous process that reduced the surfactant content required to stabilize the final microlatexes by more than 40%.

2.3 Polymerization in Oil-in-Water Microemulsions

The main difficulty encountered by most researchers working on cosurfactant-O/W microemulsion polymerization over the past decade [31–36] is the instability of microlatex produced from systems that use lower weight ratios (<1) of surfactant to monomer for a higher content of polymer (>8 wt%). The instability of the resulting microlatexes may be due to the incompatibility between the higher content of polymer formed and the cosurfactant [37]. The polymerization of a hydrophobic monomer in a ternary O/W microemulsion without a cosurfactant was first reported in 1989 by Ferrick et al [38]. This spurred a new interest in systematic polymerization studies for cationic O/W microemulsions [39–42]. The cationic surfactants can be dodecyltrimethylammonium bromide (DTAB), tetradecyltrimethylammonium bromide (TTAB), or cetyltrimethylammonium bromide (CTAB). Nonionic surfactants were also used in ternary O/W microemulsions for the polymerization of styrene and methylmethacrylate (MMA) [43] and anionic AOT microemulsion for the polymerization of tetrahydrofurfuryl methacrylate (THFM) [44]. Anionic SDS ternary O/W microemulsions have also been used to study the polymerization of butylacrylate (BUA) [45, 46], alkyl acrylates [47], and the copolymerization of BUA with acrylonitrile [48]. All of the microemulsion polymerizations produced stable microlatexes with particle sizes ranging from 20 to 60 nm in diameter. However, these ternary O/W microemulsions usually required a high surfactant concentration (7–15 wt%) to solubilize a relatively low monomer content of less than 10 wt%. These conventional O/W microemulsion polymerization recipes call for the use of at least an equal amount of surfactant and monomer, which makes the polymerization and surfactant removal processes prohibitively expensive. Nevertheless, there have been a few studies in which the formulation has been modified from these polymerization conditions in order to dramatically reduce the use of surfactant, as we will discuss in the next section.

It is generally accepted that an O/W microemulsion polymerization proceeds via a continuous particle nucleation mechanism, as in the case of inverse microemulsion polymerization [14]. The particle nucleation of polymer is generally postulated to occur in microemulsion droplets (micellar nucleation mechanism) for less water-soluble monomers, such as styrene and BUA. Homogeneous nucleation for this type of monomer may be insignificant because of an extremely large number of microemulsion droplets ($\sim 10^{16}$–10^{17} m/L) that can effectively capture the free radicals generated. The primary radicals generated in the aqueous phase probably react first with some dissolved monomers in the aqueous phase to form oligomeric radicals of higher hydrophobicity. These oligomeric radicals can then be captured more favorably by microemulsion

droplets. Therefore, the newly formed latex particles continue to grow in the microlatex through the constant supply of monomer from nucleated droplets until the chain in the particle is terminated by chain transfer to monomer [42, 49, 50]. However, Kaler's group recently consistently obtained very high molecular weights of ~15×10^6 Da for styrene O/W microemulsion polymerizations [51]. Such molecular weights are considerably higher than those typically obtained via free-radical polymerizations. In the free-radical polymerization of styrene, the chain transfer to monomer is limited and hence can only produce molecular weights of up to ~2×10^{-6} Da, as suggested by the most recent measurements of chain-transfer constants by Kukulj et al [52]. Therefore, the diffusion-limited exit of monomer radicals to the aqueous phase coupled with chain transfer to polymer are probable reasons for the enhanced molecular weight of polystyrene [51].

In contrast to emulsion polymerization, the reaction kinetics of microemulsion polymerization is characterized by two polymerization rate intervals; the interval of constant rate characteristic of emulsion polymerization is missing [42, 49, 53], as shown in Fig. 2. Polymer particles are generated continuously during the reaction by both micellar and homogeneous mechanisms. As the solubility of the monomer in the continuous domain increases, homogeneous

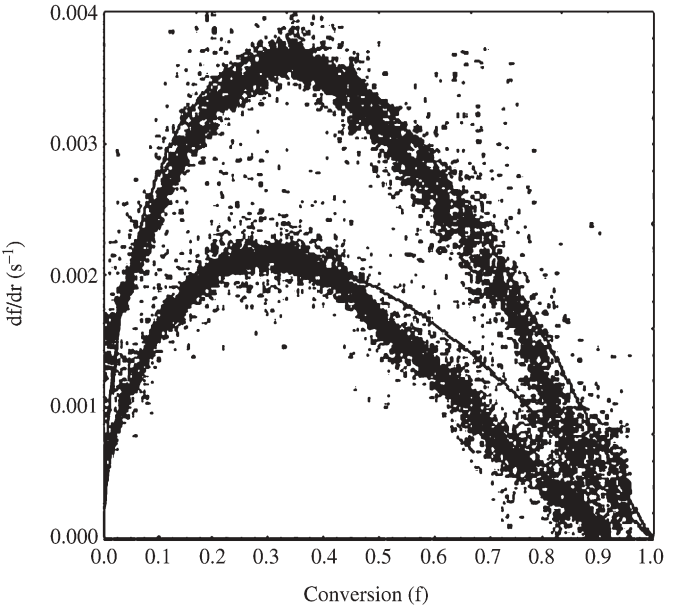

Fig. 2 Experimental and model rate versus conversion profiles for the polymerization of hexylmethacrylate in a microemulsion stabilized by the surfactant DTAB. The two curves are for initiator concentrations of 0.045 wt% (top) and 0.015 wt% (bottom) relative to the amount of monomer in the microemulsion. The solid lines are predictions from the Morgan model [56]

nucleation becomes more important [54]. In O/W microemulsion polymerization, monomer partitioning between polymer particles and uninitiated micelles via diffusion through the aqueous phase determines the concentration of monomer at the polymerization loci. This partitioning plays an important role in determining polymer particle formation and growth [55–57]. The rate of polymerization initially increases to a maximum around 20–25% of total monomer conversion (Interval I) and then decreases on further polymerization (Interval II). This is generally interpreted as indicating that the particle nucleation occurs mainly in Interval I, and polymer growth occurs in Interval II. The decreased polymerization rate in Interval II is due to the progressively depletion of monomer in the latex particles.

The growth pattern for PMMA particles was found to be different from that for styrene polymerization in ternary cationic microemulsions [58, 59] containing either TTAB, TTAC, CTAB or OTAC (octyldecyltrimethylammonium chloride). For the MMA microemulsions, the average hydrodynamic particle radius (R_h) increased continuously from about 20 to 50 nm during the polymerization. The improved interactions between the cosurfactant MMA and the cationic surfactant at interfaces may restrict the swelling of MMA-swollen PMMA particles. Hence a gradual increase in the sizes of the PMMA particles during polymerization was observed, as expected [59]. However, this was not the case for the weaker interaction between styrene and a cationic surfactant in the corresponding microemulsion. The maximum swelling of PS particles by styrene monomer, and hence the largest R_h, was attained during the early stage of polymerization (4–7% polymer conversion) [58]. As the styrene polymerization continued, R_h generally decreased due to the diminishing styrene concentration in the swollen PS particles. For some polymerized MMA-micro emulsions, particle sizes might increase significantly towards the final stage of polymerization. The agglomeration of some PMMA latex particles stabilized by TTAB was evidenced by the prolonged heating (long term storage) of microlatexes [60] at 60 °C, as shown in Fig. 3. Cationic surfactants with larger carbon chain lengths, such as OTAC or CTAB, form thicker interfacial layers which prevent latex flocculation through steric stabilization. It should be noted that the stability of PS microlatex was not affected by the alkyl chain length of the cationic surfactant due to stronger surfactant adsorption on the surface of PS particles than on PMMA particles [60]. Indeed, it is known that surfactant adsorption on the latex/water surface decreases with increasing polymer polarity [61].

Core-shell nanoparticles can also be fabricated using microemulsions. This was performed using a two-stage microemulsion polymerization beginning with a polystyrene seed [62]. Butyl acrylate was then added in a second step to yield a core-shell PS/PBA morphology. The small microlatex led to better mechanical properties than those of similar products produced by emulsion polymerization. Hollow polystyrene particles have also been produced by microemulsion polymerization of MMA in the core with crosslinking of styrene on the shell. After the synthesis of core-shell particles with crosslinked PS shells, the PMMA core was dissolved with methylene chloride [63]. The direct cross-

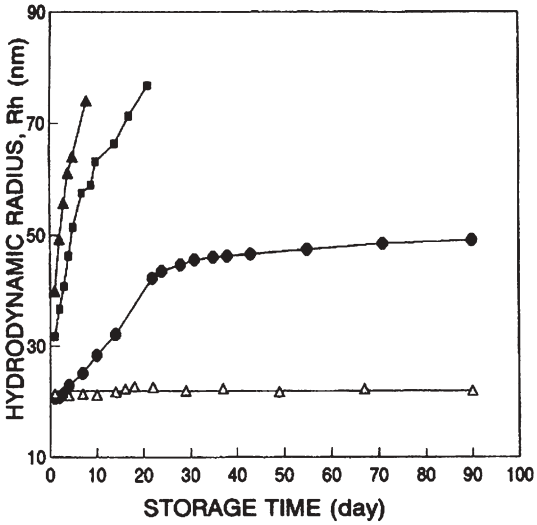

Fig. 3 Changes in PMMA particle size during long term storage at 60 °C for microlatexes stabilized by different surfactants: (filled triangles) TTAB; (filled squares) TTAC; (filled circles) CTAB; (empty triangles) OTAC

linking polymerization of styrene at the interfaces of isooctane microdroplets of microemulsion also produced hollow nanocapsules [64].

2.4 Microemulsion Polymerization for Microlatexes with High Polymer-to-Surfactant Weight Ratios

A major drawback of conventional microemulsion polymerization is the high surfactant-to-monomer ratio usually needed to form the initial microemulsion. Surfactant can be used more efficiently in semi-continuous or fed polymerization processes. Several polymerization cycles can be run in a short period of time by stepwise addition of new monomer. After each cycle of monomer addition, most of the surfactant is still available to stabilize the growing hydrophobic polymer particles, or to forms microemulsion again when a polar monomer is used. For instance, in the polymerization of vinyl acetate (VA) by a semi-continuous microemulsion process [21], latexes with a high polymer content of about 30 wt% were obtained at relatively low AOT concentrations of about 1 wt%. Moreover, their particle sizes and molecular weights were much smaller than those obtained by conventional emulsion polymerization.

A new system associated with an O/W microemulsion for styrene polymerization of up to 15 wt% solids at about 1 wt% DTAB was first reported [65] in 1994. This new two-phase system is rather similar to a Winsor I system, as depicted in Fig. 1; an organic phase containing small portions of water and surfactant in equilibrium with an O/W microemulsion in the bottom phase.

The new system consists of a pure styrene upper phase placed on top of a ternary O/W microemulsion. Strictly speaking, this new system is not identical to the Winsor I system. Hence the new polymerization system has been referred as a "Winsor I-like" system, which can be prepared by simply topping up a ternary O/W microemulsion with hydrophobic monomer without disturbing the microemulsion phase. Styrene polymerization took place only in the initial ternary microemulsion containing 0.5–1.0 wt% styrene, 1.0 wt% DTAB and a redox initiator of ammonium persulfate/tetramethylethylenediamine (APS/TMEDA). The upper styrene phase acted only as a monomer reservoir to continuously supply monomer to the polymerization loci in the lower microemulsion phase through diffusion without stirring. PS particles initially formed in the microemulsion phase became the seed for the further growth of PS particles to a more uniform size, up to about 80 nm in diameter. Therefore, microlatexes of about 15 wt% PS could be obtained using only 1 wt% DTAB. It should also be noted that the Winsor I-like system with a small amount of monomer in the upper phase becomes a milky emulsion on stirring. But this milky emulsion will transform into a transparent or bluish microlatex after polymerization.

The polymerization rate of the Winsor I-like system was very slow due to the low monomer diffusion rate through the limited interface to the polymerization loci for the unstirred system. In order to increase the interfacial areas for the infusion of monomer to the polymerization loci, hollow fiber monomer feeds were later used to polymerize not only styrene, but also MMA and butylacrylate [66]. Such a set-up using continuous monomer feeding via a hollow-fiber is shown in Fig. 4. About 100 polypropylene (PP) hollow fibers (pore size 70 nm) were bundled together. One of the openings of the hollow-fiber bundle was used for monomer feeding and the other end was sealed with epoxy resin. The initial microemulsion usually consisted of 0.5 wt% styrene or BA, or 2 wt% MMA, 1 wt% CTAB or 1.5 wt% SDS together with 0.2 wt% 1-pentanol, 4 mM equimolar redox initiator (APS/TMEDA), and water to make it up to 100 wt%. After polymerization of the microemulsion for about 15 min at room temperature with about 97–98% conversion, the additional monomer was then continuously introduced to the polymerization system via the infusion of monomer from hollow fibers connected to monomer reservoir. The rate of monomer infusion into the microemulsion could be regulated by the external nitrogen pressure applied to the monomer reservoir. The slow bubbling by nitrogen gas into the polymerizing microemulsion was to ensure homogeneous mixing. When the infusion rate of monomer was optimal, latex particles would grow to more uniform sizes at the expense of forming secondary particles via homogeneous nucleation. This method was able to produce almost uniform microlatexes of various sizes (15–65 nm) at high polymer/surfactant weight ratios up to about 15 with high molecular weights (10^6 g/mol) within 2–3 h.

Though the continuous addition of monomer via hollow fibers into a Winsor I-like system is rather novel, it is not as convenient as the drop-wise addition of monomer under a semi-continuous process. Ming et al [67, 68]

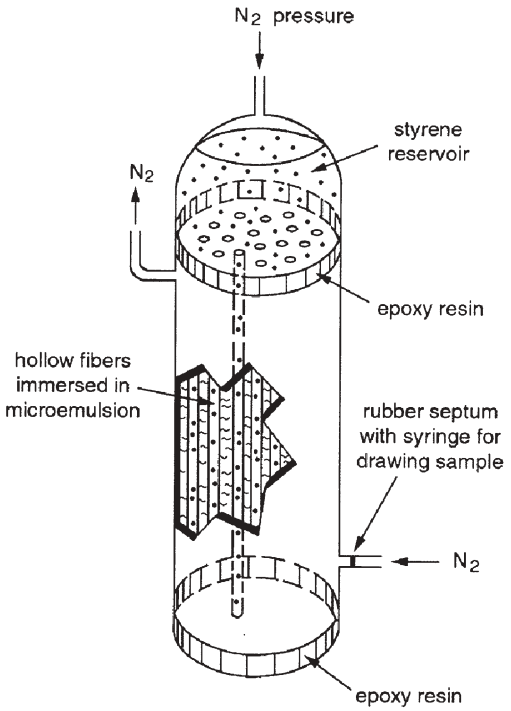

Fig. 4 Schematic presentation of the set-up (not to scale) for the polymerization of monomer in a microemulsion via hollow-fiber feeding of additional monomer

slightly modified the Winsor I-like method by directly adding monomer very slowly to pre-polymerized ternary microemulsions for producing microlatexes of PS, PMMA, poly(butyl methacrylate), or poly(methacrylate) (PMA). With 1 wt% DTAB, 24 wt% PMMA microlatexes of 33–46 nm in size were obtained. They showed that this semi-continuous process was very effective for producing small microlatexes (15 nm) containing up to 30 wt% PMA at a high PMS to SDS weight ratio of 25:1. The semi-continuous process works at the monomer-starved condition to ensure that no empty micelles exist during polymerization.

The polymerization of styrene in Winsor I-like systems by semi-continuous feeding of monomer stabilized by either DTAB, TTAB or CTAB has been systematically investigated by Gan and coworkers [69a]. Rather monodisperse polystyrene microlatexes of less than 50 nm with molecular weights of over one million were obtained at a polymer/surfactant weight ratio of 14:1. The Winsor I-like (micro)emulsion polymerization of styrene stabilized by non-ionic surfactant and initiated by oil-soluble initiators has also been reported very recently [69b]. The sizes of the large monomer-swollen particles decreased with conversion and they merged with growing particles at about 40–50% conversion.

High PMMA content (30–40%) microlatexes [70] stabilized with low concentrations of anionic SDS were also prepared by microemulsion polymeriza-

tion via semi-continuous feeding of MMA. The synthesis of monodisperse poly(dimethylsiloxane) microlatexes (<80 nm) [71] stabilized by several surfactants were also obtained at polymer/surfactant weight ratios of up to 3:1.

Nanosized polystyrene (PS) microlatexes stabilized by a mixture of cationic/cationic, anionic/anionic, or anionic/cationic surfactants of various types [72] with PS-to-surfactant weight ratios up to 10:1 have been synthesized by a semi-continuous microemulsion polymerization process. For cationic or anionic systems, spherical latex particles ranging from about 22 to 53 nm were produced almost linearly, independent of the weight ratio of the mixed surfactants of similar charges. High molecular weight (M_w) PS ranging from 1.1×10^6 to 1.9×10^6 g/mol could easily be obtained from all three systems. The present polymerization method allows one to synthesize nanoparticles of PS or other polymers with high polymer/surfactant weight ratios at some particle sizes that cannot be achieved with a single type of surfactant.

High polymer/surfactant weight ratios (up to about 15:1) of polystyrene microlatexes [73] have been produced in microemulsions stabilized by polymerizable nonionic surfactant by the semi-continuous process. The copolymerization of styrene with the surfactant ensures the long-term stability of the latexes. Nanosized PS microlatexes with polymer content (≤25 wt%) were also obtained from an emulsifier-free process [74] by the polymerization of styrene with ionic monomer (sodium styrenesulfonate, NaSS), nonionic comonomer (2-hydroxyethylmethacryalte, HEMA), or both. The surfaces of the latex particles were significantly enriched in NaSS and HEMA, providing better stabilization.

Nanoparticles of PS (M_w=1.0×10^6–3.0×10^6 mol^{-1}) microlatexes (10–30 nm) have also been successfully prepared from their respective commercial PS for the first time [75]. The dilute PS solutions (cyclohexane, toluene/methanol or cyclohexane/toluene) were induced to form polymer particles at their respective theta temperatures. The cationic CTAB was used to stabilize th microlatexes. The characteristics of these as-formed PS latex particles were quite similar to those obtained from the microemulsion polymerization of styrene as reported in literature. These microlatexes could also be grown to about 50 nm by seeding the polymerization of styrene with a monodisperse size distribution of D_w/D_n=1.08. This new physical method for preparing polymer nano-sized latexes from commercial polymers may have some potential applications, and therefore warrants further study.

3
Bicontinuous-Microemulsion Polymerization for Nanostructured Solid-Materials

Numerous attempts to prepare nanostructured materials by polymerization of suitable monomers (like MMA and styrene) in water-in-oil [76, 77] or oil-in-water [39, 51, 78–81] and bicontinuous microemulsion [27, 82–84] have been made. Polymeric materials were traditionally stabilized by non-polymerizable

surfactants, such as sodium dodecyl sulfate (SDS), and their polymerized microemulsions were usually found to be opaque and phase-separated. By incorporating polymerizable acrylic acid as co-surfactant in a microemulsion, stable transparent polymeric materials can be obtained but only at low solid contents (<15 wt%) [85]. However, the polymerized microemulsions did not reveal any microstructures when viewed by scanning electron microscope (SEM). But when SDS was replaced by a polymerizable surfactant, transparent nanoporous polymeric materials were obtained.

3.1 Nanostructured Polymers Produced by Bicontinuous-Microemulsion Polymerizations

There is increasing interest in the study of the formation of transparent nanoporous polymers (film or sheet) by bicontinuous-microemulsion polymerization [86–91a]. The real success of forming transparent solid polymers possessing various nanostructures arises from the polymerization of bicontinuous microemulsions containing a polymerizable surfactant with other monomers. The polymerizable surfactants are also known as "surfers" [91b], and they can be anionic sodium 11-(*N*-ethylacrylamindo)-undecanoate (SEAAU), cationic (acryloyloxy)-undecyltrimethylammonium bromide (AUTMAB), zwitterionic (acryloyloxy)-undecyldimethylammonioacetate (AUDMAA) or nonionic ω-methoxypoly(ethylene oxide)$_{40}$-undecyl-α-methacrylate (C_1-PEO-C_{11}-MA-40), as listed in Table 1. The polymerizable surfactants should not contain allylic hydrogens, to avoid active allylic chain transfer reactions.

The development of polymerizable microemulsions consisting of only three basic components (except a water component) for producing transparent solid polymers with nanostructure is a recent achievement [87]. For example, Fig. 5 shows the SEM micrograph of the fractured polymer prepared by the UV-initiated polymerization of a bicontinuous microemulsion consisting of 35 wt% water, 35 wt% AUDMAA and 30 wt% MMA. This micrograph reveals randomly distributed bicontinuous nanostructures of water channels and polymer domains. The widths of the bicontinuous nanostructures were about 40–60 nm. The sizes of the nanostructures can be readily reduced by adding 2-hydro-

Table 1 Some polymerizable surfactants that have been synthesized

Surfactant	Structure	CMC (mol l^{-1}, 25 °C)	Reference
SEAUU	CH_2=CHCON(C_2H_5)(CH_2)$_{10}$$COO^-Na^+$	4.2×10^{-5}	[92]
AUTMAB	CH_2=CHCOO(CH_2)$_{11}$-N^+(CH_3)$_3$$Br^-$	1.4×10^{-2}	[88]
AUDMAA	CH_2=CHCOO(CH_2)$_{11}$-N^+(CH_3)$_2$$CH_2COO^-$	9.3×10^{-3}	[87]
C_1-PEO-C_{11}-MA-40	CH_2=CHCOO(CH_2)$_{11}$-(OCH_2CH_2)$_{40}$$OCH_3$	6.6×10^{-5}	[93]

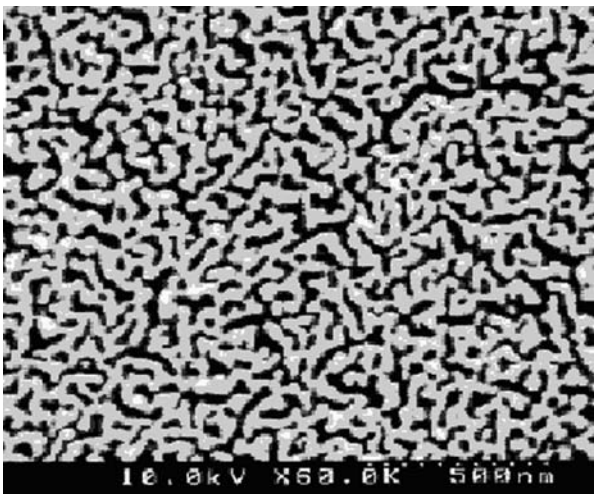

Fig. 5 SEM micrograph of a fractured polymer prepared by polymerization of a bicontinous microemulsion consisting of 35 wt% H_2O, 35 wt% AUDMAA and 30 wt% of MMA. The black and gray areas refer to water and polymer domains respectively

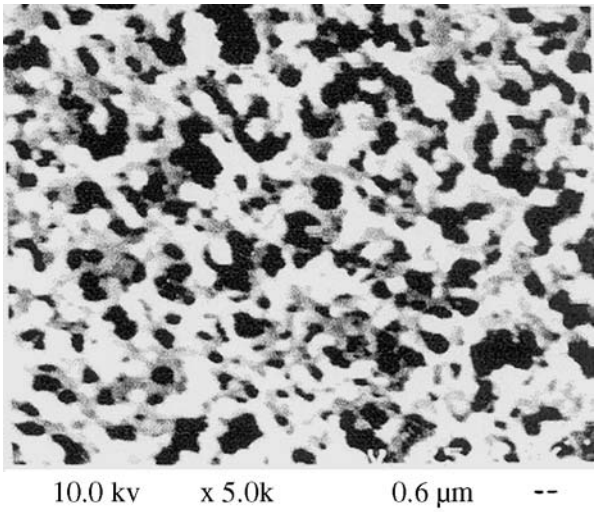

Fig. 6 SEM micrograph of a fractured polymer prepared by polymerization of a bicontinous microemulsion consisting of 30 wt% H_2O, 28 wt% AUTMAB, 38 wt% of MMA and 4 wt% HEMA. The black and gray areas refer to water and polymer domains respectively

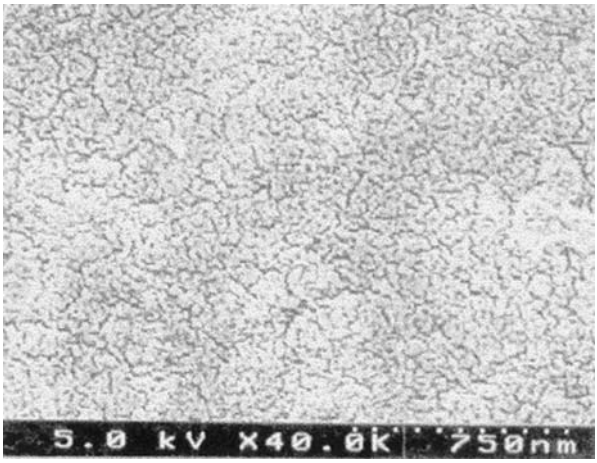

Fig. 7 SEM micrograph of a fractured polymer prepared by polymerization of a bicontinous microemulsion consisting of 40 wt% aqueous solution containing 3% NaCl, 33 wt% AUTMAB and 27 wt% of MMA. The black and gray areas refer to water and polymer domains respectively

xyethylmethacrylate (HEMA) or increased by adding 1–3 wt% NaCl solution, as shown in Figs. 6 and 7 [91a] respectively. In all of the bicontinuous microemulsions investigated, about 1 wt% of cross-linker ethyleneglycol dimethacrylate (EGDMA) was usually used to enhance the mechanical strengths of the polymers.

This type of cross-polymerization of all of the organic components (like MMA, HEMA and a polymerizable surfactant) in a bicontinuous microemulsion is an important area of recent development in microemulsion polymerization, which can be used to produce nanostructures of transparent polymer solids. The polymerization can be readily initiated using either redox or photo-initiators. The gel formation usually occurred within 20 minutes. The use of this novel type of microemulsion polymerization for preparing transparent inorganic-polymer nanocomposites in the form of films or sheets is emerging and exciting. However, very little published information about this type of nanocomposite is available, as will be described in the following sections.

3.1.1 Ion-Conductive Membranes

The development of transparent polymer electrolyte membrane from the bicontinuous-microemulsion polymerization of 4-vinylbenzene sulfonic acid lithium salt (VBSLi), acrylonitrile and a polymerizable non-ionic surfactant, ω-methoxypoly(ethylene oxide)$_{40}$-undecyl-α-methacrylate (C_1-PEO-C_{11}-MA-40) was reported in 1999 [94, 95]. The ionic conductivities of the polymer electro-

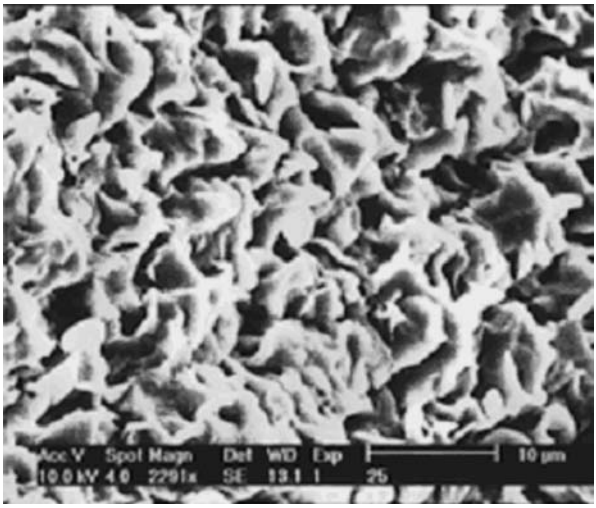

Fig. 8 SEM micrograph of the polymerized microemulsion solid, that contains the polymerizable non-ionic surfactant C_1-PEO-C_{11}-MA-40 [96], after ethanol extraction

lyte membranes were rather high, in the range of $(2–3)\times10^{-3}$ S/cm. This relatively high conductivity is attributed to the inclusion of the polymerizable ionic salt VBSLi and the existence of the interconnected aqueous channels in the polymerized bicontinuous network, which facilitate ionic conduction for the membrane electrolyte [94]. However, some unusual ionic conduction phenomena were also observed for these ion-containing membranes – large ions exhibited higher mobilities than smaller ones [95]. A possible explanation comes from the larger hydration shells of the lighter cations. This is further supported by the sharp drop in conductivity when the system is cooled below the freezing point of water.

The morphology of the microemulsion-polymerized solid after ethanol extraction, as revealed by SEM, is shown in Fig. 8. The extracted samples show globular microstructures and voids (pores). These pores might be derived from the interconnected water-filled voids generated from numerous coalescences of growing particles during polymerization.

The water in the membranes [96] could easily be replaced by polar organic solvents, such as BL, PC-EC, or EC-DMC, by immersion. The conductivities of the membranes decreased sharply (by about two orders of magnitude) with the use of organic solvents. After soaking these membranes in electrolyte solutions of 1 M $LiSO_3CF_3$/PC-EC, 1 M $LiBF_4$/BL, or 1 M $LiClO_4$/EC-DMC, their conductivities were restored to 10^{-3} S/cm [96]. This demonstrates that the water content in these microporous membranes can be freely exchanged for organic solvents or electrolyte solutions, indicating that they may be further developed as composite polymeric electrolytes for lithium/lithium ion rechargeable batteries.

3.1.2
Proton-Exchange Membranes

The bicontinuous-microemulsion polymerization technique has also been used to develop novel proton exchange membranes (PEM) for fuel cell evaluation [97]. A series of hydrocarbon-based membranes were prepared based on the formulation shown in Fig. 5, with additional ionic vinyl monomers such as VBSLi or bis-3-sulfopropyl-itaconic acid ester. After polymerization, the membranes were treated with dilute H_2SO_4 (0.5 M) to convert them to PEM membranes. The good performance of these PEM membranes in a single fuel cell is illustrated in Fig. 9.

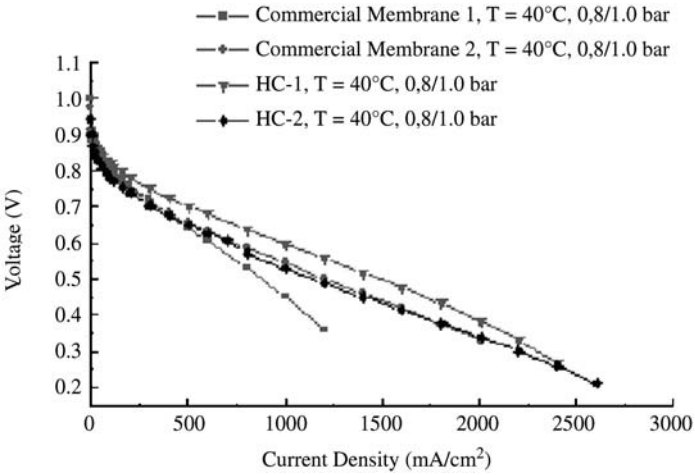

Fig. 9 Membrane performance of a single fuel cell (area: 5 cm^2, Pt loading on anode/cathode: 0.4 mg/cm^2) using commercial membranes 1 and 2, and microemulsion-synthesized membranes HC-1 and HC-2

3.2
Polymer Nanocomposites Produced by Bicontinuous-Microemulsion Polymerizations

3.2.1
Ruthenium (II) Complexes in Polymerized Bicontinuous-Microemulsions

Bicontinuous microemulsions consisting of cationic surfactant AUTMAB (30–40 wt%), MMA (30–40 wt%), and 20–40 wt% of an aqueous 50 µM solution of water-soluble metal complexes such as $Ru(dip)_3Cl_2$ (dip=4,7-diphenyl-1,10-phenanthroline) have been investigated [98]. After polymerization, the microemulsion transformed into a transparent polymer film which showed a remarkable enhancement in luminescence intensity. The emission lifetime also

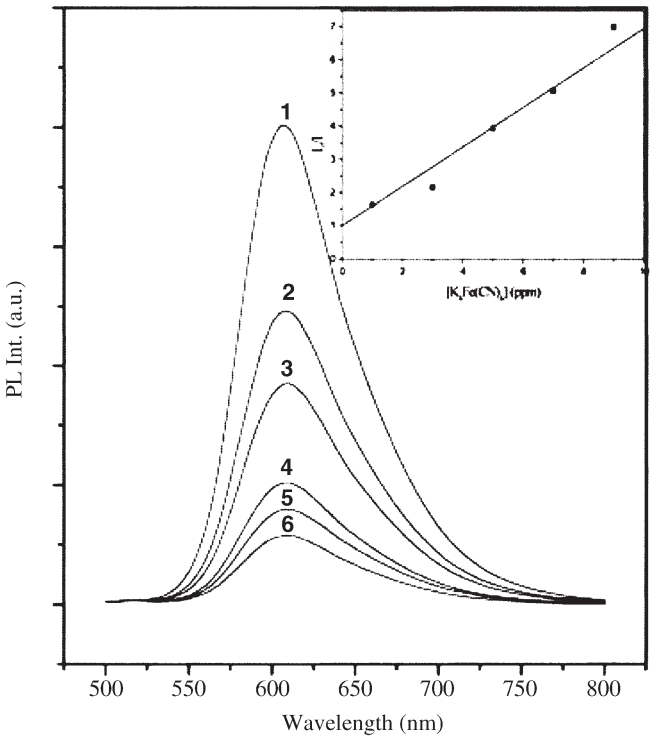

Fig. 10 The effect of potassium ferrocyanide on the luminescence spectra of $[Ru(dip)_3]^{2+}$ in polymerized cationic microemulsion: (1) 0 ppm, (2) 1 ppm, (3) 3 ppm, (4) 5 ppm, (5) 7 ppm and (6) 9 ppm. The contact time between the potassium ferrocyanide solution and the polymer film was 10 min. The insert is the Stern-Volmer plot for the quenching of $[Ru(dip)_3]^{2+}$ by potassium ferrocyanide

increased substantially from 0.98 μs (aqueous), to 2.0 μs (fluid microemulsion), to 5.8 μs for the polymerized microemulsion. The substantial increases in emission intensity and lifetime of $[Ru(dip)_3]^{2+}$ are ascribed to rigidochromism resulting from the transformation of the dynamic nanostructure of the fluid microemulsion into its solidified state after polymerization. In addition, the fluorescence of $[Ru(dip)_3]^{2+}$ could largely be quenched within 5–10 min by immersing the polymer film in a dilute (several ppm) aqueous solution of potassium ferrocyanide, as demonstrated in Fig. 10. This was possible because the polymer film possessed nanoporous open structures which enabled water and $[Fe(CN)_6]^{4-}$ ions to freely and rapidly pass through the nanochannels of the polymer network. The use of the polymerized bicontinuous microemulsion as a matrix allowed $[Ru(dip)_3]^{2+}$ complexes to be immobilized, resulting in its high sensitivity and fast response to the quencher from the external phase. This novel approach can be further developed for sensors and nanocomposites with specific functionality.

3.2.2
Aligned Nanocomposites of Ferrite-Polymer from Bicontinuous-Microemulsion Polymerization

It has been reported [99] that flame spraying of microemulsions containing nanoparticles can lead to the deposition of thin films. This is an alternative method to laser-assisted ablation and other thermal methods to evaporate metallic substrates and condense the vapors onto thin film. A novel strategy has recently been employed in the assembly of magnetic nanoparticles in polymer-nanoparticle composites using an external magnetic field [100]. A new type of hybrid colloidal assembly, combining a bicontinuous microemulsion matrix with a suspension of colloidal magnetic particles (ferrofluid), was investigated in the study. One distinct feature of this system is that the polymer matrix consists of numerous randomly interconnected channels that allow solid magnetic nanoparticles to be incorporated after the structure of the bicontinuous microemulsion matrix has been locked into place by polymerization.

The precursor, magnetic nickel ferrite nanoparticles, was prepared from mixing two W/O microemulsions, one of which contained Ni-Fe nitrate solution and the other containing ammonium hydroxide. The nickel-iron hydroxide particles formed were recovered by centrifugion followed by calcining at 500 °C for 5 h, giving the complete conversion of the hydroxide particles into magnetic nickel ferrite ($NiFe_2O_4$). The ferrofluid was then prepared by dispersing the ferrite particles in the aqueous solution stabilized by PEO-macromonomer surfactant (C_1-PEO-C_{11}-MA-40). The ferrite-microemulsion, consisting of about 33 w% water, 1–2 wt% of $NiFe_2O_4$, 35 wt% of C_1-PEO-C_{11}-MA-40, 21 wt% acrylonitrile (AN) and 9 wt% MMA was polymerized by redox initiation in a glass cell at room temperature. The transparent solid sample was microtoned to thin film, for TEM observation as shown in Fig. 11.

In the absence of a magnetic field during the polymerization, the nanoparticles of $NiFe_2O_4$ were randomly distributed in the polymerized microemulsion sample, as shown in Fig. 11a. However, under a magnetic field of a particular field strength, $NiFe_2O_4$ particles in the aqueous channels of the microemulsion could be aligned with the field without causing much agglomeration of the magnetic particles. As the polymerization of microemulsion advanced to the solidified state, the magnetic particles were locked within the water channels of the polymerized matrix along the direction of the magnetic field, as revealed by Fig. 11b. By further refining the polymerization method, magnetic particles may be patterned in polymer substrate by careful control of the external magnetic field. Many other magnetic/polymer nanocomposites can be prepared in a similar way.

This bicontinuous-microemulsion polymerization method can also be used to synthesize polymer nanocomposites containing SiO_2 [101], TiO_2, ZnO and many other semiconductors. The advantage of this method is that the nanoparticles of inorganic materials can be dispersed in the polymer matrix fairly uniformly. The only requirement is that nanomaterials should be first stabilized

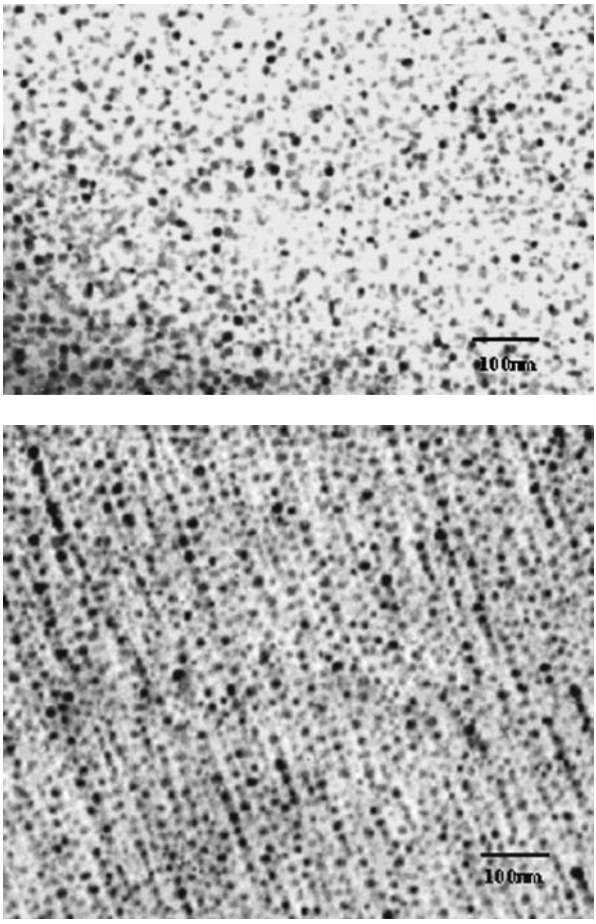

Fig. 11 TEM micrographs of polymerized ferrite-microemulsion nanocomposites containing 2 wt% $NiFe_2O_4$. **a** No magnetic field during polymerization; **b** under the influence of H=50 Oe field during polymerization

in an aqueous phase of microemulsions without causing phase separation during polymerization. Hybrid inorganic polymer materials can also be prepared from ternary microemulsions [102].

3.3 Synthesis of Nanocomposites Via In-Situ Microemulsion Polymerization

Some non-oxide nanoparticles such as PbS and CdS can be used to prepare polymer-inorganic nanocomposites by a double-microemulsion process [103]. In this case, two precursor microemulsions must be prepared separately first and then mixed together for polymerization. Using CdS-polymer nanocom-

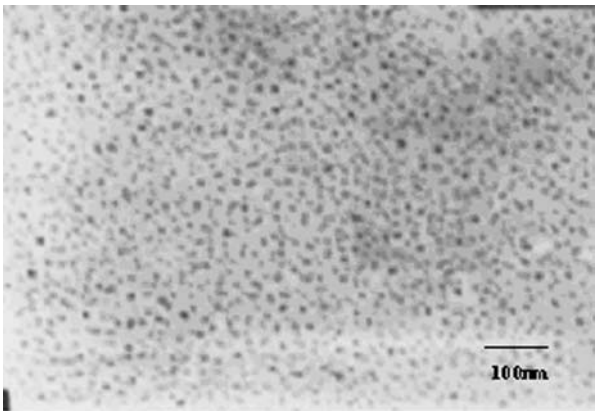

Fig. 12 TEM micrograph of Au-polymer nanocomposite prepared via in situ microemulsion polymerization

posite as an example, common compositions of two precursor microemulsions were 35 wt% MMA and 35 wt% AUDMAA. One of the microemulsions contained 30 wt% of 10 mM $CdBr_2$ aqueous solution, while the other contained 30 wt% of 10 mM $(NH_4)_2S$ aqueous solution. Two precursor microemulsions were then mixed for polymerization at 55 °C using AIBN initiator.

A dispersion of nanoparticles of Au or other metals in a polymer matrix may also be obtained by a one-pot process of microemulsion polymerization. For instance, the UV-polymerization of a microemulsion of 35 wt% MMA, 35 wt% AUDMAA and 30 wt% of 0.1 M $HAuCl_4$ aqueous solution would produce a Au-polymer nanocomposite, as shown in Fig. 12 [104]. This TEM micrograph shows a microtoned thin film of the sample. It is clearly apparent that Au particles of about 10–15 nm are well dispersed in the polymer matrix.

4
Microemulsion Reactions for Processing Inorganic Nanomaterials

The existence of microdomains or droplets with large interfacial area per unit volume in inverse and bicontinuous microemulsions opens up possibilities for controlling the inorganic reaction rates, the pathways, the stereochemistry, and the morphology of the products. By employing microemulsions, monodisperse particles of a few nanometers in diameter can be prepared for the study of quantum size effects. Many new and unusual physical and chemical properties also arise as particles attain nano-sized dimensions [105–107]. There is increasing recognition that aqueous synthesis offers growth control capabilities that can be conveniently exploited to prepare these desirable fine particles [107, 108]. The dependence of the size and polydispersity of the particles obtained on the size and concentration of the microemulsion droplets, the concentration

of the dispersed reactants, the exchange rate between the droplets, and the reactions and interactions between surfactants and metal ions or particles has already been partly addressed [109–114].

Compared to conventional solid-state reaction methods, solution-based synthesis results in higher levels of chemical homogeneity. In solution systems, mixing of the starting materials is achieved at the molecular level, and this is especially important when multi-component oxides are being prepared. As a solution-based materials synthesis technique, the microemulsion-mediated method offers a unique ability to affect particle synthesis and particle stabilization in one step. A wide variety of nanosize metal oxides – binary oxides from alumina to zirconia, as well as complex metal oxides – can be prepared by exploiting the ability of microemulsions to solubilize, compartmentalize, and concentrate reactants and products. Most of the focus in the past has been on the successful synthesis of specific metal oxide compounds as nanoparticles. Water-in-oil microemulsions (inverse microemulsions) have been the most widely used for the preparation of spherical nanoscale particles. Reagents dissolved in the water domains of an inverse microemulsion can react via intermicellar communication through dynamic collision processes. Nucleation and growth occur as the process proceeds.

Many potential applications of microemulsion-derived materials appear in the literature. The list includes catalysts, nanoporous membranes, nanocomposites and precursor powders for functional ceramics [115–139]. However, before microemulsion-derived materials become more than laboratory curiosities, two key issues must be addressed: product recovery and yield. Materials generated in microemulsion media can be used in two ways: as prepared in the fluid phase, or as recovered solids. A common practice found in the literature involves phase destabilization of microemulsions via the addition of polar solvents such as ethanol and acetone to precipitate the products. This approach works well as a laboratory technique that permits particles to be recovered for later characterization. However, it is unlikely to be an economically viable approach for practical processing, as we eventually need to separate the added solvents in order to reformulate the original microemulsion. The susceptibility of microemulsion to destabilization by electrolytes severely limits the highest concentrations that can be used for precipitation reactions. This has an adverse impact on prospects for large-scale microemulsion processing. The feasibility of microemulsion-derived synthesis depends on the availability of surfactant/oil/water formulations that give stable microemulsions during reaction, but not during precipitation reactions. Therefore, investigations that emphasize the effects of reactants and products on the stability domains of microemulsions will play an important role. Hopefully, such investigations will lead to guidelines for formulating microemulsion compositions that are compatible with large-scale material synthesis.

4.1 Synthesis of Inorganic Nanoparticles in Inverse Microemulsion

For reactions in inverse microemulsions that involve the total confinement of the reactant species within the dispersed water droplets, the exchange of reactants by the coalescence of the two droplets take place prior to their chemical reaction. The chemical reaction produces an (almost) insoluble product. The reaction medium is first saturated with this product. When the saturation exceeds a critical limit, nucleation occurs. Then the nuclei start to grow rapidly and consume the reaction product leading to a decline in the supersaturation. As soon as the supersaturation falls below the critical level, no further nucleation occurs, so only the existing particles grow beyond this point. If the time period of nucleation is short in comparision to the growth period, rather monodisperse particles are obtained.

Conceptually, these particle synthesis methods can be classified into three main groups:

1. Double inverse microemulsion
2. Inverse microemulsion plus trigger
3. Inverse microemulsion plus a second reactant, as illustrated in Fig. 13

It is apparent that a number of chemical reactions involving aqueous, organic and/or amphiphilic reagents may be accommodated in micellar systems through some of these methods or a combination of them. It is important to note that, in these processes, the reverse micelles not only serve as a passive host, but also provide hydrophobic and electrostatic interactions between the micelles. The reagents used have a profound influence on the chemical and physical properties of the resulting particles.

For the double inverse microemulsion technique, we use two separate microemulsions: reactant A solubilized in a specific microemulsion composition, and reactant B solubilized in another specific microemulsion composition. When the two microemulsions are mixed, reactants A and B will then mix within the microemulsion droplets, preventing sudden precipitation of the product AB. If reactants A and B were to be pre-mixed without using the double microemulsion technique, it would be difficult to control the particle sizes and to prevent agglomeration of particles. This is one of the principles used to produce nanoparticles with double inverse microemulsions (Fig. 13a). On the other hand, nanoparticles can also be produced in inverse microemulsions by adding a trigger (such as heat/light or a reducing/precipitating agent) to an inverse microemulsion containing the primary reactant dissolved in the aqueous core (Fig. 13b). Figure 13c shows oxide, hydroxide or carbonate precipitates formed by passing gases such as oxygen, ammonia or carbon dioxide through an inverse microemulsion containing soluble salts of the cations.

Since numerous papers have been published on the preparation of inorganic nanomaterials by microemulsions, we do not intend to review all of them here. As examples, we will describe how inverse microemulsions can be used to pre-

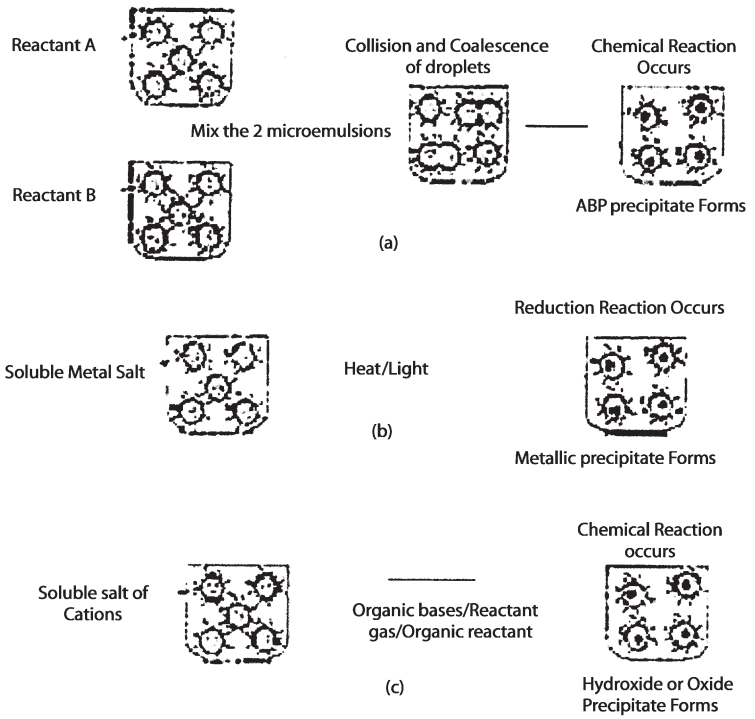

Fig. 13 Synthesis of nanoparticles in microemulsions using: **a** double inverse microemulsions; **b** inverse microemulsion plus a trigger; **c** inverse microemulsion plus reactant [122]

Table 2 Inorganic materials synthesized using inverse microemulsion

Material	Inverse microemulsion (surfactant-oil)	Investigation/results	Reference
CdS	NP-5+NP-9 and petroleum ether	To study the synthesis of CdS using hydrothermal microemulsion	[141]
PbS-coated CdS	NP-5 and petroleum ether	To study the kinetic growth and nonlinear optical response of PbS-coated CdS particles	[142]
Mn-doped ZnS	NP-5+NP-9 and	To compare the properties of Mn-ZnS particles prepared via a conventional reaction, a conventional reaction with hydrothermal treatment, a microemulsion, and a microemulsion with hydrothermal treatment	[143]

Table 2 (continued)

Material	Inverse microemulsion (surfactant-oil)	Investigation/results	Reference
$NiFe_2O_4$	NP5+NP-9 and cyclohexane	To study and characterize $NiFe_2O_4$	[144]
$BaFe_{12}O_{19}$	NP-5+NP-9 and cyclohexane	Ultrafine, high coercivity $BaFe_{12}O_{19}$ was prepared via inverse micro-emulsion and compared to that prepared using the conventional method	[145]
SiO_2	NP-5+NP-9 and cyclohexane	Influence of pH and concentration of sodium orthosilicate on the silica particle size, morphology and specific surface area	[153]
Cu-doped SiO_2	AOT+SDS and cyclohexane	To prepare and characterize Cu-SiO_2 particles	[134]
Ru-Cu-doped SiO_2	AOT+SDS and cyclohexane	The bimetallic Ru-Cu oxides supported on silica showed high catalytic conversion of N_2O	[135]
Perovskite powders	NP-5 and octane or petroleum ether	To prepare and characterize perovskites	[155]
Zirconia and zirconate	NP-5+NP-9 and cyclohexane	To produce zirconia, lead zirconate and lead zirconate titanate at much lower calcination temperatures	[158–161]
Hydroxyapetite (HA)	NP-5+NP-9 and cyclohexane	To compare differences in the sizes, morphologies and specific surface areas of HA powder prepared by W/O microemulsion, bicontinuous microemulsion and the emulsion method	[162]
Hydroxyapetite (HA)	KB6ZA and petroleum ether	To synthesize HA powders in O/W emulsion using the nonionic surfactant KB6ZA	[163]
Pt-Ru	NP-5+NP-9 and cyclohexane	To synthesize and characterize Pt-Ru catalyst for fuel cell applications	[164]

pare semiconductors, nano-sized oxide particles, and hydroxapetite nanoparticles, as illustrated in Table 2. The attraction of using nonionic polyoxyethylated alkyphenyl ether surfactants (like NP-5, NP-9, or mixture of NP-5/NP-9) is that it allow us to formulate inverse microemulsions without the need for cosurfactant; no undesirable counterions are needed. In addition, the various sizes of the hydrophilic (oxyethylene) groups or/and the hydrophobic (alkyl) groups provide flexibility during the selection of surfactant.

4.2 Materials Systems

4.2.1 Doped and Un-Doped CdS/ZnS Nanoparticles

Semiconductor nanoparticles have been extensively studied in recent years owing to their strongly size-dependent optical properties. Among these nanomaterials, CdS and PbS are particularly attractive due to their nonlinear optical behavior and unusual fluorescence or photoluminescence properties [136, 137]. A number of studies have been published recently regarding the preparation of CdS, PbS and ZnS nanoparticles in inverse microemulsion systems [138–143]. In these works, NP-5/NP-9 was the most commonly used surfactant and petroleum ether the most commonly used oil. The aqueous phase for each inverse microemulsion consisted of cadmium nitrate (0.1 M) and ammonia sulfide (0.1 M) respectively. CdS was recovered from the mixture of double microemulsions [141]. Electron microscopy revealed that the spherical particles were around 10–20 nm in diameter, as seen in Fig. 14.

The synthesis of PbS-coated CdS was conducted in a microemulsion system similar to that mentioned above, except that a third inverse microemulsion,

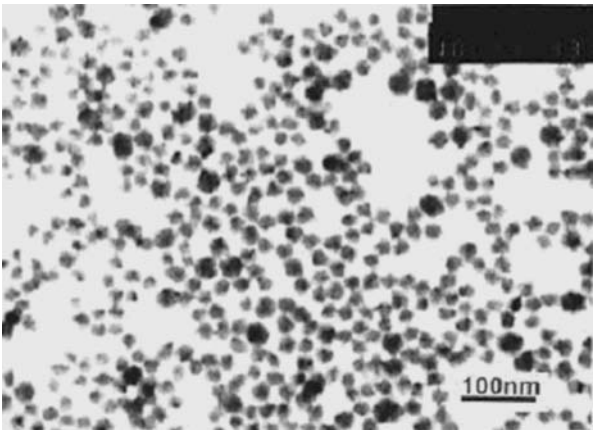

Fig. 14 Transmission electron micrograph (TEM) of a CdS cluster synthesized at 30 °C [141]

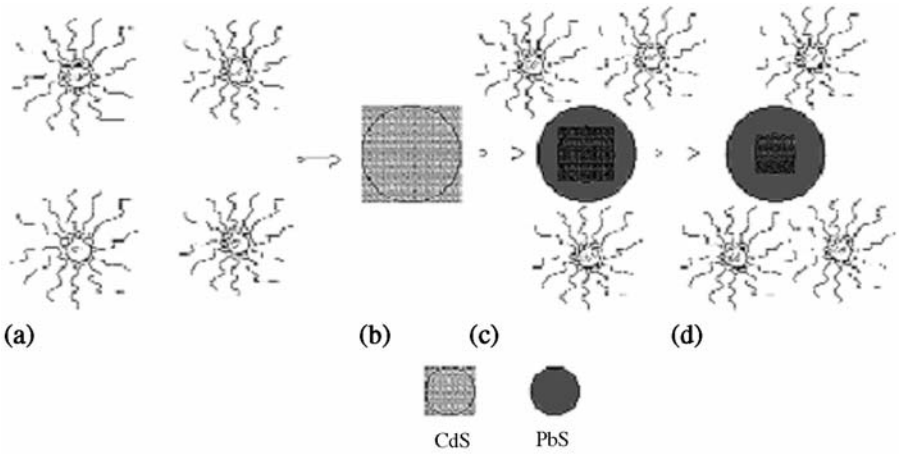

Fig. 15 Formation of PbS-coated CdS nanocomposite in microemulsion: **a** mixing of a microemulsion containing $Cd(NO_3)_2$ aqueous solution with a microemulsion containing $(NH_4)_2S$ aqueous solution; **b** formation of CdS nanoparticle in microemulsion; **c,d** Pb^{2+} ions in a third microemulsion replace the Cd^{2+} in the Cd-S band and diffuse through the PbS layer to form the PbS shell [142]

containing lead nitrate (0.1 M) in the aqueous phase, was also needed [142]. This is to encourage the formation of PbS shells around the CdS particle cores, as depicted Fig. 15. Pb^{2+} ions displaced some Cd^{2+} in the Cd–S bonds to form Pb–S bonds on the surfaces of the CdS particles. The thicknesses of the PbS shells in the PbS-coated nanocomposite could be controlled by changing the Pb^{2+} ion concentration. Absorption measurements of the mixed systems as a function of the concentration of lead nitrate solution indicated a continuous trend toward the PbS spectrum with increasing Pb^{2+} concentration. The particle sizes of the CdS, PbS and CdS/PbS composites are shown in Fig. 16. The resulting NLO properties of the CdS and PbS and CdS/PbS nanocomposite particles were determined by a femtosecond Z-scan technique. A large refractive nonlinearity in these nanocomposite particles was observed due to the optical Stark Effect and strong interfacial and inter-particle interactions. These nanoparticles with large refractive nonlinearities may find application in optical devices, such as those for optical limiting and switching.

Mn-doped ZnS powders were also prepared by inverse microemulsion under hydrothermal treatment at 120 °C [143]. This produced ultrafine and agglomerate-free particles 5–20 nm in diameter. In contrast, the particles prepared via conventional aqueous solutions often coagulated, forming large aggregated clusters. Furthermore, compared with Mn-doped ZnS materials synthesized through conventional aqueous reactions, the nanoparticles prepared in microemulsion showed significantly enhanced photoluminescence. In particular, the photoluminescence of particles prepared in microemulsion under hydrothermal treatment was found to be 60 times higher than that for material

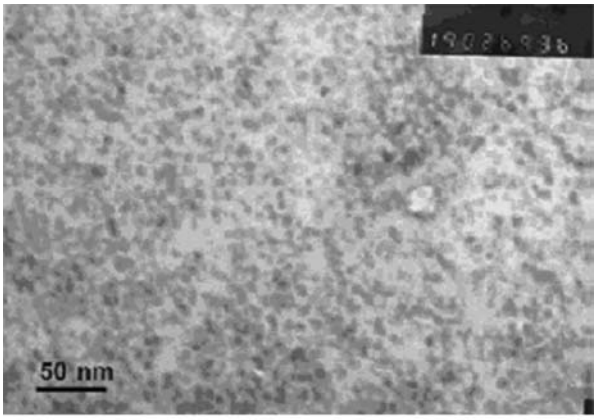

(a)

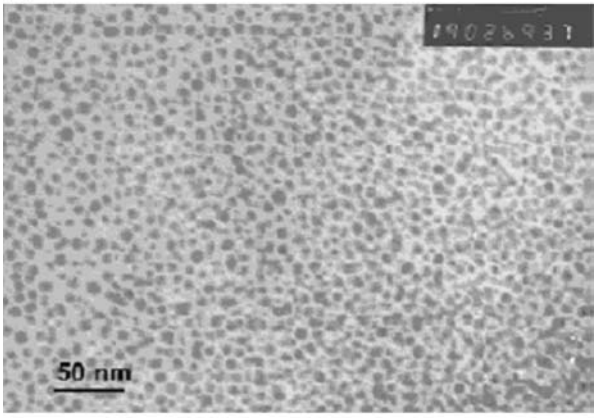

(b)

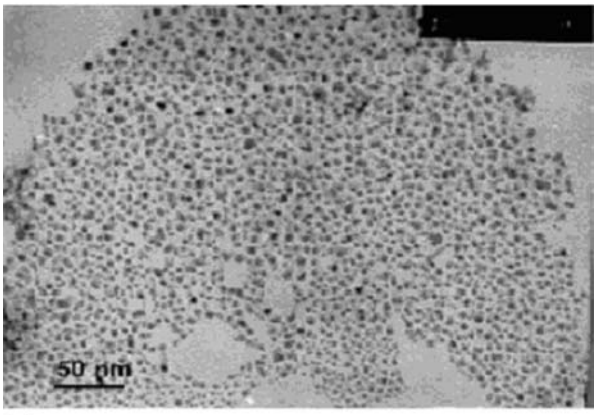

(c)

Fig. 16 Transmission electron micrographs of **a** CdS, **b** PbS nanoparticles, and **c** PbS-coated CdS nanocomposite [142]

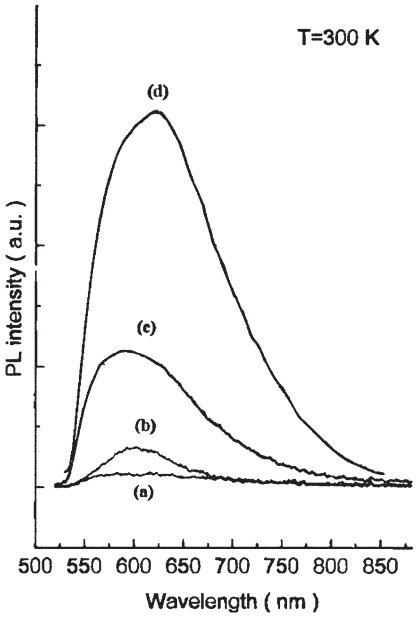

Fig. 17 Photoluminescence (PL) of ZnS:Mn^{2+} particles prepared by: **a** conventional reaction at room temperature; **b** conventional reaction with hydrothermal treatment; **c** microemulsion at room temperature; **d** microemulsion with hydrothermal treatment, with an excitation intensity of 4 W/cm^2 [143]

obtained through the direct aqueous reaction at room temperature (as shown in Fig. 17). This dramatic increase in photoluminescence yield is attributed to the surface passivation of nanoparticles by the adsorption of surfactants, the formation of sphelerite with cubic zinc blende structure, and Mn migration into the interior lattice of the ZnS host.

4.2.2 Magnetic Ferrites

Nano-sized magnetic ferrite particles are the subject of intensive research because their physical properties are quite different from those of the bulk material. The magnetic characteristics of particles used for recording media crucially depend on their sizes and shapes. So, the material used for high-quality recording media should be ultrafine, chemically homogeneous, and stable, with a narrow particle size distribution a predetermined shape. These requirements demand a reliable and reproducible preparation technique.

The formation of microhomogeneous nanoparticles of nickel and barium ferrite was carried out in a three-component microemulsion consisting of NP-5/NP-9 as the surfactant, cyclohexane as the oil, and an aqueous solution of

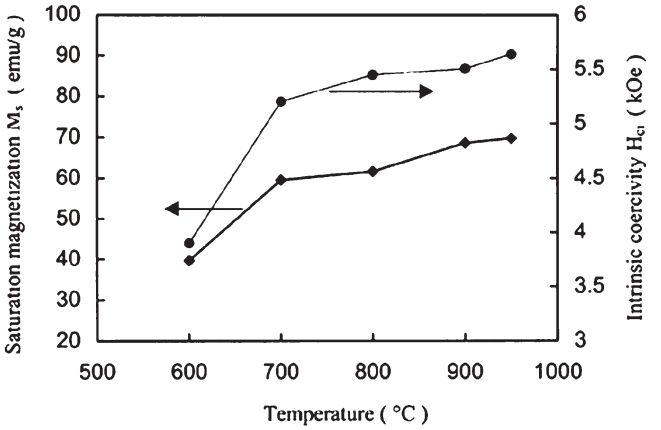

Fig. 18 The saturation magnetization and intrinsic coercivity as a function of calcination temperature for the microemulsion-derived barium ferrites [145]

nickel nitrate and ferric nitrate [144]. An immediate precipitation was affected by adding ammonia to the microemulsion, and the resulting amorphous precipitate was transformed into nickel ferrites by calcining at 600 °C. Discrete nickel ferrite particles with polyhedron shapes and an average size range from 10–20 nm were obtained. The sol-particles were identified as $NiFe_2O_4$ by Mossbauer spectroscopy, electron diffraction and X-ray spectroscopy. Magnetic measurement revealed a saturation magnetization value of 43.0 emu/g for the sample calcined at 500 °C.

Barium ferrite particles were obtained by mixing a ferric ion-containing microemulsion and a barium-containing microemulsion [145]. Precipitation of the hydroxide precursor was affected by adding ammonia solution dropwise into the microemulsions under stirring. The resulting barium ferrite particles formed at a calcination temperature of 950 °C. The round particles synthesized were well dispersed, although a limited degree of particle agglomeration was also observed. The average size of the calcined particles was in the range of 100–200 nm, which was about ten times bigger than the average size of the precursor particles. A high saturation magnetization of 69.74 emu/g and an intrinsic coercivity of 5639 Oe were obtained for the powder calcined at 950 °C (Fig. 18). These results are comparable to some of the best ever reported for fine barium ferrite powders prepared via chemistry-based processing routes. The much improved saturation magnetization and coercivity can be explained by the high phase purity and well-defined crystallinity of $BaFe_{12}O_{19}$ developed in the microemulsion-derived precursor when calcined at a temperature that is high enough.

4.2.3 Silica and Silica-Supported Ru-Cu Oxides

The vast majority of techniques published for the microemulsion-mediated synthesis of silica [146–151] are based on the alkoxide sol-gel method. The oil-soluble metal alkoxide was added to a microemulsion containing solubilized water. The alkoxide must diffuse through the oil continuous phase to the water pool where the hydrolysis and condensation reactions take place.

In our studies, the nano-sized silica was synthesized using cheap sodium orthosilicate and sodium metasilicate rather than expensive alkoxysilanes. An inverse microemulsion containing NP-5/NP-9 as surfactant and cylcohexane or petroleum ether as the oil was used to carry out the hydrolysis and condensation of sodium orthosilicate or metasilicate using an acidic medium [152, 153]. The spherical silica particles of size 10–20 nm were obtained in a system using cyclohexane as the oil and with sodium orthosilicate of 0.01–0.1 M [152]. The particle size increased as the concentration of sodium orthosilicate and the pH were increased. Silica particles prepared in basic conditions were more uniform in size than those prepared in an acidic medium. But calcined silica powders with larger specific areas (350–400 m^2/g) were obtained for those prepared in an acidic medium.

Much smaller silica particles of about 5–10 nm were formed by the controlled hydrolysis and polymerization of sodium metasilicate in bicontinuous microemulsions [153]. The bicontinuous microemulsion system consisted of NP-5/NP-9, petroleum ether, and a high concentration of sodium metasilicate solution (0.2 M). This example illustrates the feasibility of using bicontinuous microemulsion to synthesize silica powders with high specific surface areas (~400 m^2/g) and good amorphous stabilities at 600 °C. The treatment of some calcined silica powders with hexadecyltrimethylammonium hydroxide increased their specific surface areas still further, from 350 to 510 m^2/g.

The double microemulsion-mediated process also provides a convenient method for preparing a metal-containing silicate coating. The two microemulsion systems contained two common components: anionic surfactant AOT and cyclohexane [134]. The difference was that the first microemulsion consisted of an aqueous solution of sodium metasilicate (0.2 M) and 10 wt% SDS as the co-surfactant, while the second microemulsion consisted of an aqueous solution of copper nitrate (0.1 M) and 10 wt% SDS. The copper-ion microemulsion was added to the silicate-ion microemulsion with constant stirring. After 8 h of gellation, and ageing for an additional 24 h, copper nitrate crystals were identified within the silicate network. Silica-copper composite powders with various copper contents (4–20 wt%) and surface areas of 200–400 m^2/g were synthesized.

Using a variation on the microemulsion-mediated process, catalytic bimetallic Ru-Cu oxides supported by silica were made through the controlled hydrolysis/polymerization of sodium metasilicate, copper nitrate and ruthenium chloride via a single microemulsion protocol [135]. With AOT and SDS-based microemulsion, a high specific surface area (~400 m^2/g) and uniform pore size

(~38 Å) of the produced catalyst can be maintained during catalytic reactions. Moreover, tests of the catalytic activity indicated a high catalytic conversion of N_2O by the catalysts synthesized from the microemulsion process at a lower temperature (~400 °C) than that prepared from traditional impregnation processes. The uniform elemental distribution of RuO_2 on the SiO_2 produced by this microemulsion process was established by XPS and SEM/line scanning.

4.2.4 Perovskites

The complex oxides that belong to the group known as perovskites have the general formula ABO_3, where the ionic charges on the metals can assume the form $A^+B^{5+}O_3$, $A^{2+}B^{4+}O_3$ and $A^{3+}B^{3+}O_3$. The first microemulsion-mediated process to synthesize a perovskite used a double microemulsion protocol based on a nonionic surfactant Genapol OX/decane/water system [154]. A microemulsion containing $BaCl_2$ and $TiCl_4$ in the dispersed phase was mixed with an oxalic acid-containing microemulsion. However, X-ray diffraction could not confirm the presence of the intermediate barium titanyl oxalate and the calcined solid did not yield barium titanate.

The double inverse microemulsion method was also used to synthesize perovskite-type mixed metal oxides [155]. One microemulsion solution contained nitrate salts of either $Ba(NO_3)_2/Pb(NO_3)_2$, $La(NO_3)_3/Cu(NO_3)_2$ or $La(NO_3)_3/Ni(NO_3)_2$, and the other microemulsion contained ammonium oxalate or oxalic acid as the precipitant. These metal oxalate particles of about 20 nm were readily calcined into single phase perovskite-type $BaPbO_3$, La_2CuO_4 and $LaNiO_3$. The calcinations required for the microemulsion-derived mixed oxalates were 100–250 °C below the temperatures used for the metal oxalates prepared by a conventional aqueous solution precipitation method.

4.2.5 Zirconia, Lead Zirconate and Lead Zirconate Titanate

Most zirconia nanoparticles have been prepared by the microemulsion-mediated alkoxide sol-gel method [156, 157] using zirconium tetrabutoxide as the alkoxide precursor. The first step is to synthesize zirconium hydroxide precursor particles via double inverse microemulsions and then they are calcined to zirconia [158]. Three types of processing routes have been used to prepare fine lead zirconate ($PbZrO_3$) powders: a conventional solid reaction, conventional coprecipitation using either oxalic acid or ammonia solution as the precipitant, and microemulsion-refined coprecipitation using either oxalic acid or ammonia solution. The microemulsion-derived precursors exhibited a much lower formation temperature for the orthorhombic $PbZrO_3$ phase [159] than that of the conventionally coprecipitating precursors. Ammonia solution appeared to be a better precipitant than oxalic acid for reducing the formation temperature of $PbZrO_3$. It was concluded that microemulsion-derived $PbZrO_3$

powders were much finer and has less particle-particle agglomeration. The synthesis of $PbZrO_3$ powders could also be performed via a polyaniline-mediated microemulsion process [160]. A small amount (~4 wt%) of polyaniline was retained in the microemulsion-derived oxalate precursor by an in situ polymerization of lead oxalate and zirconate oxalate. The in situ polymerization of aniline on the surfaces of the oxalate particles resulted in the formation of a well-dispersed precursor powder. Upon calcination at 800 °C, ultrafine lead zirconate powder was obtained.

Low temperature synthesis of lead zirconate titanate (PZT) can also be obtained via a microemulsion process [161]. The microemulsion, containing cations of lead zirconium and titanium in the aqueous phase, was coprecipitated as hydroxide precursors by the addition of ammonium solution. Crystalline tetragonal PZT powders were then obtained by calcining the precursors at a temperature as low as 450 °C in air without forming any intermediate phases.

4.2.6 Hydroxyapetite (HA)

Hydroxyapetite ($Ca_{10}(PO_4)_6(OH)_2$) is the major constituent of human bone and teeth. The strength of HA in almost all of its applications is largely determined by its specific surface area, and so a nanocrystalline HA powder is required.

Ultrafine HA powders can be produced by reacting $CaCl_2$ and $(NH_4)_2HPO_4$ in bicontinuous microemulsion, W/O microemulsion and emulsion, which have the same basic components of cyclohexane, nonionic surfactant (NP-5/NP-9) and aqueous solution [162]. HA powder particle size, chemical homogeneity, and the degree of particle agglomeration all depend on the reaction medium. Both bicontinuous and W/O microemulsions lead to the formation of much finer HA powders than those prepared from the emulsion composition. This is because the precipitates formed in both bicontinuous and W/O microemulsions are limited in size by the dimensions of the nano-sized reaction domains. In contrast, the aqueous droplets in the emulsion are much bigger, and therefore the HA particles obtained are twice as large as those formed in nano-sized domains. It was found that the specific surface area of the powder prepared by bicontinuous microemulsion was 86.03 m^2/g, 76.64 m^2/g by W/O microemulsion, and 42.63 m^2/g by emulsion. Much smaller degrees of particle agglomeration were observed for HA powders obtained by bicontinuous and W/O microemulsions, but the powders prepared from emulsion showed a larger average agglomerate size of 1.1 μm, which was twice the size observed from the former two.

A similar study was performed on the formation of nanocrystalline HA in nonionic surfactant emulsions [163]. Instead of using NP-5/NP-9 surfactant, KB6ZA (nonionic surfactant which is a lauryl alcohol condensed with an average of 6 mol of oxyethylene oxide) was used together with petroleum ether as the oil phase to prepare HA powder in an O/W emulsion system. One of the very apparent advantages of using O/W emulsion over W/O microemulsion is

the high production yield using smaller amounts of oil and surfactant. In this study, HA was prepared by reacting $CaCl_2$ and $(NH_4)_2HPO_4$ in three reaction systems: a conventional aqueous solution, a micellar solution containing 3.2 wt% of the nonionic surfactant KB6ZA and 1.0 M $CaCl_2$ solution, and O/W emulsions containing KB6ZA with varying amounts of petroleum ether and 1.0 M $CaCl_2$ solution. For the emulsion system, the oil phase residing in the hydrophobic cores of the oil-swollen micelles lead to a large expansion in the micellar dimensions, in the form of emulsion droplets. This undoubtedly increases the reaction sites between $CaCl_2$ and $(NH_4)_2HPO_4$ at the interfaces, as shown schematically in Fig. 19. Moreover, the emulsion droplets are more stable than the surfactant micelles and the average life-span of an emulsion droplet is much longer than that of a micelle. All of these factors make an emulsion system much more suitable than a micellar system for forming HA particles of high crystallinity. The enhanced crystallinity of HA derived from the emulsion composition derives from the complexation of Ca^{2+} by oxyethylene groups of the nonionic surfactant. The resulting HA precursor powders underwent little growth in crystallite and particle sizes upon calcination at 650 °C for 6 h.

4.2.7 PtRu/C Catalysts

PtRu alloys are currently the most active anode catalysts for the oxidation of methanol or CO-contaminated H_2, (like H_2 derived from reformed methanol) in low temperature solid polymer electrolyte fuel cells such as direct methanol fuel cells (DMFC) or indirect methanol fuel cells (IMFC). High surface area catalysts are generally prepared by co-impregnation,coprecipitation, absorbing alloy colloids, or surface organometallic chemistry techniques. For both alloy and oxide promoted catalytic systems it is important that Pt and the second metal (or metal oxide) are in intimate contact. This close association of the platinum and the co-catalyst can be difficult to achieve using conventional catalyst preparation techniques because the active components may be deposited at different sites on the support surface. As the preparation details control the final composition, surface structure and morphology of the catalysts, it is not surprising to learn that catalytic activity is strongly dependent on preparation conditions.

Nano-sized PtRu catalysts supported on carbon have been synthesized from inverse microemulsions and emulsions using H_2PtCl_6 (0.025 M)/$RuCl_3$ (0.025 M)/NaOH (0.025 M) as the aqueous phase, cyclohexane as the oil phase, and NP-5 or NP-9) as the surfactant, in the presence of carbon black suspended in a mixture of cyclohexane and NP-5+NP-9 [164]. The titration of 10% HCHO aqueous solution into the inverse microemulsions and emulsions resulted in the formation of PtRu/C catalysts with average particle sizes of about 5 nm and 20 nm respectively. The RuPt particles were identified by X-ray diffraction, X-ray photoelectron, and BET techniques. All of the catalysts prepared show characteristic diffraction peaks pertaining to the Pt fcc structure. XPS analysis

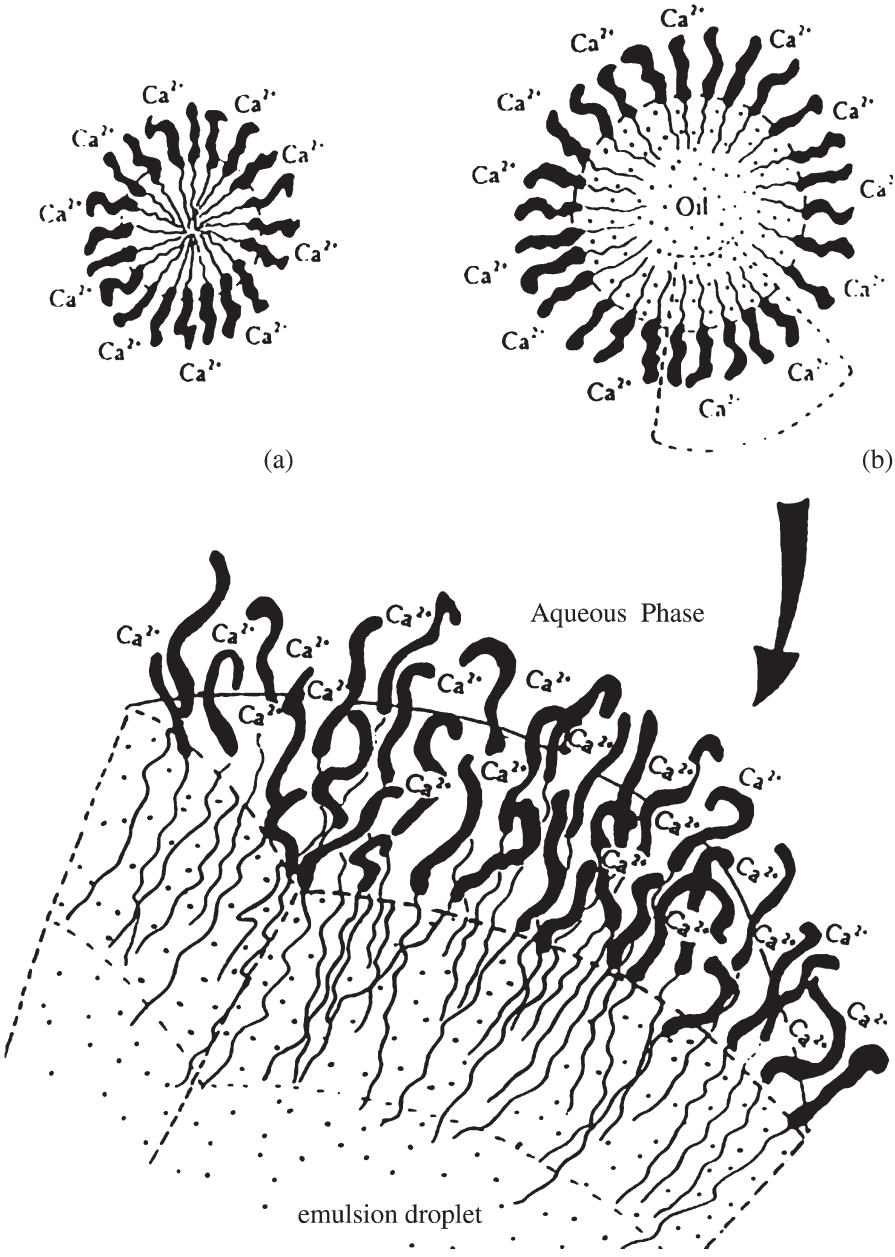

Fig. 19 Micelle and emulsion droplets in $CaCl_2$ aqueous solutions: The calcium-rich shell in the adsorbed state, at the: **a** micelle-water interface; **b** emulsion droplet surface. The surfactant molecules are represented by the zig-zag lines with Ca^{2+} heads

also revealed that the catalysts contained mostly Pt(0) and Ru(0), with a little Pt(II), Pt(IV) and Ru(IV). The double microemulsion-derived PtRu/C catalysts had higher electrocatalytic activities for methanol oxidation than that of the emulsion-derived PtRu/C electrocatalyst. The peak current density for methanol oxidation at PtRu/C obtained from the transparent inverse microemulsion was about four times higher that of the emulsion-derived PtRu/C.

4.2.8 Polymer-Coated Inorganic Nanoparticles

Nanoparticles of polyaniline/$BaSO_4$ composite, about 10–20 nm in diameter, have also been synthesized by mixing double inverse microemulsions that have some components of surfactant and oil, but different aqueous solutions [165]. The aqueous solution of one microemulsion should contain $BaCl_2$ and aniline, while the other contains $K_2S_2O_8$ and H_2SO_4. After mixing both microemulsions, nanoparticles of $BaSO_4$ are formed instantaneously with the subsequent polymerization of aniline on the surface of $BaSO_4$ particles, as verified by Rutherford backscattering measurements. The conductivity of the polyaniline/$BaSO_4$ nanocomposites increased almost linearly from 0.017 to 5 S/cm withincreasing polyaniline content in the composites (which was varied from 5 to 22 wt%). This result shows that a selection of double inverse microemulsion reactions for producing some nanocomposites of polymer/inorganic materials can be conveniently carried out by a single-step microemulsion process.

5 Conclusions

The synthesis of polymer nanomaterials by microemulsion processes is reaching maturity. Microlatexes of both hydrophilic and hydrophobic polymers can now be produced by semi-continuous microemulsion processes yielding high weight ratios of polymer to surfactant at a level attractive for to industry. However, the W/O microemulsion processes capable of producing inorganic nanomaterials with unique properties are not ready for large-scale production, because large amounts of surfactant are still needed. Bicontinuous microemulsion processes should be explored for inorganic nanomaterial production since they require lower amounts of surfactant and give higher yields.

The recent development of using polymerizable surfactants in microemulsion polymerizations has enabled the production of transparent solid polymers with some nanostructure. Randomly distributed bicontinuous nanostructures of water channels and polymer domains in solid polymers can be readily obtained from the polymerization of bicontinuous microemulsions consisting of various types of vinyl monomers and polymerizable surfactants with no allylic hydrogen.

These transparent polymers with inherent bicontinuous nanostructures may be suitable for nanofiltration, selective permeable membranes for sepa-

ration, or proton exchange membranes for fuel cell applications. The surface characteristics of the nanostructured membranes can be modified further using suitable functional monomers. New polymerizable microemulsion systems will be devised for specific copolymers and inorganic/polymer nanocomposites. Some tailor-made nanostructure polymeric materials may therefore be obtained by the polymerizable bicontinuous-microemulsion approach.

References

1. Zana R, Lang J (1987) In: Frieberg SE, Bothorel (eds) Microemulsions: structure and dynamics. CRC, Boca Raton, FL, Ch 6
2. Biasia J, Clin B, Laolanne P (1987) In: Friberg SE, Bothorel P (eds) Microemulsions: structure and dynamics. CRC, Boca Raton, FL, Ch 1
3. Frieberg SE, Bothorol P (1986) In: Friberg SE, Bothorel P (eds) Microemulsions: structure and dynamics. CRC, Boca Raton, FL
4. Winsor PA (1948) T Faraday Soc 44:376
5. Candau F (1999) In: Kumar P, Mittal KL (eds) Handbook of microemulsion science and technology. Marcel Dekker, New York, Ch 22, p 679
6. Gan LM, Chew CH (2001) In: Nalwa HS (ed) Advanced functional molecules and polymers. Gordon and Breach, New York, Ch 2, p 35
7. (a) Lopez-Quintela MA, Rivas J (1993) J Colloid Interf Sci 158:446; (b) Aikawa K, Kaneko K, Tamura T, Fujitsu M, Ohbu K (1999) Colloids Surface A 150:95; (c) Zarur AJ, Ying JY (2000) Nature 403:65; (d) Rymes J, Ehret G, Hilaire L, Boutonnet M, Jiratova K (2002) Catal Today 75:297
8. Klier J, Tucker CJ, Kalantar TH, Green DP (2000) Adv Mater 18:1751
9. Gan LM, Chew CH (1996) In: Salamone (ed) Polymeric materials encyclopedia. CRC, Boca Raton, FL, M4321
10. Candau F (1992) In: Paleos CM (ed) Polymerization in organized media. Gordon and Breach, New York, p 215
11. Candau F (1998) In: Kumar P, Mittal KL (eds) Microemulsions: fundamental and applied aspects. Marcel Dekker, New York
12. Herrera JR, Peralta RD, Lopez RG, Cesteros LC, Puig JE (2003) Polymer 44:1795
13. Candau F, Leong YS, Pouyet G, Candau SJ (1984) J Colloid Interf Sci 101:167
14. Candau F, Yong YS, Fitch RM (1985) J Polym Sci Pol Chem 23:193
15. Candau F (1987) In: Mark H, Bikales NM, Overberger CG, Menges G (eds) Encyclopedia of polymer science and engineering. Wiley, New York, 9:718
16. Vaskova V, Juranicova V, Barton J (1990) Makromol Chem 191:717
17. Vaskova V, Hlouskova Z, Barton J, Juranicova V (1990) Makromol Chem 193:267
18. Lezovic M, Ogino K, Sato H, Capek I, Barton J (1998) Polymer Int 46:269
19. Barton J, Kawamoto S, Fujimoto K, Kawaguchi H, Capek I (2000) Polymer Int 49:358
20. Barton J, Capek I (2000) Macromolecules 33:5353
21. Candau F (1989) In: El-Nokaly M (ed) ACS Sym Ser 384, Ch 4
22. Canadu F, Anquetil JY (1998) In: Shah DO (ed) Micelles, microemulsions and monolayers. Marcel Dekker, New York, p 193
23. Candau F, Zekhnini Z, Durand JP (1987) Prog Colloid Polym Sci 73:33
24. Corpart JM, Candau F (1993) Colloid Polym Sci 271:1055
25. Corpart JM, Selb J, Candau F (1993) Polymer 34:3873
26. Candau F, Buchert P (1990) Colloids Surface 48:107
27. Candau F, Pabon M, Anqueti (1999) Colloids Surface A 153:47

28. Sosa N, Peralta RD, Lopez RG, Ramos LF, Katine I, Certeros C, Mendizabal E, Puig JE (2001) Polymer 42:6923
29. Braun O, Selb J, Candau F (2001) Polymer 42:8499
30. Candau F, Braun O, Essler F, Stahler K, Selb J (2002) Macromol Symp 179:13
31. Stoffer JO, Bone T (1980) J Disper Sci Technol 1:37
32. Atik SS, Thomas JK (1981) J Am Chem Soc 103:4279
33. Tang HI, Johnson PL, Gulari E (1984) Polymer 25:1357
34. Kuo PL, Turro NJ, Tseng CM, El-Aasser MS, Vanderhoft JW (1987) Macromolecules 20:1216
35. Feng L, Ng KY (1990) Macromolecules 23:1048
36. Gan LM, Chew CH, Lye I (1992) Makromol Chem 193:1249
37. Gan LM, Chew CH, Frieberg SE (1983) J Macromol Sci Chem A 19:739
38. Ferrick MR, Murtagh J, Thomas JK (1989) Macromolecules 22:1515
39. Antonietti M, Bremser W, Muschenborn D, Rosenaur C, Schupp B, Schmidt M (1991) Macromolecules 24:6636
40. Rodriguez-Guadarrama LA, Mendizabal E, Puig JE, Kaler EW (1993) J Appl Polym Sci 48:775
41. Gan LM, Chew CH, Ng SC, Loh SE (1993) Langmuir 9:2799
42. Gan LM, Chew CH, Lee KC, Ng SC (1993) Polymer 34:3064
43. Larpent C, Tados RF (1991) Colloid Polym Sci 269:1171
44. Full AP, Puig JE, Gron LU, Kaler EW, Minter JR, Meurey TH, Texter J (1992) Macromolecules 25:5157
45. Capek I, Potisk P (1995) Eur Polym J 31:1269
46. Capek I, Fouassier JP (1997) Eur Polym J 33:173
47. Capek I, Juranicova V (1996) J Polym Sci Pol Chem 34:575
48. Capek I, Juranicova V, Barton J, Asua JM, Ito K (1997) Polymer Int 43:1
49. Guo JS, Sudol ED, Vanderhoff JW, El-Aasser MS (1992) J Polym Sci Pol Chem 30:691
50. Puig JE, Perez-Luna VH, Macias ER, Rodriguez BE, Kaler EW (1993) Colloid Polym Sci 271:114
51. Co CC, Cotts P, Burauer S, deVries R, Kaler EW (2001) Macromolecules 34:3245
52. Kukulj D, Davis TP, Gilbert RG (1998) Macromolecules 31:994
53. Hentze HP, Kaler EW (2003) Curr Opin Coll Interf Sci 8(2):164–178
54. Mendizabal E, Flores J, Puig JE, Katime I, Lopez-Serrano F, Alvarez J (2000) Macromol Chem Phys 201:1259
55. Co CC, Kaler EW (1998) Macromolecules 31:3203
56. Morgan JD, Kaler EW (1998) Macromolecules 31:3197
57. Sanghvi PG, Pokhriyal NK, Devis (2002) J Appl Polym Sci 84:1832
58. Gan LM, Chew CH, Lee KC, Ng SC (1994) Polymer 35:2659
59. Loh SE, Gan LM, Chew CH, Ng SC (1995) J Macromol Sci Pure A32:1681
60. Gan LM, Lee KC, Chew CH, Tok ES, Ng SC (1995) J Polym Sci Pol Chem 33:1161
61. Sutterline N, Kurth HJ, Markett G (1976) Angew Makromol Chem 177:1549
62. Aguiar A, Gonzales-Villegas S, Rabelero M, Mendizabal E, Puig JE (1999) Macromolecules 32:6767
63. Jang J, Ha H (2002) Langmuir 18:5613
64. Jang J, Lee K (2002) Chem Comm 1098
65. Gan LM, Lian N, Chew CH, Li GZ (1994) Langmuir 10:2197
66. Xu XJ, Siow KS, Wong MK, Gan LM (2001) Langmuir 17:4519
67. Ming W, Jones FN, Fu SK (1998) Polym Bull 40:749
68. Ming W, Jones FN, Fu SK (1998) Macromol Chem Phys 199:1075
69. (a) Xu XJ, Chew CH, Siow KS, Wong MK, Gan LM (1999) Langmuir 15:8067; (b) Chudej J, Capek I (2002) Polymer 43:1681

70. Dan Y, Yang YH, Chen SY (2002) J Polym Sci 85:2839
71. Barrere M, Silva SC, Balic R, Ganachaud F (2002) Langmuir 18:941
72. Xu XJ, Chow PY, Quek CH, Hng HH, Gan LM (2003) J Nanosci Nanotechno 3:3
73. Xu XJ, Siow KS, Wong MK, Gan LM (2001) Colloid Polym Sci 279:879
74. Xu XJ, Siow KS, Wong MK, Gan LM (2001) J Polym Sci Polym Chem 39:1634
75. Xu XY, Chow PY, Gan LM (2001) J Nanosci Nanotechno (in press)
76. Menger FM, Tsuno T, Hammond GS (1990) J Am Chem Soc 112:1263
77. Sáenz de Buruaga A, Capek I, de la Cal JC, Asua JM (1998) J Polym Sci Pol Chem 36:737
78. Antonietti M, Basten R, Gröhn F (1994) Langmuir 10:2498
79. Puig JE, Aguiar A, González-Villegas S (1999) Macromolecules 32:6767
80. Kaler EW, Co CC, de Vries R (2001) Macromolecules 34:3224
81. Kaler EW, Co CC, de Vries R (2001) Macromolecules 34:3233
82. Palani Raj WR, Sathav M, Cheung HM (1991) Langmuir 7:2586
83. Sasthav M, Cheung HM (1991) Langmuir 7:1378
84. Strey R, Lade O, Beizai K, Sottmann T (2000) Langmuir 16:4122
85. Gan LM, Chew CH (1983) J Disper Sci Technol 4:291
86. Palani Raj WR, Sasthav M, Cheung HM (1992) Langmuir 8:1931
87. Gan LM, Li TD, Chew CH, Teo WK (1995) Langmuir 11:3316
88. Gan LM, Li TD, Chew CH, Teo WK,Gan LH (1996) Langmuir 12:5863
89. Antonietti M, Hentze HP (1996) Colloid Polym Sci 274:696
90. Gan LM,Chieng TH, Chew CH, Ng SC, Pey KL (1996) Langmuir 12:319
91. (a) Gan LM, Li TD, Chew CH, Quek CH, Gan LH (1998) Langmuir 14:6068; (b) Guyot A, Tauer K (1994) Adv Polym Sci 111:44
92. Gan LM, Chieng TH, Chew CH, Teo WK, Gan LH (1996) Langmuir 10:4022
93. Liu J, Gan LM, Chew CH, Teo WK, Gan LH (1997) Langmuir 13:6421
94. Gan LM, Chow PY, Chew CH, Ong CL, Wang J, Xu G (1999) Langmuir 15:3202
95. Xu G, Ong CL, Gan LM, Ong CK, Chan HSO (1999) J Phys Chem B 10: 7573
96. Gan LM, Xu W, Siow KS, Gao Z, Lee SY, Chow PY (1999) Langmuir 15: 4812
97. Gan LM, Chow PY, Han M, Liu ZL, Yeo E (2002) In: Proc 1st Int Conf on Materials Processing for Properties and Performance, Singapore, 1–3 August 2002
98. Moy HY, Chow PY, Yu WL, Wong KMC, Yam VWW, Gan LM (2002) Chem Comm 9:982
99. Bonini M, Bardi U, Berti D, Neto C, Baglioni P (2002) J Phys Chem B 106:6178
100. Chow PY (2002) PhD Thesis, National University of Singapore, Singapore (to be published)
101. Chow PY, Gan LM (2003) J Nanosci Nanotechno 4(1–2):197–202
102. Donescu D, Fusulan L, Petcu C, Vasilescu M, Deleann C. Udrea S (2002) Macromol Symp 179:315
103. Liu B, Li HP, Chew CH, Que WX, Lam YL, Kam CH, Gan LM, Xu GQ (2001) Mater Lett 51:461
104. Quek CH, Gan LM (work to be published)
105. Andreas RP, Averback RS, Brown WL, Brus LE, Goddard III WA, Kaldor A, Louie SG, Moskovits M, Peercy PS, Riley SJ, Siegel RW, Spaepen F, Wang Y (1989) J Mater Res 4:704
106. Ichinose N, Ozaki Y, Kashu S (1988) Superfine particle technology. Springer, Berlin Heidelberg New York
107. Haruta M, Delmon B (1986) J Chem Phys 83:859
108. Brinker CJ, Scherer GW (1990) In: Sol-gel science. Academic, New York
109. Lianos P, Thomas JK (1986) Chem Phys Lett 125:299
110. Lianos P, Thomas JK (1987) J Colloid Interf Sci 125:505
111. Barnickel P, Wokaun A, Sager W, Eicke HF (1992) J Colloid Interf Sci 148:80
112. Petit C, Jain TK, Billoudet F, Pileni MP (1994) Langmuir 10:4446

113. Pileni MP (1993) Adv Colloid Interf Sci 46:139
114. Pileni MP (2003) Nat Mater 2:145
115. Inouye K, Endo R, Otsuka Y, Miyashiro K, Kaneko K, Ishikawa T (1982) J Phys Chem 86:1465
116. Fendler JH (1987) Chem Rev 87:877
117. Matson DW, Fulton JL, Smith RD (1987) Mater Lett 6:31
118. Bandow S, Kimura K, Kon-on K, Kitahara A (1987) Jpn J Appl Phys 26:713
119. Kandori K, Shizuka N, Gobe M, Kon-on K, Kitahara A (1987) J Disper Sci Technol 8:477
120. Hou MJ, Shah DO (1988) Interfacial phenomena in biology and materials processing. Elsevier, Amsterdam, p 443
121. Nagy JB (1989) Colloids Surface 35:201
122. Pillai V, Kumar P, Hou MJ, Ayyub P, Shah DO (1995) Adv Colloid Interf Sci 55:241
123. O'Sullivan EC, Patel RC, Ward AJI (1991) J Colloid Interf Sci 146:58
124. Friberg SE, Yang CC, Sjoblom J (1992) Langmuir 8:372
125. Friberg SE, Jones SM, Yang CC, Sjoblom J (1992) J Disper Sci Technol 13:65
126. Jones SM, Friberg SE (1992) J Disper Sci Technol 13:669
127. Pileni MP (1993) J Phys Chem 97:6961
128. O'Sullivan EC, Ward AJI, Budd T (1994) Langmuir 10:2985
129. Gan LM, Zhang K, Chew CH (1996) Colloid Surface A 110:199
130. Chabra V, Ayyub P, Chattopadhyay S, Maitra AN (1996) Mater Lett 26:21
131. Fang JY, Wang J, Ng SC, Chew CH, Gan LM (1997) Nanostruct Mater 8:499
132. Liu XY, Wang J, Gan LM, Ng SC, Ding J (1998) J Magn Magn Mater 184:344
133. Adair JH, Li T, Kido T, Havey K, Moon J, Mecholsky J, Morrone A, Talham DR, Ludwig MN, Wang L (1998) Mater Sci Eng R23:139
134. Zhang K, Chew CH, Xu GQ, Wang J, LM Gan (1999) Langmuir 15:3056
135. Zhang K, Chew CH, Kawi S, Wang J, Gan LM (2000) Catal Lett 64:179
136. Liu SH, Qian XF, Yin J, Ma XD, Yuan JY, Zhu ZK (2003) J Phys Chem Solid 64:455
137. Wang DB, Yu DB, Mo MS, Liu XM, Qian YT (2003) Solid State Commun 125:475
138. Tata M, Banerjee S, John VT, Waguespack Y, McPhersond GL (1997) Colloid Surface A 127:39
139. Li HP, Liu B, Kam CH, Lam YL, Que WX, Gan LM, Chew CH, Xu GQ (2000) Opt Mater 14:321
140. Fu XA, Qutubuddin S (2001) Colloid Surface A 179:65
141. Liu B, Xu GQ, Gan LM, Chew CH, Li WS, Shen ZX (2001) J Appl Phys 89:1059
142. Liu B, Chew CH, Gan LM, Xu GQ, Li HP, Lam YL, Kam CH, Que WX (2001) J Mater Res 16:1644
143. Gan LM, Liu B, Chew CH, Xu SJ, Chua SJ, Loy GL, Xu GQ (1997) Langmuir 13:6427
144. Yee KL (1998) Masters Thesis, National University of Singapore, Singapore
145. Liu XY, Wang J, Gan LM, Ng SC, Ding J (1998) J Magn Magn Mater 184:344
146. Frieberg SE, Jones SM, Sjoblom J (1994) J Mater Synth Proces 2:1994
147. Jones SM, Frieberg SE (1995) J Non-Cryst Solids 181:39
148. Chang CL, Fogler HS (1996) AICHE J 42:3153
149. Chang CL, Fogler HS (1997) Langmuir 13:3295
150. Arriagada FJ, Osseo-Asare K (1992) Colloid Surface 69:105
151. Arriagada FJ, Osseo-Asare K (1995) J Colloid Interf Sci 170:8
152. Gan LM, Zhang K, Chew CH (1996) Colloid Surface A 110:199
153. Zhang K, Gan LM, Chew CH, Gan LH (1997) Mater Chem Phys 47:164
154. Schlag S, Eicke H-F, Mathys D, Guggenheim R (1994) Langmuir 10:3357
155. LM Gan, Zhang LH, Chan HSO, Chew CH, Loo BH (1996) J Mater Sci 31:1071
156. Kusakabe K, Yamaki T, Maeda H, Morooka S (1993) ACS Prepr 38:352

157. Kawai T, Fujino A, Kon-no K (1996) Colloid Surface 109:245
158. Wang J, Ee LS, Ng SC, Chew CH, Gan LM (1997) Mater Lett 30:119
159. Fang J, Wang J, Ng SC, Gan LM, Chew CH (1998) Ceram Int 24:507
160. Fang J, Wang J, Ng SC, Gan LM, Quek CH, Chew CH (1998) Mater Lett 36:179
161. Ee LS, Wang, Ng SC, Gan LM (1998) Mater Res Bull 33:1045
162. Lim GK, Wang J, Ng SC, Chew CH, Gan LM (1997) Biomaterials 18:1433
163. Lim GK, Wang J, Ng SC, Gan LM (1999) Langmuir 15:7472
164. Liu ZL, Lee JY, Han M, Chen WX, Gan LM (2002) J Mater Chem 12:2453
165. Gan LM, Zhang LH, Chan HSO, Chew CH (1995) Mater Chem Phys 40:94

Received: September 2003

Adv Polym Sci (2005) 175: 299–328
DOI 10.1007/b100118

Dispersion Polymerization

Seigou Kawaguchi (✉)[1] · Koichi Ito[2]

[1] Department of Polymer Science and Engineering, Faculty of Engineering, Yamagata University, 4–3–16 Jonan, 992–8510 Yonezawa, Japan
skawagu@yz.yamagata-u.ac.jp
[2] Department of Materials Science, Toyohashi University of Technology, 1–1 Tempaku-cho, 441–8580 Toyohashi, Japan
itoh@tutms.tut.ac.jp

Abstract Dispersion polymerization is an attractive method for producing micron-size monodisperse polymer particles in a single batch process. Great progress in this field has been achieved over the past two decades. This article presents an overview of the recent progress in the preparation of polymeric microspheres via dispersion polymerization in organic media, focusing on the preparation of novel functional particles, the design of microspheres using macromonomers, and on understanding mechanisms for the control of particle size. Examples of functional microspheres obtained by dispersion polymerization in the presence of linear polymers, block polymers, and macromonomers are tabulated, and new developments are highlighted. Particle size control in dispersion polymerization in the presence of macromonomers is discussed, and experimental results for poly(ethylene oxide)-grafted particles are compared with theoretical expectations for ideal core-shell particles.

Keywords Functional microsphere · Macromonomer · Block copolymer · Graft copolymer · Particle size control

Symbols and Abbreviations

AIBN	2,2′-azobisisobutyronitrile
AAm	acrylamide
ATR	attenuated total reflection
BMA	*n*-butyl methacrylate
Boc-AMST	boc-*p*-aminostyrene
CMS	chloromethylstyrene
C_s	chain transfer constant
D	mean separation between PEO anchor points
DSM	dynamic swelling method
DVB	divinylbenzene
EDMA	ethylene dimethacrylate
EG	ethylene glycol
ESCA	electron spectroscopy
f	initiator efficiency
FTIR	Fourier transform infrared spectroscopy
GMA	glycidyl methacrylate
GTP	group transfer polymerization
HEMA	2-hydroxyethyl methacrylate
HLB	hydrophobic-lipophilic-balance
HPC	hydroxypropylcellulose
HPMA	2-hydroxypropyl methacrylate
$[I]_o$	initiator concentration
k_d	decomposition rate constant
k_p	propagation rate constant
k_t	termination rate constant
k_2	diffusion-controlled rate constant for coalescence between similar-sized particles
M_D	molecular weight of macromonomer
MMA	methyl methacrylate
MW	molecular weight
M_w	weight average molecular weight
N	number of particles per liter
n	number of chains grafted onto surface
N_A	Avogadro's number
NAD	nonaqueous dispersion
NIPAM	*N*-isopropyl methacrylate
NMR	nuclear magnetic resonance
NVC	*N*-vinyl carbazole
PAA	poly(acrylic acid)
PANI	polyaniline
PB	poly(1,3-butadiene)
PBMA	poly(*n*-butyl methacrylate)
PCL	poly(ε-caprolactone)
PDMAEMA	poly(2-(dimethylamino)ethyl methacrylate
PDMS	poly(dimethylsiloxane)
PDVB	polydivinylbenezene
PE	polyethylene
PEG	poly(ethylene glycol)
PEO	poly(ethylene oxide)

PGMA	poly(glycidyl methacrylate)
PHEM	Apoly(2-hydroxyethyl methacrylate)
PHSA	poly(12-hydroxystearic acid)
PIB	polyisobutylene
PLMA	poly(lauryl methacrylate)
PMA	poly(methacrylic acid)
PMMA	poly(methyl methacrylate)
PNIPAM	poly(*N*-isopropylacrylamide)
POXZ	polyoxazolines
PP	polypropylene
PS	polystyrene
P(PP-*alt*-E)	poly(propylene-*alt*-ethylene)
PTBA	poly(*t*-butyl acrylate)
PTBMA	poly(*t*-butyl methacrylate)
PVA	poly(vinyl alcohol)
PVAcA	poly(*N*-vinylacetamide)
PVME	poly(vinyl methyl ether)
PVP	poly(vinylpyrrolidone)
P4VP	poly(4-vinylpyridine)
r_i	reactivity ratio of *i* species
R	radius of particle
ρ	density
S	surface area occupied by a dispersant chain
ST	styrene
$<S^2>$	mean square radius of gyration
S_{crit}	surface area occupied by a macromonomer chain at critical point
TDI	toluene diisocyanate
TEMPO	2,2,6,6-tetramethylpiperidinyloxyl
4VBAC	4-vinylbenzyltrimethylammonium chloride
4VP	4-vinylpyridine
Vpy	vinylpyrrolidone
θ	fractional conversion of monomer
θ_{crit}	fractional conversion of monomer at critical point
θ_D	fractional conversion of macromonomer
θ_{Dcrit}	fractional conversion of macromonomer at critical point
W_D	weight of polymerized macromonomer
W_{Do}	initial weight of macromonomer
W	weight of polymerized monomer
W_o	initial weight of monomer

1 Introduction

Micron-size monodisperse polymeric microspheres are used in a wide variety of applications, such as toners, instrument calibration standards, column packing materials for chromatography, spacers for liquid crystal displays, and biomedical and biochemical analysis [1–3]. Because of the commercial and scientific interest in these particles, research into their preparation has been active

for the past two decades. Micron-size monodisperse particles were usually difficult to obtain because this size is in-between the diameter range of particles produced by conventional emulsion polymerization (0.06–0.7 μm) in a batch process and suspension polymerization (50–1000 μm). Vanderhoff et al. [4, 5] used the successive seeding method to obtain micron-size monodisperse polymer particles. The particles were also prepared by Ugelstad et al. [6, 7] by means of the two-stage swelling method. Omi et al. [8] and Kamiyama [9] used modified suspension polymerizations, and Okubo et al. [10] developed the dynamic monomer swelling method (DSM).

Dispersion polymerization is an attractive and promising alternative to other polymerization methods that affords micron-size monodisperse particles in a single batch process. Dispersion polymerization may be defined as a type of precipitation polymerization in which one carries out the polymerization of a monomer in the presence of a suitable polymeric stabilizer soluble in the reaction medium. The solvent selected as the reaction medium is a good solvent for both the monomer and the steric stabilizer polymers, but a non-solvent for the polymer being formed. Dispersion polymerization, therefore, involves a homogeneous solution of monomer(s) with initiator and dispersant, in which sterically stabilized polymer particles are formed by the precipitation of the resulting polymers. As a continuous medium, the properties of the solvent also change with increasing monomer conversion. Under favorable circumstances, the polymerization can yield, in a batch step, polymer particles of 0.1–15 μm in diameter, often of excellent monodispersity. This dispersant polymer can be formed as a reactive, polymerizable macromonomer. It can be a block copolymer in which one block has an affinity for the surface of the precipitated polymer, or it can be a soluble polymer (a "stabilizer precursor") to which grafting is thought to occur during the polymerization reaction. In all instances, this soluble dispersant polymer – a hairy layer – plays a crucial role in the dispersion polymerization process. By adsorbing or becoming incorporated onto the surface of the newly-formed precipitated polymers, it acts as a steric stabilizer, directing the particle size and colloidal stability of the system. This feature of dispersion polymerization is widely appreciated and well understood (Fig. 1).

Dispersion polymerization in organic hydrocarbon media was first developed by Osmond and coworkers at ICI [11]. They polymerized acrylic and vinylic monomers in hydrocarbons with oil soluble polymer stabilizers to produce nonaqueous dispersions (NAD) of polymer particles. Later, Almog et al. [12] extended the concept to dispersion polymerization in polar solvents as a method of forming monodisperse polymeric microspheres. Ober et al. [13–16], Tseng et al. [17], Okubo et al. [18, 19], and Paine et al. [20–24], among other authors, studied this technique in order to control particle size and achieve a narrow particle size distribution. A great deal of research has been devoted to dispersion polymerization during past two decades, as reviewed by Croucher and Winnik [25], Guyot and Tauer [26], Cawse [27], Pichot et al. [28], Asua and Schoonbrood [29], and Ito et al. [30–32]. The present article is intended to discuss state-of-the-art design of microspheres obtained by dis-

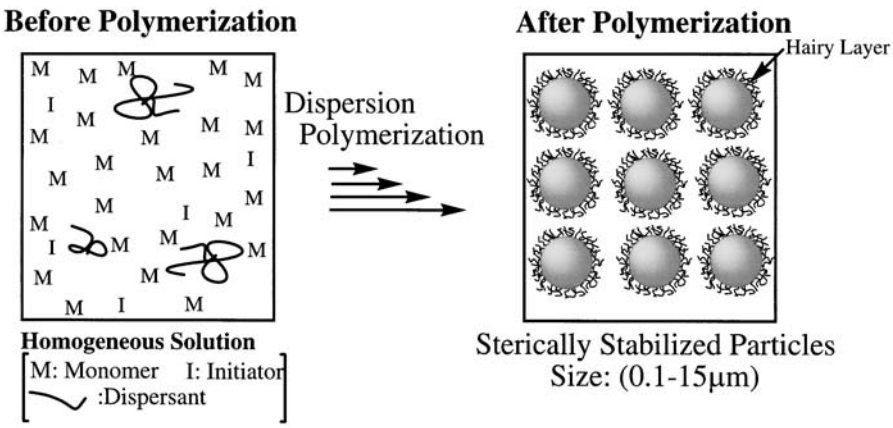

Fig. 1 Schematic description of dispersion polymerization

persion polymerization, with particular attention paid to the preparation of novel functional particles, the design of microspheres using the macromonomer technique, and to mechanistic aspects for particle size control.

2
Microsphere Syntheses by Linear and Block Polymer Dispersants

2.1
Functional Microspheres

Most research into the study of dispersion polymerization involves common vinyl monomers such as styrene, (meth)acrylates, and their copolymers with stabilizers like polyvinylpyrrolidone (PVP) [33–40], poly(acrylic acid) (PAA) [18, 41], poly(methacrylic acid) [42], or hydroxypropylcellulose (HPC) [43, 44] in polar media (usually alcohols). However, dispersion polymerization is also used widely to prepare functional microspheres in different media [45, 46]. Some recent examples of these preparations include the (co-)polymerization of 2-hydroxyethyl methacrylate (HEMA) [47, 48], 4-vinylpyridine (4VP) [49], glycidyl methacrylate (GMA) [50–53], acrylamide (AAm) [54, 55], chloromethylstyrene (CMS) [56, 57], vinylpyrrolidone (VPy) [58], Boc-*p*-aminostyrene (Boc-AMST) [59], and *N*-vinyl carbazole (NVC) [60] (Table 1). Dispersion polymerization is usually carried out in organic liquids such as alcohols and cyclohexane, or mixed solvent-nonsolvents such as 2-butanol-toluene, alcohol-toluene, DMF-toluene, DMF-methanol, and ethanol-DMSO. In addition to conventional PVP, PAA, and PHC as dispersant, poly(vinyl methyl ether) (PVME) [54], partially hydrolyzed poly(vinyl alcohol) (hydrolysis=35%) [61], and poly(2-(dimethylamino)ethyl methacrylate-*b*-butyl methacrylate)

Table 1 Examples of functional microspheres obtained by dispersion polymerization

Stabilizer	Monomer(s)	Medium	Reference
Functional particles			
PS, PMMA derivatives	HEMA	2-Butanol/toluene	[47]
Cellulose acetate butyrate	HEMA	Alcohol/toluene	[48]
PS-*b*-PB	4VP	DMF/toluene	[49]
PVP	GMA	MeOH/water or DMF	[50]
PVP	GMA/DVB	Ethanol	[51]
PVP	ST/GMA	Ethanol/water	[52]
Cellulose acetate	GMA	DMF/methanol	[53]
PVME	AAm	*t*-BuOH/water	[54]
None	AAm	*t*-BuOH/water	[55]
PVP	CMS	Ethanol/DMSO	[56]
PAA	CMS	Methoxyethanol/MeOH	[57]
PS-*b*-P(PP-*alt*-E)	VPy/EDMA	Cyclohexane	[58]
PVP	ST/Boc-AMST	*i*-Propanol	[59]
PVP	ST/NVC	Ethanol	[60]
PVA-*co*-PVAc	ST	Methanol	[61]
PDMAEMA-*b*-PBMA	ST	Alcohols	[62]
Hybrid particles			
Poly(amic acid)	ST/4VBAC	Ethanol/water	[63]
PVP	ST/polyimide prepolymer	*i*-Propanol	[64]
PVP	GMA/iron oxide	Alcohol/water	[65]
Cellulose acetate butyrate	HEMA/EDMA/iron oxide	Alcohol/toluene	[66]
PVP	HEMA/GMA/iron oxide	Alcohol/toluene	[67]
PVP	ST/SiO_2	Ethanol/water	[68]
None	4VP/HPMA/SiO_2	Water	[69]
Crosslinked particles			
PVP	DVB	Acetonitrile or Ethanol	[70]
None	DVB	Acetonitrile	[71]
None	DVB/CMS	Acetonitrile	[72]
Chitosan	NIPAM	Acetic Acid	[73]
PS-*b*-P(PP-*alt*-E)	Oxazoline methacrylate	Heptane	[74]
PVP-Aerosol-OT	ST/urethane acrylate	Ethanol	[75]
PVP	ST/2,2′-oxy-bisethanol diacrylate	Ethanol/heptane	[76]
PVP	MMA/EDMA	Ethanol/water	[77]
Dynamic swelling method (DSM)			
None	ST/DVB	Ethanol/water	[10, 78–83]

(PDMAEMA-*b*-PBMA) [62] in alcohols and polystyrene-*b*-polybutadiene (PS-*b*-PB) [49] and polystyrene-*b*-poly(propyrene-*alt*- ethylene) (PS-*b*-(PP-*alt*-E)) [58], linear PS [47], and PMMA [47] in hydrocarbon are used.

Dispersion polymerization in supercritical carbon dioxide ($scCO_2$), pioneered by DeSimone and coworkers, has recently attracted considerable attention as an environmentally friendly alternative to the use of organic solvents. A wide range of monomers have been polymerized to produce the corresponding microspheres in the presence of CO_2-philic polymers and monomers, as reviewed in another chapter.

Core-shell polystyrene-polyimide high performance particles have been successfully prepared by the dispersion copolymerization of styrene with vinylbenzyltrimethyl ammonium chloride (VBAC) in an ethanol-water medium using an aromatic poly(amic acid) as stabilizer, followed by imidization with acetic anhydride [63]. Micron-sized monodisperse polystyrene spheres impregnated with polyimide prepolymer have also been prepared by the conventional dispersion polymerization of styrene in a mixed solvent of isopropanol/2-methoxyethanol in the presence of L-ascorbic acid as an antioxidant [64].

A recent interesting example is the preparation of organic/inorganic hybrid particles by dispersion polymerization. Horák et al. [65–67] have prepared cross-linked poly(2-hydroxyethyl methacrylate) (PHEMA)- and poly(glycidyl methacrylate) (PGMA)-based magnetic microspheres by incorporating iron oxide into cellulose acetate butyrate stabilizer or PVP. Polymer encapsulation of small silica particles has also been achieved using the dispersion polymerization of styrene in ethanol-water medium with PVP [68]. Silica-polymer hybrid particles have also been prepared very recently by the precipitation copolymerization of 4-vinylpyridine with 2-hydroxypropyl methacrylate (HPMA) in water [69]. These organic/inorganic hybrid particles would be expected to lead to a new generation of nanostructured materials with diverse applications such as catalysts, electronic or phonic devices, and sensors.

Highly cross-linked monodisperse polydivinylbenzene (PDVB) microspheres have been prepared in acetonitrile with or without PVP stabilizer [70–72]. Interestingly, PDVB microspheres are very stable without any stabilizer in acetonitrile, possibly due to their highly crosslinking rigid surface. Other examples of the syntheses of crosslinked microspheres [73–77] are listed in Table 1.

The dynamic swelling method (DSM) [10] has also been described for the preparation of crosslinked microspheres with free vinyl groups [78]. Therefore, polystyrene seed particles (1.9 μm) prepared by dispersion polymerization are dispersed in ethanol-water (7/3, w/w) containing divinylbenzene (DVB), benzoyl peroxide, and poly(vinyl alcohol) (PVA). The slow drop-wise addition of water to the mixture causes the DVB phase to separate, and it is continuously imbibed by seed particles to produce relatively large swollen particles (4.3 μm), which are then polymerized to afford the respective PS-PDVB composite particles with free vinyl groups. DSM has recently been developed in order to prepare hollow microspheres and various oddly-shaped polymer particles, including a rugby ball, red blood cells, or snowman structures [79–83].

2.2 Living Dispersion Polymerization

Living dispersion (co-) polymerization is interesting due to its straightforward control of molecular weight with a narrow distribution, and also the functionalization of living end groups that occurs. Living anionic dispersion polymerization of styrene or α-methylstyrene has been achieved in hydrocarbon solvents with block copolymer stabilizers such as PS-*b*-poly(4-trimethylsilylstyrene) [84], PS-*b*-PB [85–87], PS-*b*-poly(4-*tert*-butylstyrene) [88, 89], poly(vinyl ethyl ether) [90], and PS-*b*-polyisobutylene (PS-*b*-PIB) [91], and PS-*b*-P(PP-*alt*-E) [92]. Jenkins and coworkers [93] polymerized methyl methacrylate in *n*-heptane via group transfer polymerization (GTP). Highly crosslinked microspheres have also been prepared by the living anionic copolymerization of *t*-butylstyrene and divinylbenzene in heptane [94].

Living radical dispersion polymerization is a promising way to expand the design and scope of functional polymer colloids to a wider range of other monomers. The 2,2,6,6-tetramethyl-1-piperidinyloxy (TEMPO)-mediated living radical dispersion polymerization of styrene has been carried out in presence of PS-*b*-P(PP-*alt*-E) in decane at 135 °C [95] or PVP in alcohol-water at 130 °C [96] in order to produce microspheres with a very broad size distribution, consisting of relatively low molecular weight polystyrene (M_w=10^4) with M_w/M_n=1.1.

Table 2 Examples of microspheres obtained by living dispersion polymerization

Stabilizer	Monomer	Medium	Reference
Living anionic dispersion polymerization			
PS-poly(4-trimethylsilylstyrene)	ST	Hexane	[84]
PS-*b*-PB	ST	Hexane	[85, 86]
None	ST/butadiene	Pentane	[87]
PS-*b*-Poly(4-*tert*-butylstyrene)	ST	Hexane	[88, 89]
Poly(vinyl ethyl ether)	α-methylstyrene	Heptane	[90]
PS-*b*-PIB	ST	Hexane	[91]
PS-*b*-P(PP-*alt*-E)	ST	Hydrocarbon	[92]
PS-*b*-P(PP-*alt*-E)	MMA	Heptane	[93]
None	*t*-butylstyrene/DVB	Heptane	[94]
Living radical dispersion polymerization			
PS-*b*-P(PP-*alt*-E)	ST	Decane	[95]
PVP	ST	Alcohol/water	[96]
Ring opening dispersion polymerization			
Poly(dodecyl methacrylate)-*g*-poly(ε-caprolactone)	ε-caprolactone and lactide	Heptane/dioxane	[97,98]

Dispersion polymerization has also been applied to the ring opening polymerization of ε-caprolactone and lactide in heptane-dioxane (4/1 v/v) with poly(dodecyl methacrylate)-*g*-poly(ε-caprolactone) as stabilizer [97]. Diethylaluminium ethoxide and tin(II) 2-ethylhexanoate were used as initiators in these two systems, respectively, to obtain functional microspheres with a narrow particle size distribution and a narrow molecular weight distribution [98]. Table 2 provides an overview of microspheres obtained by living dispersion polymerization.

2.3 Microspheres from Non-Vinyl Monomers

Microspheres have been prepared by the dispersion polymerization of monomers other than vinyl monomers, such as styrene and (meth-)acrylates. Polyaniline (PANI) is one of the most frequently studied electrically conducting polymers. Since the paper by Armes and Aldissi [99] in 1989, there have been numerous reports on the preparation of PANI dispersions by oxidative

Table 3 Examples of microspheres of monomers other than vinyl monomers obtained by dispersion polymerization

Stabilizer	Monomer	Medium	Reference
Oxidative polymerization			
PVP	Aniline	Alcohol/water	[100, 101]
PVME	Aniline	Alcohol/water	[102, 103]
PVA	Aniline	Water/alcohol	[104–106]
Poly(styrenesulfonic acid)	Aniline	Water	[107]
Methycellulose	Aniline	Water/alcohol	[108]
HPC	Aniline	Water	[109]
PVA	3,5-Xylidine	Water	[110, 111]
Ethylhydroxycellulose	Pyrrole	Ethanol/water	[112, 113]
PVME	Pyrrole	Ethanol/water	[114]
Enzymatic polymerization			
PVME, PVA, PEG	Phenol	Dioxane/phosphate buffer	[115, 116]
PVME	*p*-Phenylphenol	Dioxane/phosphate buffer	[115, 116]
Polyurethane			
Poly(lauryl methacrylate) diol	TDI/EG	Paraffin oil	[117]
Polyester			
Poly(2-ethylhexyl acrylate-*co*-styrene-*co*-acrylic acid)	4-Acetoxybenzoic acid + 2,6-acetoxynaphthoic acid	–	[118]

polymerization. Colloidally-stable submicron-sized PANI particles are produced in the aqueous-alcohol media by the dispersion polymerization of aniline in the presence of a suitable steric stabilizer such as PVP [100, 101], PVME [102, 103], PVA [104–106], poly(styrenesulfonic acid) [107], methycellulose [108], and HPC [109]. The oxidative dispersion polymerization of 3,5-xylidine [110, 111] produced needle-shaped particles in water. Polypyrrole particles were also prepared in aqueous ethanol using $FeCl_3$ and ammonium persulfate as the oxidant [112–114].

Uyama and Kobayashi et al. [115, 116] were first to prepare nearly monodisperse sub-micron polyphenol particles by the enzyme-catalyzed dispersion polymerization of phenol and *p*-phenylphenol in a mixture of 1,4-dioxane and phosphate buffer using a water-soluble polymer as stabilizer (such as PVME, PVA, and PEG).

Polyurethane [117] and polyester [118] particles have also been prepared by the dispersion polyaddition of ethylene glycol (EG) and toluene diisocyanate (TDI) in paraffin, and the polycondensation of acid and ester at a high polymerization temperature, respectively. Table 3 provides an overview of microspheres of monomers other than vinyl monomers obtained by dispersion polymerization.

3
Microsphere Syntheses by Reactive Dispersants, Macromonomers, Inimers, and Transurfs

Macromonomers are polymers or oligomers with polymerizable end groups, widely investigated for the preparation of functional polymers and polymer microspheres by dispersion polymerization. For microspheres, the macromonomers should be designed to copolymerize with the main monomers in such a way as to produce graft chains that serve as efficient stabilizers; in other words, their main chain should be firmly bound to the particle surface and the graft chains should extend into the polymerization medium.

Examples of dispersion polymerizations using macromonomers are summarized in Table 4. Non-aqueous dispersion (NAD) polymerization of polar

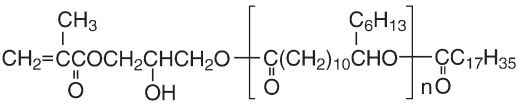

1

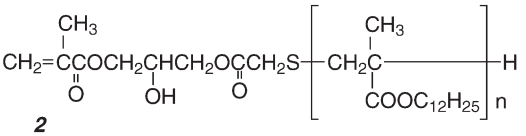

2

Table 4 Examples of dispersion copolymerization with reactive dispersants

Reactive dispersant	Monomer	Medium	Reference
PHSA **1**	MMA	Hydrocarbon	[11]
PLMA **2**	MMA	Hydrocarbon	[11]
PE **3**	MMA	Dodecane, PE	[119]
PDMS 4	ST	Silicone oil	[120]
POXZ **5**	MMA	MeOH/H_2O	[121]
POXZ **5**	ST	EtOH/H_2O	[122]
POXZ **5**	CH_2=CHNHCHO	MeOH	[123]
POXZ **6**	MMA	MeOH/H_2O	[124]
PEO **7** (*m*=1)	MMA, ST	EtOH/H_2O	[126, 127]
PEO **8** (*m*=3, 5, 7)	ST	Ethanol/H_2O	[128]
PEO **9a**	ST	EtOH/H_2O	[129]
PEO **9a, 11**	ST	EtOH/H_2O	[130]
PEO **7** (*m*=1, 4, 7)	ST, MMA, BMA	MeOH/H_2O	[131–133]
PEO **9b** (*m*=11)	ST	EtOH/H_2O	[134]
PEO **10** (*m*=2.6, 4.1, 6.8)	ST	MeOH/H_2O	[135]
PEO **9a, 9b** (*m*=6, 10)	ST, MMA	MeOH/H_2O	[125, 137]
PEO **12**	ST	EtOH/H_2O	[136]
PEO **13**	ST	EtOH/H_2O	[138]
PVP **14**	ST, MMA	EtOH	[139]
PVAcA **15**	ST	EtOH	[140]
PVA **16**	MMA	EtOH/Water	[141]
P4VP **17**	ST	EtOH	[142]
PNIPAM **18**	ST	EtOH	[143]
PTBMA **19**	ST	EtOH	[144]
PAA **20**	MMA	EtOH/H_2O	[145]
PDMS **4**	MMA, ST	CO_2	[146]
PCL **21**	L,L-Lactide	Heptane/dioxane	[97, 98]
PMA **22**	MMA	EtOH/H_2O	[147]
PMA **23**	ST	MeOH/H_2O	[148]
PDMAEMA **24**	ST	Alcohols	[150]
PEO **25**	ST	MeOH/H_2O	[151]
Inimer **26**	ST, MMA	Ethanol/H_2O	[155]
Transurf **27**	ST	Ethanol/H_2O	[156]

monomers was first carried out in aliphatic hydrocarbon media with the hydrophobic macromonomers **1** and **2** [11]. These were copolymerized with MMA or other polar monomers to produce comb-graft copolymers, which have limited solubility in pure aliphatic hydrocarbons but adequate solubility in hydrocarbon-monomer mixtures. It is particularly effective in stabilizing PMMA NAD particles. Polyethylene (PE) macromonomers **3** have been used

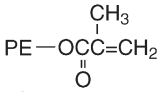

3

for the dispersion copolymerization of MMA in dodecane and in PE melts to produce stable PMMA dispersions at a high temperature [119]. In the latter case, nanocomposite materials in which submicron-sized fine PMMA particles are uniformly dispersed in the PE bulk can be prepared during the copolymerization. Monodisperse PS particles (0.70 μm), prepared by the dispersion copolymerization of styrene with the poly(dimethylsiloxane) PDMS macromonomer **4** in PDMS-diol (MW=7,500), was allowed (together with trimethylolpropane) to react with hexamethylene diisocyanate using dibutyltin dilaurate as a catalyst. The product of the polyaddition was a tough elastomeric composite with polystyrene particles finely dispersed and strongly anchored in a PDMS-polyurethane matrix [120].

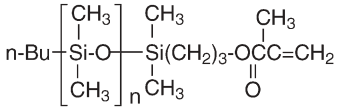

4

This technique has been extended to polar media, especially alcohols and their mixtures with water as a continuous phase.Kobayashi and Uyama et al. [121– 124] reported that poly(2-oxazoline) macromonomers such as **5** and **6** are very effective for dispersion copolymerization with styrene, MMA, and *N*-vinylformamide in methanol, ethanol, and mixtures of these alcohols with water. They reported that the particle size decreased with increasing initial macromonomer concentration and that graft-copolymerized poly(2-oxazoline) chains are concentrated on the particle surface to act as steric stabilizers.

Dispersion copolymerizations that use the poly(ethylene oxide) (PEO) macromonomers **7–13** in alcoholic media have been intensively studied by

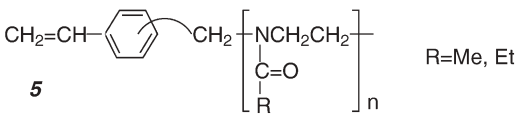

R=Me, Et

5

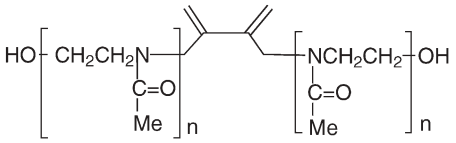

6

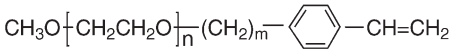

7 (m = 1, 4, 7)

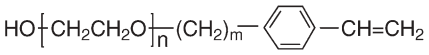

8 (m = 3, 5, 6)

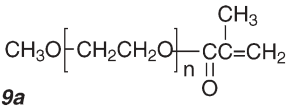

9a

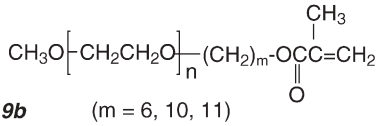

9b (m = 6, 10, 11)

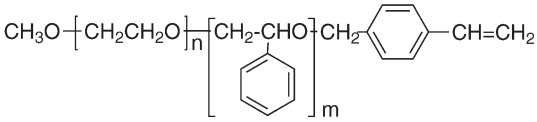

10 (m=2.6, 4.1, and 6.8)

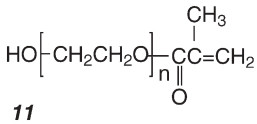

11

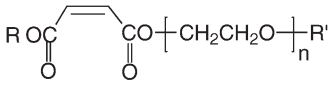

R=H, $C_{12}H_{25}$
R'=H, CH_3

12

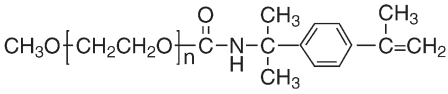

13

many researchers [125–138]. They produce nearly monodisperse polymeric microspheres of submicron to micron sizes, covered with PEO chains on their surface. Several factors that affect the particles' size and the polymerization kinetics have been studied. Theoretical models for particle nucleation in these systems have also been developed and compared with the experimental observations, as will be discussed later.

Several other hydrophilic macromonomers including **14–20** have been applied to the dispersion polymerization [139–145]. These macromonomers were synthesized by radical polymerization in the presence of appropriate chain transfer agents, followed by transformation of the end group, as previously summarized [30]. Akashi et al. [143] used poly(*N*-isopropylacrylyamide) (PNIPAM) macromonomer **18** in ethanol and prepared thermosensitive microspheres 0.4–1.2 μm in diameter consisting of a PS core and PNIPAM branches on their surface. The particles are particularly useful for many biomedical applications. Indeed, the particles have been reported to flocculate and change in light transmittance with increasing temperature.

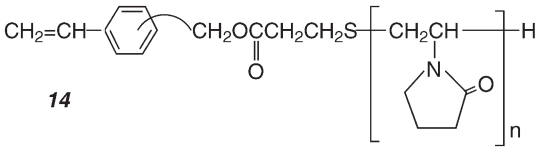

14

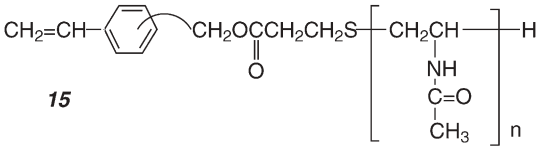

15

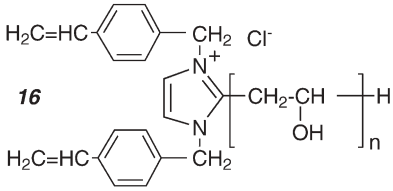

16

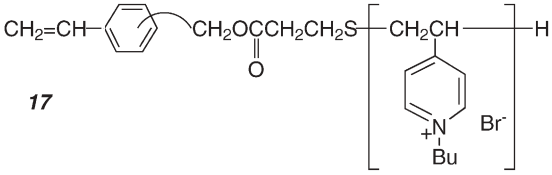

17

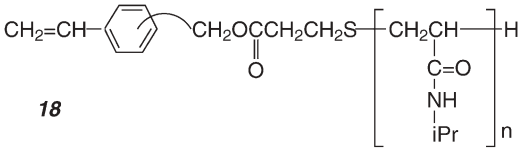

18

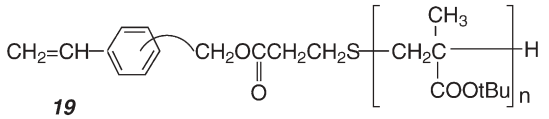

19

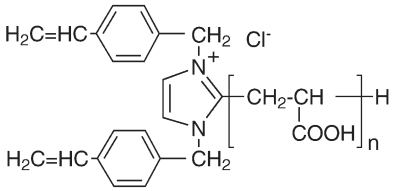

20

DeSimone and his co-workers have intensively studied polymerization reactions in an environmentally friendly solvent, CO_2. In the presence of the CO_2-philic silicone-based macromonomer **4**, relatively monodisperse micron-sized polymer particles were obtained by the polymerization of MMA and styrene in supercritical CO_2, as shown in another chapter [146].

Sosnowski et al. [97, 98] have reported that uniform biodegradable polymeric particles with diameters of less than 5 μm can be prepared by ring-opening dispersion polymerization of L,L-lactide in heptane-dioxane mixed solvent in the presence of poly(dodecyl acrylate)-*g*-poly(ε-caprolactone), which were synthesized by the copolymerization of dodecyl acrylate with the poly(ε-caprolactone) macromonomers **21**. Note that the polymer particles consist of well-defined poly(L,L-lactide) polymers with $M_n \approx 1 \times 10^4$ and $M_w/M_n \approx 1.0_6$.

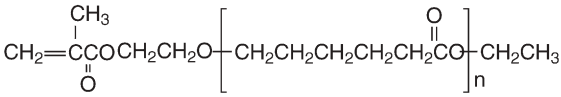

21

The polyelectrolyte macromonomers **17**, **20**, **22**, and **23** [142, 143, 147, 148] were prepared and applied to dispersion copolymerizations to produce polymeric particles covered with polyelectrolyte chains. Evidently, the dependence of the conformational properties of polyelectrolyte brush chains attached to the latex surface on the pH, the degree of neutralization, and the salt concentration have been the subject of growing experimental and theoretical effort.

22

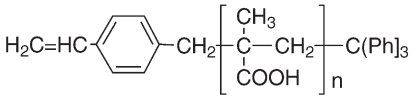

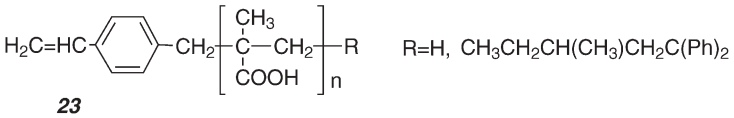

23

Some novel water soluble macromonomers, **24**, have been synthesized by the oxyanionic polymerization [149] of 2-(dimethylamino)ethyl, 2-(diisopropylamino)ethyl, and 2-(*N*-morpholino)ethyl methacrylate, and conducted to dispersion copolymerization of styrene in alcohol media [150]. Sufobetaine-based macromonomer was prepared by the polymer reaction of **24** (R=CH_3) with propane sultone, and was found to be useful in the dispersion polymerization of styrene even at high electrolyte levels (up to 1 M NaCl). Ito et al. [151] synthesized new PEO macromonomers with a cationic charge at the ω-end, **25**, and examined the influence of the charge on the particles' size in dispersion copolymerization with styrene in alcohol media.

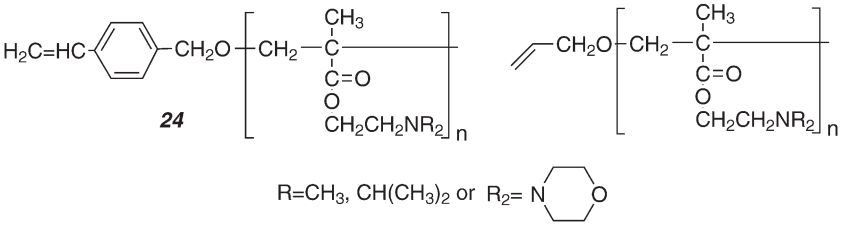

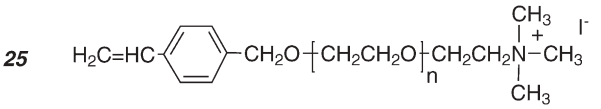

Poly(HEMA-*co*-MMA-*g*-PMMA) graft copolymer was also prepared with a commercially available poly(methyl methacrylate) (PMMA) macromonomer, HEMA, and MMA, and used as an efficient dispersant for the dispersion polymerization of styrene in ethanol [152].

Recently, Akashi and coworkers [153, 154] synthesized novel spherical particles on which nano-projections are uniformly distributed over the whole surface like "confetti" by the one-step dispersion terpolymerization of acrylonitrile, styrene, and the PEO macromonomer **9a** in ethanol/water media. The control of nanoparticle morphology by a one-step synthetic procedure is important to self-organization at the polymer chain level, which is a basis for the formation of biological nanoconstructs such as viruses and organelles.

Dispersion polymerization in the presence of reactive surfactants including surfmers, inisurfs and transurfs is also a versatile method for producing functional microspheres [26]. For example, the macromonomeric azoinitiator **26** is an effective inisurf in the preparation of PS and PMMA particles [155].

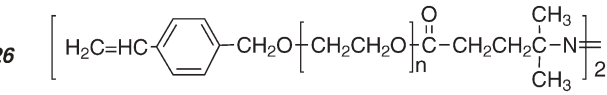

Similarly, the thiol-ended transurf **27** shows higher stabilizing efficiency than PVP in the dispersion polymerization of styrene and MMA in water-ethanol [156].

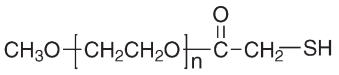

In all instances of the dispersion polymerization, amphiphilic graft copolymers produced in a selective solvent for the branches play a crucial role. Schematically, a microsphere obtained by copolymerization in this way with a small amount of macromonomer has a core-shell structure as given in Fig. 2, with the core occupied by the insoluble substrate polymer chains and the shell by the soluble, graft-copolymerized macromonomer chains. The backbone chains of the graft copolymers, which must be insoluble in the medium, serve as the anchors into the core. The following section presents general criteria for the size control of polymeric microspheres by dispersion copolymerization using macromonomers.

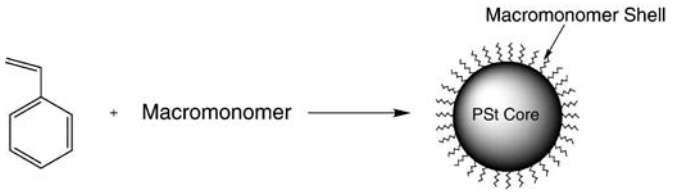

Fig. 2 Schematic description of dispersion copolymerization of styrene with macromonomer

4
Particle Size Control in Dispersion (Co-)Polymerization

4.1
Theoretical Model

According to the aggregative and coagulative nucleation theories [157] which all originally derive from the homogeneous nucleation theory [158], the most important point when determining particle number is the instant at which sterically-stabilized particles form [159]. After this point, coagulation between similar-sized particles no longer occurs, and the number of particles present in the reaction medium remains constant. Sufficient particle stabilization may be achieved with physically adsorbed stabilizers in the case of linear soluble polymers, copolymers, and block copolymers. For covalent bonding, polymerization is performed in the presence of macromonomer stabilizers, which copolymerize with monomer(s) to graft stabilizer on the particles' surface [26, 31]. The graft copolymer may be also produced by the chain transfer reaction of a propagating radical with a soluble polymer chain.

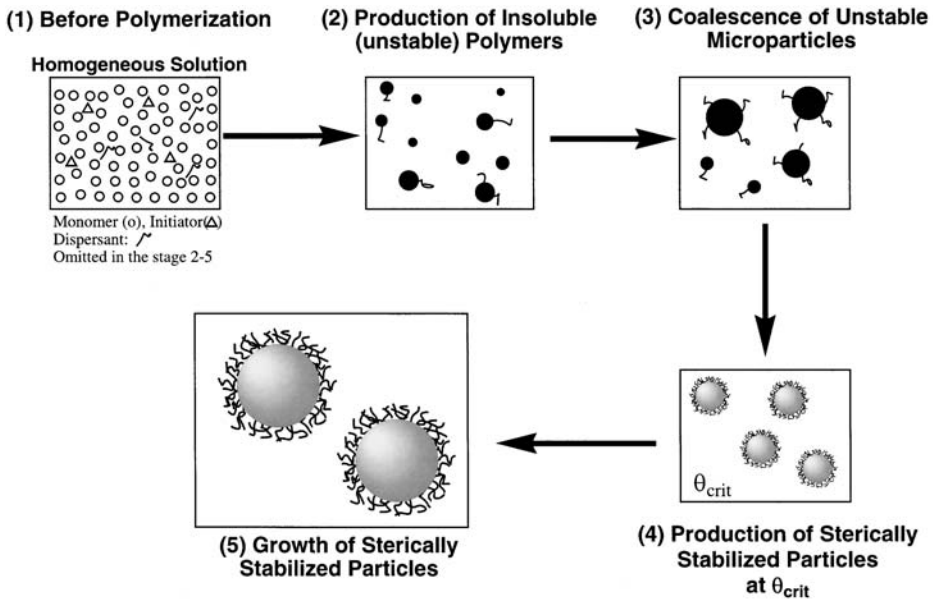

Fig. 3 Schematic model for the particle nucleation and growth of sterically-stabilized particles in dispersion polymerization

As shown in Fig. 3, the dispersion polymerization is considered to proceed as follows:

1. Before polymerization, the reaction mixture dissolves completely into the continuous phase.
2. When the reaction mixture is heated, free radicals are formed by initiator decomposition and grow in the continuous phase to produce linear oligomer, polymers, and/or graft copolymers. The solubility of these polymers is a function of their molecular weight (MW) and the composition of the graft copolymers. Polymers with a MW larger than a certain critical value precipitate and begin to coagulate to form unstable particles.
3. These particles coagulate on contact, and the coagulation among them continues until sterically-stabilized particles form.
4. This point is referred to as the critical point, and it occurs when all of the particles contain sufficient stabilizer polymer chains on the surface to provide colloidal stability.
5. After this point, no new nuclei or particles are formed and the particles may grow both by the diffusive capture of oligomers and the coagulation of very small unstable particles (nuclei, precursors) produced in the continuous phase and by the polymerization of the monomer included within the particles until all of the monomer is consumed. The total number of such sterically-stabilized particles remains constant so that their size is only a function of the amount of polymer produced.

In 1990, Paine [24] first developed a multibin kinetic model for the aggregation of precipitated radicals or unstabilized particles in dispersion polymerization, based on diffusion-controlled particle aggregation, which was described by Smoluchowski [160] and Frenklach [161]. The stabilized particles whose surfaces are completely covered with grafted polyvinylpyrrolidone (PVP) chains do not aggregate. This was the first model that quantitatively simulated the role of the stabilizer molecules at the particle formation stage. Assuming ideal core-shell structures in which the main monomer forms the core, and dispersant the shell, one can readily establish a basic relationship between microsphere size and weights of main core polymer and stabilizer polymer attached on the particle surface, as given by the following equations:

$$W = W_o\theta = \frac{4}{3}\pi R^3 \rho N \tag{1}$$

and

$$nS = \frac{W_{Do}\theta_D N_A S}{NM_D} = 4\pi R^2 \tag{2}$$

Here, W (g/l) is the weight of monomer polymerized, W_o is the weight of monomer feed, θ is the fractional conversion of monomer, R is the particle core radius (cm), ρ is the core polymer density, N is the particle number per liter, n is the number of dispersant molecules on one particle, S is the area of particle surface covered by one dispersant molecule, W_{Do} is the weight (in g/l) of dispersants in feed, M_D is the molecular weight of dispersant, θ_D is the fraction of adsorbed or grafted dispersant on particle surface, and N_A is Avogadro's number. Combining Eqs. 1 and 2 produces a universal relationship between the particle radius and the extent of polymerization for the microspheres obtained by an ideally grafted steric stabilizer:

$$R = \frac{3W_o\theta}{\rho N_A W_{Do}\theta_D\left(\frac{S}{M_D}\right)} \tag{3}$$

In spite of different mechanisms of particle formation and growth, Eq. 3 predicts larger particles with increasing amounts of main polymer, and with lower surface coverage by individual dispersant molecules (S/M_D), but smaller particles with increasing amounts of dispersant. Also, S/M_D increases with the solvency of the dispersion medium, and hence the particle radius should be smaller in media that are good solvents for the dispersant.

One problem is the estimation of θ_D and S with respect to the monomer conversion (θ) and the attachment of the dispersant to particles. For adsorbed dispersants, θ_D is determined by the partition of dispersant between the particle surface ($4\pi R^2 N$) and the continuous medium. For chemical grafting via chain transfer, Paine [24] derived the equation

$$R = \theta^{\frac{1}{3}} \left(\frac{3W_o}{\rho N_A}\right)^{\frac{2}{3}} \left(\frac{M_D}{C_S W_{Do} S_{crit}}\right)^{\frac{1}{2}} \left(\frac{0.386 k_2}{4\pi k_t}\right)^{\frac{1}{6}} \left(\frac{k_t}{2k_d f[I]_o}\right)^{\frac{1}{12}} \quad (4)$$

where C_s is the chain transfer constant to dispersant polymer chains, S_{crit} is S at critical point, k_2 is the diffusion-controlled rate constant for coalescence between similar-sized particles ($M^{-1}s^{-1}$), k_p is the propagation rate constant ($M^{-1}s^{-1}$), k_t is the termination rate constant ($M^{-1}s^{-1}$), $[I]_o$ is the initiator concentration (M), and f is the initiator efficiency and k_d is the initiator decomposition rate constant (s^{-1}).

Equation 4 was found to explain particle size data fairly well, with reasonable kinetic and coverage parameter values (k's and S_{crit}), in the dispersion polymerization of styrene in ethanol with PVP dispersant [24]. Many other dispersion polymerization systems with homopolymer dispersants appear to be explained by Eq. 4, except for the frequently observed direct particle size dependence on initiator concentration [27].

For dispersion polymerization with macromonomer stabilizers, we use Eq. 5 and Eq. 6 [31, 32, 131–133].

$$R = \theta^{\frac{1}{3}} \left(\frac{3W_o}{\rho N_A}\right)^{\frac{2}{3}} \left(\frac{M_D r_1}{W_{Do} S_{crit}}\right)^{\frac{1}{2}} \left(\frac{0.386 k_2}{4\pi k_p}\right)^{\frac{1}{6}} \left(\frac{k_t}{2k_d f[I]_o}\right)^{\frac{1}{12}} \quad (5)$$

$$S = \theta^{-\frac{1}{3}} \left(\frac{3W_o}{\rho N_A}\right)^{\frac{1}{3}} \left(\frac{M_D S_{crit}}{r_1 W_{Do}}\right)^{\frac{1}{2}} \left(\frac{4\pi k_p}{0.386 k_2}\right)^{\frac{1}{6}} \left(\frac{2k_d f[I]_o}{k_t}\right)^{\frac{1}{12}} \left(\frac{\theta}{\theta_D}\right) \quad (6)$$

Here r_1 is the reactivity ratio ($=\theta_{crit}/\theta_{Dcrit}$) of the monomer ($M_1$) in a copolymerization with the macromonomer (M_2) at critical stabilization.

In Eqs. 4 and 5, one sees that the radius of the latex particle follows simple scaling relationships with the key parameters in the system: $\theta^{1/3}$, $[\text{monomer}]_o^{2/3}$, $[\text{dispersant}]_o^{-1/2}$, $[\text{initiator}]_o^{-1/12}$, where $[]_o$ means initial concentration. These equations predict that the particle size and stabilization are determined by the magnitude of r_1. In addition, looking at Eq. 6, it is apparent that the surface area occupied by a stabilizer chain follows $\theta^{-1/3}$, and in the case of azeotropic copolymerization, $\theta=\theta_D$. This means that the chain conformation for the grafts on the latex particle will change with grafting density. The S value is closely related to the conformation of a single polymer chain as a stabilizer grafted onto the surface of a latex particle. According to de Gennes' "mushroom" model [162] for a polymer grafted to a noninteracting surface, the polymer chain occupies a volume determined by its mean-squared radius of gyration $<S^2>$. When the surface becomes crowded with chains, additional energy is needed to deform the polymer mushrooms into brushes. When the particle surfaces are completely covered with random coils of the polymer, they are also sterically-stabilized against coagulation with other particles. One, therefore, defines S_{crit} as the maximum surface area occupied by a single polymer chain in the continuous phase.

4.2 Comparison of Experiment with Theory

For dispersion copolymerization with PEO macromonomers, the power law exponents in Eq. 5 have been experimentally determined and compared, as summarized in Table 5. Initial monomer concentration has a major influence on the final particle radius. The experimental power law exponents (0.82–1.02) are usually significantly larger than those in Eqs. 4 and 5, except for 0.63 for styrene as a monomer with **7** (m=4, n=45). This is likely to be due to a solvency effect of the monomer. The values of the exponents for the macromonomer and initiator concentration dependences in the polymerization of hydrophobic monomer, styrene and *n*-butyl methacrylate are in good agreement with those from Eq. 5. Figure 4a shows a comparison of Eq. 5 with the particle radius obtained for the dispersion copolymerization of styrene with the PEO macromonomer **7** (m=4, n=45), in methanol-water medium (9/1 v/v). One sees that the experimental particle radius is quantitatively described by the model with reasonable constants, θ=1, ρ=1.05 g cm^{-3}, N_A=6.02×10^{23}, k_2=10^9 L mol^{-1} s^{-1}, k_p=352 L mol^{-1} s^{-1}, k_t=6.1×10^7 L mol^{-1} s^{-1}, k_d=3.2×10^{-7} s^{-1}, f=1, and S_{crit}/r_1= 10 nm^2, r_1=1.

In remarkable contrast, unusually high exponent values (~1.2) have been obtained in the dispersion copolymerization of a polar monomer, MMA in methanol-water (8:2 and 7:3 v/v) media. The value of the exponent drops to 0.51 when the water content is increased to higher than 40%, as shown in

Table 5 Values of the exponents in $R=K$ [Monomer] [a][Macromonomer] [b][Initiator] [c] (see also Eq. 5) for dispersion copolymerizations with macromonomers

Macromonomer	Monomer	Medium	*a*	*b*	*c*	Reference
Theory (Eq. 5)	–	–	0.67	–0.50	–0.083	–
7, m=4, n=45	ST	MeOH/H_2O (9:1)	0.63	–0.52	–0.068	[131]
7, m=1, 4, 7, n=53, 110	BMA	MeOH/H_2O (8:2)	0.82	–0.54	–0.10	[132]
9b, m=11, n=40	ST	EtOH/H_2O (9:1)	1.02	–0.60	–0.090	[134]
10, m=2.6, n=41	ST	MeOH/H_2O (9:1)	–	–0.47	–	[135]
10, m=4.1, n=41	ST	MeOH/H_2O (9:1)	–	–0.40	–	[135]
10, m=2.6, n=41	ST	MeOH/H_2O (9:1)	–	–0.59	–	[135]
8, m=3,5,6, n=50	ST	MeOH/H_2O (9:1)	–	–0.50	–	[128]
4, n=130	ST	Silicone oil (M=2700)	–	–0.40	–	[120]
7, m=1, n=45	MMA	MeOH/H_2O (8:2)	–	–1.17	–	[133]
7, m=1, n=45	MMA	MeOH/H_2O (7:3)	0.85	–1.15	–0.030	[133]
7, m=1, n=45	MMA	MeOH/H_2O (6:4)	–	–0.51	–	[133]
7, m=1, n=45	MMA	MeOH/H_2O (5:5)	–	–0.52	–	[133]
7, m=1, n=36	ST/AN	Ethanol/H_2O (8:2)	–	–0.68	–	[153]

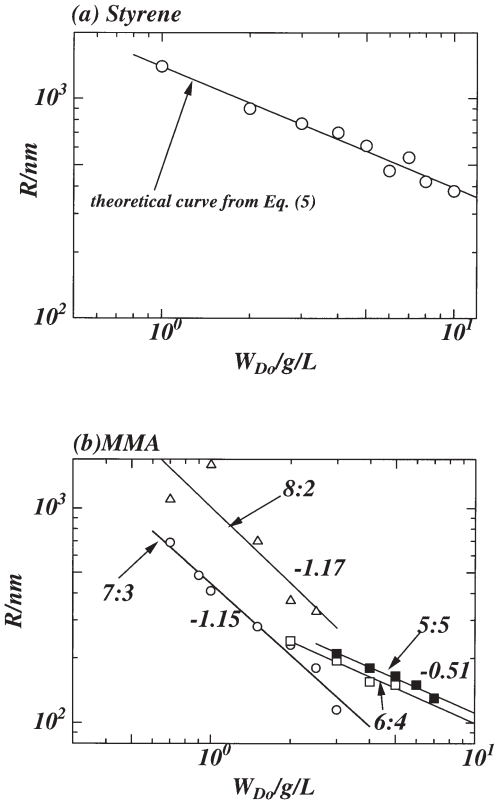

Fig. 4 Double logarithmic plots of average particle radius (R) as a function of weight (W_{Do}) of PEO macromonomer. **a** Styrene **7** (m=4 and n=45), W_o=100 g/L, $[I]_0$=0.0122 mol/L, θ=1 at 60 °C. The straight line is a theoretical curve calculated from Eq. 5 with the parameters in the text. **b** MMA **7** (m=1 and n=45), W_o=100 g/L, $[I]_0$=0.012 mol/L, θ=1 at 60 °C in methanol: water=8:2 (empty triangles), =7:3 (empty circles), =6:4 (empty squares), and =5:5 (filled squares)

Fig. 4b. The significant change in the value of the exponent with the polarity of the continuous phase cannot be simply explained by the current model, so further refinements [163–165] are needed.

The criteria for designing PEO macromonomers to be used as efficient dispersants in dispersion polymerization have been thoroughly studied by Ito et al. [128, 131, 135, 151], who examined the effects of the length of spacer (m), the degree of polymerization of PEO chain (n) of **7**, and charge group at the ω-end of **25** on particle size.

5
Chain Conformation of Grafted Polymer Chains at the Particle Surface

Polymer adsorption has been a subject of both theoretical and experimental interest, because the adsorption behavior of the polymer at the solid-liquid interface is strongly connected with many technologically important processes such as flocculation, adhesion, coating, and lubrication in addition to the colloidal stabilization already discussed above. This subject has been recently reviewed by Cosgrove, Griffiths [166], Fleer et al. [167], and Kawaguchi and Takahashi [168]. Among a variety of adsorbed polymers, two are of particular interest with respect to macromonomers. One is the adsorption of comb and graft copolymers with highly grafted chain density onto the solid surface, which is referred to as "brush adsorption", as illustrated in (a) of Fig. 5. Another is the attachment of the double bond of the macromonomer with the solid surface by chemical reaction, which is referred to as "terminally-attached

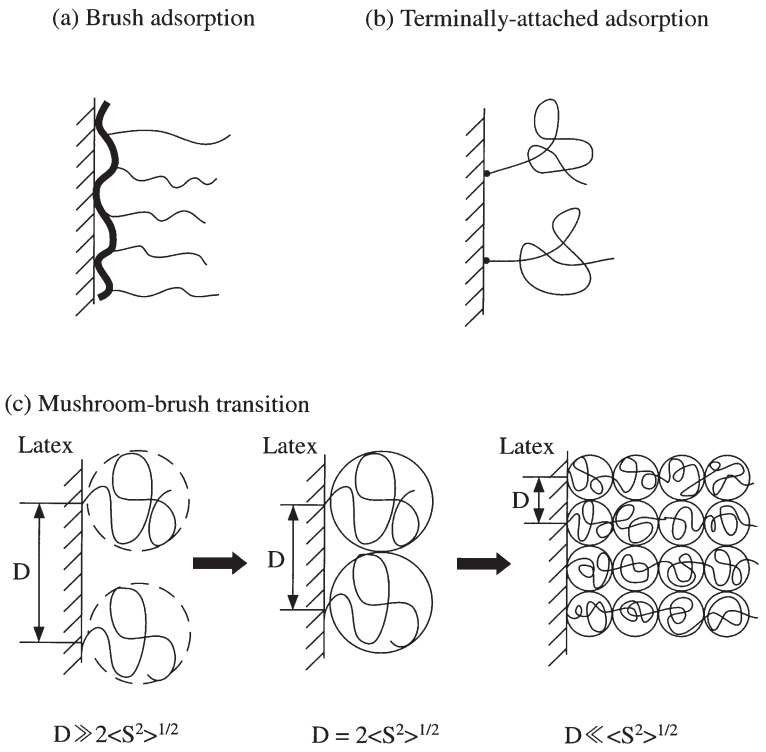

Fig. 5 Schematic representation of the possible conformations of adsorbed (co)polymers prepared using the macromonomer technique. **a** Brush adsorption of graft copolymer; **b** terminally-attached adsorption, and; **c** the mushroom-brush transition for strongly overlapping chains as proposed by de Gennes [162] and Alexander [170]

adsorption", as illustrated in (b) of Fig. 5. The conformational properties of these grafted polymer chains have been the subject of growing attention, from the point of view of the "mushroom-brush" transition proposed by de Gennes [162, 169] and Alexander [170], as shown in (c) of Fig. 5.

While there have been many studies on the conformational properties of terminally-attached polymer chains, prepared either by the adsorption of block copolymers in a selective solvent onto a solid surface [171] or by the reaction of a solid surface with reactive groups of polymer [172], little has been reported for graft copolymer chains prepared from macromonomers. Cairns et al. [173] carried out a SANS study of a non-aqueous dispersion system comprised of deuterated PMMA latex grafted with poly(12-hydroxystearic acid), **1.** The thickness of the layer was found to correspond to about 2/3 of the extended chain length. Comb-like PEO gradient surfaces were grafted onto low density PE sheets by corona discharge treatment followed by the homopolymerization of the PEO macromonomers **9b** (n=1, 5 and 10) and the gradient PEO concentration at the surface was characterized by measuring the water contact angle, by FTIR-ATR, and by ESCA [174]. The gradient surfaces can be used to investigate the interactions between biological species and the surface PEO chains. Hadziioannou and coworkers [175] prepared a terminally-attached cationic polyelectrolyte brush on a gold-coated Si-wafer by end-grafting styryl-terminated poly(vinylpyridine) macromonomer, followed by quarternarization with methyl iodide. The surface was characterized by means of scanning force microscopy, ellipsometry, and FTIR-ATR.

Wu et al. [176] studied the surface properties of PS and PMMA microspheres stabilized by the PEO macromonomer **7** (m=1) using dynamic light scattering, and claimed that for PMMA microspheres the surface area occupied by a PEO molecule is nearly twice as large as that for PS microspheres, assuming that 100% macromonomer is copolymerized to attach to the latex surface. However, this is not the case for styrene copolymerization with PEO macromonomers in which only 10% PEO macromonomer was copolymerized [131]. In contrast, it was confirmed that 100% of PEO macromonomers were copolymerized for the MMA and BMA dispersion copolymerization [132, 133].

^{1}H NMR studies have been carried out for the dispersion copolymerization of BMA with the PEO macromonomer **7** (m=7), in a deuterated methanol-water medium [177]. The fractional composition and surface-grafted PEO concentration were monitored as functions of conversion and particle size. In Fig. 6, the mobile fraction of PEO chains incorporated into the particles is plotted against the interchain spacing D, as shown in (c) of Fig. 5, which can be calculated using particle size values and conversions. One sees that the values of the mobile fraction increase sharply with decreasing D in the region of D<1.6 nm and become constant below D=1.4 nm. The radius of gyration of the PEO chain coil in methanol is calculated to be 1.6 nm, which corresponds to the D value at which a sharp increase in mobile fraction occurs. This result may suggest that the onset of a pancake-to-brush transition of grafted chains at the interface

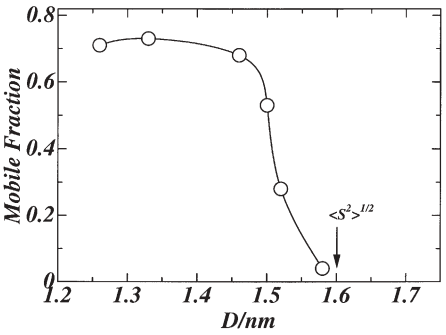

Fig. 6 Plots of mobile fraction of surface anchored PEO chains against the estimated mean separation D between PEO anchor points on the surface of the particles. The D values were calculated from the particle size and number, assuming that all PEO chains were located at the surface

occurs when, say, $D \approx \langle S^2 \rangle^{1/2}$, as expected by theory [162, 169, 170]. This subject should lead to a better understanding of the true nature of the steric stabilization that exists in many dispersion systems.

6 Conclusions and Future

A wide variety of polymer microspheres can be made by dispersion polymerization. A key component in all of these systems is the stabilizer (dispersant) both during particle formation and for the stability of the resulting colloidal particles. Functionality can be introduced into colloidal particles in various ways: by copolymerization of functional monomers (like HEMA), or incorporation of functional dispersants, initiators, chain transfer agents, or macromonomers. Many different types of macromonomer are prepared and used to prepare functional microspheres. Amphiphilic macromonomers provide a particularly versatile component in these systems, being the source of both stabilizer and functional residue. They act as stabilizer because they are covalently grafted onto the particles' surface by copolymerization with main monomers, and form tightly bound hairy shells on the particles' surface.

The experimental details of dispersion polymerization with various polymeric dispersants and macromonomers are fairly well established. A basic expression for particle size control has also been derived for the formation of clear-cut core-shell particles based on highly incompatible core-shells such as polystyrene-PVP and polystyrene-PEO. However, results deviate considerably from theory in compatible polymers such as PMMA with PEO macromonomer. The detailed structures of the "hairy" shells need to be discovered in order to better understand the exact mechanism of their formation and stabilizing function.

References

1. Ugelstad J, Mørk PC, Mfutakanba HR, Soleimany E, Nordhuus I, Schmid R, Berge A, Ellingsen T, Aune O, Nustad K (1983) In: Poehlein GW, Ottewill RH, Goodwin JW (eds) Science and technology of polymer colloids. Nijhoff, Boston, MA
2. Ober CK, Lok KP (1986) US Pat 4617249
3. Ugelstad J, Berge A, Ellingsen T, Schmid R, Nilsen T-N, Mørk PC, Stenstad P, Hornes E, Olsvik Ø (1992) Prog Polym Sci 17:87
4. Vanderhoff JV, El-Aasser MS, Micale FJ, Sudol ED, Tseng CM, Silwanowicz A, Kornfeld DM, Vicente FA (1984) J Dispers Sci Technol 5:231
5. Vanderhoff JV, El-Aasser MS, Micale FJ, Sudol ED, Tseng CM, Silwanowicz A, Sheu HR, Kornfeld DM (1986) Polym Mater Sci Eng 54:1986
6. Ugelstad J, Mørk PC, Kaggerud KH, Ellingsen T, Berge A (1980) Adv Coll Interfac Sci 13:101
7. Ugelstad J, Mørk PC, Kaggerud KH, Ellingsen T, Khan AA (1982) In: Piirma (ed) Emulsion polymerization. Academic, New York, Ch 11
8. Omi S, Katami K, Yamamoto A, Iso M (1994) J Appl Polym Sci 51:1
9. Kamiyama M, Koyama K, Matsuda H, Sano Y (1993) J Appl Polym Sci 50:107
10. Okubo M, Shiozaki M, Tsujihiro M, Tsukada Y (1991) Coll Polym Sci 269:222
11. Barret KEJ (ed) (1975) Dispersion polymerization in organic media. Wiley, London
12. Almog Y, Reich S, Levy M (1982) Brit Polym J 14:131
13. Lok KP, Ober CK (1985) Can J Chem 63:209
14. Ober CK, Lok KP, Hair ML (1985) J Polym Sci Pol Lett 23:103
15. Ober CK, Hair ML (1987) J Polym Sci Pol Chem 25:1395
16. Ober CK, Lok KP (1987) Macromolecules 20:268
17. Tseng CM, Lu YY, El-Aasser MS, Vanderhoff JW (1986) J Polym Sci Pol Chem 24:2995
18. Okubo M, Ikegami K, Yamamoto Y (1989) Colloid Polym Sci 267:193
19. Okubo M, Katayama Y, Yamamoto Y (1991) Colloid Polym Sci 269:217
20. Paine AJ, McNulty J (1990) J Polym Sci Pol Chem 28:2569
21. Paine AJ (1990) J Colloid Interf Sci 138:157
22. Paine AJ (1990) J Polym Sci Pol Chem 28:2485
23. Paine AJ, Luymes W, McNulty (1990) Macromolecules 23:3104
24. Paine AJ (1990) Macromolecules 23:3109
25. Croucher MD, Winnik MA (1990) In: Candau F, Ottewill RH (eds) An introduction to polymer colloids. Kluwer Academic, Dordrecht, p 35
26. Guyot A, Tauer K (1994) Adv Polym Sci 111:43
27. Cawse JL (1997) In: Lovell PA, El-Aasser MS (eds) Emulsion polymerization and emulsion polymers. Wiley, Chichester, UK, p 743
28. Pichot C, Delair T, Elaissari A (1997) In: Asua JM (ed) Polymeric dispersions: principles and applications. Kluwer Academic, Dordrecht, p 515
29. Asua JM, Schoonbrood HAS (1998) Acta Polym 49:671
30. Ito K (1998) Prog Polym Sci 23:581
31. Ito K, Kawaguchi S (1999) Adv Polym Sci 142:129
32. Ito K, Cao J, Kawaguchi S (2002) In: Arshady R, Guyot A (eds) Functional colloids (MML Series, Vol 4). Citus, London, p 109
33. Sáenz J, Asua J M (1995) J Polym Sci Pol Chem 33:1511
34. Sáenz J, Asua J M (1995) J Polym Sci Pol Chem 34:1977
35. Bamnolker H, Margel S (1996) J Polym Sci Pol Chem 34:1857
36. Horák D, Švec F, Fréchet JMJ (1995) J Polym Sci Pol Chem 33:2961
37. Kiatkamjornwong S, Kongsupapsiri C (2000) Polym Int 49:1395

38. Yang W, Yang D, Hu J, Wang C, Fu S (2001) J Polym Sci Pol Chem 39:555
39. Takahashi K, Nagai K (1996) Polymer 37:1257
40. Shen S, Sudol ED, El-Aasser MS (1994) J Polym Sci Pol Chem 32:1087
41. Horák D, Švec F, Fréchet JMJ (1995) J Polym Sci Pol Chem 33:2329
42. Takahashi K, Uyama H, Kobayashi S (1998) J Macromol Sci Pure A35:1473
43. Ho C-H, Chen S-A, Amiridis MD, Zee JWV (1997) J Polym Sci Pol Chem 35:2907
44. Chen Y, Yang H-W (1992) J Polym Sci Pol Chem 30:2765
45. Arhady R (1999) In: Arshady R (ed) Microspheres, microcapsules & liposomes, vol 1. Citus, London, p 11
46. Margel S (1999) In: Arshady R (ed) Microspheres, microcapsules & liposomes, vol 2. Citus, London, p 11
47. Takahashi K, Miyanori S, Uyama H, Kobayashi S (1996) J Polym Sci Pol Chem 34:175
48. Horák D (1999) J Polym Sci Pol Chem 37:3785
49. Takahashi K, Miyamori S, Uyama H, Kobayashi S (1997) Macromol Rapid Commun 18:471
50. Takahashi K, Uyama H, Kobayashi S (1998) Polym J 30:684
51. Park KY, Jeong WW, Suh KD (2003) J Macromol Sci A50:617
52. Yang W, Hu J, Tao Z, Li L, Wang C, Fu S (1999) Colloid Polym Sci 277:446
53. Horák A, Shapoval P (2000) J Polym Sci Pol Chem 38:3855
54. Ray B, Mandal BM (1999) J Polym Sci Pol Chem 37:493
55. Lee K, Lee S, Song B, Lee D (2000) Polymer (Korea) 24:629
56. Margel S, Nov E, Fisher I (1991) J Polym Sci Pol Chem 29:347
57. Bahar T, Tuncel A (1999) Polym Eng Sci 39:1849
58. Horák A, Kryštůfek M, Spěváček J (2000) J Polym Sci Pol Chem 38:653
59. Covolan VL, D'Antone S, Ruggeri G, Chiellini E (2000) Macromolecules 33:6685
60. Yang W, Zhou H, Tao Z, Hu J, Wang C, Fu S (2000) J Macromol Sci Pure A37:659
61. Dawkins JV, Neep DJ, Shaw PL (1994) Polymer 35:5366
62. Baines FL, Dionisio S, Billingham NC, Armes SP (1996) Macromolecules 29:3096
63. Watanabe S, Ueno K, Kudoh K, Murata M, Masuda Y (2000) Macromol Rapid Commun 21:1323
64. Omi S, Saito M, Hashimoto S, Nagai M, Ma G-H (1998) J Appl Polym Sci 68:897
65. Horák D (2001) J Polym Sci Pol Chem 39:3707
66. Horák D, Boháček J, Šubrt M (2000) J Polym Sci Pol Chem 38:1161
67. Horák D, Semenyuk N, Lednicky F (2000) J Polym Sci Pol Chem 41:1848
68. Bourgeat-Lami E, Lang J (1998) J Colloid Interf Sci 197:293
69. Percy MJ, Michailidou V, Armes SP, Perruchot C, Watts JF, Greaves SJ (2003) Langmuir 19:2072
70. (a) Li K, Stöver HDH (1993) J Polym Sci Pol Chem 31:2473; (b) Li K, Stöver HDH (1993) J Polym Sci Pol Chem 31:3257
71. (a) Downey JS, Frank RS, Li W-H, Stöver HDH (1999) Macromolecules 32:2838; (b) Li W-H, Stöver HDH (2000) Macromolecules 33:4354
72. Li WH, Li LK, Stöver HDH (1999) J Polym Sci Pol Chem 37:2295
73. Lee C-F, Wen C-J, Chiu Q-Y (2003) J Polym Sci Pol Chem 41:2063
74. Hölderle M, Bar G, Mülhaupt R (1997) J Polym Sci Pol Chem 35:2539
75. Kim J-W, Suh K-D (1998) Colloid Polym Sci 276:878
76. Huang J, Zhang H, Hou J, Jiang P (2002) React Funct Polym 53:1
77. Huang J-X, Yuan X-Y, Yu X-L, Zhang H-T (2003) Polym Int 52:819
78. Okubo M, Nakagawa T (1992) Colloid Polym Sci 270:853
79. Okubo M, Minami H (1996) Macromol Symp 101:509
80. Okubo M, Minami H (1996) Colloid Polym Sci 274:433

81. Okubo M, Konishi Y, Minami H (1998) Colloid Polym Sci 276:638
82. Okubo M, Minami H (1997) Colloid Polym Sci 275:992
83. Okubo M, Yamashita T, Minami H, Konish Y (1998) Colloid Polym Sci 276:887
84. Schneider M, Mülhaupt R (1994) Polym Bull 32:545
85. Awan MA, Dimonie VL, El-Aasser MS (1996) J Polym Sci Pol Chem 34:2633
86. Awan MA, Dimonie VL, El-Aasser MS (1996) J Polym Sci Pol Chem 34:2651
87. Tausendfreund I, Bandermann F, Siesler HW, Kleimann M (2002) Polymer 43:7085
88. Kim J, Jeong SY, Kim KU, Ahn YH, Quirk RP (1996) J Polym Sci Pol Chem 34:3277
89. Murray JG, Schwab FC (1982) Ind Eng Chem Prod Res Dev 21:93
90. Stampa GB (1970) J Appl Polym Sci 14:1227
91. Keki S, Deak G, Daroczi L, Kuki A, Zsuga M (1999) Macromol Symp 157:217
92. Schwab FC, Murray JG (1985) Anionic dispersion polymerization of styrene. In: Culbertson BM, McGrath JE (eds) Advances in polymer synthesis. Plenum, New York
93. Jenkins AD, Maxfield D, dos Santos CG, Walton DRM, Stejskal J, Kratochvil P (1992) Makromol Chem Rapid Commun 13:61
94. Okay O, Funke W (1990) Macromolecules 23:2623
95. Holderle M, Baumert M, Mülhaupt R (1997) Macromolecules 30:3420
96. Gabaston LI, Jackson RA, Armes SP (1998) Macromolecules 31:2888
97. Sosnowski S, Gadzinowski M, Slomokowski S, Penczek S (1994) J Bioact Compat Pol 9:345
98. Sosnowski S, Gadzinowski M, Slomokowski S (1996) Macromolecules 29:4556
99. Armes SP, Aldissi M (1989) J Chem Soc Chem Commun 88
100. Eisazadeh H, Gilmore KJ, Hodgson AJ, Spinks G, Wallace GG (1995) Colloid Surface A 103:281
101. Eisazadeh H, Gilmore KJ, Wallace GG (1995) Polym Int 37:87
102. Banerjee P, Mandal BM (1995) Synth Met 74:257
103. Banerjee P, Digar ML, Bhattacharyya SN, Madal BM (1995) Langmuir 11:2414
104. Armes SP, Aldissi M, Hawley M, Berry JG, Gottesfeld S (1991) Langmuir 7:1447
105. Nagaoka T, Nakano H, Suyama T, Ogura K, Oyama M, Okazaki S (1997) Anal Chem 69:1030
106. Stejskal J, Kratochvíl P, Gospodinova N, Terlemezyan L, Mokreva P (1992) Polymer 33:4857
107. Shannon K, Fernandez JE (1994) J Chem Soc Chem Commun 643
108. Chattopadhyay D, Mandal BM (1996) Langmuir 12:1585
109. Stejskal J, Špírková M, Riede A, Helmstedt M, Mokreva P, Prokeš J (1999) Polymer 40:2847
110. Okubo M, Masuda T, Mukai T (1998) Colloid Polym Sci 276:96
111. Minami H, Okubo M, Murakami K, Hirano S (2000) J Polym Sci Pol Chem 38:4238
112. Mandal TK, Mandal BM (1995) Polym Commun 36:1911
113. Mandal TK, Mandal BM (1999) J Polym Sci Pol Chem 37:3723
114. Digar ML, Bhattacharyya SN, Mandal BM (1994) Polymer 35:377
115. Uyama H, Kurioka H, Kobayashi S (1995) Chem Lett 795
116. Kobayashi S, Uyama H, Ohmae M (2001) Bull Chem Soc Jpn 74:613
117. Ramanathan LS, Shukla PG, Sivaram S (1998) Pure Appl Chem 70:1295
118. Bunn A, Griffin BP, MacDonald WA, Rance DG (1992) Polymer 33:3066
119. Kawaguchi S, Okada T, Tano K, Ito K (2000) Des Monomers Polym 3:263
120. Uchida T, Kawaguchi S, Ito K (2002) Des Monomers Polym 5:285
121. Kobayashi S, Uyama H, Choi JH, Matsumoto Y (1991) Proc Jpn Acad Ser B 67:140
122. (a) Kobayashi S, Uyama H, Lee SW, Matsumoto Y (1993) J Polym Sci Pol Chem 31:3133; (b) Shimano Y, Sato K, Kobayashi S (1995) J Polym Sci Pol Chem 33:2715

123. Uyama H, Kato H, Kobayashi S (1993) Chem Lett 261
124. (a) Kobayashi S, Uyama H, Narita Y (1992) Makromol Chem Rapid Commun 13:337; (b) Koyabashi S, Uyama H (1993) Kobunshi Ronbunshu 50:209
125. Furuhashi H, Kawaguchi S, Itsuno S, Ito K (1997) Colloid Polym Sci 275:227
126. Akashi M, Chao D, Yashima E, Miyauchi N (1990) Appl Polym Sci 39:2027
127. Capek I, Riza M, Akashi M (1992) Polym J 24:959
128. (a) Shen R, Akiyana C, Senyo T, Ito K (2003) C R Chim 6:1329; (b) Shen R, Senyo T, Akiyana C, Atago Y, Ito K (2003) Polymer 44:3221
129. Prestige C, Tadros ThF (1988) J Colloid Interf Sci 124:660
130. (a) Capek I, Riza M, Akashi M (1992) Makromol Chem 193:2843; (b) Riza M, Capek I, Kishida A, Akashi M (1993) Angew Makromol Chem 206:69; (c) Capek I, Riza M, Akashi M (1997) J Polym Sci Pol Chem 35:3131; (d) Capek I, Nguyen SH, Berek D (2000) Polymer 41:7011
131. Nugroho M, Kawaguchi S, Ito K (1995) Macromolecular Reports A32:593
132. Kawaguchi S, Winnik MA, Ito K (1995) Macromolecules 28:1159
133. (a) Ito K (1994) Kobunshi Kako 30:510; (b) Hattori T, Nugroho MB, Kawaguchi S, Ito K (1996) Polym Prepr Jpn 45:157
134. (a) Liu J, Gan LM, Chew CH, Quek CH, Gan LH (1997) J Polym Sci Pol Chem 35:3575; (b) Liu J, Chew CH, Wong SY, Gan LM, Lin J, Tan KL (1998) Polymer 39:283
135. Imai H, Kawaguchi S, Ito K (2003) Polym J 35:528
136. (a) Lacroix-Desmages P, Guyot A (1996) Macromolecules 29:4508; (b) Lacroix-Desmages P, Guyot A (1996) Colloid Polym Sci 274:1129
137. (a) Akashi M, Yanagi T, Yashima E, Miyauchi N (1989) J Polym Sci Pol Chem 27:3521; (b) Serizawa T, Takehara S, Akashi M (2000) Macromolecules 33:1759; (c) Chen M-Q, Serizawa T, Kishida A, Akashi M (1999) J Polym Sci Pol Chem 37:2155
138. Shay JS, English RJ, Spontak RJ, Balik CM, Khan SA (2000) Macromolecules 33:6664
139. Akashi M, Yanagi T, Yahsima E, Miyauchi N (1989) J Polym Sci Pol Chem 27:3521
140. Iwasaki I, Yashima E, Akashi M, Miyauchi N, Marumo K (1991) Polym Prepr Jpn 40:2597
141. (a) Ishizu K, Tahara N (1996) Polymer 37:1729; (b) Ishizu K, Yamashita M, Ichimura A (1997) Macromol Rapid Commun 18:639
142. Riza M, Tokura S, Kishida A, Akashi M (1993) Polym Prepr Jpn 42:4617
143. Chen MQ, Kishida A, Akashi M (1996) J Polym Sci Pol Chem 34:2213
144. Riza M, Tokura S, Iwasaki M, Yashima E, Kishida A, Akashi M (1995) J Polym Sci Pol Chem 33:1219
145. Ishizu K, Yamashita M, Ichimura A (1997) Polymer 38:5471
146. Shaffer KA, Jones TA, Canelas DA, Desimone JM, Wilkinson SP (1996) Macromolecules 29:2704
147. Ishizu K, Tahara N (1996) Polymer 37:2853
148. Obayashi N, Kawaguchi S, Ito K (1997) Polym Prepr Jpn 46:162
149. Nagasaki Y, Sato Y, Kato M (1997) Macromol Rapid Commun 18:827
150. Lascelles SF, Malet F, Mayada R, Billingham NC, Armes SP (1999) Macromolecules 32:2462
151. (a) Senyo T, Atago Y, Kiang H, Shen R, Ito K (2003) Polym J 35:513; (b) Senyo T, Atago Y, Shen R, Ito K (2003) Polym Prepr Jpn 52:1224
152. Fujioka M, Ma G-H, Du Y-Z, Ogino K, Nagai M, Omi S (2003) J Polym Sci Pol Chem 41:1788
153. Chen M-Q, Kaneko T, Chen C-H, Akashi M (2001) Chem Lett 1306
154. Kaneko T, Hamada K, Chen M-Q, Akashi M (2004) Macromolecules 37:501
155. (a) Yilidiz U, Hazer B, Capek I (1995) Angew Makromol Chem 231:135; (b) Yilidiz U, Hazer B (2000) Polymer 41:539

156. (a) Bourgeat-Lami E, Guyot A (1997) Colloid Polym Sci 275:716; (b) Schipper ETWM, Sindt O, Hamaide T, Lacroix-Desmazes P, Müller B, Huyot A, van den Enden MJWA, Vidal F, van Es JJGS, German AL, Montaya Goñi AM, Sherrington DC, Schoonbrood HAS, Asua JM, Sjöberg M (1998) Colloid Polym Sci 276:402
157. Feeney PJ, Napper DH, Gilbert RG (1987) Macromolecules 20:2922
158. Fitch RM, Tsai CH (1971) In: Fitch RM (ed) Polymer colloids. Plenum, New York
159. Gilbert RG (1995) In: Emulsion polymerization: A mechanistic approach. Academic, New York
160. Smoluchowski MV (1917) Z Phys Chem 192:129
161. Frenklach M (1985) J Colloid Interf Sci 108:237
162. de Gennes PG (1980) Macromolecules 13:1069
163. Yasuda M, Yokoyama H, Seki H, Ogino H, Ishimi K, Ishikawa H (2001) Macromol Theor Simul 10:54
164. Yasuda M, Seki H, Yokoyama H, Ogino H, Ishimi K, Ishikawa H (2001) Macromolecules 34:3261
165. Lacroix-Desmazes P, Guillot J (1998) J Polym Sci Pol Phys 36:325
166. Cosgrove T Griffiths PC (1992) Adv Colloid Interfac 42:175
167. Fleer GJ, Cohen Stuart MA, Scheutjens JMHM, Cosgrove T, Vincent B (1993) In: Polymers at interfaces. Chapman & Hall, London
168. Kawaguchi M, Takahashi A (1992) Adv Colloid Interfac 37:219
169. de Gennes PG (1987) Adv Colloid Interfac 278:189
170. Alexander S (1977) J Phys (Paris) 38:983
171. Auroy P, Auvray L, Leger LL (1991) Physica A 172:269
172. Taunton HJ, Toprakcioglu C, Fetters LJ, Klein J (1990) Macromolecules 23:571
173. Cairns RJR, Ottewill RH, Osmond DWJ, Wagstaff I (1976) J Colloid Interf Sci 54:45
174. Jeong BJ, Lee JH, Lee HB (1996) J Colloid Interf Sci 178:757
175. Werts MPL, van der Vegte EW, Hadziioannou G (1997) Langmuir 13:4939
176. Wu C, Akashi M, Chen MQ (1997) Macromolecules 30:2187
177. Kawaguchi S, Winnik MA, Ito K (1996) Macromolecules 29:4465

Received: March 2004

Adv Polym Sci (2005) 175: 329–346
DOI 10.1007/b100114

Heterogeneous Polymerization of Fluoroolefins in Supercritical Carbon Dioxide

Karen A. Kennedy[1] · George W. Roberts[1] · Joseph M. DeSimone (✉)[1,2]

[1] Department of Chemical Engineering, North Carolina State University, Raleigh, NC 27695–7905, USA
kakenne2@eos.ncsu.edu, groberts@eos.ncsu.edu
[2] Department of Chemistry, University of North Carolina at Chapel Hill, Chapel Hill, NC 27599–3290, USA
desimone@unc.edu

Abstract In recent years, carbon dioxide has been investigated for its potential to replace the aqueous and organic solvents used in polymerization processes. Carbon dioxide has several benefits, including being environmentally benign, a tunable solvent, resistant to chain transfer, and of low viscosity which facilitates high initiator efficiencies and fluid handling. Homo- and copolymerization of fluoroolefins such as tetrafluoroethylene (TFE), vinylidene fluoride (VF2), hexafluoropropylene (HFP), and perfluorinated vinyl ethers in carbon dioxide are particularly interesting because of the significant waste reduction and the elimination of potentially harmful processing agents. This review focuses on recent developments in polymerizing fluoroolefins via heterogeneous polymerization in carbon dioxide. At least one CO_2-based polymerization process has recently been commercialized, and additional research is underway to understand the kinetics associated with polymerizing fluoroolefins

in carbon dioxide. As researchers improve their understanding of CO_2-based polymerizations, and as industry continues to look for more economically and environmentally-sound alternatives to existing processes, it will become more and more common to employ carbon dioxide as a polymerization medium.

Keywords Supercritical carbon dioxide · Fluoropolymers · Tetrafluoroethylene · Vinylidene fluoride

Abbreviations

AIBN	2,2′-azobis(isobutyronitrile)
APFO	ammonium perfluorooctanoate
BPPP	Bis(perfluoro-2-*N*-propoxypropionyl) peroxide
C8	ammonium perfluorooctanoate
CMC	Critical micelle concentration
CSTR	Continuous stirred tank reactor
CTFE	Chlorotetrafluoroethylene
DEPDC	Diethyl peroxydicarbonate
EPA	Environmental Protection Agency
FEP	Poly(tetrafluoroethylene-co-hexafluoropropylene)
FMG	Fluoropolymers Manufacturers Group
FTIR	Fourier transform infrared spectroscopy
HFP	Hexafluoropropylene
LDPE	Low-density polyethylene
M_n	Number-average molecular weight
MAC	Maleic acid
MAN	Maleic anhydride
MFI	Melt flow index
MWD	Molecular weight distribution
NMR	Nuclear magnetic resonance spectroscopy
PFA	Poly(tetrafluoroethylene-co-perfluoro(propyl vinyl ether))
PMVE	Perfluoro(methyl vinyl ether)
PPVE	Perfluoro(propyl vinyl ether)
PTFE	Poly(tetrafluoroethylene)
PVDF	Poly(vinylidene fluoride)
$scCO_2$	Supercritical carbon dioxide
SCF	Supercritical fluid
TFE	Tetrafluoroethylene
VF	Vinyl fluoride
VF2	Vinylidene fluoride

1 Introduction

The first application of supercritical fluids (SCFs) to the polymer industry occurred in the 1930s, with the development of a free-radical bulk polymerization of supercritical ethylene to produce low-density polyethylene (LDPE) [1, 2]. LDPE is synthesized by a high-pressure process, at 180–300 °C and 1000–

Table 1 Critical temperatures and pressures of substances useful as supercritical fluids [9]

	Critical temperature T_c (°C)	Critical pressure P_c (bar)
Carbon Dioxide (CO_2)	31.1	73.8
Water (H_2O)	374.4	221.2
Ethane (C_2H_6)	32.4	48.8
Propane (C_3H_8)	96.8	42.5
Ammonia (NH_3)	132.4	113.5
Nitrous Oxide (N_2O)	36.6	72.4
Fluoroform (CHF_3)	26.3	48.6

3000 bar, in which the polymer is soluble in supercritical ethylene monomer [3]. However, inert SCFs have only recently been exploited in a wide range of polymer applications. Research with supercritical carbon dioxide ($scCO_2$) has outpaced research with other SCFs because carbon dioxide is inexpensive, has a critical point (Table 1) at conditions lower than that of most other SCFs (increasing the range of tunability), and is environmentally benign. Supercritical carbon dioxide has found particular application as a polymerization medium because of its inertness to free radicals [4] (in other words, there is no chain transfer to CO_2), and because of CO_2's high initiator efficiencies. DuPont has built a commercial-scale facility for the production of tetrafluoroethylene-based polymers, including Teflon™ FEP (a copolymer of tetrafluoroethylene and hexafluoropropylene), in carbon dioxide [5]. Significant research [6–8] into the use of $scCO_2$ as a polymerization medium has been reported. This review will focus on recent developments in the polymerization of fluoroolefins, such as tetrafluoroethylene, via heterogeneous polymerization in $scCO_2$. The particular challenges and rewards associated with polymerizing fluoroolefins in CO_2 will be discussed.

2 Conventional Polymerization of Fluoroolefins

The major commercial fluoropolymers are made by homopolymerization of tetrafluoroethylene (TFE), chlorotrifluoroethylene (CTFE), vinylidene fluoride (VF2), and vinyl fluoride (VF), or by co-polymerization of these monomers with hexafluoropropylene (HFP), perfluoro(propyl vinyl ether) (PPVE), perfluoro(methyl vinyl ether) (PMVE), or ethylene. The polymers are formed by free-radical polymerization in water or fluorinated solvents.

Currently, there is concern about the use of ammonium perfluorooctanoate (APFO), also known as "C8", which is necessary for the manufacture of fluorinated plastics and elastomers in water. C8 is a perfluorinated anionic surfactant used as a dispersing agent in the polymerization and copolymerization of many fluoropolymers, including poly(tetrafluoroethylene) (PTFE), poly(vinylidene

fluoride) (PVDF), poly(tetrafluoroethylene-co-hexafluoropropylene) (FEP), poly(tetrafluoroethylene-co-perfluoro(propyl vinyl ether)) (PFA), and poly-(tetrafluoroethylene-co-perfluoro(methyl vinyl ether)) [10]. It is necessary to use a perfluorinated anionic surfactant for two important reasons. First, fluorinated anionic surfactants have the right interfacial properties to disperse hydrophobic particles like fluoropolymers in water. Second, fluorinated carbon-centered radicals are extremely electrophilic and will react (via chain transfer) with any hydrocarbon-based species in solution, including the surfactant. Hence, the surfactant chosen needs to be hydrogen free.

Earlier this year, the Environmental Protection Agency (EPA) released a preliminary risk assessment of C8 and other fluorochemicals [10]. Although the EPA refers to C8 as a persistent organic pollutant, there have been no reported adverse health affects in humans. However, because of these potential environmental and health problems, 3 M, who was the leading manufacturer of C8, exited the C8 business [11]. DuPont and other members of the Fluoropolymers Manufacturers Group (FMG) have conducted research over the last 30 years to identify alternatives to C8 for economic reasons, and because C8 persists in the body. However, no viable, alternative dispersing agent has been identified. Carbon dioxide is the only known alternative that can eliminate the need for C8 in the manufacturing process.

Polymers made from TFE and VF2 dominate the fluoropolymer market. Existing methods for synthesizing these polymers will be reviewed in the following sections.

2.1 Tetrafluoroethylene

Poly(tetrafluoroethylene) is a fluorinated analog of polyethylene with chains that are arranged into a helical twisting conformation in which the carbon backbone is shielded by fluorine atoms. This results in a polymer with superior chemical resistance. Additionally, PTFE has high thermal stability and a very low coefficient of friction. This makes PTFE an ideal polymer to use as an anti-stick coating and to use with aggressive chemicals. In 2001, the U.S. consumed 39.7 million pounds of PTFE – it was the most widely consumed of any fluoropolymer [12]. PTFE is sold as a granular resin, fine powder, or an aqueous dispersion for use in a variety of applications, including coatings, chemical processing equipment, and wire insulation.

PTFE is synthesized via either suspension or dispersion polymerization in water, depending on the particle size required. Both processes are run at 70–120 °C and 1–6 MPa using a water-soluble initiator such as ammonium persulfate [13]. In the dispersion polymerization, a dispersing agent, such as ammonium perfluorooctanoate (C8), and mild agitation are used to produce a stable dispersion of fine PTFE particles of average particle size 0.2 µm. Hydrocarbon wax can be added to prevent coagulation of the particles. Because the amount of dispersing agent is typically less than the critical micelle concen-

tration (CMC), the polymerization is not a true emulsion polymerization. However, the polymerization does possess characteristics of an emulsion polymerization. After the polymerization is complete, the particles may be precipitated to form a fine powder or the dispersion may be concentrated for direct use as a coating. Fine powder PTFE is commonly mixed with a lubricant such as kerosene to perform paste extrusion of tubing and wire insulation.

In suspension polymerization, little or no dispersing agent and vigorous agitation is used to produce a coagulated granular resin with particles 1–2 mm in size. The particles are dried and ground to varying particle sizes for molding or ram extrusion into precision parts.

Conventional wisdom suggests that PTFE homopolymer cannot be melt-processed to form molded parts due to its extremely high molecular weight and high melt viscosity. Grades of PTFE, known as micropowders, with low molecular weight and low melt viscosity are typically used as additives in coatings and thermoplastics [14]. However, these grades cannot be melt-processed due to their brittleness. Tervoort et al [15] recently reported that PTFE with medium viscosities (melt flow rate 0.2–2.6 g/10 min) and bimodal molecular weight distributions can be melt processed. PTFE grades with high and low viscosity are blended in a twin-screw extruder to form a blend exhibiting a pseudobimodal molecular weight distribution. The blend retains the mechanical strength of the high viscosity material, but the presence of the low viscosity material enables melt-processing of the material into a variety of parts and also suggests the possible recycling of PTFE.

2.2 Vinylidene Fluoride

Poly(vinylidene fluoride) is a semi-crystalline polymer that is produced commercially by a free-radical emulsion or suspension polymerization of vinylidene fluoride (CH_2=CF_2) in water [16–18]. PVDF exhibits a unique combination of mechanical and electrical properties due to the alternating spatial arrangement of CH_2 and CF_2 groups along the polymer backbone. PVDF is the fluoropolymer consumed in the greatest quantities aside from PTFE [12], because of its (1) high mechanical and impact strength, (2) resistance to environmental stress, (3) ease of melt-processability, and (4) low cost compared to other fluoropolymers. PVDF is used in architectural coatings (~40%), semiconductor manufacture and chemical processing (~40%), and wire and cable insulation (~20%) [19]. A small, but increasing amount of PVDF is used as electrodes in lithium batteries [12, 20].

Polymerization of vinylidene fluoride by emulsion or suspension polymerization in water is conducted at conditions of 10–130 °C and 10–200 bar. In the emulsion polymerization, either water-soluble peroxides or monomer-soluble peroxy or organic peroxides are used as initiators [17]. Fluorinated surfactants, such as ammonium perfluorooctanoate, are used as dispersing agents. Chain transfer agents, such as acetone, chloroform, or trichlorofluoromethane, may be

used to control the molecular weight [13]. The resulting latex of dispersed particles is coagulated, washed, and spray dried to form a fine powder. The powder consists of spherical agglomerates 0.2–0.5 μm in diameter.

The suspension polymerization is conducted using monomer-soluble peroxy initiators. Water-soluble polymers, such as poly(vinyl alcohol), are typically used as suspending agents to reduce the coalescence of the polymer particles [17]. A slurry of polymer particles 30–100 μm in diameter is formed during the polymerization. The particles are washed and dried before further processing.

The effect of polymerization conditions on the polymer morphology in PVDF has been studied [16, 21]. Regioisomer defects in the form of reversed head-to-tail addition are common in the polymerization of vinyl monomers [22]. These defects affect the crystallinity and final properties of the polymer. The fraction of defects in PVDF ranges from 3.5 to 6 mol%, increasing with reaction temperature [22]. The α-phase crystal is the most common crystal observed in PVDF. However, an increase in defects leads to a greater amount of β-phase crystals in the polymer [16, 23], which gives PVDF its piezoelectric properties. An increase in the amount of β crystals formed was observed for different initiating systems [23]. Additionally, enhancement of the β crystals in PVDF is achieved by applying tensile forces or mechanical stretching to the polymer [24]. The γ and δ crystal phases may be generated from the α-phase using heat or an electric field, respectively. The γ-phase crystal has also been formed by crystallization under high pressure [25].

Commercial PVDF is sold in powder form or may be compression molded into pellets. Depending on the polymerization conditions, differing properties of PVDF may be produced. PVDF exhibiting a multimodal molecular weight distribution has been reported due to its improved melt flow characteristics [26] and its use in lithium batteries [24]. Dohany [26] reports the formation of a distinct bimodal molecular weight distribution that is strongly dependent on the addition of the initiator to the reaction. The initiator is continuously fed to the reaction until about 50% of the total monomer feed is added to the reactor. At that point, the addition of the initiator is stopped and the remaining monomer is continuously fed to the reactor. The high molecular weight peak measured by gel permeation chromatography is more than 30% of the overall molecular weight distribution. The high molecular weight portion allows processing of the polymer at high shear rates for improved productivity. The use of these polymers in lithium batteries is largely the result of their relatively high defect structure, which promotes ionic conductivity in the electrochemical cell [24].

2.3 Copolymers

PVDF and PTFE have wide application in industry due to their strength, chemical and wear resistance, and dielectric properties. However, VF2 and TFE may be copolymerized with comonomers such as hexafluoropropylene (HFP) and

vinyl ethers to modify the properties of the polymer. For example, copolymerizing VF2 with HFP improves the flexibility of the polymer without compromising the electrical properties. Therefore, VF2-HFP copolymers are used more commonly in cable insulation than VF2 homopolymer. Copolymers of TFE with perfluoroalkyl vinyl ethers have properties very similar to the TFE homopolymer except that the copolymer may be processed by injection molding because of its lower melt viscosity. Copolymers of TFE and VF2 can also be made to form fluorinated elastomers and perfluorinated elastomers when cure site monomers are used. Important examples of such elastomers include terpolymers of VF2, TFE, and either HFP or PMVE along with a cure site monomer such as bromotetrafluorobutene [19].

Copolymers are produced by aqueous copolymerization of the monomers in a manner similar to the homopolymerizations. Nonaqueous polymerizations of TFE with PPVE may be conducted in water or in fluorinated solvents at lower temperatures (30–60 °C) using a soluble organic initiator such as perfluoropropionyl peroxide. The molecular weight is controlled by addition of chain transfer agents such as methanol in nonaqeuous polymerizations or hydrogen in aqeous polymerizations.

3
Supercritical Carbon Dioxide as a Polymerization Medium

3.1
Properties of Supercritical Carbon Dioxide

Supercritical fluids possess characteristics that make them interesting for use as polymerization media. A supercritical fluid exists at temperatures and pressures above its critical values. In the supercritical state, the fluid exhibits physical and transport properties intermediate between the gaseous and liquid state. This is illustrated in Table 2. SCFs have liquid-like densities, but gas-like diffusivities. These intermediate properties can provide advantages over liquid-based processes. In particular, the higher diffusivities of SCFs reduce mass transfer limitations in diffusion-controlled processes. Additionally, lower energy is required for processing the supercritical fluid because its viscosity is lower than that of most liquids, and because the need to vaporize large quantities of liquid is avoided.

Table 2 Comparison of typical SCF, liquid, and gas properties [27]

	Liquid	SCF	Gas
Density (g/cm^3)	1	0.1–0.5	10^{-3}
Viscosity (Pa s)	10^{-3}	10^{-4}–10^{-5}	10^{-5}
Diffusivity (cm^2/s)	10^{-5}	10^{-3}	10^{-1}

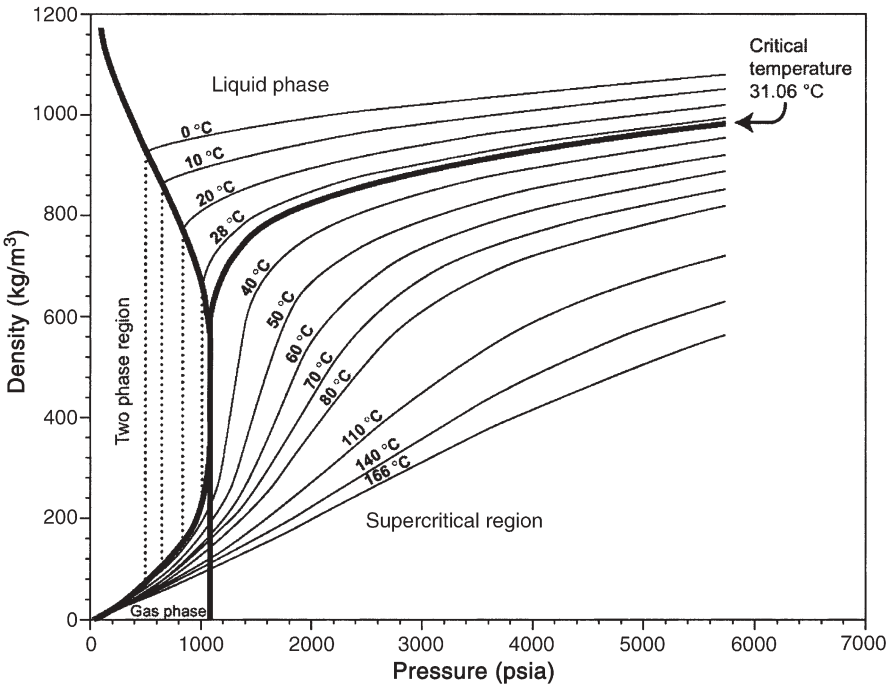

Fig. 1 Density versus pressure isotherms for carbon dioxide [28]

SCFs have a tunable density that may offer further advantages in reaction and processing applications. This tunability is illustrated in Fig. 1 for carbon dioxide. Near the critical point, even small changes in the temperature or pressure of carbon dioxide dramatically affect its density. Similarly, the viscosity, dielectric constant, and diffusivity are also tunable parameters, which allows specific control of systems involving supercritical fluids.

Carbon dioxide is inexpensive and widely available. The main source of carbon dioxide is from chemical manufacturing. For example, it is a major byproduct in the production of ammonia, ethanol, and hydrogen. Finally, carbon dioxide is non-toxic, nonflammable, and easily recycled.

3.2 Advantages of Using Supercritical Carbon Dioxide

Supercritical carbon dioxide is a very good solvent for small molecules, but a poor solvent for most high molecular weight polymers at mild conditions (T<100 °C, P<350 bar). Amorphous fluoropolymers and silicones are the only polymers known to be soluble in CO_2 at mild conditions [6]. This difference in solubilities is an advantage for CO_2-based polymerizations, as it can be used to reduce the energy requirements necessary to separate and purify a polymer after synthesis. Consider, for example, a batch precipitation polymerization in

CO_2. Initially, the reactor contains a homogeneous solution of monomer and initiator (and perhaps a chain transfer agent) in CO_2. As the polymerization proceeds, the polymer precipitates to form a separate phase. When the polymerization is complete, the polymer is separated from the reaction mixture by a conventional fluid/solid separation process (sedimentation, filtration, centrifugation). The fluid phase contains unreacted monomer and initiator, which can be recycled. When the polymer is depressurized, the CO_2 escapes, leaving a dry polymer. This contrasts with water-based processes in which the polymer must be dried to remove water. The drying step can be quite energy intensive. Additionally, CO_2 can remove residual monomer from the polymer by supercritical fluid extraction. Significant energy savings may be realized in a CO_2-based polymerization.

Other advantages of CO_2-based polymerizations are that there is no chain transfer to the solvent, and that the production of unstable end groups can be dramatically reduced. Guan et al [4] studied the decomposition of 2,2′-azobis-(isobutyronitrile) (AIBN) in $scCO_2$. It was found that initiator efficiencies greater than 80% were possible due to the low viscosity of CO_2 and negligible solvent cage effects. Additionally, analysis of the decomposition products showed that there was no chain transfer to CO_2.

Reactive end groups, such as acyl fluoride and carboxylic acid end groups, are commonly formed in the aqueous polymerization of fluoroolefins, especially the copolymerization of TFE with HFP and PPVE [13]. These unstable end groups may decompose during melt processing of the polymer and cause defects in the final application. Generally, finishing steps are required after the polymerization to remove these end groups by hydrolysis or fluorination. Using CO_2 as a polymerization medium eliminates the need for these finishing steps and additional control of the polymerization is achieved with the absence of chain transfer to solvent.

The feasibility of using $scCO_2$ in polymerizations has been demonstrated by the commercial production of Teflon^{TM} in CO_2 [29] using methods developed by DeSimone and Romack [30–35]. Polymerization in carbon dioxide does not require the use of C8, which has received negative publicity for being persistent in the blood. DuPont has built a $40 million development facility for the production of Teflon FEP using CO_2-based technologies [5]. Poly(vinylidene fluoride) (PVDF) is another fluoropolymer that may be manufactured in supercritical carbon dioxide. DeSimone and co-workers [36, 37] reported the first continuous polymerization of vinylidene fluoride in $scCO_2$. Subsequently, Solvay Corporation submitted a patent application on a process for making poly(vinylidene fluoride) in $scCO_2$ [38]. As researchers continue to improve their understanding of CO_2-based polymer applications, and as industry continues to look for more economical and environmentally-sound alternatives to existing processes, the use of supercritical carbon dioxide in commercial polymer reactions and processing will increase.

4
Precipitation Polymerization in Supercritical Carbon Dioxide

4.1
Introduction

The first reported polymerization of fluoroolefins in carbon dioxide was by Fukui and coworkers [39, 40]. Tetrafluoroethylene, chlorotrifluoroethylene, and other fluoroolefins were polymerized in the presence of CO_2 using ionizing radiation [39, 40] and free-radical initiators [40]. DeSimone and coworkers reported the homogeneous telomerization of tetrafluoroethylene [41] and vinylidene fluoride [42] in CO_2 using AIBN as an initiator. The kinetics of AIBN decomposition in CO_2 is well understood [4]. However, peroxide initiators are preferred over azo initiators for producing stable endgroups in fluoroolefins [43]. The peroxy initiators bis(perfluoro-2-*N*-propoxypropionyl) peroxide (BPPP) and diethyl peroxydicarbonate (DEPDC) have had the greatest application in the heterogeneous polymerization of fluoroolefins in CO_2.

DeSimone and coworkers have studied the decomposition kinetics of BPPP [44] and DEPDC [45] in CO_2. The decomposition of DEPDC was studied [45] by a technique in which the decomposition rate constant, k_D, and the initiator efficiency, f, were determined from a single set of experiments using a continuous stirred tank reactor (CSTR). It was found that the decomposition was first order and that the rate constant was independent of the pressure. The activation energy of the decomposition rate constant in CO_2 was consistent with those in other solvents. It was concluded that the nature of the solvent did not affect the decomposition kinetics. The decomposition kinetics of BPPP [44] in CO_2 and fluorinated solvents was measured using FTIR. Based on results from the effect of viscosity on the observed decomposition rate constant, it was concluded that the decomposition mechanism was a single-bond homolysis. Additionally, it was concluded that the decomposition rate constants in CO_2 and fluorinated solvents should be similar. The studies of BPPP and DEPDC decomposition in CO_2 set the stage for a better understanding of the overall kinetics of polymerizations in CO_2. The next section contains a discussion of recent research into the polymerization of fluoroolefins in CO_2 using BPPP, DEPDC, and ionizing radiation.

4.2
Polymerization of Tetrafluoroethylene

Several alternative polymerization media have been proposed for reducing the amount of unstable end groups in poly(tetrafluoroethylene). These include chlorofluorocarbons, which are detrimental to the environment, perfluorocarbons, hydrofluorocarbons, and perfluoroalkyl sulfide acids, which are all expensive. Supercritical carbon dioxide has been identified as a viable alternative to aqueous and fluorocarbon reaction media [31]. Furthermore, mixing

tetrafluoroethylene with carbon dioxide increases the safety of handling the monomer [46]. Pure tetrafluoroethylene (TFE) is susceptible to autopolymerization and may be explosive without proper handling. Storing and shipping TFE in a mixture with CO_2 makes handling safer.

The polymerization of TFE in CO_2 [31–35, 41, 47] has been studied extensively. Polymerizations were typically run at 35 °C using BPPP as an initiator. This particular initiator was selected to produce stable end groups in the polymer made in CO_2. The selection of initiators for polymerization of fluoromonomers in CO_2 that would produce stable end groups had not been reported previously. The reaction produced up to a 100% yield and a 160,000 g/mol molecular weight polymer. This work set the stage for commercialization of a CO_2-based process for making TFE-based polymers by DuPont [5]. DuPont has started to sell melt-processible polymers with enhanced performance capabilities [29] that are polymerized in a CO_2-based process.

4.3 Polymerization of Vinylidene Fluoride

The current means for commercial production of poly(vinylidene fluoride) generates large amounts of wastewater due to water-based suspension or emulsion polymerization. Additionally, large amounts of energy are required to remove the water from the polymer before downstream processing. The use of $scCO_2$ as a polymerization medium for vinylidene fluoride has been previously demonstrated in batch polymerizations [42, 48]. A CO_2-based system has the advantage of eliminating wastewater generation during the polymerization. Because the polymer is readily separated from CO_2, significant energy savings may be realized. Recently, Charpentier et al have developed a system for polymerizing vinyl monomers, including vinylidene fluoride, in $scCO_2$ using a continuous stirred tank reactor [36]. The technical viability of continuously polymerizing vinylidene fluoride in $scCO_2$ was demonstrated with this system. Furthermore, Solvay Corporation has recently submitted a patent application for the continuous polymerization of vinylidene fluoride and other halogenated monomers in $scCO_2$ [38].

The first demonstration of vinylidene fluoride polymerization in $scCO_2$ was the homogeneous telomerization of vinylidene fluoride with perfluorobutyl iodide and AIBN [42]. Several batch studies [48, 49] then were conducted to identify appropriate initiators for the CO_2-based synthesis of high molecular weight PVDF. Kipp [48] used several different peroxy and azo initiators and found that the azo initiators, AIBN and 2,2′-azobis(2,4-dimethyl-methoxypentanitrile), were ineffective in producing significant amounts of PVDF. Amongst the peroxy initiators studied, Kipp found that BPPP was very effective as an initiator for vinylidene fluoride. Number-average molecular weights (M_n) upwards of 24,000 g/mol and conversions of up to 85% were reported. Brothers [49] found that dimethyl(2,2′-azobisisobutyrate) was better than other azo initiators, such as AIBN, for initiating the polymerization of vinylidene

fluoride in CO_2. Brothers reported reaction yields of 22.8%, compared to only 2.6% for an AIBN-initiated system.

Galia and coworkers [50] used γ-radiation to initiate the polymerization of VF2 in CO_2. Reactions were run at 20–40 °C at pressures less than 25 MPa. Number-average molecular weights as high as 607,000 g/mol were observed in polymerizations with initial monomer concentrations ranging from 3.4 to 4.7 mol/L. The polydispersity ranged from 2.5 to 8.8. Conversions were 20–42%. At the highest monomer concentration studied (6.2 mol/L), a conversion of 73% was observed. Galia concluded from rheological measurements of the polymers that increasing the monomer concentration increased the degree of branching and crosslinking in the polymer. The effect of temperature and system density on the kinetics and polymer properties was also studied. There was no observable impact of the system density on the kinetics or polymer properties. However, the polymer properties were very sensitive to the reaction temperature.

Recently, Charpentier et al. [36] demonstrated the synthesis of PVDF by a continuous precipitation polymerization in $scCO_2$, using diethyl peroxydicarbonate (DEPDC) as an initiator. Low molecular weight polymers (M_n<20,000 g/mol) were reported in this first work. However, subsequent research has yielded PVDF with number-average molecular weights upwards of 79,000 g/mol [51, 52]. PVDF made in the continuous CO_2-based system had molecular weights comparable to commercial polymers, but also exhibited unique properties not observed in PVDF made by conventional processes.

4.3.1 Continuous Polymerization

In a typical continuous polymerization [36, 51–54], vinylidene fluoride (VF2), carbon dioxide, and initiator are continuously fed to a continuous stirred tank reactor (CSTR). The initiator is dissolved in a solvent such as (other solvents possible) Freon-113 and the ratio of initiator to monomer was typically less than 0.01 g/g. This initial reaction mixture is homogeneous over the full range of monomer concentrations evaluated (up to 6 M or 50 wt% VF2 in CO_2). As the reaction proceeds, the polymer precipitates from the fluid phase to form a solid polymer phase. The effluent exiting the reactor consists of polymer particles suspended in a fluid mixture of carbon dioxide, unreacted monomer, and unreacted initiator. The effluent is passed through a heat exchanger to quench the reaction. The polymer is collected in one of three filters, depending on whether the reactor is running at unsteady state or steady state. Finally, after the polymer is separated, the effluent is vented into a hood. Conceivably, the effluent may be recycled back to the reactor. A schematic of the polymerization system is shown in Fig. 2. Typical conversions in the reactor are 7–25%. A range of reaction conditions were studied at 30–80 °C, 130–280 bar, and with average residence times of 12– 50 minutes.

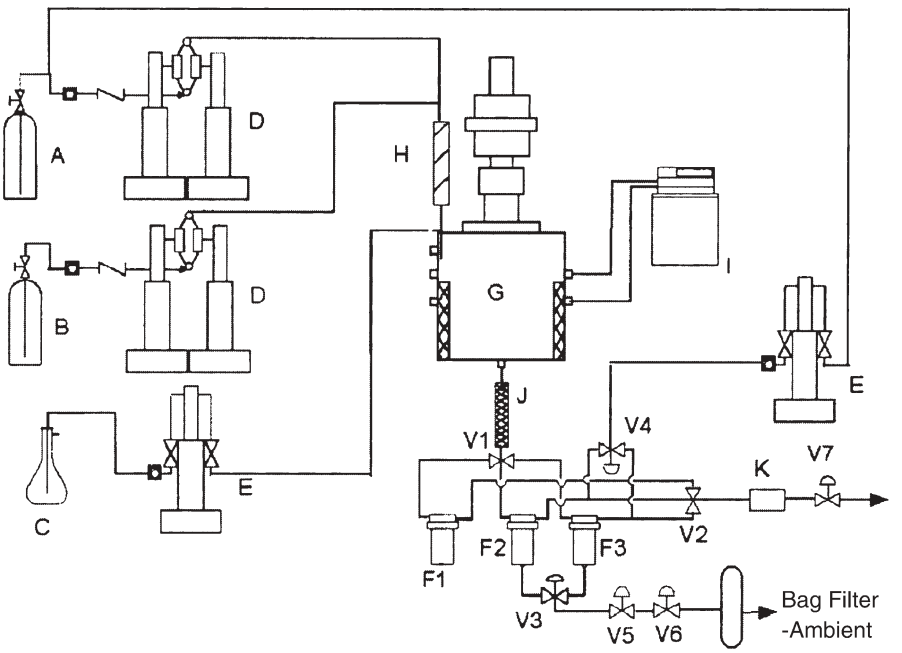

Fig. 2 Continuous polymerization apparatus: A, CO_2 cylinder; B, monomer; C, initiator solution; D, continuous syringe pumps; E, syringe pumps; F1, steady-state filter; G, thermostated autoclave; H, static mixer; I, chiller/heater unit; J, effluent cooler; K, gas chromatograph; V1, V2, four-way valves; V4, three-way valves; V5, V6, two-way valves; V7, heated control valve [51]

A kinetic model based on homogeneous polymerization was developed to describe the polymerization in CO_2 [51, 54]. A model based on the reaction scheme in Fig. 3 adequately described the polymerization rates and the polydispersity of the polymer. Monomer inhibition was incorporated into the model to account for the observed deviation from first-order kinetics. However, imperfect mixing of the higher viscosity medium is an alternative explanation. It was concluded that termination was by combination, for three reasons. First, there was no existing literature to support termination by disproportionation for PVDF. Second, the polydispersity was approximately 1.5 at low monomer concentrations. Third, NMR studies showed no evidence of unsaturation.

Chain transfer to the polymer was proposed to account for the broadening of the molecular weight distribution at high monomer concentrations. However, as discussed in the next section, the model failed to predict the bimodal character that is unique to PVDF polymerized in $scCO_2$ at high monomer concentrations.

$$I \xrightarrow{k_D} 2fR^{\bullet} \quad \text{(Initiator decomposition)}$$

$$R^{\bullet} + M \xrightarrow{k_M} P_1^{\bullet} \quad \text{(Chain initiation)}$$

$$P_n^{\bullet} + M \xrightarrow{k_p} P_{n+1}^{\bullet} \quad \text{(Propagation)}$$

$$P_n^{\bullet} + P_m^{\bullet} \xrightarrow{k_{tc}} P_{n+m} \quad \text{(Termination by combination)}$$

$$P_n^{\bullet} + M \xrightarrow{k_Q} P_n + M^{*} \quad \text{(Inhibition)}$$

$$P_n^{\bullet} + P_m \xrightarrow{mk_{tp}} P_m^{\bullet} + P_n \quad \text{(Chain transfer to polymer)}$$

Fig. 3 Kinetic scheme to model the continuous polymerization of vinylidene fluoride in supercritical carbon oxide [51]

4.3.1.1 Polymer Properties

A comparison was made between the properties of PVDF synthesized in CO_2 and a commercial PVDF sample. The polymers synthesized in CO_2 had molecular weights similar to the commercial polymer and the melt flow indices (MFIs) were similar [54]. For PVDF synthesized in CO_2 with a weight-average molecular weight of 150,000 g/mol, the MFI was 2.6 g/10 min. The MFI for a commercial sample with a weight-average molecular weight greater than 195,000 was 1.4 g/10 min.

Unique PVDF properties have been observed after polymerization in supercritical carbon dioxide [38, 51–53, 55] at certain conditions. The polymer synthesized in supercritical carbon dioxide exhibits a bimodal molecular weight distribution (MWD), as illustrated in Fig. 4 [52]. At molar VF2 feed concentrations less than about 1.9 M, the polymer has a unimodal distribution, at the conditions of Fig. 4. As the monomer concentration is increased, the distribution becomes broader and bimodal. Changes in temperature, pressure, and residence time also have an effect on the MWD [51, 52]. In Fig. 4, τ is the average residence time (the reactor volume divided by the inlet volumetric flow rate).

Several hypotheses were investigated to explain the bimodal character of the polymer. These include: (1) imperfect mixing, (2) long chain branching, and (3) heterogeneous polymerization. A heterogeneous polymerization is characterized by polymerization in both the fluid and precipitated polymer phases, so that the phase equilibrium is an important element of kinetics and polymer properties. It was stated that neither imperfect mixing nor a homogeneous polymerization with long chain branching due to chain transfer to polymer could explain the bimodal nature of the CO_2-polymerized PVDF [51, 52]. However, it was recently demonstrated that a combination of chain branching and heterogeneous polymerization could produce the bimodal MWDs observed experimentally [56].

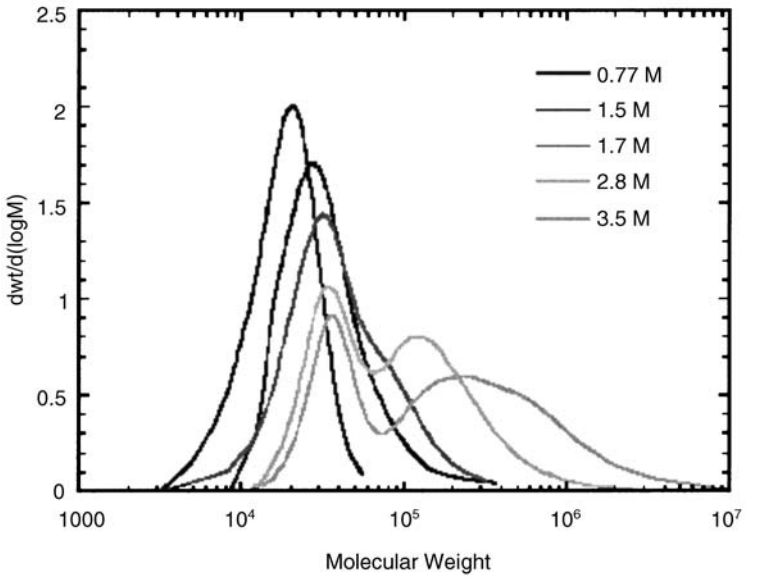

Fig. 4 Effect of inlet monomer concentration on molecular distributions. Polymerization conditions are 75 °C, 4000 psig, τ=20–22 min, [I]o=2.8–3.3 mmol/L [52]

4.4 Synthesis of Copolymers

Copolymerizations of TFE [31, 47, 57–61] and VF2 [57, 58, 61, 62] in $scCO_2$ have been reported. Romack and coworkers [47, 60] did early work to perform precipitation polymerizations of TFE with HFP and TFE with perfluoropropyl vinyl ether (PPVE) at 35 °C and moderate pressures (<133 bar). A chain transfer agent, methanol, was necessary to limit the molecular weight to a range of commercial interest. Hydrogen chloride and hydrogen bromide have also been reported as effective chain transfer agents for these polymerizations in CO_2 [58]. Romack and coworkers concluded that the significantly higher molecular weights produced in CO_2 were due to the fact that chain transfer and β-scission reactions occurred to a lesser extent in $scCO_2$, especially at the lower temperatures used. These undesirable reactions are commonplace in the copolymerization of TFE/PPVE conducted at elevated temperatures in conventional solvents. The limited β-scission reactions were attributed to the enhanced diffusion of TFE into the polymer phase to improve the rates of radical cross-propagation with TFE. It was demonstrated that conducting the polymerization in CO_2 at lower temperatures improved the effectiveness of the propagation reaction over that of the chain transfer reactions to produce high molecular weight polymers.

The research group of Shoichet [57, 59] also has demonstrated that using CO_2 as a polymerization medium can improve the effectiveness of the propagation reaction over chain transfer reactions in fluoroolefin synthesis. Shoichet's

group polymerized vinyl acetate with fluoroolefins in CO_2 with [59] and without [57] surfactants. The copolymers formed in CO_2 were linear, compared to the highly branched copolymers formed by aqueous polymerization. They concluded that because radical hydrogen abstraction from vinyl acetate was significantly reduced in CO_2, branching of the polymer was practically eliminated.

There has been research on new, novel fluoroolefin-based copolymers that benefit from synthesis in $scCO_2$. In 2000, Wheland and Brothers [61] described novel copolymers of fluoroolefins with maleic anhydride (MAN) and maleic acid (MAC) for use as coatings and as adhesives or compatibilizing agents for fluoropolymers. Currently, maleic anhydride must be grafted onto existing fluoropolymers to achieve the desired properties. Maleic acid does not readily copolymerize with fluoroolefins in the presence of water. Therefore, polymerization of MAN or MAC with fluoroolefins in CO_2 provides a way to synthesize the desired fluoropolymer directly. There is an interest in using 157 nm photoresists in microchip manufacturing to create smaller and smaller features in circuitry. Zannoni and DeSimone [62] have copolymerized fluoroolefins with norbornene and a norbornene analog for use as 193 nm and 157 nm photoresists. Ultimately, these photoresists may be synthesized, processed and developed entirely in CO_2, with dramatically reduced solvent use, revolutionizing the manufacture of microchips.

5 Conclusions

Supercritical carbon dioxide shows promise as a polymerization medium for the synthesis of fluoroplastics and fluoroelastomers. CO_2 offers the benefit of an environmentally friendly process that reduces the amount of waste generated and energy required when processing polymers. Additionally, polymerization kinetics and polymer properties may be enhanced by polymerization in CO_2. DuPont has already commercialized a process for making fluoropolymers in CO_2. Use of CO_2 as a polymerization medium for certain grades of fluoropolymers eliminates the need for C8, which has received a lot of controversy in recent years. It remains to be seen whether many of the current grades of fluoropolymers can be synthesized in carbon dioxide. For PTFE, to date only granular forms of PTFE have been achieved. It is important to find a way to synthesize fine powders of PTFE, which should be feasible through process variable manipulations, and other fluoropolymers in CO_2 to eliminate the C8 problem. As researchers continue to enhance their understanding of CO_2-based polymer applications, and as industry continues to look for more economically and environmentally-sound alternatives to existing processes, supercritical carbon dioxide should become a technology of choice for new and improved commercial polymerization processes.

References

1. Swallow JC (1960) The history of polyethene. In: Renfrew A, Morgan P (eds) Polyethene: The technology and uses of ethylene polymers. Interscience, New York, p 1
2. Kirby CF, McHugh MA (1999) Chem Rev 99:565
3. Folie B, Radosz M (1995) Ind Eng Chem Res 34:1501
4. Guan Z, Combes JR, Menceloglu YZ, DeSimone JM (1993) Macromolecules 26:2663
5. McCoy M (1999) Chem Eng News 77:10
6. Canelas DA, DeSimone JM (1997) Adv Polym Sci 133:103
7. Cooper AI (2000) J Mater Chem 10:207
8. Kendall JL, Canelas DA, Young JL, DeSimone JM (1999) Chem Rev 99:543
9. Manivannan G, Sawan SP (1998) The supercritical state. In: McHardy J, Sawan SP (eds) Supercritical fluid cleaning: fundamentals, technology and applications. Noyes, Westwood, NJ, p 1
10. EPA (2003) Federal Register: Perfluorooctanoic acid (PFOA) and fluorinated telomers. US EPA, Washington, DC (http://www.epa.gov/opptintr/pfoa/)
11. Lee J (2003) Chemical might pose health risk to younger women and girls. New York Times, New York
12. Ring K-L, Kalin T, Kishi A (2002) Fluoropolymers. Chemical economics handbook. SRI International, Menlo Park, CA
13. Feiring AE (1994) Fluoroplastics. In: Banks RE, Smart BE, Tatlow JC (eds) Organofluorine chemistry: Principles and commercial applications. Plenum, New York, p 339
14. Gangal SV (1985) Polytetrafluoroethylene, homopolymer of tetrafluoroethylene. In: Mark HF, Bikales NM, Overberger CG, Menges G (eds) Encyclopedia of polymer science and engineering, vol 16. Wiley, New York, p 577
15. Tervoort T, Visjager J, Graf B, Smith P (2000) Macromolecules 33:6460
16. Lovinger AJ (1982) Poly(vinylidene fluoride). In: Bassett DC (ed) Developments in crystalline polymers, vol 1. Applied Science, London, p 195
17. Dohany JE (1994) Poly(vinylidene fluoride). In: Kroschwitz JI (ed) Kirk-Othmer encyclopedia of chemical technology, vol 11. Wiley, New York, p 694
18. Seiler DA (1997) PVDF in the chemical process industry. In: Scheirs J (ed) Modern fluoropolymers: High performance polymers for diverse applications. Wiley, Chichester, UK, p 487
19. Scheirs J (2001) Fluoropolymers: Technology, markets, and trends. Rapra Technology Limited, Shawbury, UK
20. Atofina Chemicals (2003) Internet brochure: Kynar PVDF for lithium batteries. Atofina Chemicals, Philadelphia, PA (http://www.atofinachemicals.com/kynarglobal/kynar-literature.cfm)
21. Kochervinskii VV, Danilyuk TY, Madorskaya LY (1986) Polym Sci USSR 28:690
22. Dohany JE, Humphrey JS (1985) Vinylidene fluoride polymers. In: Mark HF, Kroschwitz JI (eds) Encyclopedia of polymer science and engineering, vol 17. Wiley, New York, p 532
23. Jo SM, Lee WS, Oh HJ, Park S, Ahn BS, Park KY (1999) Polymer (Korea) 23:800
24. Wille RA, Burchill MT (1998) WO 9838687
25. Doll WW, Lando JB (1968) J Macromol Sci Phys 2:219
26. Dohany JE (1978) US 4076929
27. Savage PE, Gopalan S, Mizan TI, Martino CJ, Brock EE (1995) AIChE J 41:1723
28. DeSimone JM (2002) Science 297:799
29. DuPont (2002) Press Release: DuPont introduces fluoropolymers made with supercritical CO_2 technology. DuPont, Wilmington, DE
30. DeSimone JM (1996) US 5496901

31. DeSimone JM, Romack T (1997) US 5618894
32. DeSimone JM, Romack T (1997) US 5674957
33. DeSimone JM, Romack T (1999) US 5981673
34. DeSimone JM, Romack T (1999) US 5939501
35. DeSimone JM, Romack T (1999) US 5939502
36. Charpentier PA, Kennedy KA, DeSimone JM, Roberts GW (1999) Macromolecules 32:5973
37. DeSimone JM, Charpentier PA, Roberts GW (2001) WO 0134667
38. Blaude J-M, Chauvier J-M, Martin R, Bienfait C (2002) WO 02055567
39. Fukui K, Kagiya T, Yokota H (1970) JP 45003390
40. Fukui K, Kagiai T, Yokota H (1971) JP 46011031
41. Romack TJ, Combes JR, DeSimone JM (1995) Macromolecules 28:1724
42. Combes JR, Guan Z, DeSimone JM (1994) Macromolecules 27:865
43. Hintzer K, Lohr G (1997) Melt processable tetrafluoroethylene-perfluoropropylvinyl ether copolymers (PFA). In: Scheirs J (ed) Modern fluoropolymers: High performance polymers for diverse applications. Wiley, Chichester, UK, p 223
44. Bunyard WC, Kadla JF, DeSimone JM (2001) J Am Chem Soc 123:7199
45. Charpentier PA, DeSimone JM, Roberts GW (2000) Chem Eng Sci 55:5341
46. Bramer DJV, Shiflett MB, Yokozeki A (1994) US 5345013
47. Romack TJ (1997) Polymerization of fluoroolefins in liquid and supercritical carbon dioxide (free radical). PhD Thesis, University of North Carolina at Chapel Hill, Chapel Hill, NC
48. Kipp BE (1997) The synthesis of fluoropolymers in carbon dioxide and carbon dioxide/aqueous systems. PhD Thesis, University of North Carolina at Chapel Hill, Chapel Hill, NC
49. Brothers PD (2000) US 6103844
50. Galia A, Caputo G, Spadaro G, Filardo G (2002) Ind Eng Chem Res 41:5934
51. Saraf MK, Gerard S, Wojcinski.II LM, Charpentier PA, DeSimone JM, Roberts GW (2002) Macromolecules 35:7976
52. Saraf MK (2001) Polymerization of vinylidene fluoride in supercritical carbon dioxide: Molecular weight distribution. Masters Thesis, North Carolina State University, Raleigh, NC
53. DeSimone JM, Charpentier PA, Roberts GW (2001) WO 0190206
54. Charpentier PA, DeSimone JM, Roberts GW (2000) Ind Eng Chem Res 39:4588
55. Saraf MK, Wojcinski LM, Kennedy KA, Gerard S, Charpentier PA, DeSimone JM, Roberts GW (2002) Macromolecular Symp 182:119
56. Saraf MK (2002) Personal communication
57. Baradie B, Shoichet MS (2002) Macromolecules 35:3569
58. Farnham WB, Wheland RC (2001) WO 0146275
59. Lousenberg RD, Shoichet MS (2000) Macromolecules 33:1682
60. Romack TJ, DeSimone JM, Treat TA (1995) Macromolecules 28:8429
61. Wheland RC, Brothers PD (2000) US 6107423
62. Zannoni LA, DeSimone JM (2002) Polym Mater Sci Eng 87:197

Received: April 2004

Author Index Volumes 101 – 175

Author Index Volumes 1 – 100 see Volume 100

Subject Index